NASA/CP-1999-209704/VOL2/PT1

1999 NASA High-Speed Research Program Aerodynamic Performance Workshop

Volume II—High Lift

Edited by
David E. Hahne
Langley Research Center, Hampton, Virginia

December 1999

The NASA STI Program Office . . . in Profile

Since its founding, NASA has been dedicated to the advancement of aeronautics and space science. The NASA Scientific and Technical Information (STI) Program Office plays a key part in helping NASA maintain this important role.

The NASA STI Program Office is operated by Langley Research Center, the lead center for NASA's scientific and technical information. The NASA STI Program Office provides access to the NASA STI Database, the largest collection of aeronautical and space science STI in the world. The Program Office is also NASA's institutional mechanism for disseminating the results of its research and development activities. These results are published by NASA in the NASA STI Report Series, which includes the following report types:

- TECHNICAL PUBLICATION. Reports of completed research or a major significant phase of research that present the results of NASA programs and include extensive data or theoretical analysis. Includes compilations of significant scientific and technical data and information deemed to be of continuing reference value. NASA counterpart of peer-reviewed formal professional papers, but having less stringent limitations on manuscript length and extent of graphic presentations.

- TECHNICAL MEMORANDUM. Scientific and technical findings that are preliminary or of specialized interest, e.g., quick release reports, working papers, and bibliographies that contain minimal annotation. Does not contain extensive analysis.

- CONTRACTOR REPORT. Scientific and technical findings by NASA-sponsored contractors and grantees.

- CONFERENCE PUBLICATION. Collected papers from scientific and technical conferences, symposia, seminars, or other meetings sponsored or co-sponsored by NASA.

- SPECIAL PUBLICATION. Scientific, technical, or historical information from NASA programs, projects, and missions, often concerned with subjects having substantial public interest.

- TECHNICAL TRANSLATION. English-language translations of foreign scientific and technical material pertinent to NASA's mission.

Specialized services that complement the STI Program Office's diverse offerings include creating custom thesauri, building customized databases, organizing and publishing research results . . . even providing videos.

For more information about the NASA STI Program Office, see the following:

- Access the NASA STI Program Home Page at ***http://www.sti.nasa.gov***

- Email your question via the Internet to help@sti.nasa.gov

- Fax your question to the NASA STI Help Desk at (301) 621-0134

- Telephone the NASA STI Help Desk at (301) 621-0390

- Write to:
  NASA STI Help Desk
  NASA Center for AeroSpace Information
  7121 Standard Drive
  Hanover, MD 21076-1320

NASA/CP-1999-209704/VOL2/PT1

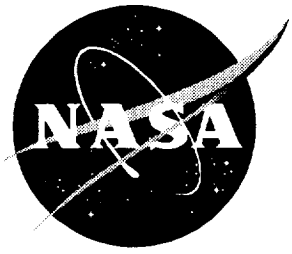

1999 NASA High-Speed Research Program Aerodynamic Performance Workshop

Volume II—High Lift

Edited by
David E. Hahne
Langley Research Center, Hampton, Virginia

Proceedings of a workshop sponsored by
the National Aeronautics and Space
Administration, Washington D.C., and
held in Anaheim, California
February 8–12, 1999

National Aeronautics and
Space Administration

Langley Research Center
Hampton, Virginia 23681-2199

December 1999

The use of trademarks or names of manufacturers in this report is for accurate reporting and does not constitute an official endorsement, either expressed or implied, of such products or manufacturers by the National Aeronautics and Space Administration.

Available from:

NASA Center for AeroSpace Information (CASI)
7121 Standard Drive
Hanover, MD 21076-1320
(301) 621-0390

National Technical Information Service (NTIS)
5285 Port Royal Road
Springfield, VA 22161-2171
(703) 605-6000

PREFACE

The High-Speed Research Program sponsored the NASA High-Speed Research Program Aerodynamic Performance Review on February 8-12, 1999 in Anaheim, California. The review was designed to bring together NASA and industry High-Speed Civil Transport (HSCT) Aerodynamic Performance technology development participants in areas of: Configuration Aerodynamics (transonic and supersonic cruise drag prediction and minimization) and High-Lift. The review objectives were to: (1) report the progress and status of HSCT aerodynamic performance technology development; (2) disseminate this technology within the appropriate technical communities; and (3) promote synergy among the scientist and engineers working HSCT aerodynamics. The HSR AP Technical Review was held simultaneously with the annual review of the following airframe technology areas: Materials and Structures, Environmental Impact, Flight Deck, and Technology Integration. Thus, a fourth objective of the Review was to promote synergy between the Aerodynamic Performance technology area and the other technology areas within the airframe element of the HSR Program.

The work performed in the Configuration Aerodynamics (CA) element of the High-Speed Research Program during 1998 was presented in the following sessions:

Propulsion Integration
Analysis Methods
Design Optimization
Testing

The work performed in the High Lift (HL) element of the High-Speed Research Program during 1998 was presented in the following sessions:

High-Lift Configuration Development
Tools and Methods Development

The proceedings for the Aerodynamic Performance Annual Review are published in three volumes:

Volume I, Parts 1 and 2	Configuration Aerodynamics
Volume II, Parts 1 and 2	High Lift

AP Review Chairperson: David Hahne
NASA Langley Research Center

CONTENTS

*Part 2 is presented under separate cover.

Data Corrections and Wind-Tunnel Data Comparisons of a 5% TCA model in the NASA Ames 12-ft. Pressure Tunnel

Fanny A. Zuniga
NASA Ames Research Center

HSR Airframe Technical Review
Anaheim, CA
February 9-11, 1999

This figure lists the outline of the paper.

Outline

- Test Objectives
- Test Summary
- Model Geometry
- Data Corrections
- Comparison of WICS vs. Classical Corrections
- Repeatability
- Test to Test Comparisons
- Summary

This figure lists the primary test objectives of the 5% TCA test. The objectives are listed in order of priority.

Test Objectives

- Determine the effect of geometric variations near the inboard leading-edge flap on high-lift and stability and control performance data.
- Determine Re effects on TCA high-lift configuration for optimum high-lift and stability and control performance at takeoff, climbout, approach and landing conditions.
- Obtain flow-visualization data on upper surface of wing for CFD validations.

This figure summarizes the TCA-3 test. It shows the test occupancy dates, number of runs, range of conditions, model instrumentation, leading-edge flap configurations and data taken.

TCA-3 Test Summary

- 5% TCA model tested in ARC's 12-ft. PWT tunnel
  - Occupancy Dates: Jan. 22 - Feb. 23, 1998
  - Data Runs: 464 Runs
- Range of Conditions

Mach number	0.24
Total Pressure	1 to 4.7 atm.
Reynolds number	7.13 to 36.8 million
Dynamic Pressure	85 to 386 psf
Angle of Attack	-4° to 31° (1 atm.)
	-4° to 24° (4.7 atm.)

TCA-3 Test Summary

- Leading-Edge Flaps
  - Plain, Cambered, Drooped, Sealed-Slats
- 380 Model Surface Pressures
- Pressure Sensitive Paint
- Model Deformation Data
- Color Oil Flow Visualization
- Skin Friction Oil Interferometry Data

This figure shows a side-view of the 5% TCA model in the 12-ft. tunnel test section. It shows the model at two angles-of-attack, 0° and 31° (max alpha at 1 atm.). At max alpha, the nose of the model was 14.1 in. from the ceiling and the tail was 23.1 in. from the tunnel floor. The model pitched up and down through deflection of the aft pitch strut. The figure is drawn to scale.

Model Geometry

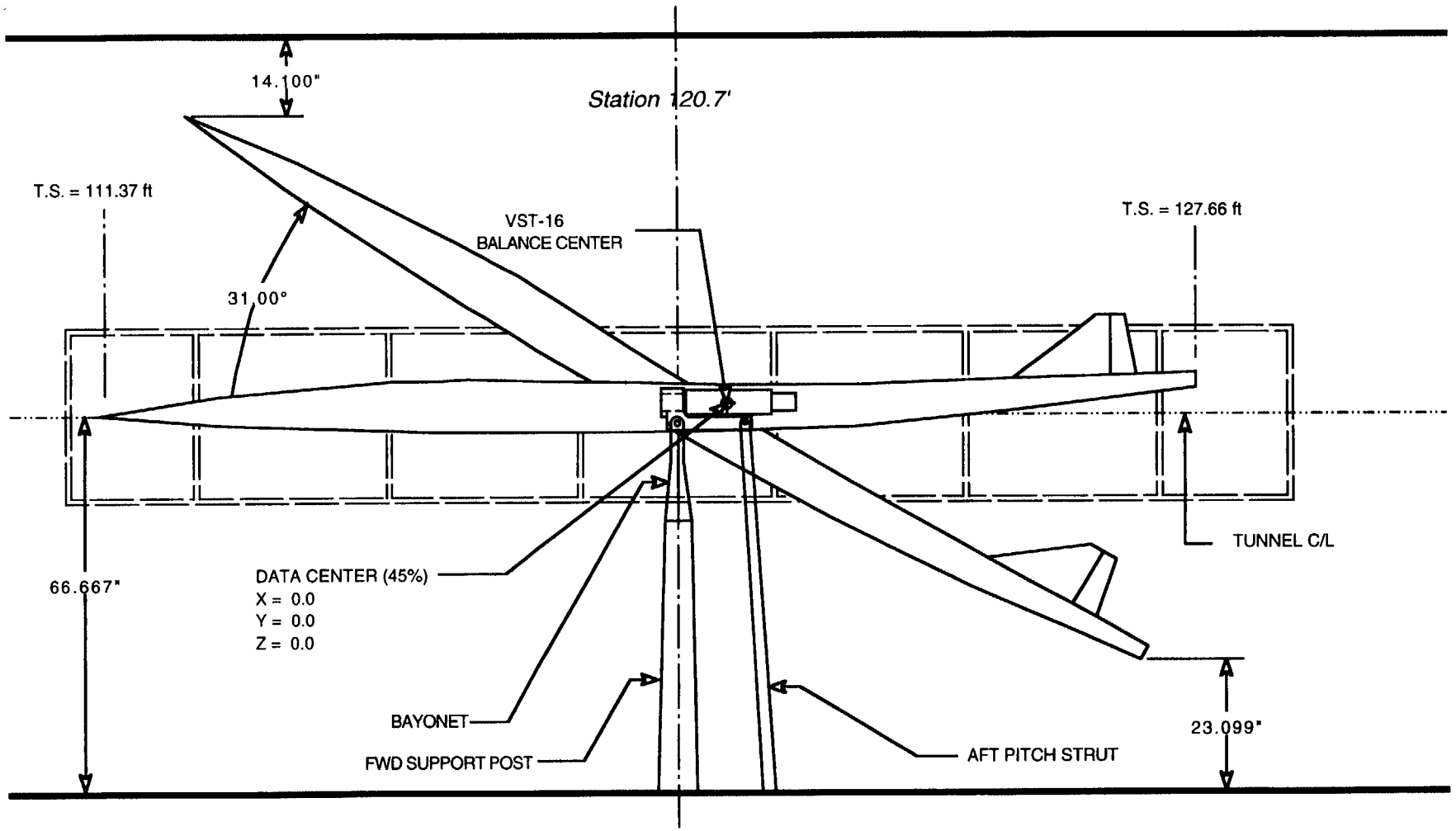

This figure shows a forward-view looking aft of the 5% TCA model in the 12-ft. tunnel test section. It shows the model at 31° angle of attack (max alpha at 1 atm.). At max alpha, the wingtips were 2.37 ft. from the flat section of the wall. The post was 6.6 in. in diameter at the tunnel floor. The total solid body blockage of the model and the post was 15% at max alpha. The figure is drawn to scale.

5% TCA Model in 12-ft Tunnel

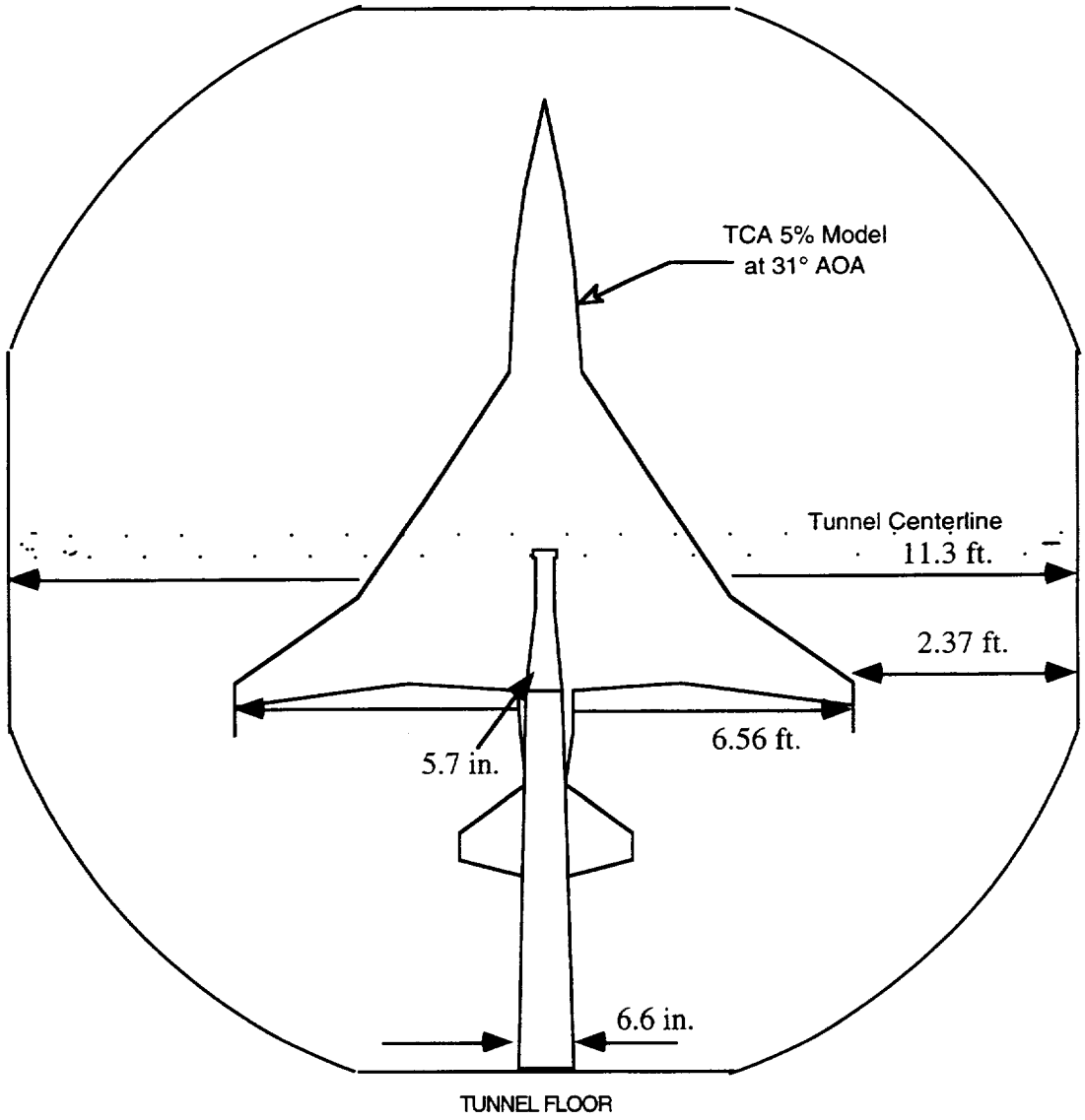

VIEW LOOKING AFT

This figure shows all the data corrections applied to the data. The left-hand column lists the correction type and the right-hand term lists the corresponding correction term. The difference between the classical and WICS correction methods will be described in the following charts.

12-ft. Data Corrections

Correction Type	Correction Term
Blockage (solid and wake)	ΔM and ΔQ (Classical and WICS)
Wall correction	$\Delta\alpha$ (Classical and WICS)
Buoyancy	ΔAF
Cavity Pressure	ΔNF and ΔPM
Nacelle Base	ΔNF, ΔAF and ΔPM
Nacelle Internal Drag	ΔNF, ΔAF and ΔPM

This figure describes the difference between the classical and the WICS correction methods. The classical method is based on 3 reports: NACA Report TR995[1], Maskell[2] reference and Sivells and Salmi[3] reference. The solid body blockage is determined by source-sink method as outlined in TR995. The wake blockage for attached and separated flow is determined by a semi-empirical method as outlined in Maskell's reference. This method is based on a flat-plate estimate. The angle-of-attack correction is described in the Sivells and Salmi reference. This method was specifically developed for closed-circular test sections similar to the 12-ft. tunnel test section.

The Wall Interference Correction System (WICS) is based on potential flow theory and uses wall pressure data in combination with lift force data to obtain blockage factor and angle-of-attack correction terms. The WICS method is described in Ulbrich's[4] reference. Since the WICS method uses wall pressure data in its estimate of the corrections, this method has been proven to be more accurate in estimating wake blockage due to separation than the classical method for the 12-ft. tunnel. However, during the TCA3 test, only the classical corrections were available real-time online to the user. Therefore, the classical corrections were used as the primary coefficient set during the test.

[1]J.G. Herriot, Blockage Corrections for Three Dimensional-Flow Closed-Throat Wind Tunnels with Consideration of the Effect of Compressibility, NACA TR 995, 1950.

[2]E.C. Maskell, A Theory of the Blockage Effects on Bluff Bodies and Stalled Wings in a Closed Wind Tunnel, ARC R&M 3400, 1965.

[3]J.C. Sivells and R.M. Salmi, Jet Boundary Corrections for Complete and Semispan Swept Wings in Closed Circular Wind Tunnels, TN 2454, 1951.

[4]N. Ulbrich, The Real-Time Wall Interference Correction System of the NASA Ames 12-Foot Pressure Wind Tunnel, NASA/CR-1998,208537, July 1998.

"Classical" Method

- Solid body blockage determined by source-sink system as outlined in NACA Report TR995
- Wake blockage for attached and separated flow determined by semi-empirical method as outlined in Maskell reference
- Angle-of-attack correction for closed-circular test sections is described in Sivells and Salmi reference

Wall Interference Correction System (WICS)

- Blockage and AOA correction based on method described in Ulbrich's report NASA/CR-1998-208537
- Uses wall pressure data in combination with lift force data to obtain blockage factor and AOA correction

This figure shows a comparison of the dynamic pressure corrections for the classical and WICS methods at high and low Reynolds numbers. The data shown was taken for plain flaps with leading-edge flaps deflected at 35°, trailing-edge flaps deflected at 15°/15°/15/10° and horizontal tail set at 0°.

The data showed good agreement for alphas up to 15° at low Reynolds number and good agreement up to 10° at high Reynolds number. Above these alphas, the differences between the classical and WICS corrections grew greater with increasing alpha. At max alpha, the classical corrections were about twice as big as the WICS corrections. These differences can be due to the different methods in estimating wake blockage due to separated flow used in the classical and WICS methods. As stated earlier, the WICS method does a better job in estimating the wake blockage than the classical method and should be the preferred correction set at these higher angles-of-attack.

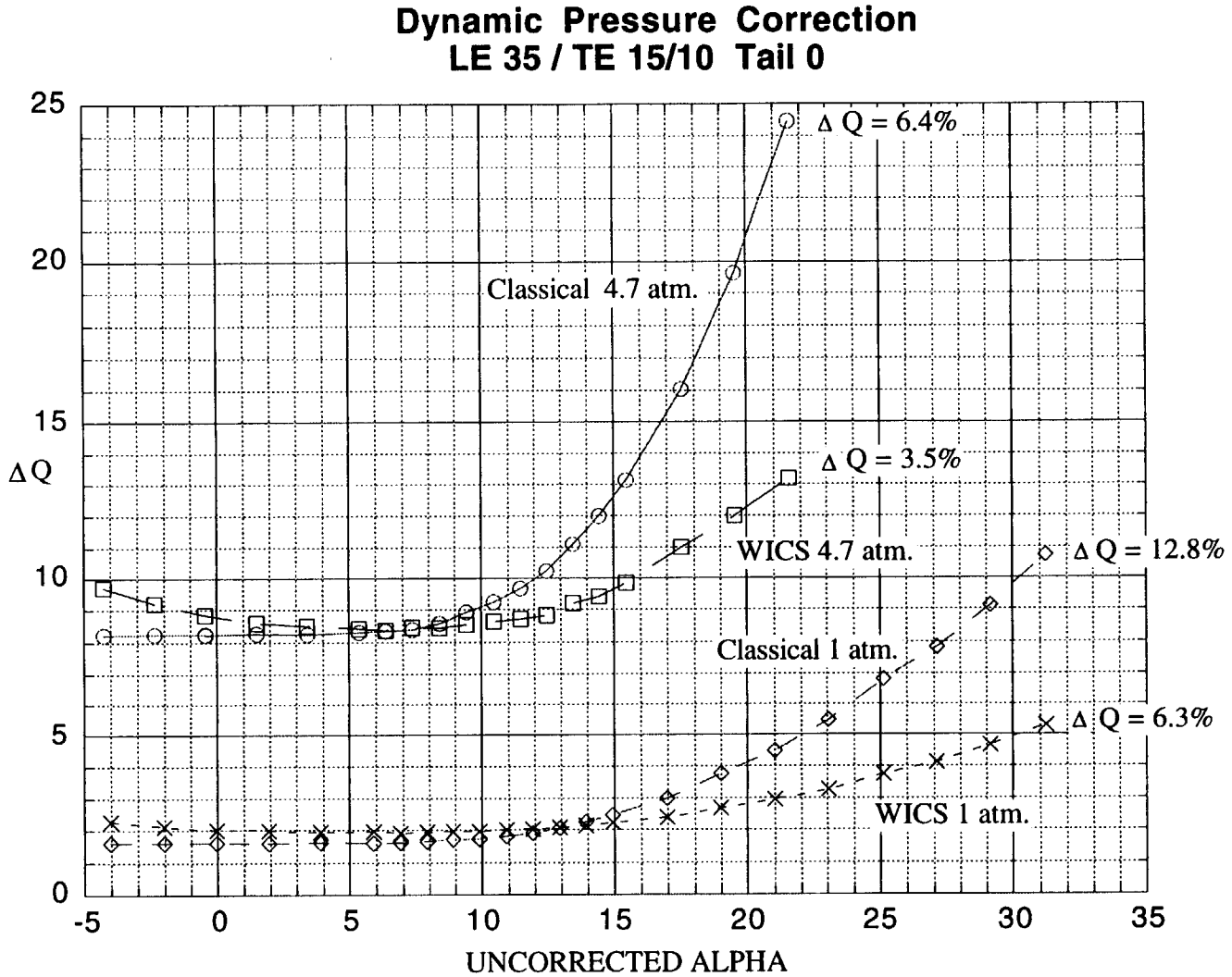
Dynamic Pressure Correction
LE 35 / TE 15/10 Tail 0
ΔQ
UNCORRECTED ALPHA
25
20
15
10
5
0
-5
0
5
10
15
20
25
30
35
Δ Q = 6.4%
Classical 4.7 atm.
Δ Q = 3.5%
WICS 4.7 atm.
Δ Q = 12.8%
Classical 1 atm.
Δ Q = 6.3%
WICS 1 atm.

This figure shows a comparison of the angle-of-attack corrections using the classical and WICS methods at high and low Reynolds numbers. The data shows very good agreement between the two correction methods for alphas up to 15°. At the nominal alpha of 10°, the alpha correction is slightly less than 1° for high and low Reynolds numbers.

Angle-of-Attack Correction
LE 35/ TE 15/10 Tail 0

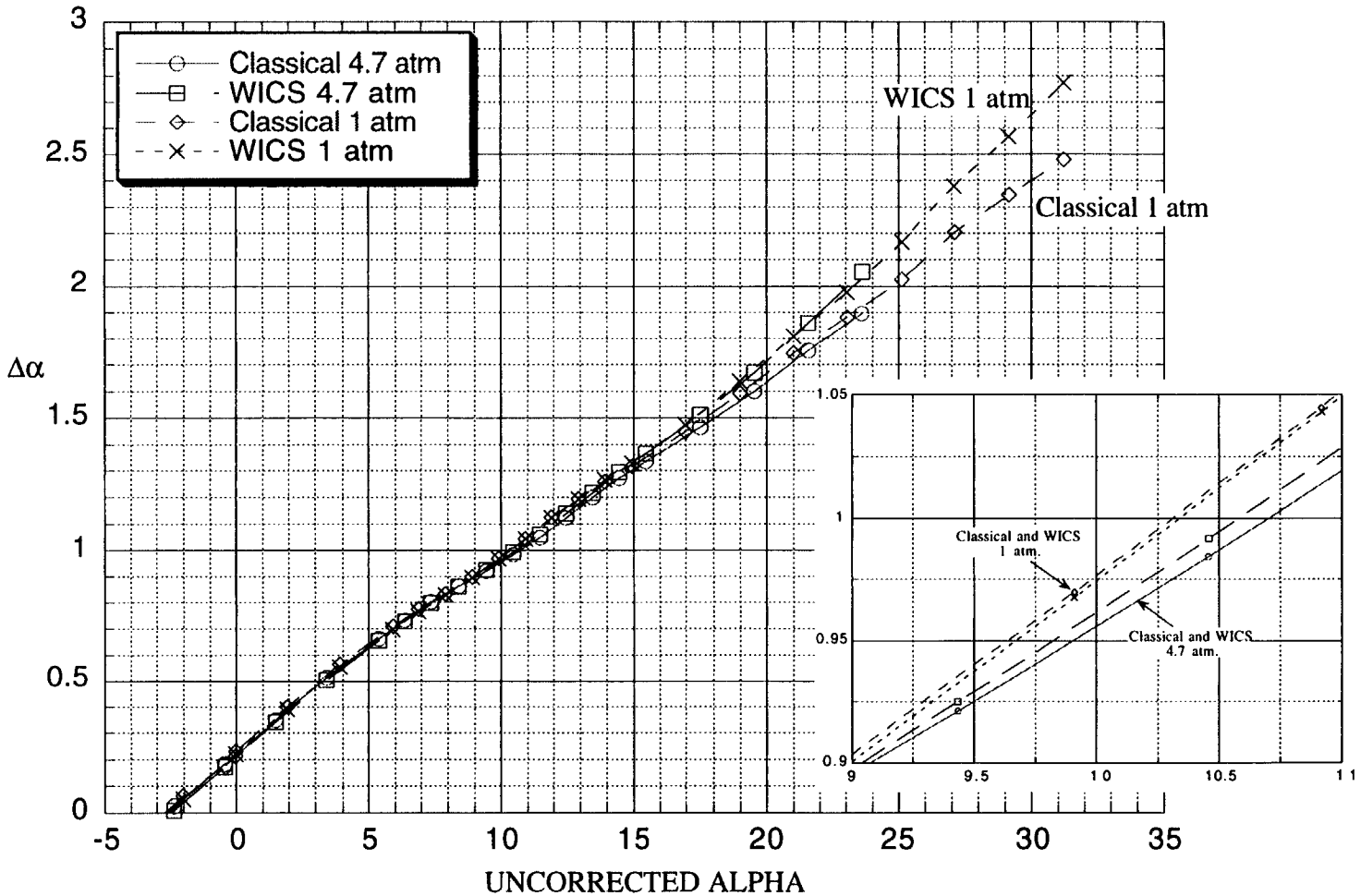

This figure shows force and moment correction data for high Reynolds number and nominal CL=0.5. The correction terms included in this figure are cavity, nacelle base, buoyancy and nacelle internal drag. These correction terms in general were very small. The total change in lift and pitching moment coefficient was 0.2%. The change in drag coefficient was -2.5%.

Sample Force and Moment Correction Data

Data from Run 119 at 4.7 atm and CL=0.5
LE 35 TE 15/10 and Tail 0

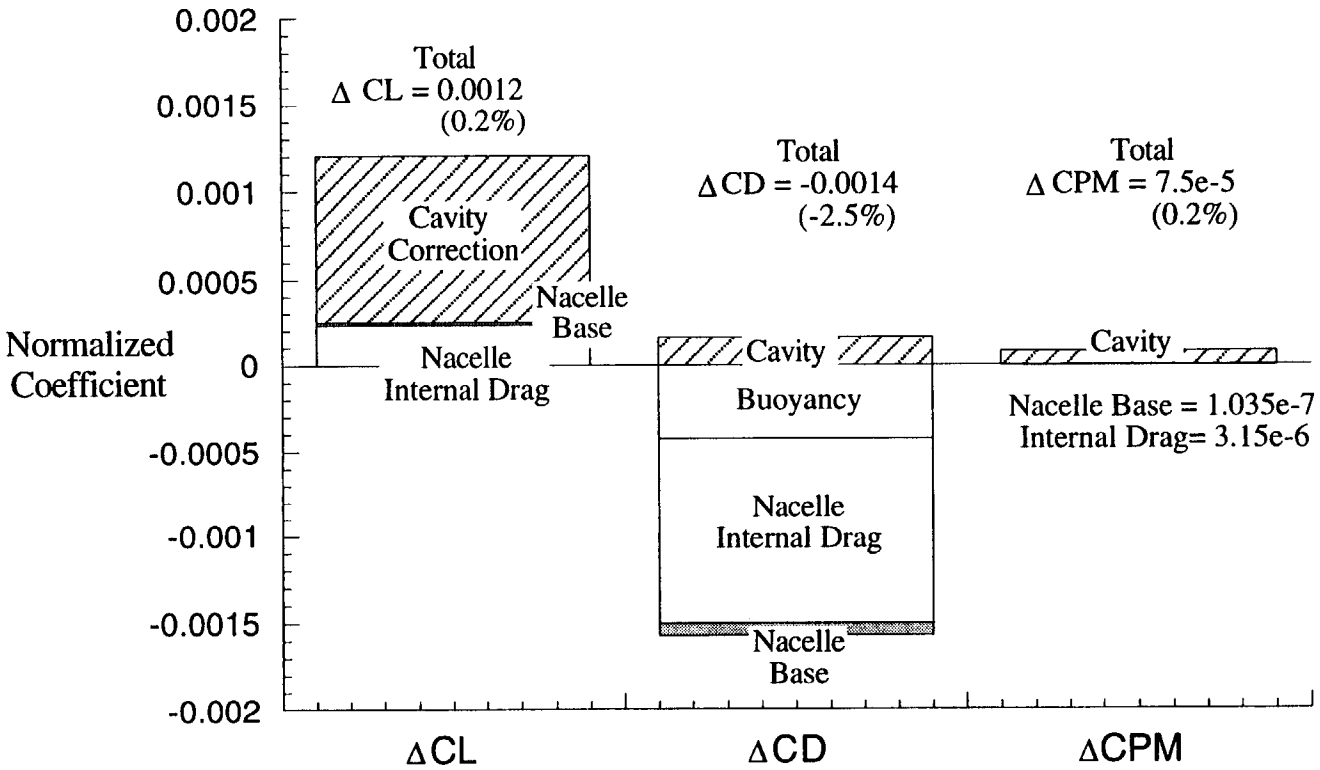

This figure shows a comparison of lift coefficient corrections using classical and WICS methods at high Reynolds number. The data shows good agreement up to 10° alpha. As before, the WICS method resulted in a smaller correction than the classical method.

Lift Coefficient Correction

Classical vs. WICS at 4.7 atm.

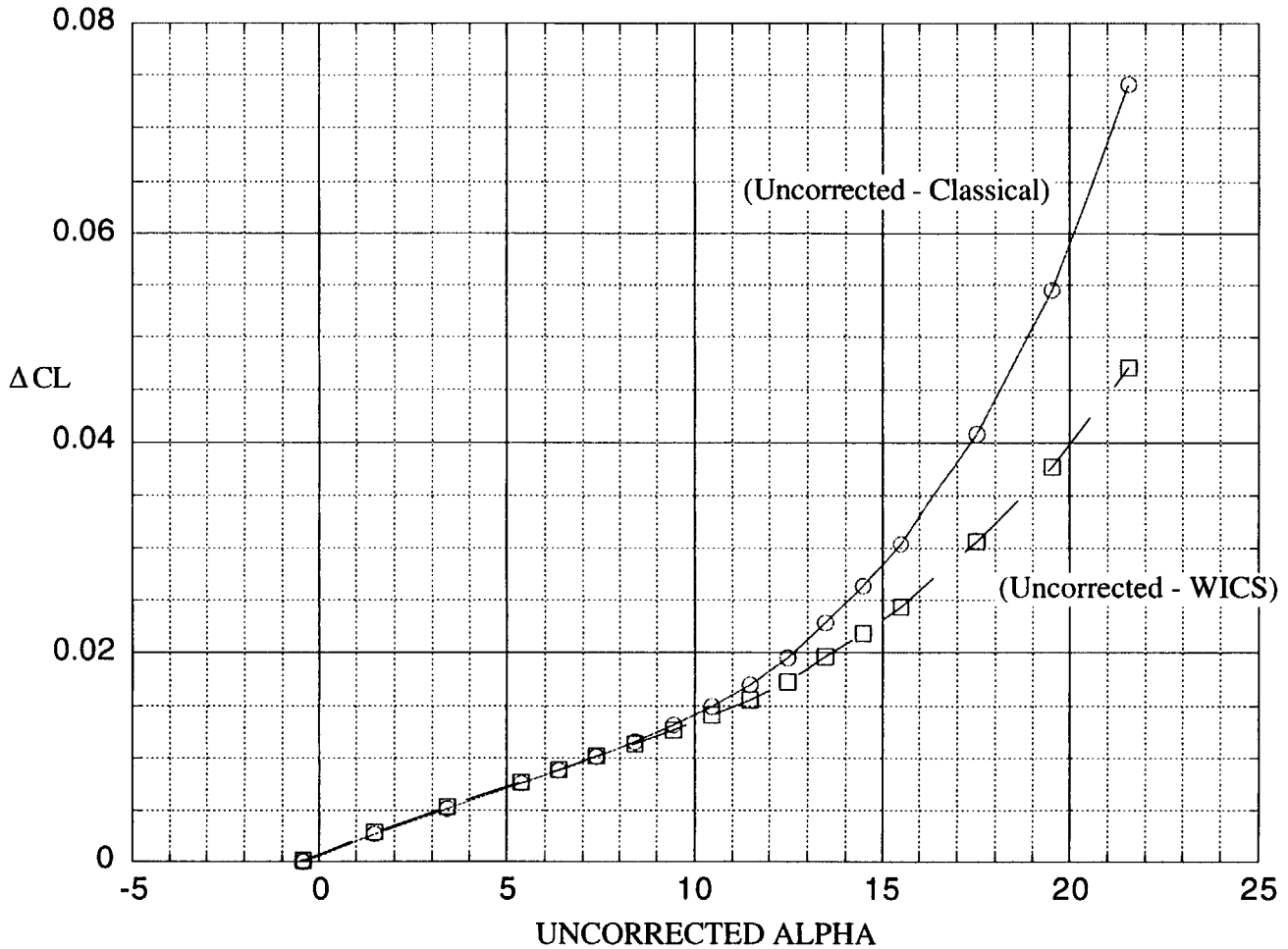

This figure shows a comparison of drag coefficient corrections using classical and WICS methods at high Reynolds number. The data shows good agreement up to 12° alpha.

Drag Coefficient Correction

Classical vs. WICS at 4.7 atm.

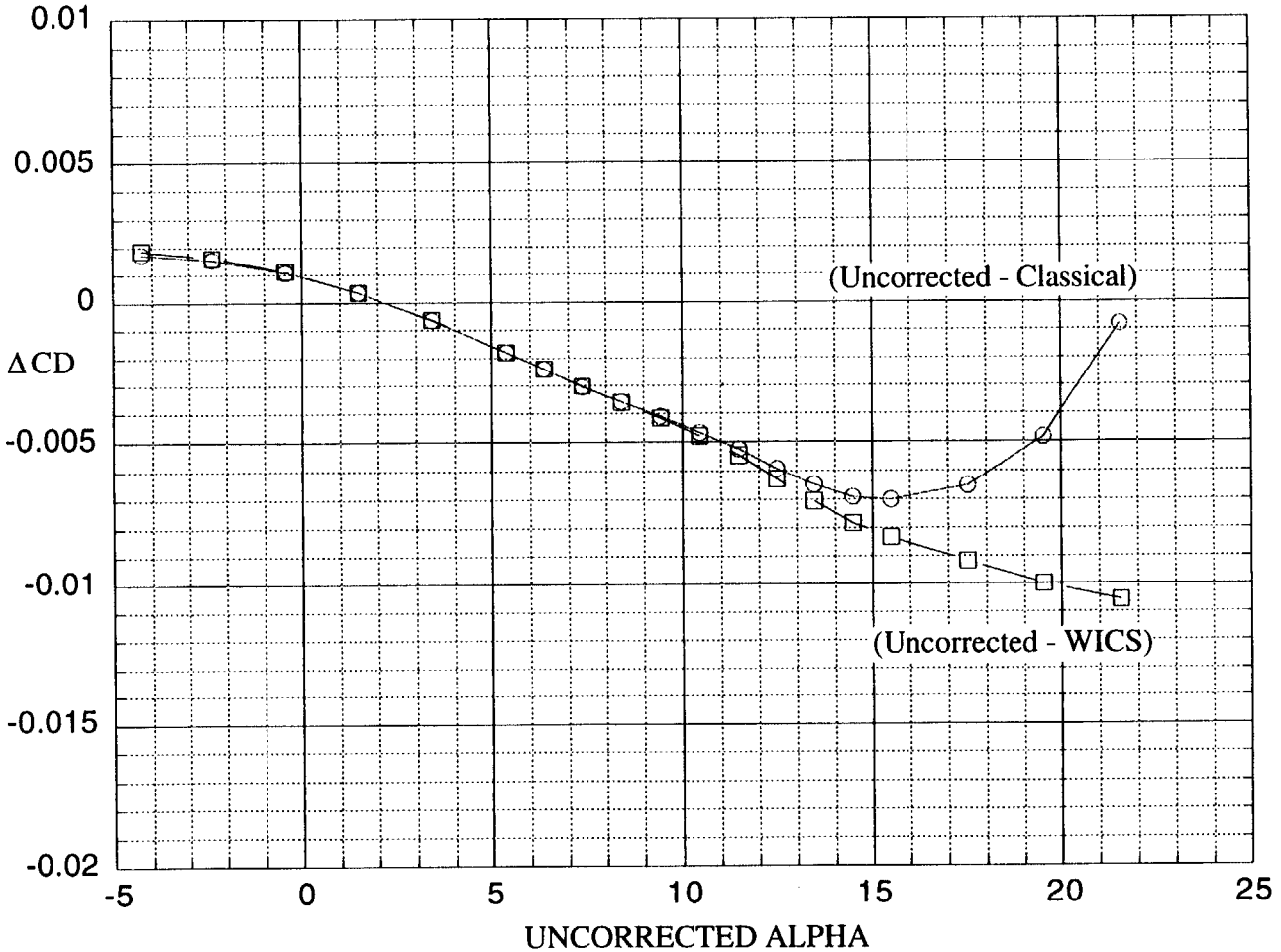

This figure shows a comparison of pitching moment coefficient corrections using classical and WICS methods at high Reynolds number. The data shows good agreement up to 14° alpha.

Pitching Moment Coefficient Correction

Classical vs. WICS at 4.7 atm.

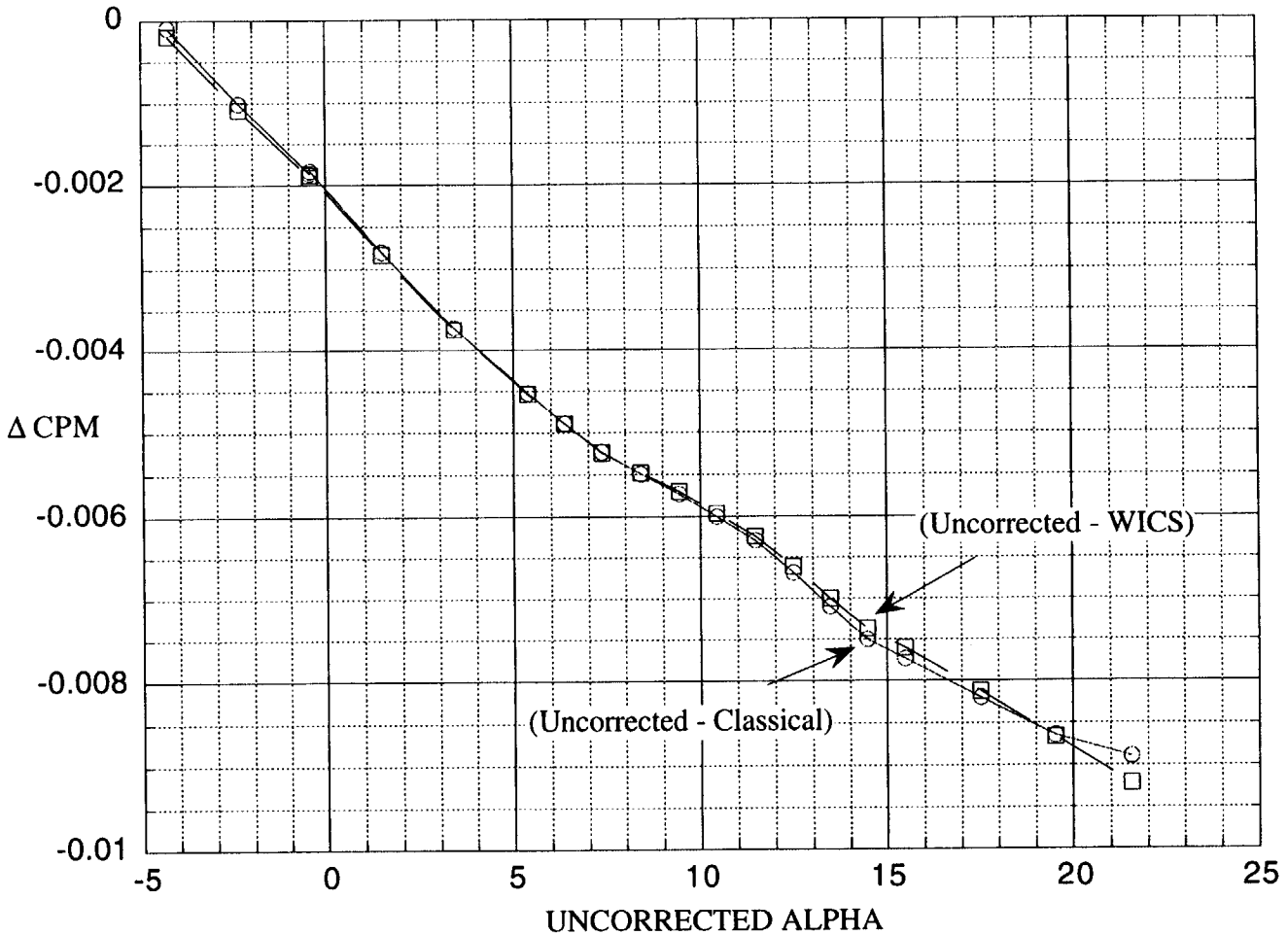

This bar graph summarizes the force and moment correction terms for the classical and WICS methods. This data shows the percentage difference between the corrected and uncorrected coefficient. This chart shows little difference between the classical and WICS corrections at the nominal condition of CL=0.5 and at high Reynolds number. It should be noted that the differences between the correction terms are much greater at high alphas as was seen in the previous charts. It is therefore recommended that the WICS data be used at alphas greater than 15° at low Reynolds number and at alphas greater than 10° at high Reynolds number.

Comparison of WICS and Classical Corrections on Aerodynamic Coefficients at CL = 0.5 and 4.7 atm.

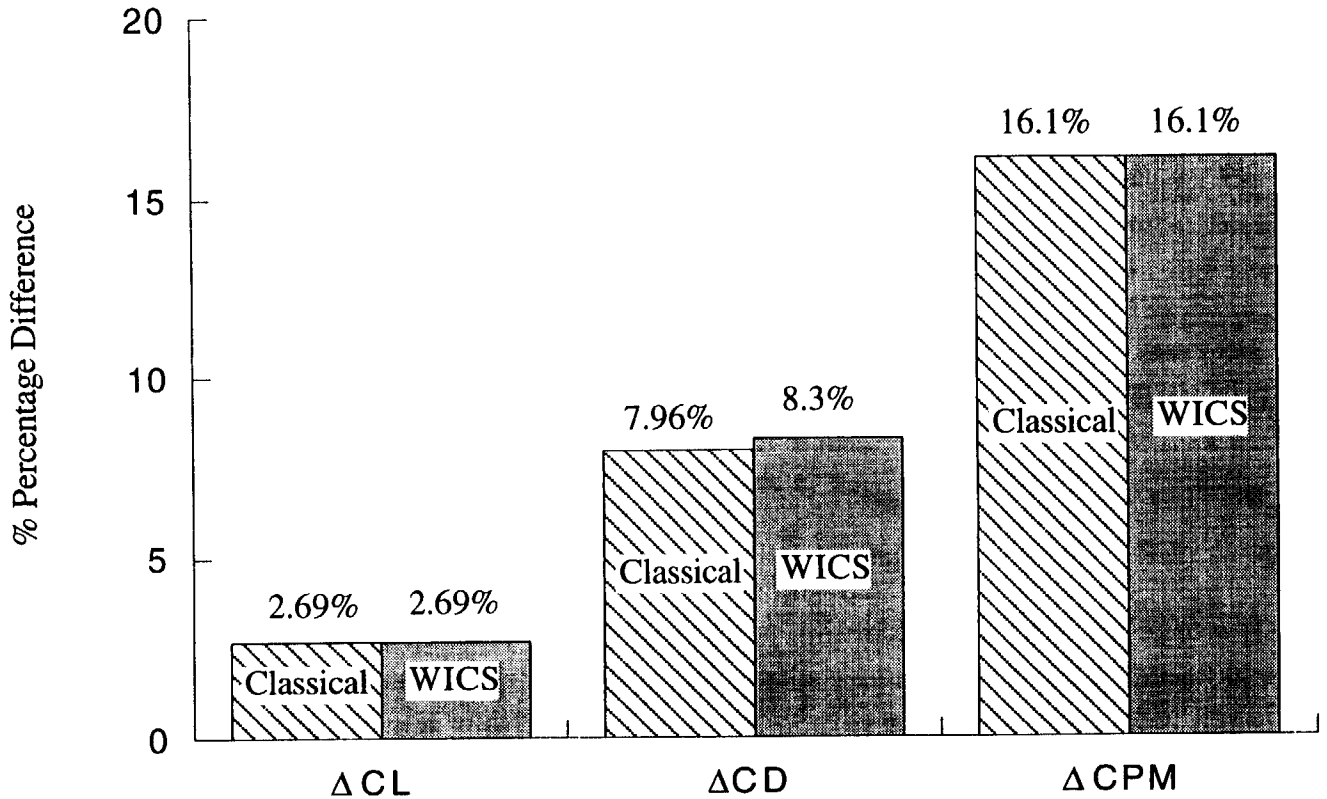

This figure shows repeatability data for lift coefficient at high Reynolds number for runs 104, 105, 227, 295 and 346 which included runs at the beginning, middle and end of the test. The model configuration for these runs were the baseline plain flaps (LE 30 TE 15/10). The data shows very good repeatability up to max alpha. At the nominal alpha of 10°, the data scatter was within ±0.0025 CL.

TCA3 Repeat Runs
Lift Coefficient Comparison

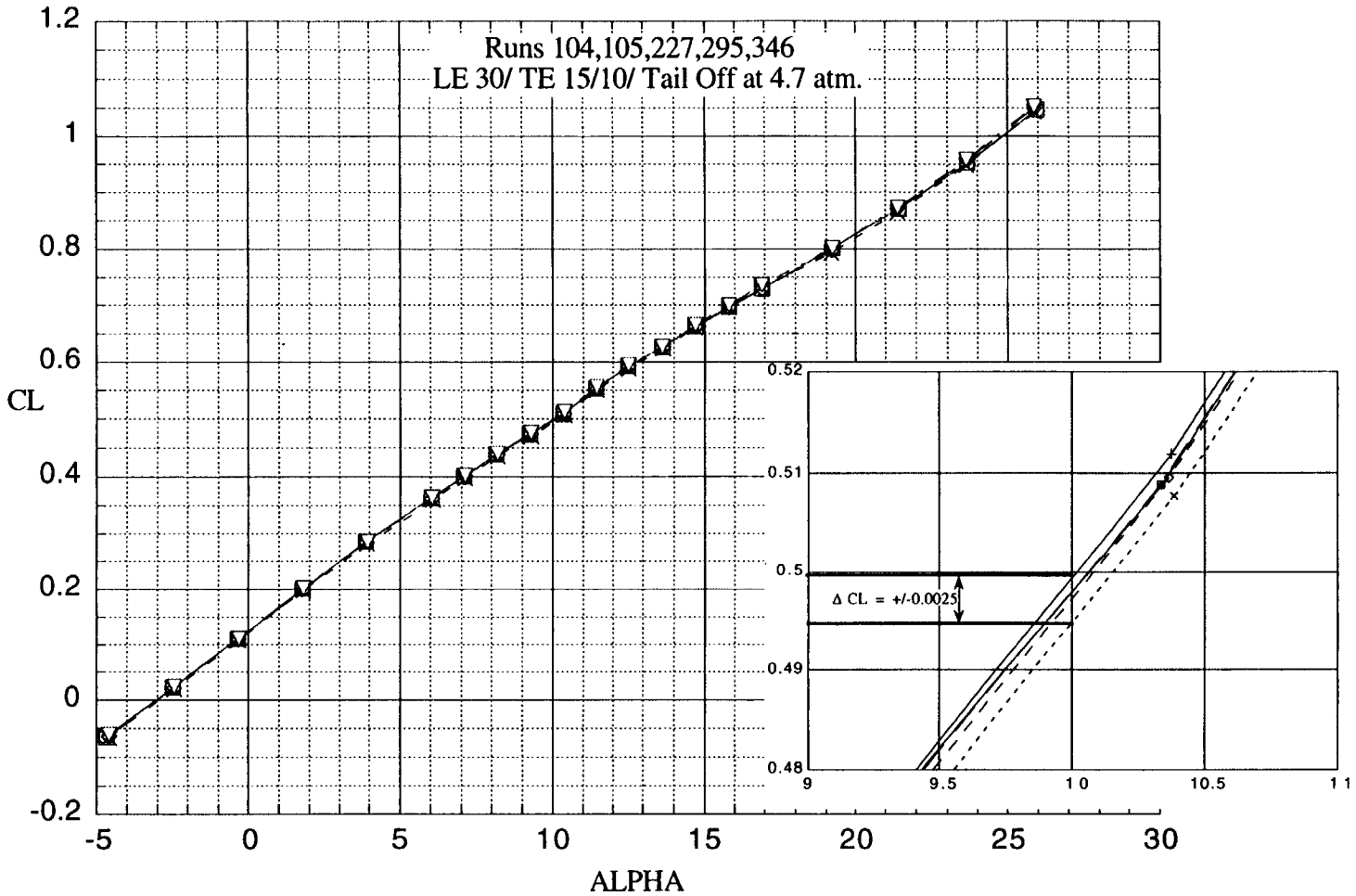

This figure shows repeatability data for drag coefficient at high Reynolds number for runs 104, 105, 227, 295 and 346 which included runs at the beginning, middle and end of the test. The model configuration for these runs were the baseline plain flaps (LE 30 TE 15/10). The data shows very good repeatability up to max alpha. At the nominal alpha of 10°, the data scatter was within ±2 drag counts.

TCA3 Repeat Runs
Drag Coefficient Comparison

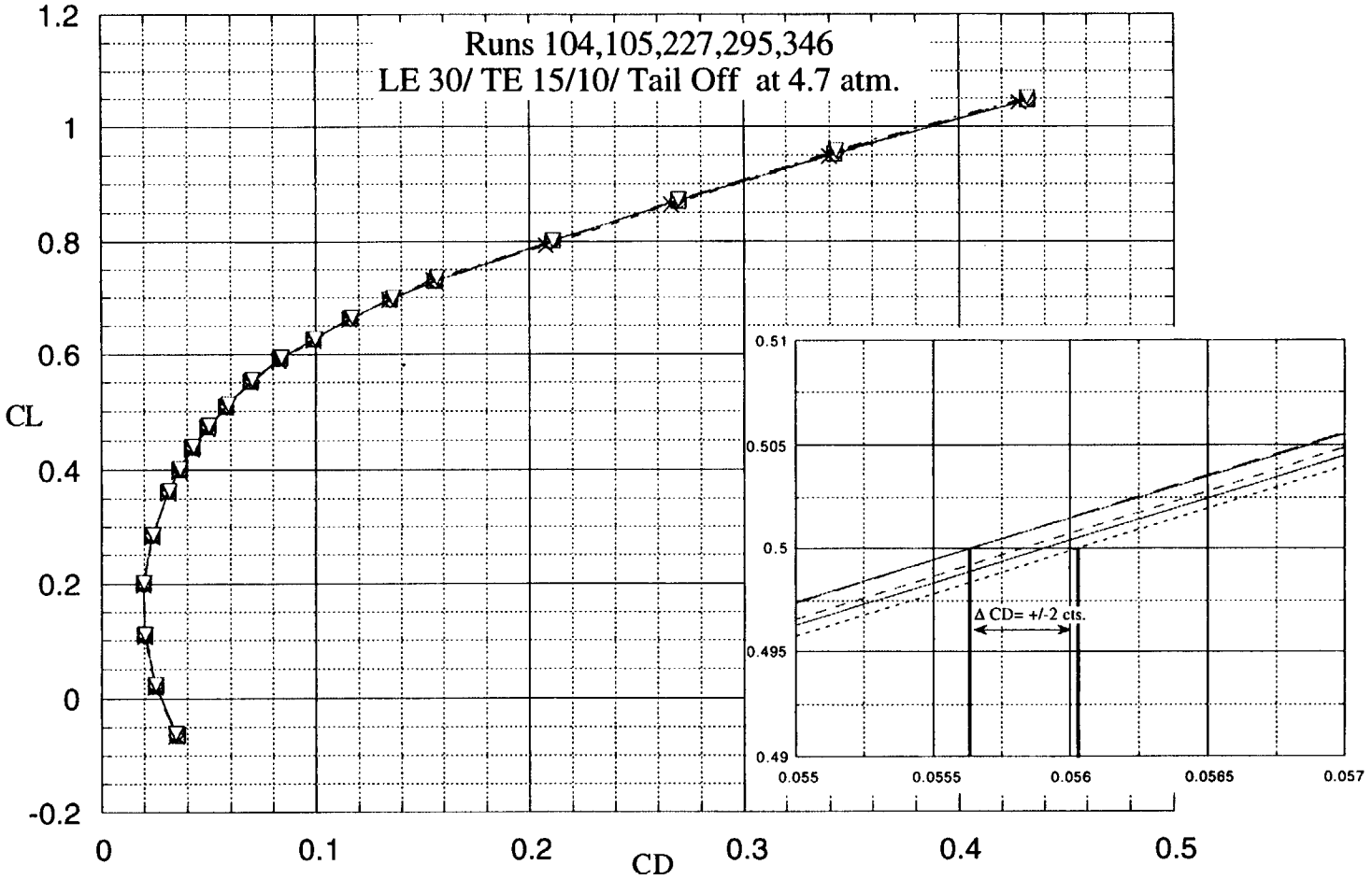

This figure shows repeatability data for lift-to-drag ratio at high Reynolds number for runs 104, 105, 227, 295 and 346 which included runs at the beginning, middle and end of the test. The model configuration for these runs were the baseline plain flaps (LE 30 TE 15/10). The data shows very good repeatability up to max alpha. At the nominal alpha of 10°, the data scatter was within ±0.032 L/D.

TCA3 Repeat Runs
Lift-to-Drag Ratio Comparison

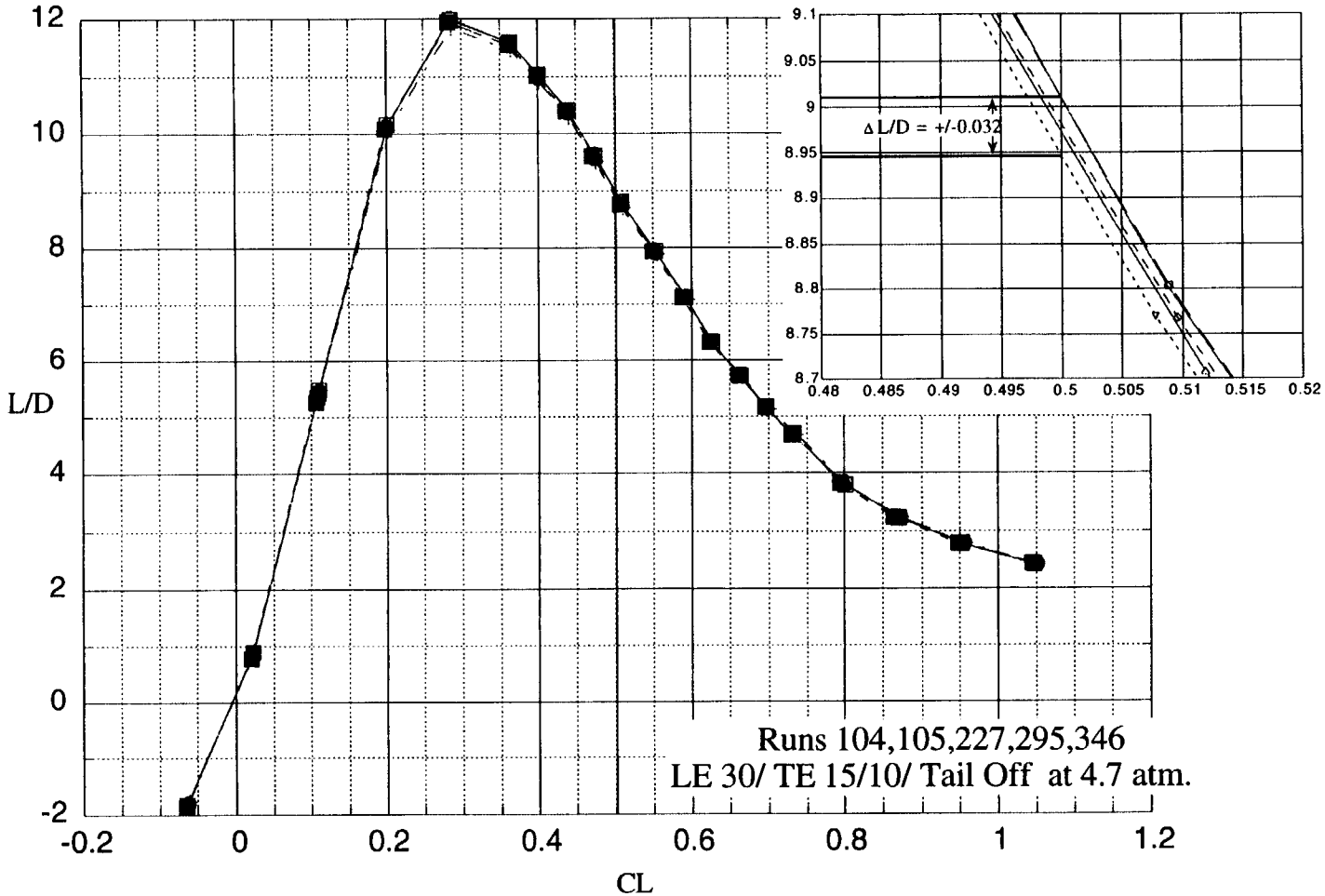

This figure shows repeatability data for pitching moment coefficient at high Reynolds number for runs 104, 105, 227, 295 and 346 which included runs at the beginning, middle and end of the test. The model configuration for these runs were the baseline plain flaps (LE 30 TE 15/10). The data shows very good repeatability up to max alpha. At the nominal alpha of 10°, the data scatter was within ±0.00028 CPM.

TCA3 Repeat Runs
Pitching Moment Coefficient Comparison

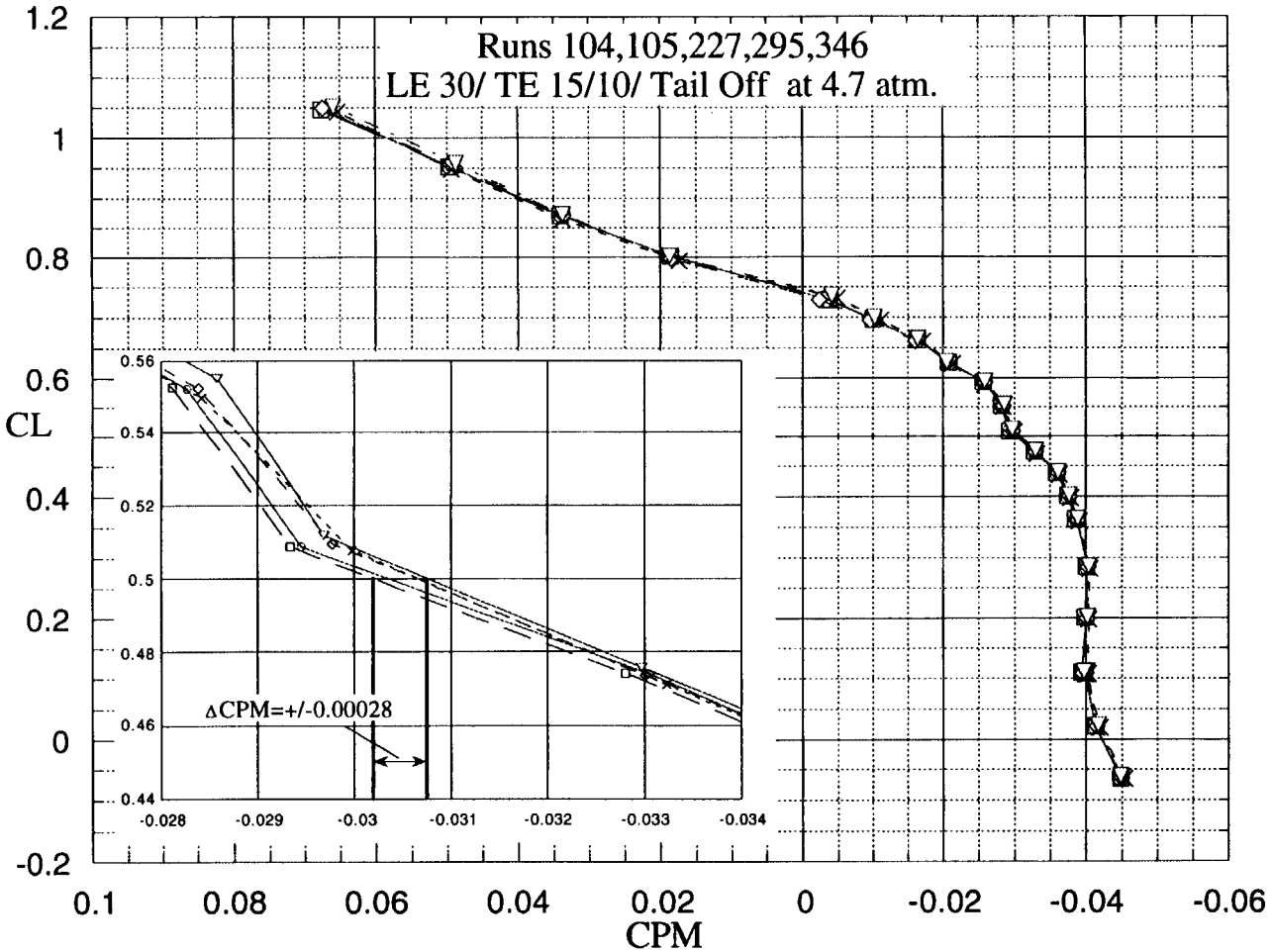

This figure summarizes the repeatability data at high and low Reynolds number. The data scatter at high Reynolds number is less than at low Reynolds number. This was expected since the loads at the high Reynolds number case were designed to use the full range of the balance capacity.

Summary of Repeatability Data

	TCA-3 4.7 atm.	TCA-3 1 atm.
ΔCL	±0.0025	±0.015
ΔCD	± 2 cts.	± 3.5 cts.
ΔCPM	±0.00028	±0.0005
ΔL/D	±0.032	±0.06

This figure summarizes the corrections applied at ARC's 12-ft. and LaRC's 14x22-ft. tunnel. The methods used to determine blockage and wall corrections are different at each tunnel. The equations used to determine cavity, nacelle internal drag, and nacelle base were the same for each tunnel. The 12-ft. applies a buoyancy correction which is a drag force produced as a result of a variation of longitudinal static pressure along the test section. The 14x22-ft. does not account for this correction since this correction term is very small in the 14x22-ft. test section.

One final difference in the data corrections between the 12-ft. and 14x22-ft. is the mount support system interference correction. Only the 14x22-ft. accounts for this correction. This correction term is based on 6% Ref H data from Langley's test #442. There was no upflow and support interference data available for the 12-ft. tunnel.

12-ft. vs. 14x22-ft. Corrections

12-ft.	14x22-ft.
Solid and Wake Blockage (Maskell)	Solid and Wake Blockage
Wall correction (Sivells and Salmi)	Wall correction (Heyson)
Cavity	Cavity
Nacelle Internal Drag	Nacelle Internal Drag
Nacelle Base	Nacelle Base
Buoyancy	Mount system interference

This figure compares the lift coefficient curves between the TCA-3 and TCA-4 tests. The TCA-3 (12-ft.) fully-corrected data was compared to the TCA-4 (14x22-ft.)data with and without the mount support system interference correction. The interference correction was not added to the 12-ft data since this correction was determined from data on the 6% Ref H model in the 14x22-ft. using a different support post.

The figure shows better agreement between the 12-ft. and 14x22-ft. fully-corrected data than with the 14x22-ft. data without the interference correction. Since there was no upflow and support interference data available for the 12-ft., no assumptions were made to estimate the magnitude and sign of this correction term for the 5% TCA model in the 12-ft. test section.

Test-to-Test Comparison

TCA-3 and TCA-4 Tests

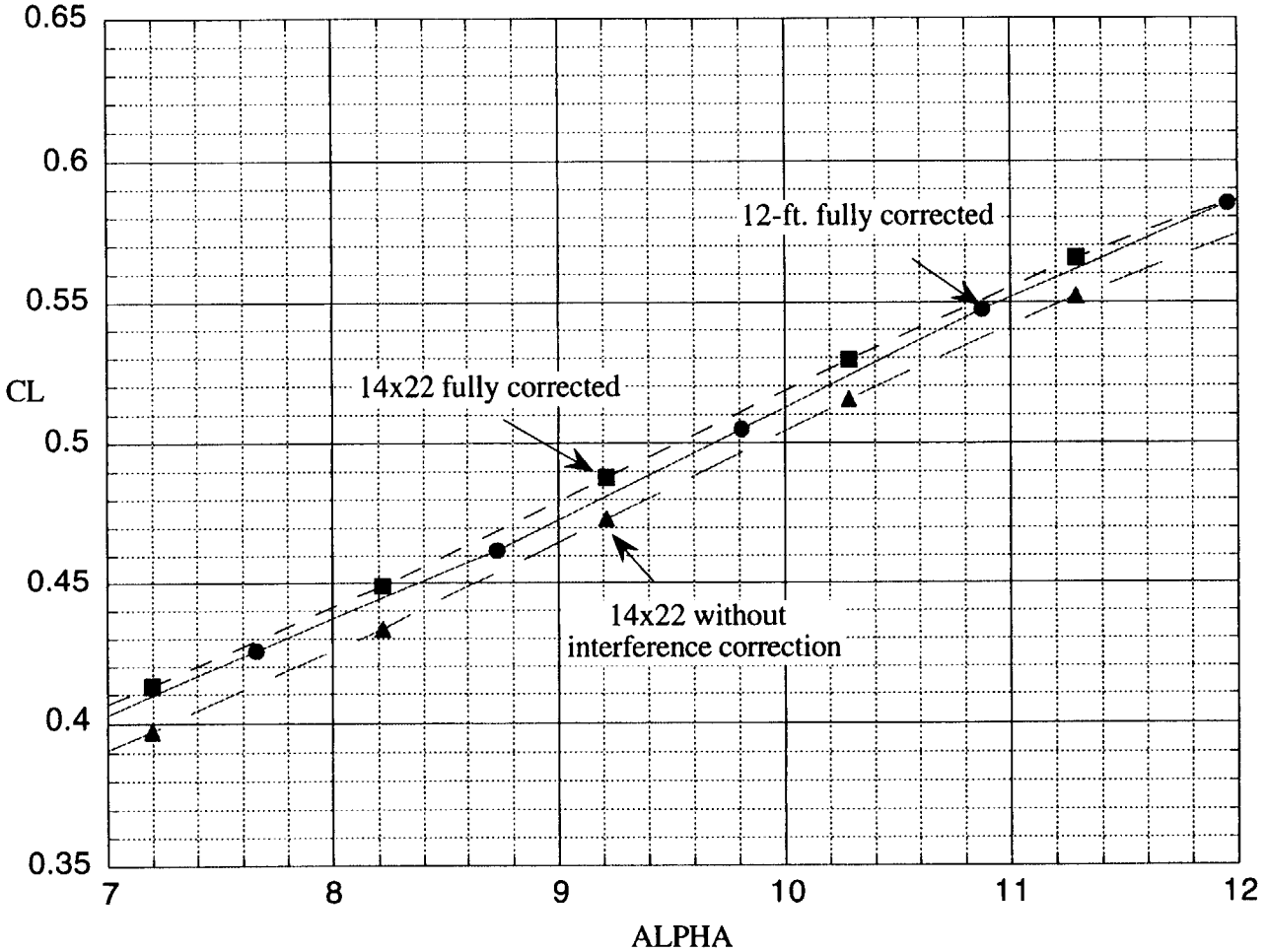

This figure compares the lift-to-drag ratios between the TCA-3 and TCA-4 tests. The figure shows little difference between the 14x22-ft. fully-corrected data and the 14x22-ft. data without the interference correction.

Test-to-Test Comparison

TCA-3 and TCA-4 Tests

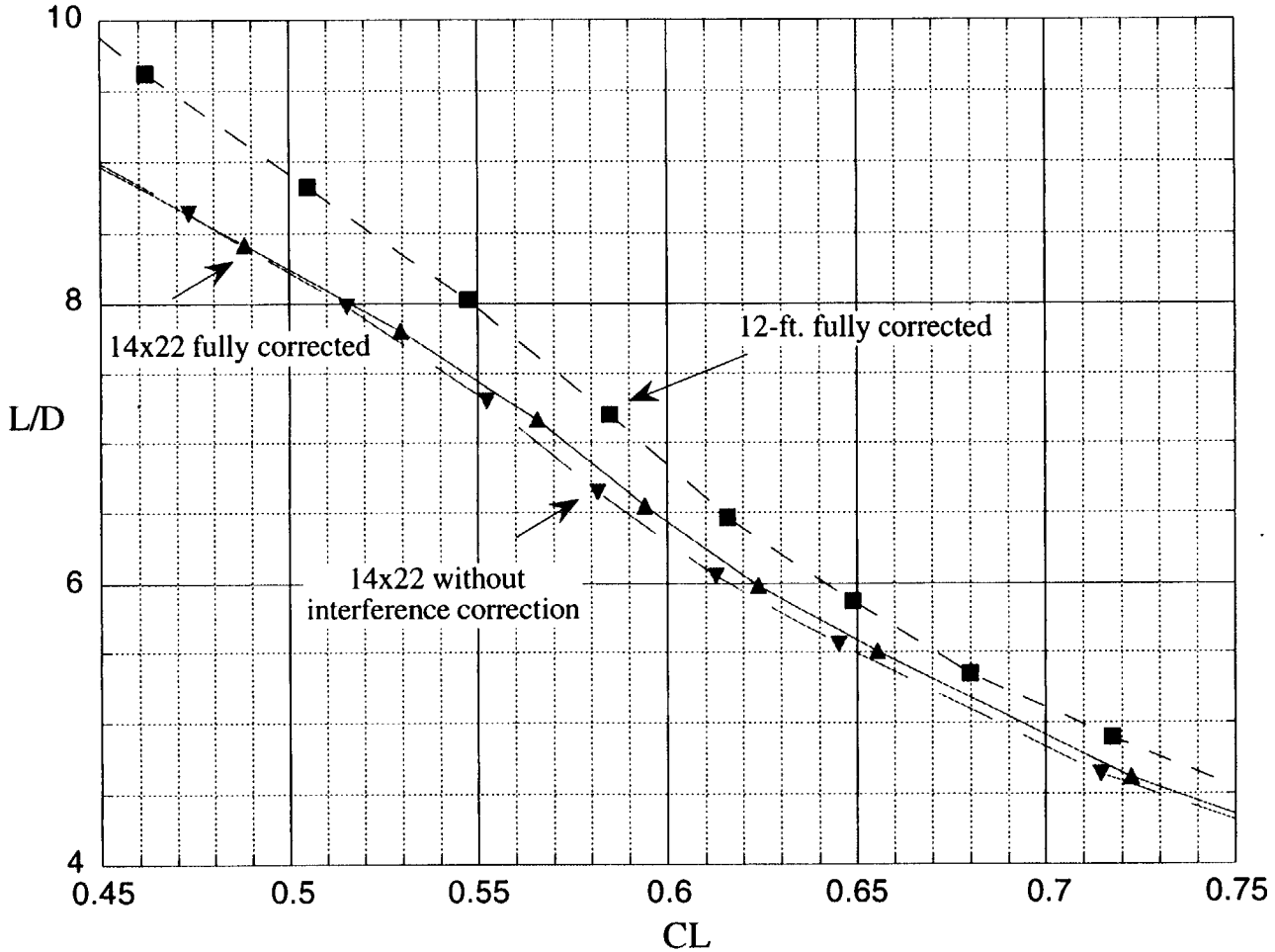

This figure compares the drag polars between the TCA-3 and TCA-4 tests. The figure shows very little difference between the 14x22-ft. fully-corrected data and the 14x22-ft. data without the interference correction.

Test-to-Test Comparison

TCA-3 and TCA-4 Tests (Fully-Corrected Data)

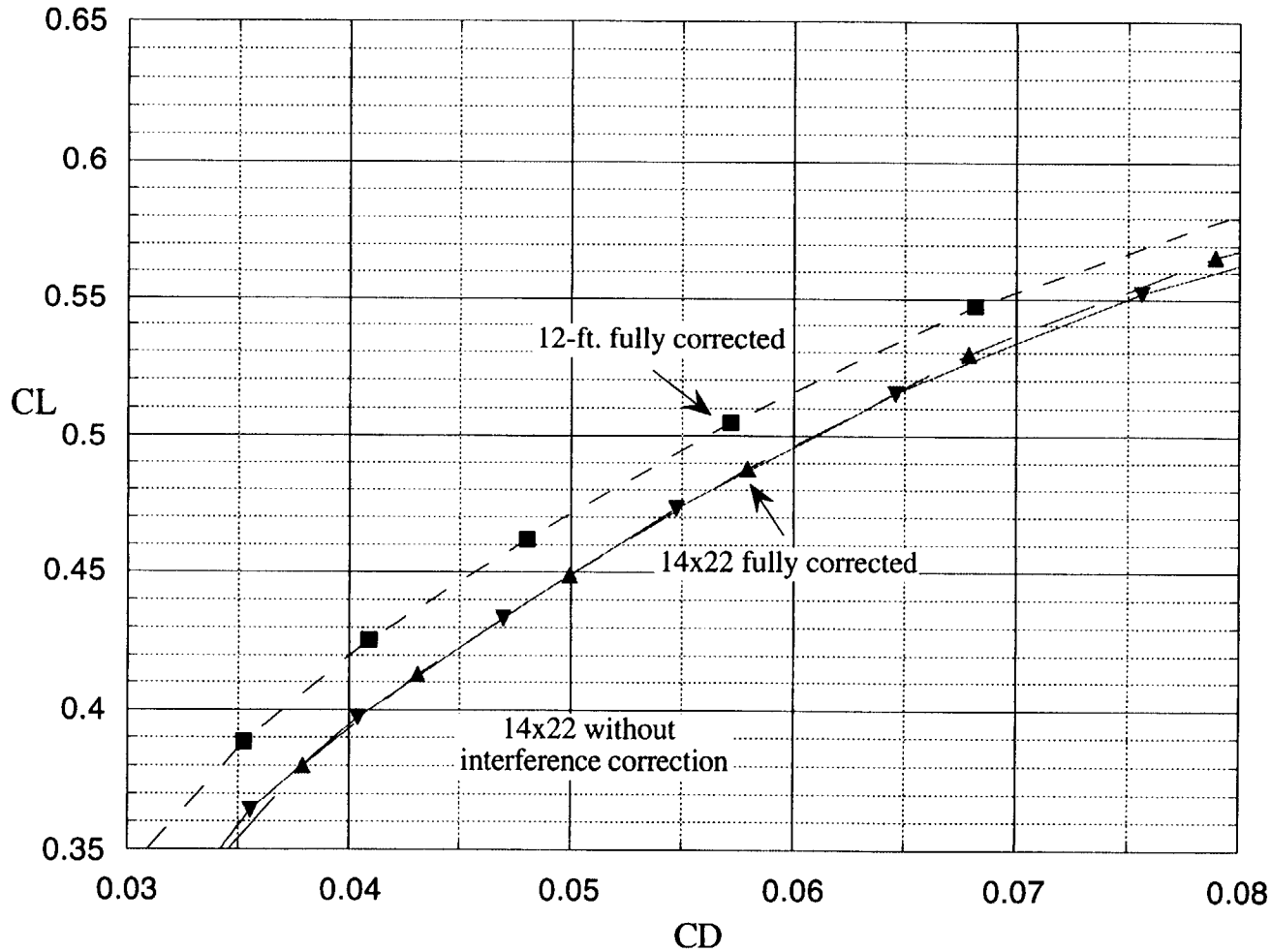

This figure compares the lift coefficient curves between the TCA-3 and TCA-4 tests with fully-corrected data for both tests. The figure compares data for two flap configurations. The flap configurations compared were the baseline plain flaps (LE 30 TE 15/10) and flaps up configuration (LE 0/TE 0).

The figure shows good agreement for both flap configurations.

Test-to-Test Comparison

TCA-3 and TCA-4 Tests (Fully-Corrected Data)

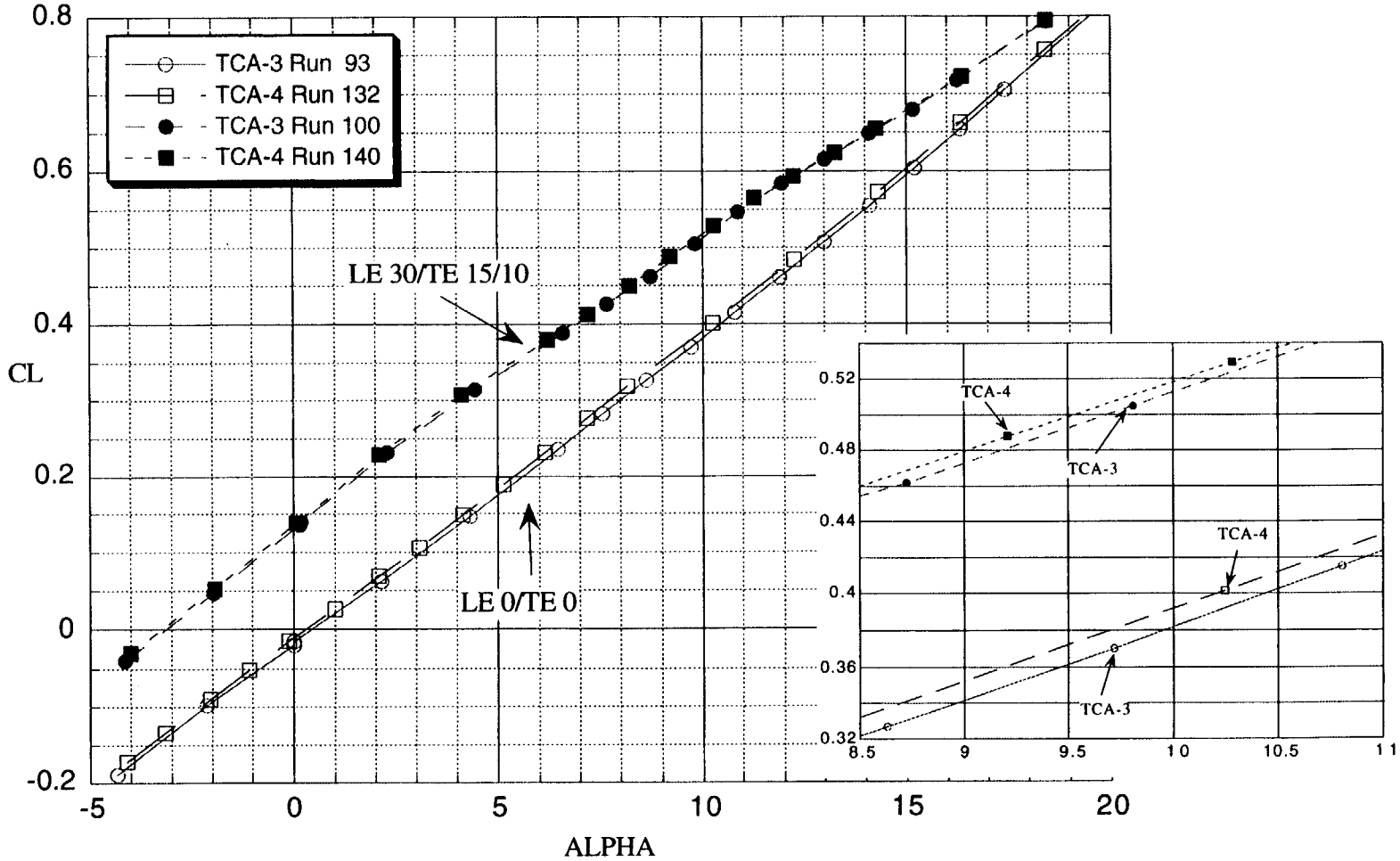

This figure compares the drag polars between the TCA-3 and TCA-4 tests with fully-corrected data for both tests. The figure compares data for two flap configurations. The flap configurations compared were the baseline plain flaps (LE 30 TE 15/10) and flaps up configuration (LE 0/TE 0).

The TCA-3 data in general had less drag than the TCA-4 data for a given CL. At the nominal CL=0.5, the TCA-3 data was at 50 counts less drag than the TCA-4 data. This difference could be due to the different methods in computing blockage and wall effects at the 12-ft. and 14x22-ft. tunnels in addition to the support interference correction term. However, without upflow and support interference data from the 12-ft., it is difficult to conclude with certainty what is causing this 50 drag count difference between tests.

Test-to-Test Comparison

TCA-3 and TCA-4 Tests (Fully-Corrected Data)

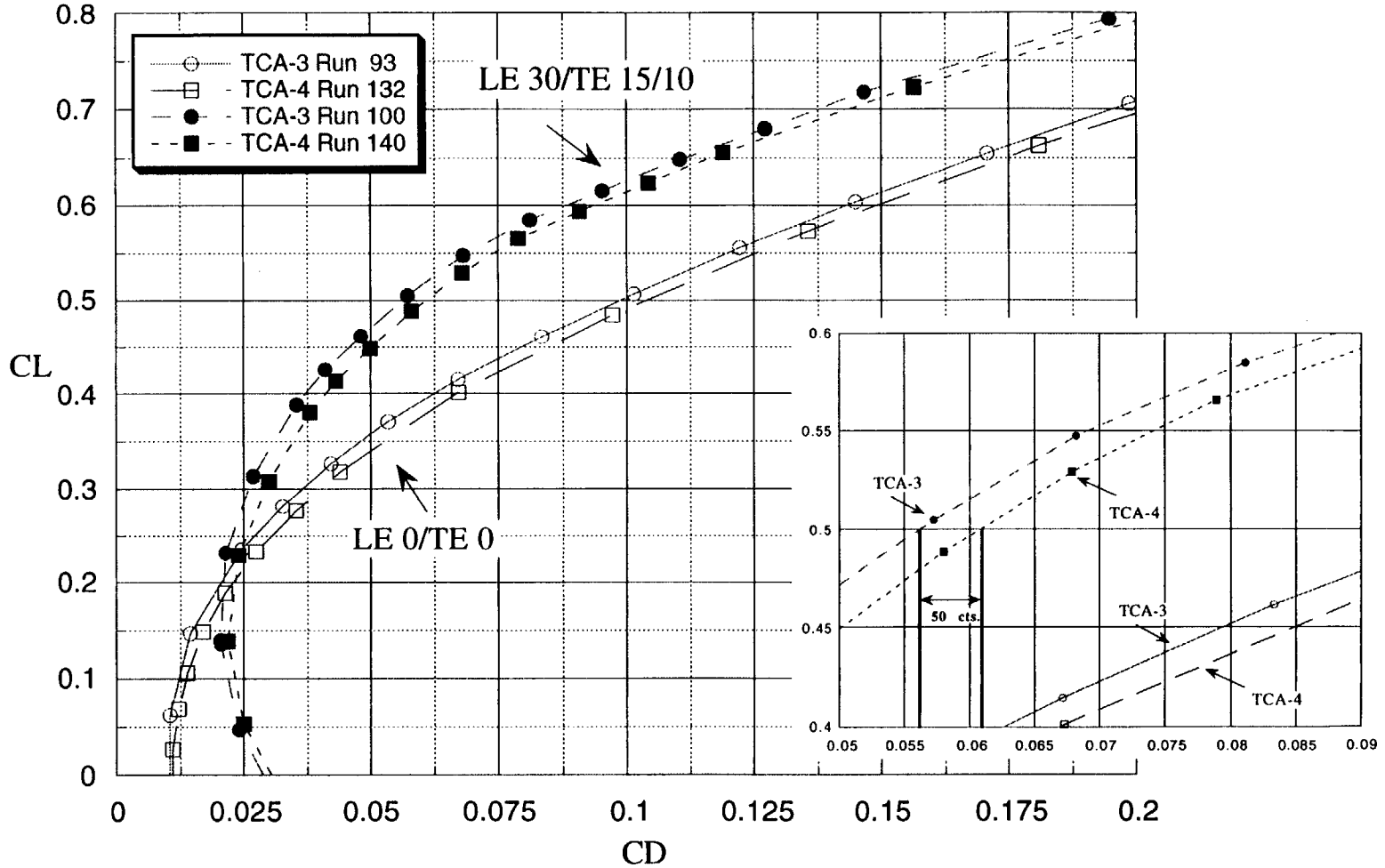

This figure compares the lift-to-drag ratios between the TCA-3 and TCA-4 tests with fully-corrected data for both tests. The figure compares data for two flap configurations. The flap configurations compared were the baseline plain flaps (LE 30 TE 15/10) and flaps up configuration (LE 0/TE 0).

The TCA-3 data in general had higher lift-to-drag ratios than the TCA-4 data for a given CL. At the nominal CL= 0.5, the TCA-3 data showed a greater L/D of 0.7 units greater than the TCA-4 data at the baseline flap configuration. Again, this difference could be due to the different methods in computing blockage and wall effects at the 12-ft. and 14x22-ft. tunnels and also to the support interference correction term.

Test-to-Test Comparison

TCA-3 and TCA-4 Tests (Fully-Corrected Data)

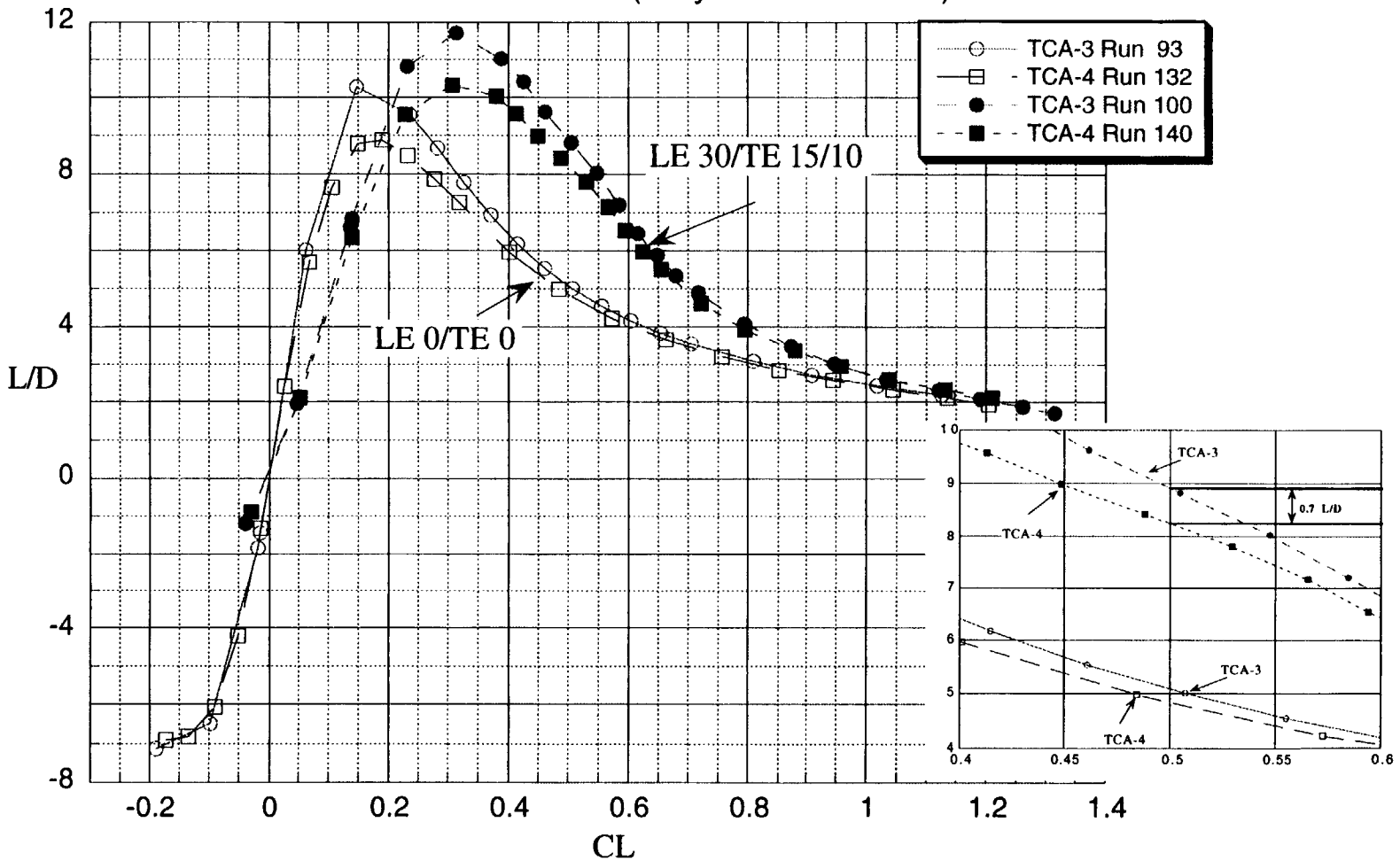

The following summarizes the main conclusions of this paper:

- TCA-3 data corrections were presented
  - Blockage, wall, buoyancy, cavity, nacelle base and internal drag
- Classical vs. WICS corrections
  - Good agreement up to α=15° at low Reynolds number
  - Good agreement up to α =10° at high Reynolds number
  - Recommend to use WICS data above these angles-of-attack
- Good repeatability data
  - ΔCD = ±2 cts. and ΔL/D = ±0.032
- Test-to-Test Comparisons
  - Uncertainty in using mount system interference correction
  - TCA-3 and TCA-4 data show very good agreement in CL
  - TCA-3 shows 50 cts. less drag than TCA-4 at CL=0.5
  - TCA-3 shows greater L/D of 0.7 than TCA-4 at CL=0.5

Summary

- TCA-3 data corrections were presented
  - Blockage, wall, buoyancy, cavity, nacelle base and internal drag
- Classical vs. WICS corrections
  - Good agreement up to $\alpha = 15°$ at low Reynolds number
  - Good agreement up to $\alpha = 10°$ at high Reynolds number
  - Recommend to use WICS data above these angles-of-attack
- Good repeatability data
  - $\Delta CD = \pm 2$ cts. And $\Delta L/D = \pm 0.032$
- Test-to-Test Comparisons
  - Uncertainty in using mount system interference correction
  - TCA-3 and TCA-4 data show very good agreement in CL
  - TCA-3 shows 50 cts. less drag than TCA-4 at CL=0.5
  - TCA-3 shows greater L/D of 0.7 than TCA-4 at CL=0.5

Wind Tunnel Test of a 5% HSCT (TCA) Model in the NASA Ames 12 FT Pressure Tunnel

Robin Edwards, Roger Clark,
David Yeh and Ryan Polito

The Boeing Company
Phantom Works, Long Beach

Presented at
HSR Airframe Annual Review
Anaheim,California Feb 1999

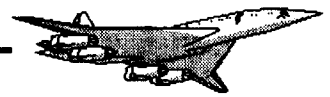

This figure shows the test objectives for the test of the 5% TCA model in the NASA 12 ft Pressure Tunnel

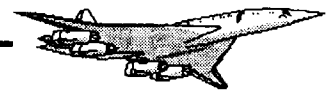

OBJECTIVES

- DETERMINE THE EFFECT OF GEOMETRIC VARIATIONS OF THE INBOARD LEADING EDGE FLAP ON HIGH LIFT, STABILITY AND CONTROL PERFORMANCE DATA
- DETERMINE THE REYNOLDS NUMBER EFFECTS ON TCA HIGH LIFT CONFIGURATION FOR OPTIMUM HIGH-LIFT AND STABILITY AND CONTROL PERFORMANCE AT TAKE-OFF, CLIMBOUT, APPROACH AND LANDING CONDITIONS

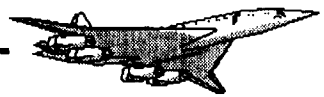

OBJECTIVES (CONT)

- OBTAIN FLOW VISUALIZATION DATA ON THE UPPER SURFACE OF THE WING FOR CFD VALIDATION AND FLOW PHYSICS
  - PRESSURE SENSITIVE PAINT (ARC)
  - MINI TUFT DATA (BCAG)
  - OIL FLOW (ARC)
  - WING DEFORMATION DATA AT HIGH AND LOW REYNOLDS NUMBERS USING AN OPTICAL SYSTEM (LaRC AND ARC)

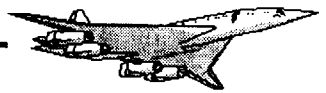

This figure shows the 5% model (6.5 ft span) in the NASA Ames 12 ft pressure tunnel

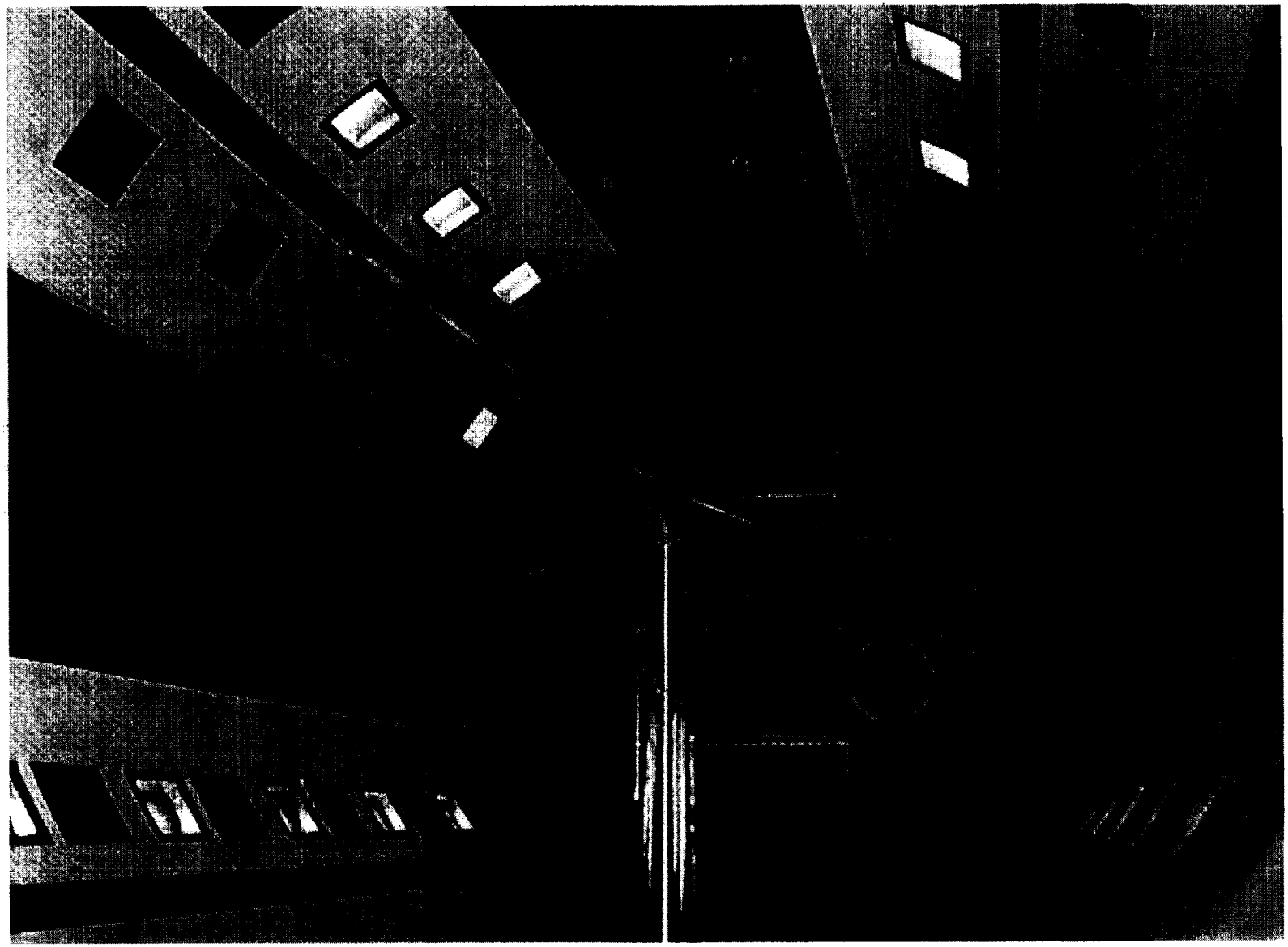

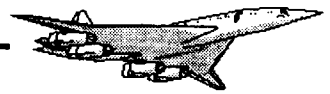

This figure shows the the principal geometric details of the 5% Technology Concept Aircraft (TCA)

5% TCA Model Planform and Parts

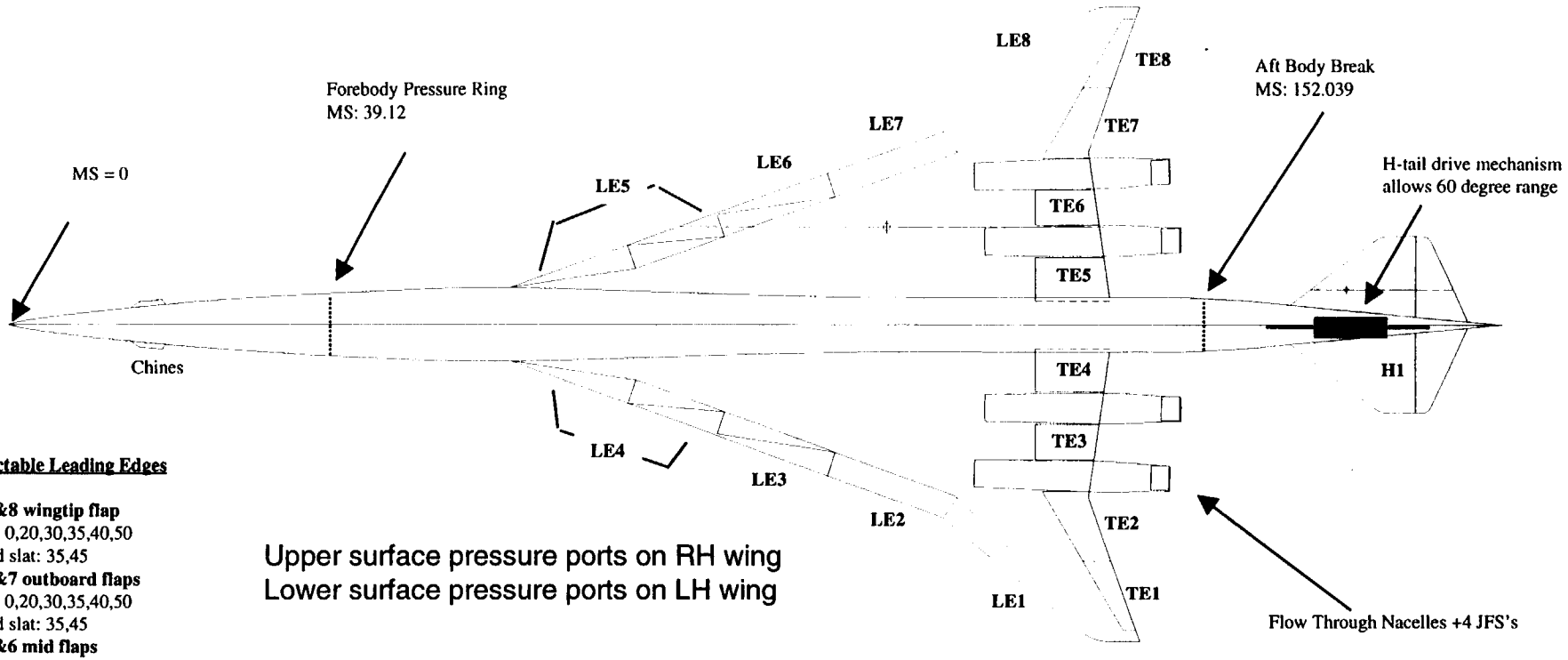

Upper surface pressure ports on RH wing
Lower surface pressure ports on LH wing

Deflectable Leading Edges

LE 1&8 wingtip flap
plain: 0,20,30,35,40,50
sealed slat: 35,45
LE 2&7 outboard flaps
plain: 0,20,30,35,40,50
sealed slat: 35,45
LE 3&6 mid flaps
plain: 0,20,30,35,40,50
plain: 0-0,0-30,30-30,35-35,
0-40,40-40,0-50
(transition from X to X)
sealed slat: 35,45
camber: 0,30,35,40
droop: 0,30,35,40
LE 4&5 inboard flaps
plain: 0,20,30,35,40,50
plain: 0-0,0-30,30-30,35-35,
0-40,40-40,0-50
sealed slat: 35,45
camber: 35
droop: 35

Deflectable Trailing Edges

TE1, 2, 7, 8
0, +-10, +-15, +-20, +-30
TE3 & 6
5 deg increments (-? to +30)
TE4 and 5
0, +5, +10, +15, +20, +30

W1: TCA Baseline
AR: 2.027
I/B sweep: 71 degrees
O/B sweep: 52 degrees
Sref: 21.25 sq ft
Cbar: 56.972 in.
50% mac: 115.236 in.
Span: 78.757 in.
Length: 195.6 in.

Vertical Tail

Fixed Vertical Tail
V1
Sref: 1.0175 sq ft
Deflectable Rudder
0,+10,+20, +25,+30

Horizontal Tail

Remotely Actuated, +-30
H1
Sref: 2.0 sq ft (exposed)
25% mac: 175.386 in
Deflectable Elevator
0,+-10,+-20,+-25,+-30
Cbar=18.588 in

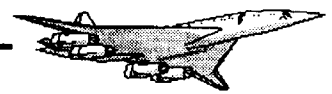

Three alternate leading-edge geometries were examined in addition to the baseline leading-edge simple hinged flaps. Two concepts consisted of modifications to the inboard flap segments (LE4 and LE5), to evaluate the effects of local modifications to the leading edge with the aim of improving the performance of the "part-span" flap in which only the three outboard flap segments are deflected (LE1-LE3 and LE6-LE8). The third concept is a sealed slat configuration in which some limited amount of Fowler motion is introduced into the flap. This concept was successfully tested on the outboard wing panel in the LaRC14x22-foot tunnel on both the 6% Ref H model (LaRC 437) and on the 5% TCA mode (LaRC 449). The current test extended this concept to the inboard wing.

This figure shows some cross-sectional cuts through the cambered and the drooped modifications to the inboard flap segment.

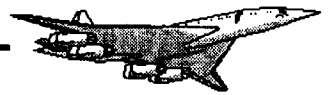

Cambered and Drooped Leading-Edge Flaps

Cambered Leading-Edge

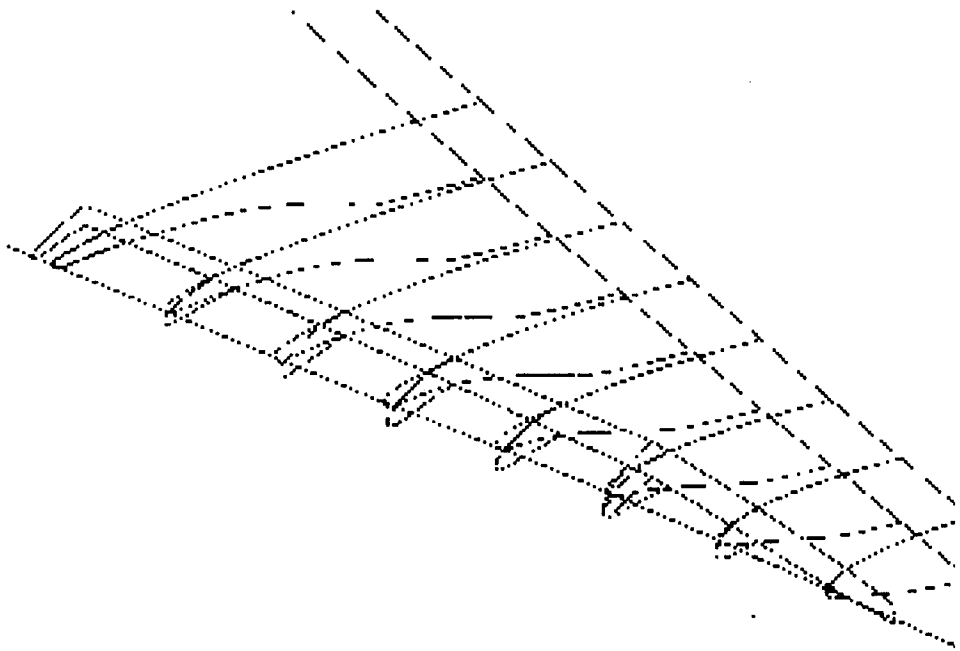

Drooped Leading-Edge

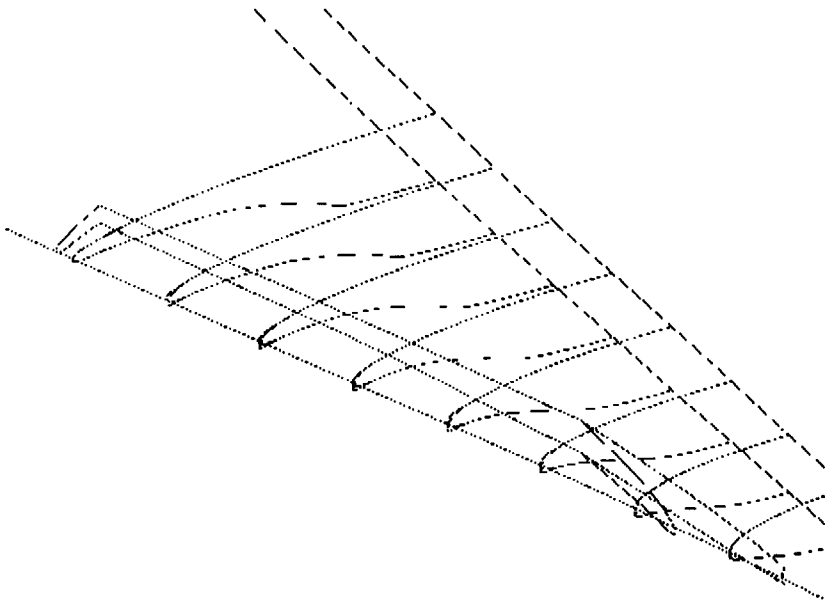

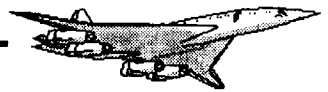

This figure shows a schematic view of the various leading edge flap geometries tested. The cambered and the drooped modifications were applied to the inboard flap segments only as seen in the previous slide. The sealed slat was tested both as a full span sealed slat, and on the outboard wing panel only (with the plain flap used on the inboard wing panel).

All of the flap sections shown here are from the inboard wing panel.

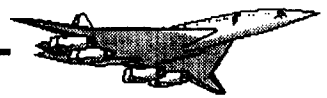

LEADING-EDGE FLAP GEOMETRY SCHEMATIC

- PLAIN

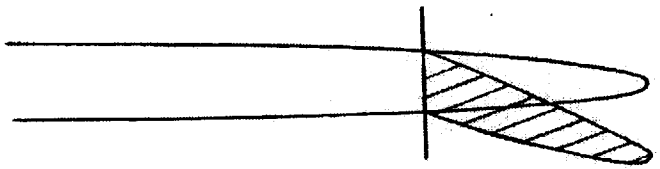

- CAMBERED

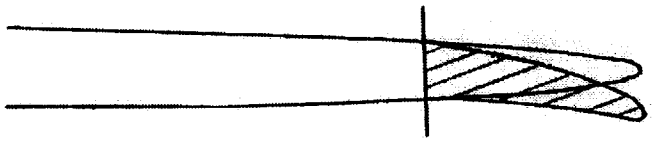

- DROOPED

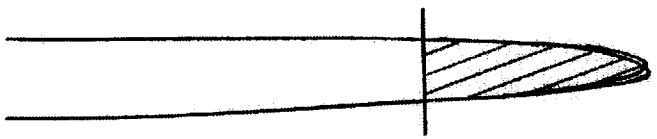

- SEALED SLAT

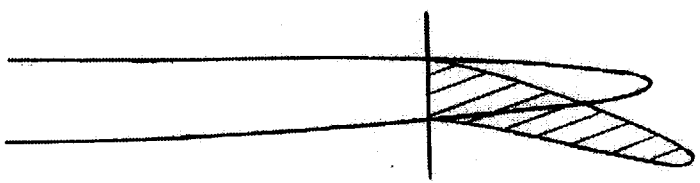

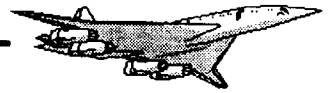

This figure shows the main details of the test of the 5% TCA model in the 12 ft pressure tunnel.

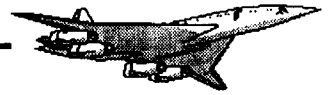

TEST DETAILS

- TESTED 22 JANUARY - 23 FEBRUARY 1998
- 464 RUNS IN 360 HOURS (1.30 RUNS/ HOUR)
- MACH NUMBER 0.24
- Re No RANGE
  - 1.50 - 7.75 MILLION PER FT
  - 7.13 - 36.8 MILLION
- PRESSURE RANGE 1.0 TO 4.7 ATMOSPHERES
- SUPPORTED BY BOEING (LONG BEACH AND SEATTLE), LMAS, ARC AND LaRC

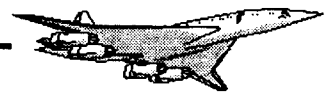

This figure shows the topics to be discussed in the test results.

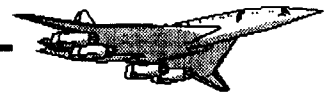

TEST RESULTS

- REPEATABILITY
- TEST TO TEST COMPARISONS
- LEADING EDGE PERFORMANCE
- REYNOLDS NUMBER EFFECTS
- FLOW VISUALIZATION
  - OIL FLOW
  - PRESSURE SENSITIVE PAINT
- MODEL DEFORMATION

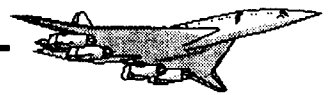

REPEATABILITY

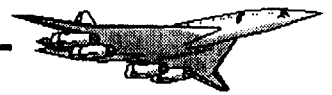

This figure shows the repeatability for Lift Coefficient at high Reynolds Number for the baseline plain flap (LE/TE = 30/15/10) configuration throughout the test. Very good repeatability is shown with a scatter in CL of + or - 0.003 at alpha = 10 degs..

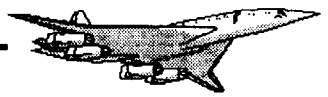

LIFT COEFFICIENT COMPARISON

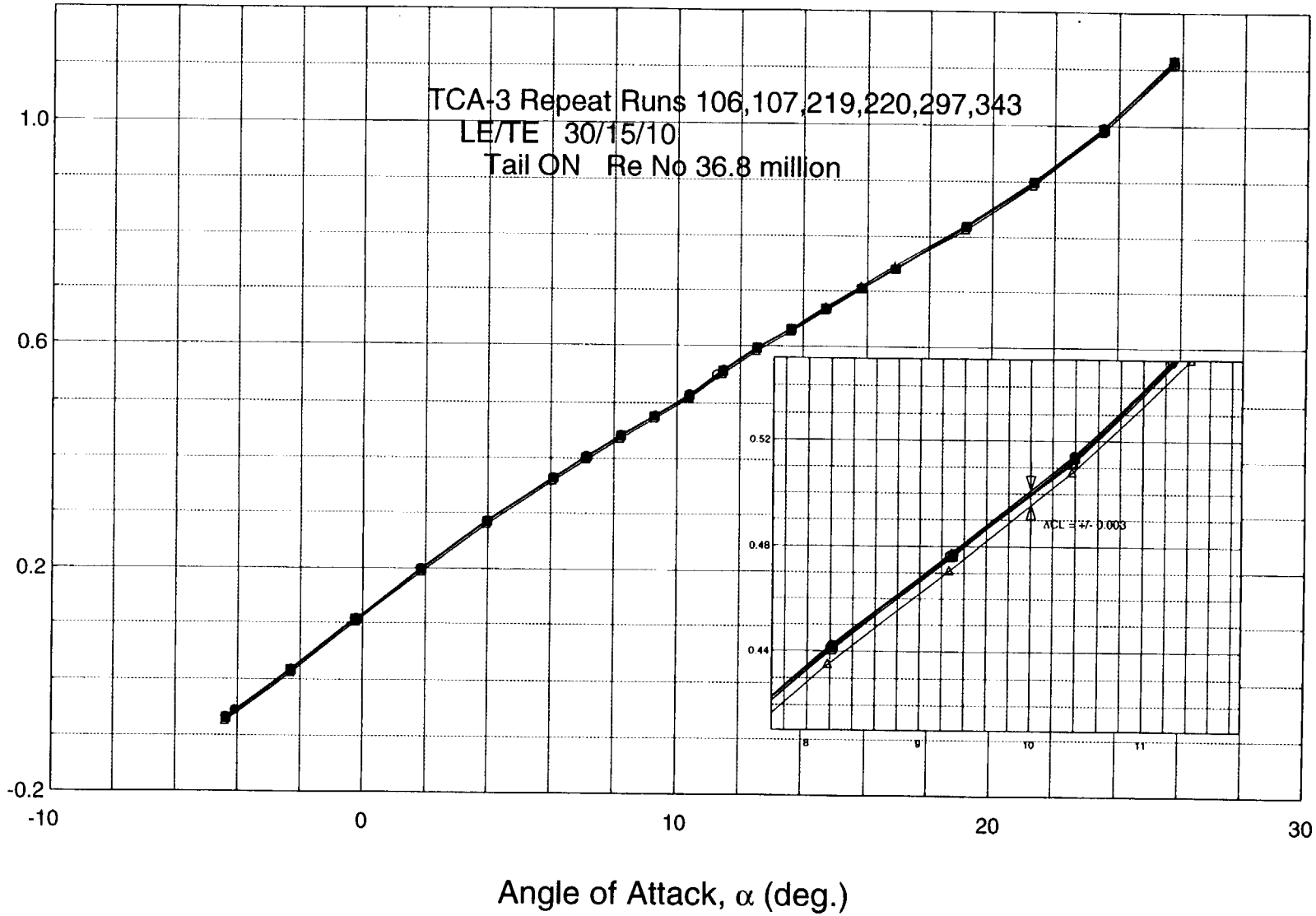

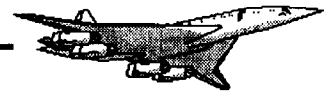

Repeatability of the Drag Coefficient for the baseline configuration at high Reynolds Number is shown in this figure. The scatter in Cd is + or - 2.5 counts at CL = 0.50.

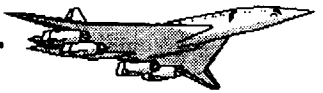

DRAG COEFFICIENT COMPARISON

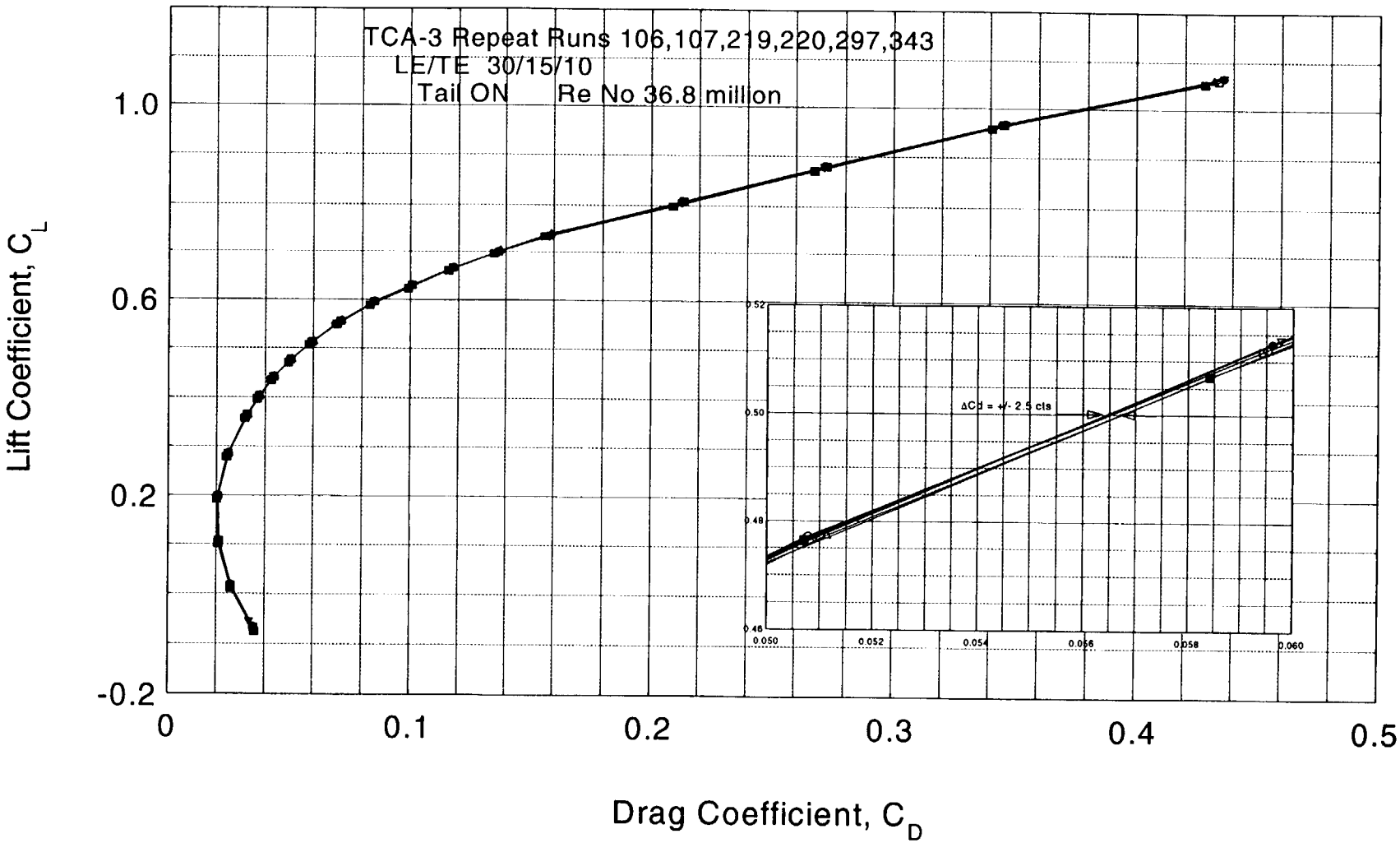

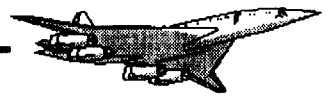

This figure shows repeatability of Pitching Moment Coefficient for high Reynolds Number data. At CL = 0.50 the scatter in Cm is + or - 0.0004.

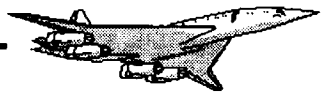

PITCHING MOMENT COMPARISON

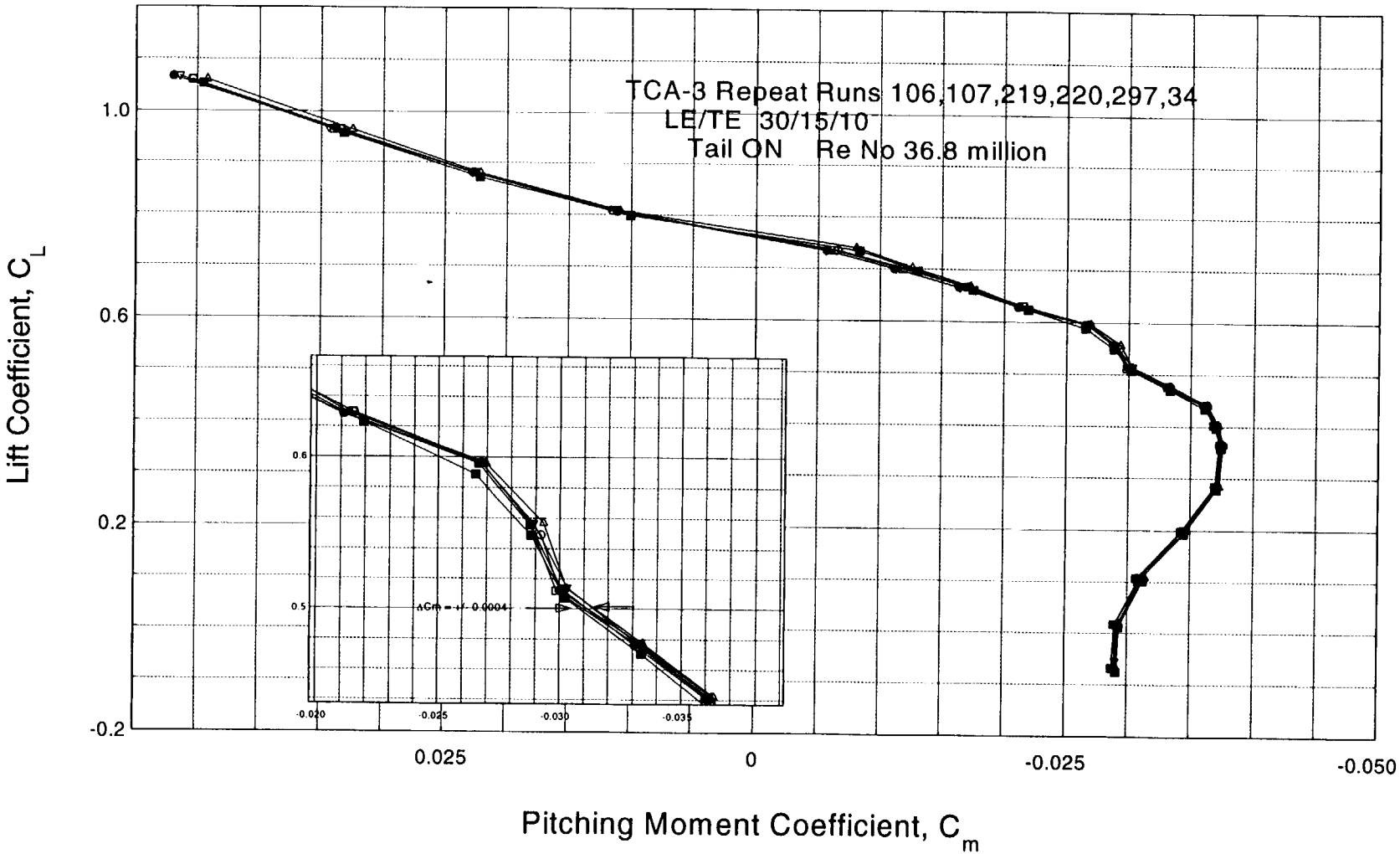

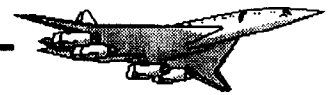

The repeatability for L/D of the baseline configuration at high Reynolds Number throughout the test is shown in this figure. At CL = 0.50 the scatter in L/D is + or - 0.025.

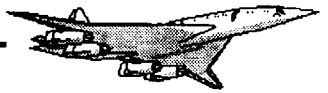

LIFT-TO DRAG RATIO COMPARISON

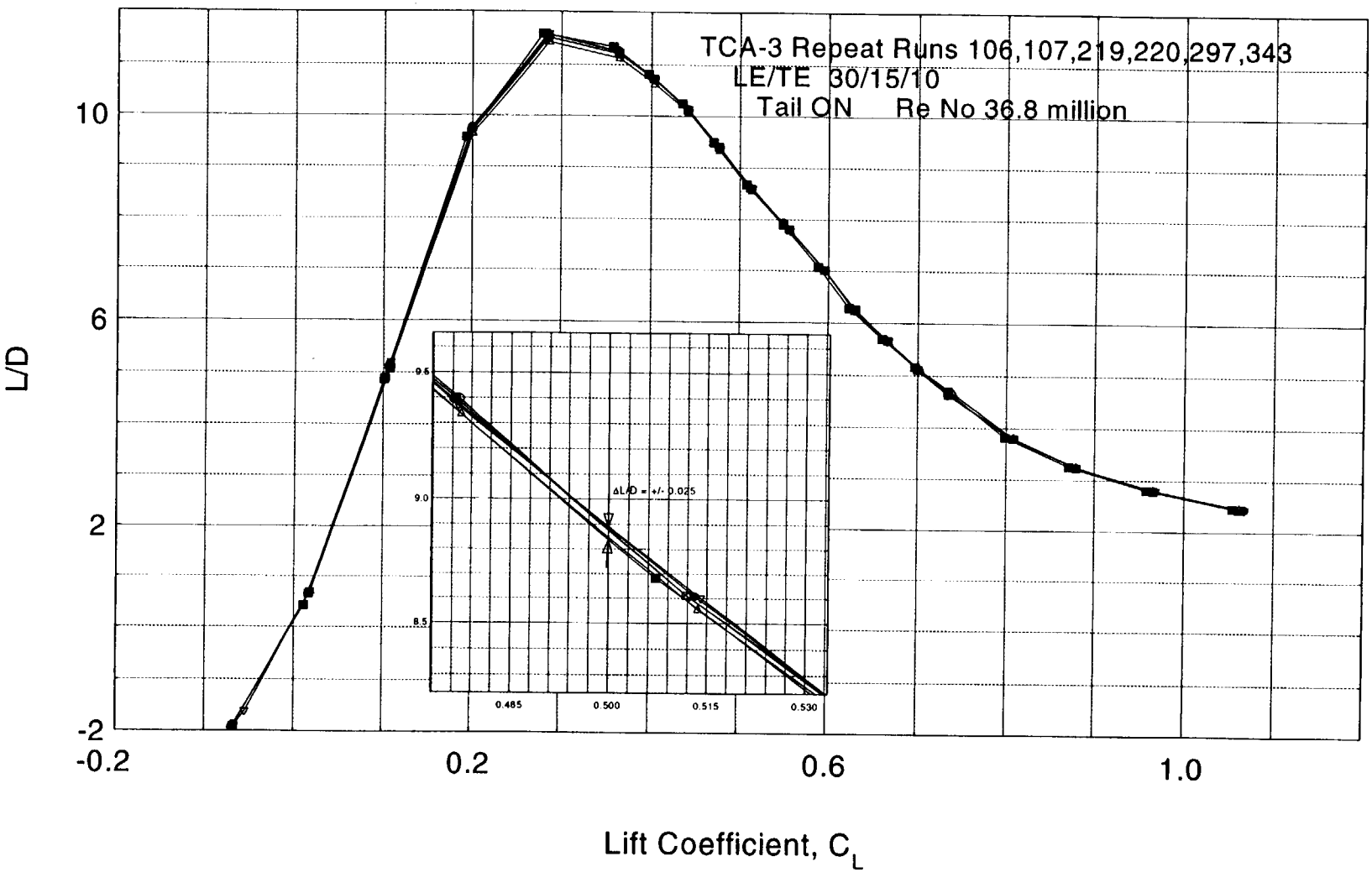

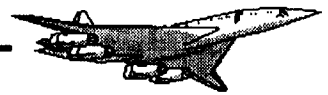

This figure summarizes the repeatability of the various coefficients for the baseline configuration throughout the test for both high and low Reynolds Number. The scatter percentage difference is less than 2% except for Pitching Moment which is just over 3.5% at low Reynolds Number. This overall repeatability is considered very good.

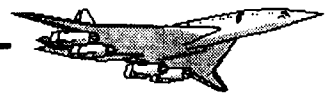

Summary of Repeatability Data at CI = 0.5
LE/TE = 35/15/10 Tail ON

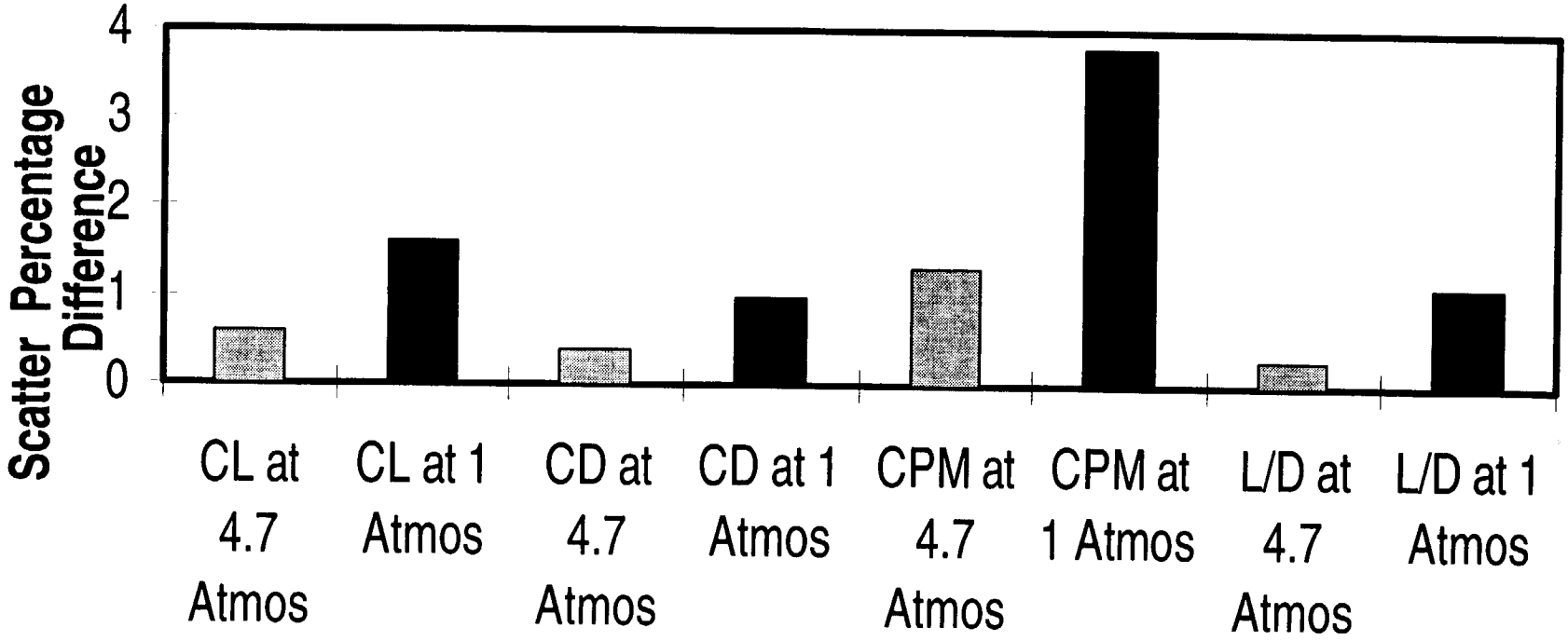

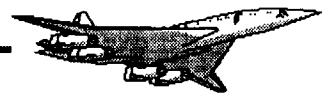

TEST TO TEST COMPARISONS

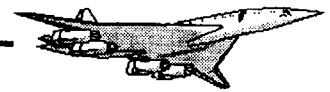

This figure shows a test to test comparison of the data obtained in the Ames 12 ft tunnel (TCA-3) with that obtained in the Langley 14 x 22 ft low speed wind tunnel (TCA-1). The figure shows the lift curves for tail on with LE/TE flaps 0/0 and tail off with LE/TE flaps 30/15/10. Also shown is the data from TCA-4 for the flaps down, tail off configuration obtained in the Langley 14 x 22 ft tunnel. This TCA-4 data has been corrected for model support post effects. Similar corrections to the TCA-3 data have not been made as this effect is unknown at this time.

The TCA-3 data is seen to be consistently higher in lift than that measured in TCA-1 but comparisons with data obtained from the latest 14 x 22 ft test, TCA-4, indicate a closer agreement in lift levels between the two tunnels.

TCA 5% MODEL - TUNNEL COMPARISONS 1 ATMOSPHERE q = 85 PSF

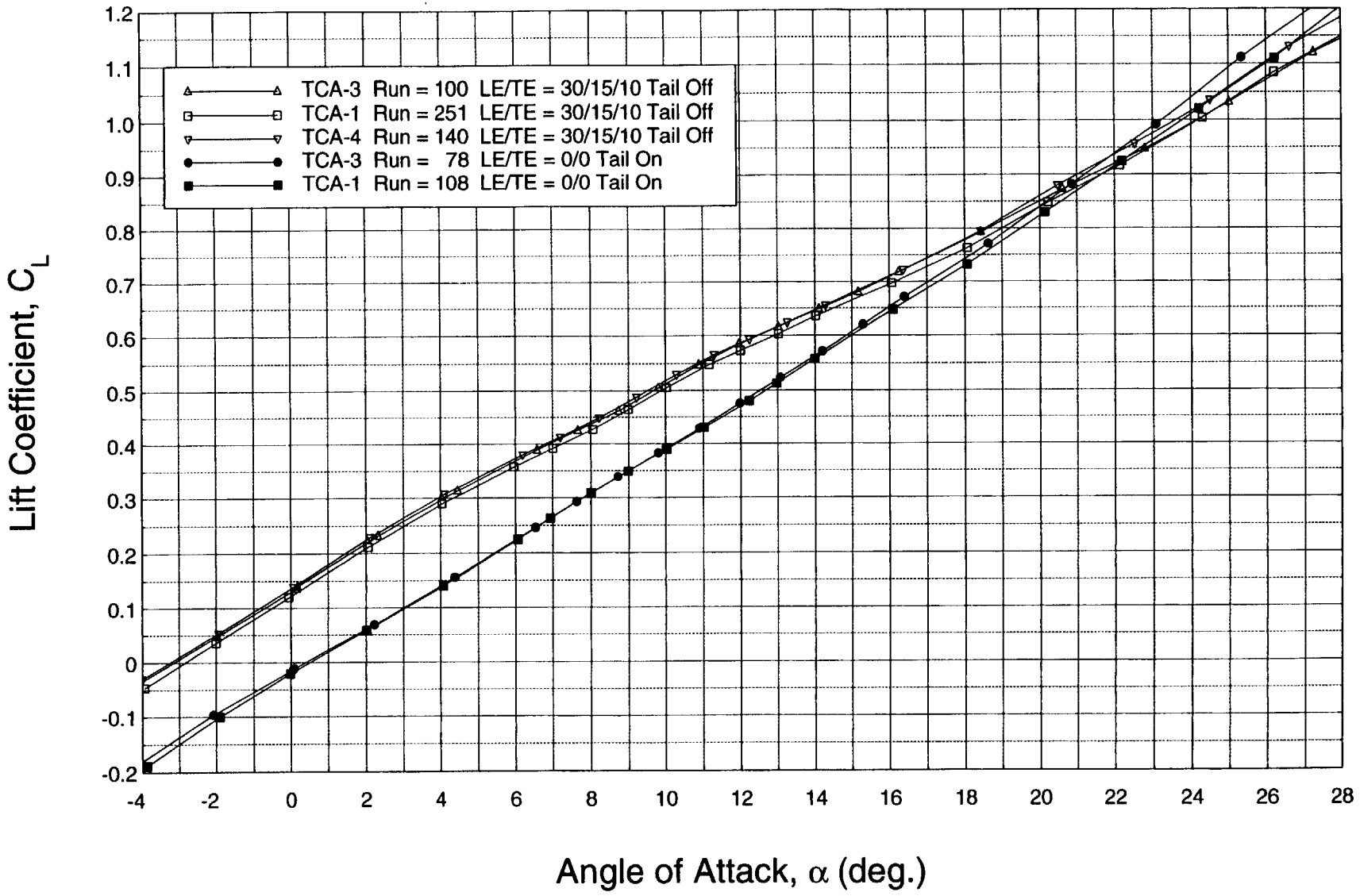

This figure shows the test to test comparisons of the drag polar for the same configurations as shown previously. The comparison for drag is not as good as lift because the 14 x 22 ft drag data (TCA-1) is known to be suspect because of drift problems in the axial force measurement.

TCA 5% MODEL - TUNNEL COMPARISONS 1 ATMOSPHERE q = 85 PSF

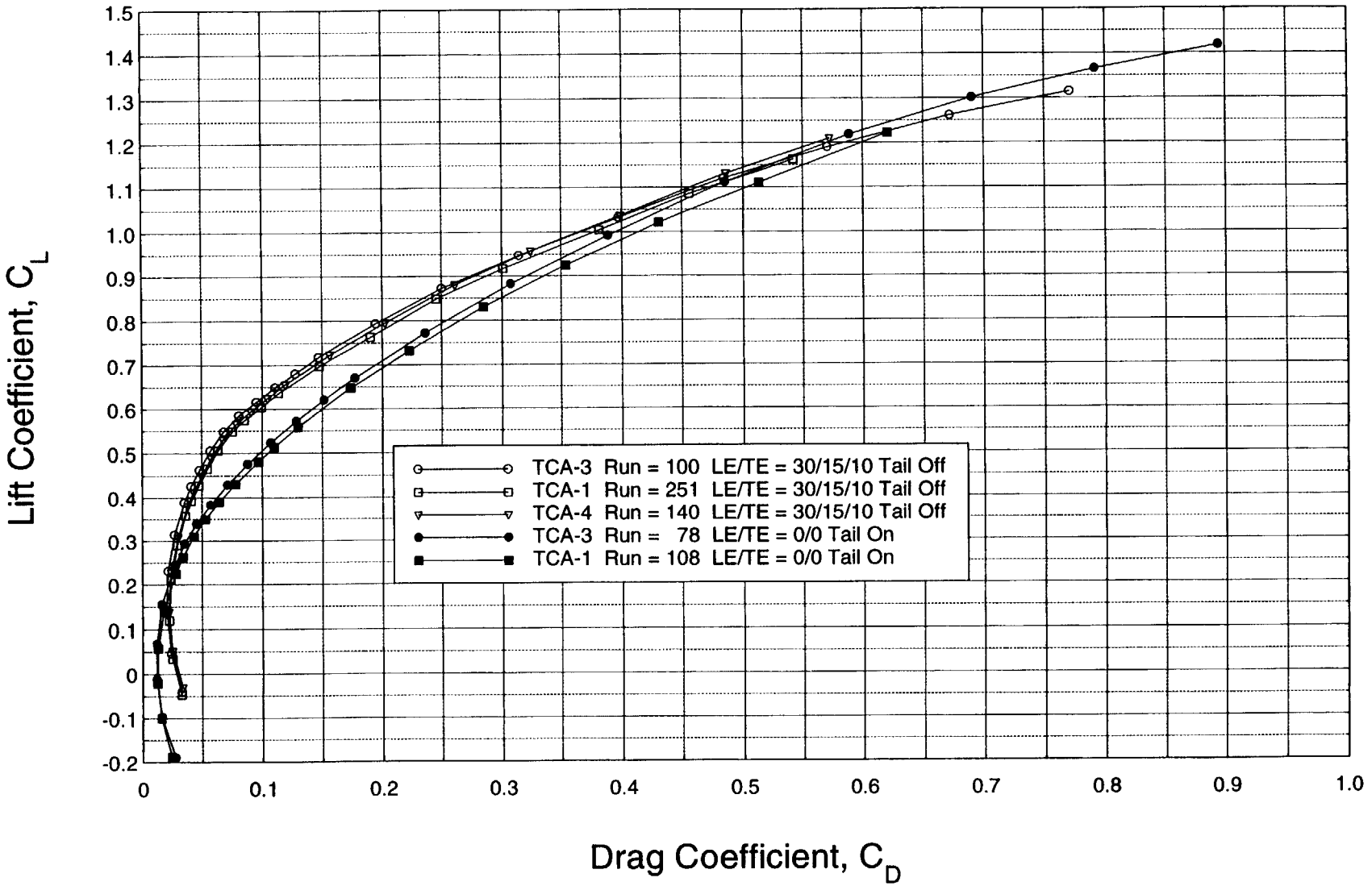

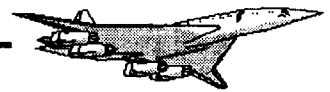

This figure shows the test to test comparison of the pitching moment for the baseline configuration. While the lift data shown previously show some small differences between the two tunnels the pitching moment shows a bigger difference. This difference is believed to be due to model support post interference which as stated previously has not been accounted for in the TCA-3 data. The Ames 12 ft model support is much smaller than the 14 x 22 ft tunnel so the interference will be much less.

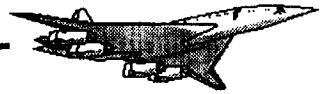

TCA 5% MODEL - TUNNEL COMPARISONS 1 ATMOSPHERE q = 85 PSF

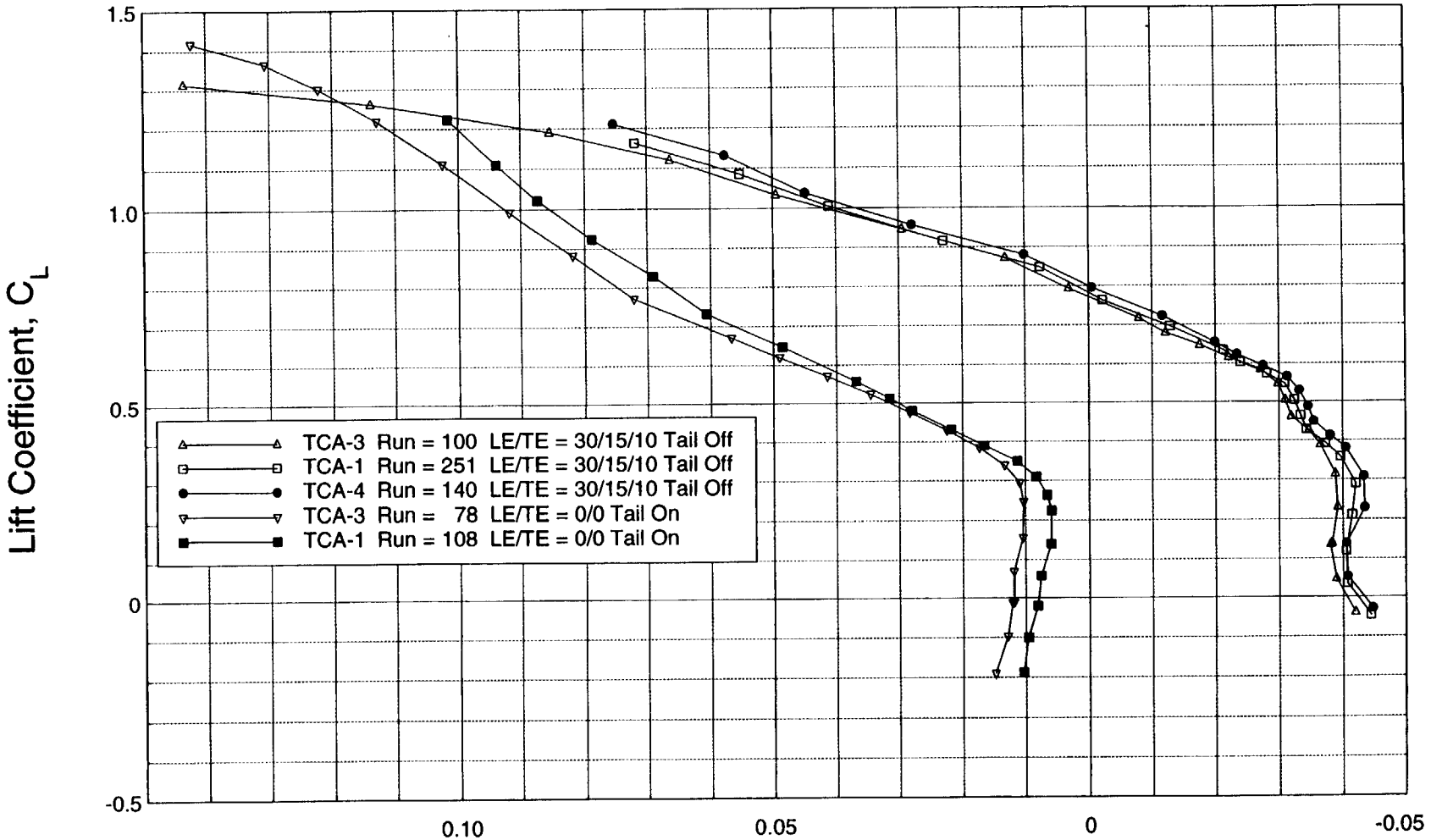

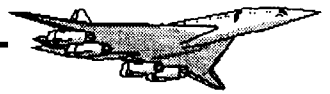

This figure shows the test to test comparisons of L/D for the baseline configurations. This parameter is very sensitive to changes in drag so it is not surprising that a better comparison is not shown because of the drift in axial force for the TCA-1 test data mentioned in the previous drag figure.

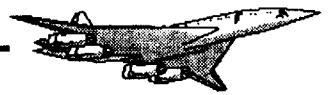

TCA 5% MODEL - TUNNEL COMPARISONS 1 ATMOSPHERE q = 85 PSF

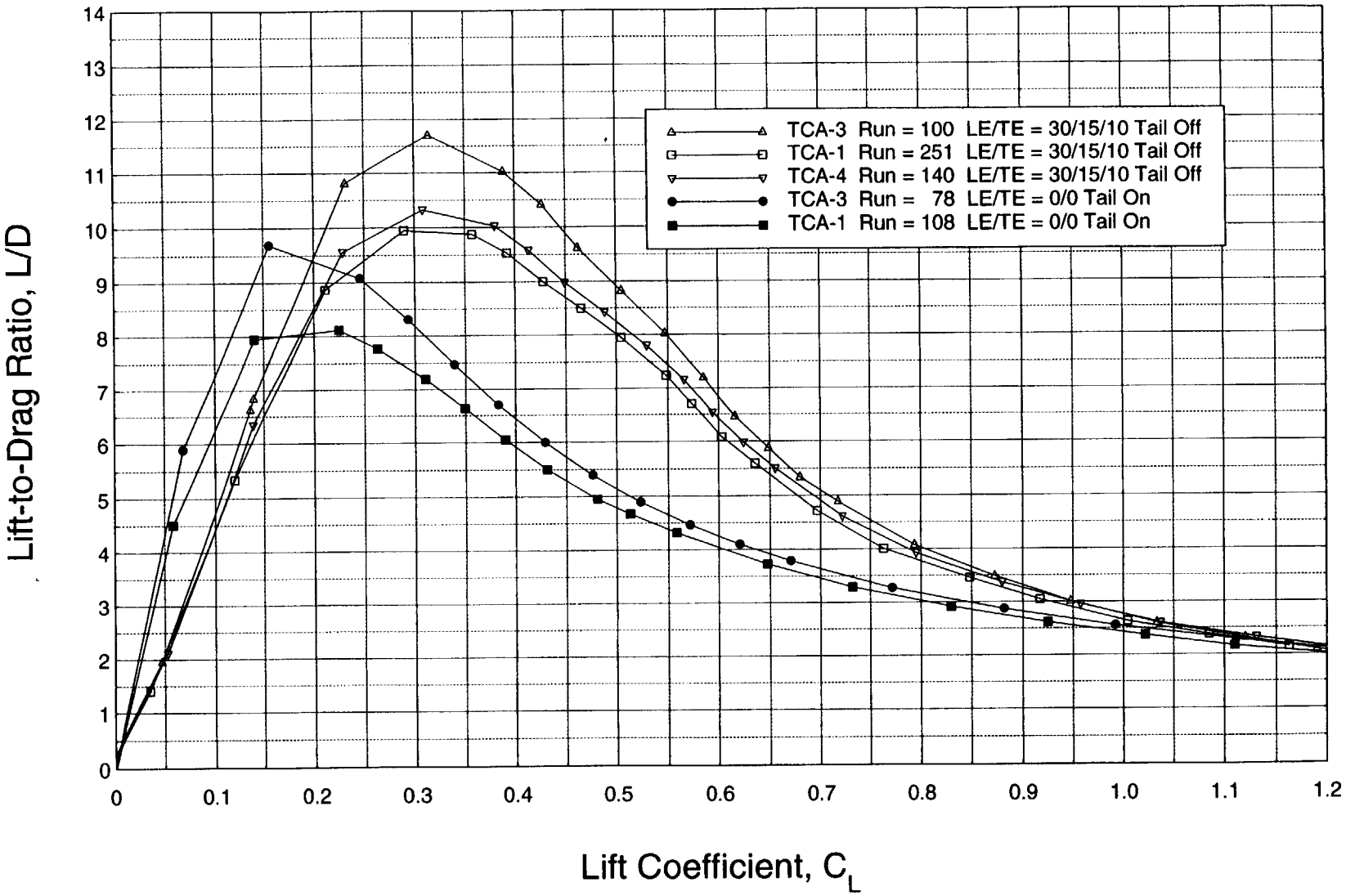

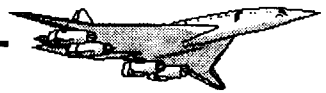

LEADING EDGE PERFORMANCE

This figure shows the performance of the various LE plain flaps tested at high and low Reynolds Number together with a comparison of a plain flap tested in the 14 x 22 ft tunnel. The measure of performance is chosen to be L/D at a climb-out CL = 0.50. The TE flaps are 15/15/15/10 and the horizontal tail is on. It can be seen that at both low and high Reynolds Number conditions, the 30 deg. flap performs better than the 35 deg. flap deflection. The poor performance of the 14 x 22 ft tunnel run reflects the drift in axial force already mentioned.

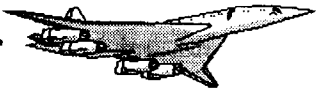

PLAIN FLAP PERFORMANCE AT 30 AND 35 DEGS AT HIGH AND LOW Re No

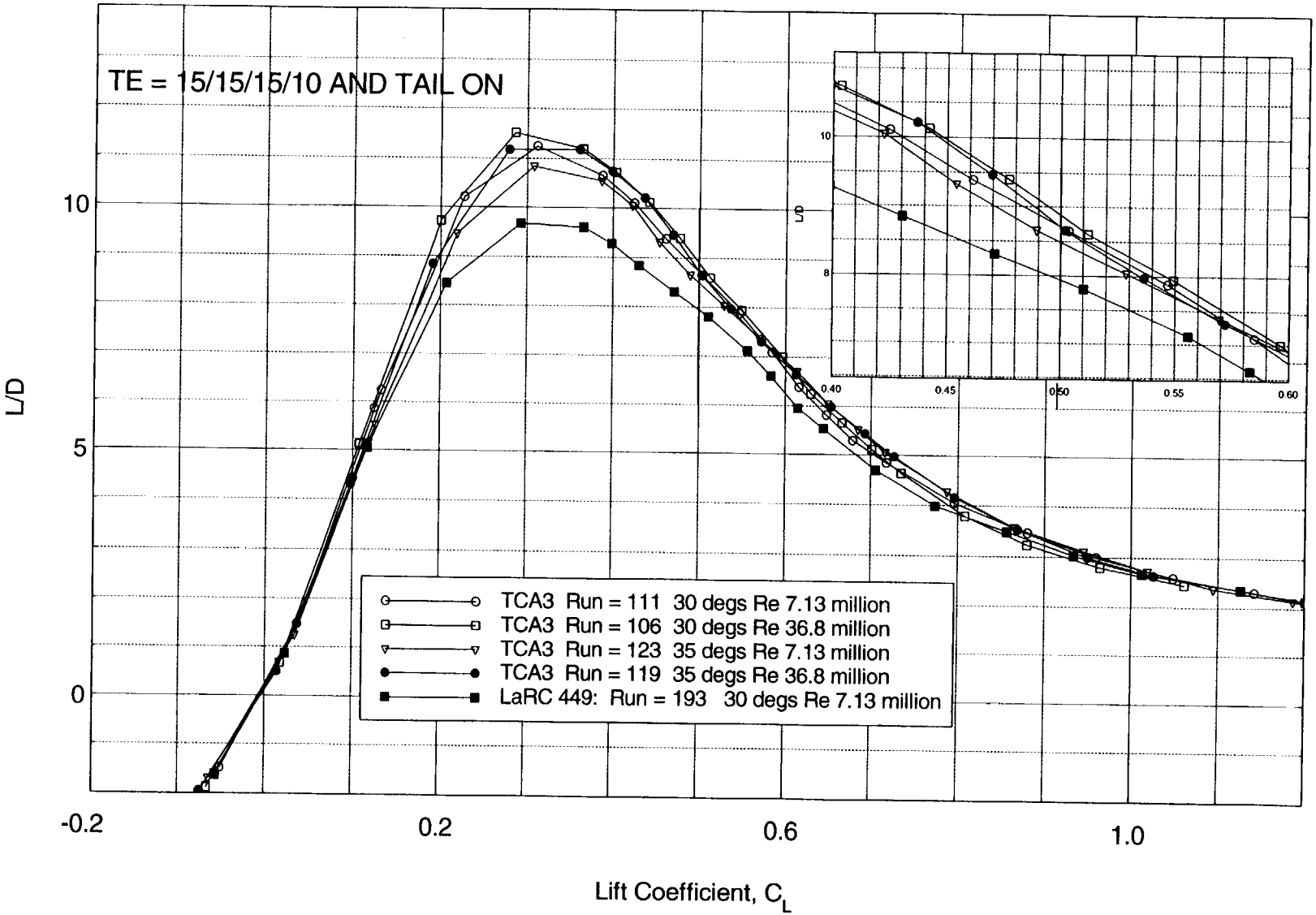

This figure shows the L/D performance for drooped leading edge flaps at 30, 35 and 40 degs. deflection at high and low Reynolds Number. The trailing edge flaps are 15/15/15/10 and the horizontal tail is on. For this drooped leading edge configuration the best performance is generated by a 30 deg. deflection at both high and low Reynolds Number.

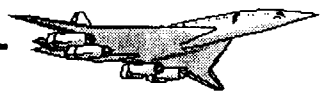

DROOPED FLAP PERFORMANCE AT 30,35 AND 40 DEGS AT HIGH AND LOW Re No

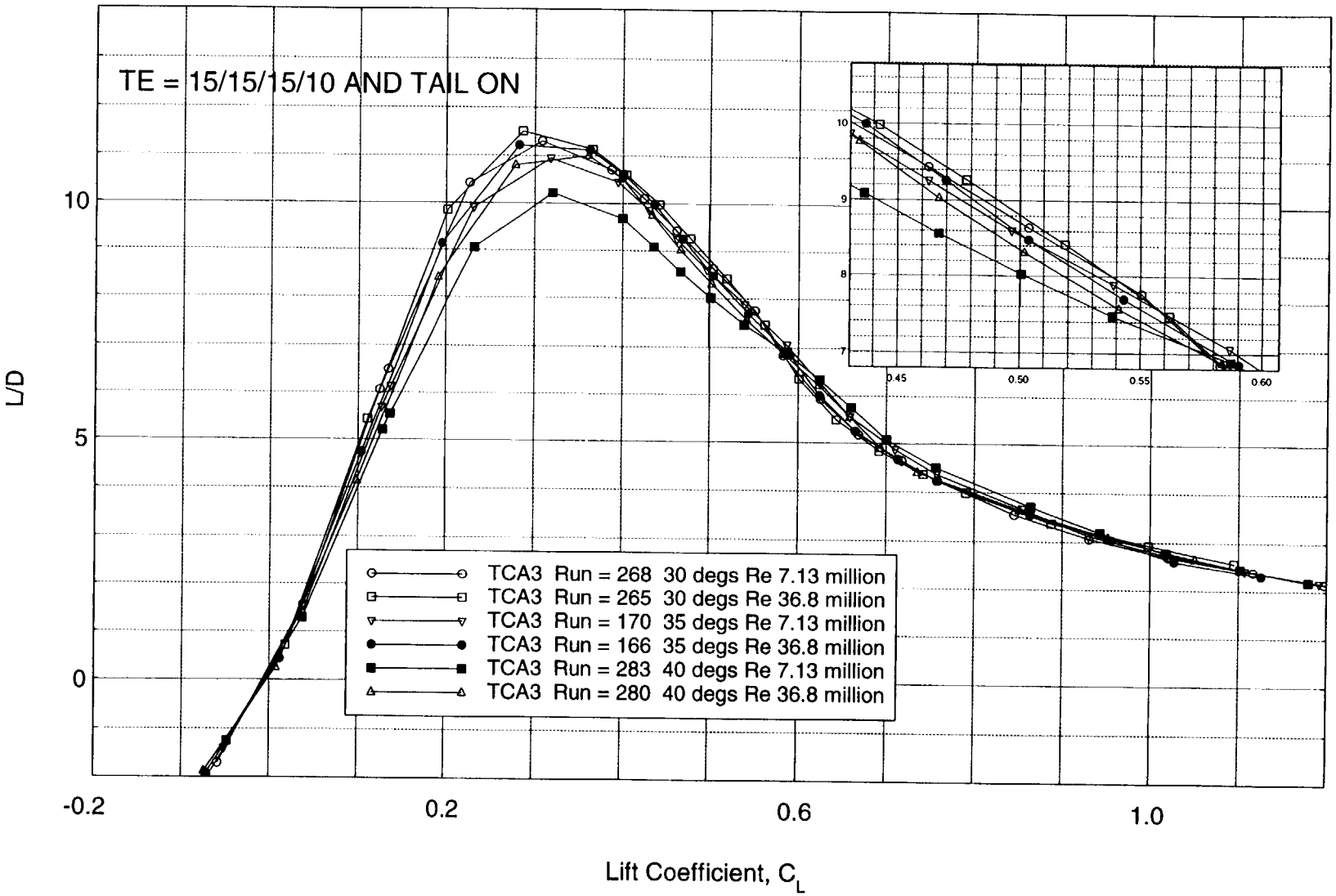

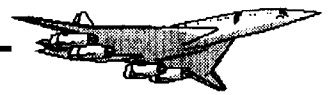

The cambered leading edge flap performance is shown in this figure for deflections of 30, 35 and 40 degs. at high and low Reynolds Number. Again a deflection of 30 degs. at both high and low Reynolds Number produces the best performance. The leading edge is clearly over deflected at 40 degs, which shows particularly poor performance at the low Reynolds Number.

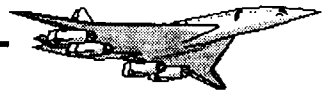

CAMBERED FLAP PERFORMANCE AT 30, 35 AND 40 DEGS AT HIGH AND LOW Re No

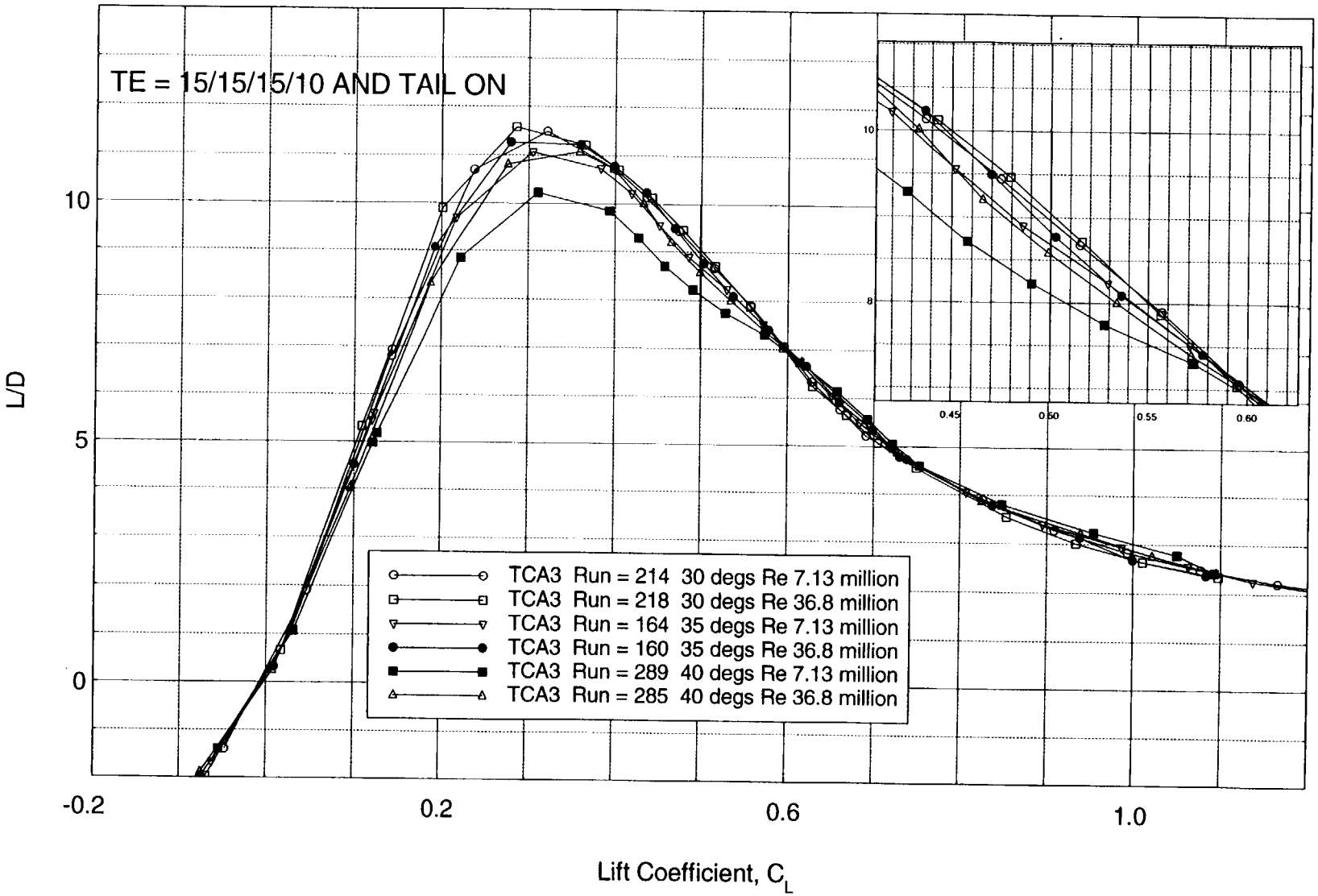

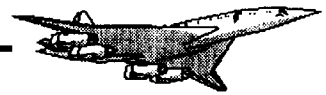

Leading- edge sealed slats were tested at deflections of 35 and 45 degs, both full span and inboard with a plain flap outboard. Both high and low Reynolds Number data is shown in this figure. The best L/D performance is generated by either full span sealed slats at 35 or 45 degs. deflection at high Reynolds Number. The worst performance comes from the inboard sealed slat configuration at 45 degs, probably because the outboard plain flap was deflected 40 degs., thus causing a mismatch at the wing crank junction.This mismatch was a result of the available leading edge parts.

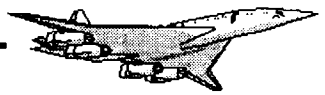

SEALED SLAT PERFORMANCE AT 35 AND 45 DEGS AT HIGH AND LOW Re No

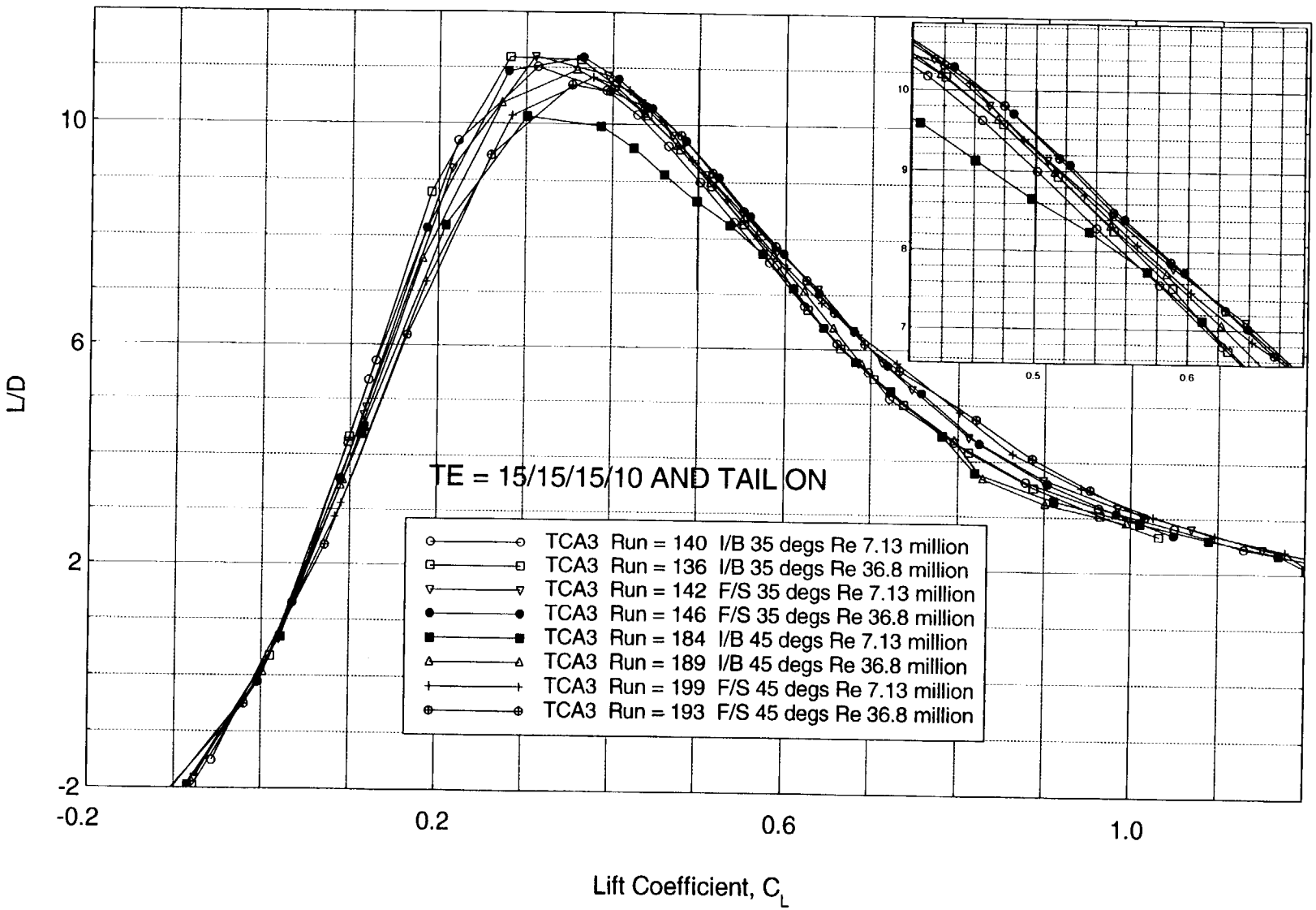

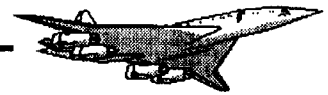

This figure compares the best L/D performance at high Reynolds Number for each of the various leading edges tested, plain flaps, drooped flaps, cambered flaps and full span or inboard span sealed slats. The clear winner is the full span sealed slat at 35 deg.deflection, followed by the inboard sealed slats at 35 degs. Relative to a plain flap deflected 30 degs. the full span sealed slat improves L/D by 0.60 units.

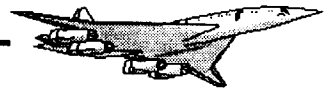

SUMMARY OF BEST PERFORMING FLAPS AT HIGH Re

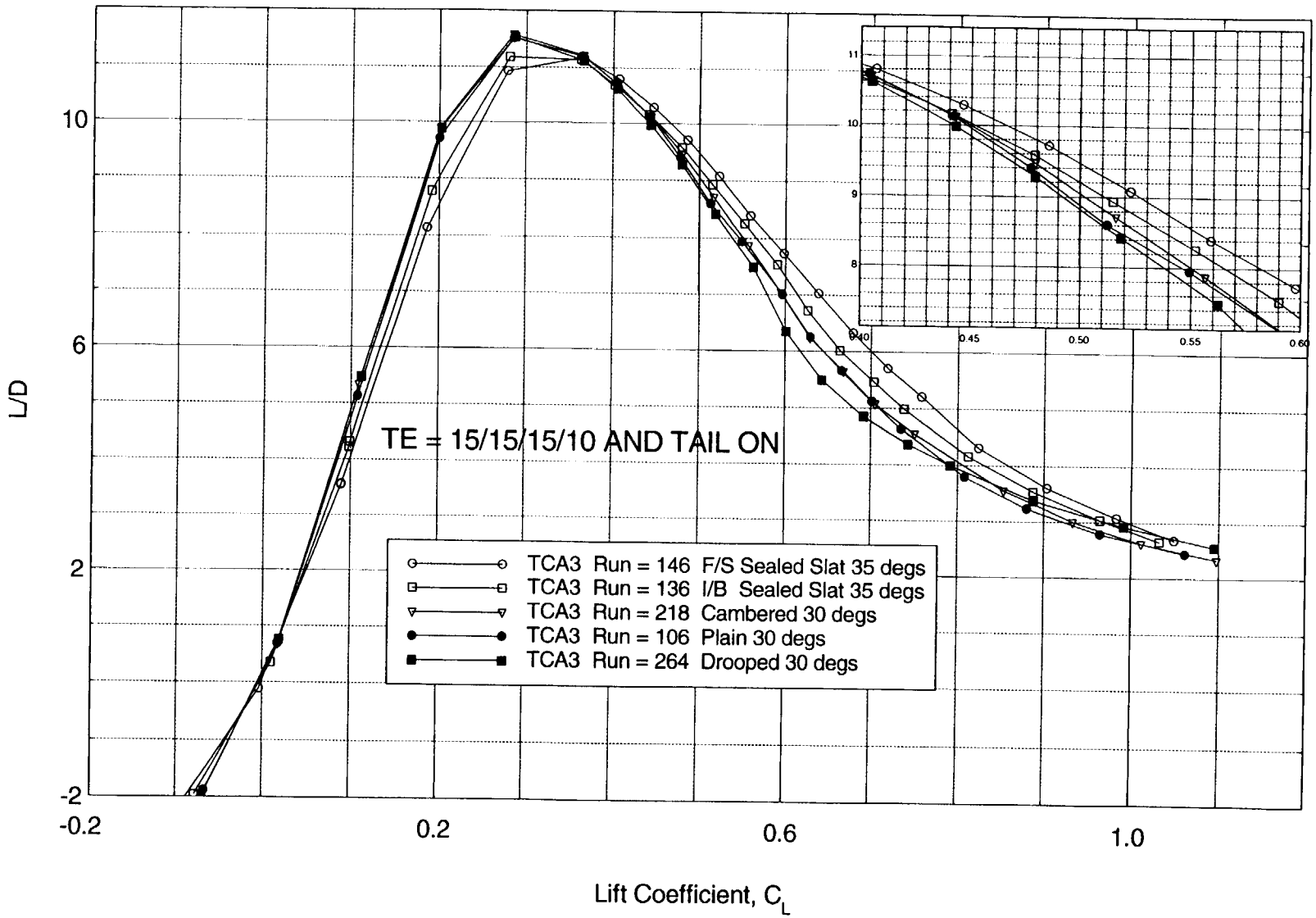

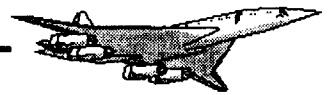

The effect of leading edge flap deflection on L/D for the various flaps tested at high and low Reynolds Number is shown in this figure. For the plain flaps, cambered flaps and drooped flaps the best performance is attained at a deflection of 30 degs. The sealed slats indicate no performance gain between leading edge deflections of 35 and 45 degs. The lower value of L/D at 45 deg. inboard sealed slat deflection has already been explained by the flap mismatch at the wing leading edge crank point.

This data suggests that a lower sealed slat deflection of 30 degs. could possibly perform as well as any of the sealed slats tested.

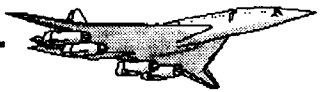

EFFECT OF LEADING EDGE FLAP DEFLECTION ON

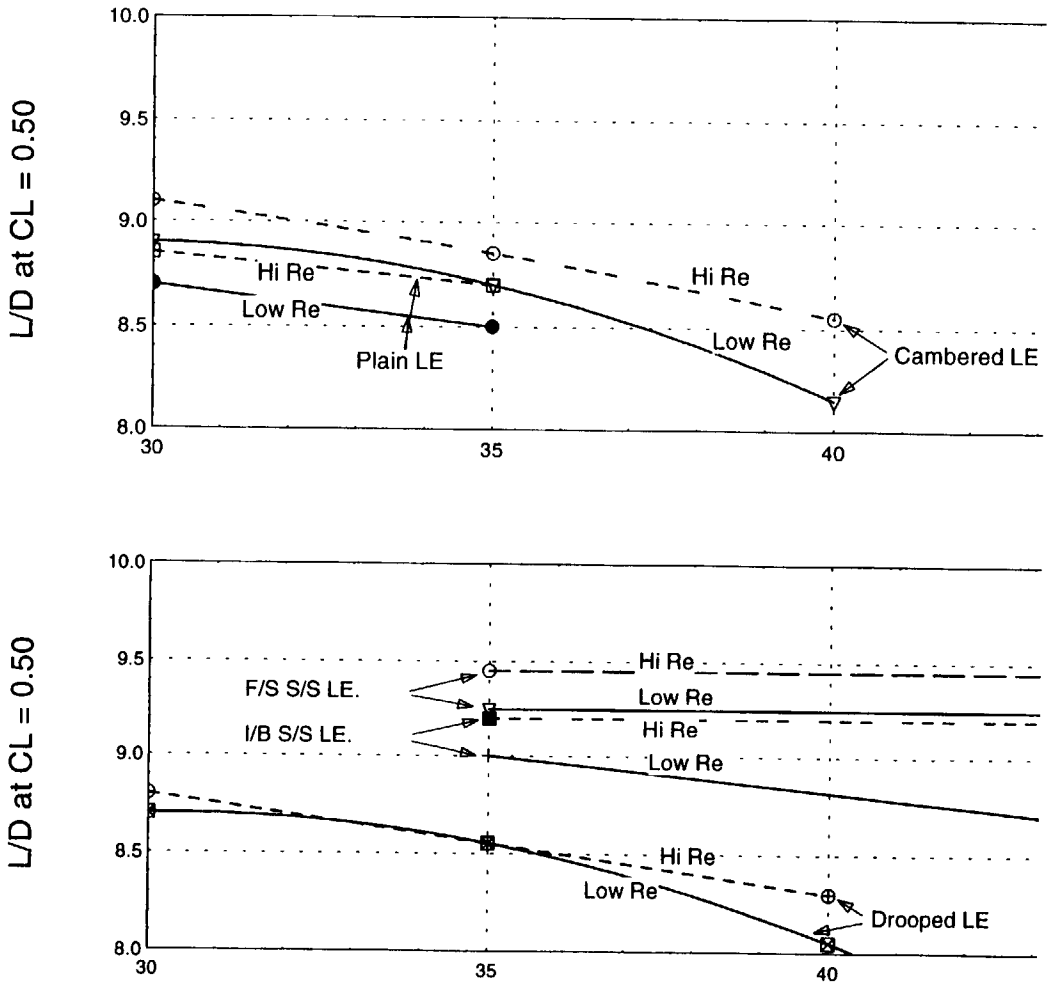

LEADING EDGE FLAP DEFLECTION-DEGS

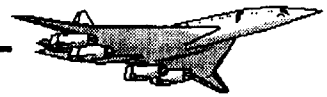

This bar chart shows L/D at the climb-out CL = 0.50 for high and low Reynolds Number for plain flaps, drooped flaps and cambered flaps at 30 degs. deflection, together with inboard and full span sealed slats at 35 degs. deflection. All data has been trimmed and this trim drag penalty amounts to an addition of approximately 45 drag counts. In addition, skin friction drag adjustments have been made to account for a full scale aircraft. These skin friction adjustments are -35 counts of drag for low Reynolds Number to to full scale Reynolds Number and -11 counts for high Reynolds Number to full scale Reynolds Number. As will be seen the full span sealed slat continues to reflect the best performance.

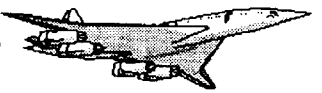

L / D at CL = 0.5 (Extrapolated, tunnel trim)
LE = 30 deg., TE = 15/10 deg.

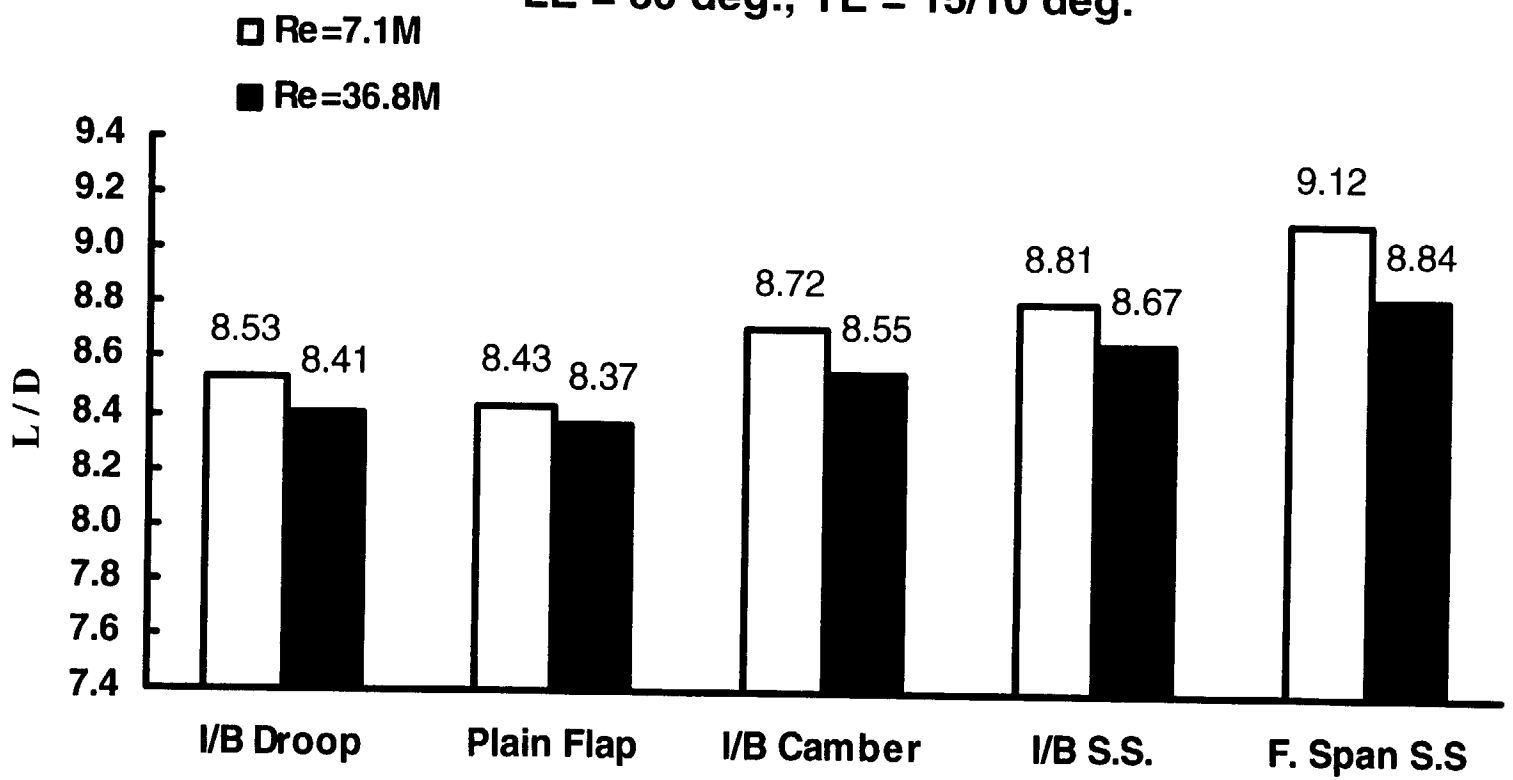

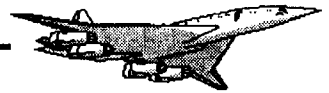

This bar chart shows a further refinement of L/D at the climb-out CL = 0.50 for high and low Reynolds Numbers. Based on historical trim data it was felt that a more realistic value for trim drag would be 20 drag counts and this value is reflected in the values of L/D shown. The full span sealed slat continues to provide the best performance and the L/D = 9.30 at high Reynolds Number is close to the predicted level of L/D shown on the TCA Projection Milestone Schedule reported at the Airframe Annual Review in February 1998.

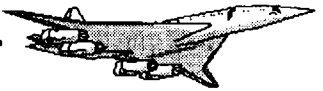

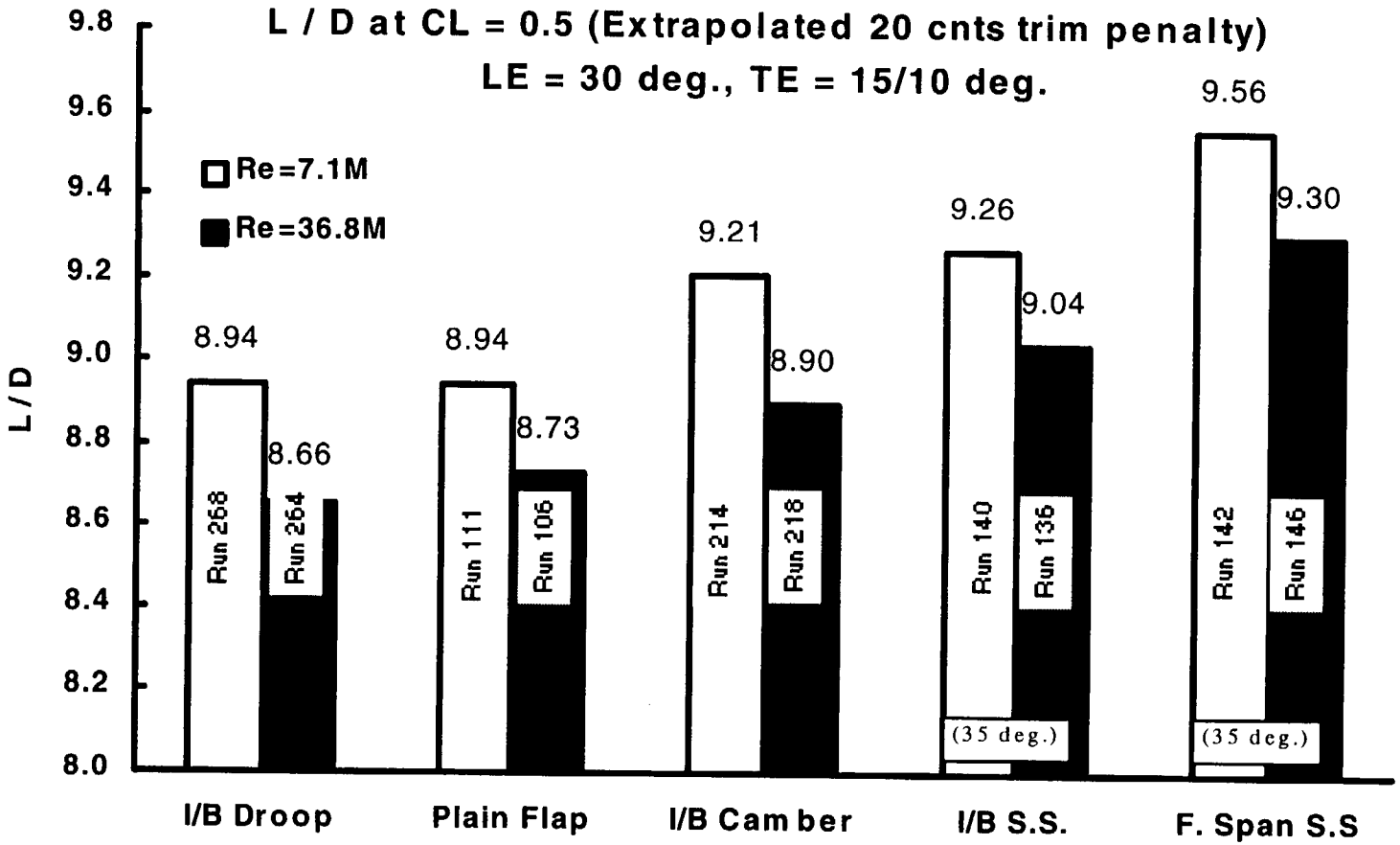
L / D at CL = 0.5 (Extrapolated 20 cnts trim penalty)
LE = 30 deg., TE = 15/10 deg.
Re=7.1M
Re=36.8M
L/D
9.8
9.6
9.4
9.2
9.0
8.8
8.6
8.4
8.2
8.0
8.94
8.66
8.94
8.73
9.21
8.90
9.26
9.04
9.56
9.30
Run 268
Run 264
Run 111
Run 106
Run 214
Run 218
Run 140
Run 136
Run 142
Run 146
(35 deg.)
(35 deg.)
I/B Droop
Plain Flap
I/B Camber
I/B S.S.
F. Span S.S

REYNOLDS NUMBER EFFECTS

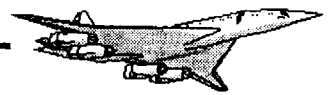

This figure shows the effect of Reynolds Number on the lift and drag coefficients for the baseline (LE/TE = 0°/0°) configuration, tail-off.
There is little variation of the lift with Reynolds number, except at the upper angle-of-attack limit at the higher Reynolds number where the balance load was approaching the allowable limit.
The drag polar indicates a reduction in minimum drag of nearly 10 counts as the Reynolds number increases from 7.13 Million to 36.8 Million. Based on the NTF 2.2% Ref H data, we would expect to see some laminar flow at zero lift conditions at the lower Reynolds number conditions, while at 36.8 Million Reynolds number boundary layer should be fully turbulent. The reduction in CD0 is consistent with this expectation. However, at higher angles-of-attack, the drag increases with Reynolds number. The reason for this increase is not clear.

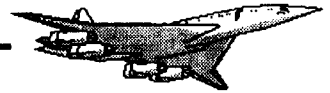

Effect of Reynolds Number on Lift and Drag
Baseline Configuration LE/TE = 0°/0° Tail Off

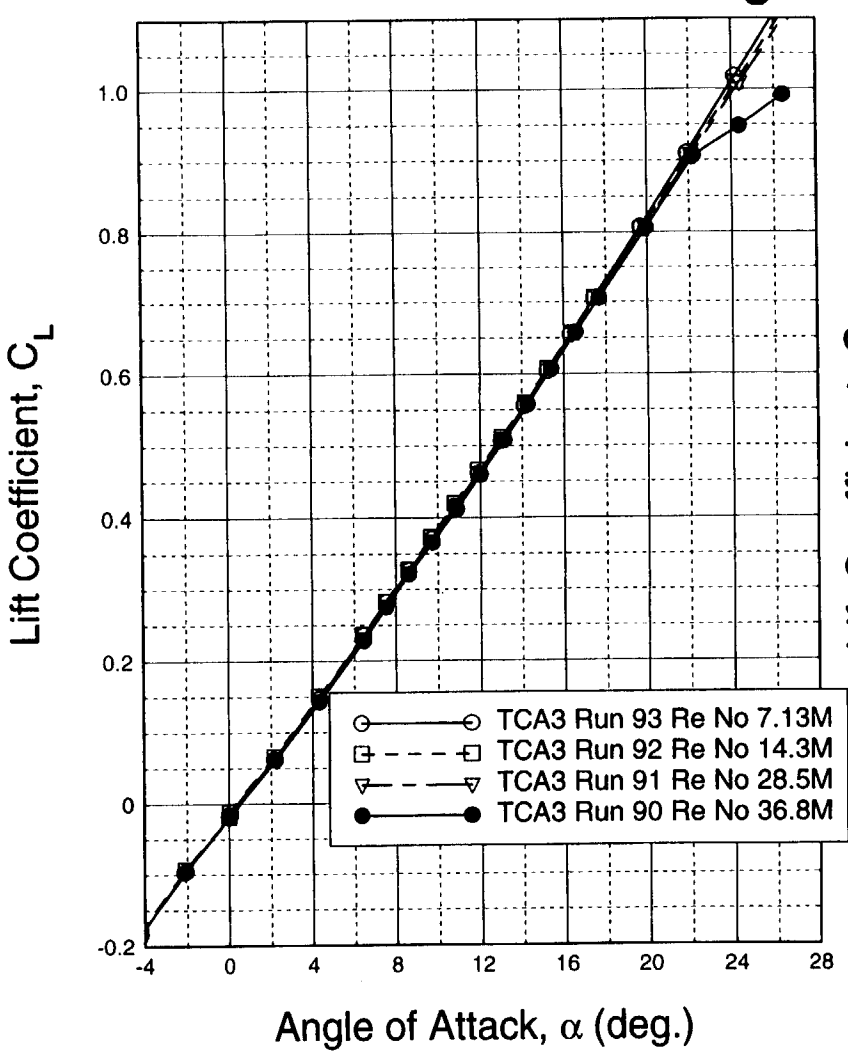

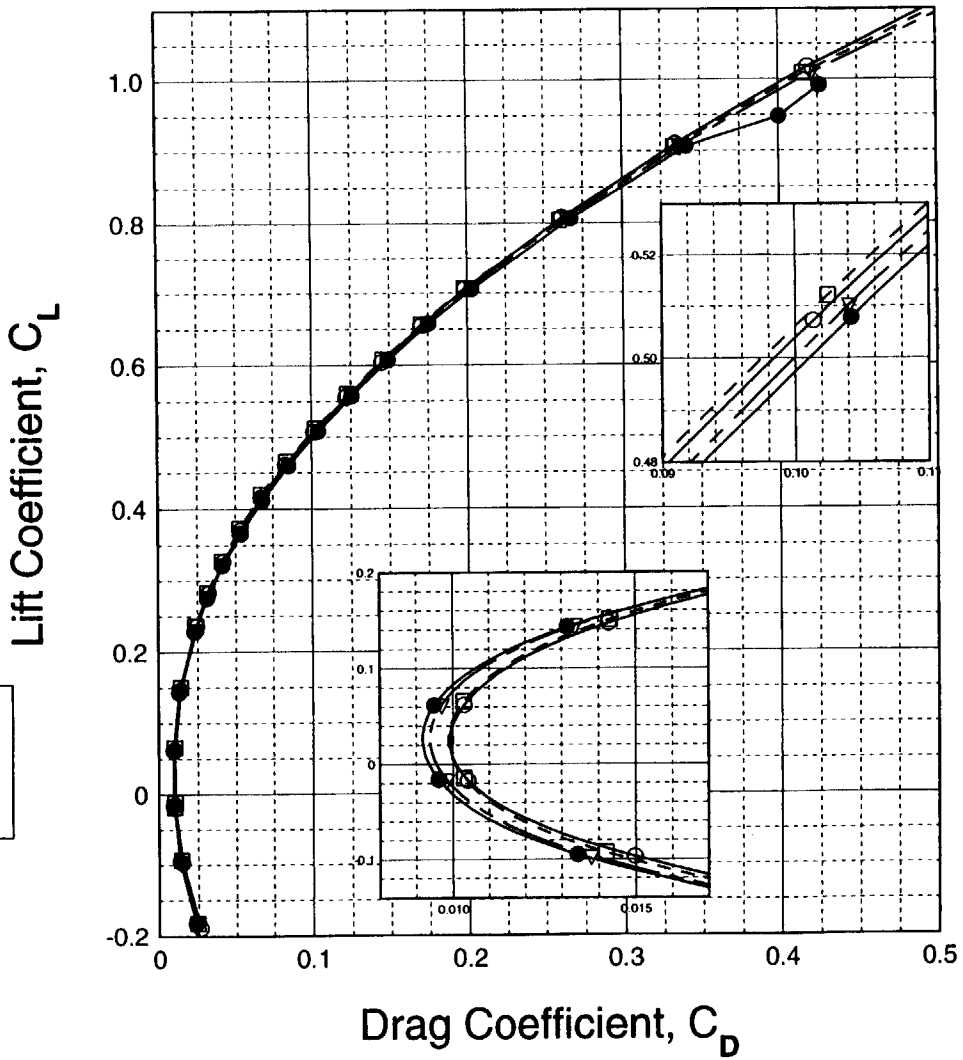

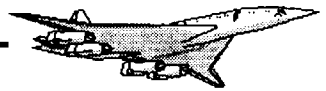

This figure shows the effect of Reynolds Number on the pitching moment and L/D for the baseline (LE/TE = 0°/0°) configuration, tail off.
There is an increase in nose-up pitching moment as the Reynolds number increases. Typically, this would indicate the presence of a stronger leading-edge vortex at the higher Reynolds number conditions, which would be consistent with the drag polar presented on the previous slide. This result is however contrary to the NTF data in which there is more nose-down pitching moment as the Reynolds number increases.

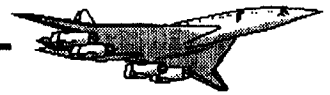

Effect of Reynolds Number on Pitching Moment and L/D
Baseline Configuration LE/TE = 0°/0° Tail Off

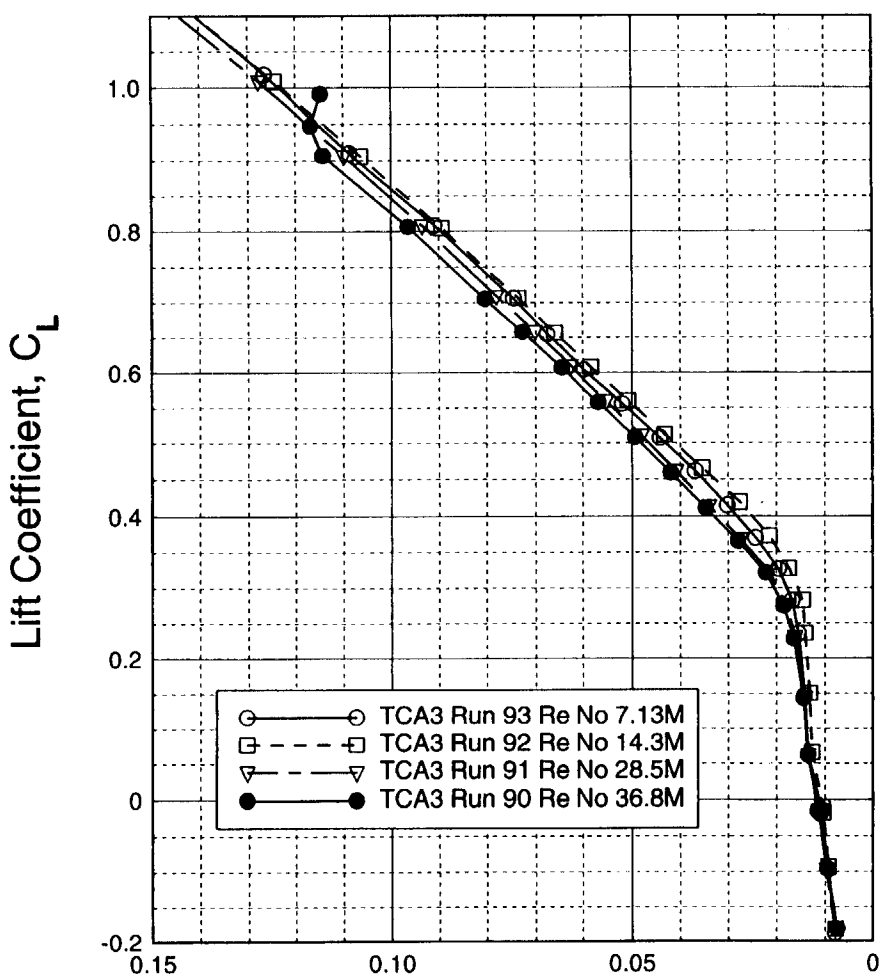

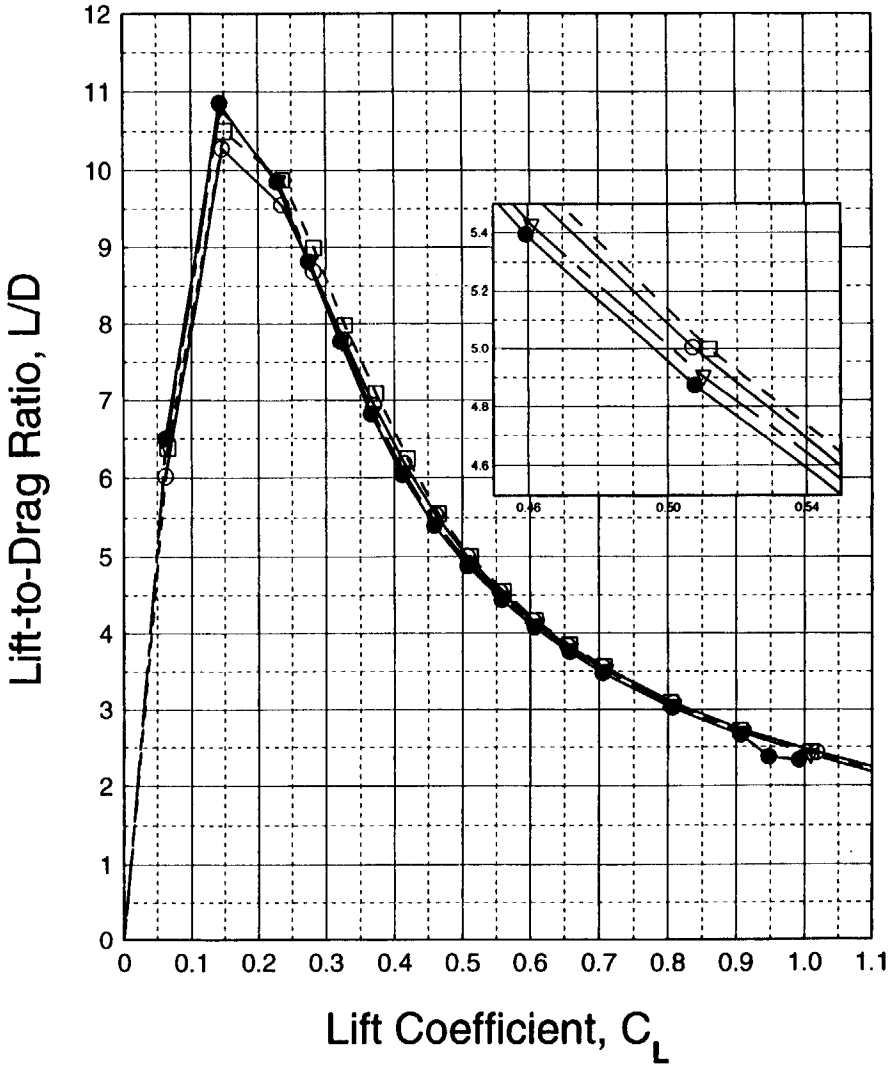

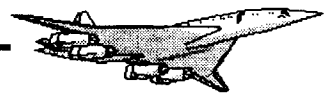

This figure shows the effect of Reynolds Number on the lift and drag coefficients for the baseline (LE/TE = 0°/0°) configuration with horizontal tail incidence 0°. This data is similar to the tail-off data presented in the previous two slides. The reduction in minimum drag from low to high Reynolds number is a little over 10 counts. However, there is again an increase in drag of about 20 counts at CL=0.5. The reason for this increase is not clear at this time.

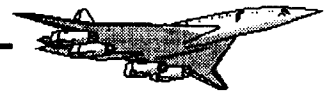

Effect of Reynolds Number on Lift and Drag
Baseline Configuration LE/TE = 0°/0° Tail = 0°

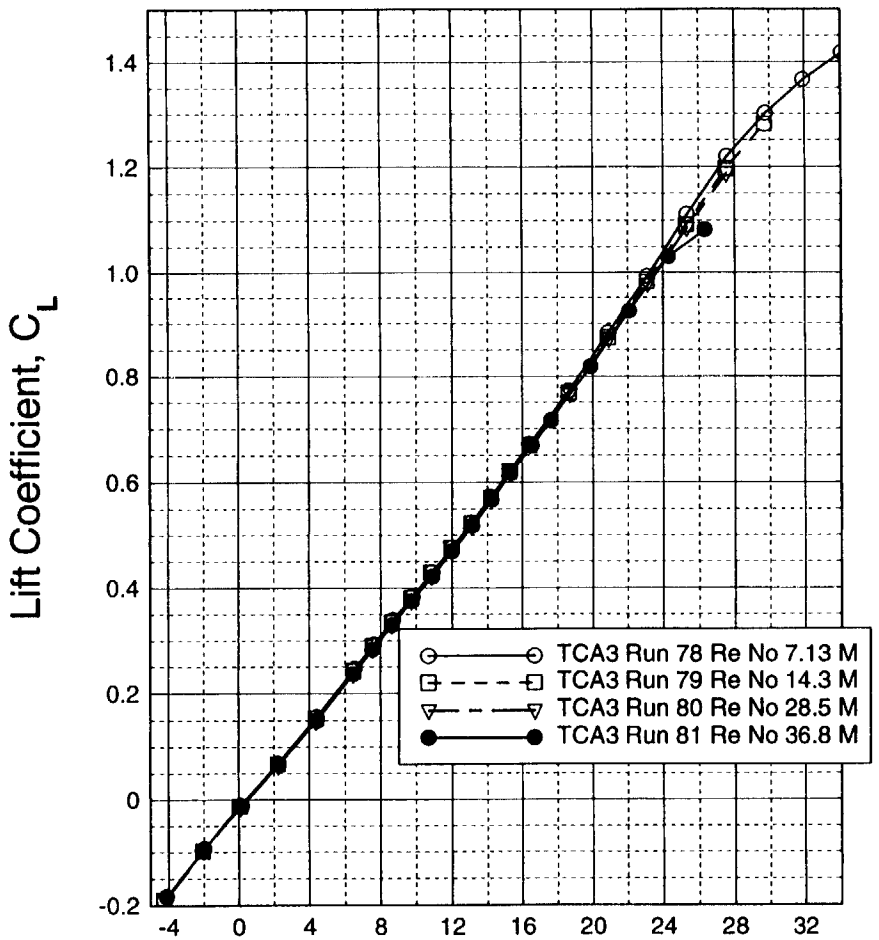

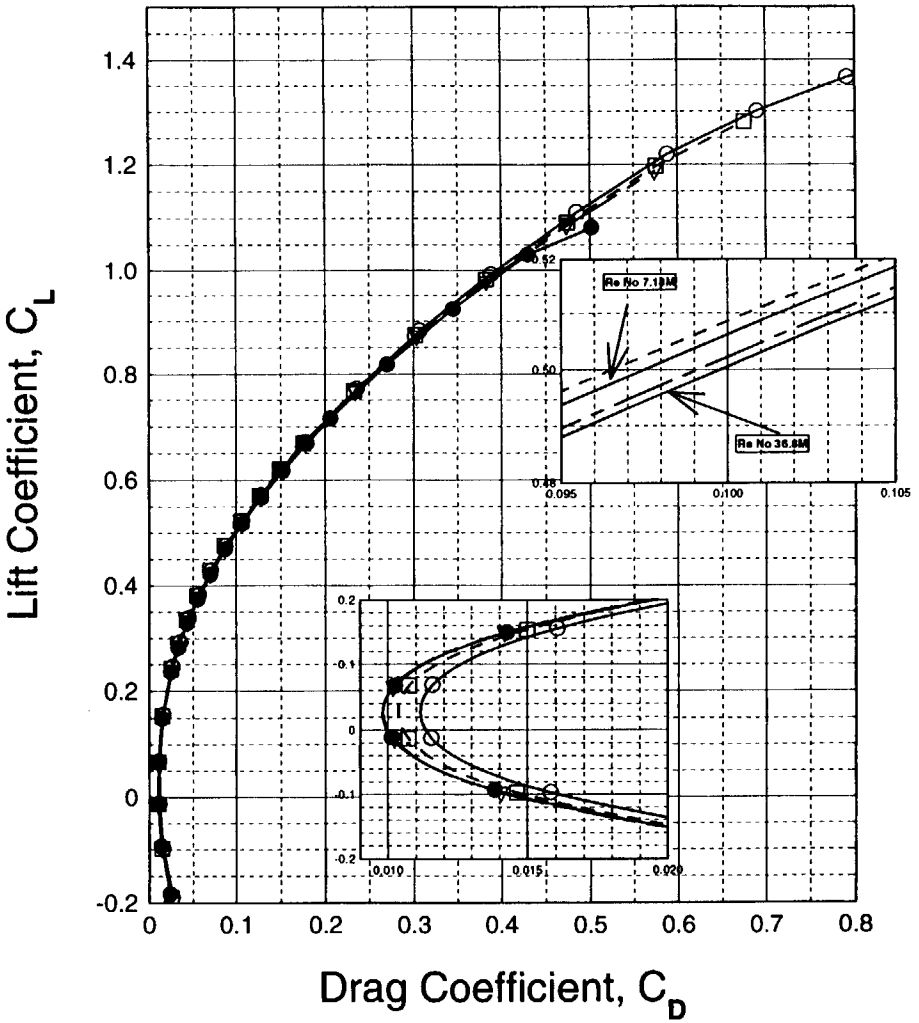

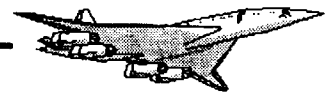

This figure shows the effect of Reynolds Number on the pitching moment and L/D for the baseline (LE/TE = 0°/0°) configuration.
As was seen in the tail-off data, the higher Reynolds number data has a stronger nose-up pitching moment, while the L/D is actually slightly lower at the higher Reynolds number. The change in pitching moment is greater than was seen with the tail-off configuration, indicating that this effect could be associated with the support post. There will be a reduction in the viscous wake behind the support post as the Reynolds number increases which could cause more nose-up pitching moment. However, since the post effect observed in the 14x22-foot Upflow and Interference Test was fairly uniform across the angle-of-attack range, any Reynolds number effect would also be expected to be present at all angles-of-attack.

Effect of Reynolds Number on Pitching Moment and L/D
Baseline Configuration LE/TE = 0°/0° Tail = 0°

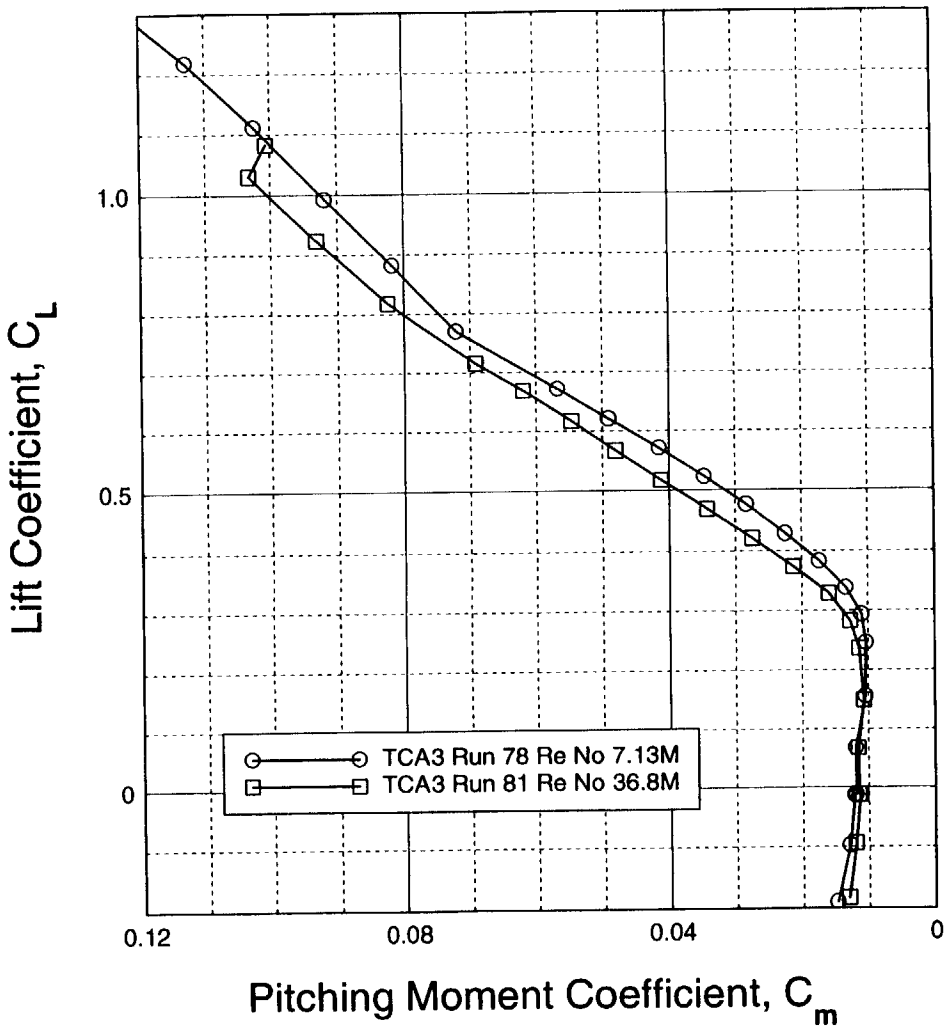

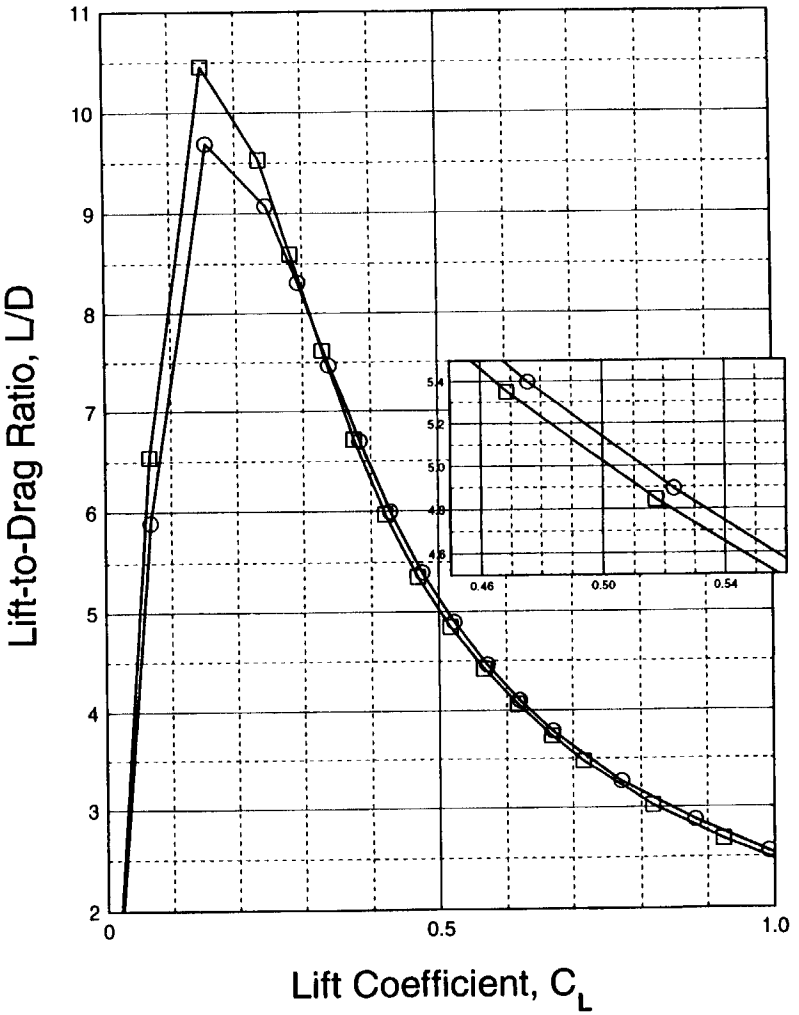

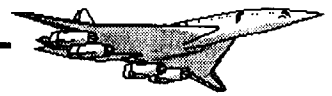

This figure shows the effect of Reynolds Number on the lift and drag coefficients for the high-lift configuration with plain leading-edge flaps. The leading-edge flaps are deflected 30° (full span) and the trailing-edge flaps are deflected 15° for the 3 outboard flaps, and 10° inboard.

Up to about 16° angle-of-attack, the lift does not vary much with Reynolds number. At higher angles-of-attack, there is some decrease in lift which could be associated with model elastic effects.

The drag polar indicates a reduction of about 10 counts in minimum drag which is still present at CL=0.5. This drag reduction observed at Cl=0.5 is less than would be expected from the reduction in skin friction drag.

The data from back to back repeat runs is plotted here showing a good level of repeat quality.

Effect of Reynolds Number on Lift and Drag
LE/TE = 30°/15°/10° Plain Flaps Tail = 0°

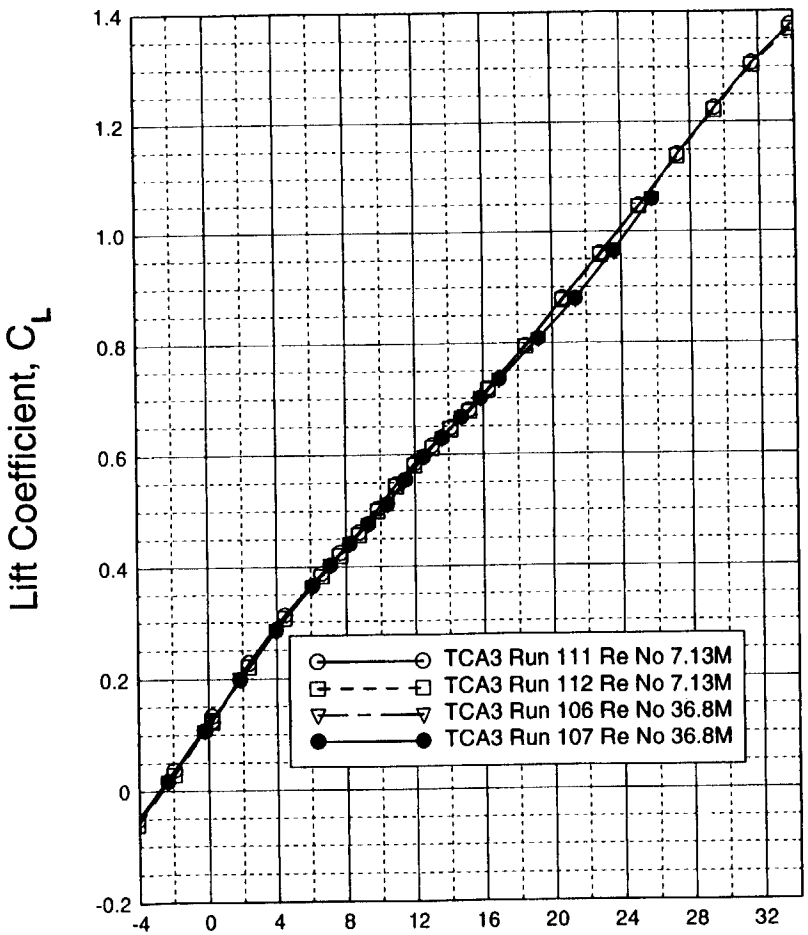

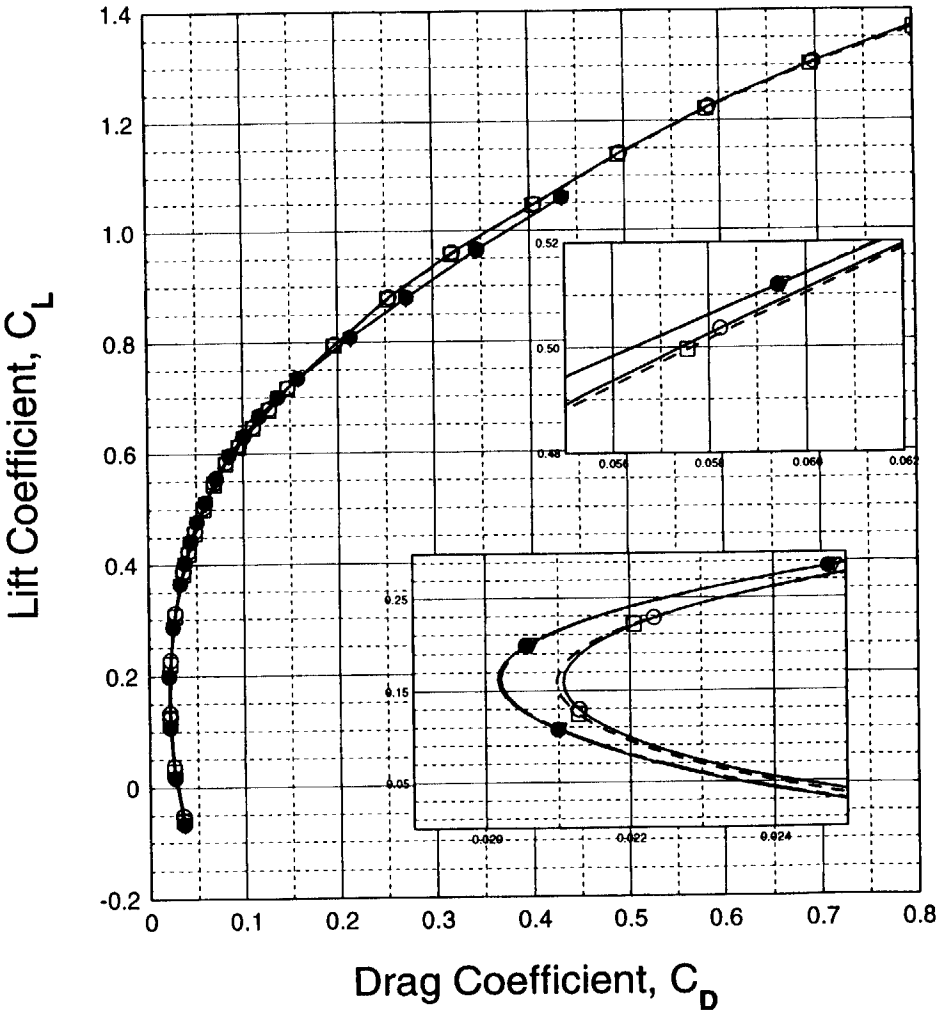

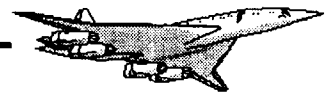

This figure shows the effect of Reynolds Number on the pitching moment and the L/D for baseline high-lift configuration. The leading-edge flaps are deflected 30° (full span) and the trailing-edge flaps are deflected 15° for the 3 outboard flaps, and 10° inboard.

There is less effect on pitching moment due to Reynolds number for the high-lift configuration than was seen for the flaps-up configuration up to a Cl of about 0.8, which corresponds to the point at which the lift curves were seen to begin to differ, possibly due to model elastic effects. This data differs from the flaps up configurations where there was a significant increase in pitching moment with Reynolds number.

The increase in L/D with Reynolds number is about 0.2 at CL=0.5, which is less than that seen in the NTF data for the 2.2% Ref H model.

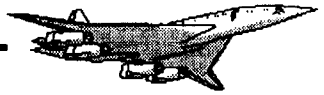

Effect of Reynolds Number on Pitching Moment and L/D
LE/TE = 30°/15°/10° Plain Flaps Tail = 0°

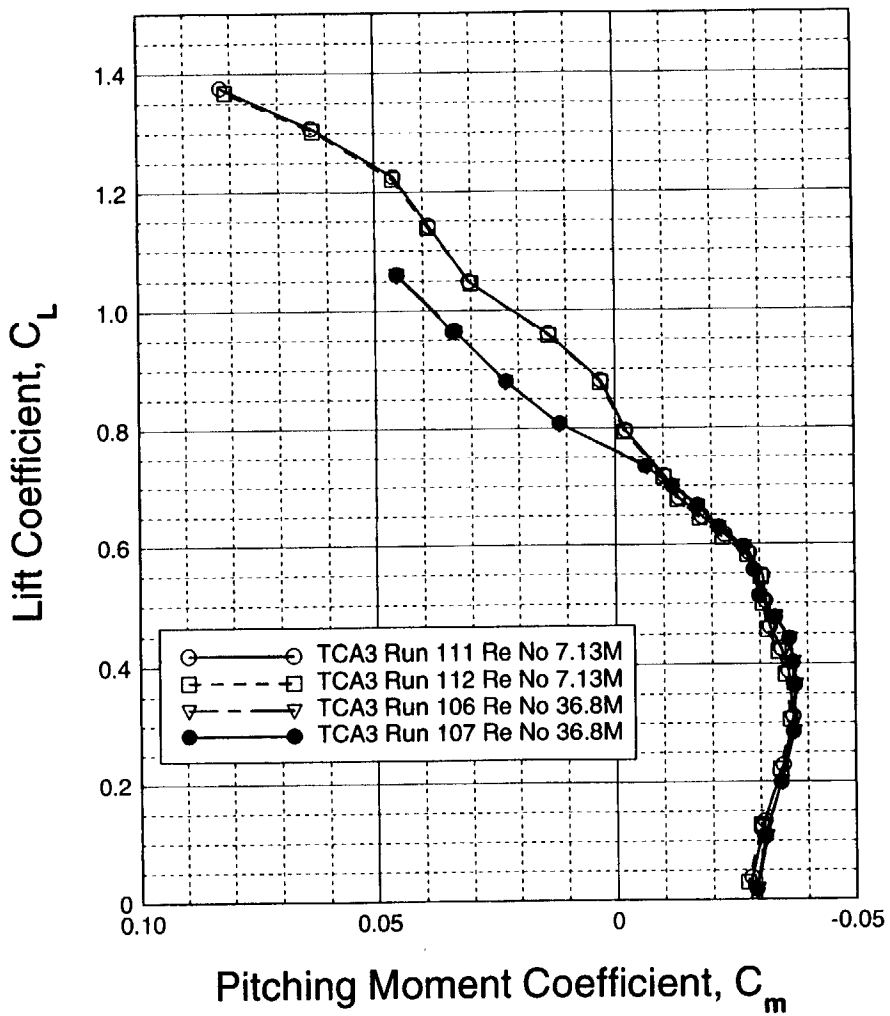

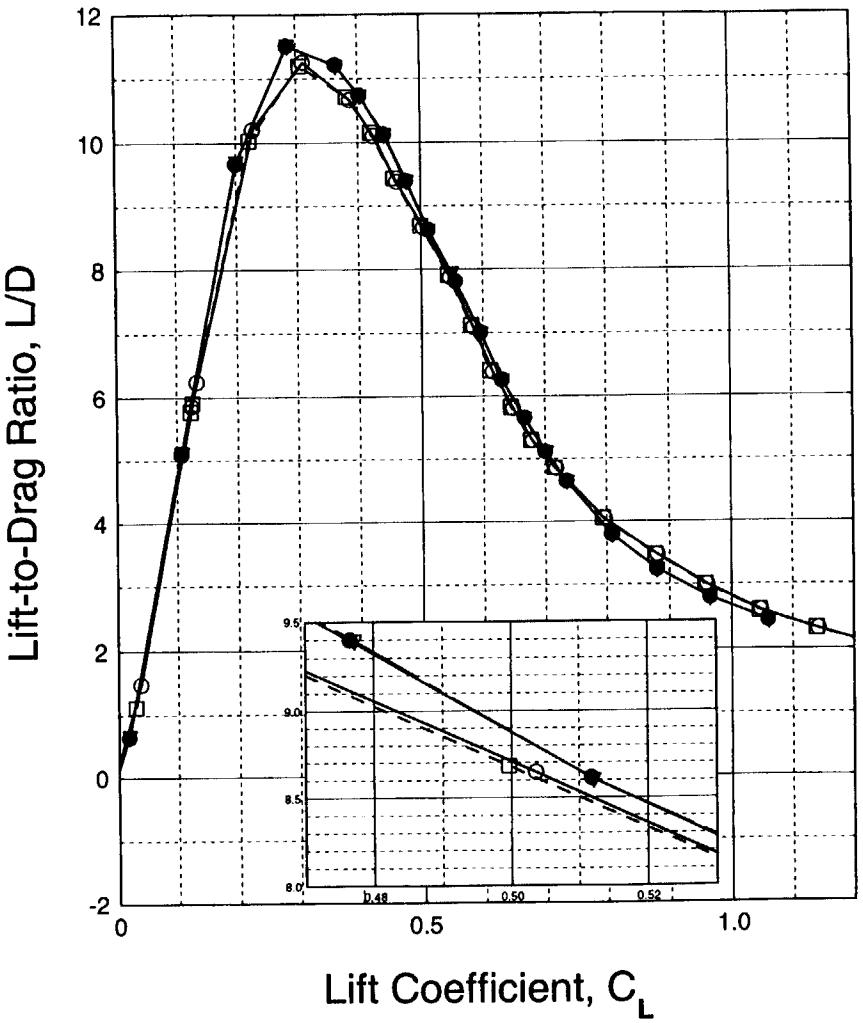

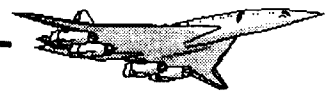

This figure compares the measured variation in minimum drag between the low Reynolds number and the high Reynolds number data for the flaps up and high-lift (LE/TE=30°/15°/10°) configurations. Data is plotted for the wing/body, wing/body/nacelle/vertical and wing/body/nacelle/vertical/horizontal configurations.

The error bars shown represent an error of +/- 2.5 drag counts which was the data repeatability level reported earlier for the high Reynolds number data. Examination of the repeat runs for the full high-lift configuration indicated that the scatter in the Reynolds number increment is comparable to the errors in the absolute drag levels. This seems to be reasonable, since the Reynolds number increments were obtained from back-to-back runs in which only the tunnel test conditions were changed.

The measured increments are compared with the analytical trends which would be expected if we assume a fully turbulent boundary-layer development for both the high- and low-Reynolds number data. Based on the NTF data, we would expect to see some laminar flow for the flaps-up configuration at zero-lift conditions. For this reason, the NTF data point shown here for the flaps up configuration shows a Reynolds number increment of about half that to be expected from the analytical approximation. For the high-lift configuration, the measured increment is comparable to the analytical levels.

However, it is not clear why the Reynolds number increments from the current test are so much lower than the fully turbulent boundary-layer predictions.

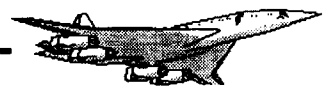

Reynolds Number effect on CD0

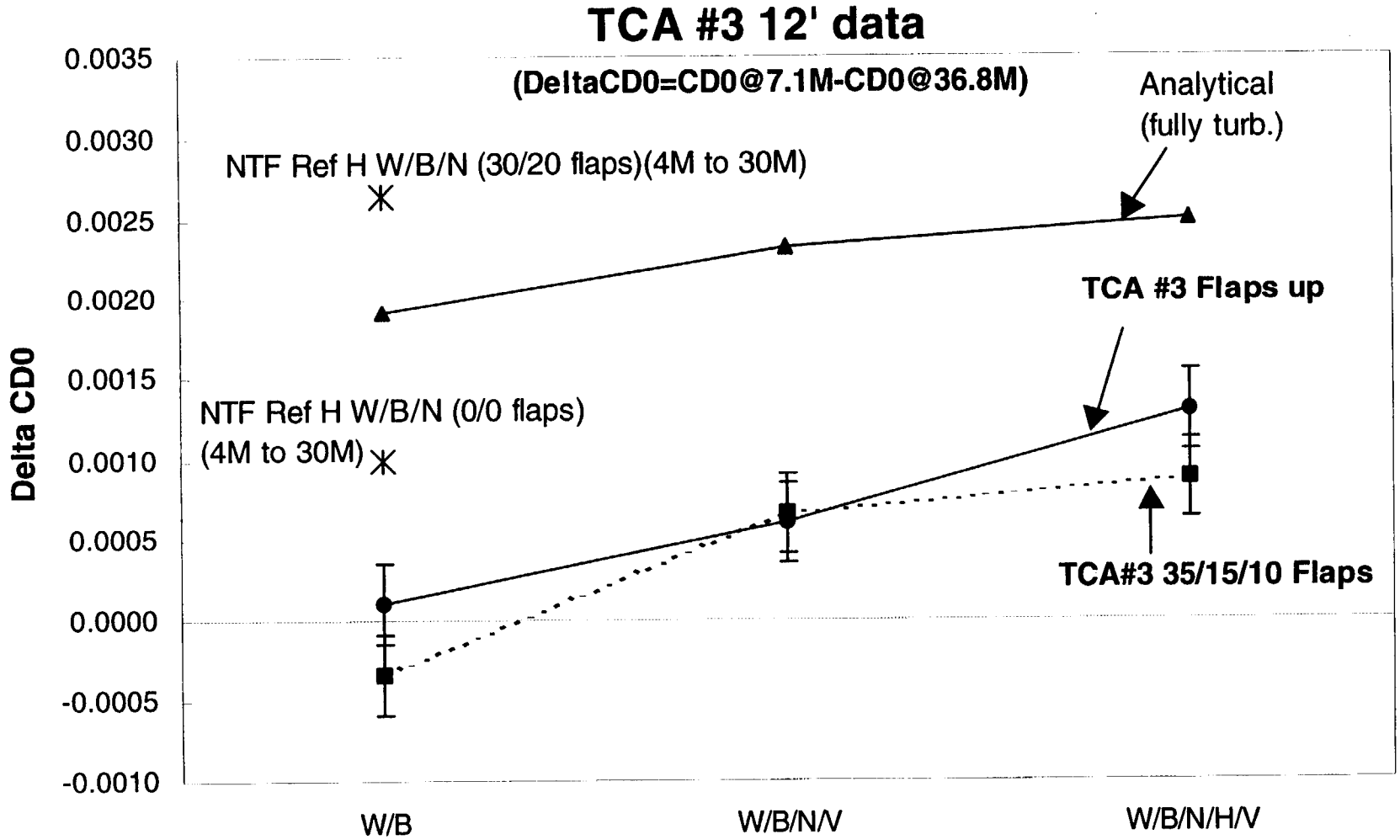

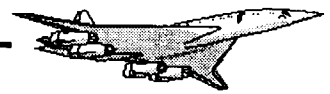

FLOW VISUALIZATION

OIL FLOW
PRESSURE SENSITIVE PAINT

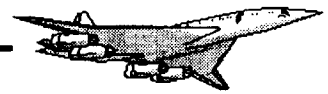

This figure indicates the oil flow and interferometry testing which was done during this test and the configurations investigated.

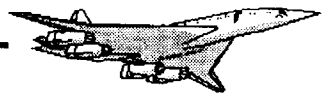

OIL FLOW AND INTERFEROMETRY (ARC)

- OIL FLOW PICTURES TAKEN OF THE WING/BODY COMBINATION AT 3 FLAP CONFIGURATIONS
  - F/S LE SEALED SLATS AT 35 DEG
  - CAMBERED LE AT 30 DEG
  - DROOPED LE AT 30 DEG
- INTERFEROMETRY PICTURES TAKEN OF THE WING/BODY COMBINATION AT 2 FLAP CONFIGURATIONS
  - F/S LE SEALED SLAT AT 35 DEG
  - CAMBERED LE AT 30 DEG

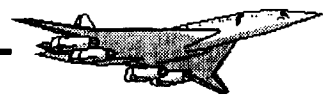

This figure shows an example of the oil flow pictures taken during this test. The pattern was obtained by mixing mineral oil and artists paint and striping the wing with alternate colors and then running the tunnel for about five minutes. This particular example configuration had full span leading edge sealed slats deflected 35 degs. and trailing edge flaps of 15/15/15/10 degs. The horizontal tail and nacelles were off and the angle of attack was 10 degs. The Reynolds Number was 36.8 million.

Separation can be seen at the hinge line of the leading edge flap and a vortex emanating from the leading edge fuselage intersection flowing across the inboard panel of the wing. The results are somewhat disappointing since the different colored paints merge into a multicolor blur where no distinct flow features are evident. Because of this result, the technique using mineral oil and lamp black which produces well defined striations is recommended for future oil flow studies.

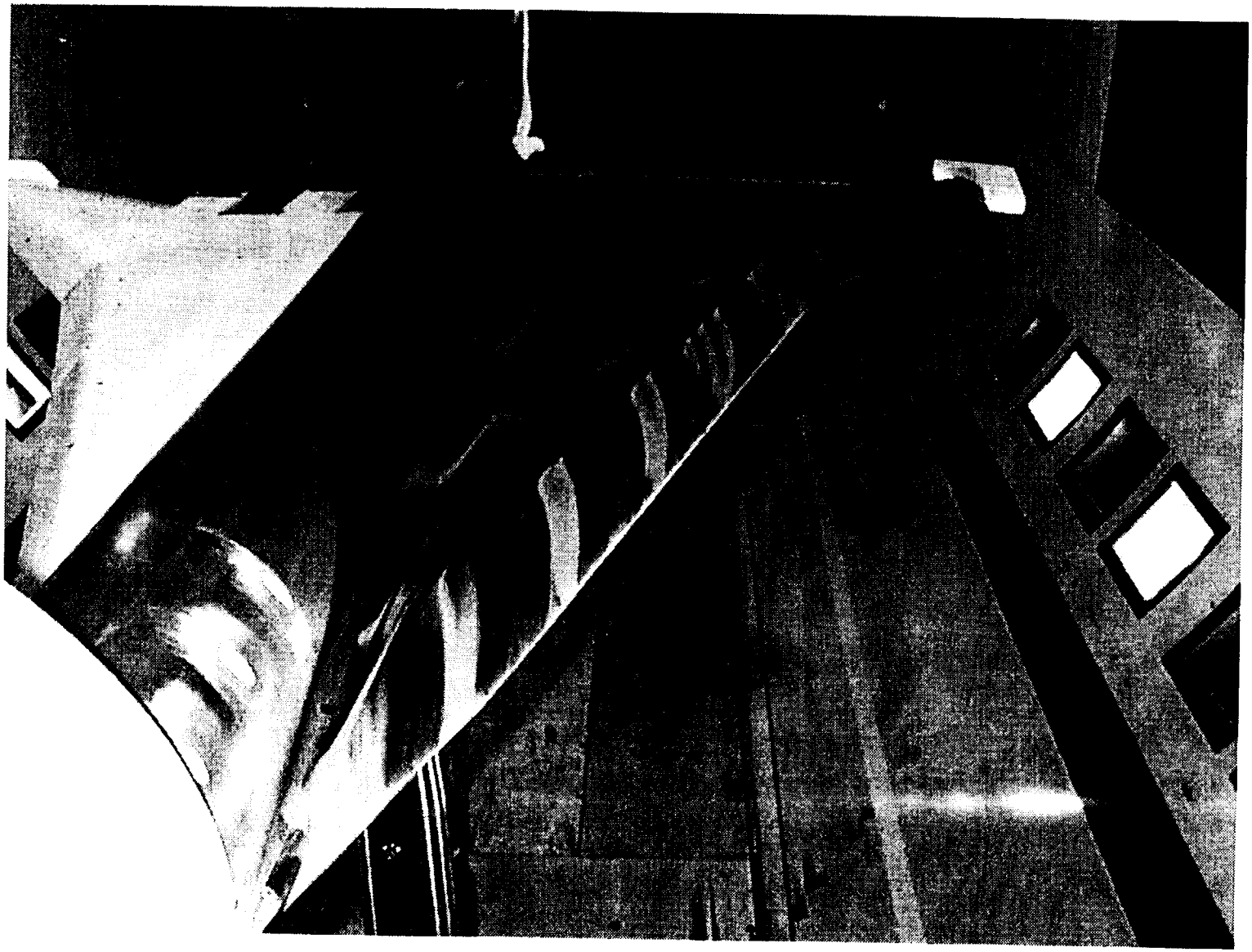

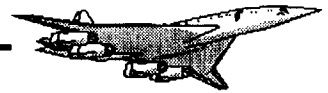

This chart describes the setup procedure required in order to measure the skin friction coefficient by the interferometry technique. This is a recent innovation and is described more fully in SAE Conference Paper 932550 by Mateer and Monson and dated 1996. The experiment for this wind tunnel test was run, and the results produced by, David Driver of NASA Ames.

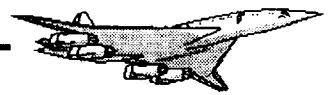

INTERFEROMETRY TECHNIQUE

- MYLAR WITH ADHESIVE BACKING IS APPLIED TO THE MODEL TO PROVIDE A SMOOTH OPTICAL SURFACE
- SILICONE OIL IS APPLIED TO THE MYLAR PRIOR TO EACH RUN
- OIL FLOWS DUE TO SURFACE SHEAR AND BECOMES THIN (1 TO 2 MICRONS) AFTER 5 MINS
- INTERFERENCE PATTERNS (FRINGES) ARE VISIBLE IN THE OIL AND DISTANCE BETWEEN FRINGES IS PROPORTIONAL TO SKIN FRICTION COEFF. Cf

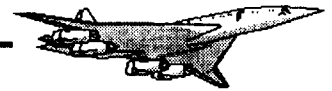

This chart shows a schematic of the interference phenomena and the results obtained using the interferometry technique on a NACA 0012 wing. These results are from the paper already referenced.

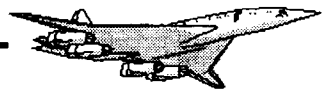

OIL FILM INTERFEROMETRY TECHNIQUE

OIL FLOW DUE TO SURFACE SHEAR

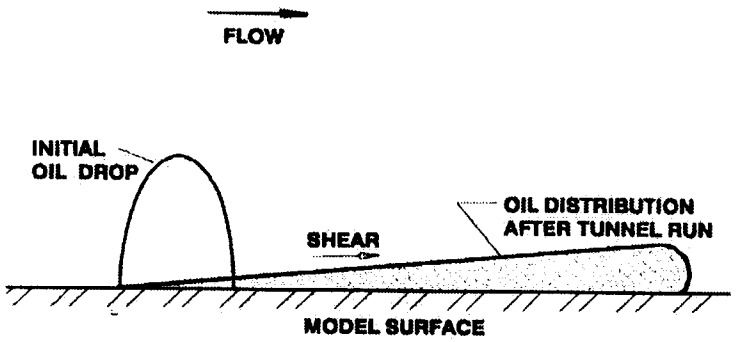

INTERFERENCE PATTERN SCHEMATIC

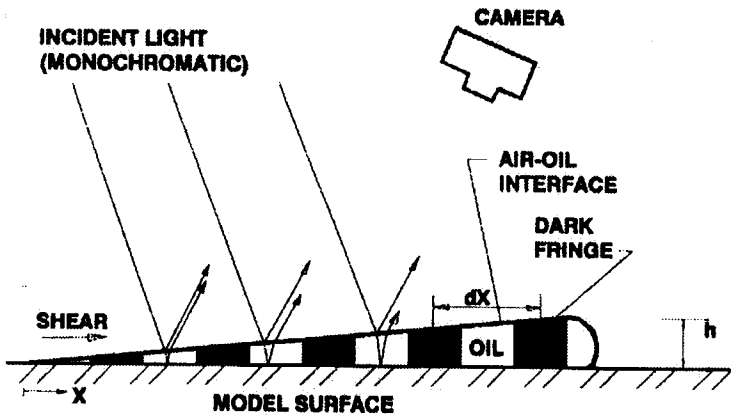

$$C_f=(2n_oCos(\theta_r)dx/\lambda) / \int^t q(t)/\mu(t)\,dt$$

OIL PATCHES ON NACA 0012 WING

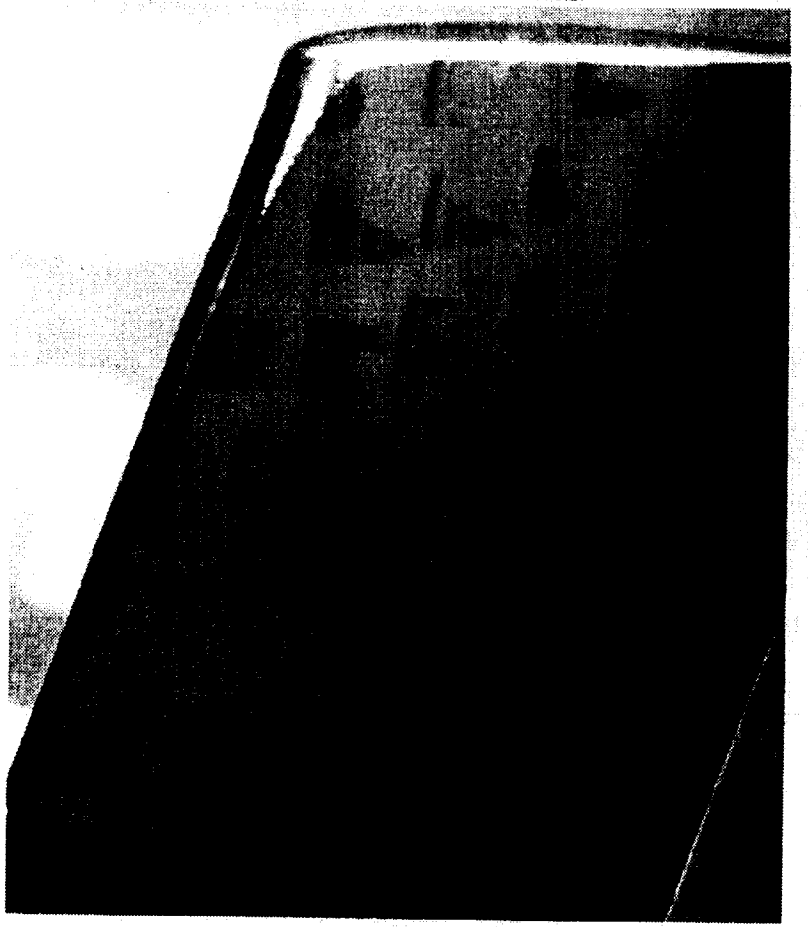

TECHNIQUE OF MATEER & MONSON AIAA J. 1996
MONSON & MATEER SAE CONFERENCE PAPER 932550

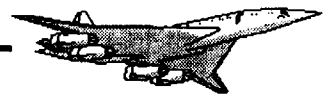

This chart shows an example of the interferometry technique results obtained on the TCA model fore-body during the test. Note the three interference fringe patterns produced where the silicone oil has sheared due to the air flow.

OIL-FILM INTERFEROMETRY APPLIED TO THE FORE BODY

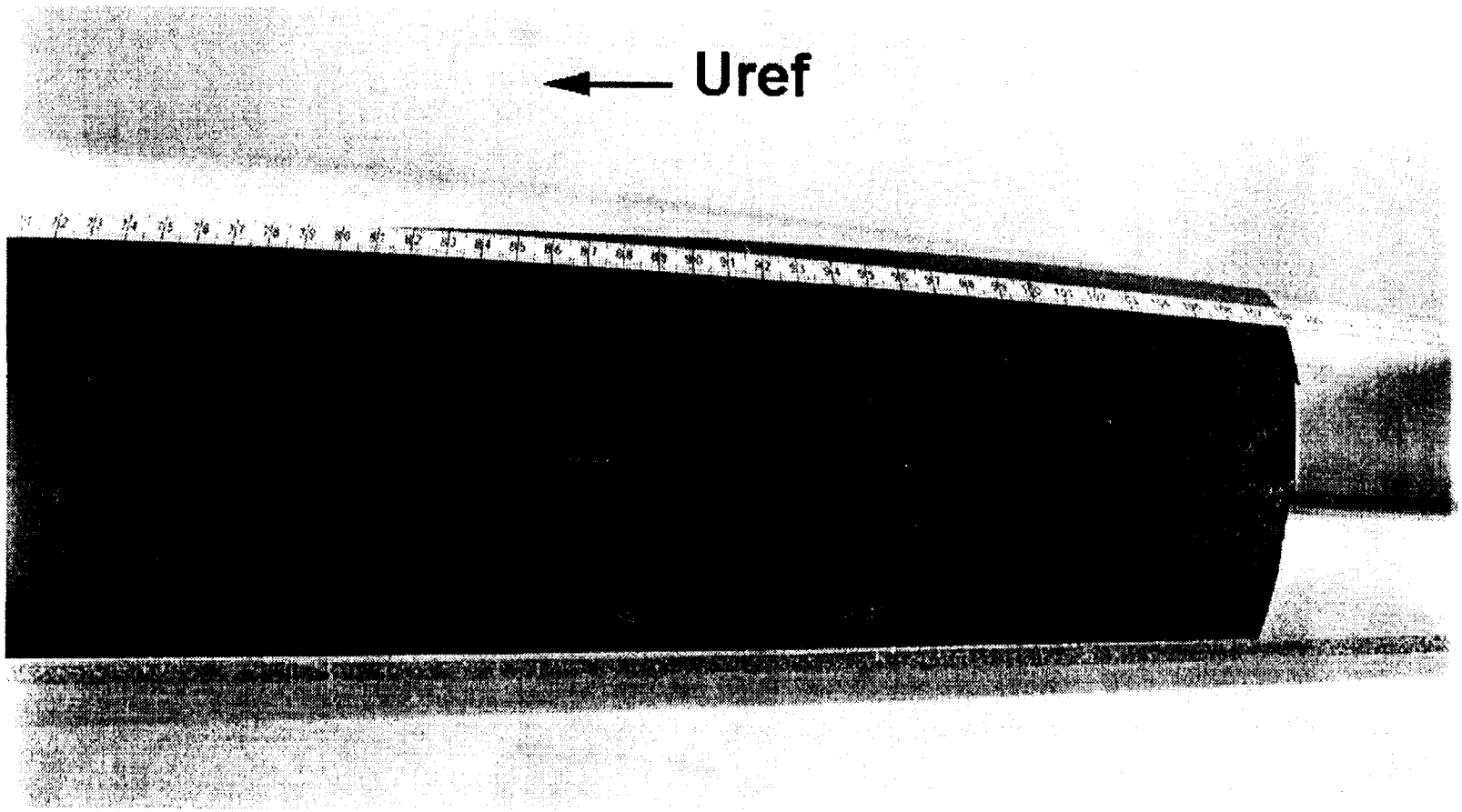

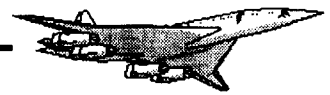

This figure shows the results obtained for the skin friction coefficient, Cf, at various locations along the TCA model fore-body for high and low Reynolds Numbers. It is not known why there is a rise in value of Cf between 30 and 40 inches along the fore-body but the relationship of high Reynolds Number and low Cf and vice versa is very evident.

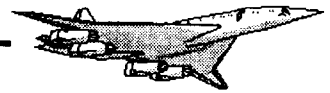

SKIN-FRICTION DISTRIBUTION ON THE FORE BODY @CONSTANT Phi=60°

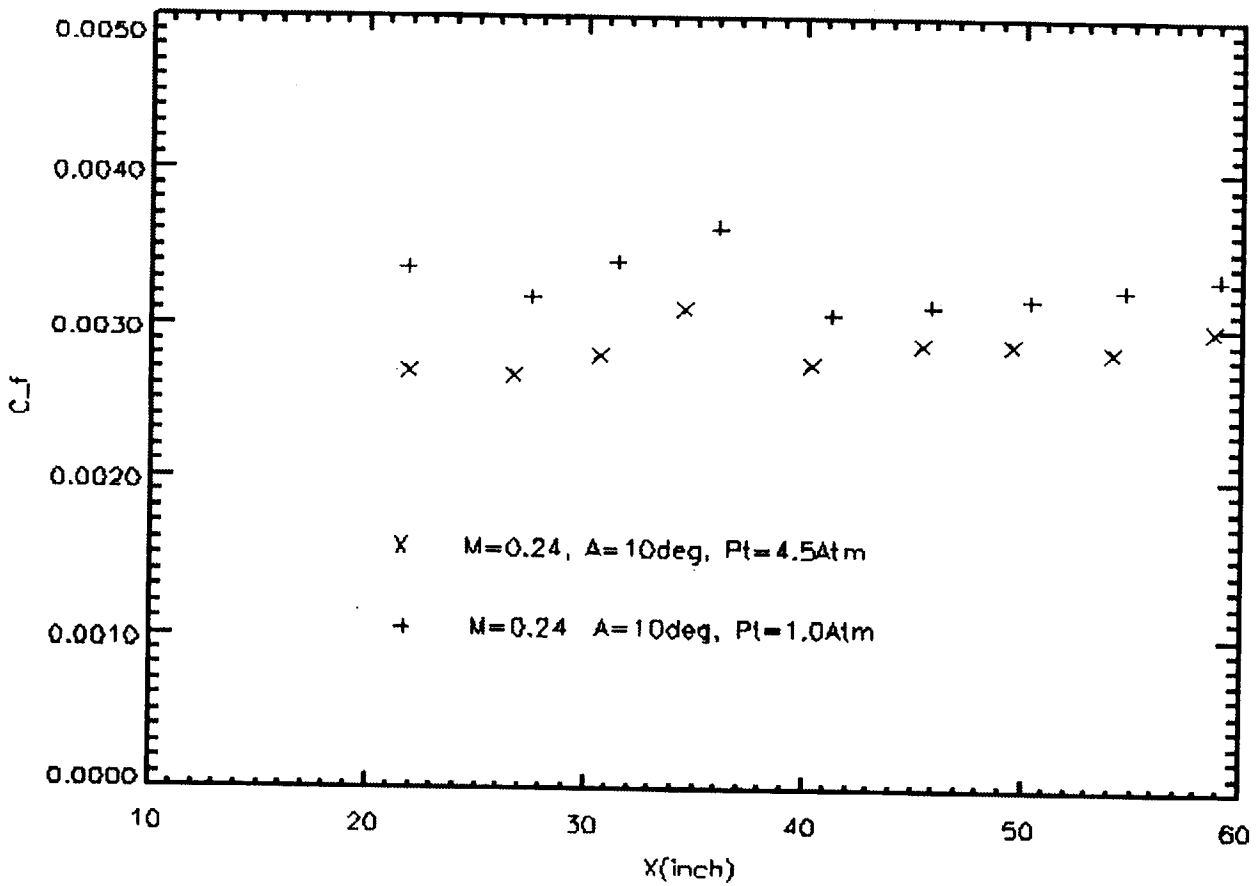

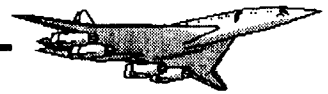

This chart shows the condition and configurations for the wing surface pressure investigation using the pressure sensitive paint technique. The data was gathered by observing the painted upper surface of the right hand wing. The experiment and production of pressure plots shown in this report were the result of work by James Bell of NASA Ames.

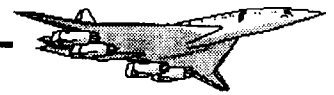

PRESSURE SENSITIVE PAINT (ARC)

- PAINTED UPPER SURFACE OF RIGHT HAND WING
- TWO VIEWING STATIONS
  - TOP VIEW OF WING
  - CLOSE-UP VIEW OF LEADING EDGE
- ACQUIRED DATA AT TWO PRESSURES FOR SIX DIFFERENT LEADING EDGE CONFIGURATIONS, MOSTLY WITH NACELLES AND EMPENNAGE OFF

This chart shows the pressures observed for the configuration with inboard leading edge sealed slats and outboard plain flaps deflected 35 degs. The trailing edge flaps were deflected 15/15/15/10 degs, the nacelles were off and the Reynolds Number was 7.13 million.The angle of attack was close to 15 degs.

Clearly seen is the wing apex vortex which sweeps over the inboard wing panel and trailing edge flaps. A small vortex is seen to develop on the wing leading edge upstream of the wing crank point and then travelling over the inboard part of the outboard trailing edge flaps. Finally a vortex is generated at the wing crank point and travels along the outboard wing panel leading edge before sweeping over the outboard trailing edge flap. The small white oblong area near the trailing edge flaps is caused by missing paint on the adjustment mechanism for the trailing edge flap.

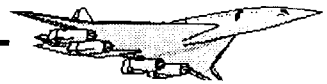

TCA 5%
Plain/Sealed 35-15 Full

Test	120037	Mach	0.2426	PSTAT	2039.
Run	492	Alpha	14.61	PTOT	2124.
Point	9	RN	1.698	TF	49.78
Camera	1	Q	83.96	TTF	55.78

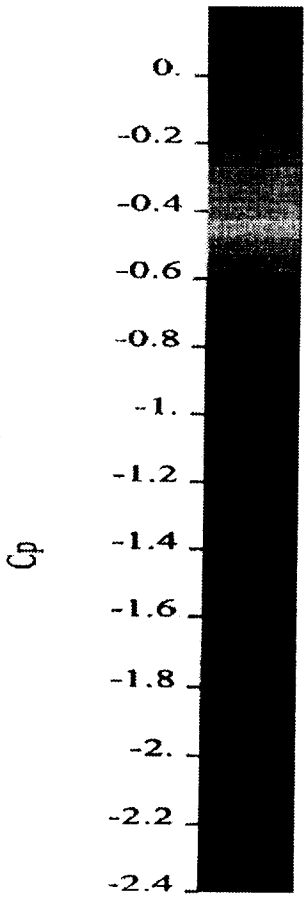

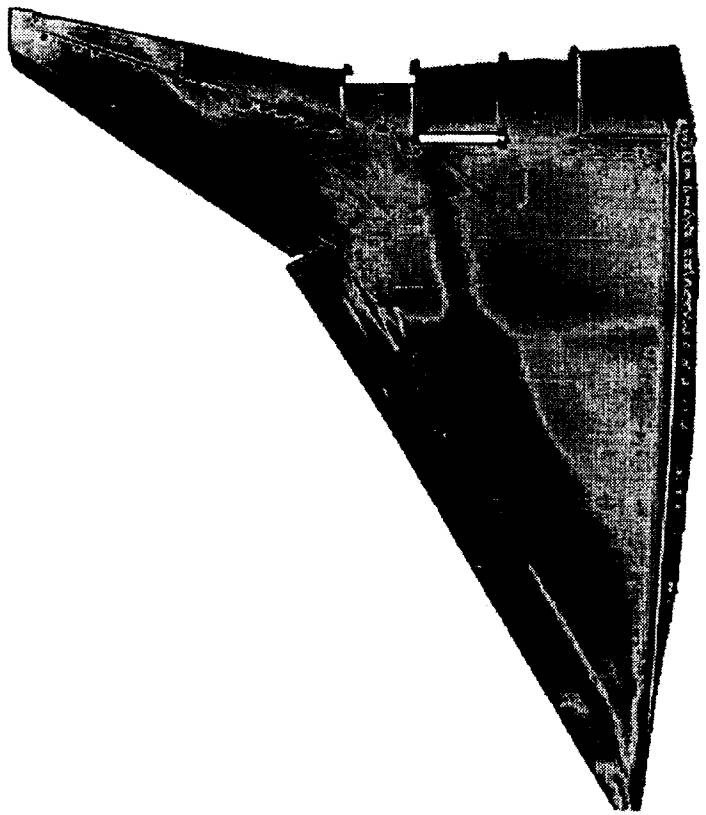

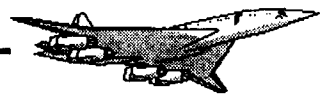

This chart shows the pressures observed for the same configuration as the previous chart but the Reynolds Number is now 36.8 million. In general the same vortices as before are seen to form over the inboard and outboard wing panels.

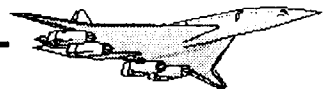

TCA 5%
Plain/Sealed 35-15 Full

Test	120037	Mach	0.2434	PSTAT	9549.
Run	490	Alpha	14.74	PTOT	9950.
Point	9	RN	7.868	TF	55.42
Camera	1	Q	396.	TTF	61.53

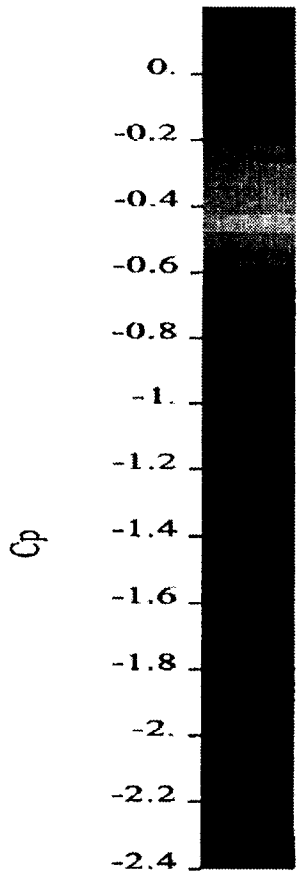

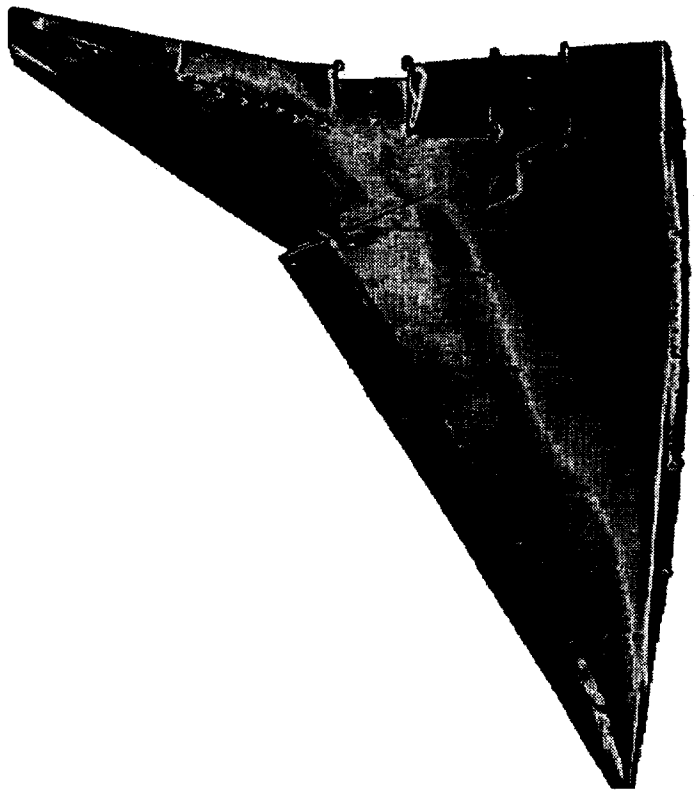

MODEL DEFORMATION

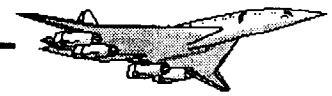

This chart summarizes the configurations and conditions where wing deformation data was gathered. This procedure has been developed and refined by Al Burner at NASA Langley and for this model test was conducted by John Schreiner of NASA Ames.

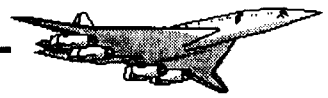

DEFORMATION CONFIGURATIONS

HIGH AND LOW REYNOLDS NUMBER

- PLAIN FLAP LE/TE = 30/20 TAIL ON
- PLAIN FLAP LE/TE = 40/20/15 TAIL ON
- PLAIN FLAP LE/TE = 40/20/15 TAIL OFF
- PLAIN FLAP LE/TE = 0/30 TAIL ON
- PLAIN FLAP LE/TE = 30/10 TAIL OFF NACS OFF
- PLAIN FLAP P/S LE/TE = 30/0/10 TAIL OFF NACS OFF

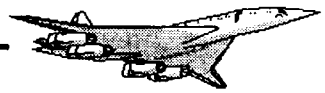

This figure shows the location of the retro-reflective targets placed on the left hand wing. Six locations in all were used, four on the outboard wing panel and two on the nacelles with a reference line of targets on the side of the fuselage.

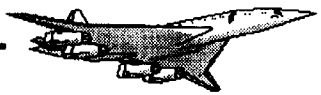

Retro-Reflective Target Placement

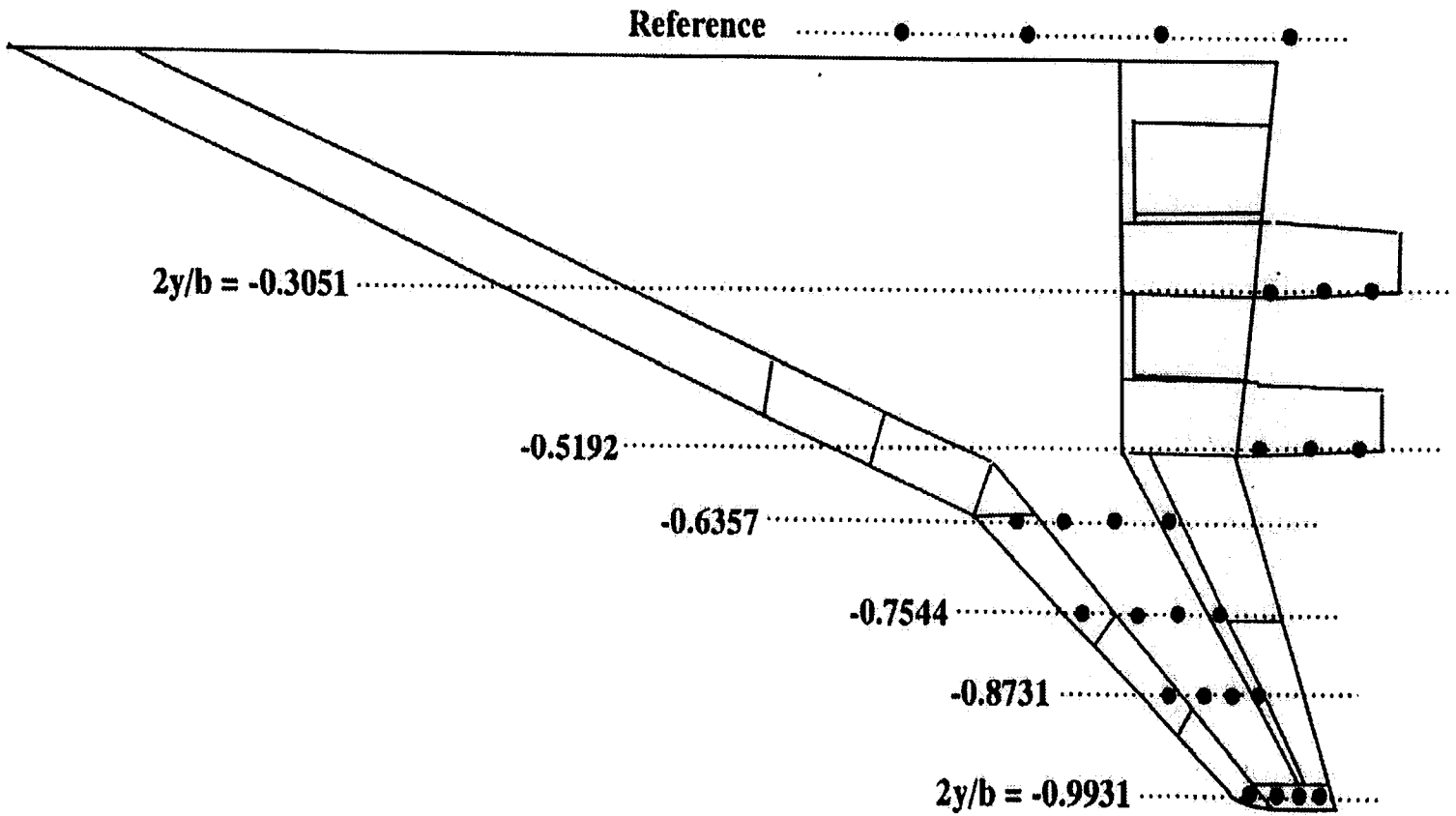

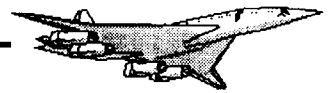

The data for wing deformation was gathered by use of a camera whose field of view included the retro-reflective targets already described.Also shown in this chart are the model locations in the tunnel for three angles of attack. Because of constraints on where the camera could be placed and the size of the model, the ideal camera viewing angle of 20 to 60 degs. was not attained. This made it necessary to do additional manipulation of the data to ensure satisfactory results.

Imaging Geometry

TCA model at three angle-of-attack positions. View looking downstream in 12-foot PWT.
Ideal viewing angle = 20 to 60 Degrees

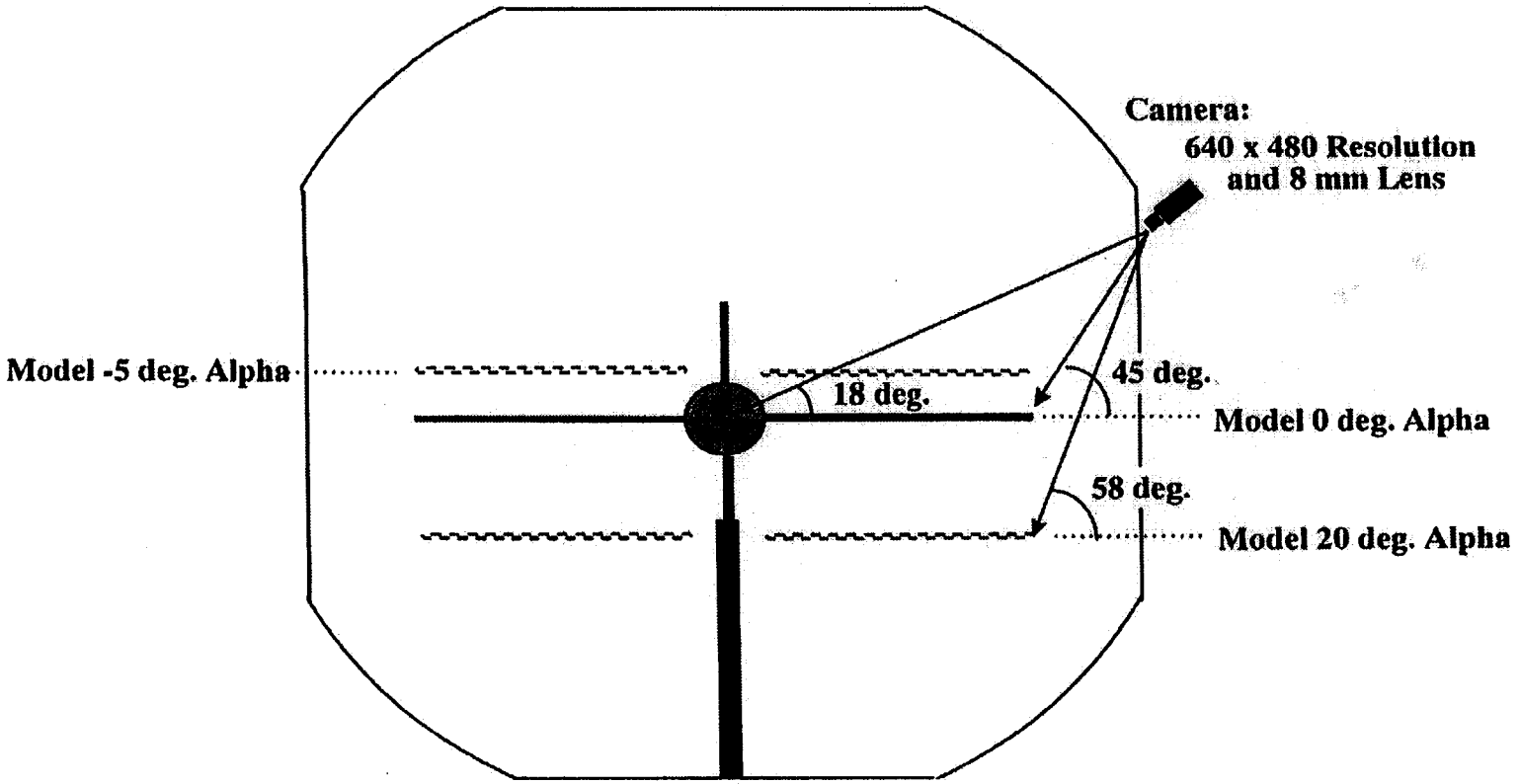

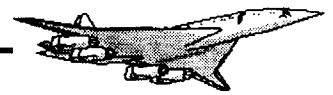

This figure shows an example of the deformation data results for a tail off, nacelles off configuration with LE/TE flaps = 30/10 and high and low Reynolds Number. The figure shows displacement (inches) plotted against body angle of attack(degs) where the displacement was measured at the wing trailing edge. The four spanwise stations shown are all located on the outboard wing panel.

The displacement appears to be fairly linear up to about 13 degs.body alpha and then either falls slightly or maintains a constant value. As expected the higher Reynolds Number data produces the higher displacement.

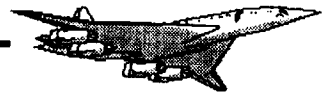

DEFORMATION DATA LE/TE = 30/10 TAIL OFF NACELLES OFF
Run 466 Re 36.8 million = Solid line
Run 469 Re 7.13 million = Dashed line

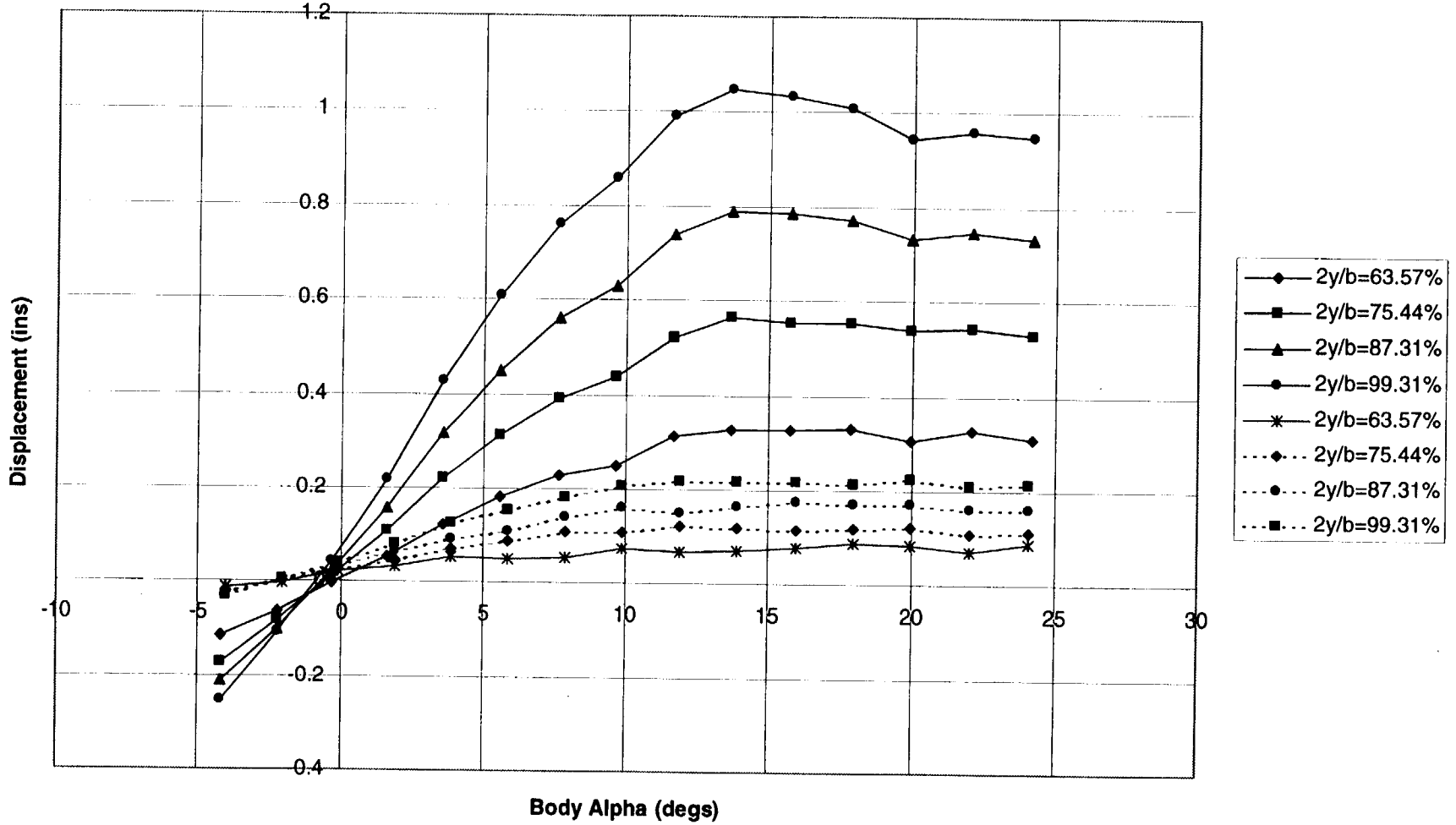

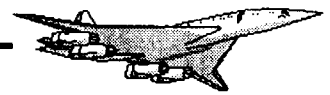

This figure shows the wing twist data for the same conditions shown in the previous figure. The high Reynolds Number data shows a similar trend in twist data as the displacement data, with linear increases to about 13 degs. body alpha and constant or slightly decreasing values thereafter. The low Reynolds Number data is very oscillatory above about 5 degs. body alpha but with much smaller twist angles, less than -0.30 degs.

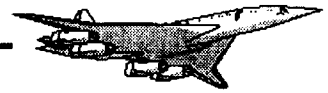

DEFORMATION DATA LE/TE = 30/10 TAIL OFF NACELLES OFF
Run 466 Re 36.8 million = Solid line
Run 469 Re 7.13 million = Dashed line

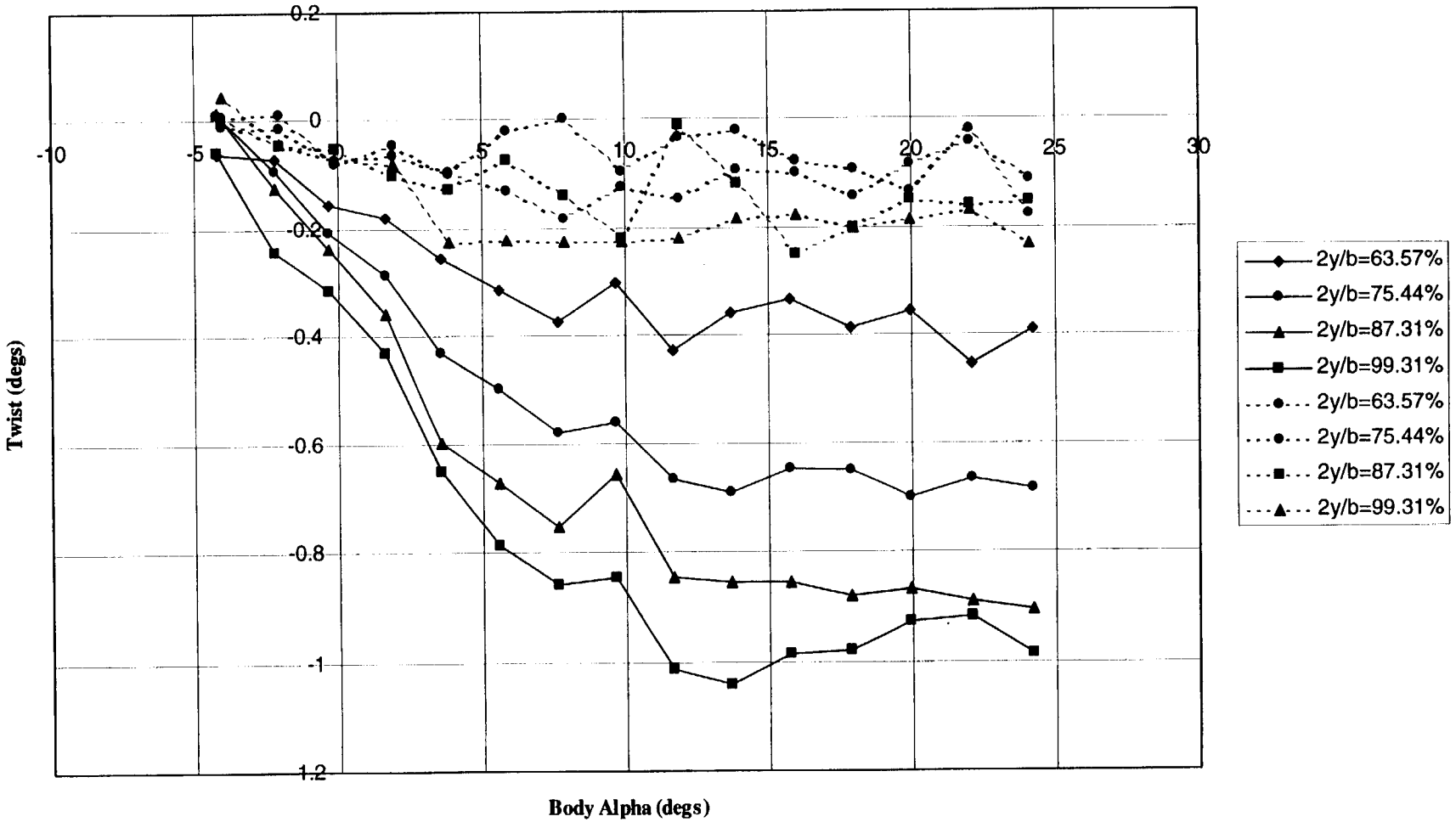

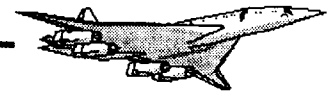

This chart lists the main conclusions from this test.

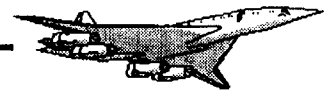

SUMMARY

- GOOD REPEATABILITY WITHIN TEST
- REASONABLE TUNNEL TO TUNNEL COMPARISON EXCEPT FOR DRAG
- BEST L/D AT DESIGN CONDITION OBTAINED WITH SEALED SLAT CONFIGURATION
  - SEALED SLAT TESTED WAS POSSIBLY OVER DEFLECTED
  - FALL BACK CONFIGURATION WOULD BE LEADING EDGE CAMBERED AT 30 DEGS
- SOME REYNOLDS NUMBER EFFECTS SHOWN TO BE SMALL AND SOME EFFECTS NOT FULLY UNDERSTOOD

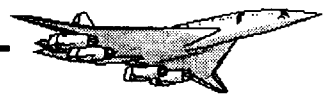

This chart concludes the main conclusions from this test.

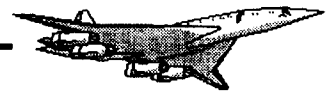

SUMMARY (CONTINUED)

- MINI-TUFT DATA UNOBTAINABLE DUE TO EQUIPMENT FAILURE
- OIL FLOW TECHNIQUE VERY USEFUL FOR COMPARISON WITH CFD ANALYSIS (BLACK PAINT NOT COLORED PAINT)
- DEFORMATION DATA VERY USEFUL, FURTHER WORK NEEDED TO UNDERSTAND RELATIONSHIP WITH REYNOLDS NUMBER
- PRESSURE SENSITIVE PAINT HAS POTENTIAL TO ENHANCE PRESSURE FIELD DATA, PARTICULARLY IN REGIONS WHERE PRESSURE PORTS ARE NOT AVAILABLE

Wind Tunnel Test of a 5% HSCT TCA Model in the NASA Ames 12-ft Pressure Tunnel (Stability & Control Summary)

TCA-3

Paul T. Glessner
Paul Kubiatko

Airframe Systems Review
February 9, 1999

BOEING

This presentation highlights the stability and control findings of the third entry of the 5% HSCT TCA scale model. TCA-3 was performed at NASA Ames' 12' pressurized wind tunnel.

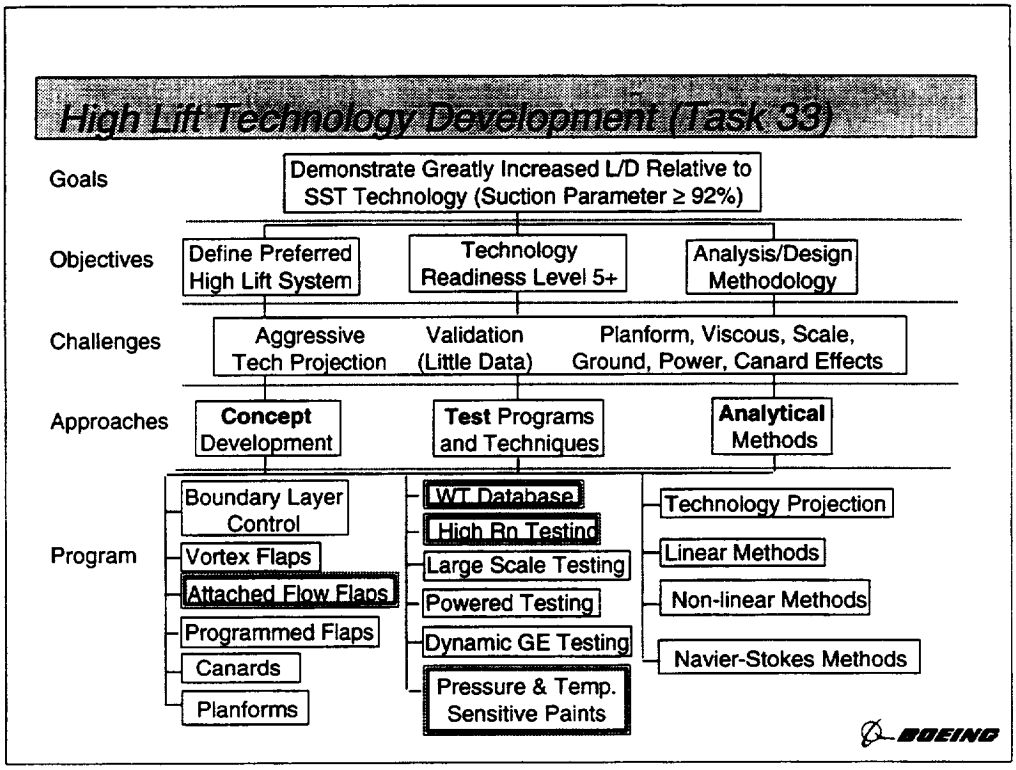

This slide shows an outline of the High-Lift Technology program.

Outline

- **Test Objectives**
- **Test / Configuration Description**
- **Test Results:**
  - Plain Flaps
    - Repeatability
    - Comparison to 14x22
    - Reynolds number effects
  - Increased Camber LE Flaps
  - Drooped LE Flaps
  - Sealed LE Flaps
    - Part-span / Full-span
- **Summary**

BOEING

The test objectives, test/configuration description, test results and summary are included in this presentation. The TCA-3 Final Test Summary document for contractual deliverable Subtask 4.3.2.1 of Task 33 has other plots that are not presented here. The more significant stability and control plots are presented here. This presentation is a shortened version of the document mentioned above.

TCA-3 Stability & Control Test Objectives

- Determine the effects on longitudinal and lateral-directional S&C characteristics of several High Lift leading-edge flap geometry variations.

And

- Determine the Reynolds number effects on the S&C characteristics of those leading-edge flap geometry variations.

BOEING

The test objectives of the Ames 12' (TCA-3) test were to: 1) determine the effect of geometric variations of the inboard leading edge flap on high-lift (HL) performance and stability & control (S&C) characteristics, 2) determine Re effects on the Technology Concept Airplane (TCA) configuration for optimum performance at takeoff (TO), climbout (CO), approach (AP), and landing (LDG) conditions, 3) obtain flow-visualization (flo-viz) data on the upper surface of the wing for comparison to computational fluid dynamic (CFD) results, 4) obtain video deformation and pressure sensitive paint (PSP) data. Additionally, data obtained at low Reynolds number could be compared to data obtained on similar configurations in the NASA LaRC 14' x 22' (LaRC 449) to evaluate model installation effects and data correction trends between the two facilities.

TCA-3 S&C Test Details

- Tested 22 January - 23 February 1998
- 464 runs in 360 hours (1.30 runs/ hour)
- Mach number = 0.24
- Reynolds number range:
  - 1.50 - 7.75 million/ft
  - 7.13 - 36.8 million
- Pressure range: 1.0 to 4.7 atmospheres
- Dynamic pressure range: 85 TO 386 lb/ft^2
- Pitch polars at $\beta = 0$ and +4 degrees
- Yaw polars at $\alpha = 20$ degrees
- Supported by Boeing (Long beach and Seattle), LMAS, ARC and LaRC

BOEING

The TCA-3 test was performed at NASA Ames' 12' pressurized tunnel from January 28th to February 23rd, 1998. The average run rate with two, ten-hour shifts, including model changes was 1.14 runs per hour.

The 12' wind tunnel at NASA Ames is a closed circuit, single return, variable density, closed throat, wind tunnel with exceptionally low turbulence. The desired Mach, Re, and total temperature (Tt) were set in the tunnel and total pressure (Pt) was calculated from the other three. This was true for all Re numbers except the lowest one. The lowest Re number is obtained with the tunnel at atmospheric Pt. The model was supported by the dual-strut turntable mechanism typically used for high-lift testing in this facility. This dual-strut support (bi-pod) differs from the dual strut support used at NASA LaRC. Additional tunnel specifications and pictures can be obtained from NASA ARC's World Wide Web-site located at "http://aocentral.arc.nasa.gov/".

The tunnel had both the Balance Load Alarm Monitoring System (BLAMS) and the Wall Interference Correction System (WICS) programs available to reduce the chances of over-exceeding balance limits and to reduce the data with the correct wall interference corrections applied, respectively

5% TCA Model in the Ames 12 FT Tunnel

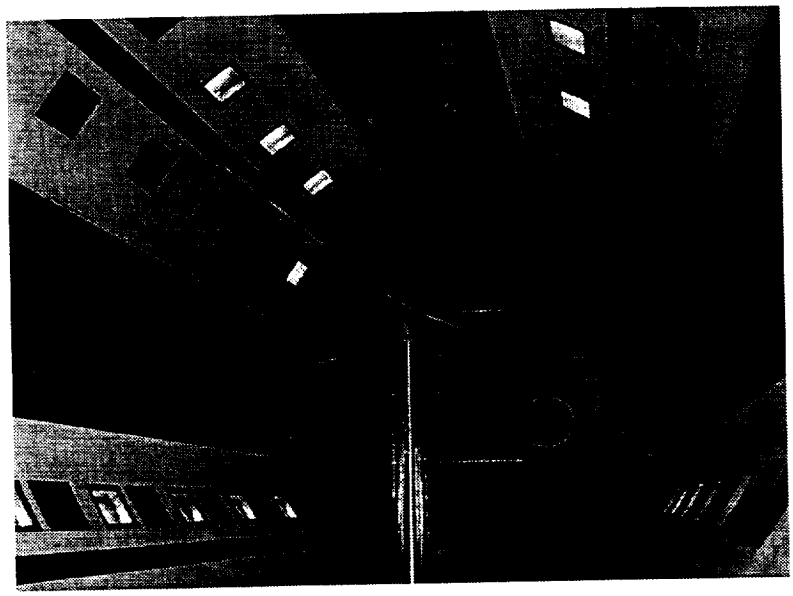

BOEING

The octagonal 12' cross-section is easily viewed in the pictured above. The rectangular shape of the 14' x 22' (not shown) and the octagonal shape of the 12' results in dissimilar wall interference and blockage corrections being applied to the data at each facility.

Comparison of Model Support Hardware

Ames 12 FT

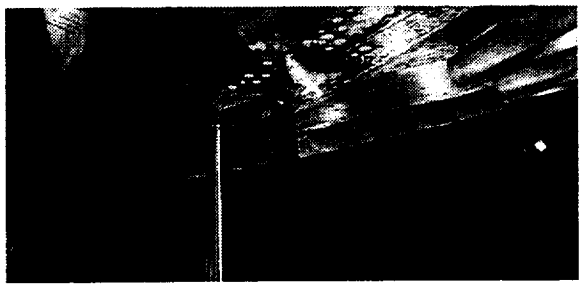

LaRC 14'x22'

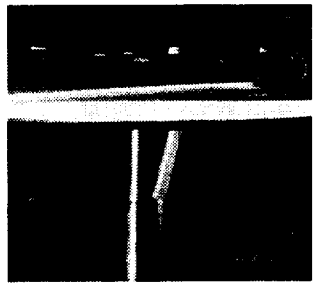

BOEING

The two pictures directly above are of the 5% TCA model installed in both the Ames 12' and the Langley 14'x 22' facilities, respectively. The picture above shows a close-up of the Ames' bi- pod mounting system. The aft mast is considerably larger in diameter than that of the pitch link used at LaRC pictured to the right.

Diameter at model bottom:	Main Post	Pitch Link
Ames 12'	2.75 in.	2.25 in.
LaRC 14' x 22'	3.8 in.	1.45 x 2.45 in.

This difference in the mounting hardware may result in a shift in the pitching moment coefficients when comparing tunnel to tunnel data.

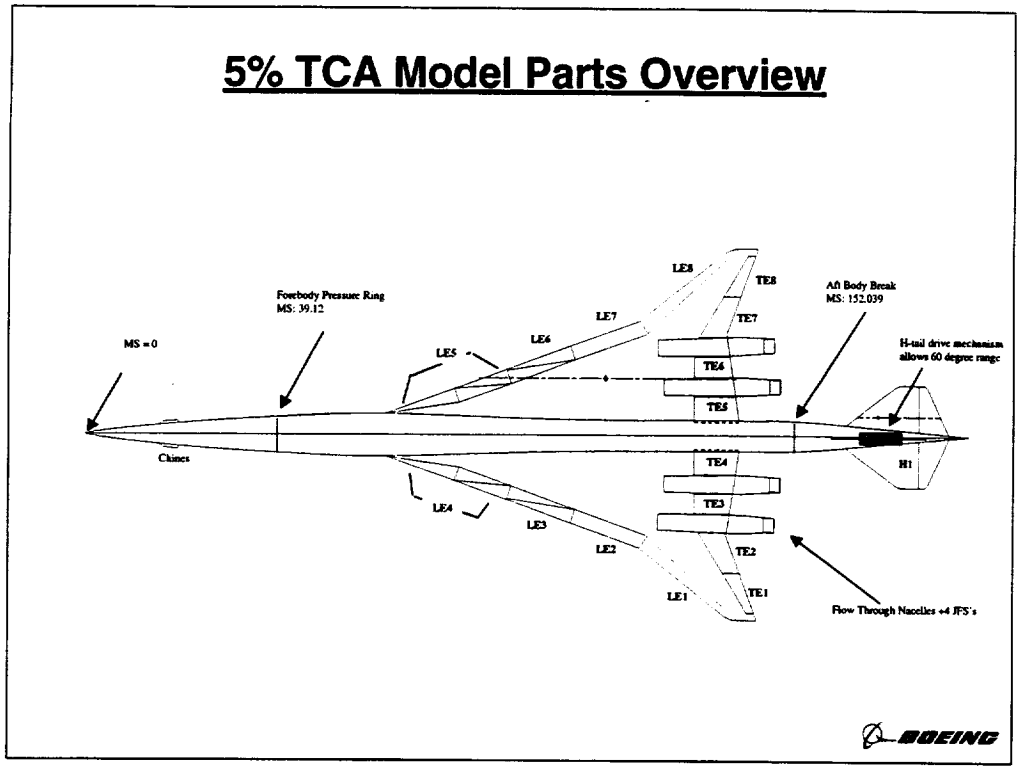

The test matrix* consisted of the following leading edge (LE) flap configurations with various combinations of tails(horizontal and vertical) off and on: plain flaps, full and partial** span, plain flaps, full span and gear down, increased camber, partial*** span, drooped leading edge, partial*** span, sealed le slat, full and partial*** span, and specific psp and cfd configurations. Tails Off for both Plain and Leading Edge Slats for various Wing, Body, Nacelles (on and off), and Chine (Full and Partial) configurations were run.

* *All data runs included the chine on the model.*

** *Plain partial LE flaps were obtained when LE flaps #3 and #6 (see model parts picture) were used to transition to LE 0 degrees, inboard. This was an issue for two runs: #94 and #95. All other plain flap configurations runs were tested the whole length of the LE.*

*** *Partial 'sealed slat' deflections were defined as and effected only the inboard wing as outboard panels had deflected plain flaps. The TCA model's LE flaps #3 and #6 (actual TCA airplane: LE #5 and #10) were used to transition to a different partial LE geometry variation to side-of-body (SOB).*

The final summary document has a more extensive parts picture and list.

Leading-Edge Flap Geometry Comparison

- PLAIN
- CAMBERED
- DROOPED
- SEALED SLAT

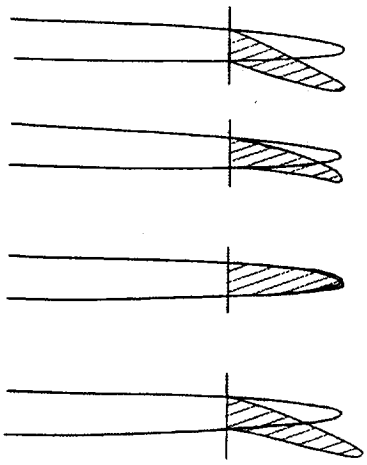

BOEING

The various leading edge flap configurations tested are shown above. The plain flap is the original leading edge flap configuration tested earlier in TCA-1 and TCA-2. The sealed slats were tested earlier in TCA-1 and on the outboard locations only. The cambered and drooped were first tested on the 5% in TCA-3.

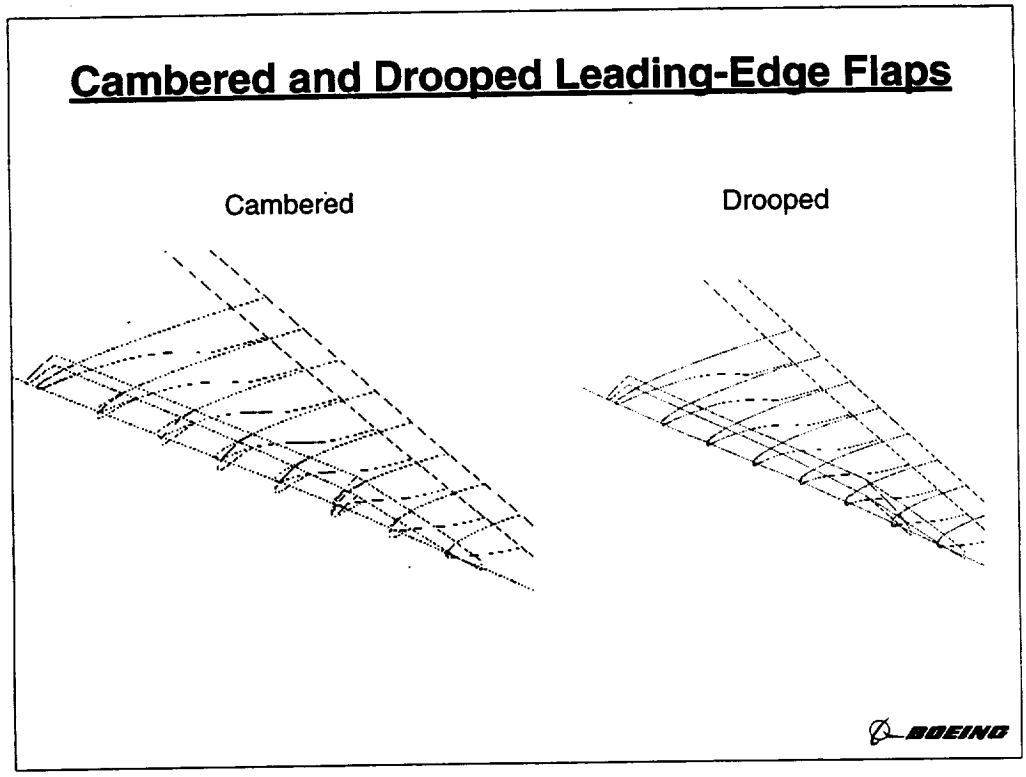

The above pictures of the cambered and drooped leading edge configurations show the amount of change that was made to the initial design to create the two different leading shapes. The slight variation from the original plain leading edge to the drooped leading edge configuration can just be seen as a second line delineates the original shape.

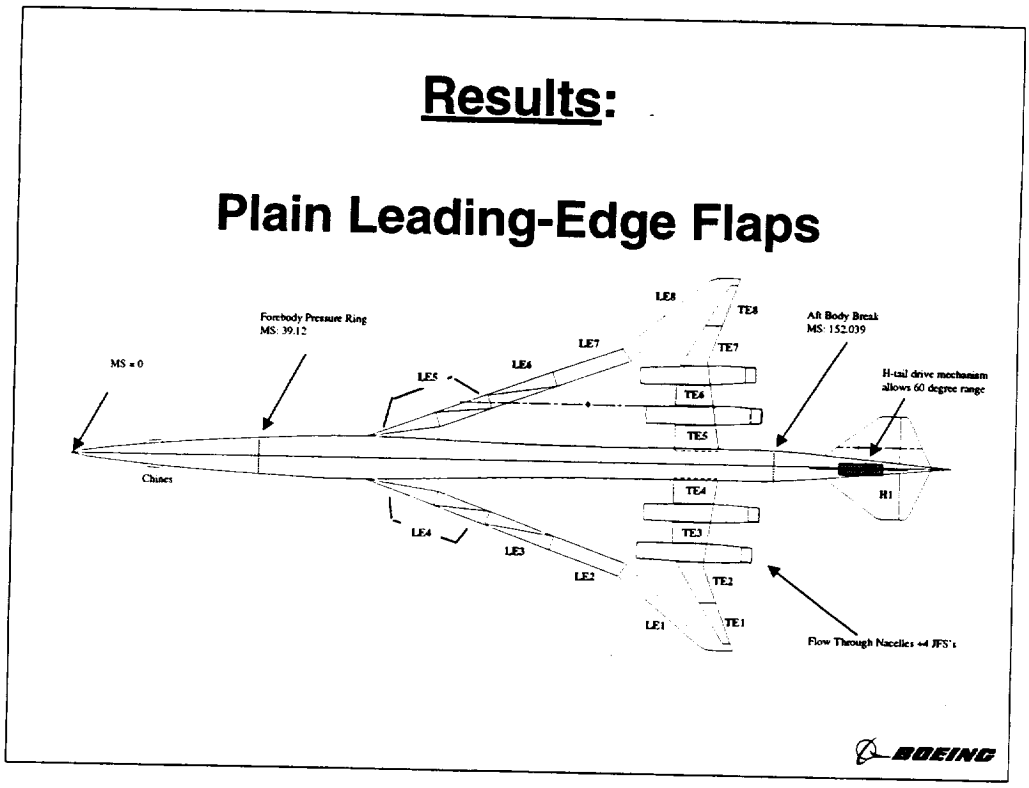

Plain flaps were run the whole length of the leading edge as stated before.

TCA-3 Pitching Moment Repeatability

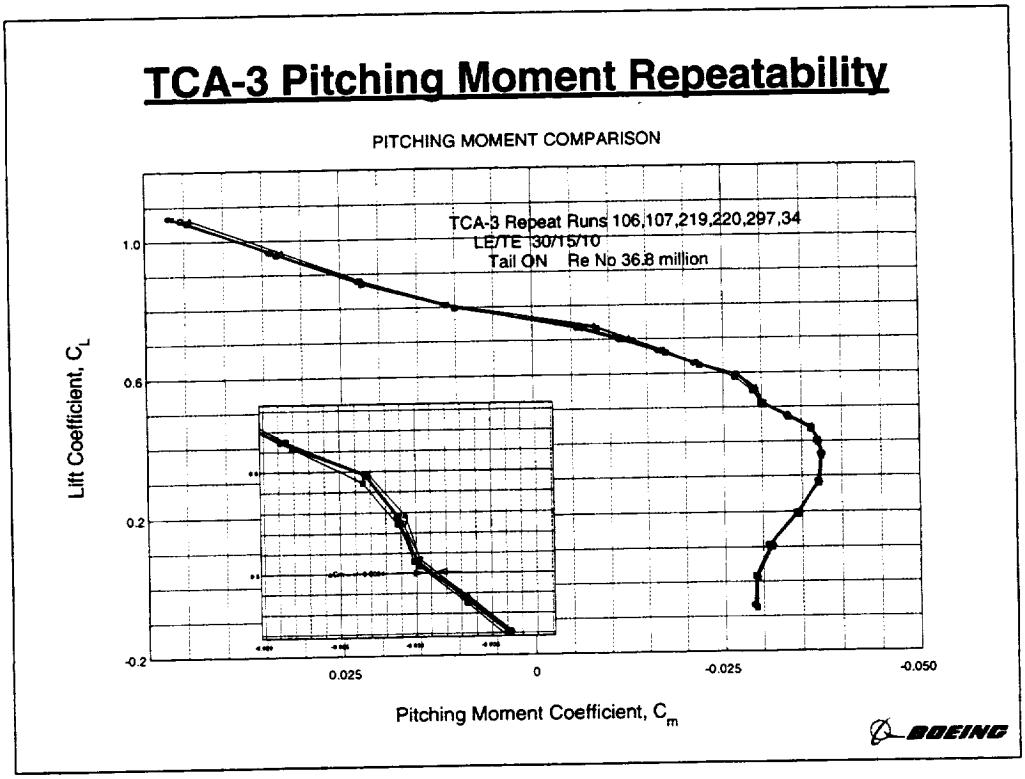

The repeatability is considered well within industry agreed upon S&C parameter constraints. The 0.0004 pitching moment coefficient translates into approximately 0.15 of a degree of stabilizer movement.

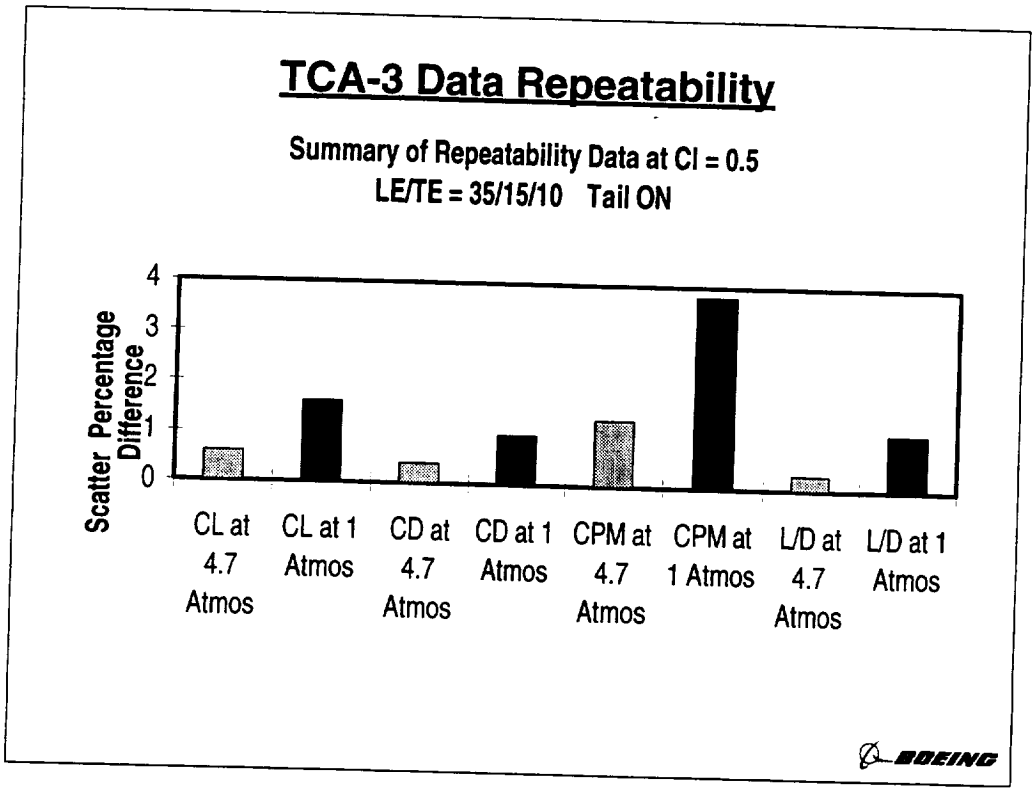

The repeatability of pitching moment coefficient is very good at the higher Reynolds number and slightly worse for atmospheric runs. Again, this is considered within industry agreed upon parameter constraints for both situations.

Ames 12' to LaRC 14'x22' Pitching Moment Repeatability Comparison and Re Effects

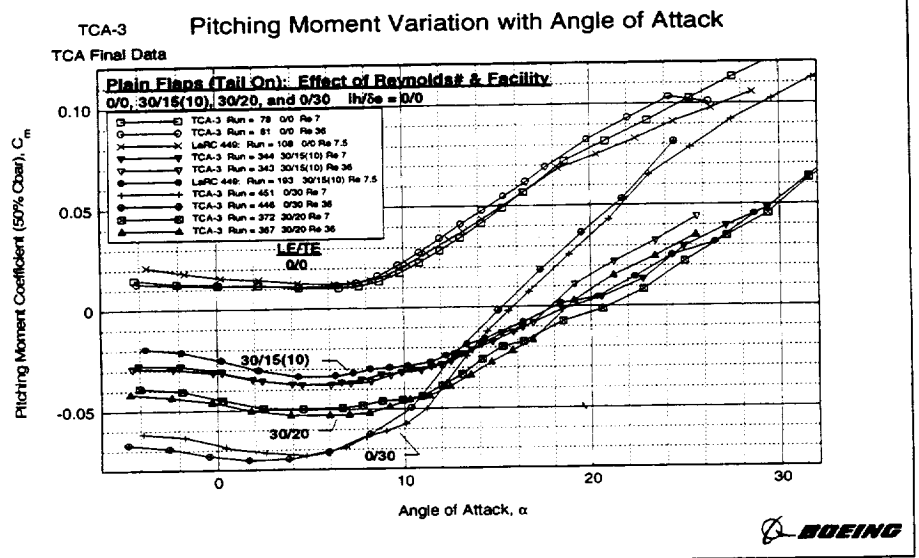

The plot above shows the effect of Re for tail-on, plain LE flap configurations of 0/0, 30/15(10), 30/20, and 0/30. Similar to the tail-off configurations shown on previous pages, pitch stability reduces when Re increases. The decrease in stability varies with flap deflection, particularly at higher alphas. The 0/30 configuration appears to have the least amount of pitch stability at both Re. This is expected, because without the LE flaps deflected, flow over the wing separates at moderate angles of attack, especially when there is significant aft camber (deflected trailing-edge flaps).

The comparison between the 14' x 22' and the 12' tail-on data show similar stability trends; however, there is a reduction in pitch stability for the TCA-3 data when compared to the TCA-1 test data. This stability decrease is prevalent in most facility-to-facility comparisons.

Ames 12' to LaRC 14'x22' Yawing Moment Repeatability Comparison and Re Effects

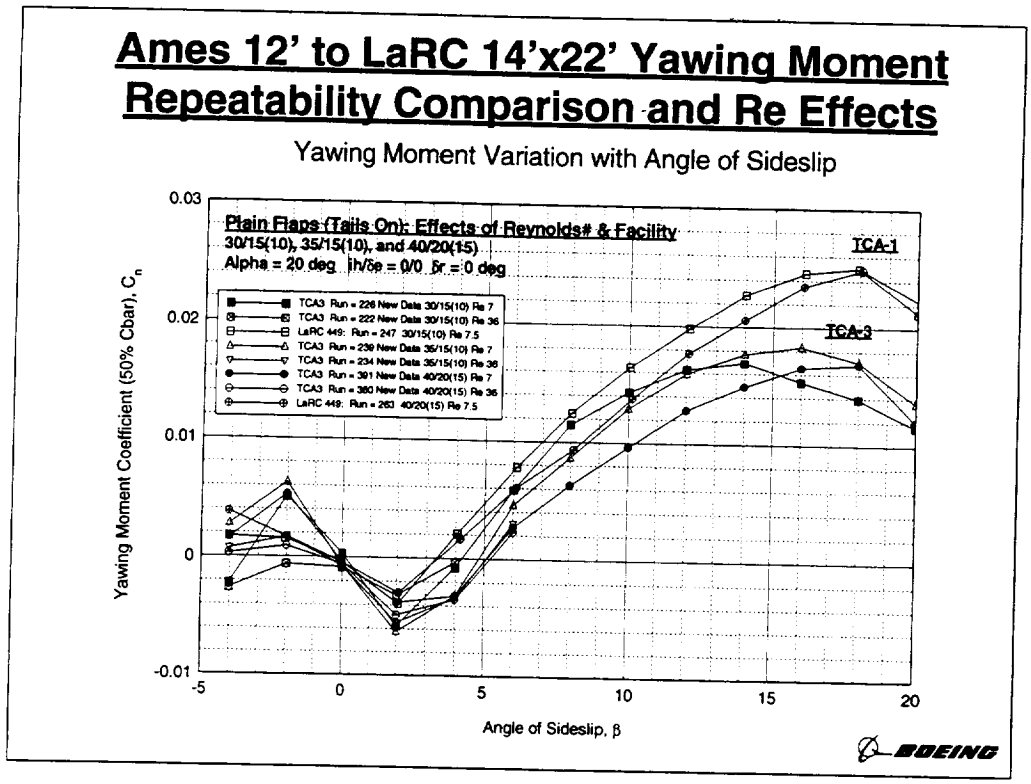

The plot above shows the Re effects on the tail-on directional stability (slope of yawing moment with sideslip angle) at a constant 20 degrees of alpha for the 30/15(10), 35/15(10), and 40/20(15) plain LE flap configurations. Tunnel-to-tunnel comparisons for 30/15(10) and 40/20(15) plain LE flap configurations are also shown. At this large alpha, all configurations have negative directional stability (unstable) from –2 to +2 degrees of sideslip at both Re numbers tested. Beyond 2 degrees of sideslip, the slope of yawing moment with sideslip reverses and all configurations become statically stable until large sideslip angles are reached. Data obtained at Re=36 was limited to no more than 6 degrees of sideslip because of the large forces and moments encountered at this high angle of attack. The plot on the next page is an enlargement (sideslip angles between –4 and 10 degrees) of the plot above and provides a better look at the effects of Re.

Although the overall trends are similar, there are significant differences in the yawing moment due to sideslip when the data from the 12' and 14'x22' tunnels are compared at Re=7 million. A significant reduction in yawing moment coefficient is seen for both the 30/15(10) and the 40/20(15) flap configuration data obtained at the 12'.

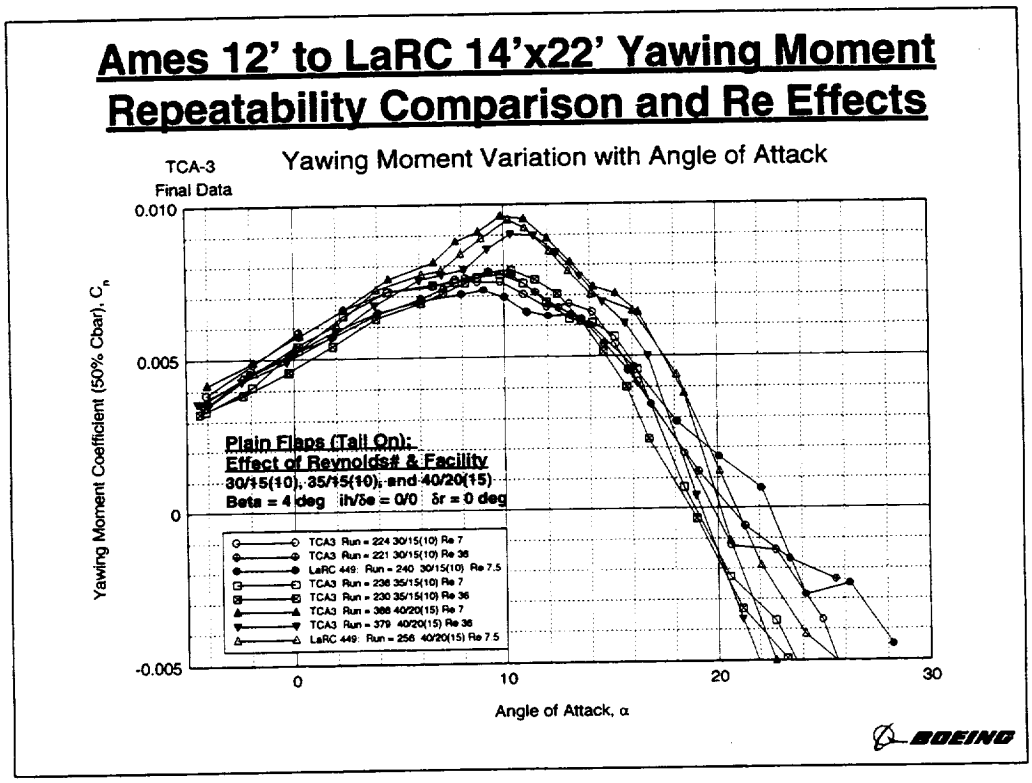

The plot above plot shows the effect of Re on the variation of yawing moment coefficient with angle of attack, at a constant sideslip angle of 4 degrees, for tail-on plain LE flap configurations of 30/15(10), 35/15(10) and 40/20(15). All flaps deflected configurations exhibit increasing positive directional stability (yawing moment at an alpha divided by the sideslip angle) up to 10 degrees alpha. After 10 degrees alpha, directional stability begins to reduces rapidly with alpha until yawing moments become negative (directionally unstable) between 18 to 23 degrees of alpha, depending on the flap deflection. For the configurations shown, the effect of Re on directional stability does not appear to be consistent, rather the effect of Re appears to vary depending on alpha and flap deflection. However, for all three plain LE flap configurations there is a noticeable reduction in directional stability at the higher Re up to moderate alphas. The 40/20(15) configuration appears to have significantly more directional stability at all alphas, particularly at alpha = 10 degrees. The 35/15(10) configuration, tested in TCA-3 only, appears to have the lowest level of directional stability at both small and high alphas, but reasonable stability levels at moderate alphas.

The comparison between the 14' x 22' and the 12' data shows similar directional stability trends over the entire alpha range, although the level varies between the two.

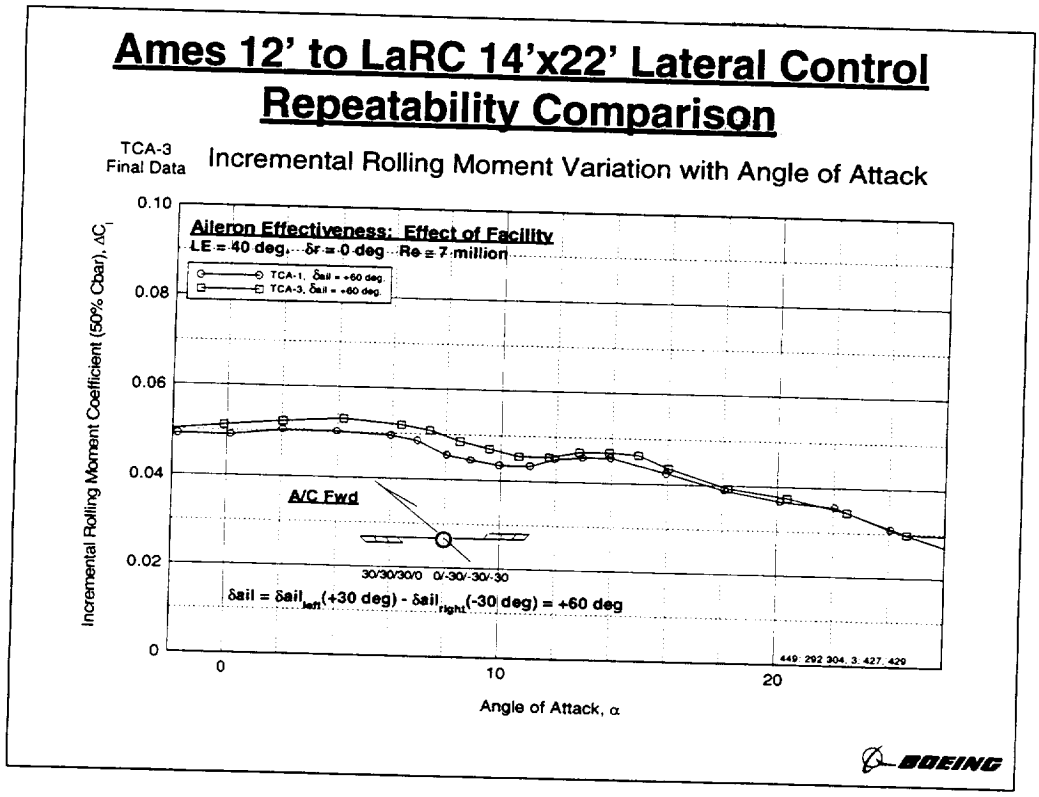

The plot above shows a comparison, between the LaRC 14' x22' and Ames 12' data, of the the rolling moment coefficient variation with alpha for the plain LE flaps deflected 40 degrees and the TE flaps (#1-#3 and #6-#8) deflected asymmetrically 30 degrees (for maximum lateral control). While both curves exhibit similar characteristics with respect to alpha, the data obtained at the 12' facility indicates an increase in maximum lateral control effectiveness. Although at high angles of attack, the maximum lateral control effectiveness is the same at both facilities.

The effect of Re on maximum lateral control effectiveness was not able to be determined due to the high forces and moments encountered at Re=36 million.

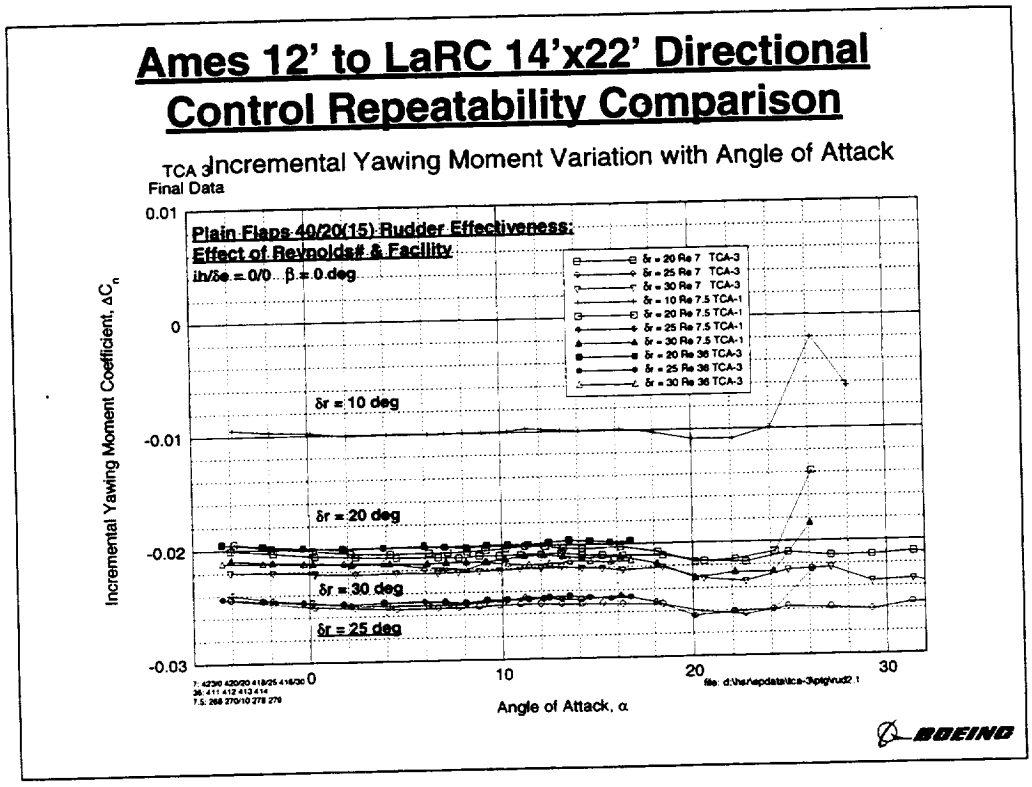

The plot above shows the effects of Re on incremental yawing moment coefficient due to rudder deflection (rudder effectiveness) in pitch for the 40/20(15) plain LE flap configuration. These curves were derived by subtracting rudder undeflected data from rudder deflected data at zero degrees sideslip and are fairly constant with alpha. Rudder effectiveness increases and is fairly linear (per degree of deflection) up to 25 degrees of rudder deflection. The 30 degree rudder deflected data being less effective than the 25 degree rudder deflected data indicates that the rudder reaches its maximum effectiveness between 25 and 30 degrees of rudder deflection. When Re was increased from 7 to 36 million, rudder effectiveness was reduced slightly for all three rudder deflections tested.

The rudder effectiveness data obtained in TCA-3 agrees well with TCA-1 data. The source of the large spikes in the TCA-1 data, at high alphas, is unknown.

Results:

Increased Camber Leading-Edge Flaps

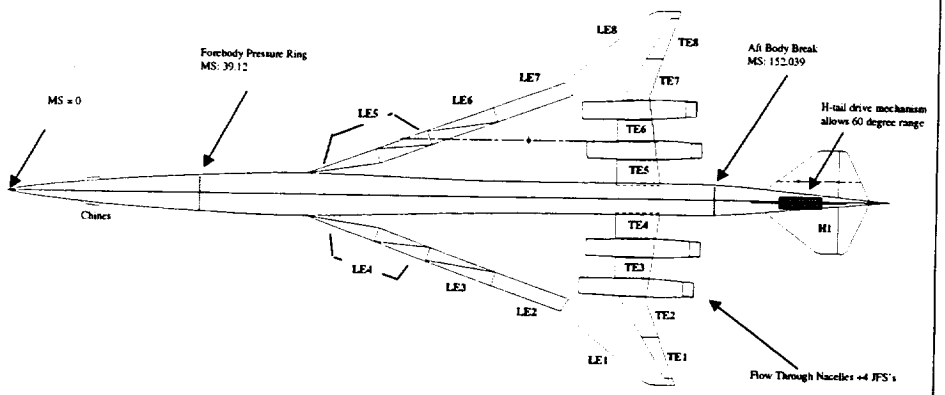

The increased leading edge camber configurations were only run on the first inboard set of flaps (LE 4 and 5) transitioning into their respective aft following neighbors (LE 3 and 6).

Increased Camber LE Flaps Longitudinal Characteristics

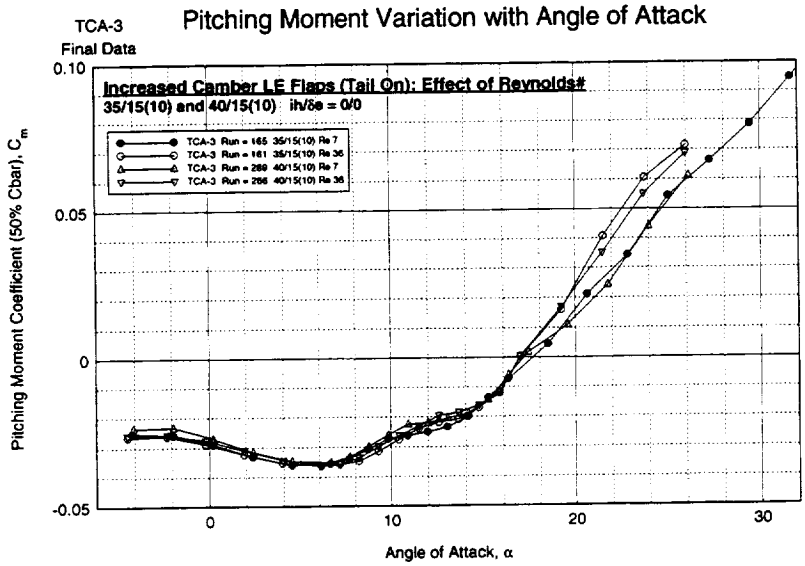

The plot above shows tail-off pitch stability characteristics as a function of alpha and Re for the increased camber LE flap configurations of 35/15(10) and 40/15(10). Increasing LE flaps from 35 to 40 degrees only gained a minimal amount of nose-down moment for the Vmin recovery maneuver. Increasing Re number reduces pitch stability as angles of attack increase above 16 degrees. At either Re, increasing the LE deflection from 35 to 40 degrees while holding the TE fixed at 15(10) does not result in any additional nose-down pitching moment.

Results:

Drooped Leading-Edge Flaps

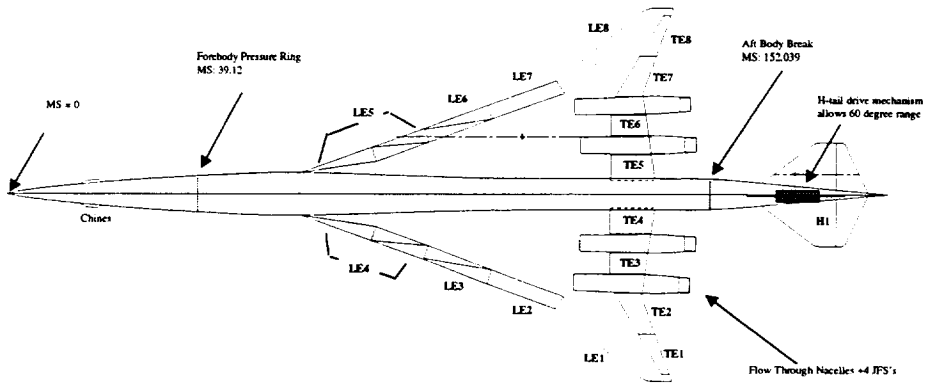

The drooped leading edge configurations were only run on the first inboard set of flaps (LE 4 and 5) transitioning into their respective aft following neighbors (LE 3 and 6).

Drooped LE Flaps
Longitudinal Characteristics

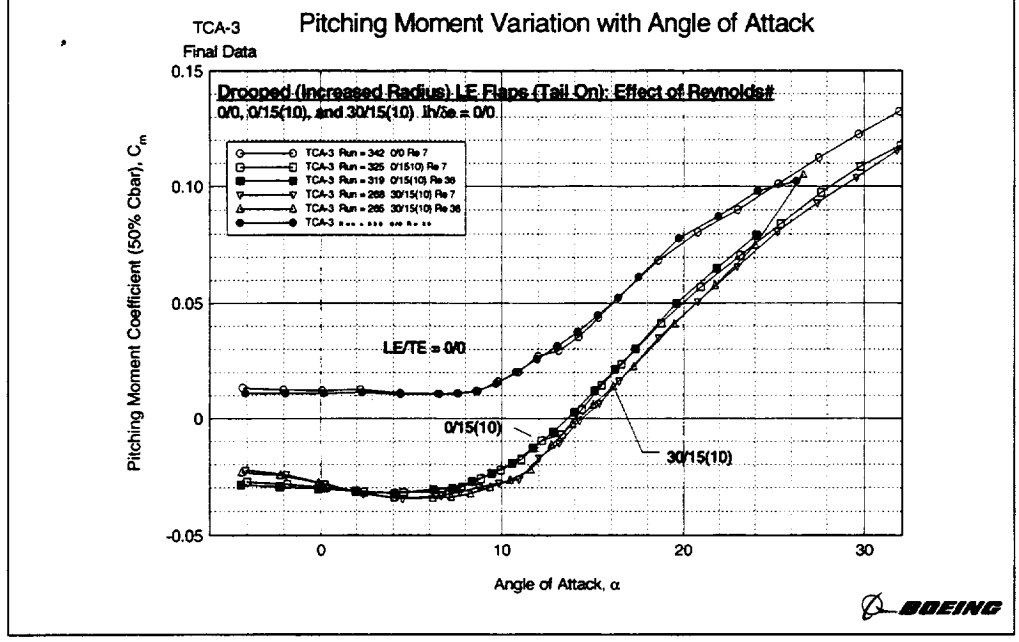

The plot above shows the variation of tail-on pitching moment coefficient with angle of attack and Re for the drooped LE flap configurations of 0/0, 0/15(10), and 30/15(10). All three tail-on configurations exhibit similar pitch characteristics over the entire alpha range.

The effects of Re do not become apparent until 20 degrees of alpha, at which time, the typical reduction in pitch stability at higher Re is seen. This was also seen for the drooped LE flap configurations with the horizontal tail-off. There is, however, a slight pitch stability increase at the lower alphas when the LE deflection is increased from 0 to 30 degrees with the TE flaps fixed at 15(10).

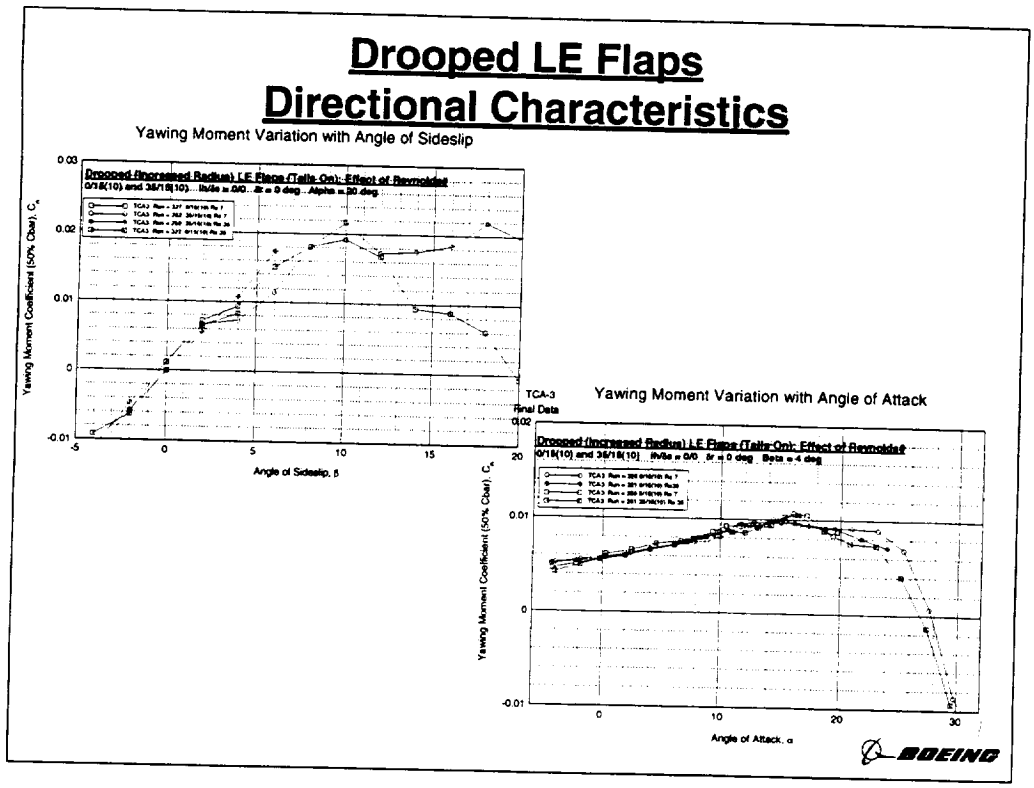

The left-hand plot above shows the variation of tail-on yawing moment coefficient with sideslip angle and Re for the drooped LE flap configurations of 0/15(10) and 35/15(10) at a constant 20 degrees of alpha. Both drooped LE flap configurations show positive directional stability at both Re for the first few degrees of sideslip. This is in contrast to the negative directional stability observed for the plain LE flap configuration at this high alpha. At the lower Re number, the 0/15(10) flap configuration shows a rapidly degrading directional stability above 10 degrees of sideslip, while the 35/15(10) flap configuration appears to maintain a somewhat constant level of yawing moment (neutrally stable). Although the high Re data was limited in sideslip angle by balance load limits, it does show, relative to the lower Re data, a small negative shift in yawing moment around zero sideslip angle.

The right-hand plot above shows the variation of tail-on yawing moment coefficient with angle of attack and Re number, at a constant sideslip angle of four degrees, for the drooped LE flap configurations of 0/15(10) and 35/15(10). The directional stability at small sideslip angles, seen in the previous plot, is maintained out to very large angles of attack. This drooped LE flap configuration stands out, when compared to the other configurations tested, as having the best directional stability at high alpha and sideslip angles. Re is shown to not have any significant or consistent effect on directional stability characteristics over the range of angles of attack tested.

Results:

Sealed Leading-Edge Flaps

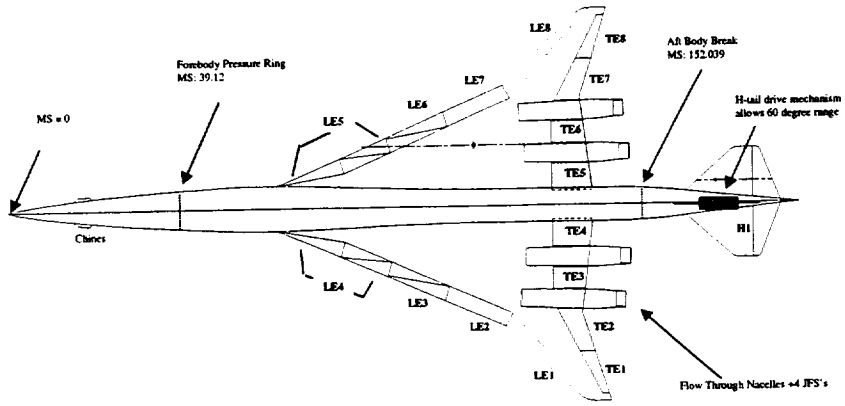

The sealed leading edge slats were tested at the inboard locations only on this test. Their transition to the side-of-body is similar to that of the plain flaps. The transition for both flap configurations take place at flap segments 4 and 5.

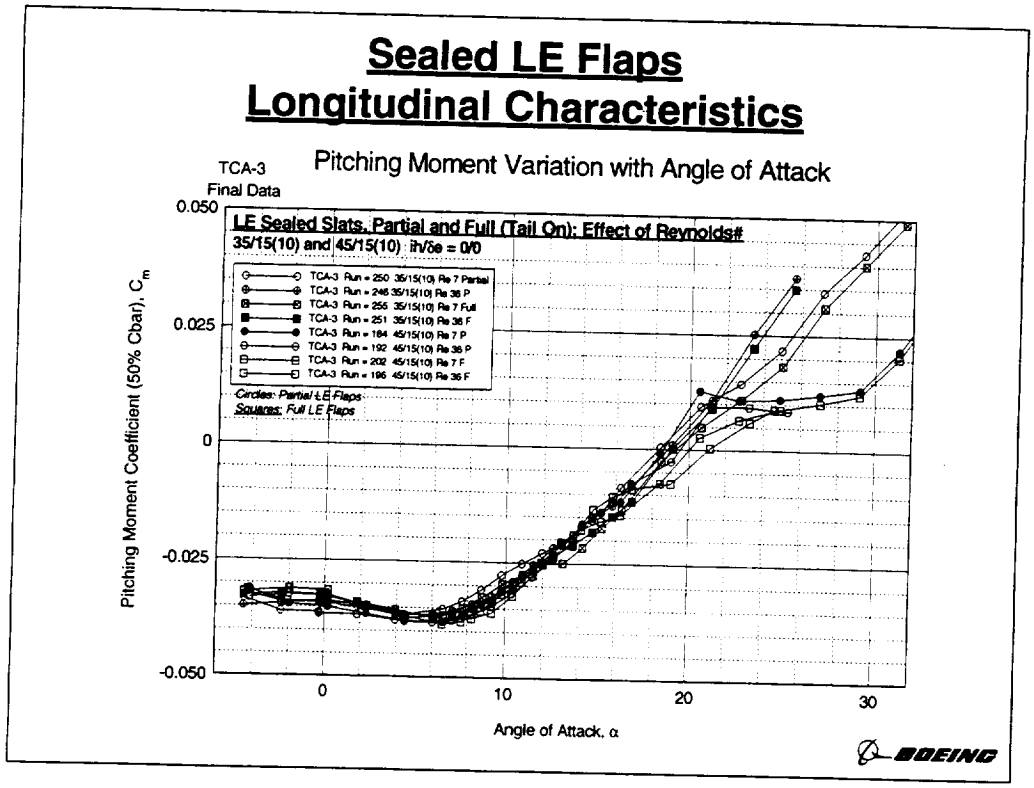

The plot above shows the variation of tail-on pitching moment coefficient with angle of attack and Re for the part-span and full-span sealed LE flap configurations of 35/15(10) and 45/15(10). The 45/15(10) part-span and full-span sealed LE flap configuration exhibit significantly less "pitch-up" at both Re for alphas above 20 degrees. In fact, the 45/15(10) part-span configuration, at low Re, has a dramatic pitch stability reversal at 20 degrees of alpha.

Note: Both the 35 and 45 degree part-span sealed LE flap data shown here have a 40 degree plain LE flap deflection on the outboard wing.

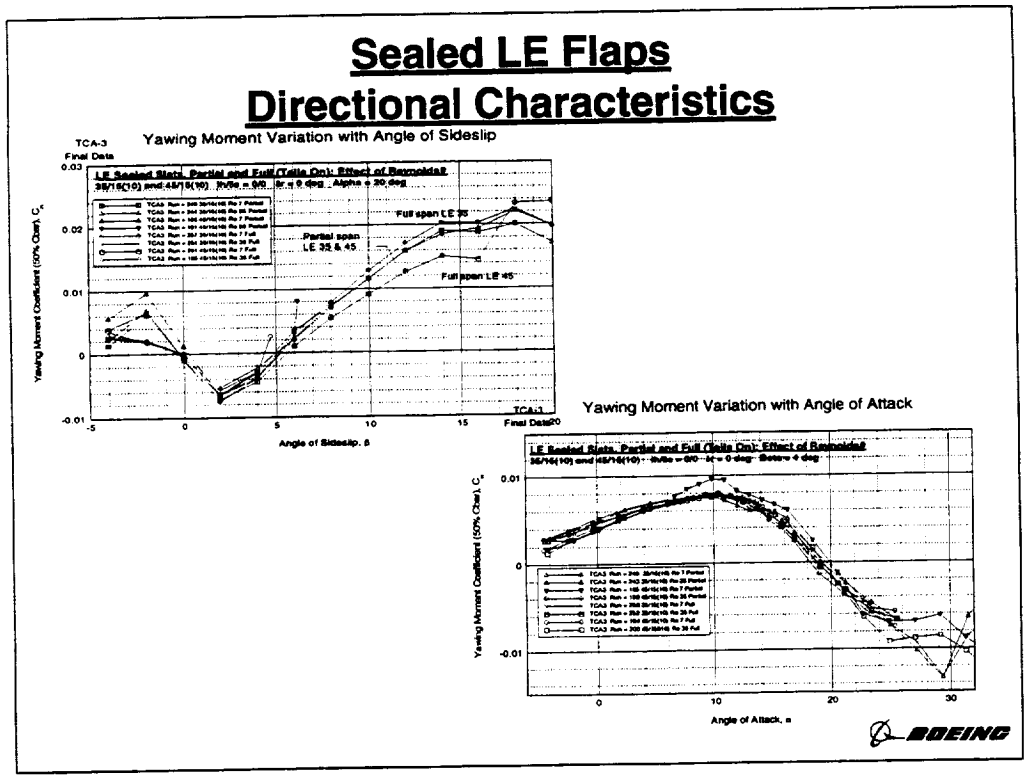

The left-hand plot above shows the variation of tail-on yawing moment coefficient with sideslip angle and Re for the part-span and full-span sealed LE flap configurations of 35/15(10) and the 45/15(10) at a constant 20 degrees of alpha. Similar to the plain LE flap configurations shown earlier, both partial and full-span sealed LE flap configurations have negative directional stability (unstable) from –2 to +2 degrees of sideslip. Beyond 2 degrees of sideslip, the slope of yawing moment with sideslip reverses and all configurations become statically stable until large sideslip angles are reached. Above 6 degrees sideslip, yawing moment is positive for all configurations. Re number effects are hard to determine due to the limited amount of data taken at Re=36 million. For the part-span configuration, deflecting the LE from 35 to 45 degrees does not appear to have much effect on yawing moment. However, for the full-span configuration, deflecting the LE from 35 to 45 degrees results in significantly lower yawing moment levels, particularly at higher sideslip angles. The cause of the rapid increase in yawing moment level, after 16 degrees of sideslip, for the 45 degree full-span configuration is unknown.

The right-hand plot above shows the variation of tail-on yawing moment coefficient with angle of attack and Re, at a constant sideslip angle of four degrees, for the sealed LE flap configurations of 35/15(10) and 45/15(10). All of the sealed slat configurations show increasing positive directional stability up to 10 degrees of alpha. Beyond 10 degrees of alpha, all of the configurations show a rapid decrease in directional stability but are directionally stable up to 18 degrees of alpha at both Re. There does not appear to be any significant directional stability changes due to Re effects. There are also no significant differences in directional stability between the partial and full span configurations; although at low angles of attack, the partial span configurations are a little more stable.

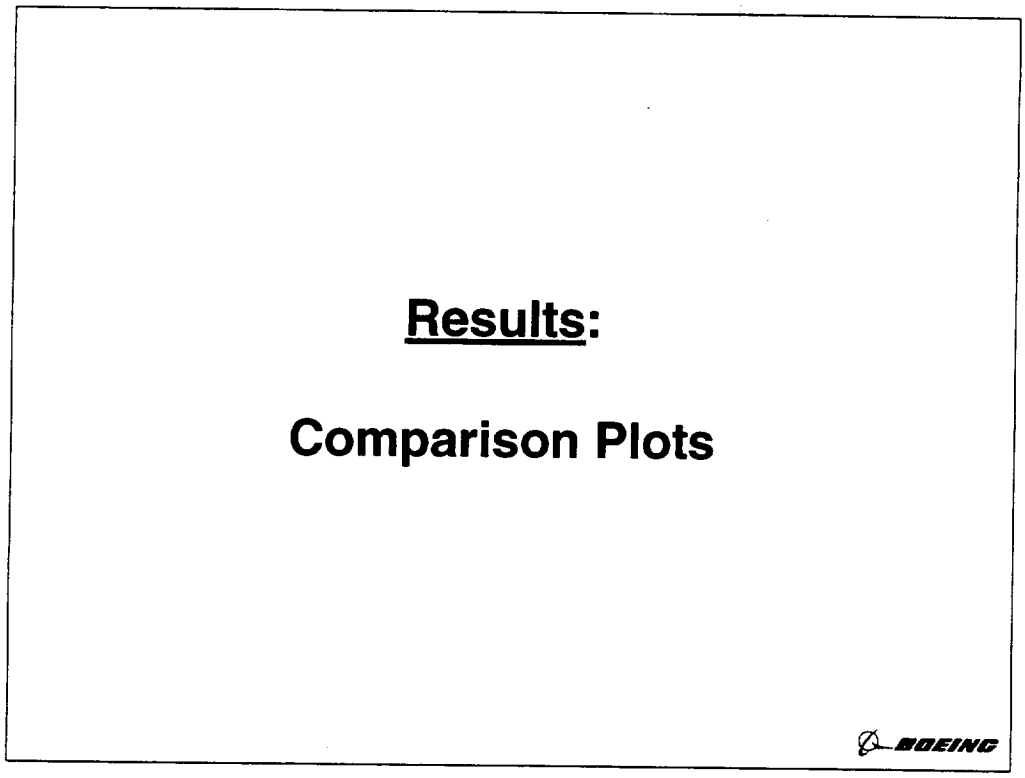

The following plots are from the test summary document as well and represent four out of the five that were originally plotted.

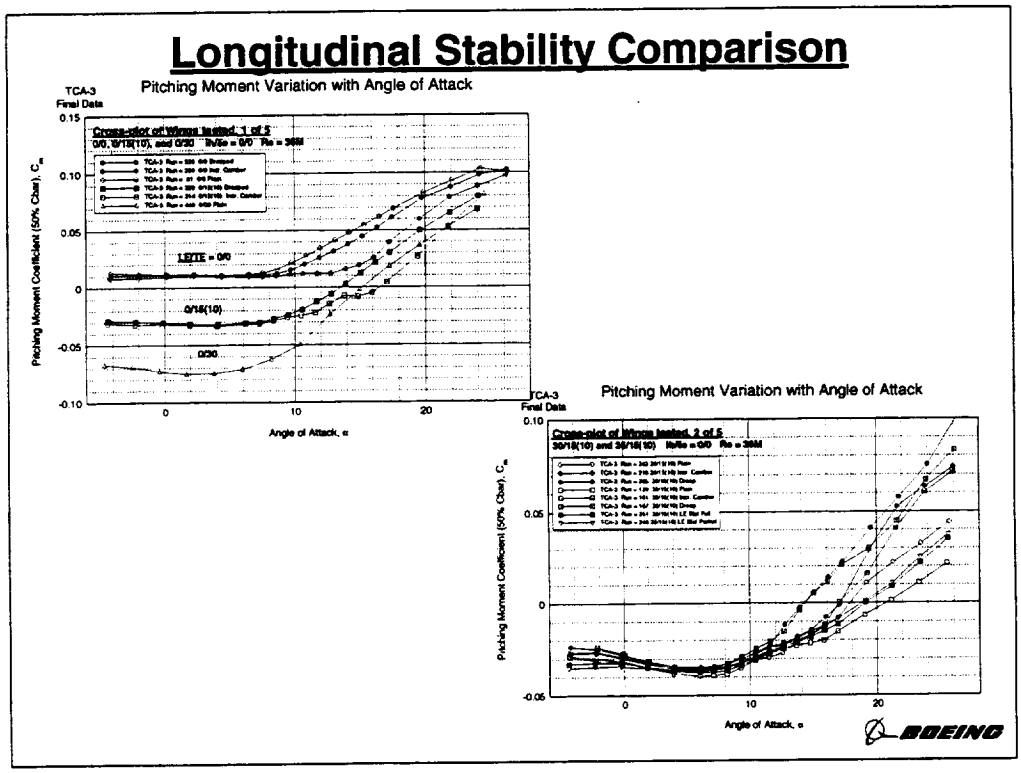

The left-hand plot above shows the pitch characteristics, at Re=36 million, of the plain, the drooped, and the increased camber LE flap configurations that were tested with zero LE flap deflection and various TE flap deflections. The increased camber LE flap configurations are shown to have the most significant effect on pitch characteristics, delaying the angle of attack at which "pitch-up" begins. This effect is more prominent for the 0/0 configuration than for the 0/15 configuration. The 0/30 plain LE flap configuration is shown for comparison to the other plain LE flap configurations.

The plot above shows the pitch characteristics of various LE flap geometry configurations that were tested with similar LE and TE flap deflections at Re=36 million. The 35/15(10) plain flap configuration, at high angles of attack, has the most nose-down pitching moment (favorable for Vmin recovery) and the least amount of "pitch-up" of the configurations shown. On the other hand, both drooped LE flap configurations exhibit "pitch-up" at a significantly lower angle of attack than the rest of the configurations shown. The increased camber LE flap configurations have a significantly more pronounced "pitch-up" at 17 degrees angle of attack.

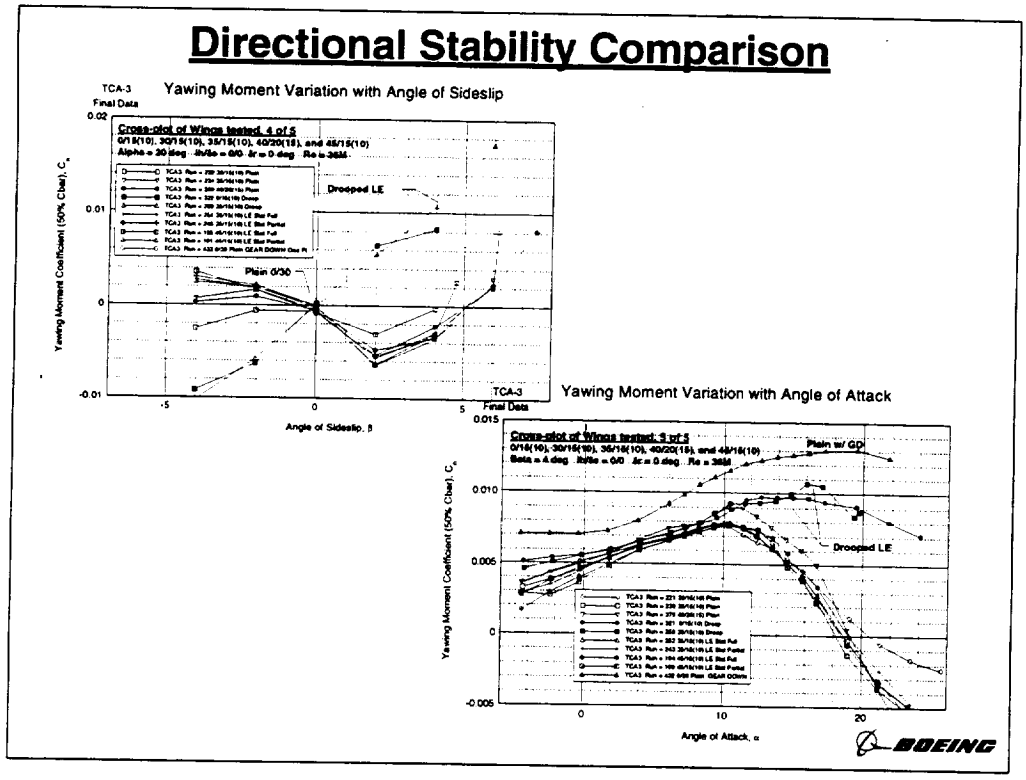

The plot above shows, for several of the LE flap geometries tested at Re=36million, the variation of yawing moment coefficient with sideslip angle at a constant fuselage angle of attack of 20 degrees. For the limited amount of sideslip data obtained at this high angle of attack and Re, the drooped LE flap configuration clearly exhibits exceptionally linear and stable directional characteristics compared to the rest of the configurations shown.

The plot above shows, for several of the LE flap geometries tested at Re=36million, the variation of yawing moment coefficient with sideslip angle at a constant fuselage angle of attack of 20 degrees. For the limited amount of sideslip data obtained at this high angle of attack and Re, the drooped LE flap configuration clearly exhibits exceptionally linear and stable directional characteristics compared to the rest of the configurations shown.

TCA-3 Stability & Control Summary

- **Data Repeatability:**
  - Very Good between TCA-3 repeat runs.
  - Good between ARC 12' and LaRC 14'x22' except:
    - Reduced pitch stability, reduced yawing moment level at high α.
- **Reynolds number Effects:**
  - Effects observed due to increase in Re:
    - Reduced pitch stability (aeroelastic effect at high α)
    - Small reduction in directional stability
    - No effect on rudder effectiveness

BOEING

Data obtained at the Ames 12' (at atmospheric Re) was compared to data obtained at the LaRC 14'x22' for similar plain LE flap configurations. The Ames 12' data showed relative to the 14'x22' data:

- A consistent reduction in pitch stability.
- A significant reduction in yawing moment at high angles of attack.
- A small increase in the maximum lateral control power.
- Nearly identical levels of rudder effectiveness.

Reynolds Number (Re) effects on either longitudinal or lateral-directional stability and control characteristics were not significant for all of the LE flap geometry configurations tested. Although Re effects were small, trends due to Re number were seen. These trends include:

- Increasing Re number reduces pitch stability, particularly at the higher alphas.
- In general, directional stability was reduced when Re was increased.
- Increasing Re had no effect on rudder effectiveness.
- Increasing Re reduced the magnitude of the nose-down pitching moment increment due to the landing gear.

TCA-3 Stability & Control Summary
(Continued)

- **Alternate LE Flap Configurations:**
  - Increased Camber
    - Pitch-up delayed for undeflected LE but more severe pitch-up for LE deflected 35 degrees.
  - Drooped
    - Significant improvement in high α directional stability but also more severe pitch-up (earlier).
  - Sealed
    - Improved high α pitch stability
    - No significant difference in pitch or directional stability between part-span and full-span

BOEING

The increased camber leading edge proved to delay pitch-up more than drooped and plain for similar deflections. No sideslip data was taken for the increased camber configurations.

The drooped LE flap configuration was shown to have superior directional stability characteristics over the other configurations tested, particularly at high angles of attack. However, the drooped LE flap configuration was shown to have more severe "pitch-up" at higher angles of attack.

The part-span and the full-span 45/15(10) sealed LE flap configurations were shown to have favorable high angle of attack pitch stability characteristics. There were no significant differences observed in either the longitudinal or lateral directional stability and control characteristics between the part-span and full-span sealed LE flap configurations.

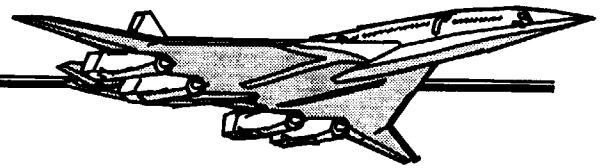

TCA-4 / NASA473 Test Results

A High-Lift and Stability & Control Test of the HSR 5% Model Including Planform Variations, Canard and 3-Surface Configurations

Michael B. Elzey / Robert C. Griffiths
The Boeing Company

February 9, 1999

HSR

TCA-4 High-Lift Test

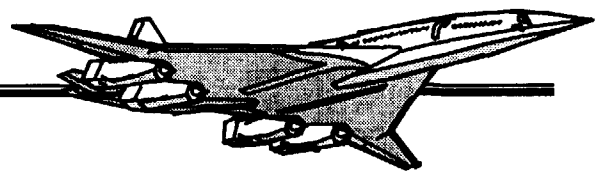

The TCA 5% model is shown in the NASA-Langley 14'x22' low-speed wind tunnel facility. The test was conducted between June 24 and July 29, 1998.

HSR

TCA-4 High-Lift Test

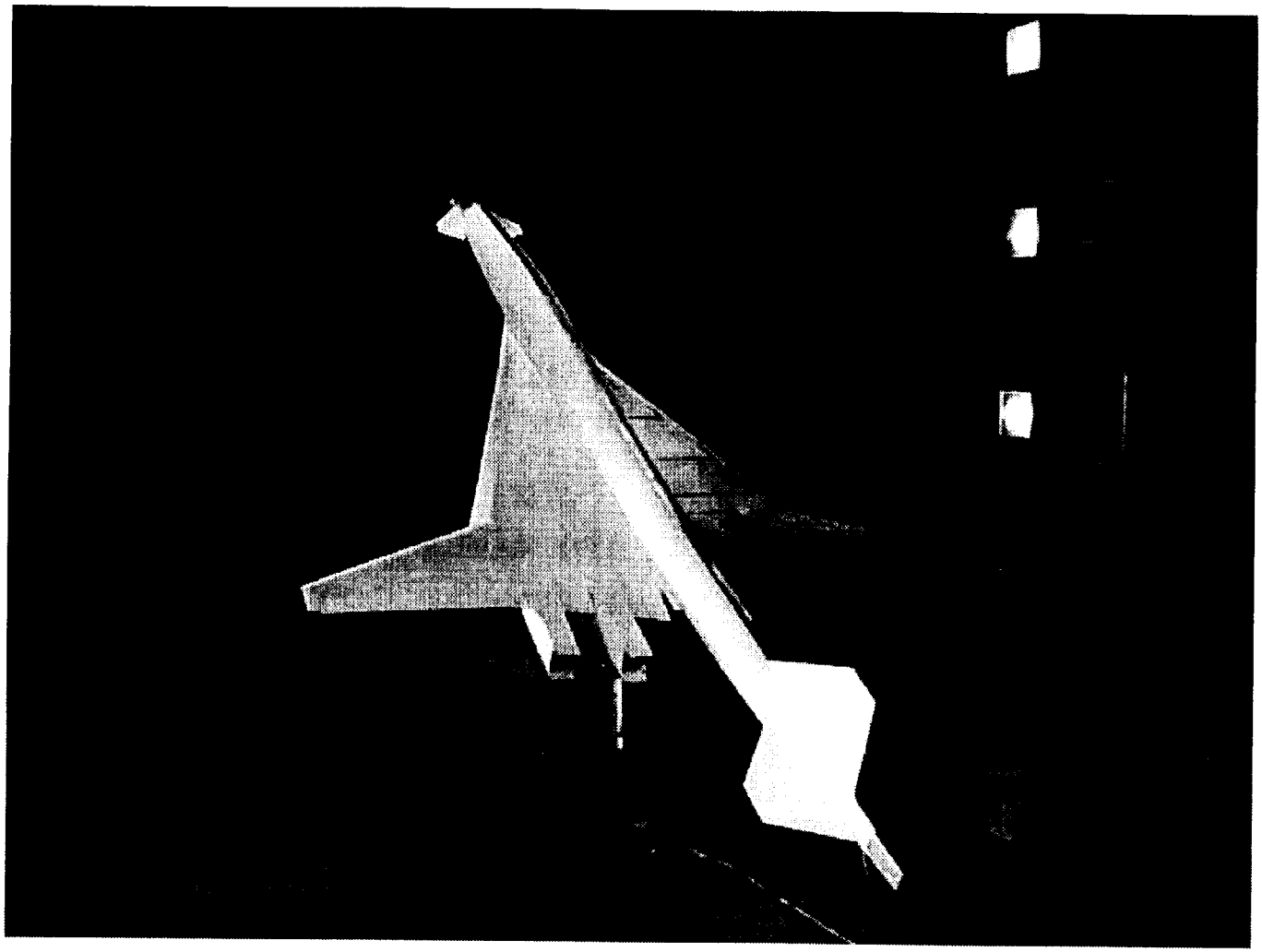

HSR Test Team

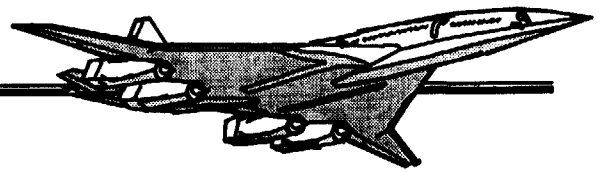

The TCA-4 (NASA473) pre-test planning was supported by HSR partners NASA-Langley (LaRC), NASA-Ames (ARC), Boeing Commercial Aircraft Group (BCAG) and Lockheed-Martin Aeronautical Systems (LMAS). ARC and LMAS were not available to staff the test.

In addition to the HSR partners, the model designer and fabrication shop - Advanced Technologies Inc. (ATI) and Tri-Models - were available during the pre-test planning activities.

HSR Test Team

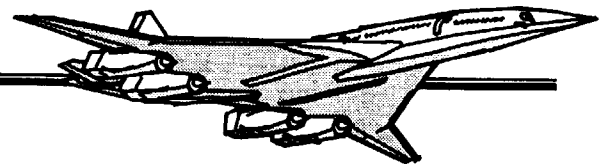

- Boeing - Seattle
  - wind tunnel support, instrumentation
- Boeing - Long Beach
- Lockheed-Martin
- NASA-Ames
- NASA-Langley
- Advanced Technologies Inc. / Tri-Models

HSR Test Team

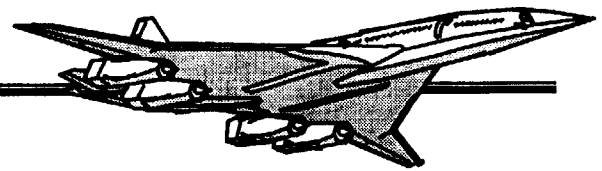

Researchers

- Boeing - Seattle
  - Katie Byrnes
  - Mike Elzey
  - Bob Griffiths
  - Eric Roth
  - Christine Titzer
- Boeing - DPD
  - Robin Edwards
  - Ryan Polito
  - Art Powell
  - Paul Glessner
- NASA-Langley
  - Linda Bangert
  - Bryan Campbell
  - Lewis Owen
- NASA-Ames
  - Brian Smith
  - Fanny Zuniga
- Lockheed-Martin
  - Bill Evans
  - Dave Hoyle

HSR Test Team

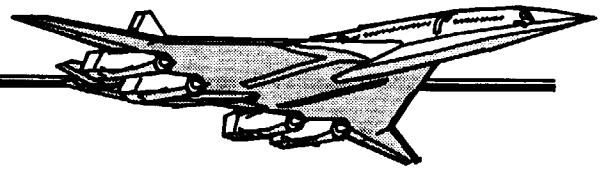

Model Design / Fabrication

- ATI
  - Don Barr
  - Bruce Bailey
  - Ron Calis
  - Chris Carter
  - Paul Coburn
  - Danny Ewton
  - Don Ewton
  - Steve Jones
  - Jason Lenakos
  - Robert Moreland
  - Ed Reel
  - Tim Shekoski
  - Wise Simones
- Tri-Models
  - Doug Carr
  - Ron D'Falco
  - Dennis Herzog
  - Sergio Mendoza
  - Al Roberts
  - Anthony Stulpin
- Boeing - Seattle
  - Barry Bowers

HSR Test Team

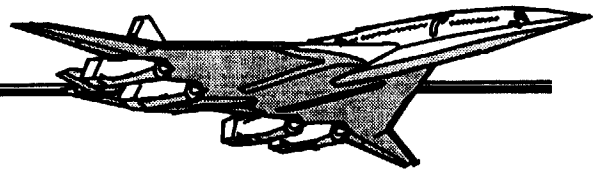

Data System Support

- NASA-Langley
  - Nettie Orie (lead)
  - Bruce Wells
  - Kevin Beard (CSC)
  - Mark Calvin (CSC)
  - Kurt Hitke (CSC)
  - Ben Trower (CSC)
  - Sharnita McKay (Wyle Labs)
- Boeing - Seattle
  - Richard Bell
  - Danny Delcarpio

Instrumentation

- NASA-Langley
  - Tom Jones
  - Trent Kite
  - Alven Clark (Wyle Labs)
- Boeing - Seattle
  - Larry Barstow
  - Hugh Beck
  - Tom Butler
  - Steve Hatten
  - Marty Neubauer

HSR Test Team

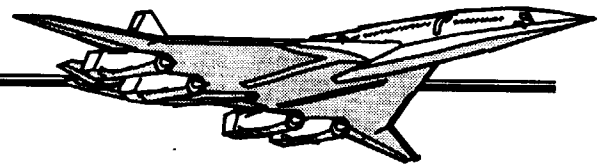

Wind Tunnel Support

NASA-Langley

test engineers

Bill Abeyounis
Walker Smith

technicians

Jim Anderson
Barry Askew
Tom Bryant
Patricia Christian
Jimmy Clark
Clinton Duncan
Ed Durham
Holly Elliott
Jim Gayton
Dick Hartman
Mike Henshaw
Wendy Johnson
Betsy Kennedy
Carl Maddox
Jody Matthews
George Miles
Mike Ramsey
Cassandra Stevens
John Treier (test director)

Boeing - Seattle

test engineers

Richard Bell (TE/ DE)
Earl Patterson (TE)

technicians

Ed Giboney
Lloyd Laws

HSR

TCA-4 High-Lift Test

Road Map

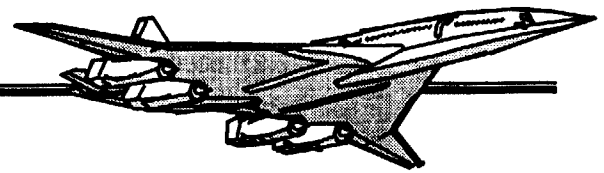

This material will be presented as follows:

First, test objectives and background will be discussed. Background material includes part description, test statistics and progress made.

Second, general test results will be discussed, including data quality and test-to-test comparisons.

Third, high-lift results will be presented, followed by stability and control. Each section will summarize respective conclusions.

Finally, general recommendations will be presented and discussed.

Road Map

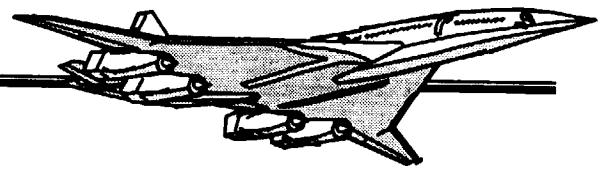

- Test objectives
- Background
  - test setup, test statistics, "HowGozIt" chart
- Results
  - Data quality
  - Test-to-test
  - High-lift
  - Stability & control
- Concluding remarks

Objectives

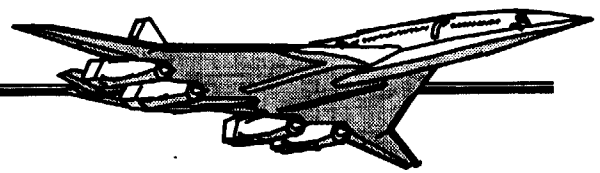

The objectives for the TCA-4 test were as follows:

1. Evaluate wing planform and 3-surface effects on high lift performance, longitudinal and lateral / directional stability and control.
2. Identify showstoppers to TC configuration.
3. Obtain data for a configuration buildup database.
4. Obtain on surface flow visualization and static pressure data for better understanding of flow physics and CFD validation.
5. Achieve enough testing to better optimize TCA-5 test planning.
6. Evaluate the path of the canard tip vortices to address issues concerning the possibility of inlet ingestion, as well as possible directional control problems.

Objectives

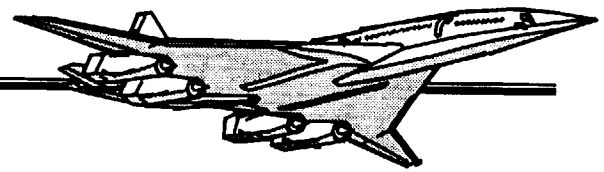

- Evaluate wing planform and 3-surface effects on high lift performance, long. & lat./dir. stability & control
- Determine showstoppers
- Obtain data for a configuration database
- Obtain flow viz and pressure data for better understanding of flow physics / CFD validation
- Achieve enough testing to allow intelligent follow-on test planning (TCA-5)
- Evaluate path of canard tip vortices (PAI)

The PTC

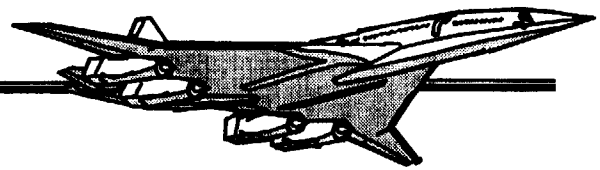

The development of new parts for the TCA-4 test was driven by the HSR baseline configuration at the time of model part definition, the PTC. The differences between the TCA baseline, to which the original model was designed, and the PTC are shown on the chart. The biggest impact on TCA-4 model design was the addition of a chinfin, canard, smaller horizontal tail, aspect ratio and outboard panel sweep change. The last two resulted in two new outboard panels constructed, with outboard sweeps that would bracket the proposed PTC outboard panel sweep of 32°. Both new panels were designed to give a resultant aspect ratio of 2.8.

The PTC

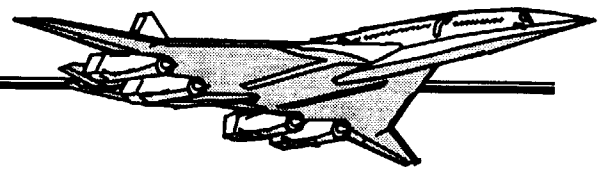

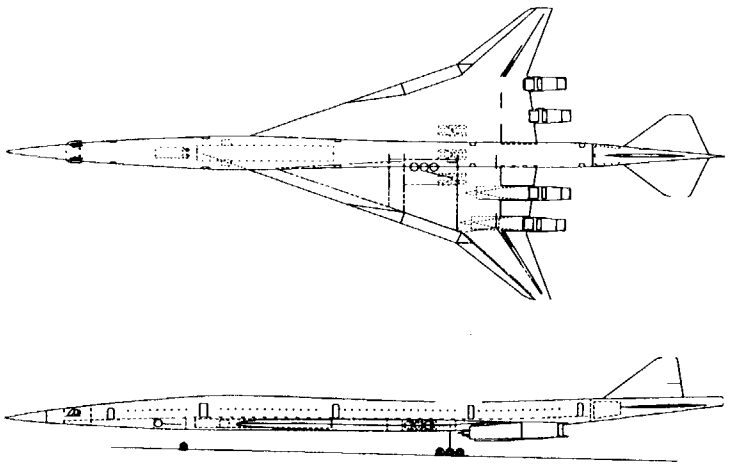

Model 2.0-52

Wing Area	8500 sq. ft.
Wing Span	131.3 sq. ft.
Aspect Ratio	2.0
MAC	1139.4 in.
Indb. Sweep	71 deg.
Outbd. Sweep	52 deg.
H-tail Area	800 sq. ft.
V-tail Area	407 sq. ft.

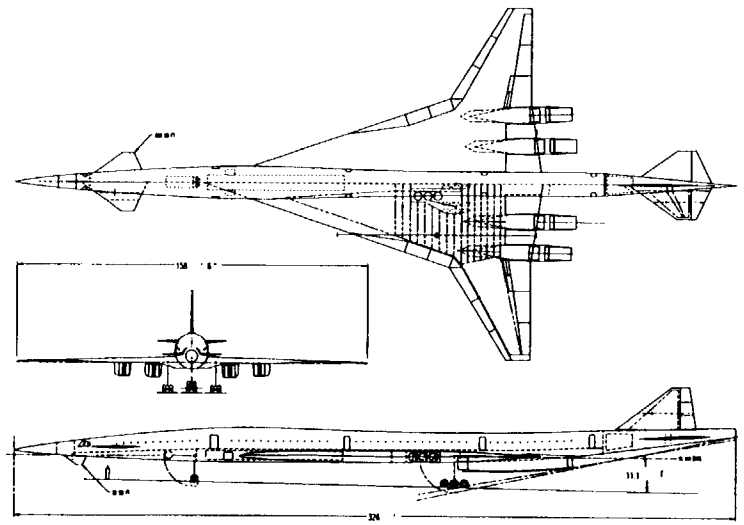

PTC Cycle 2

Wing Area	9200 sq. ft.
Wing Span	158.5 ft.
Aspect Ratio	2.73
MAC	1077.9 in.
Inbd. Sweep	71.0 deg.
Outbd. Sweep	32.0 deg.
H-tail Area	545 sq. ft.
V-tail Area	415 sq. ft.
Canard	220 sq. ft.
Chin fin	25 sq. ft.

New Parts for TCA-4

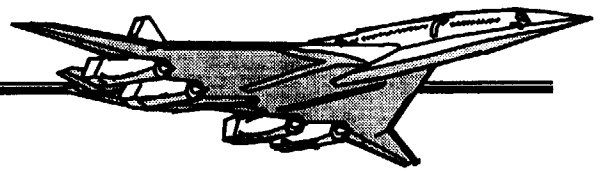

Close to 100 new parts were designed and fabricated in preparation for TCA-4. Aerodynamic designers worked closely with the chosen model design shop (ATI-Hampton, VA) to turn out high quality parts on time and on budget. Tri-Models out of Huntington Beach, CA, performed most of the fabrication work.

ATI continued to support the test after part delivery. A suggestion and subsequent forebody modification conducted at the ATI shop resulted in a significant time savings during in-tunnel canard installation and removal.

HSR

TCA-4 High-Lift Test

New Parts for TCA-4

HSR

TCA-4 High-Lift Test

The Three Outboard Panels

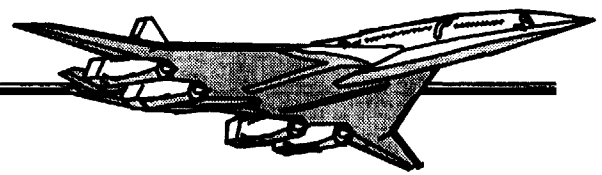

Planform effects were investigated by testing a total of three outboard panels.

The existing TCA 2.027-52, or "Wing 1", was used to establish the baseline performance characteristics. Two new outboard panels were built to provide higher aspect ratio (increased span) and lower outboard leading & trailing edge sweep. These two panels were the 2.8-28, or "Wing 2" and the 2.8-38, or "Wing 3".

"X.X-YY": X.X aspect ratio with YY degrees outboard leading edge sweep.

HSR

TCA-4 High-Lift Test

The Three Outboard Panels

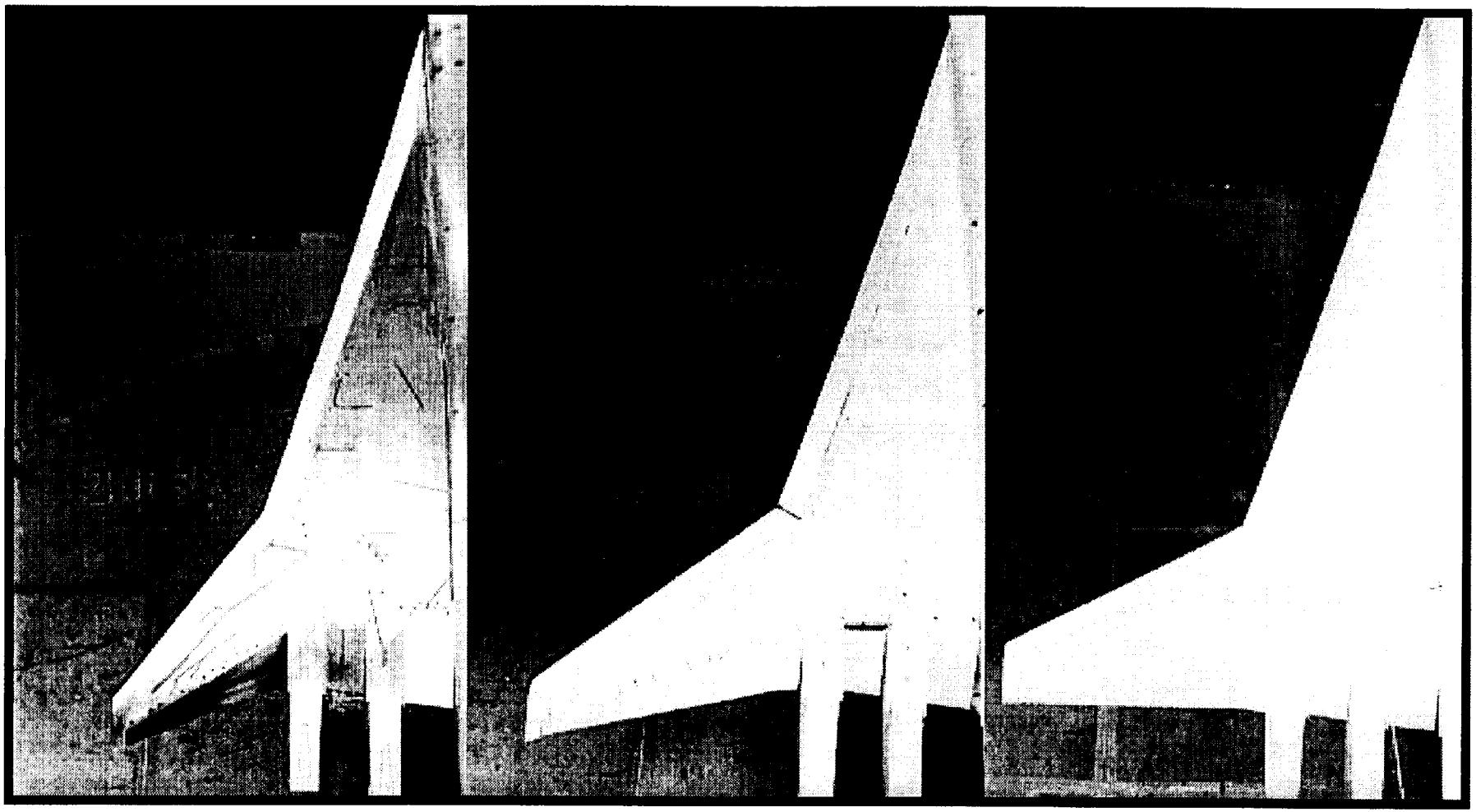

Occupancy

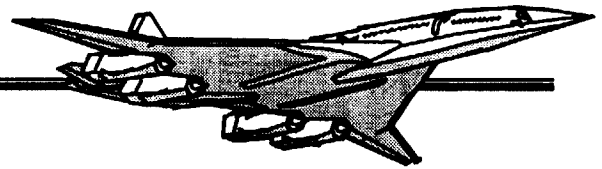

A total of 521 productive wind-on runs were obtained over 54 shifts, for a run rate of 1.17 per occupancy hour.

One measure of the productivity of a test can be determined, once occupancy has been established, by breaking out the productive and the non-productive hours as shown. These hours were closely tracked by the test engineers from Boeing and Langley.

Occupancy

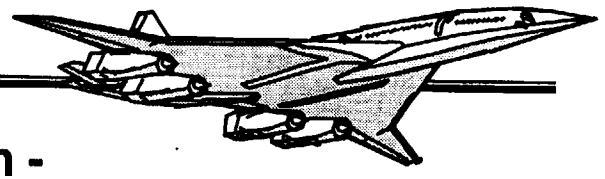

TCA-4 Occupancy Breakdown - 447.2 Total Hours

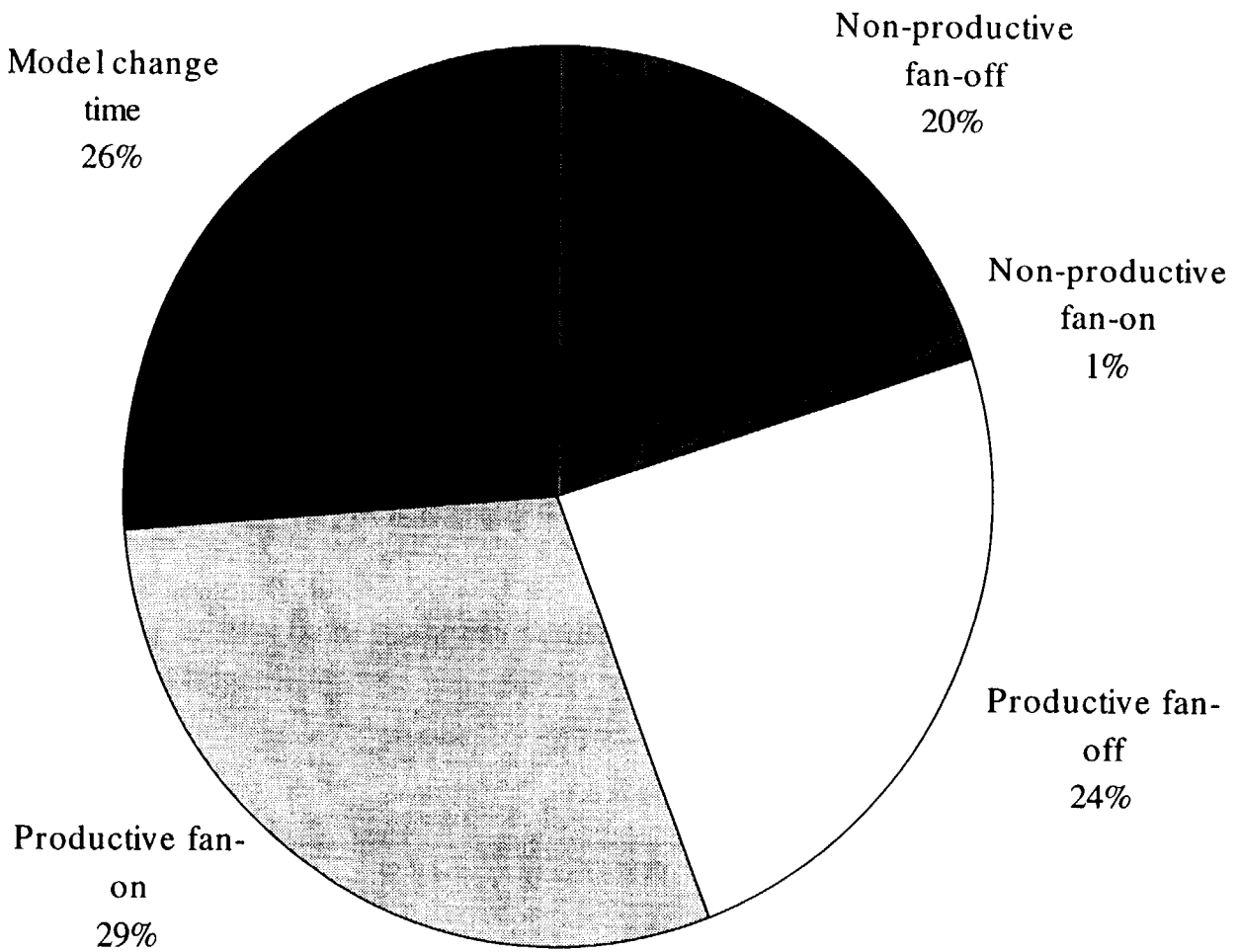

Occupancy

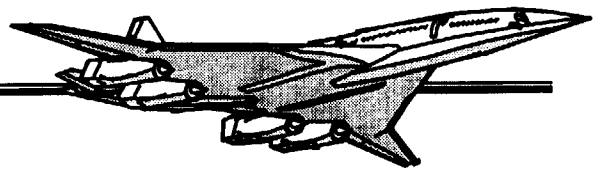

Another measure is the percentage of fan-on vs. the percentage of productive fan-off time. Productive fan-off in this case does not include:

1. model change times to make this a model independent measure,
2. facility problems,
3. model problems.

These non-productive hours are then subtracted from the total occupancy hours to calculate total productive fan-on/fan-off hours.

Looking at tunnel productivity in this fashion is indicative of what it takes for a facility to get up and running. In a perfect world the fan-on percentage would equal 100% (impossible, of course). For TCA-4, total productive fan-on time was 55% of productive fan-on/fan-off occupancy hours.

The other tests shown are two representative tests in the DeRA facility as well as an early 1998 Boeing 777 entry in the Ames 12'.

HSR

TCA-4 High-Lift Test

Occupancy

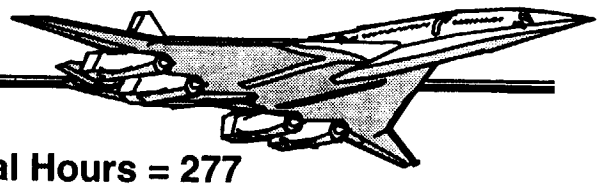

Total Hours = 237

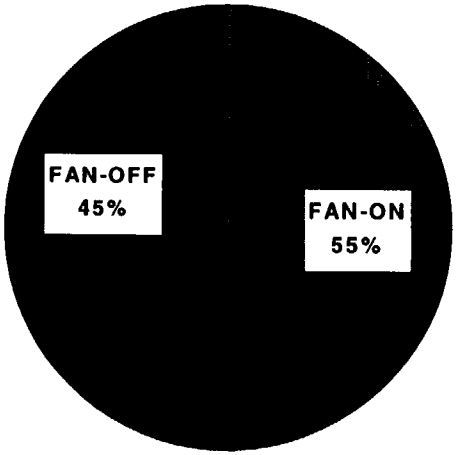

LaRC 14'x22'

Total Hours = 277

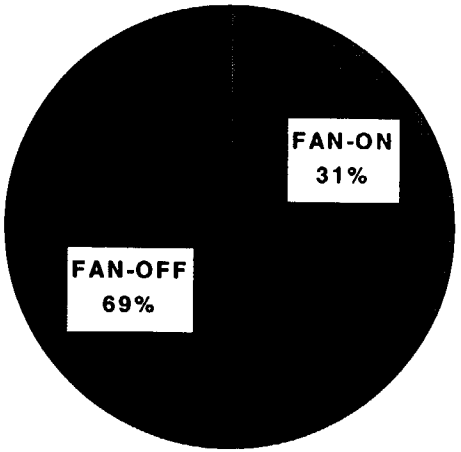

ARC 12'

Total Hours = 408

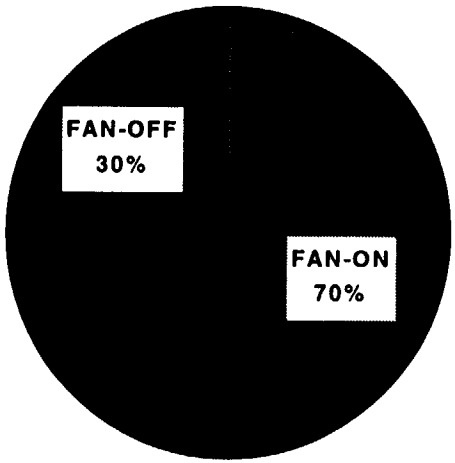

DeRA #1

Total Hours = 306

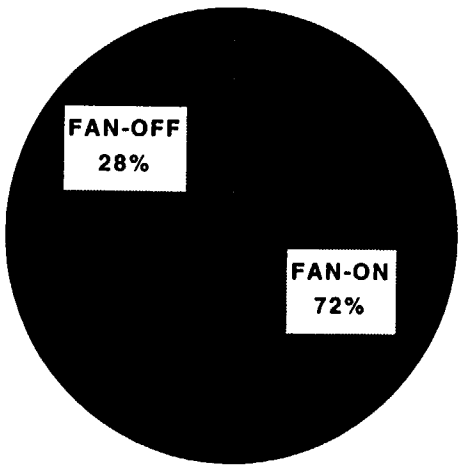

DeRA #2

HSR

TCA-4 High-Lift Test

"HowGozIt"

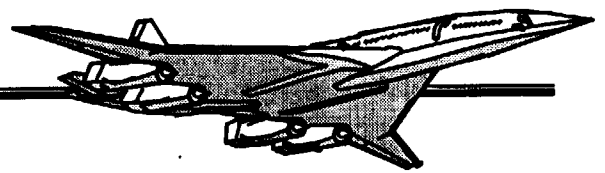

The "HowGozIt" chart tracks the progress of test objectives against time allotted on a shift-by-shift basis. Based on how well pre-test time estimates are tracking against the actual time, adjustments can be made to the plan of test.

The TCA-4 plan of test was reduced nearly 50% before the wind was turned on for the first time due to facility and model problems, and an earlier exit date than anticipated. Due to increased productivity as the test progressed, nearly 90% of the original test plan was completed.

HSR

TCA-4 High-Lift Test **"HowGozIt"**

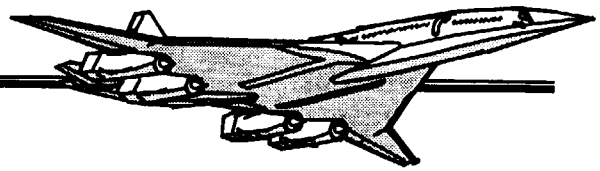

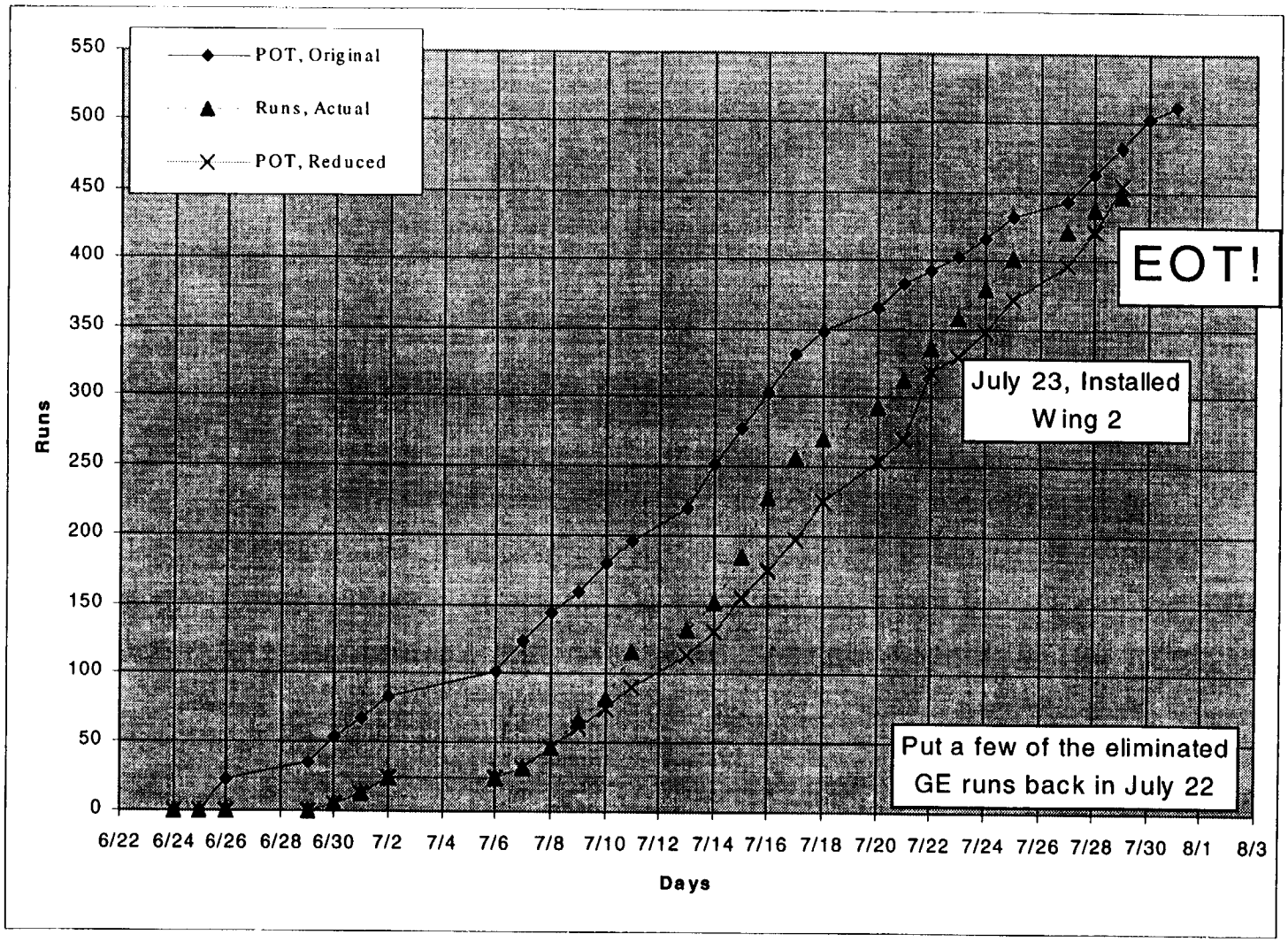

HSR

TCA-4 High-Lift Test

Repeatability

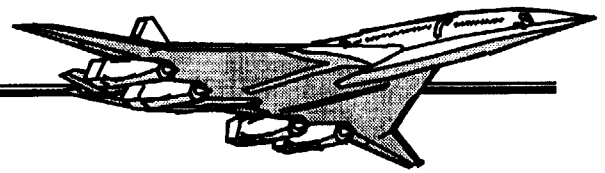

The within test data repeatability was excellent. As can be seen in the figure, total scatter of C_D about the data mean is less than ±4 drag counts below a C_L of 0.6. The 95% confidence interval for the entire polar is ±2 drag counts. The confidence interval gets even smaller if C_L's above 0.6 are excluded.

Repeatability

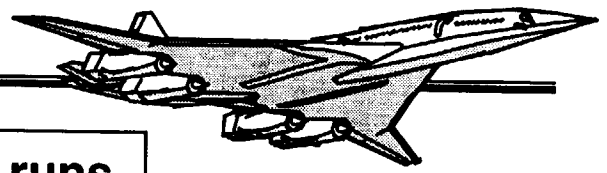

Wing 3, Flaps 30/10, Tail off, 11 runs

first run: 269; last run: 714

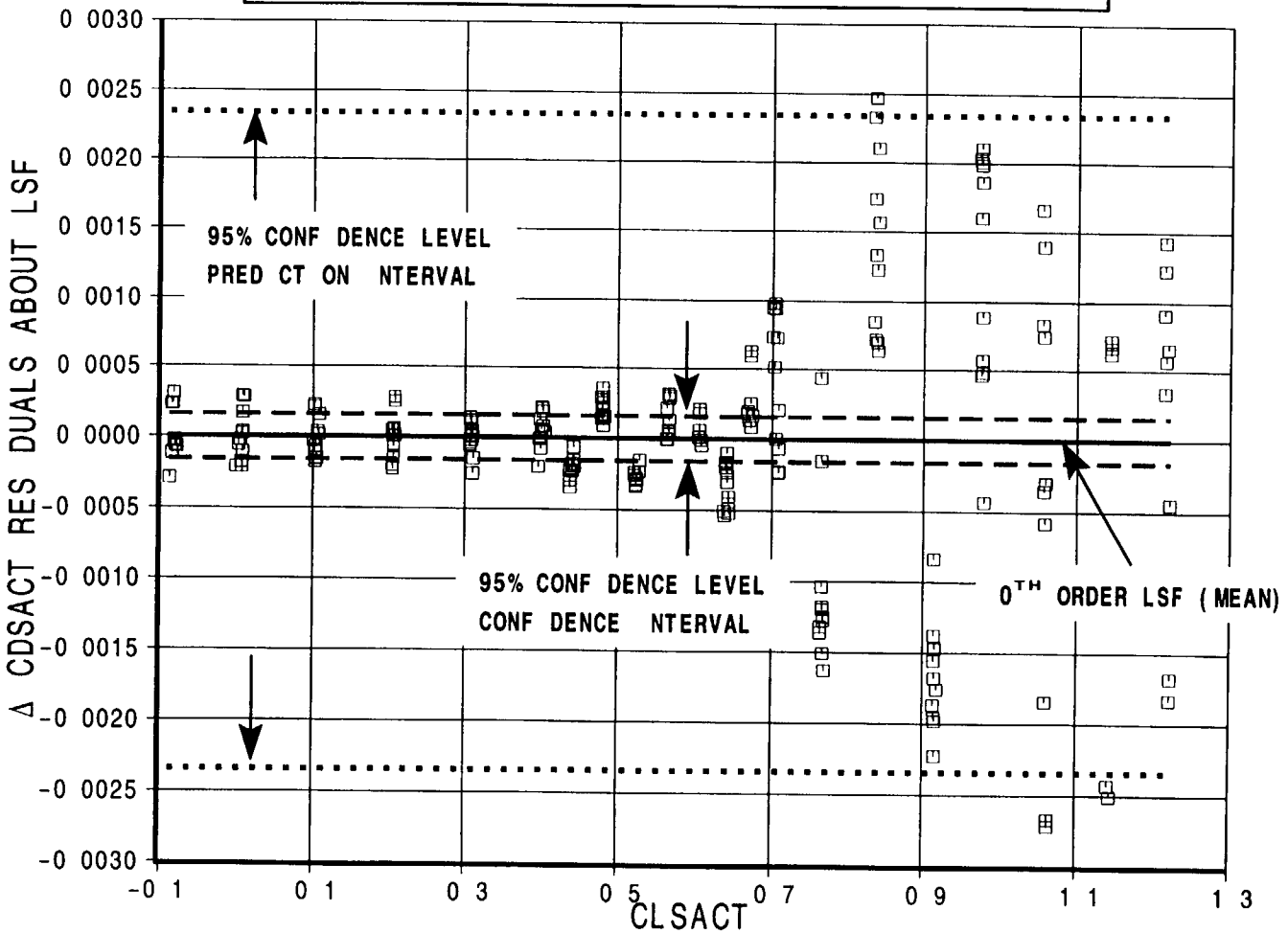

Repeatability

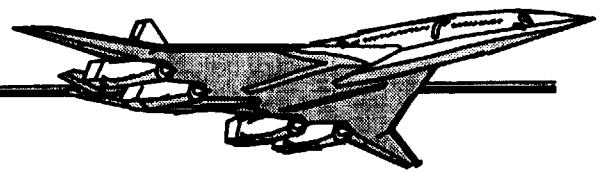

Data repeatability was consistently excellent for the 3 wings tested. The figure shows 95% CI levels for C_L as a f(α), C_D as f(C_L) and C_M as f(C_L) for each of the 3 planforms. These data represent all repeat runs for each wing's chosen climbout flap configuration.

Repeatability

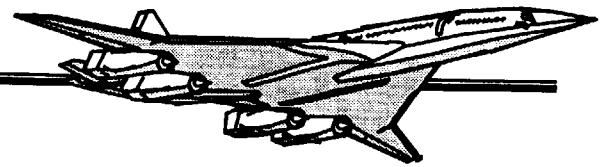

95% Confidence Intervals

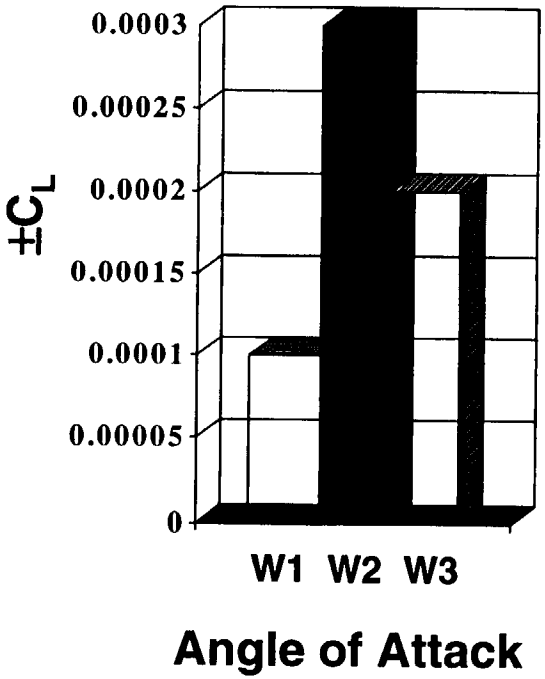

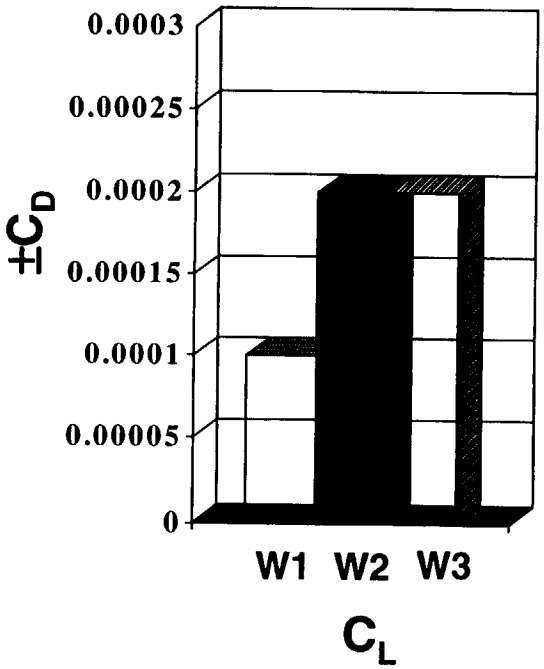

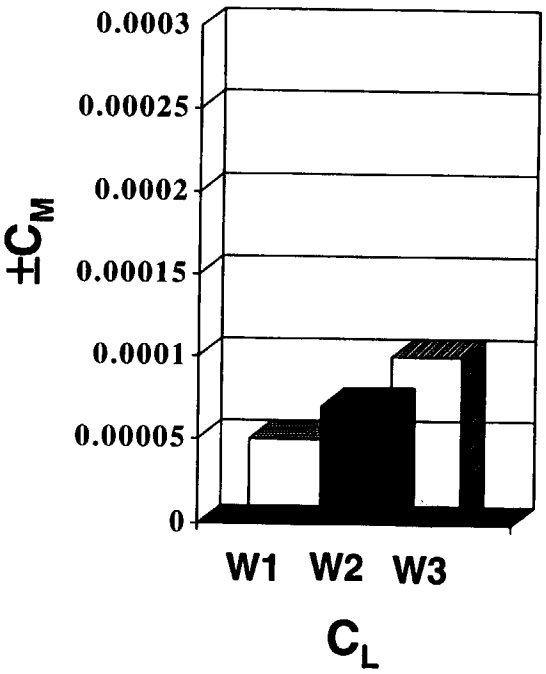

HSR

TCA-4 High-Lift Test

Test-to-Test

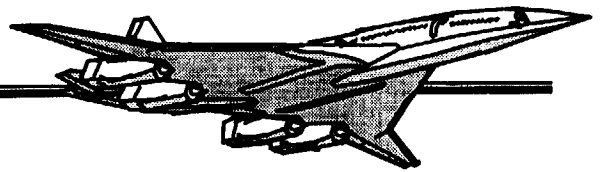

The purpose of making a test-to-test comparison is to determine long term repeatability & facility differences and, if possible, correct data to obtain absolute levels.

Tunnel differences were analyzed between the 14'x22 and the ARC 12' using the TCA (W1) 5% model, and the 14'x22' and NTF facilities using the RefH 6% model.

When making comparisons, every effort was made to adjust tunnel data to consistent levels of corrections. In the analysis, 14'x22' and Ames 12' data did not contain upflow corrections while NTF did.

Test-to-Test

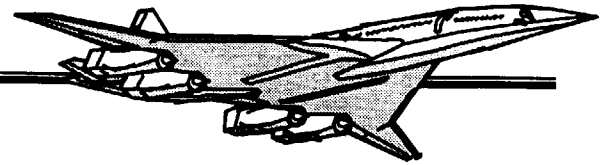

- Purpose of test-to-test comparison:
  - long term repeatability (same tunnel)
  - facility differences
  - search for absolute levels

- Tests compared:
  - TCA-4 to TCA-3 (14'x22' to Ames 12')
  - NASA #421 & #437 to NTF078 (14'x22' to NTF)

HSR

TCA-4 High-Lift Test

Test-to-Test

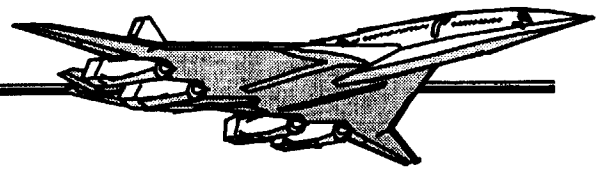

The 2 tunnels for which HSR has low speed data for the TCA5% model, W1, are the NASA-Langley 14'x22' and the NASA-Ames 12' facilities. Both tunnels make an attempt to correct the data to a freeair condition, employing wall, nacelle base and internal drag, body cavity, wake blockage, and solid blockage corrections, among others. Support interference is available for the TCA 5% model using increments measured with the 6% RefH model, assuming that the RefH increments are similar to TCA5% levels. Planform specific upflow is unknown in both facilities. Different correction methodologies are employed between the 2 facilities for effect of walls and some blockage terms.

Each and every production wind tunnel facility would like to think that, within the limitations of their corrections, the final data from a wind tunnel entry is truly "final", and that ideally these data could be applied to building up flight data. Both the 14'x22 and 12' have final datasets for the TCA 5% model, yet the data levels do not match. Determining where the real answer lies depends on knowing all possible corrections, including upflow and support interference. Without this information, collapsing the data is arbitrary.

LaRC 14'x22'

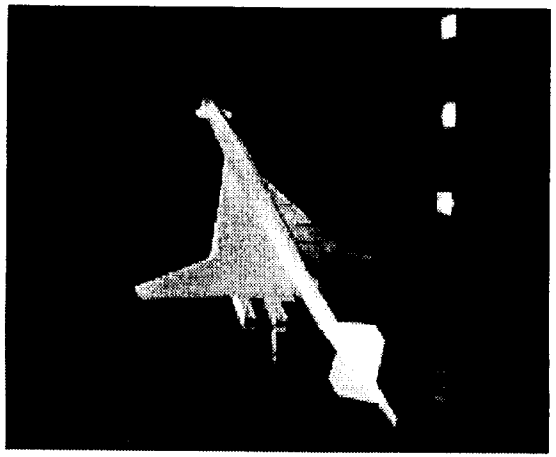

- support interference measured
- wall corrections
- nacelle base & internal; cavity
- wake blockage approx.
- solid blockage
- planform specific upflow unknown
- tunnel biases

The answer is somewhere in here

ARC 12'

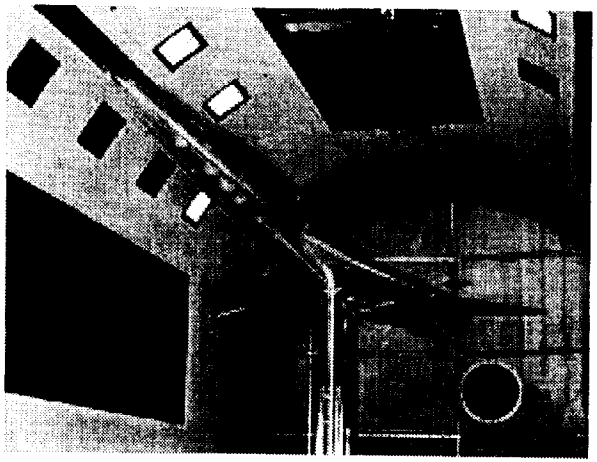

- support interference unknown
- wall corrections
- nacelle base & internal; cavity
- wake blockage approx.
- solid blockage
- planform specific upflow unknown
- tunnel biases

Given the known corrections, closing the data is arbitrary. We need more information.

Test-to-Test

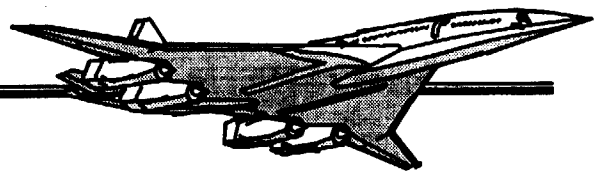

These data have not been corrected for support interference or upflow; all other available corrections have been applied. The two tests shown are the 12' TCA-3 and the 14'x22' TCA-4 entries.

The TCA-3 lift curve is offset above TCA-4 by $\Delta C_L \approx +.01$, or $\Delta\alpha \approx 0.3°$. This offset is nearly constant from zero lift to angles of attack above 14°.

No relative rotation seen between lift curves, implying that the dynamic pressures used to reduce the coefficients was consistent between the 2 facilities.

Possibilities: support interference differences, relative change in tunnel flow angularity, other?

Test-to-Test

2.027-52, Flaps 30/15(10)

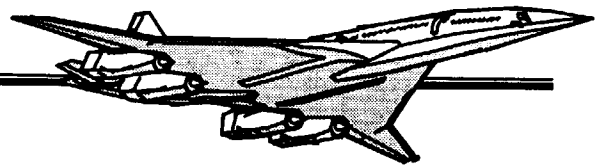

These curves are east square representat ons of a repeat runs for each nd v dua test/conf gurat on

	Ames 12	14 x22
cav ty	y	y
nt drag	y	y
base pressure	y	y
support nt	u	n
upf ow	u	u
wa	y	y

y=yes n=no u=unknown

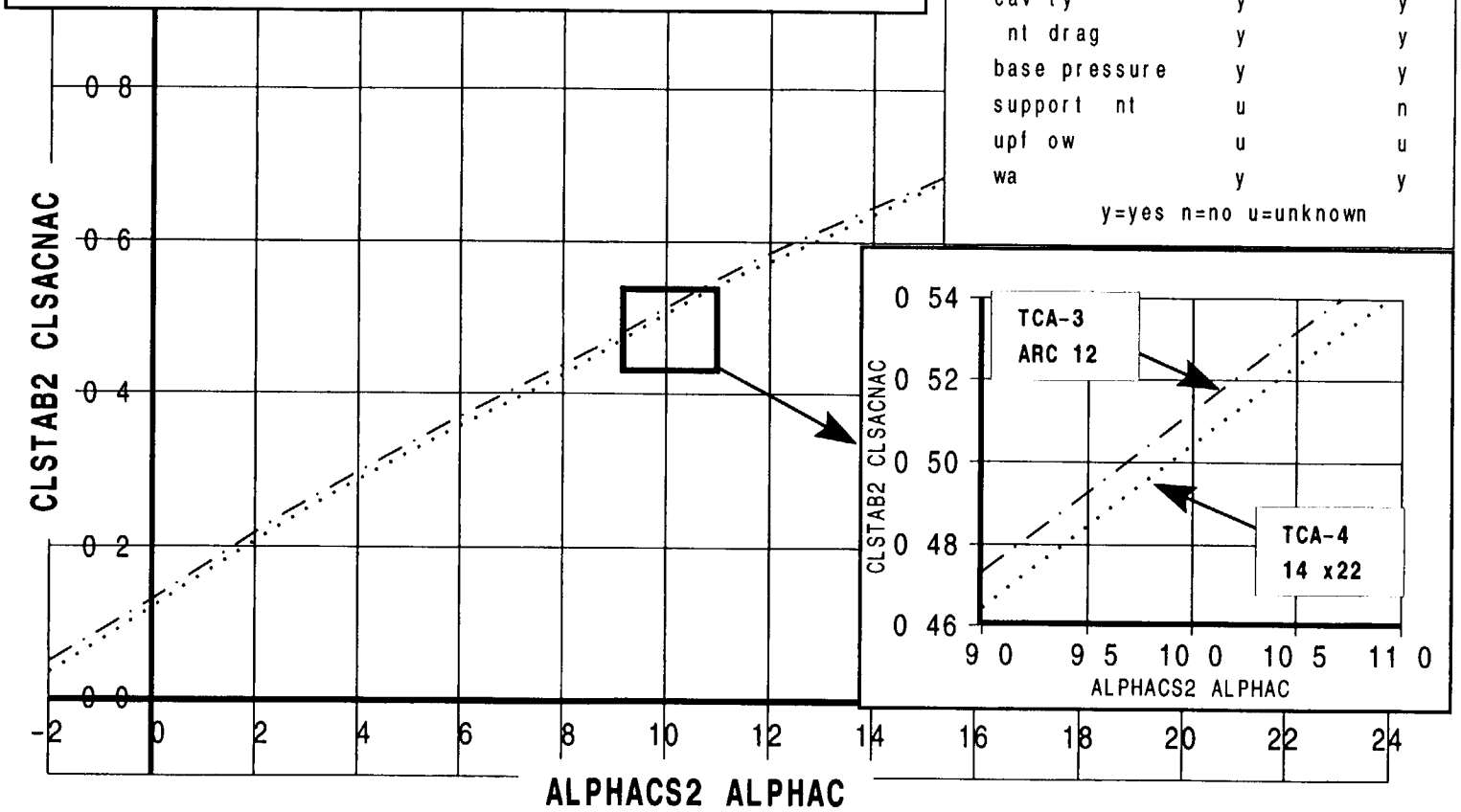

Test-to-Test

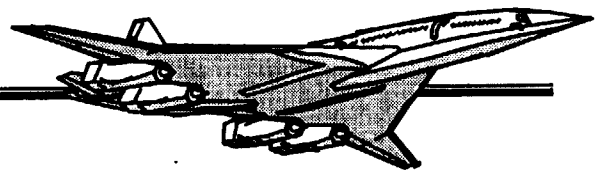

A large polar rotation about zero lift is evident between the Ames 12' data and the 14'x22' data. At a lift coefficient of 0.5 TCA-3 has approximately 50 counts less drag than TCA-4.

It should be noted that above CL's of 0.6 the drag polar rotation can be seen to lessen between the two datasets. This de-rotation effect is likely due to differences in the way the 12' and 14'x22' correct for wake blockage: the 12' uses Maskell's separated flow correction while the 14'x22' uses Maskell's attached flow simplification. The attached flow version would tend to under-correct the drag due to wake blockage at the higher lift coefficients. Since upflow is inferred in the attached flow region, this de-rotation does not impact upflow assumptions based on drag polar rotation.

Test-to-Test

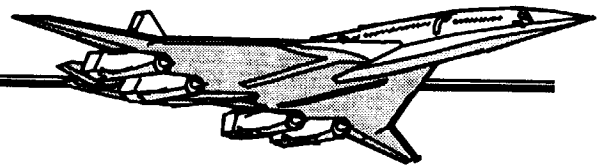

2.027-52, Flaps 30/15(10)

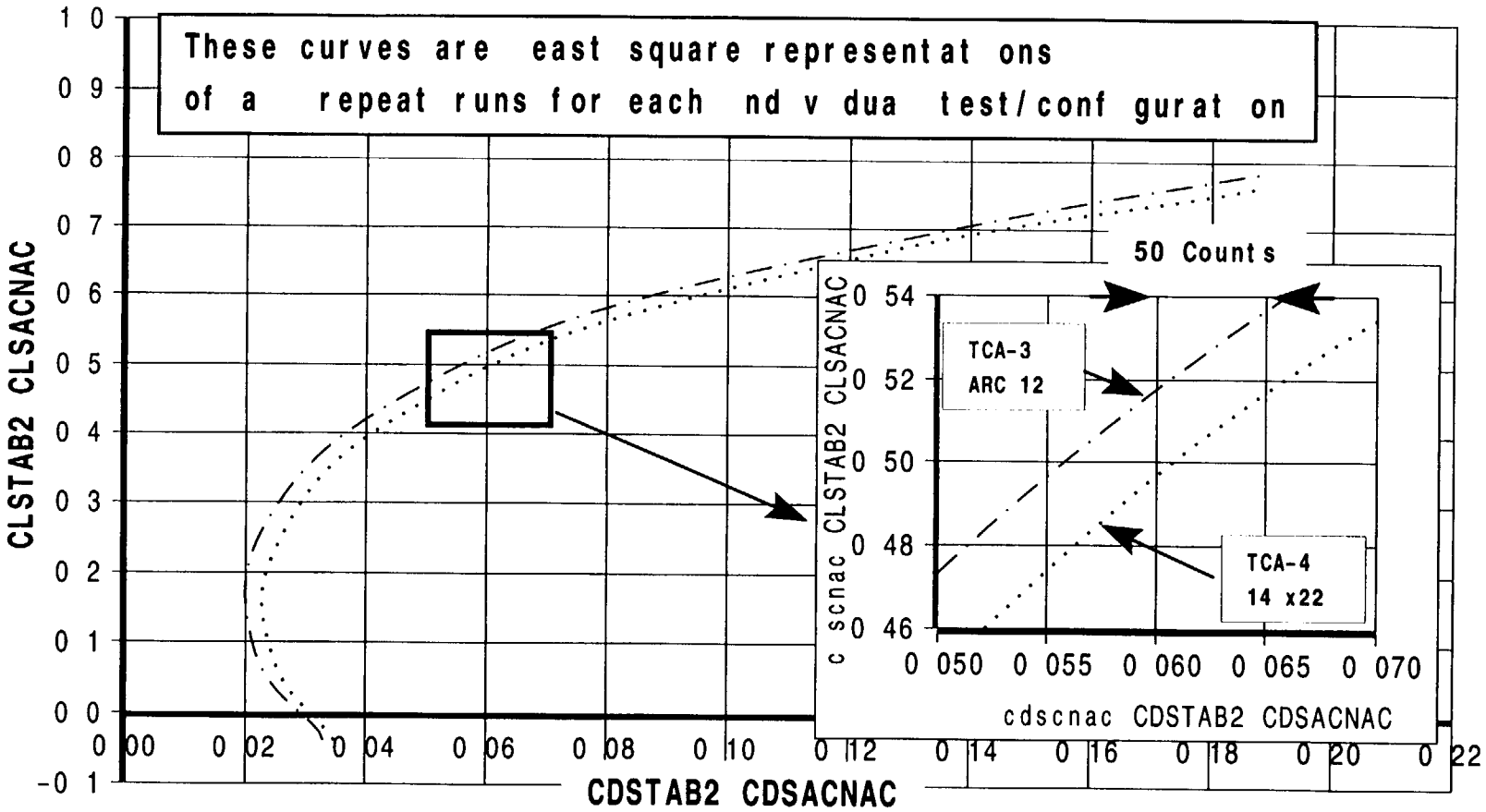

Test-to-Test

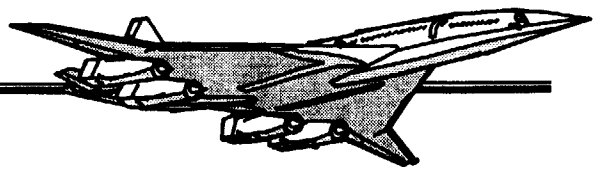

As expected from the lift curves and drag polars, TCA-3 (12') has an L/D higher than TCA-4 (14'x22') by approximately .7 units at a lift coefficient of 0.5.

Test-to-Test

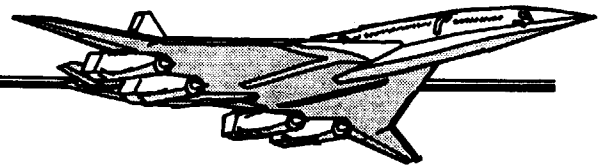

2.027-52, Flaps 30/15(10)

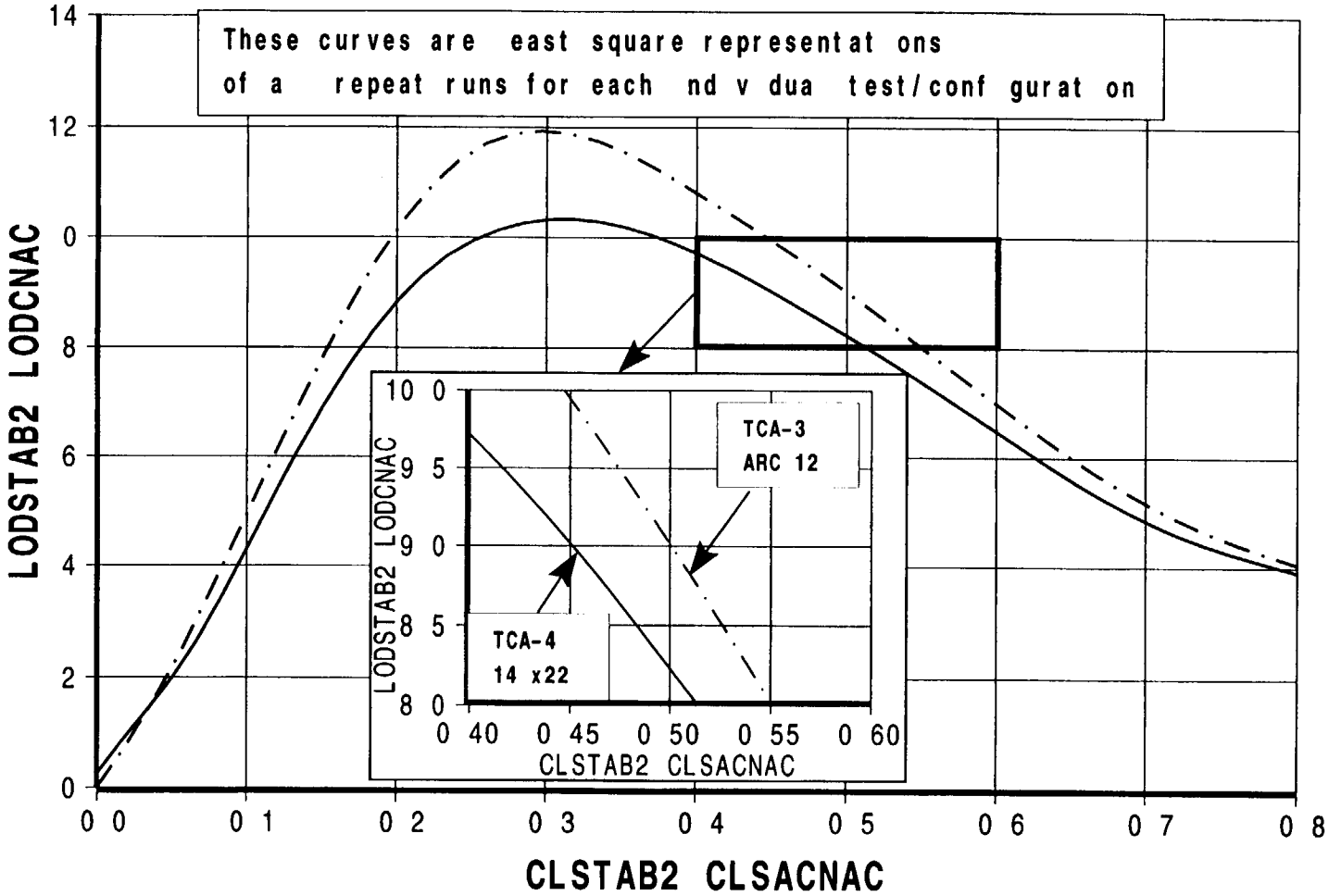

Test-to-Test

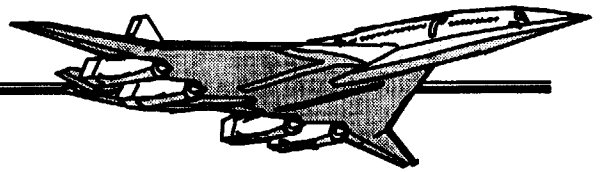

The RefH **0/0** (flaps undeflected) and **30/10** (climbout flaps) were used to make comparisons between NTF (NTF078) and three 14'x22' tests: NASA421, NASA429 and NASA437. Only a flaps up comparison between NTF and NASA421 and NASA437 is shown here. The other test data shows a similar result.

11.5 counts were added to the NTF drag data to account for aftbody and vertical fin skin friction.

This figure shows 2 effects:

First, the drag difference as a function of lift between the NTF and 14'x22' for both flap configurations. Both charts agree to first order that the 14'x22' data is approximately 20 drag counts higher than the NTF, at least at moderate C_L's.

Second, there is no evidence from the data of a significant polar rotation between the 14'x22' and NTF at C_L's below 0.55.

RefH 6%, flaps 0/0, tail off, comparable level of corrections, repeat runs averaged

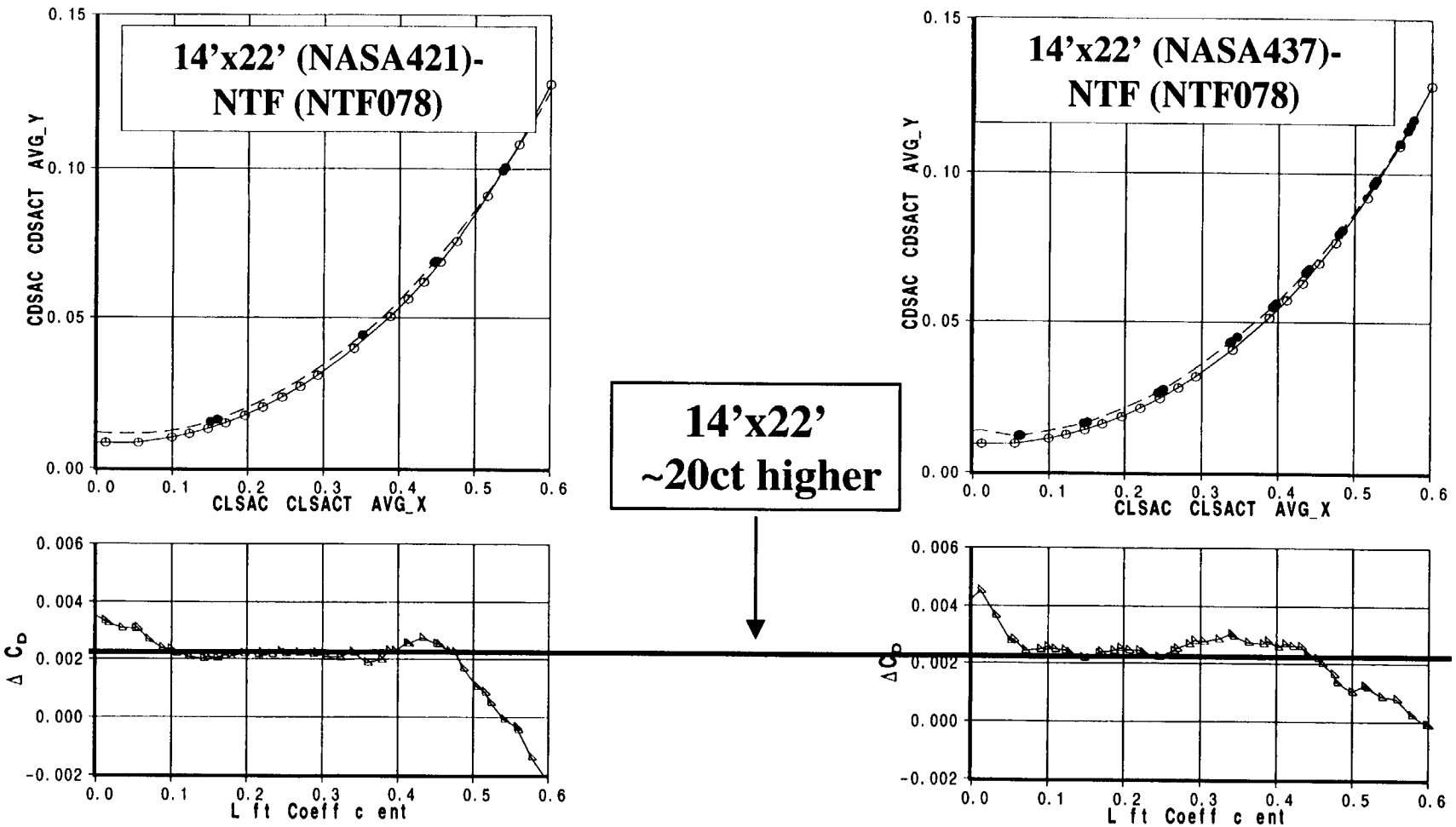

Test-to-Test

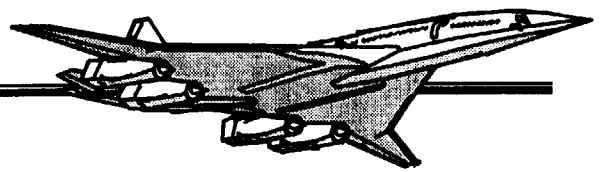

Since there is no evidence of a polar rotation between the NTF and 14'x22', and since the NTF data is upflow free, the argument could be made that the Ames 12' data facility has an unaccounted for upflow.

Referring back to the earlier lift curve comparison between Ames and the 14'x22' which showed an offset in lift curves between the two facilities, it can be seen that a correction to the 12' data of .3° tends to collapse the lift curves, as shown here.

Test-to-Test

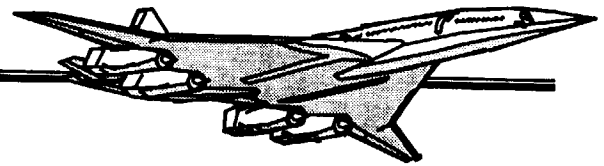

2.027-52, Flaps 30/15(10)

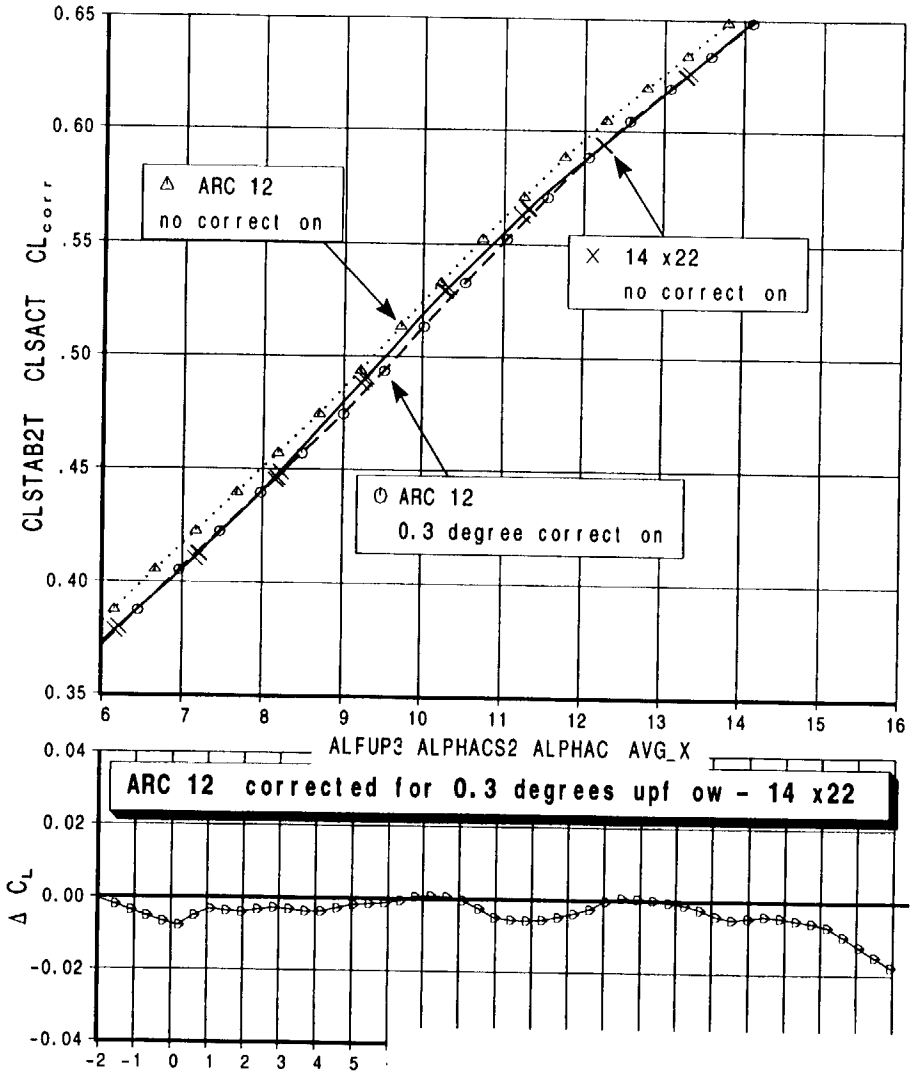

Ames 12', TCA-3

and

14'x22, TCA-4

Test-to-Test

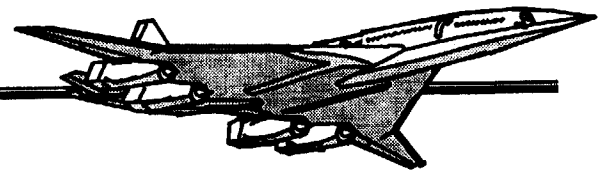

Continuing the .3° upflow correction to the Ames data results in similar drag polar shapes between the 14'x22' and Ames 12' as seen here.

There is still an offset of about 20 drag counts evident between the two facilities at moderate lift levels, C_L's < 0.55. Adjusting the 14'x22' drag levels to be consistent with the NTF levels as seen earlier would result in a 20 count shift in the 14'x22' data, bringing the 14'x22' data to Ames 12' drag levels.

Test-to-Test

2.027-52, Flaps 30/15(10)

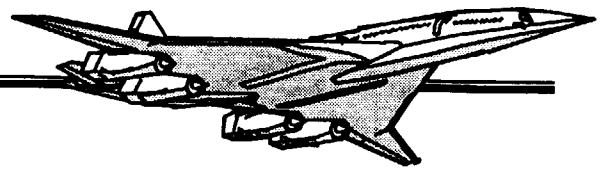

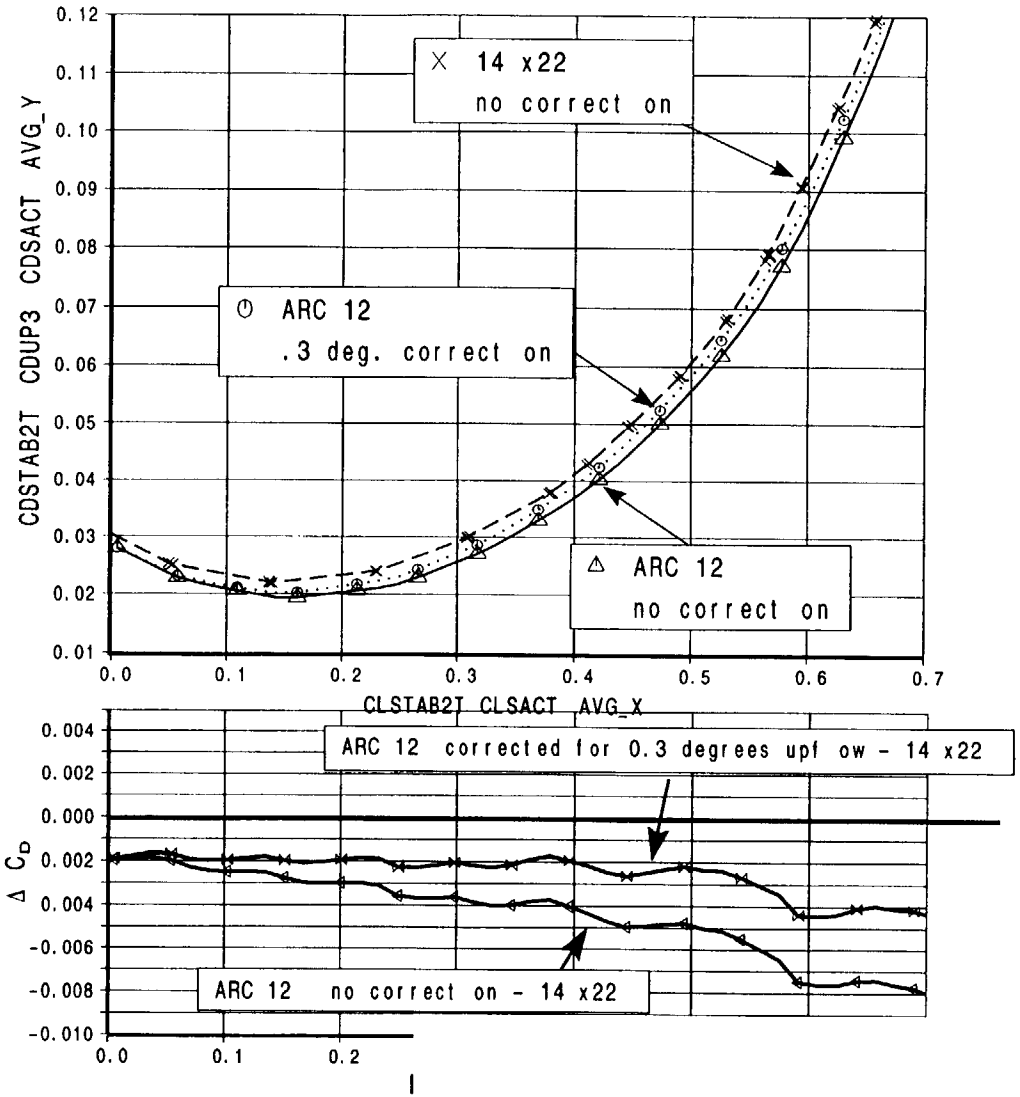

Ames 12', TCA-3

and

14'x22, TCA-4

HSR

TCA-4 High-Lift Test

Test-to-Test

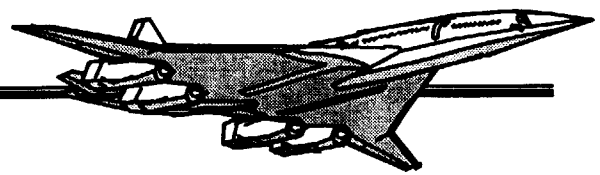

The L/D's shown here include the TCA-3 (12') and TCA-4 (14'x22') data. These data include the final data from the tunnels, as well as the Ames 12' data corrected for 0.3° upwash and the 14'x22 drag levels corrected 20 counts to NTF levels.

Note that while there are an infinite number of ways that 2 datasets can be made to collapse, the method presented here relies on making the connection between the NTF facility and the 14'x22' facility, and then applying the appropriate corrections to the Ames 12' and Langley 14'x22' datasets.

HSR

TCA-4 High-Lift Test

Test-to-Test

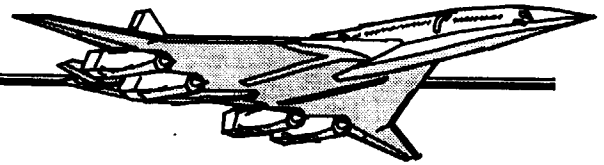

2.027-52, Flaps 30/15(10)

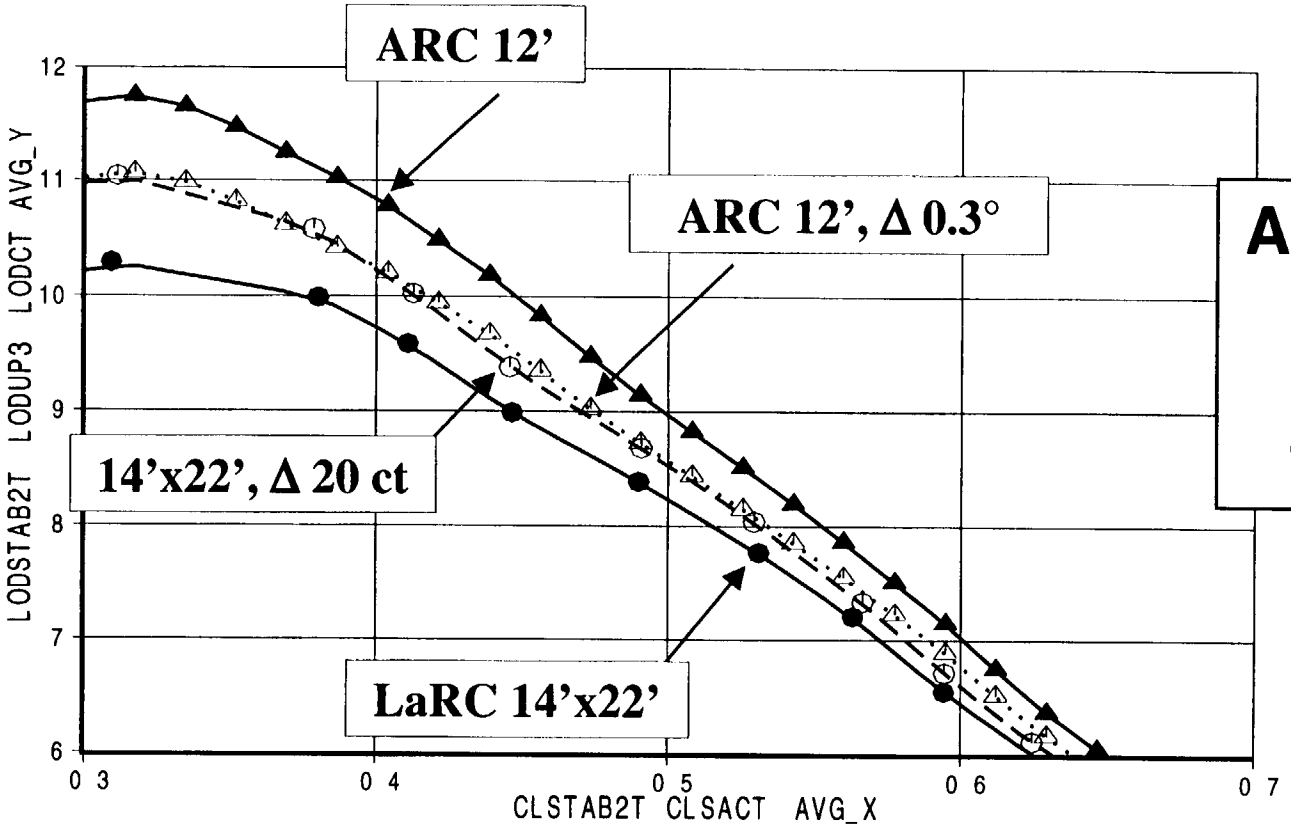

Ames 12', TCA-3

and

14'x22, TCA-4

The BLRS

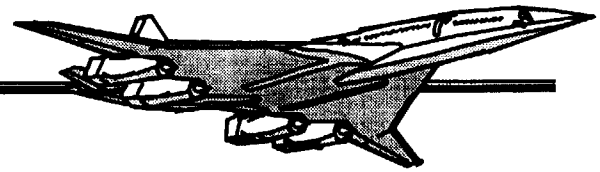

Due to the proximity of the model to the tunnel boundary layer removal system, or BLRS, there has been some concern that the open cavity (BLRS off) was influencing tunnel angularity. A quick check was done at model max height by comparing data results with the BLRS open (nominal) and taped over. Three back-to-back polars were run for each BLRS setting. The open/closed BLRS runs were conducted one right after the other to minimize meteorological and other influences out of our control.

HSR

TCA-4 High-Lift Test

The BLRS

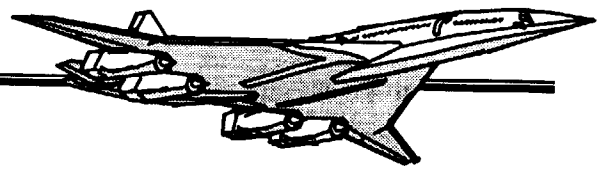

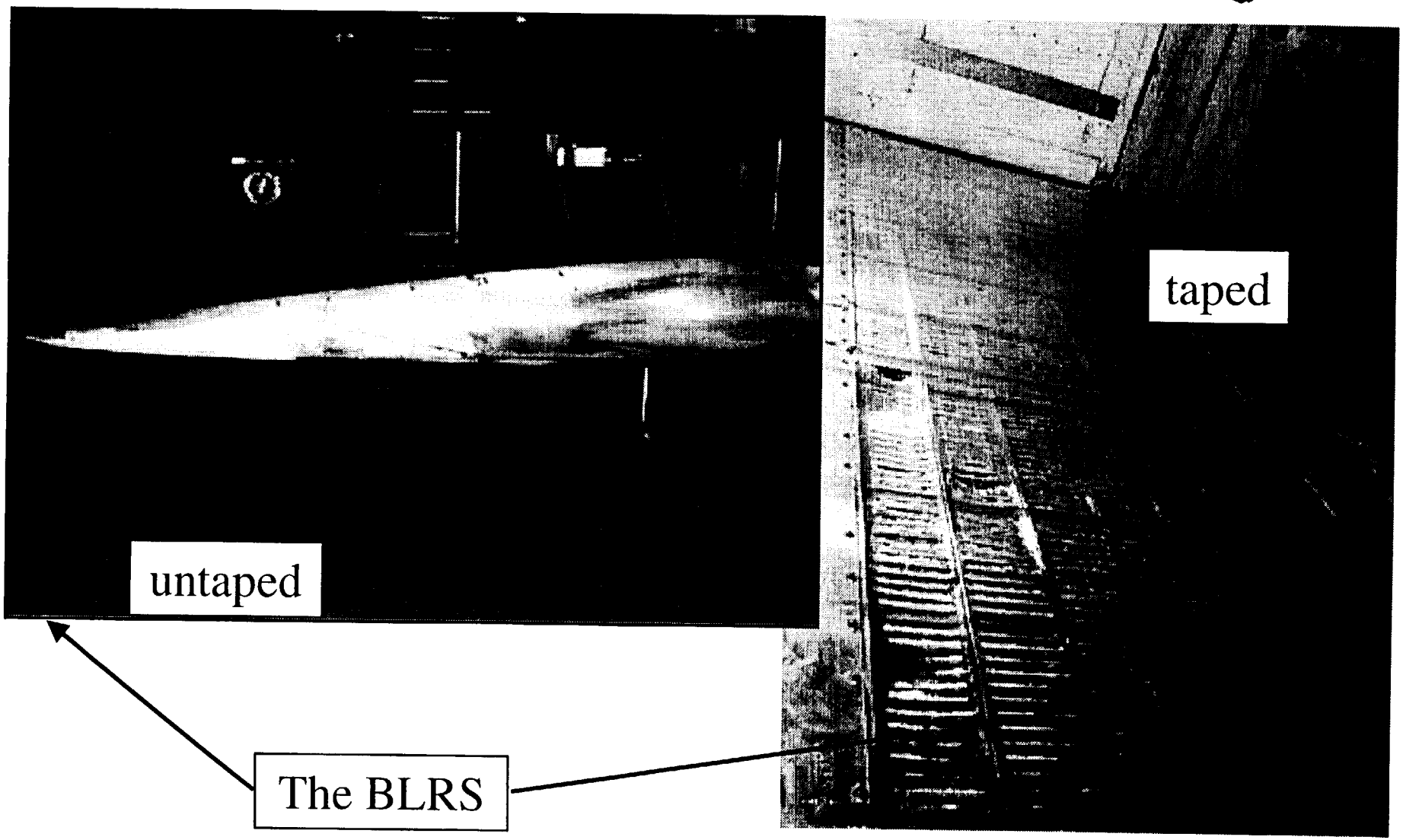

The BLRS

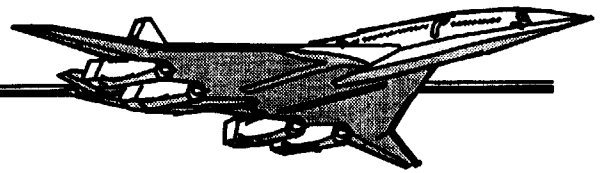

The BLRS resulted in an upwash at the model of .08°. While interesting, this result was not applied to the data in the form of a correction. A detailed tunnel calibration would be necessary to truly understand the impact of these results. It is possible that this effect is only seen with models that extend near the BLRS. Additionally, it is also possible that this BLRS effect is a function of airplane pressure field (configuration).

The results were passed over to the 14'x22' facility for further possible study.

The BLRS

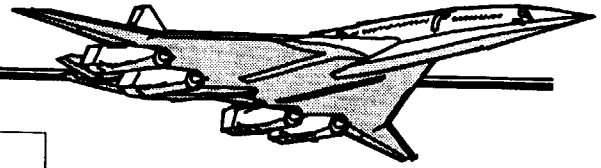

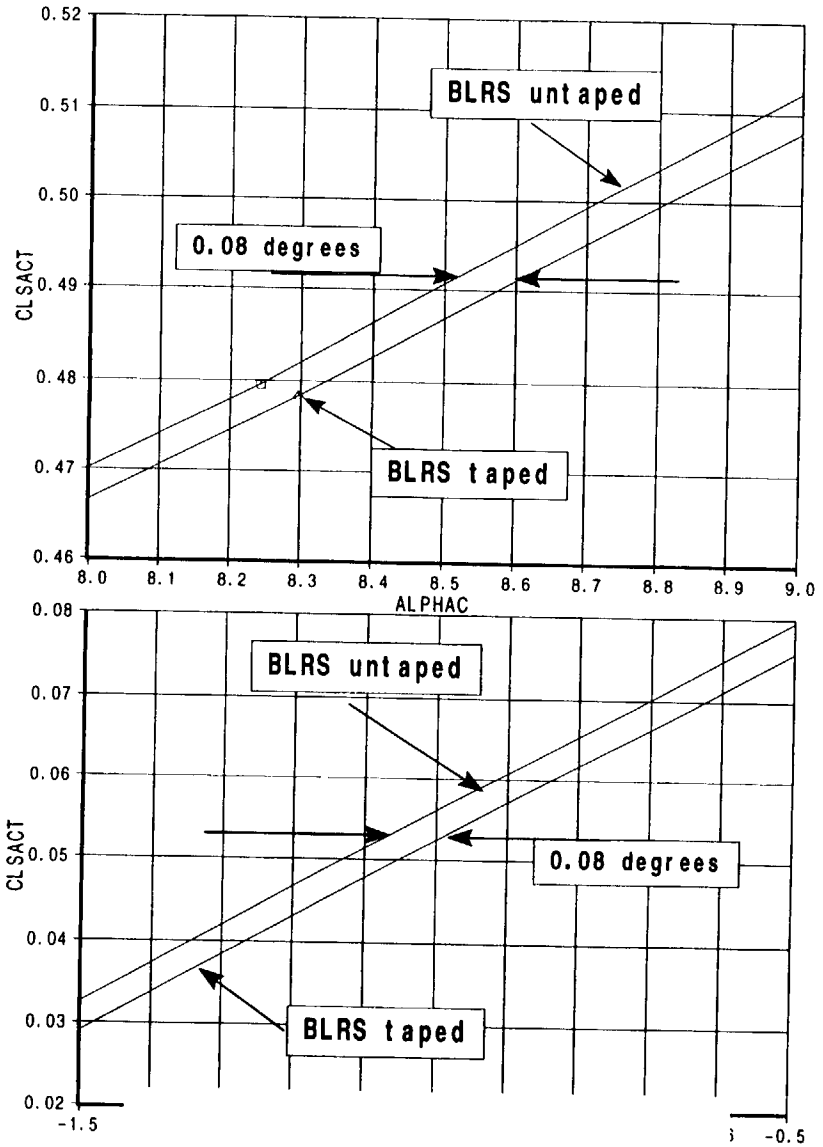
0.52
0.51
0.50
0.49
0.48
0.47
0.46
CLSACT
BLRS untaped
0.08 degrees
BLRS taped
8.0
8.1
8.2
8.3
8.4
8.5
8.6
8.7
8.8
8.9
9.0
ALPHAC
0.08
0.07
0.06
0.05
0.04
0.03
0.02
CLSACT
BLRS untaped
0.08 degrees
BLRS taped
-1.5
-0.5

High-lift Results

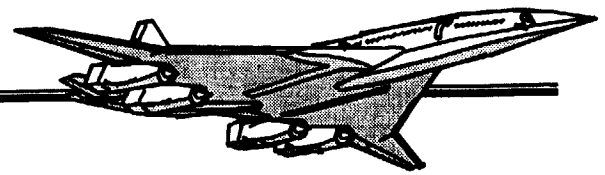

A selected set of high-lift results will be included here.

High-lift Results

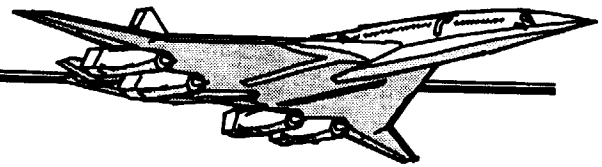

- Selected high-lift results
  - planform effects (lift, drag, buffet)
  - trimming methodology
  - buildup results
  - canard effectiveness
  - compare to CFD results
  - canard tip vortices

Test Progression

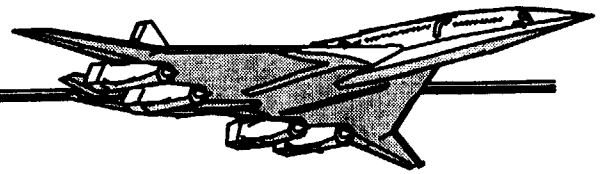

The test progressed in a fairly linear fashion: first, the baseline TCA (W1) was tested to re-establish our within test baseline. Then, as our primary planform, W3 (2.8-38) was tested next. A large matrix of flaps were tested back-to-back (29 total) both for the Common Process buildup database as well as to find our best W3 flap configuration to use for the rest of W3 testing, including S&C and 3-surface. The best flap was determined with the help of an analytical trimming methodology, which was applied to each untrimmed flap tested in-tunnel to determine analytical 3-surface trimming characteristics - specifically, best 3-surface trimmed L/D was compared between each flap configuration, and a winner chosen. This method will be discussed shortly. Care was taken to ensure that the chosen flap did not exhibit undesirable stability characteristics.

Finally, W2 was tested in a similar manner as W3.

Test Progression

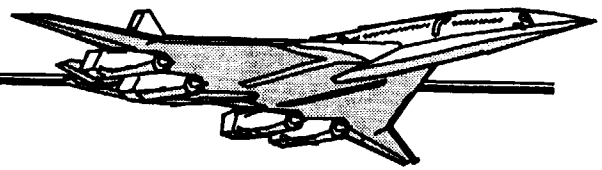

TCA Baseline W1

establish within test baseline

Wing 3 (2.8-38)

Flap matrix (29 flap combinations)

Choose flap

3-surface trimming, S&C, ground effect, flow viz

Wing 2 (2.8-28)

Flap matrix (29 flap combinations)

Choose flap

3-surface trimming, S&C, flow viz

Time

Flap chosen using analytical trimming method for best 3-surface trimmed L/D

Drag Polars

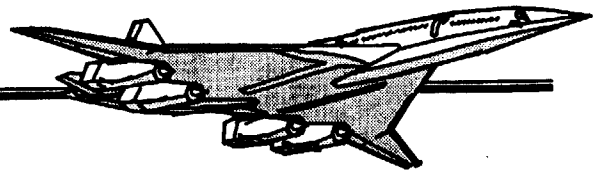

This figure plots both total C_D and $C_{D,P}$ (C_D - ideal induced drag) as a function of C_L. It can be seen that above C_L's of 0.3 in particular, subtracting ideal induced drag from total drag tends to collapse the drag polars. This means that the drag difference between the 3 planforms is due primarily to aspect ratio related induced drag; pressure drag associated with vortex formation and separated flow dominates the flaps up configuration above moderate angles-of-attack.

HSR

TCA-4 High-Lift Test

Drag Polars

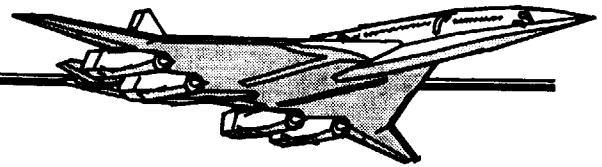

W1, W2 and W3, Flaps Up

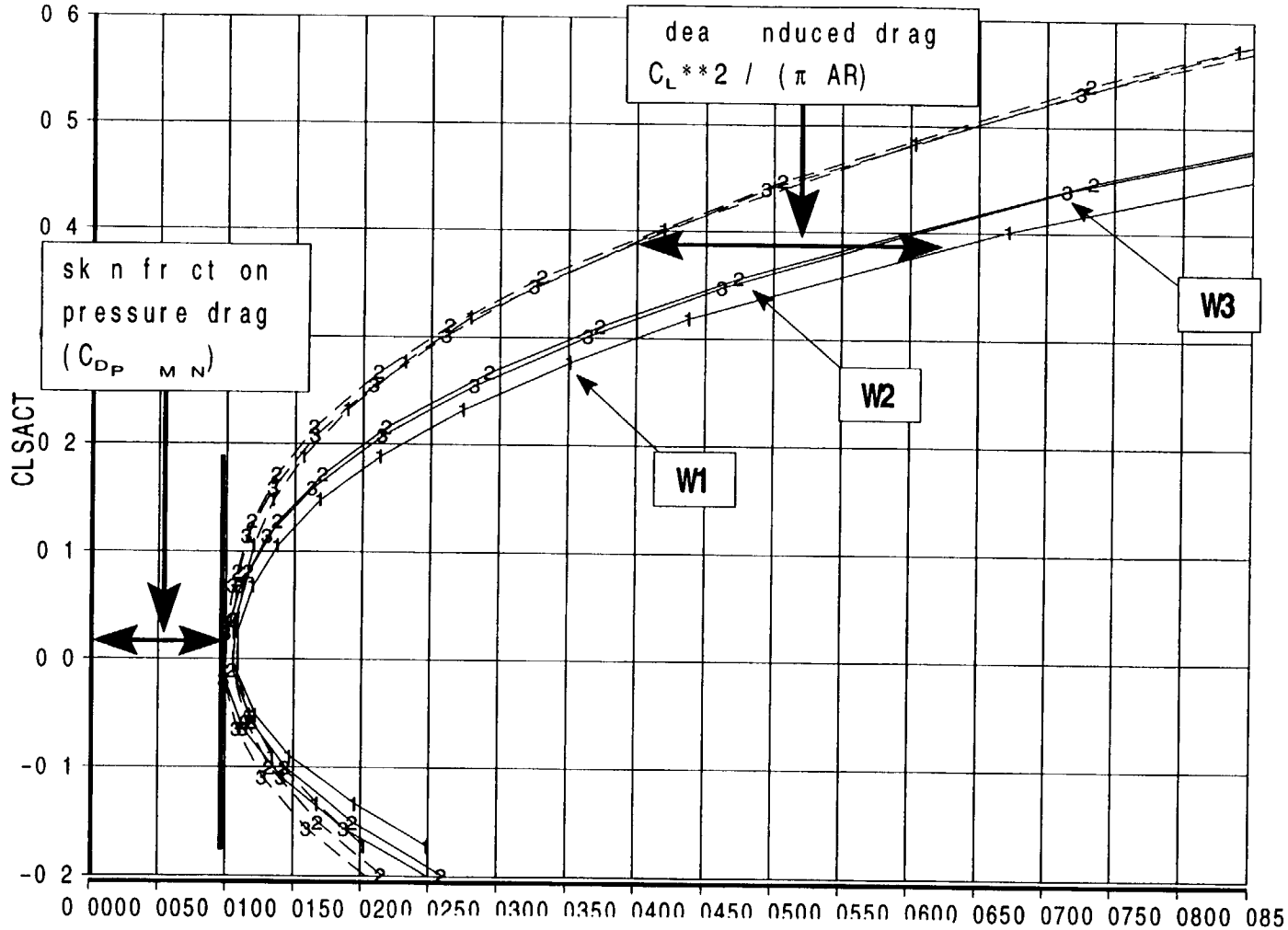

Drag Polars

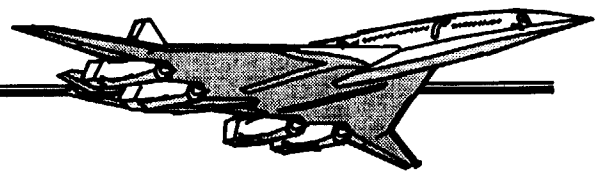

This figure plots both total C_D and $C_{D,P}$ (C_D - ideal induced drag) as a function of C_L. It can be seen that W2 and W3 provide a drag benefit beyond that associated with aspect ratio adjusted ideal induced drag (otherwise, as seen with the flaps up configuration, the $C_{D,P}$ polars for all 3 wings would collapse). There is an additional benefit in the pressure or viscous drag for the flaps down configurations associated with the change in aspect ratio and outboard panel sweep.

Also seen is the room left for aerodynamic improvements at a $C_L = 0.5$ (assuming a 100% span efficiency). Improvements can be gained by optimizing LE deflection (reduce LE separation / vortex formation), optimizing TE deflection (optimize span load) and designing more aerodynamically efficient flaps (for example, sealed slats or variable camber flaps).

Drag Polars

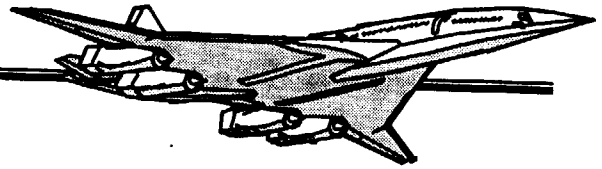

W1, W2 and W3, Climbout Flaps

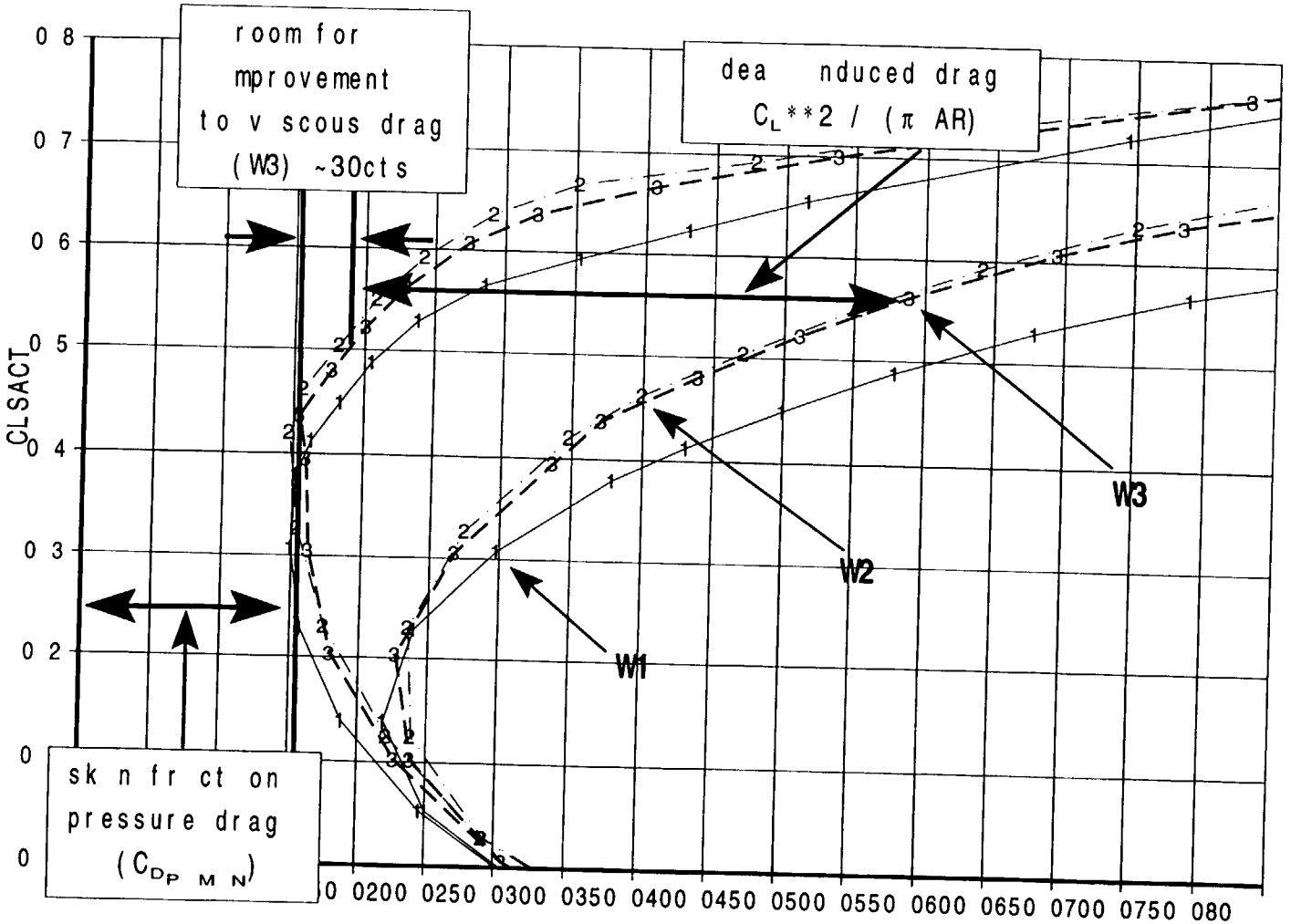

Lift Curves

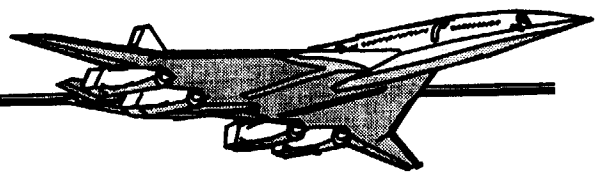

Adjusting W1 lift data from an aspect ratio of 2.027 to 2.8 using simple lifting line theory accounts for most of the difference in the lift curve slopes. The zero lift offset is due primarily to the increased W1 trailing edge flap deflection.

HSR

TCA-4 High-Lift Test

Lift Curves

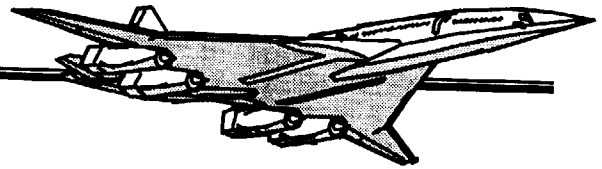

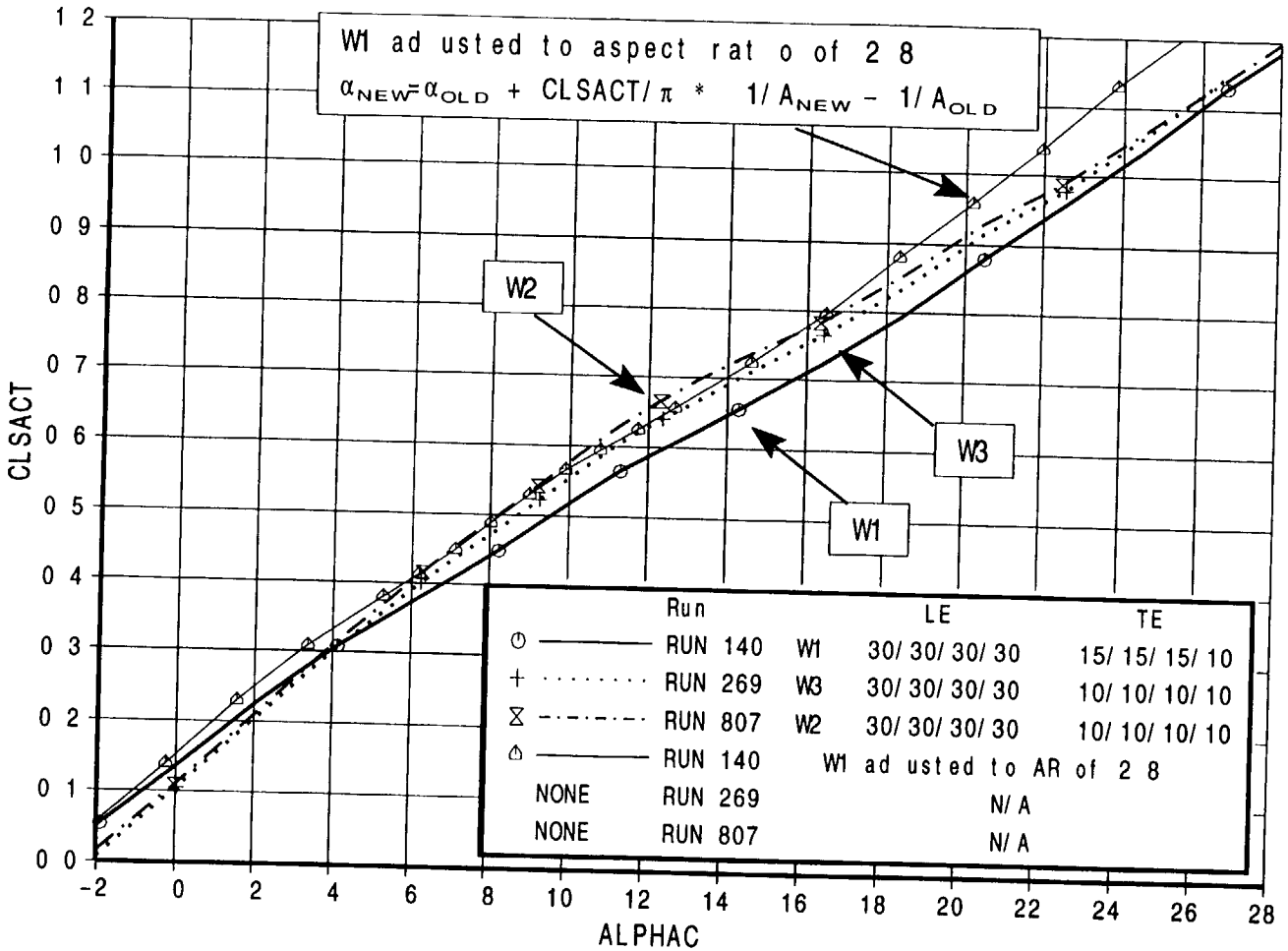

HSR

TCA-4 High-Lift Test

L/D, untrimmed

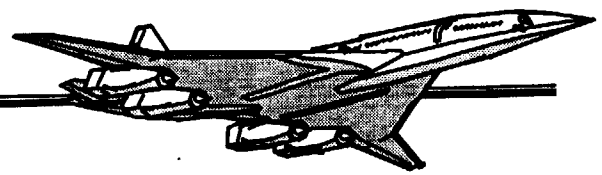

Lift-to-drag curves are shown here for 4 different configurations: the best climbout flap configuration for each wing planform plus one additional for comparative purposes.

W2 was found to have the highest L/D at the design C_L of 0.5 when the inboard LE's were deflected to a constant 30° and outboard LE's at 25° (TE constant 10°). When the W2 outboard LE's were deflected to 30° L/D decreased by 0.3 units. This was most likely due to an over-deflection of the LE flap on the reduced outboard sweep of W2.

HSR

TCA-4 High-Lift Test

L/D, untrimmed

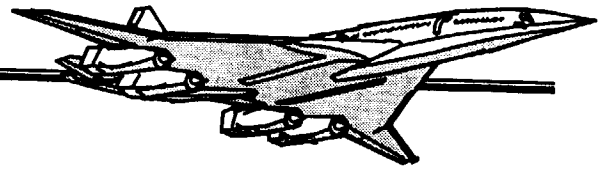

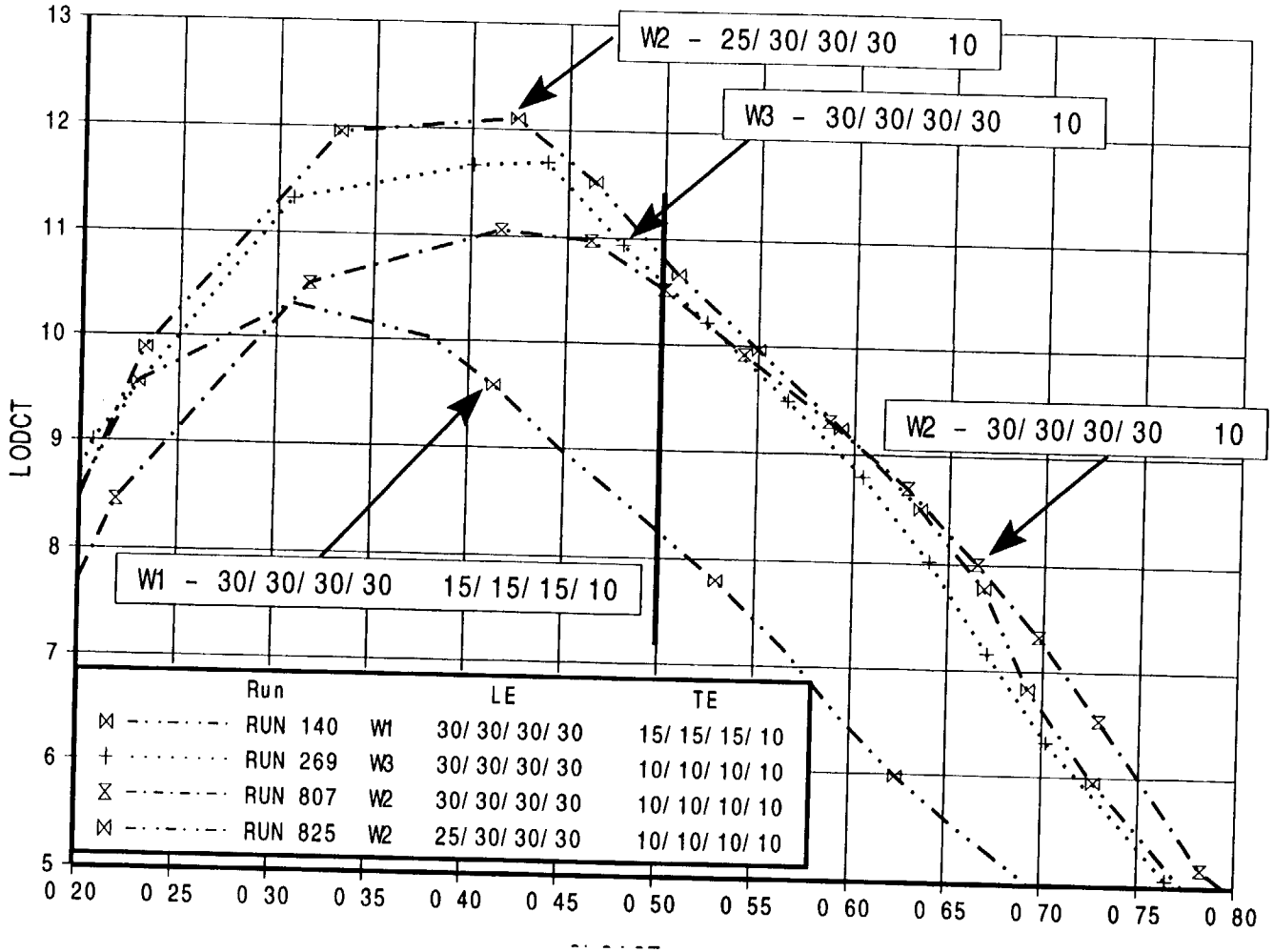

W3 Pressures

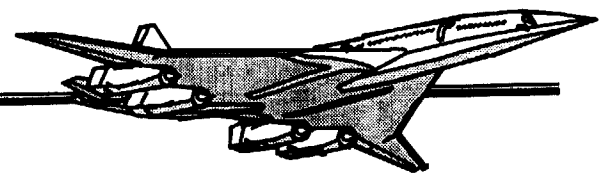

For the 30/10 configuration, W3 outboard leading edges can be seen to be slightly over-deflected at an angle-of-attack of 8 degrees (near the design CL of 0.5) at sections WD and WF, but nearly aligned at section WE.

HSR

TCA-4 High-Lift Test

W3 Pressures

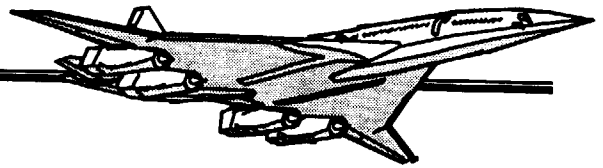

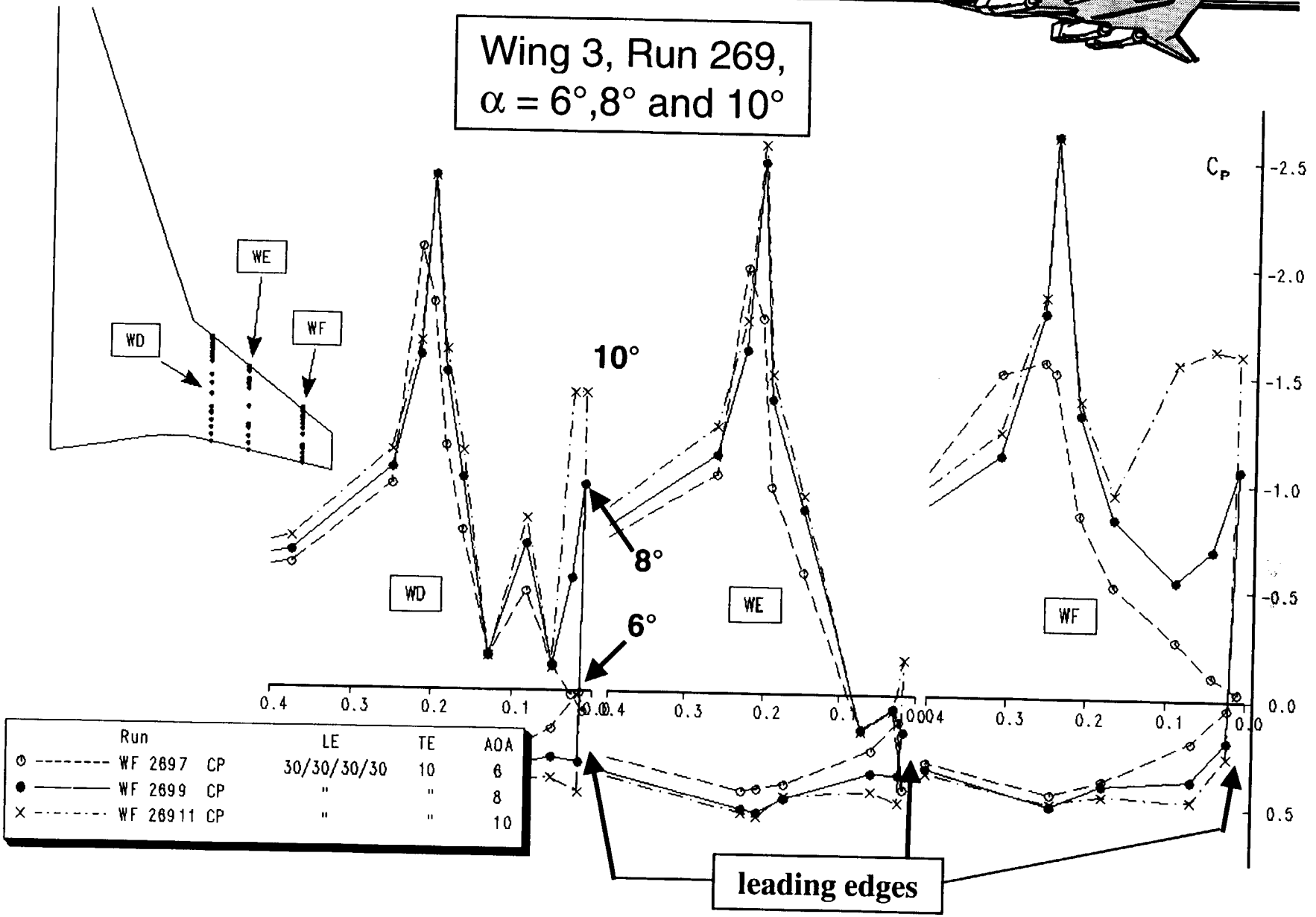

HSR

TCA-4 High-Lift Test

On Surface Flow Viz

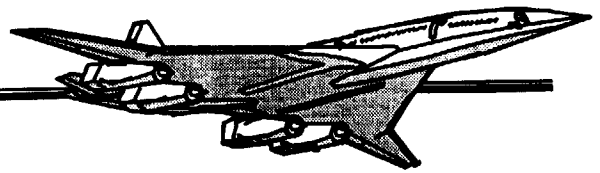

On surface flow characteristics were captured successfully with a mixture of black tempera, mineral oil and oleic acid. The ratio of tempera to mineral oil was determined by trial and error in the tunnel; earlier non-flow viz runs were used to ensure a good mix was available for the dedicated flow visualization runs.

The configuration in the figure below is of the 30/10 W3 flaps. Ten degrees angle-of-attack is about 2 degrees higher than optimum but shown here to more clearly show surface flow characteristics. Leading edge separation, reattachment line on the leading edge flap, hingeline separation and again an attachment line just aft of the hingeline can be clearly seen here.

HSR

TCA-4 High-Lift Test

On Surface Flow Viz

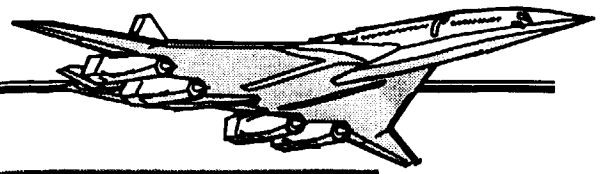

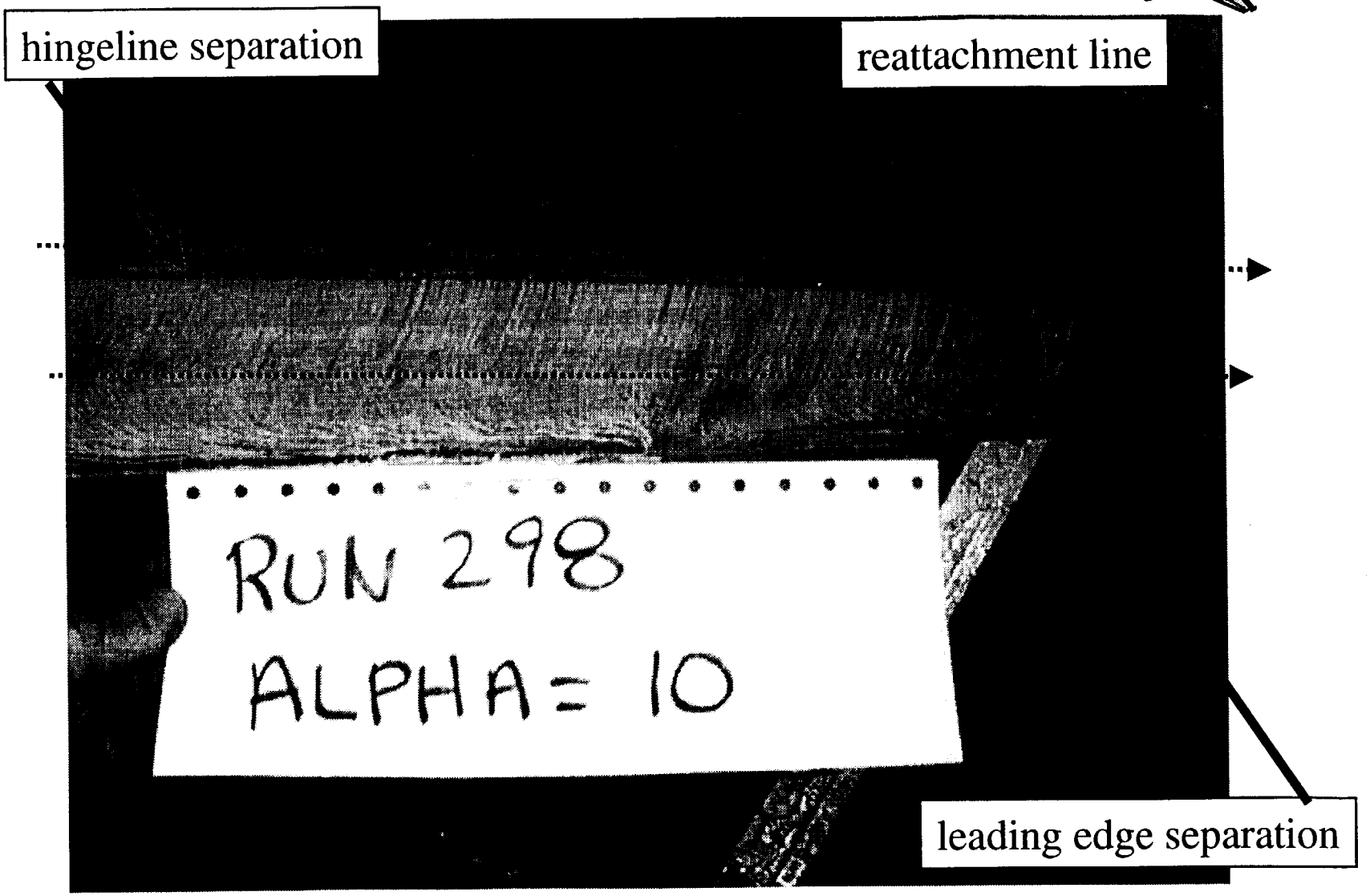

HSR

TCA-4 High-Lift Test

Analytical Trimming Method

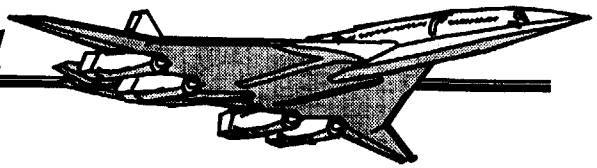

One difficulty in trimming 3-surface configurations is that there are an infinite number of canard and tail loadings which will trim the W/B pitching moment. An analytical method was developed which gives the optimum canard and tail loads. The figure shows tail + trim drag as a function of W/B C_M.

One of the judgment calls necessary during the test was to choose a W/B configuration that would give us the best 3-surface trimmed L/D. Since we did not have wind tunnel data (early on in the test) to buildup a 3-surface configuration, the analytical method was used to calculate the optimum 3-surface trim for each W/B configuration in the flap matrix. The method adds calculated optimum canard drag and pitching moment contributions to the W/B polar and pitching moment then trims any remaining C_M using the horizontal tail with tail polars and downwash extracted from previous wind tunnel data.

The two experimentally determined points shown lie on the analytically derived curves thus validating the analytical method.

Analytical Trimming Method

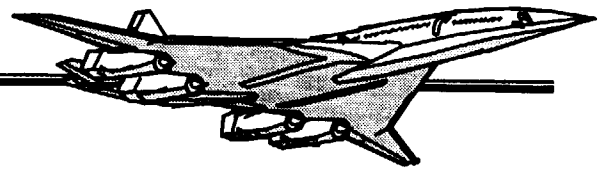

Approximate Optimum Trimming Results - 2.8-38

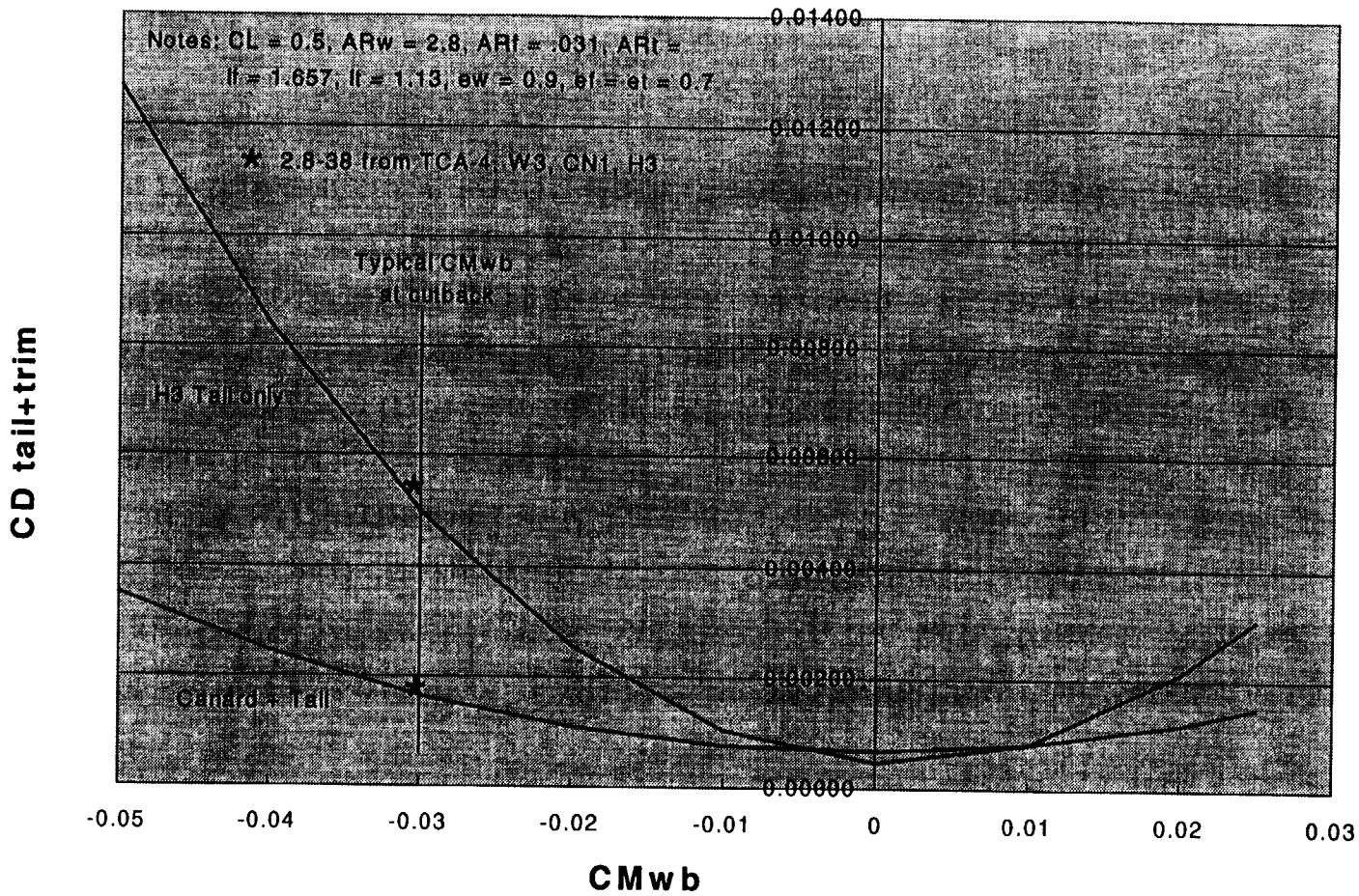

Trimming Methods

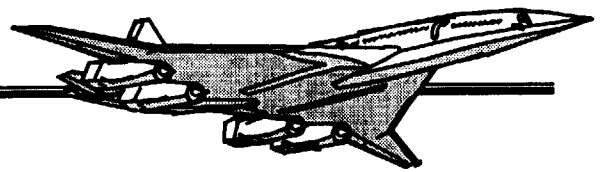

This figure shows the result of applying the analytical trimming method to thirteen W3 wing/body/ flap configurations tested in the wind tunnel. Also on this chart are the untrimmed configurations, one 3-surface configuration (full span LE 30° , full span TE 10°) trimmed in tunnel, and one 2-surface (tail on, canard off) configuration (also full span LE 30° , full span TE 10°) trimmed in tunnel. The in-tunnel 3-surface trim run had a canard incidence of -5°, canard elevator of +15° and was trimmed with the H3 horizontal tail. The 2-surface trim run was trimmed using the same 2/3-size H3 horizontal tail. Since H3 was sized for a 3-surface configuration, this L/D trim level would be expected to increase slightly with H1, but not to the 3-surface level. Both of the in-tunnel trim runs were trimmed at 52% mac.

It can be seen that for the chosen 30/10 flaps for W3, the analytical trimming method predicted the 3-surface trim levels to within .05 units of L/D.

HSR

TCA-4 High-Lift Test

W3 (2.8-38) Various Trimming Methods by Flap Configuration
Trimmed at 52% mac

W3 Flap Configurations

HSR

TCA-4 High-Lift Test

L/D, trimmed in tunnel

2-surface, 3-surface as function of CG

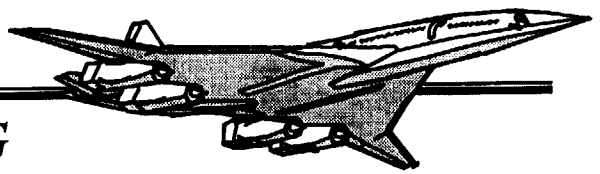

The figure below shows in-tunnel trimmed L/D as a function of airplane CG, from 45% to 55% mac, for both W2 and W3. Flap configurations were those determined during the test to be the best for climbout.

W2 and W3 were trimmed in the 3-surface configuration using both the canard and the H3 tail. W2 and W3 were also trimmed in the 2-surface configuration using the H3 tail. Both W2 and W3 achieved their highest trimmed L/D points when trimming with H3 at a fixed canard incidence of -5° and canard elevator of +15°. Since 52% mac is near the airplane neutral point, it is not unexpected that the best trim condition would happen at this CG. This was seen for all methods of trimming.

HSR

TCA-4 High-Lift Test

L/D, trimmed in tunnel

2-surface, 3-surface as function of CG

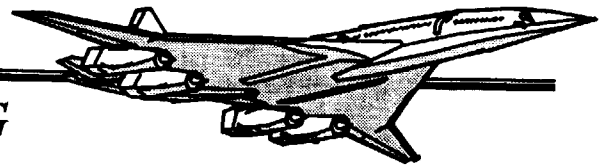

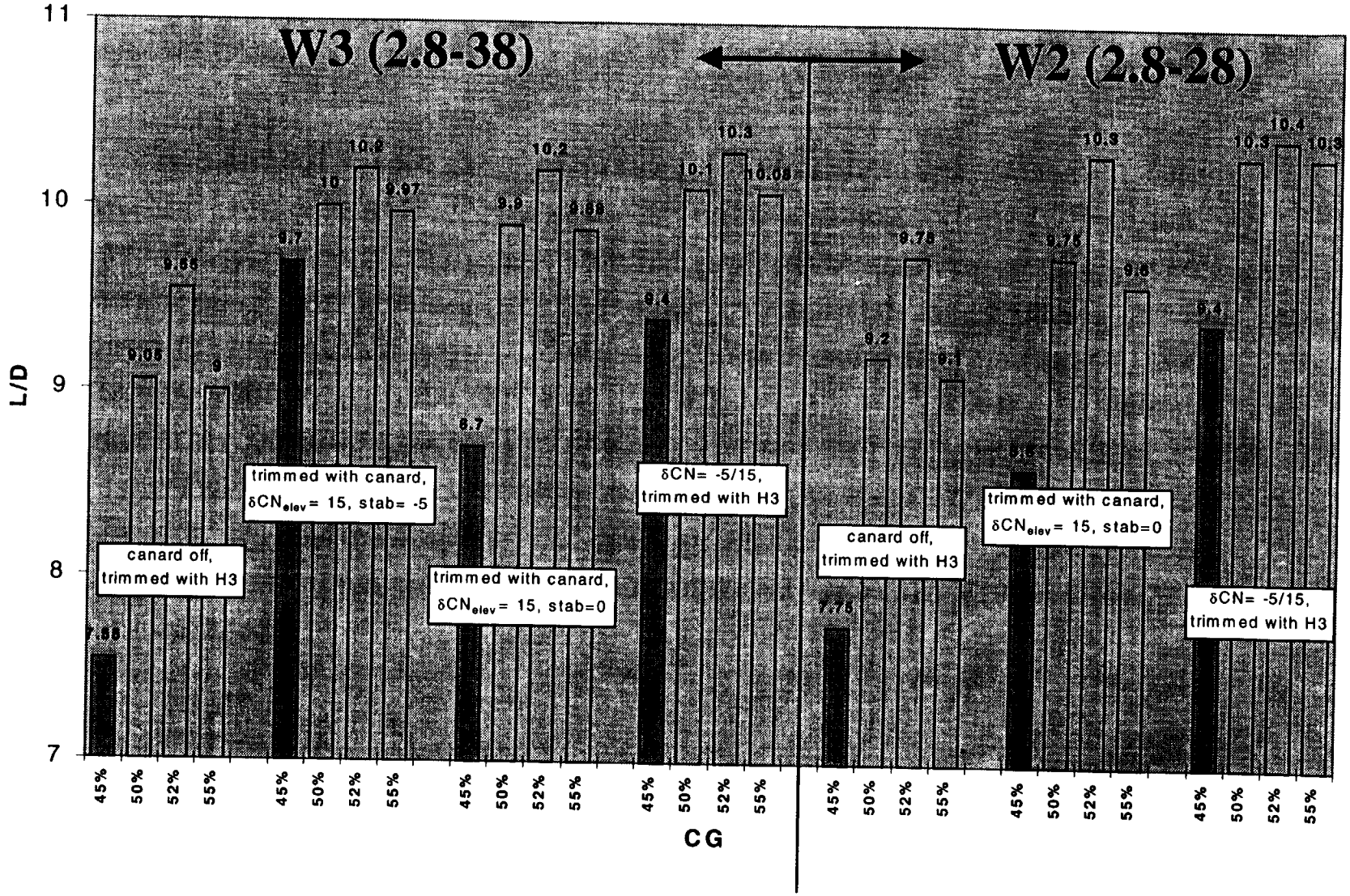

Build-Up Results

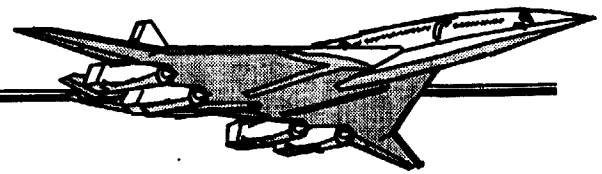

Using the Common Process buildup methodology, W3 performance levels (14'x22' Re) were predicted pre-test. Buildups were done using both W1 (TCA) and RefH as wind tunnel base data. This chart shows the difference between Common Process predicted C_D values and TCA-4 measured values for W3 with 30/10 flaps. C_L's of 0.3, 0.5 and 0.7 are shown. Ideally, if the buildups are perfect, the vertical bars would be lines (bars with zero height) sitting on 0. This was not the case. The TCA buildup was closer in level to W3 than the RefH by a significant amount, but still underpredicted W3 levels by 35 drag counts at a C_L of 0.5. Trailing edge flap deflections larger than 10° (not shown here) were even further off of experimentally measured values.

HSR

TCA-4 High-Lift Test

Build-Up Results

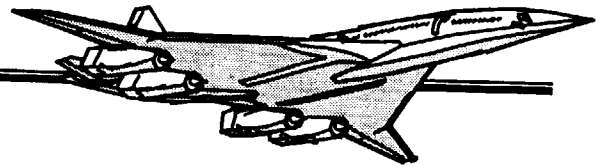

C_D Build-up to Wing 3 (2.8-38) - 3-sfc, trimmed, Comparing the use of W1 and RefH as base data

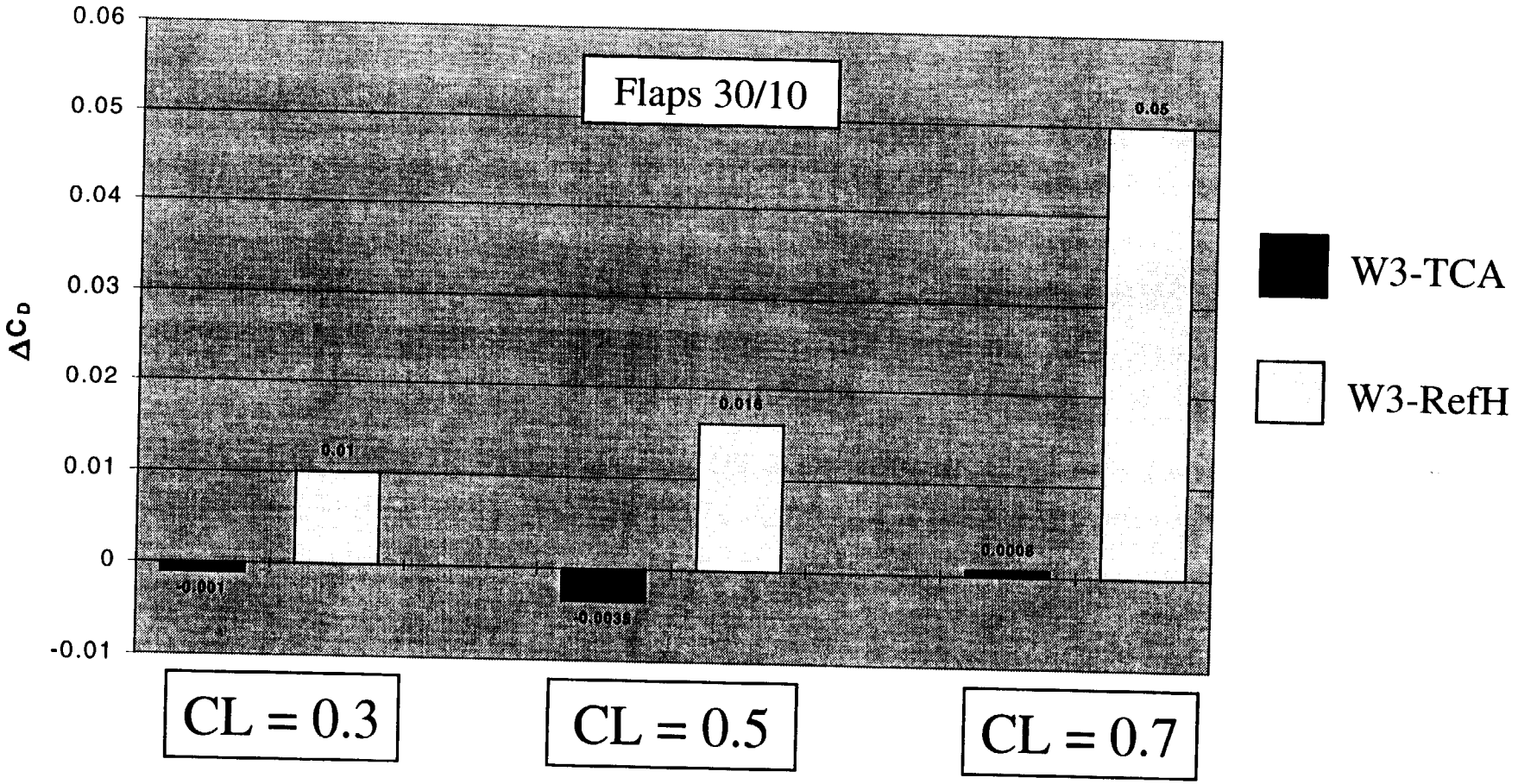

Wing Buffet Results

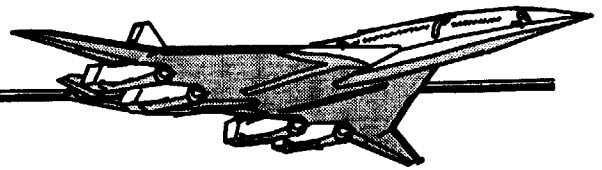

Two strain gage bridges were installed on the model wings with the objective of measuring the effect of planform and flap configuration on wing buffet onset.

Buffet onset was seen to be dependent on planform, flaps up, as seen in the first figure below. However, the flaps up trend is not well understood.

Buffet onset was seen to be delayed as a function of decreasing outboard sweep. Additionally, onset was delayed beyond the climbout C_L of 0.5 for all three wings.

Buffet onset was seen to occur prior to the stall recovery C_L of 0.9 for W2 and W3. Further study of this condition may be warranted.

HSR

TCA-4 High-Lift Test

Wing Buffet Results

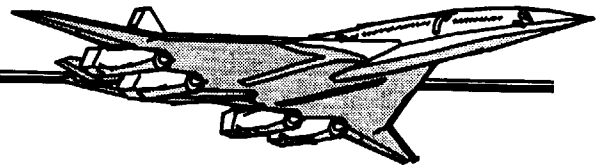

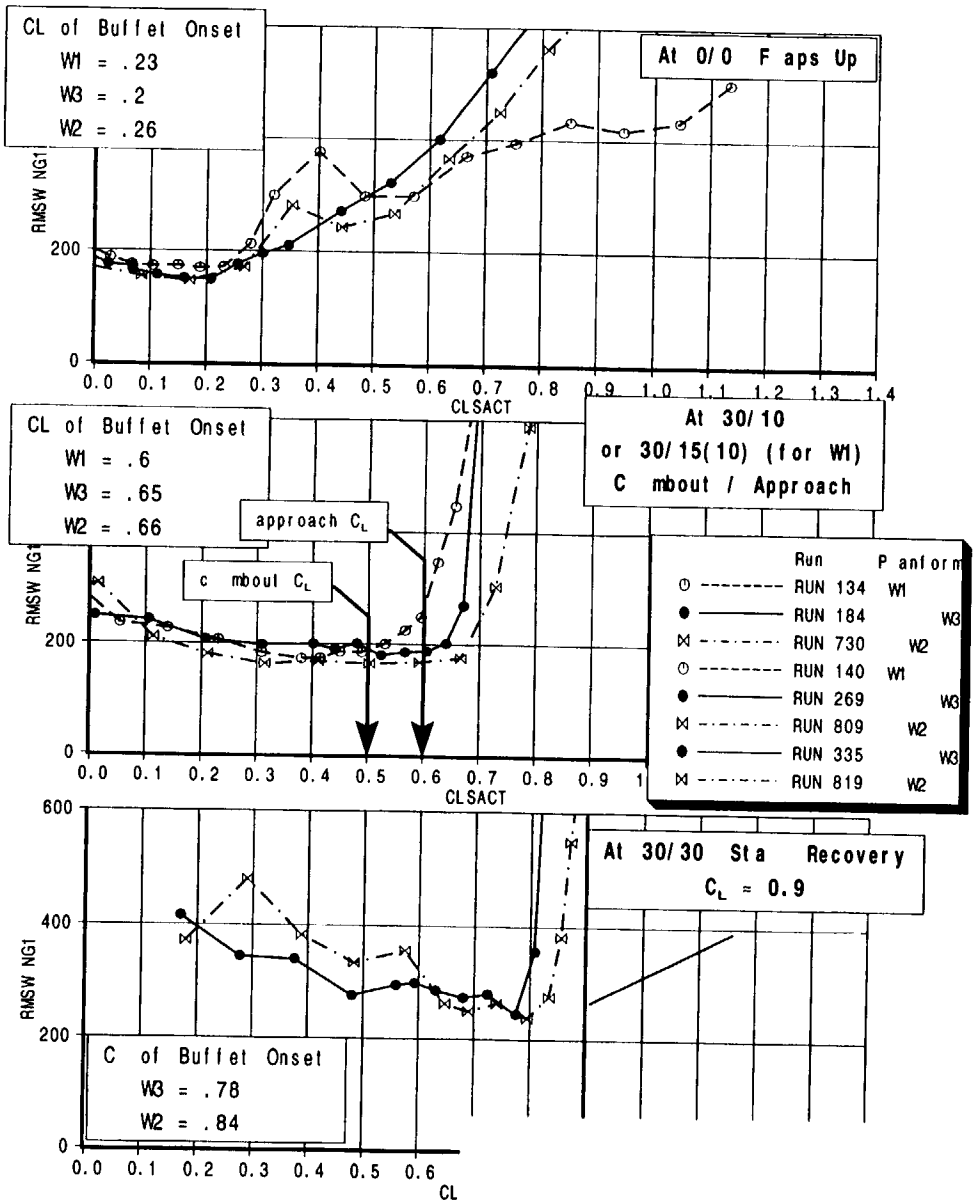

Horizontal Tail Off,

Canard Off

Gear Off

HSR

TCA-4 High-Lift Test

CFD - Wind Tunnel

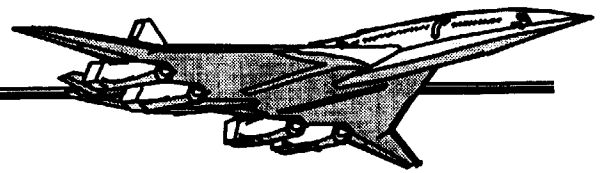

This figure the shows the lift comparison between CFL3D, TLNS and 14x22 wind tunnel data. The wind tunnel data is from TCA-4 (NASA473) with nacelles and tail off, and is fully corrected. The CFL3D data includes runs at 10° angle-of-attack using both a C-O grid topology and an H-grid topology. The TLNS data includes runs at several angles-of-attack, all using an H-grid topology.

Both CFL3D results show good agreement with the test data, with a negligible effect on lift due to the grid topology. TLNS also matches the test data quite well, with just slightly lower lift at the operating condition (alpha = 10°)

CFD - Wind Tunnel

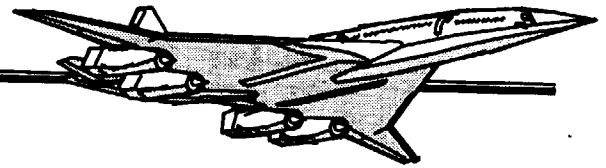

TCA 2.8-38 L30T10
CFL3D vs TLNS vs Test Data
Lift Curves

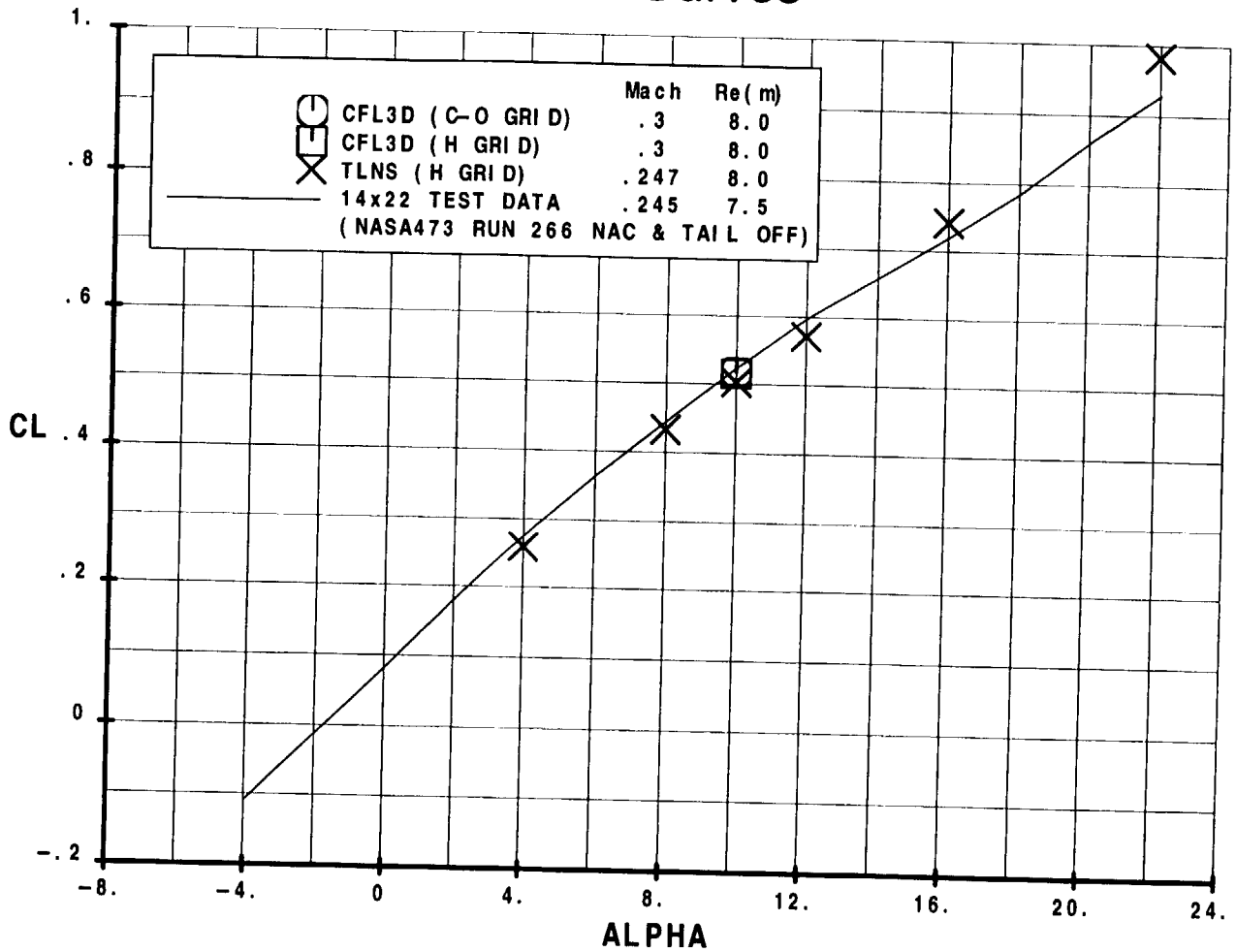

CFD - Wind Tunnel

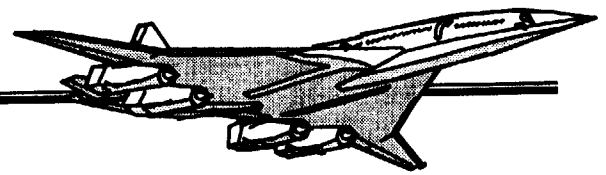

This figure the shows the lift-to-drag ratio comparison between CFL3D, TLNS and 14x22 wind tunnel data. The wind tunnel data is from TCA-4 (NASA473) with nacelles and tail off, and is fully corrected. The CFL3D data includes runs at 10° angle-of-attack using both a C-O grid topology and an H-grid topology. The TLNS data includes runs at several angles-of-attack, all using an H-grid topology.

In the case of L/D, the CFL3D runs again bracket the test data, with the C-O grid having the lower L/D because of the higher drag. The TLNS data falls well below the test data at lower C_Ls, again due to the higher drag, but then matches the test data quite well at the highest C_Ls.

CFD - Wind Tunnel

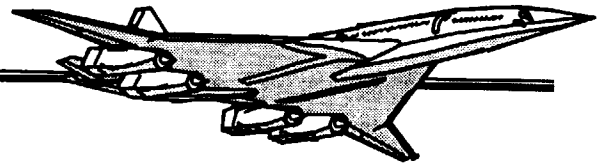

TCA 2.8-38 L30T10
CFL3D vs TLNS vs Test Data
Lift-to-Drag Ratio

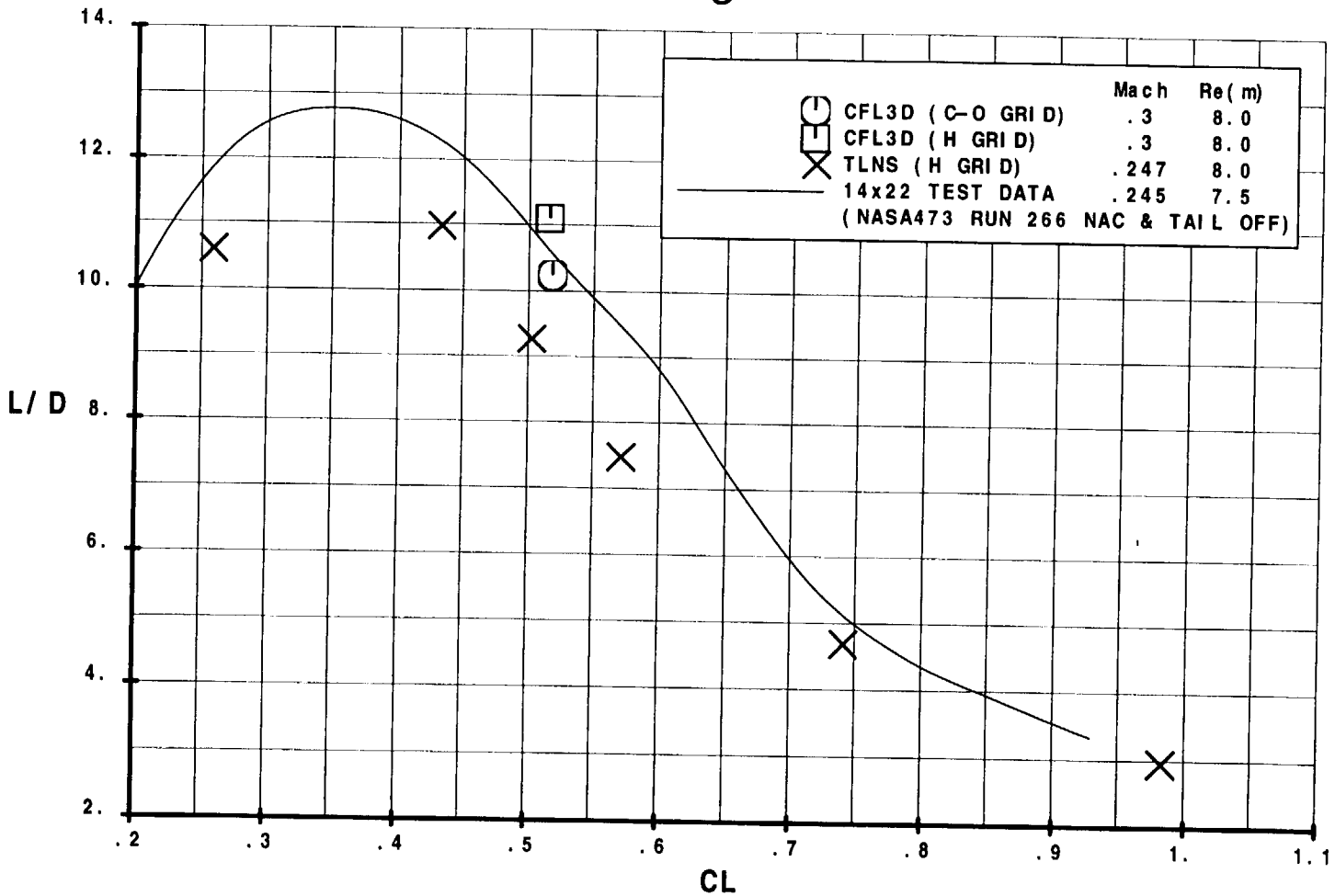

HSR

TCA-4 High-Lift Test

CFD & W/T Flow Patterns

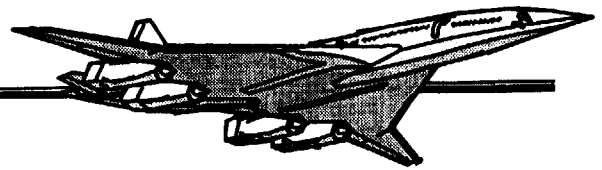

On surface flow patterns are shown by CFD (left) and oil flow (right), both for the TCA 2.8-38 (W3) 30/10 configurations.

HSR

TCA-4 High-Lift Test

CFD & W/T Flow Patterns

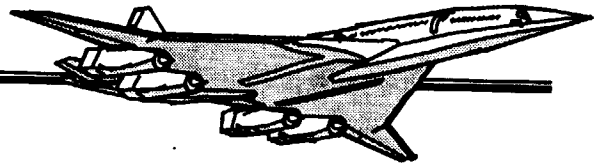

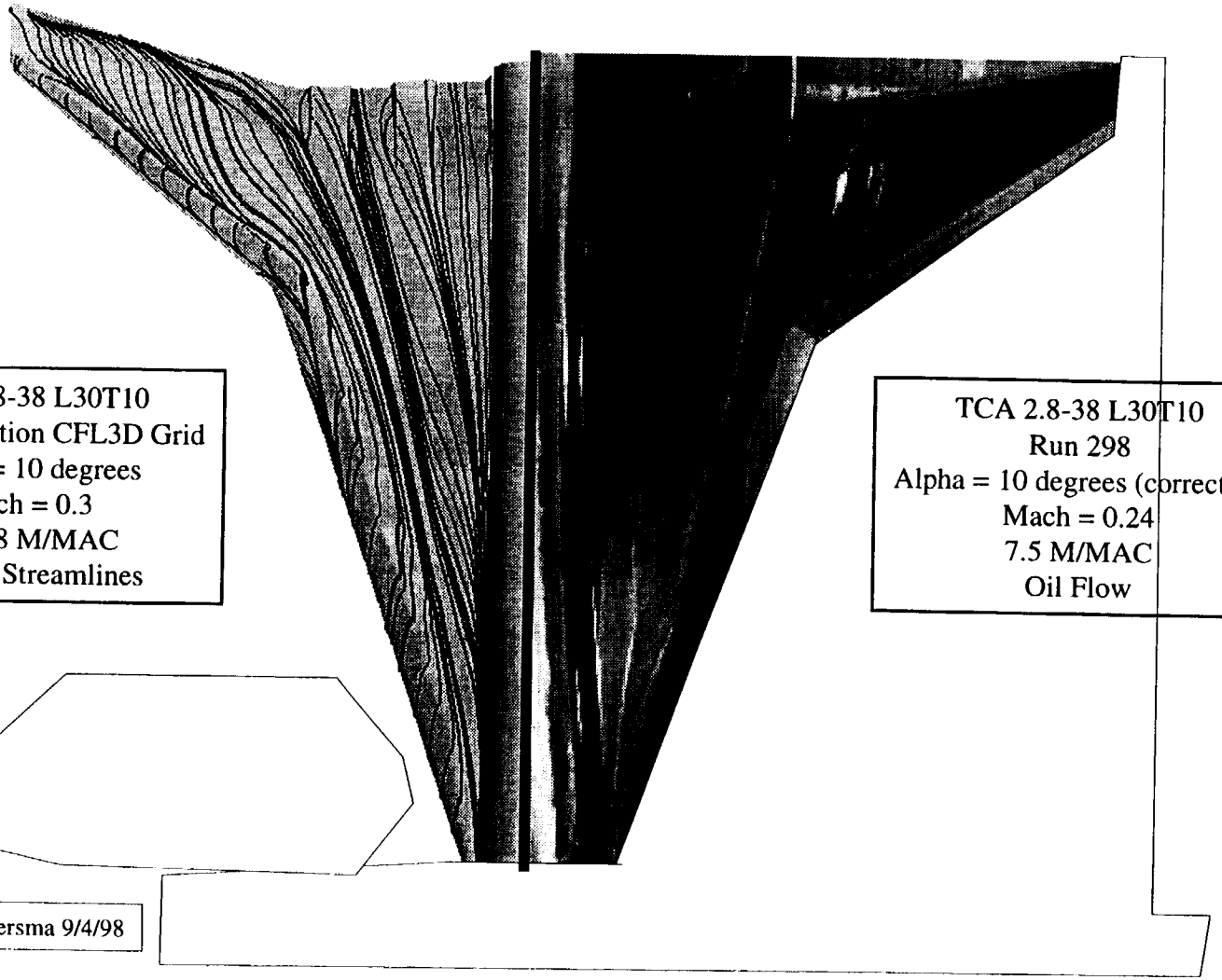

TCA 2.8-38 L30T10
CFL3D Solution CFL3D Grid
Alpha = 10 degrees
Mach = 0.3
Re = 8 M/MAC
Surface Streamlines

TCA 2.8-38 L30T10
Run 298
Alpha = 10 degrees (corrected)
Mach = 0.24
7.5 M/MAC
Oil Flow

Siebersma 9/4/98

Canard Contribution to Lift

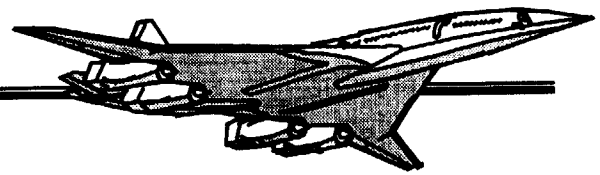

This figure shows a variety of canard / canard elevator deflection combinations, plotting the canard lift contribution against model angle-of-attack. Model configuration is W3, 30/10, tail off.

Note that at moderate airplane angles-of-attack with a positively loaded canard, a resultant loss of lift to the airplane can occur. The canard / wing interaction results in a local reduction of wing upwash inboard.

HSR

TCA-4 High-Lift Test

Canard Contribution to Lift

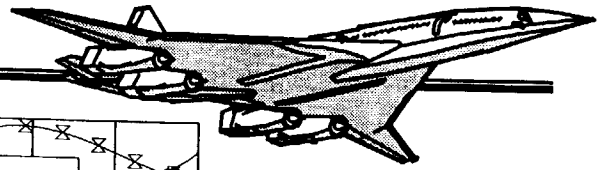

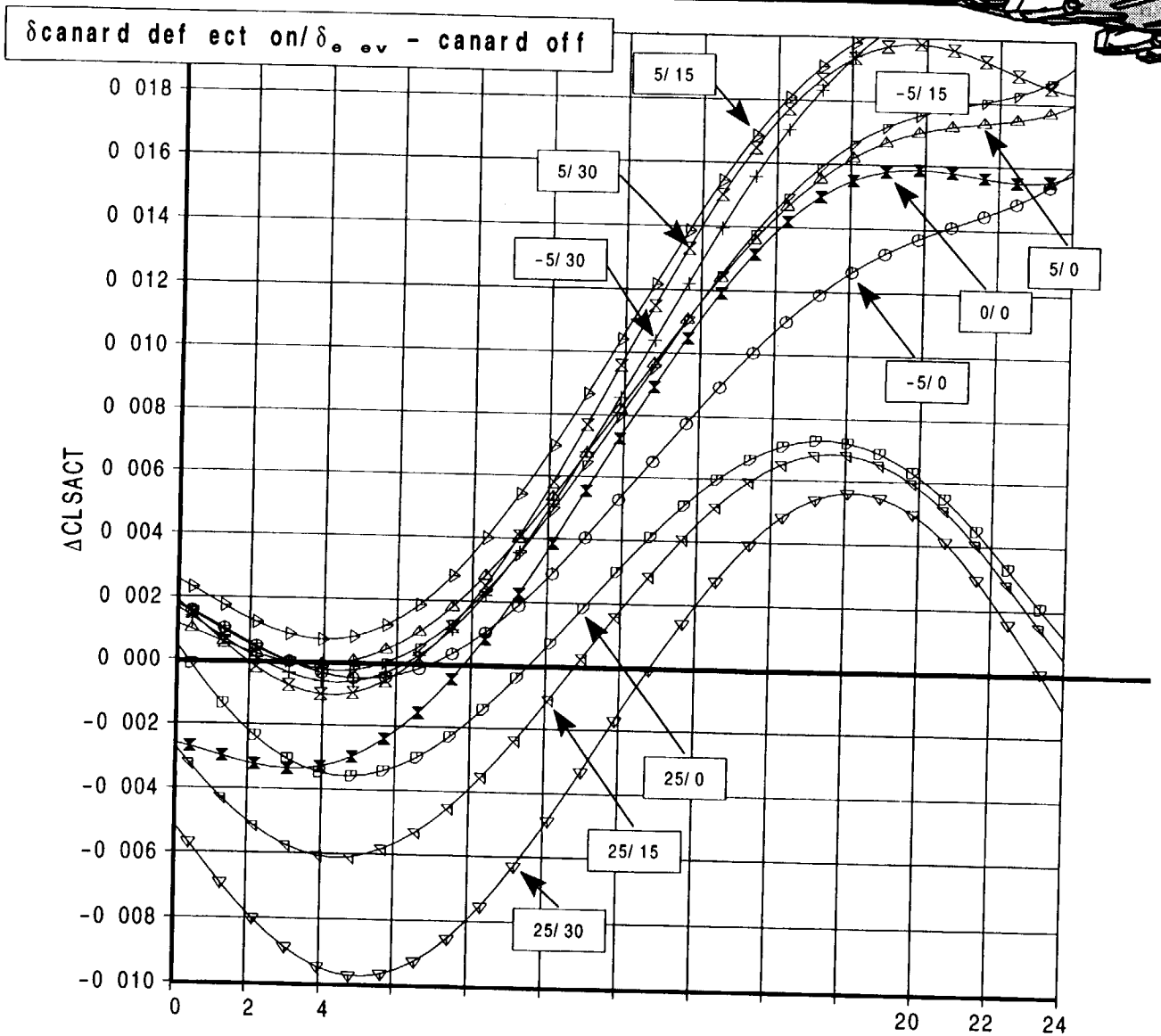

Pink String Technology

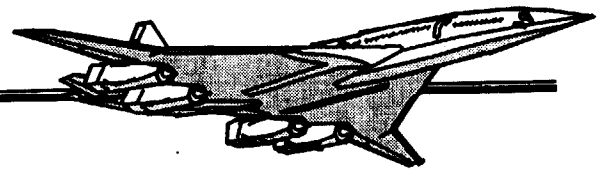

"PST"

A length of string was attached to the canard tip in an attempt to qualitatively determine the downstream location of the canard tip vortices. The method worked quite well. However, the ability of the string to remain within the vortex core was a function of both mass (thickness or weight) and length.

HSR

TCA-4 High-Lift Test

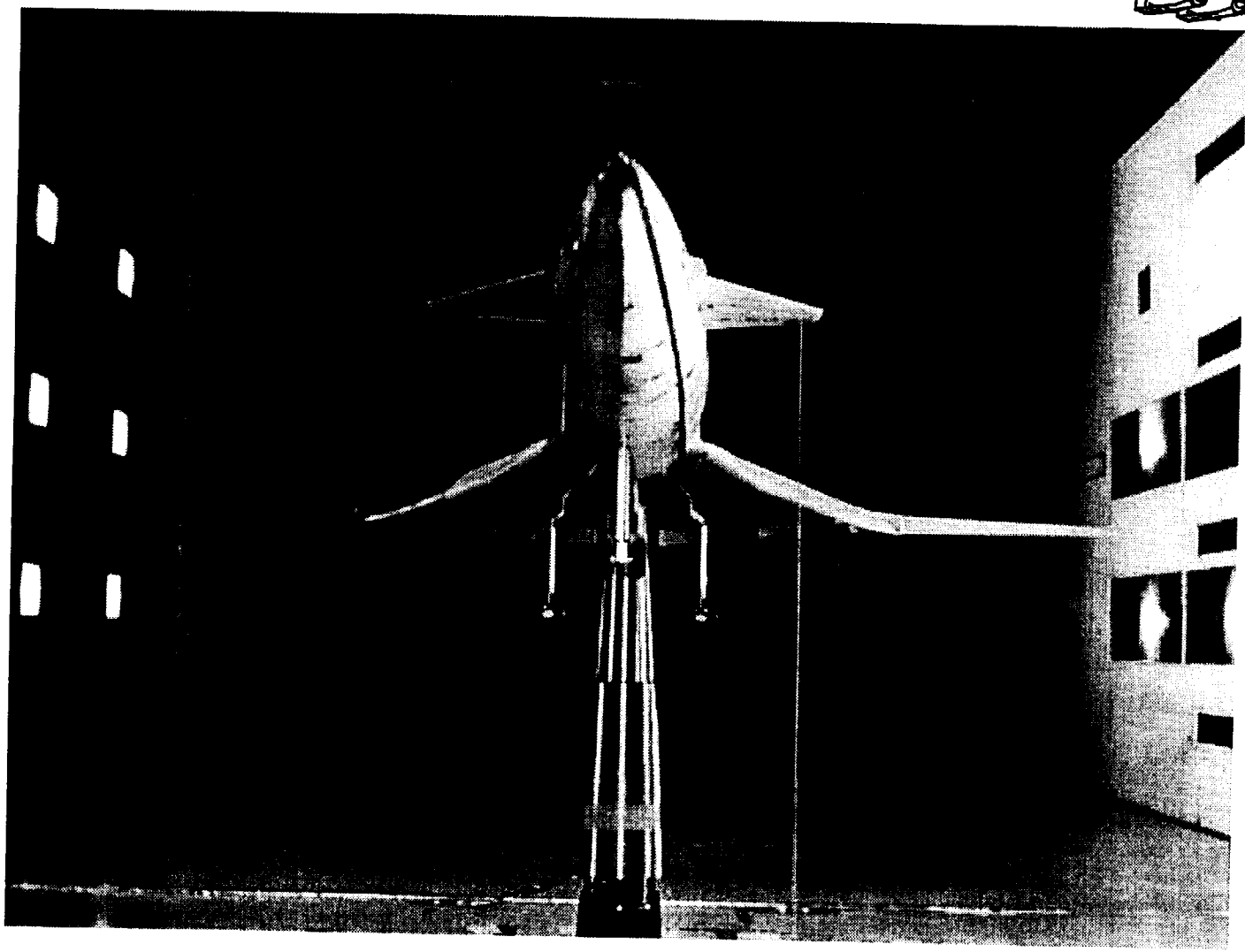

Canard Vortices

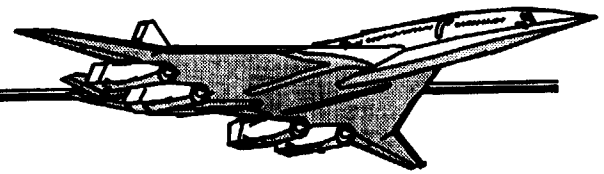

The canard tip vortex (pink string) can be seen entering the inboard nacelle at this low alpha, positively loaded canard operating condition. This will need to be studied further.

HSR

TCA-4 High-Lift Test

Canard Vortices

α = -0.9, β = 0, HGT = 78.3,
Q=85.1, δCN = +5°, δCNelev = 0°

Conclusions (1/2)

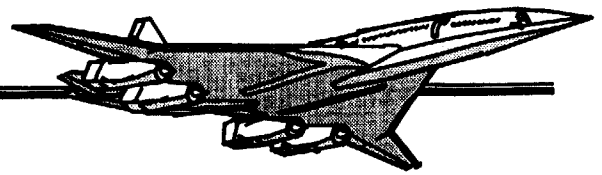

- Within test data repeated very well.
- Tunnel-to-tunnel drag polar differences are likely due to differences in tunnel upflow and unknown tunnel biases.
- As expected, increasing aspect ratio and reducing outboard sweep resulted in L/D improvements.
- A 3-surface configuration results in a higher trimmed L/D than a conventional wing/tail configuration through CG range.

Continued ...

Conclusions - (2/2)

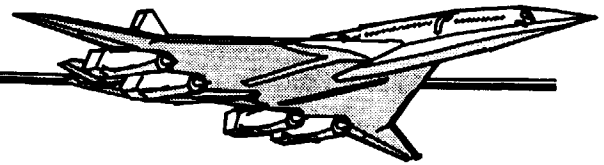

- The analytical optimum trimming method did a good job predicting in-tunnel 3-surface trimming results.
- The Common Process buildup needs improvement to database and analytical tools methodology.
- Buffet measurements indicate onset occurs after climbout and approach regimes, further study is warranted for stall recovery.
- Positive canard loading can result in loss of airplane lift.
- Canard tip vortices appear to be ingested into the inlets at low angles of attack; further study warranted.

HSR

TCA-4 High-Lift Test

Recommendations

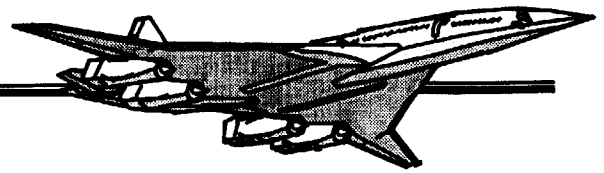

- Buildup process:
  - Panel code not good at predicting large incremental configuration changes, especially relating to viscous effects.
  - Establish and maintain a large experimental database OR
  - Incorporate N-S tools

- Navier-Stokes
  - Utilize N-S tools more for pre-test predictions
  - Further use of N-S tools as diagnostic tool

- Tunnel-to-tunnel
  - If absolute levels are required, detailed tunnel calibrations must be performed; consistent tunnel calibration model

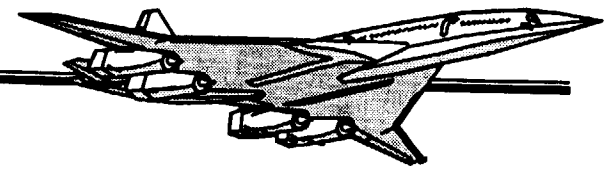

TCA-4 / NASA 473 Test Results

A High-Lift and Stability & Control Test of the HSR 5% Model Including Planform Variations, Canard and 3-Surface Configurations

Michael B. Elzey / Robert C. Griffiths
The Boeing Company

February 9, 1999

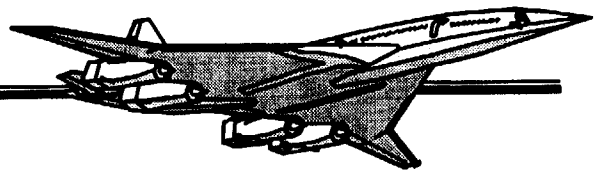

TCA-4 TEST RESULTS
STABILITY & CONTROL

Michael Elzey
February, 1999

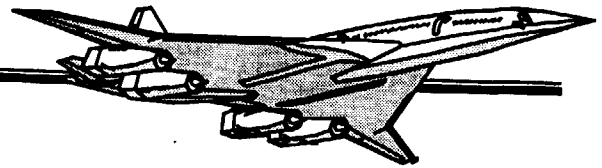

TCA-4 Test Results ~ S&C
Agenda

1. Longitudinal Stability
2. Longitudinal Control
3. Lateral-Directional Stability
4. Lateral-Directional Control
5. Repeatability
6. Conclusions

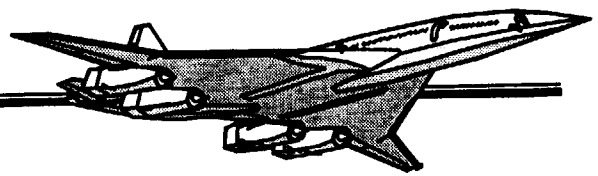

TCA-4 Test Objectives ~ S&C

1. Determine if there are any "showstoppers" for the PTC configuration:
    a. Reduced outboard wing sweep/increased aspect ratio
    b. 3 surface/canard configurations

2. Develop a database to size PTC control surfaces:
    a. Canard and horizontal tail effectiveness
    b. Ground effects

3. Understand the effects of various configuration changes:
    a. Outboard wing sweep and aspect ratio
    b. Leading and/or trailing edge flap deflections
    c. Canard and horizontal tail effectiveness and effects
    d. Chin fin effectiveness
    e. Flaperon effectiveness
    f. Rudder effectiveness

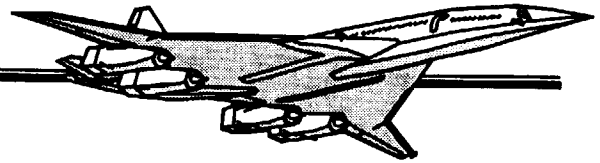

Longitudinal Stability

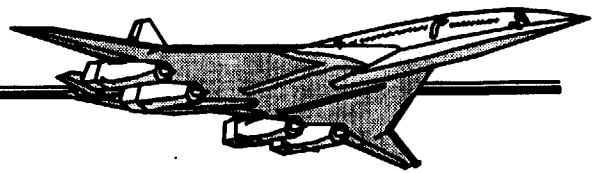

Baseline Longitudinal Characteristics -- Wing W3

Baseline longitudinal characteristics for wing W3 are presented. Canard off and on, horizontal tail off and on data are displayed. Note that the canard is very destabilizing, while the horizontal tail is only mildly stabilizing. These data are for a $\delta_{LE}/\delta_{TE} = 30°/10°$ flap setting in free air.

Longitudinal Stability

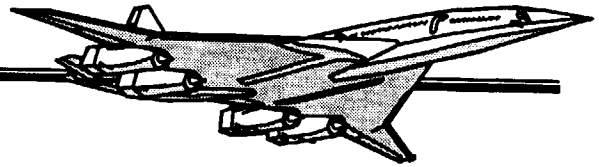

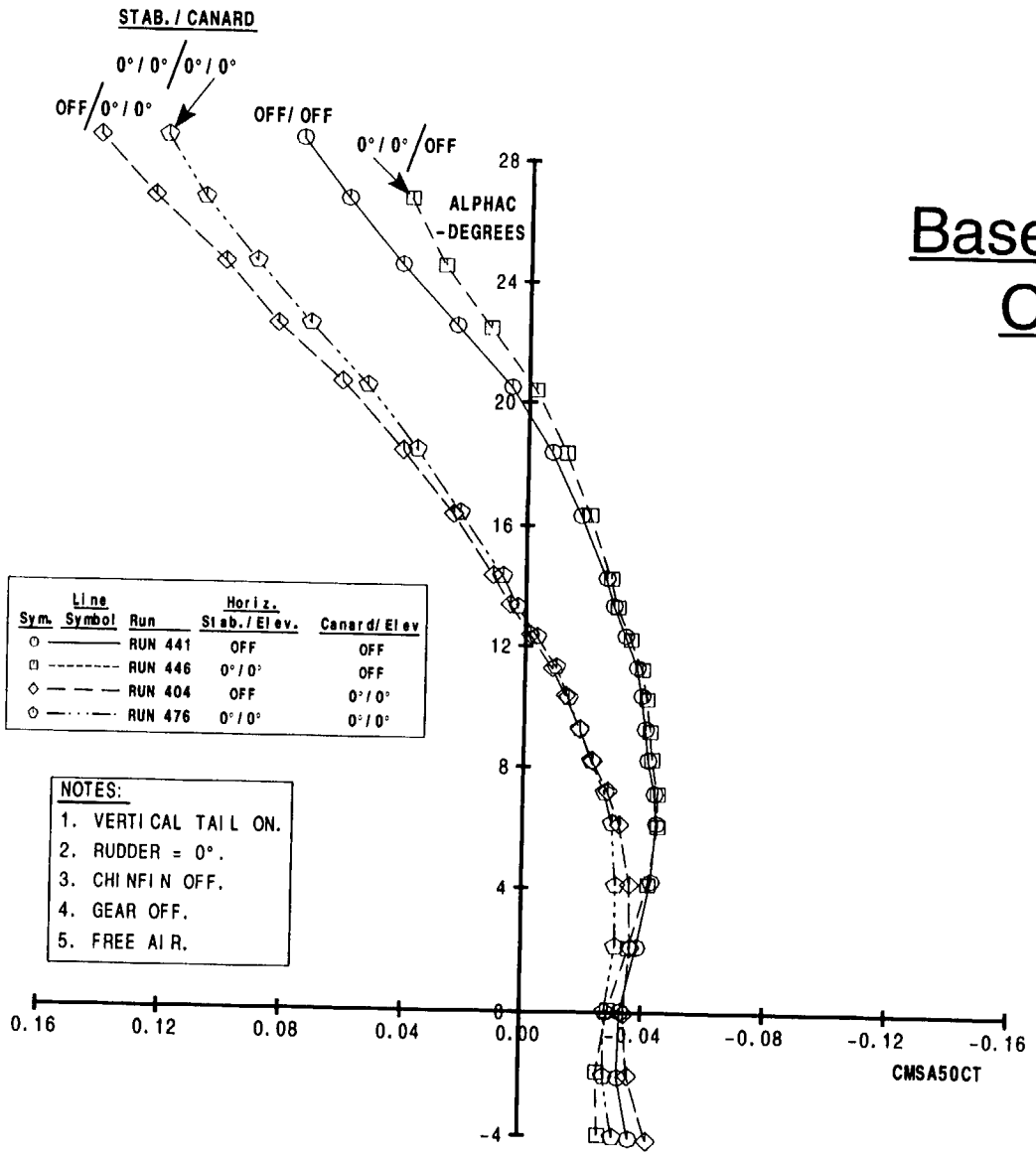

Baseline Longitudinal Characteristics

Wing W3

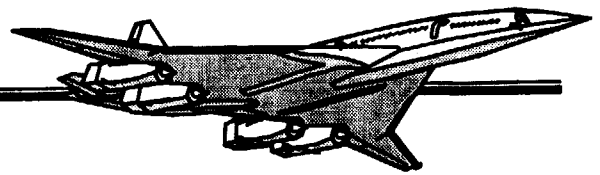

Baseline Longitudinal Characteristics -- Wing W2

Baseline longitudinal characteristics for wing W2 are seen below. The effects of the canard and horizontal tail, as well as the baseline stability and C_{m_o} levels, are shown to be very similar to the wing W3 data displayed on the previous chart. The outboard W2 wing leading edge panel was deflected 25°, rather than the 30° of wing W3.

Longitudinal Stability

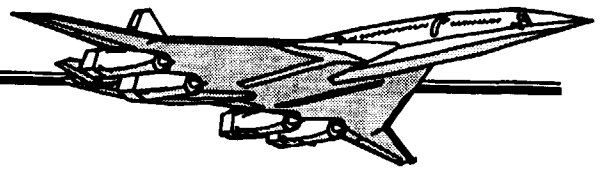

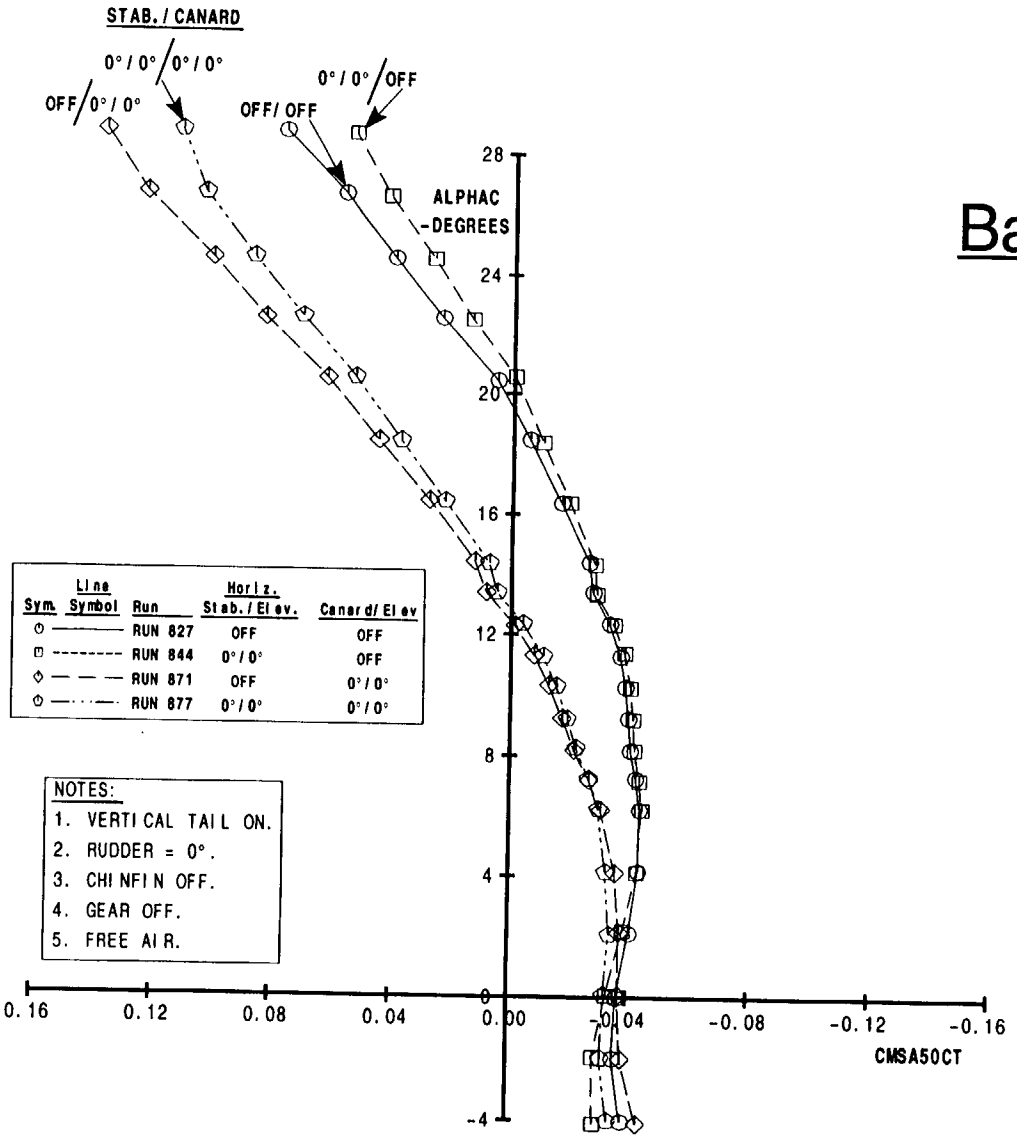

Baseline Longitudinal Characteristics

Wing W2

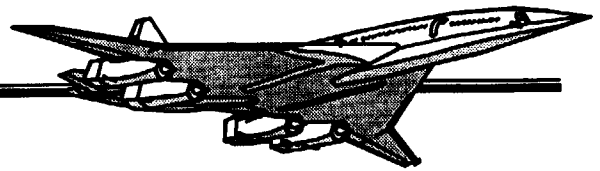

Effect of Outboard Wing Planform

Canard Off/Horizontal Tail Off

Longitudinal data for wings W1, W2 and W3 are compared. Model geometry for the three wings are:

Wing	Aspect Ratio	Outboard Sweep-Deg.	SREF-Ft^2	MAC-In.
W1	2.027	52	21.25	56.972 (TCA Baseline)
W2	2.8	28	22.57	54.323
W3	2.8	38	22.71	54.175

Note that the longitudinal stability and C_{m_o} levels are similar for the three wings.

Longitudinal Stability

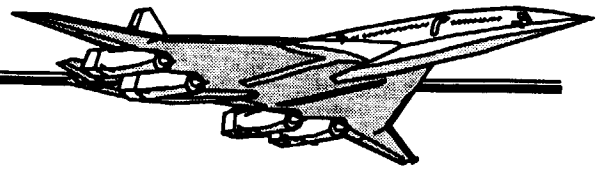

Effect of Outboard Wing Planform

Canard Off/ Horizontal Tail Off

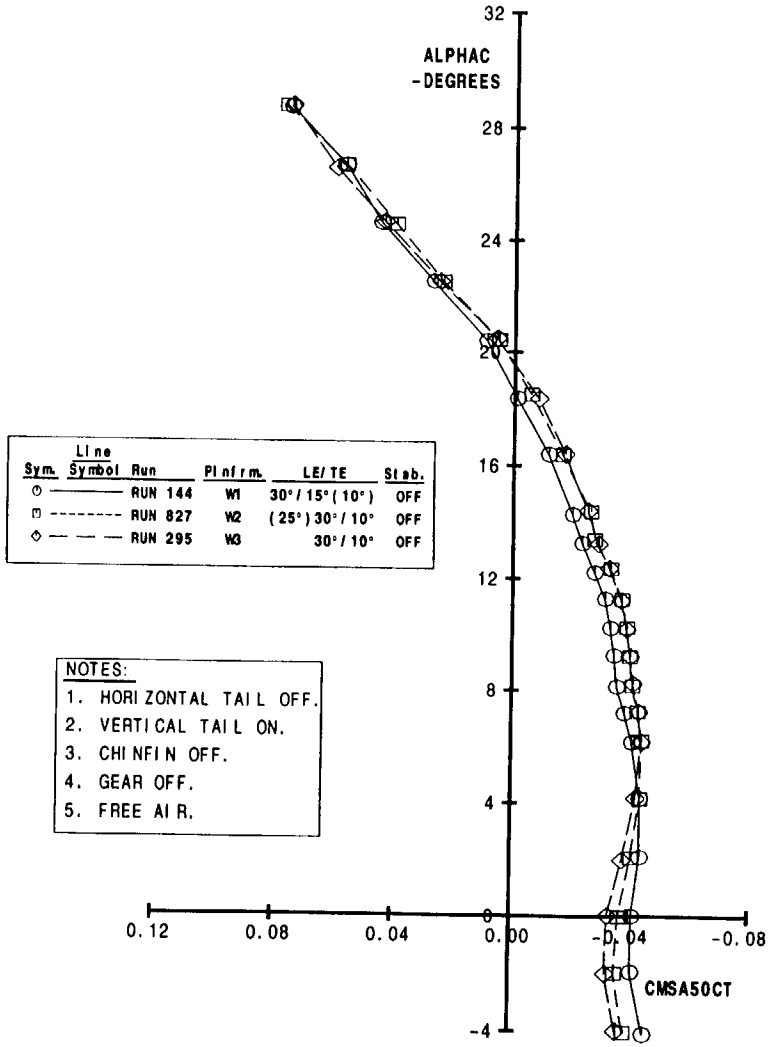

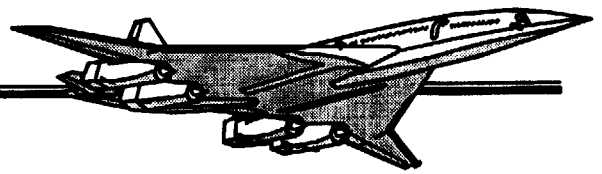

Effect of Outboard Wing Planform
Canard Off/Horizontal Tail On

Longitudinal stability and C_{m_o} characteristics shown with the horizontal tail on are very similar to the the tail off trends shown in the previous chart.

Longitudinal Stability

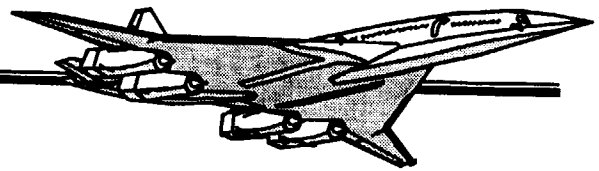

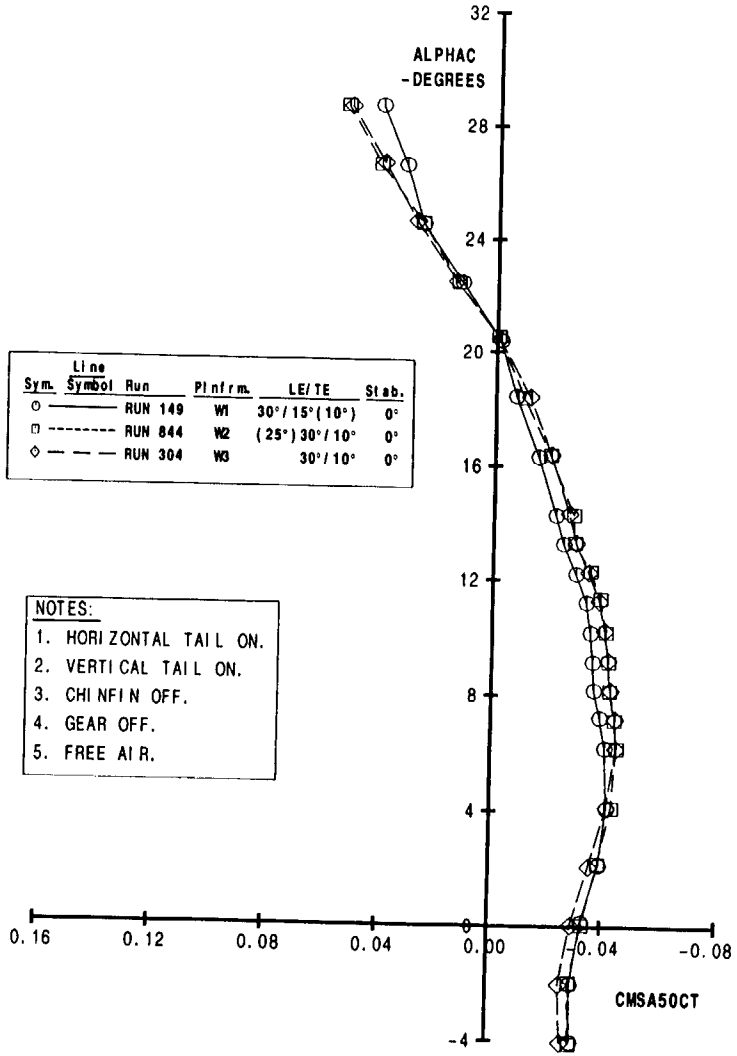

Effect of Outboard Wing Planform

Canard Off/ Horizontal Tail On

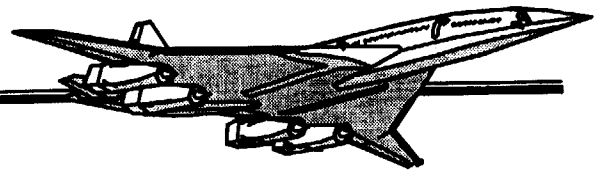

Effect of Trailing Edge Flap Deflection -- L.E. Flaps = 30°

Canard Off/Horizontal Tail On -- Wing W3

These data show the effects of increasing the trailing edge flap deflection on wing W3 from 0° through 30° by 10° increments. The $\Delta C_{m_{FLAP}}$ due to an increase from δ_{FLAP} =20° to δ_{FLAP} = 30° is seen to be approximately half the value seen for lower flap deflections. Also note that the $\Delta C_{m_{FLAP}}$ is significantly reduced for higher angles of attack (α >14°). Similar data were taken for wing W2, with comparable results.

HSR

TCA-4 Stability & Control Test **Longitudinal Stability**

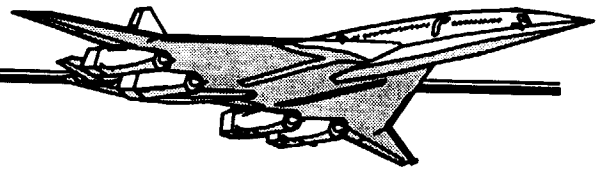

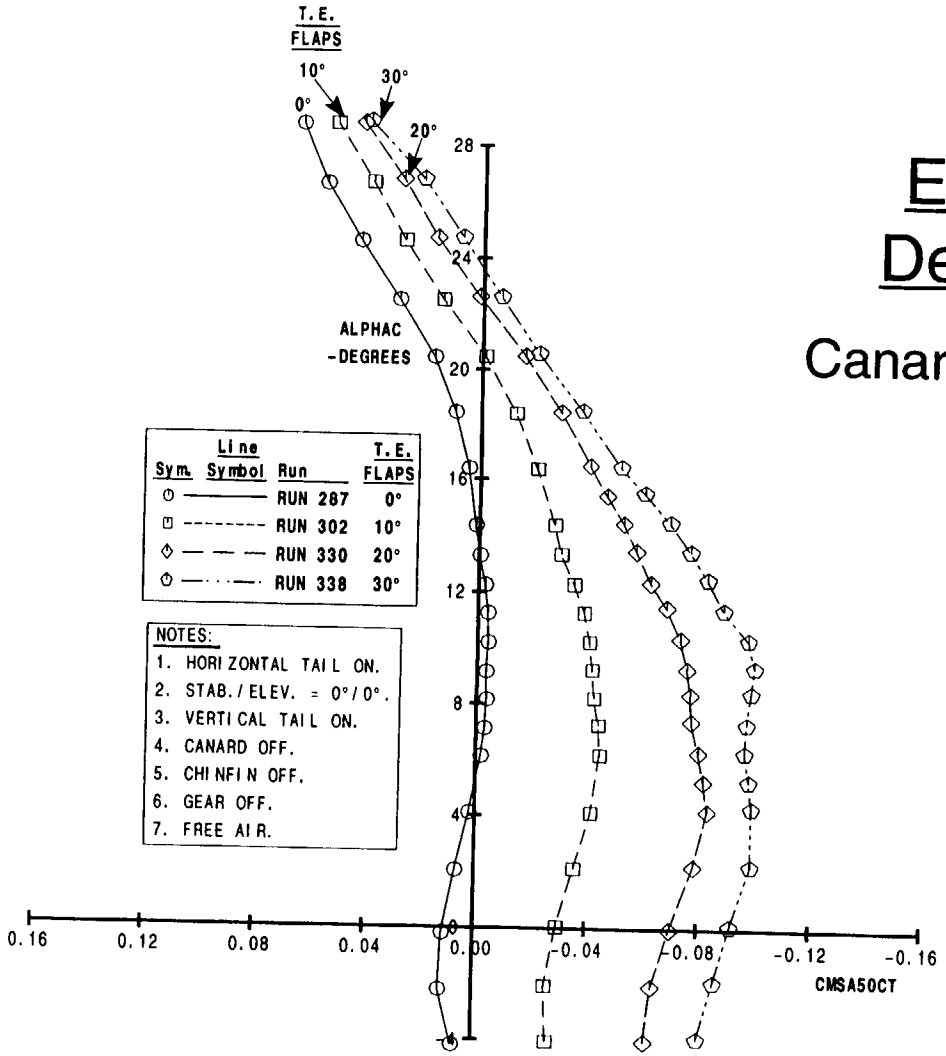

Effect of Trailing Edge Flap Deflection -- L.E. Flaps = 30°

Canard Off/ Horizontal Tail On--Wing W3

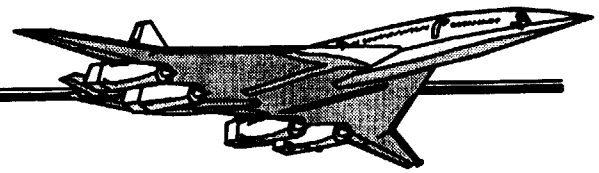

Effect of Leading Edge Flap Deflection -- T.E. Flaps = 0°

Canard Off/Horizontal Tail On -- Wing W3

The facing chart displays the effect of varying the leading edge flap deflection from 0° to 30°. The 30° of leading edge deflection allows an additional 10° angle of attack before the onset of the unstable force break. This delay produces a favorable ΔC_m of -0.048 at α =28°.

Longitudinal Stability

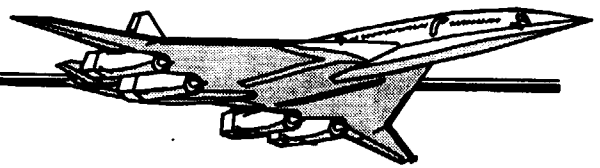

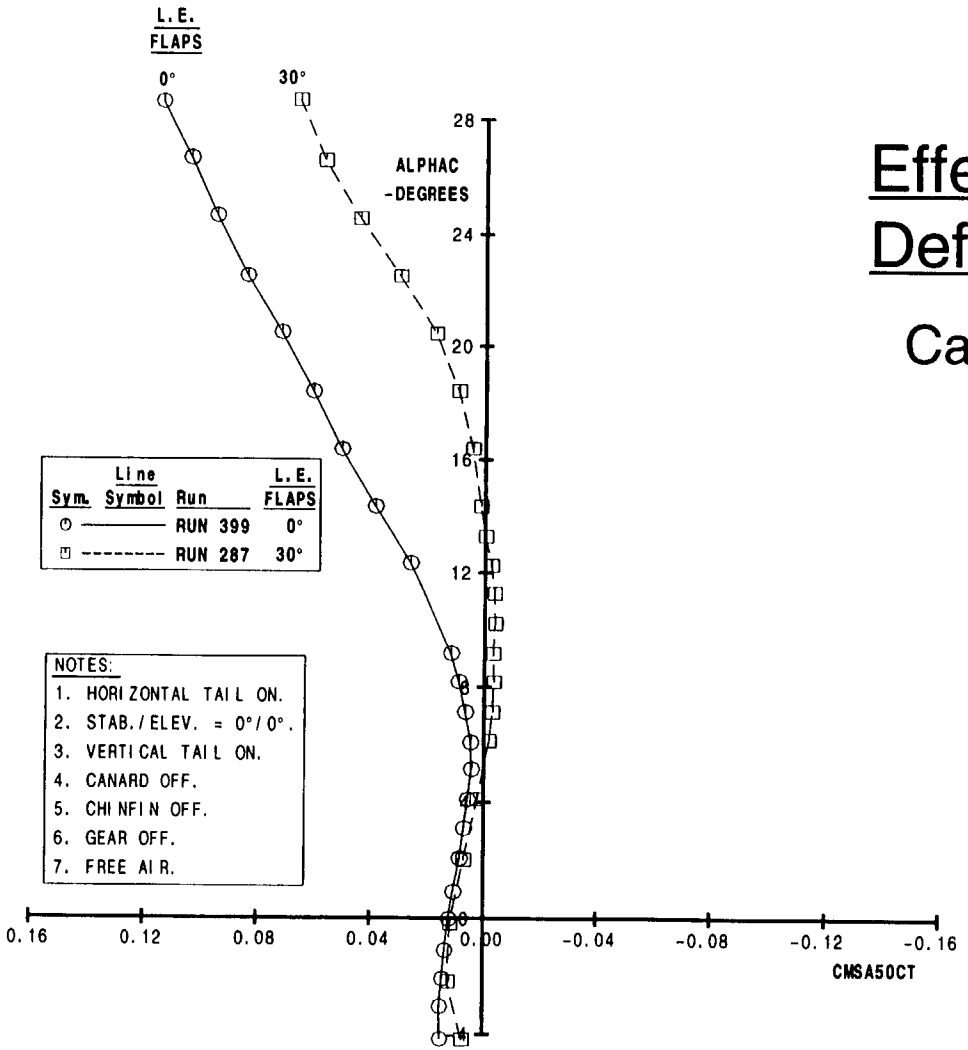

Effect of Leading Edge Flap Deflection -- T.E. Flaps = 0°

Canard Off/ Horizontal Tail On
-- Wing W3

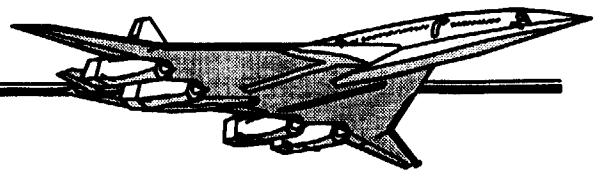

Effect of Ground Height -- Wing W3

Canard Off -- Wing LE/TE = 30°/10°

Data are presented for the maximum (MAX) and minimum (MIN) heights for determining ground effects. Both horizontal tail off and on data are displayed. It is evident that bringing the model into ground effect produces a large stabilizing influence longitudinally for the horizontal tail on configuration. This is because the downwash over the horizontal tail is significantly reduced when the model is brought into ground effect (see next chart). Ground effect data were not taken with wing W2 or W1 installed.

Longitudinal Stability

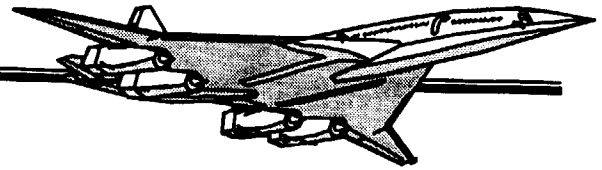

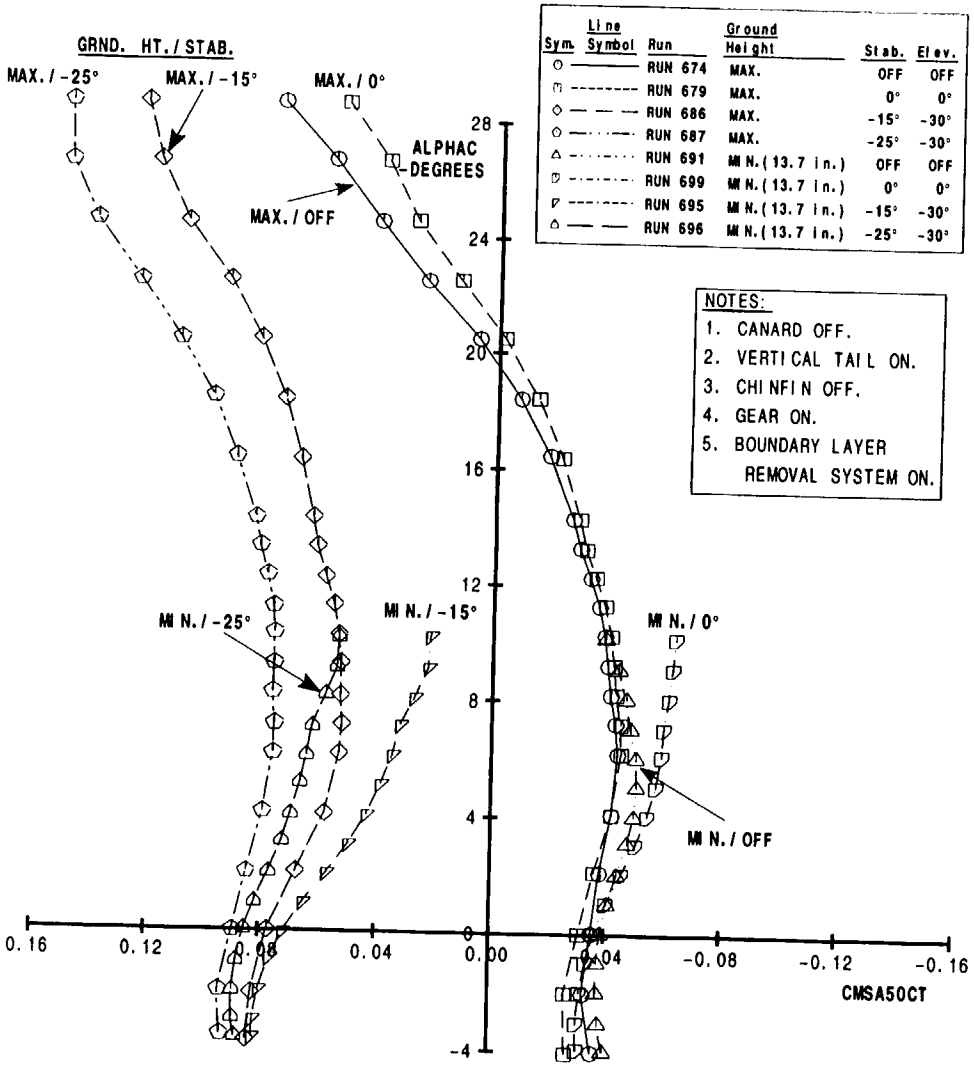

Effect of Ground Height -- Wing W3

Canard Off -- Wing LE/TE =30°/10°

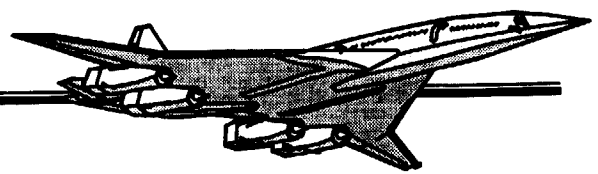

Effect of Ground Height on Downwash -- Wing W3

Horizontal Tail On -- Wing LE/TE = 30°/10°--Canard Off

Downwash values for wing W3 with a $\delta_{LE}/\delta_{TE} = 30°/10°$ were calculated from the wind tunnel data for the MAX and MIN heights. The dramatic difference in ε/α (which contributes directly into longitudinal stability) is evident.

Longitudinal Stability

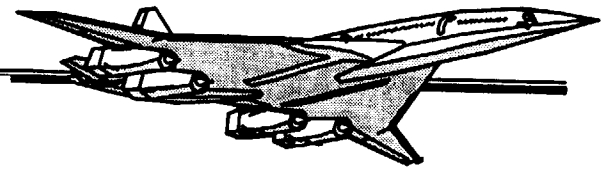

NOTES:
1. WING W_3.
2. CANARD OFF.
3. CHIN FIN OFF.
4. FOREBODY CHINE ON.
5. LANDING GEAR ON.
6. $\delta_{LE} / \delta_{TE} = 30° / 10°$.
7. VERTICAL TAIL ON.
8. RUDDER = 0°
9. q = 85 PSF.
10. $\beta = 0°$
11. HORIZONTAL TAIL H_3.

LINE SYM.	GROUND HEIGHT
———	MAX.
- - - - - - -	MIN. (13.7 WL)

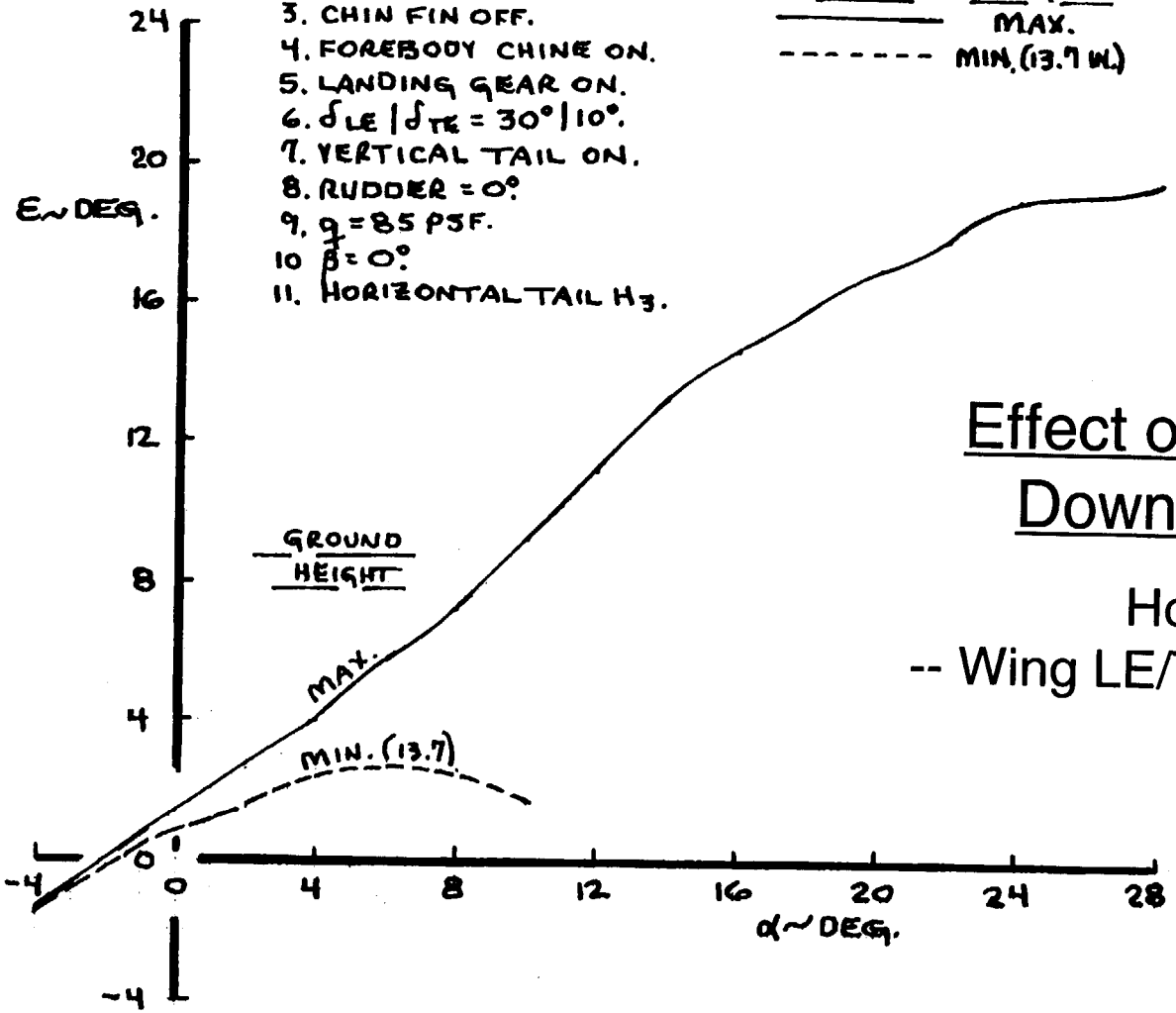

Effect of Ground Height on Downwash -- Wing W3

Horizontal Tail On
-- Wing LE/TE = 30°/10° -Canard Off

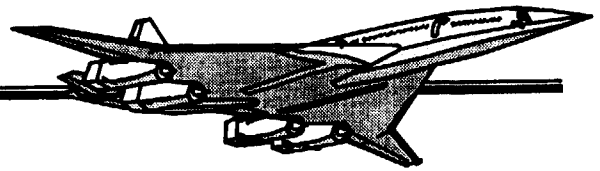

Effect of Boundary Layer Removal System -- Wing W3

Min. Height -- Horizontal Tail and Canard Off -- Wing LE/TE = 30°/10°

A suction system is installed in the 14 x 22 wind tunnel floor to remove the unwanted, thickened boundary layer. This boundary layer removal system (BLRS) is normally operating when ground effect data are being acquired. The effect of this BLRS on longitudinal stability characteristics is displayed on the next page. It is shown that turning the BLRS off degrades longitudinal stability.

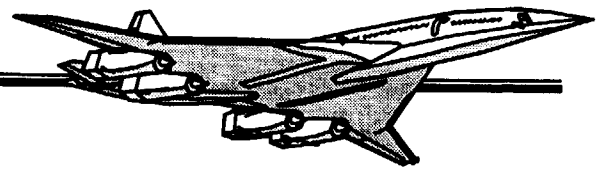

Effect of Boundary Layer Removal System -- Wing W3

Min. Height -- Horiz. Tail and Canard Off -- Wing LE/TE = 30°/10°

Line Sym.	Symbol	Run	BLRS
○	———	RUN 707	OFF
□	--------	RUN 706	ON

NOTES:
1. HORIZONTAL TAIL OFF.
2. VERTICAL TAIL ON.
3. CANARD OFF.
4. CHINFIN OFF.
5. GEAR ON.
6. MIN. HGT. (13.71 IN.).

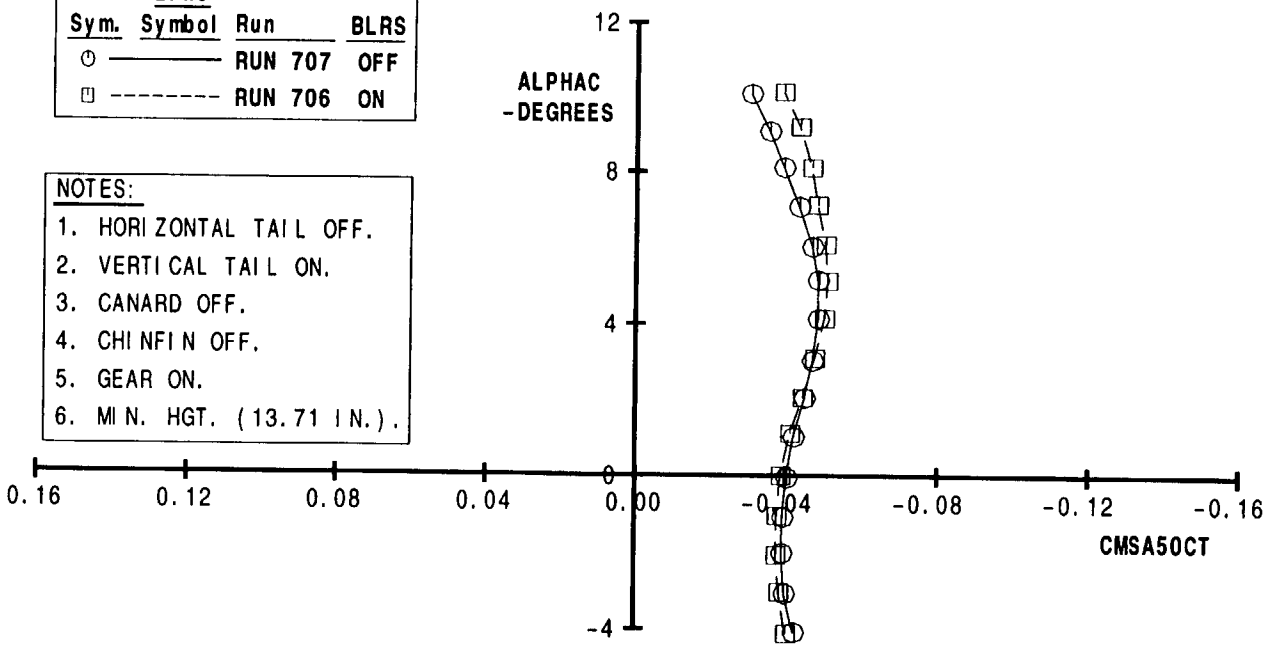

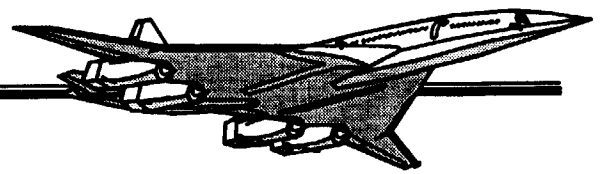

Effect of BLRS Taping -- Wing W3

Max. Height -- Horizontal Tail and Canard Off -- Wing LE/TE = 30°/10°

The Boundary Layer Removal System (BLRS) sucks boundary layer air in through a grate ahead of the model when operating in ground effect. During the test, concern was voiced that even when the system was not operating, there could be flow through this grate. It was taped up, and the effect of this taping on aerodynamic characteristics was measured. The effect on pitching moment was negligible.

Longitudinal Stability

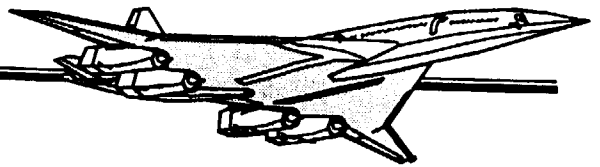

Effect of BLRS Taping -- Wing W3

Max. Height -- Horiz. Tail and Canard Off - - Wing LE/TE = 30°/10°

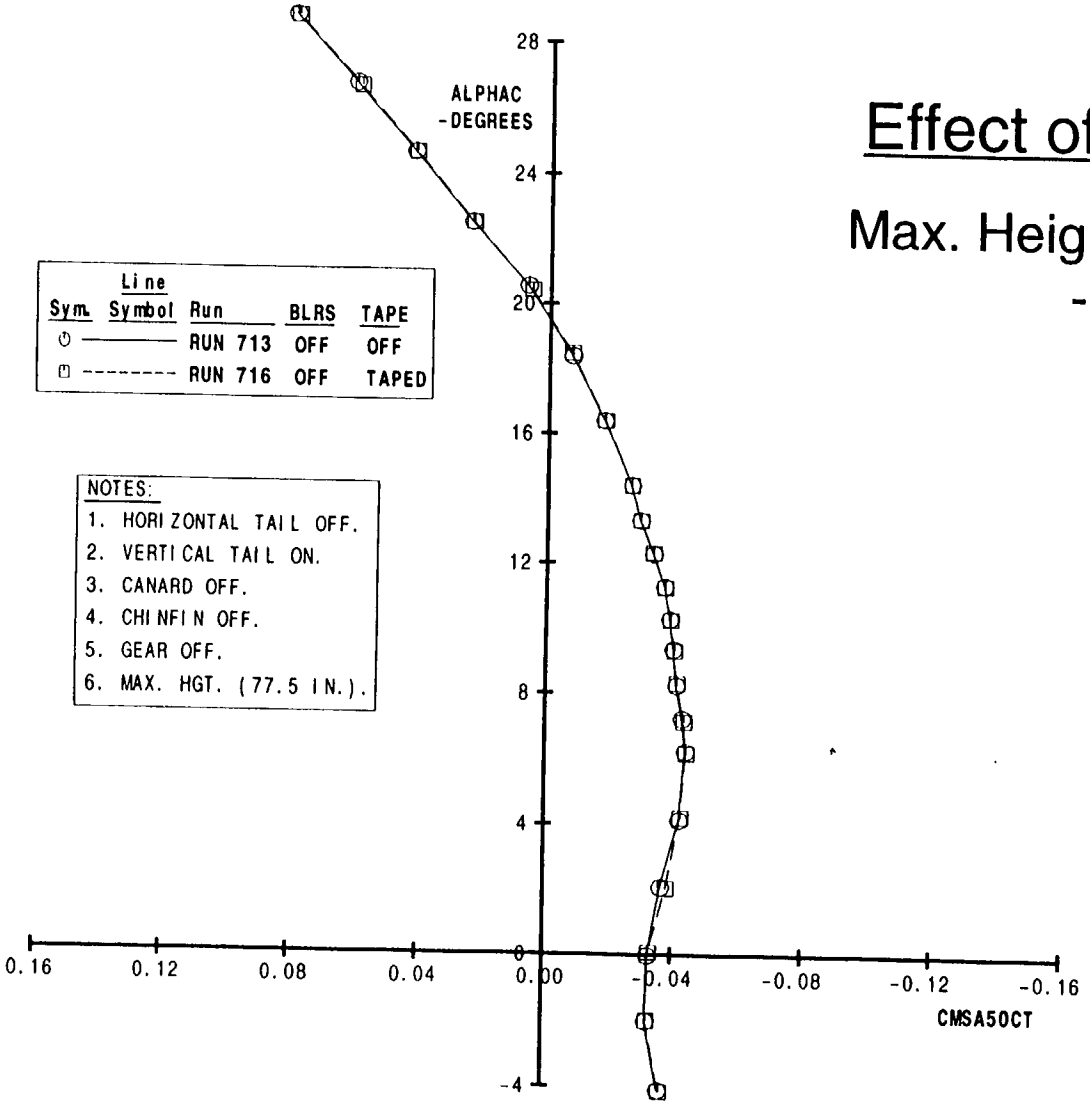

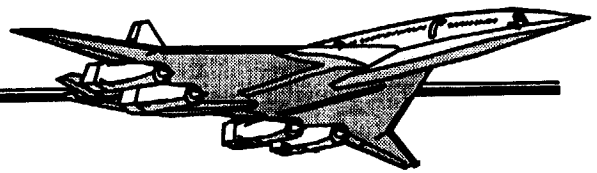

Longitudinal Control

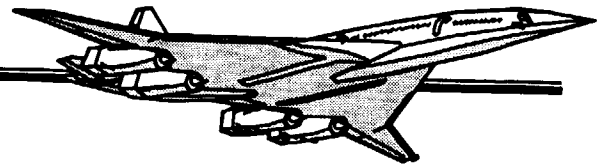

Stabilizer Effectiveness

Effect of Wing Planform ~ Canard Off

Stabilizer effectiveness (Cm_s ~ i.e., $\delta Cm/\delta_{STAB}$) is plotted versus angle of attack for wings W1, W2 and W3 on the adjacent chart. It is evident that when W1 is corrected for planform geometry, the stabilizer effectiveness levels tend to collapse. Note that the data for wings W2 and W3 utilize the H3 horizontal tail, while H1 is used with wing W1.

HSR

TCA-4 Stability & Control Test **Longitudinal Control**

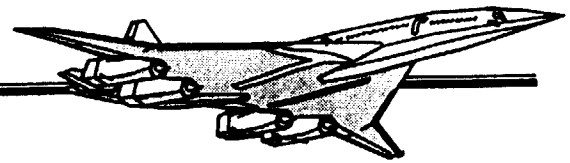

LINE SYM.	WING	HORIZ.	L.E./T.E. FLAPS
———	W_1	H_1	30°/15°(10°)
— —	W_2	H_3	(25°)30°/10°
- - - - - - -	W_3	✓	30°/10°
— — — *	W_1	H_1	30°/15°(10°)

NOTES:
1. CANARD OFF.
2. CHIN FIN OFF.
3. FREE AIR.
4. FOREBODY CHINE ON.
5. LANDING GEAR OFF.
6. VERTICAL TAIL ON.
7. RUDDER = 0°.
8. q = 85 PSF.
9. β = 0°.
10. δ_{FRL} = 0° ⟶ -10°

* THESE W_1H_1 DATA ARE MULTIPLIED BY $\frac{\bar{V}_H W_3H_3}{\bar{V}_H W_1H_1}$

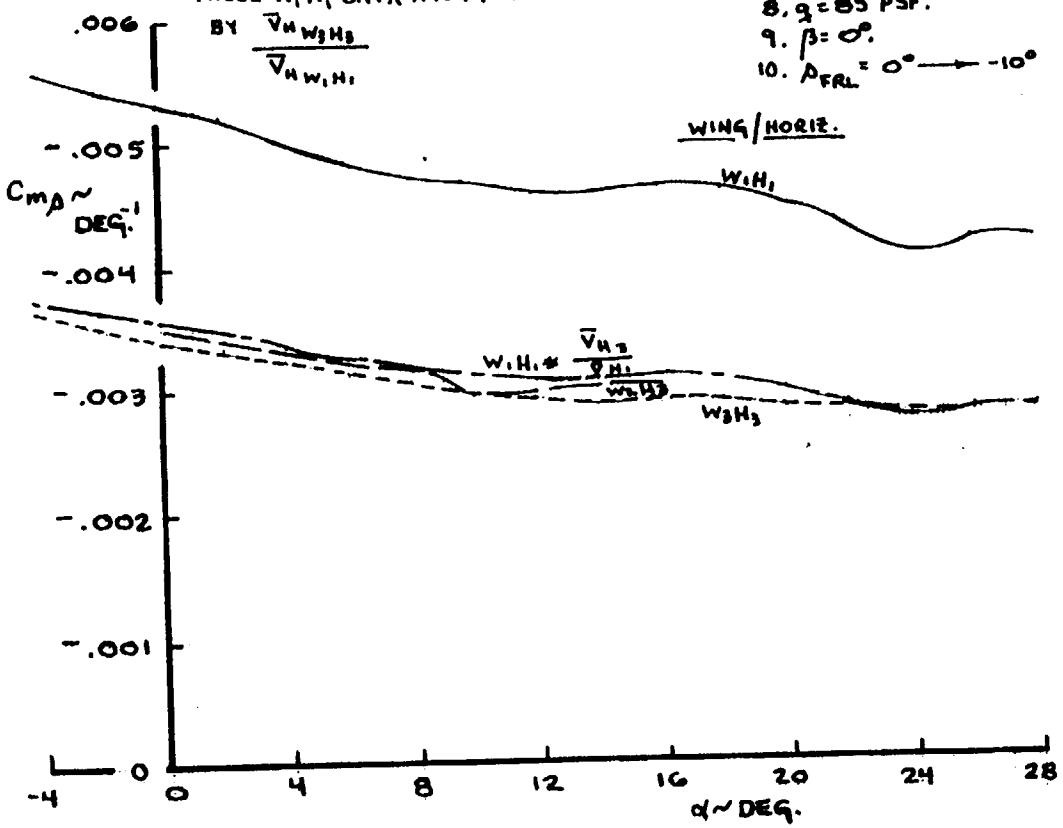

Stabilizer Effectiveness

Effect of Wing Planform
~ Canard Off

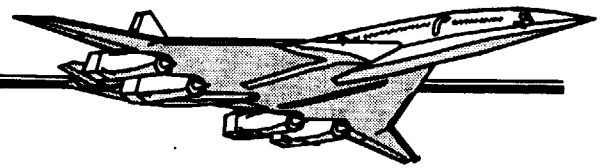

Canard Effectiveness

Small A/P Nose-Up Deflections ~ Horizontal Tail On

The effect of the CN1 canard on longitudinal control for small positive deflection angles is shown. The horizontal tail is on at 0° deflection and both elevators are neutral. Note that the 10° canard deflection has reduced effectiveness above $\alpha = 20°$. Also observe the strong de-stabilization with the canard on.

HSR

TCA-4 Stability & Control Test **Longitudinal Control**

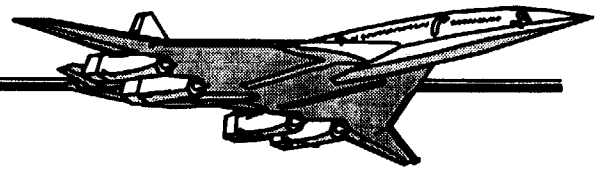

Canard Effectiveness

Small A/P Nose-Up Deflections

~ Horizontal Tail On

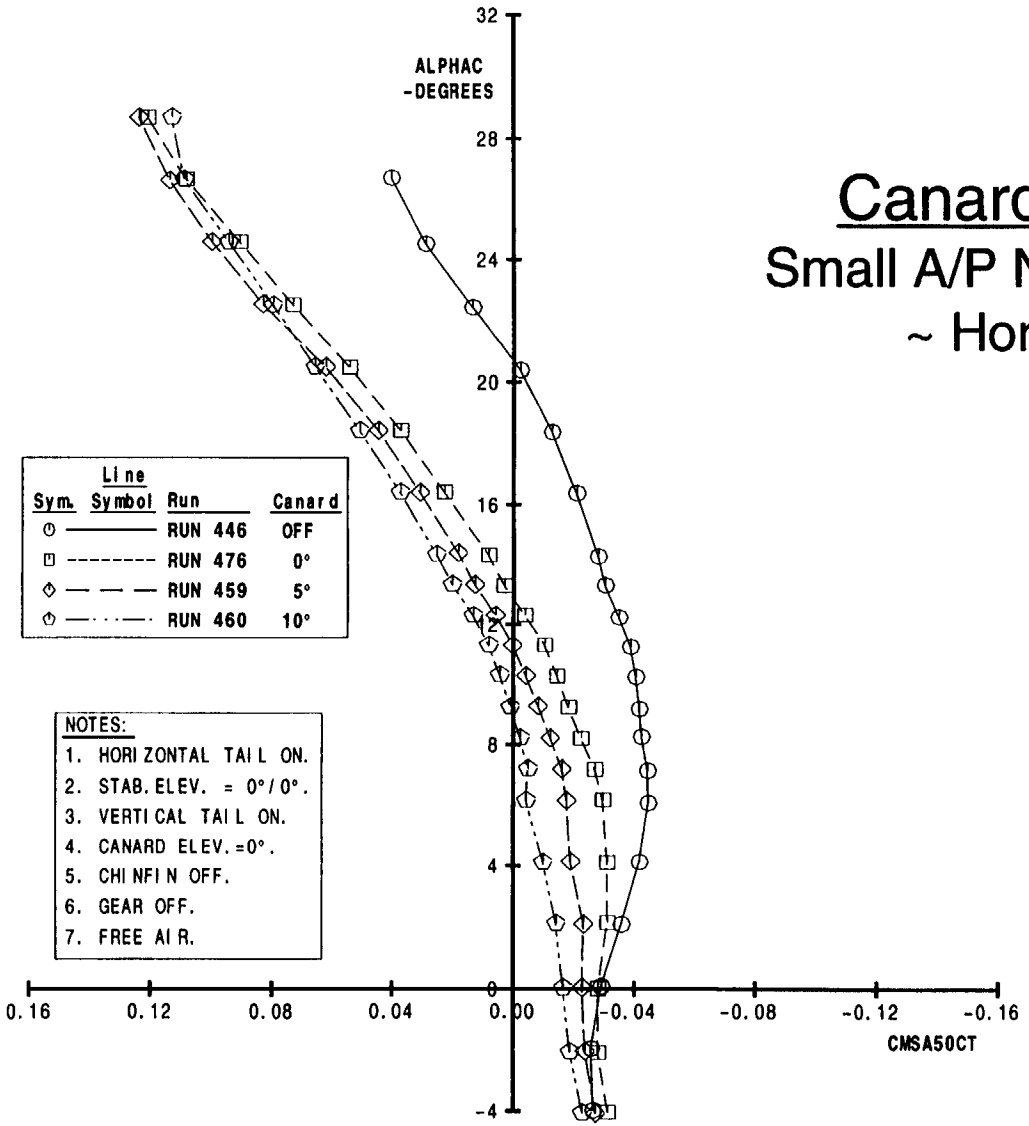

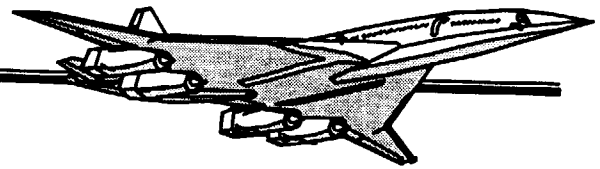

Canard Effectiveness

Large A/P Nose-Up Deflections ~ Horizontal Tail On

Canard effectiveness for conditions with large positive deflections is displayed. Note that there is a progressive reversal with increasing angle of attack for canard deflections > $\delta_c = +15°$. Also, the pitch data are quite non-linear between $\alpha = 2°$ and $\alpha = 8°$.

Longitudinal Control

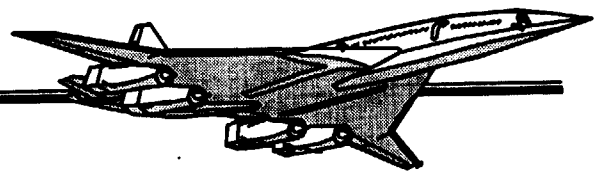

Canard Effectiveness

Large A/P Nose-Up Deflections
~ Horizontal Tail On

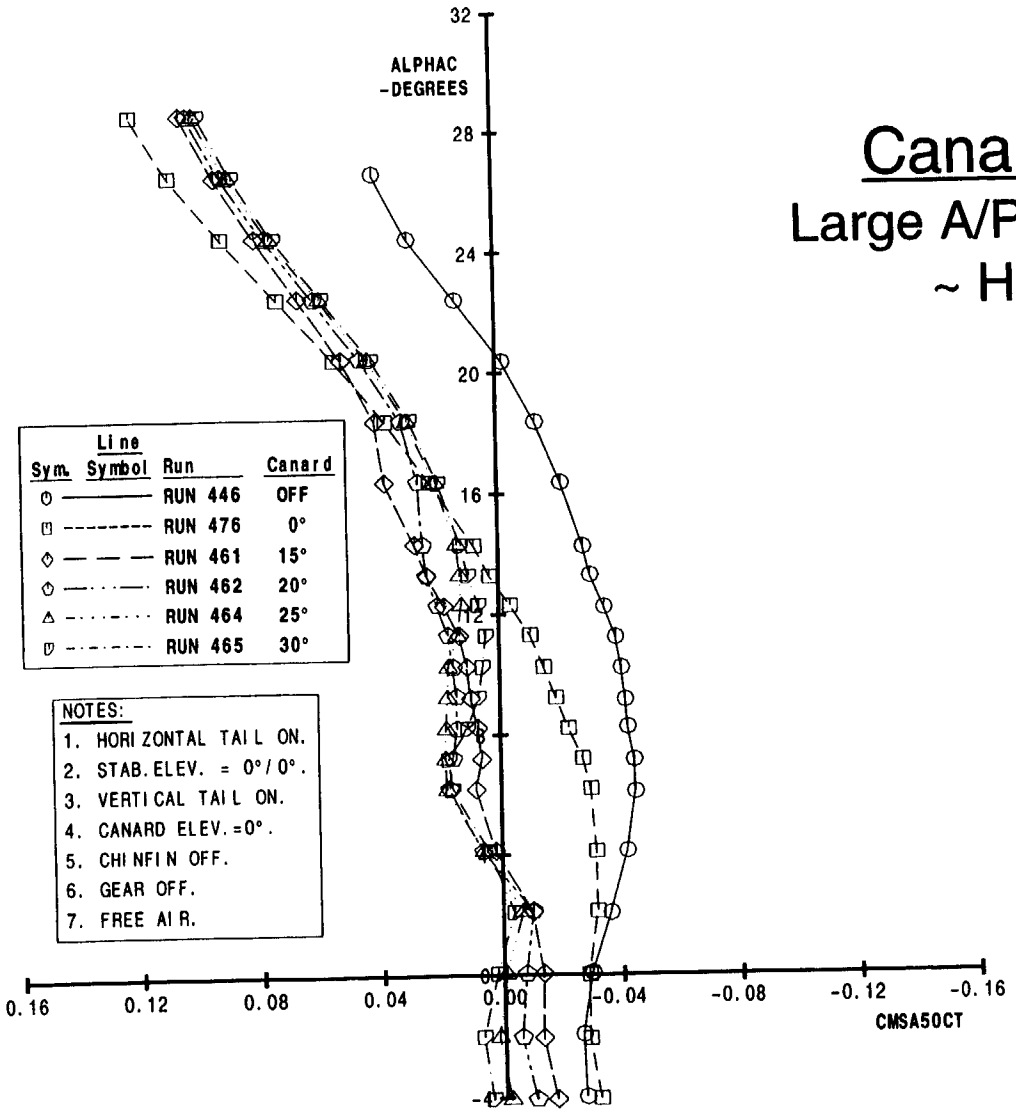

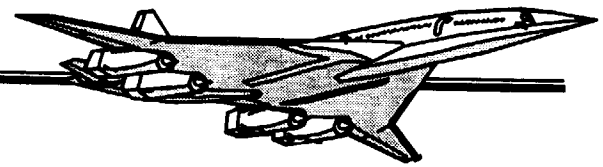

Canard Effectiveness

Small A/P Nose-Down Deflections ~ Horizontal Tail On

Smaller negative canard control data are displayed. Observe that these data are more linear and canard reversal does not occur through $\delta_c = -15°$ and $\alpha = 28°$.

Longitudinal Control

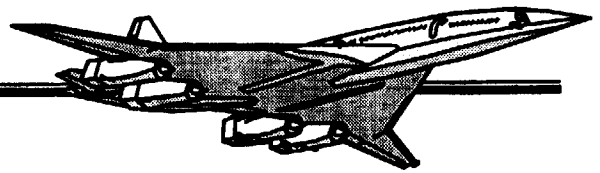

Canard Effectiveness

Small A/P Nose-Down Deflections
~ Horizontal Tail On

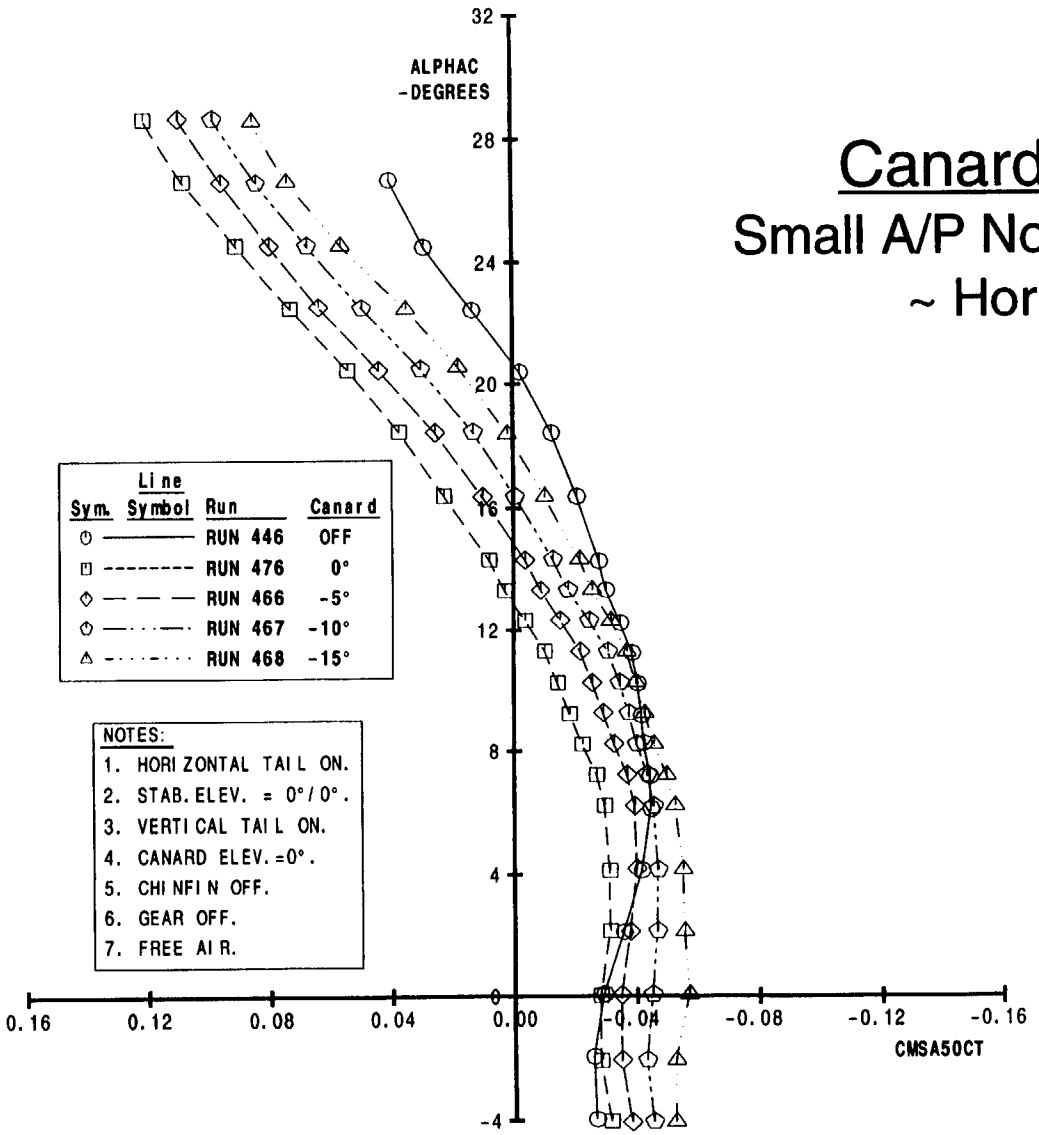

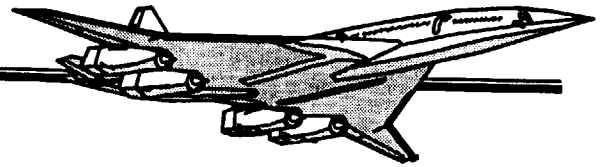

Canard Effectiveness

Take-Off Rotation ~ In Ground Effect ~ Horizontal Tail On

Positive canard deflections were tested in ground effect to assess their capability to provide take-off rotation control. The data are somewhat non-linear. However, for take-off rotation, $\alpha \approx 0°$, and here the data are more regular as a function of canard deflection.

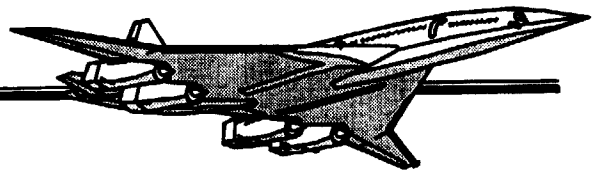

Canard Effectiveness

Take-Off Rotation ~ In Ground Effect ~ Horizontal Tail On

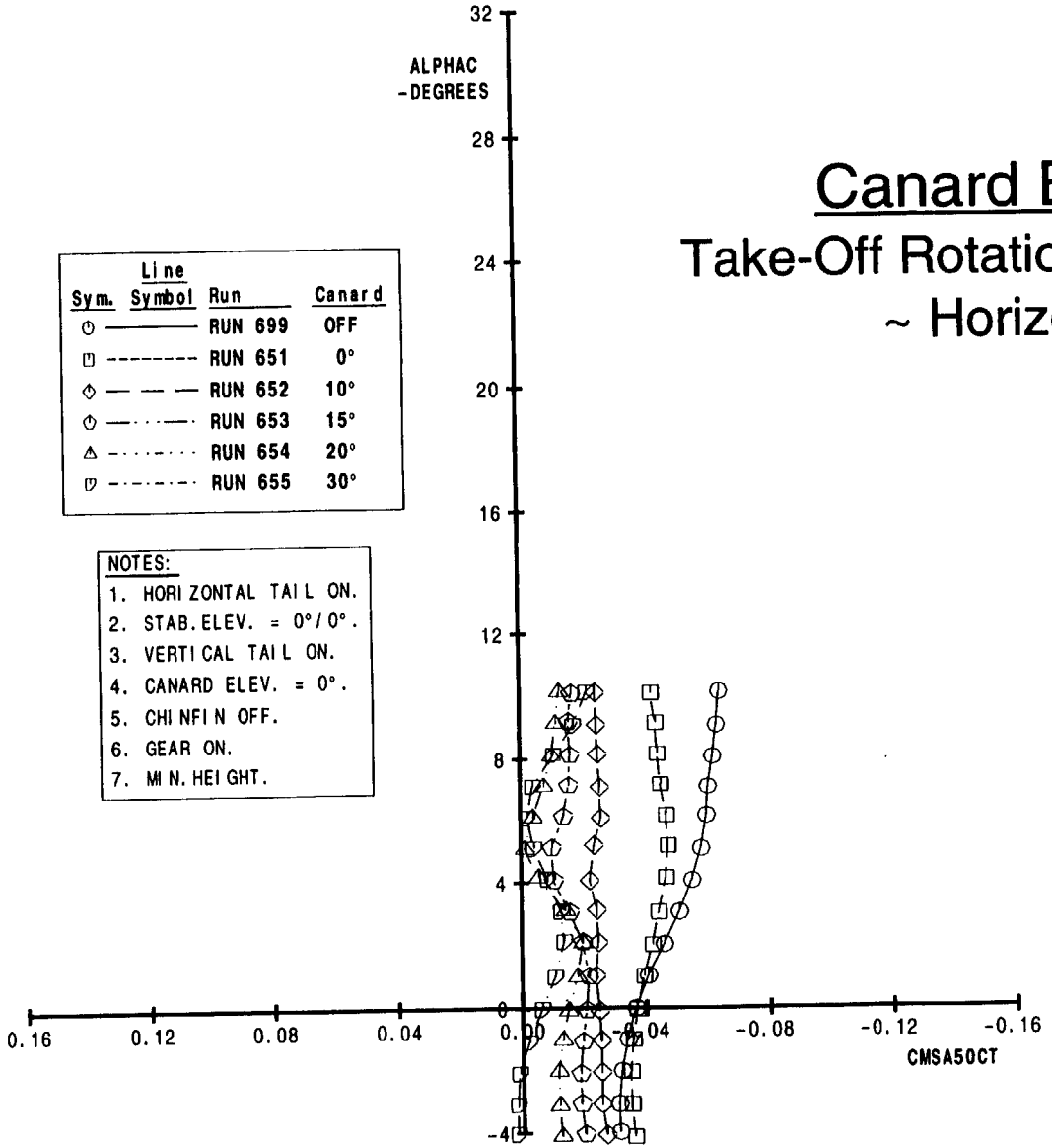

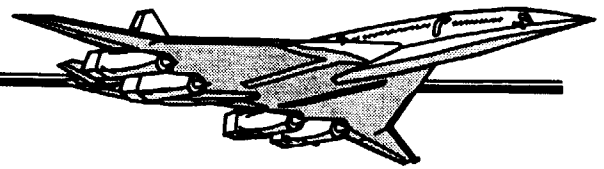

Canard Effectiveness

Stall Recovery ~ Free Air ~ Horizontal Tail On

Canard effectiveness for the stall recovery configuration was also examined. The wing W3 stall recovery leading/trailing edge flap condition was 30°/30°. The horizontal/elevator was set to 0°/0°. The data show that -45° of canard deflection provides a significant nose-down pitching moment ($\Delta Cm = -.074$) at $\alpha = 26°$. However, -30° of elevator only generates another -.01 ΔCm for this condition.

HSR

TCA-4 Stability & Control Test

Longitudinal Control

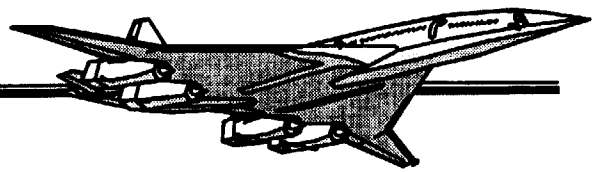

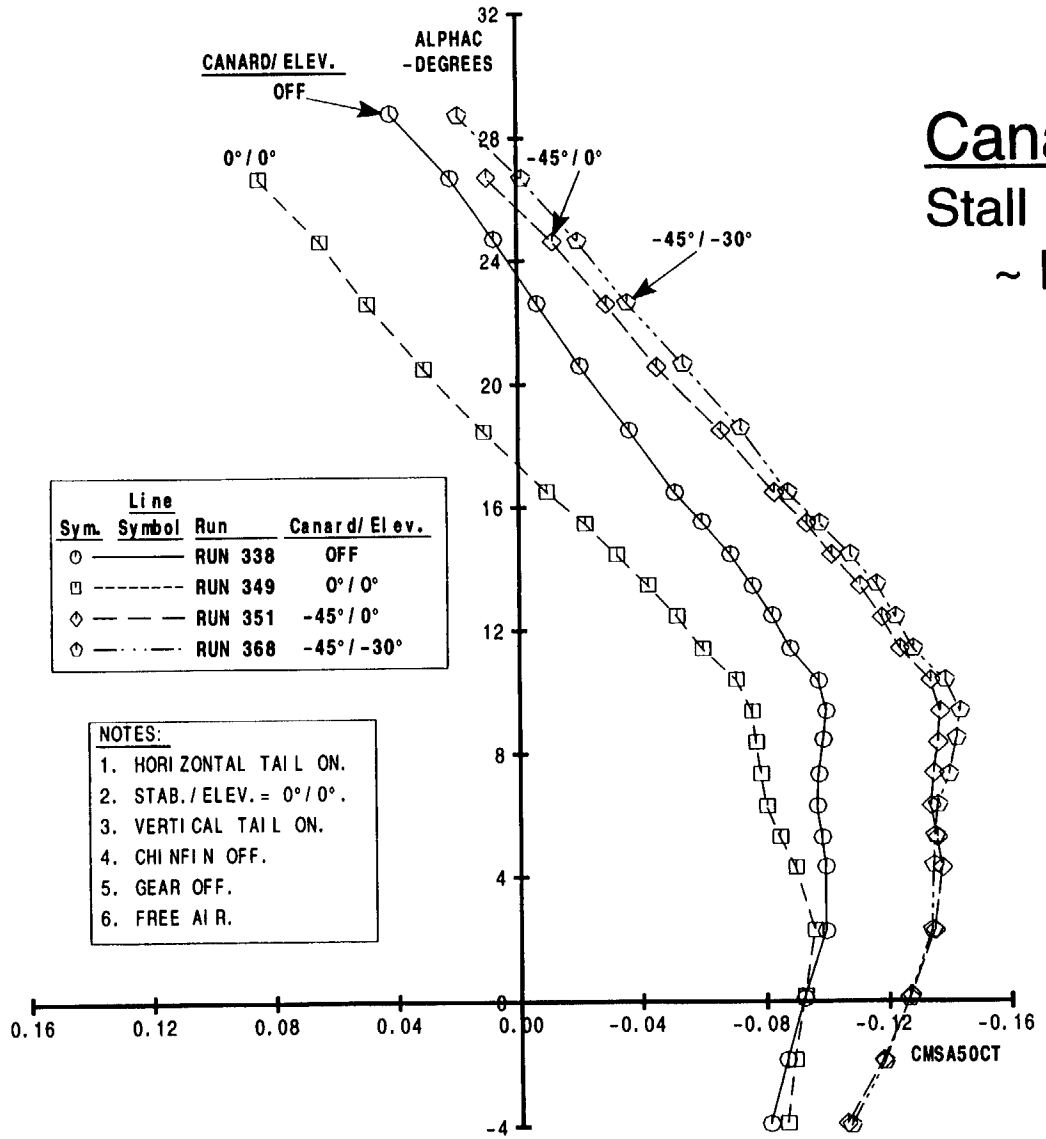

Canard Effectiveness

Stall Recovery ~ Free Air
~ Horizontal Tail On

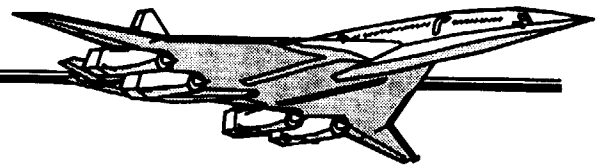

Horizontal Tail Effectiveness

Effect of Canard Deflection

The effect of the canard and canard elevator deflection on horizontal tail effectiveness is shown in the attached figure. Observe that there is a canard induced non-linearity in the data between $\alpha = 4°$ and 14°. Otherwise, the canard and/or canard elevator deflection do not produce much of an effect on the stabilizer effectiveness data.

HSR

TCA-4 Stability & Control Test

Longitudinal Control

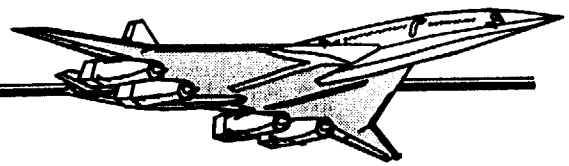

NOTES:
1. WING W3.
2. CANARD DEFLECTION = +5°
3. CHIN FIN OFF.
4. FREE AIR.
5. FOREBODY CHINE ON.
6. LANDING GEAR OFF.
7. VERTICAL TAIL ON.
8. RUDDER = 0°.
9. $\delta_{LE}/\delta_{TE} = 30°/10°$.
10. $q = 85$ PSF.
11. $\beta = 0°$.
12. HORIZONTAL H3.
13. $\rho_{FRL} = 0° \rightarrow -10°$

LINE SYM.	$\delta_{CANARD}/\delta_{ELEV.}$
————	OFF
— — —	+5°/0°
- - - - - - -	+5°/+15°

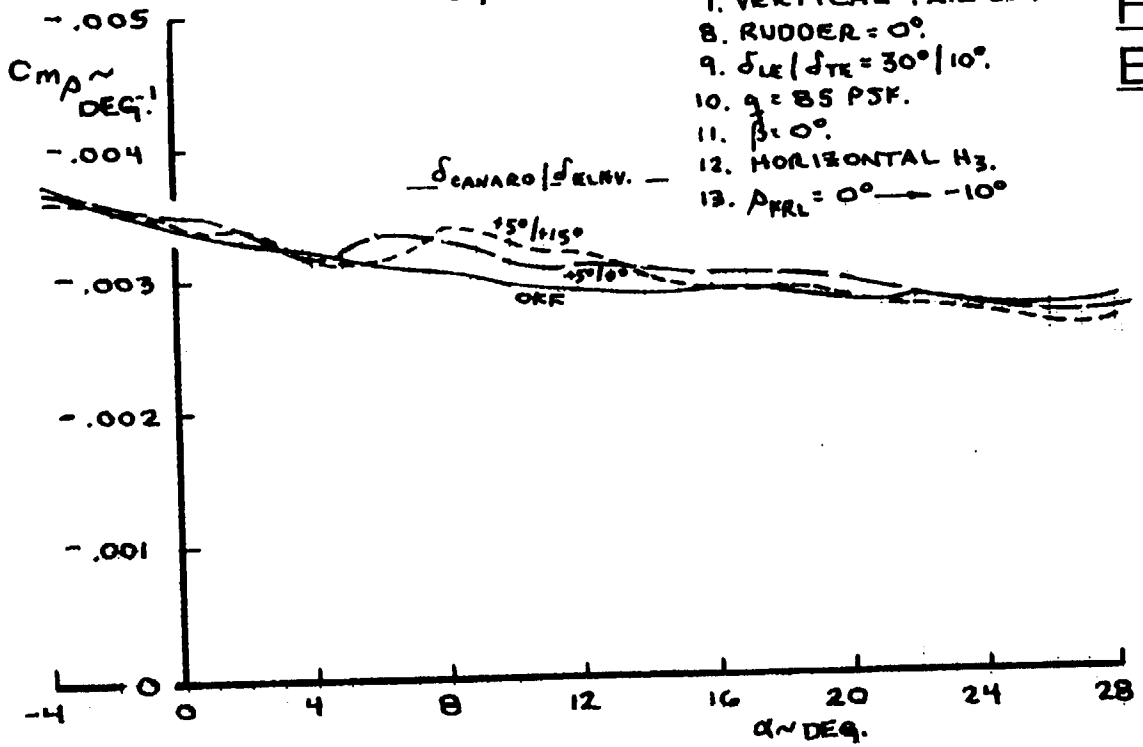

Horizontal Tail Effectiveness
Effect of Canard Deflection

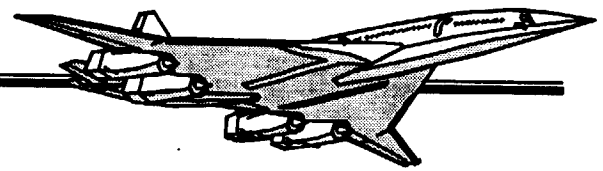

Effects of Canard on Downwash

$\delta_{canard}/\delta_{elev.}$ = OFF, 0°/0°, +5°/0°, -5°/0°

The effect of small canard deflections on downwash measured at the horizontal tail is displayed. A non-linearity between $\alpha = 3°$ and 8° due to a positive 5° of deflection is observed. This phenomenon is not seen with $\delta_{canard} = 0°$ or -5°.

Longitudinal Control

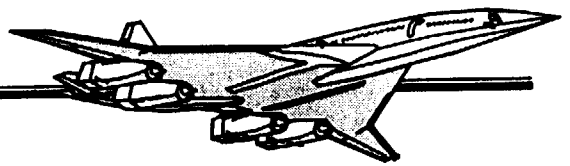

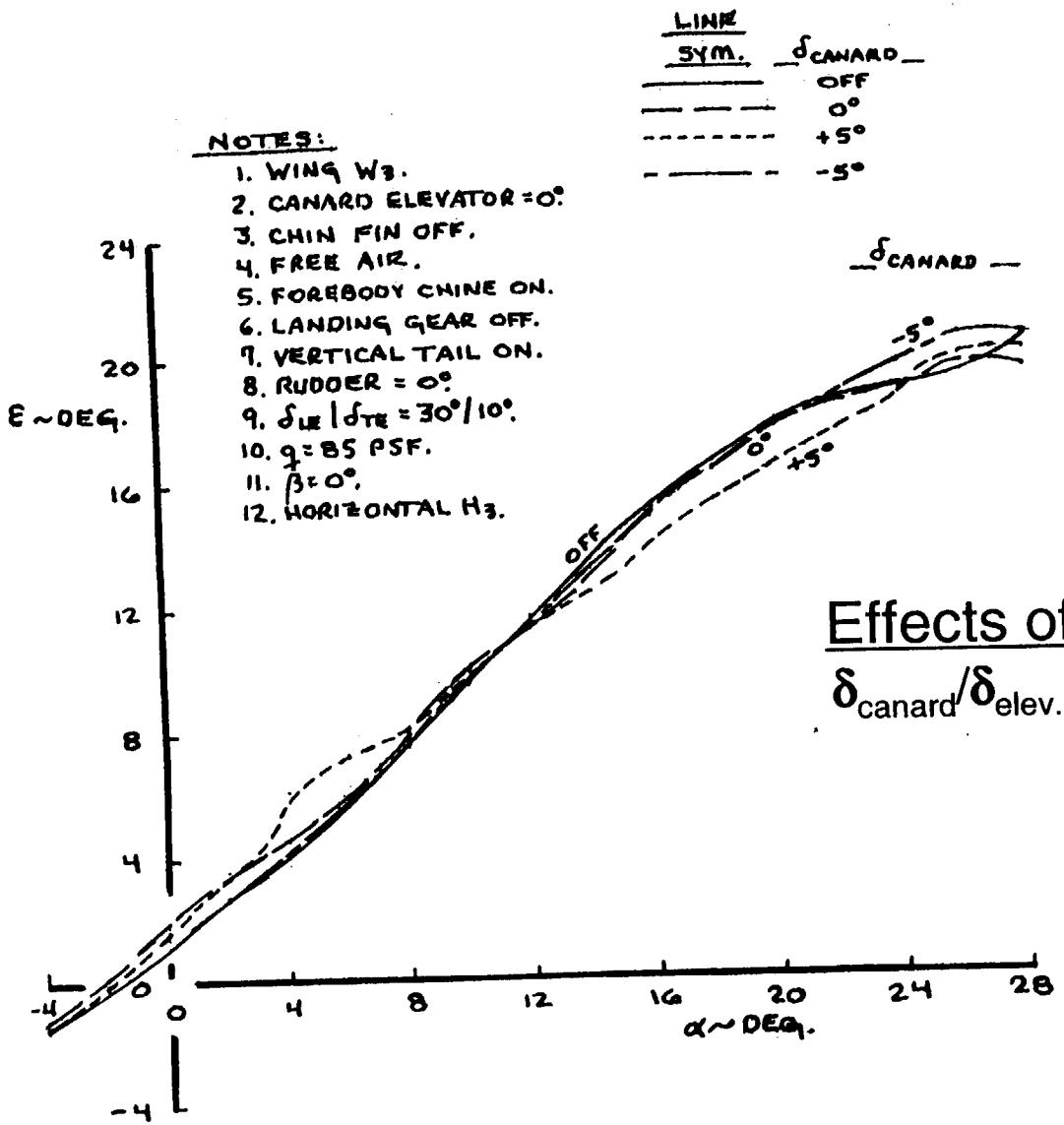

Effects of Canard on Downwash

$\delta_{canard}/\delta_{elev.}$ = OFF, 0°/0°, +5°/0°, -5°/0°

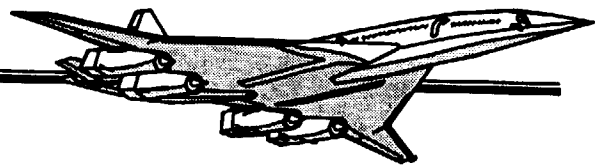

Effects of Canard on Downwash

$\delta_{canard}/\delta_{elev.}$ = OFF, -5°/0°, -5°/+15°

The addition of a +15° elevator to a -5° canard setting has produced a somewhat larger ($\alpha = 0° \rightarrow 11°$) non-linearity in the downwash data.

Longitudinal Control

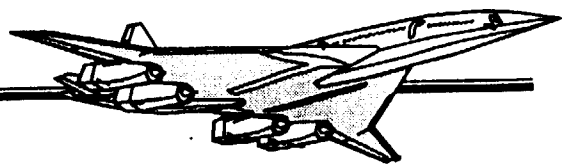

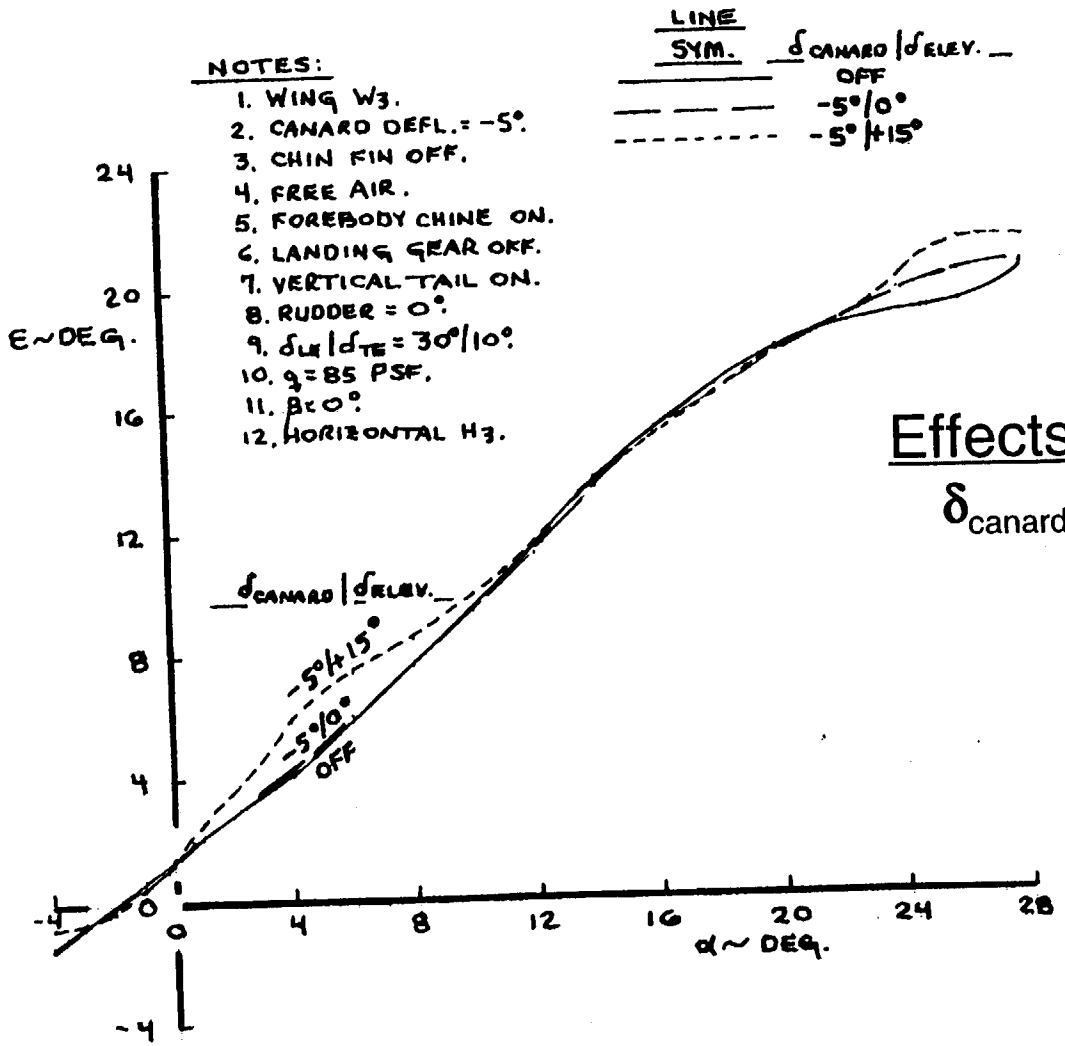

Effects of Canard on Downwash

$\delta_{canard}/\delta_{elev.}$ = OFF, -5°/0°, -5°/+15°

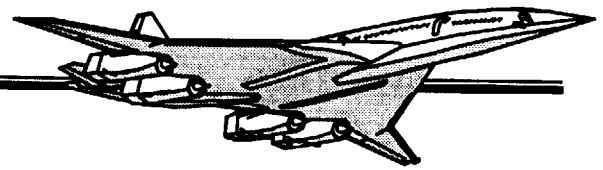

Effects of Canard on Downwash

$\delta_{canard}/\delta_{elev.}$ = OFF, +5°/0°, +5°/+15°

When a +15° elevator is added to an already non-linear data producing +5° canard, the resultant downwash is extremely non-linear between $\alpha = 2°$ and 12°. Clearly, positive canard/elevator deflections are introducing some change into the inboard wing flowfield which causes a disruption to the downwash at the horizontal tail.

Longitudinal Control

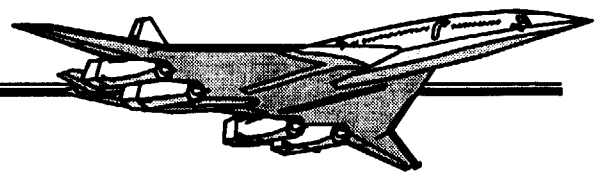

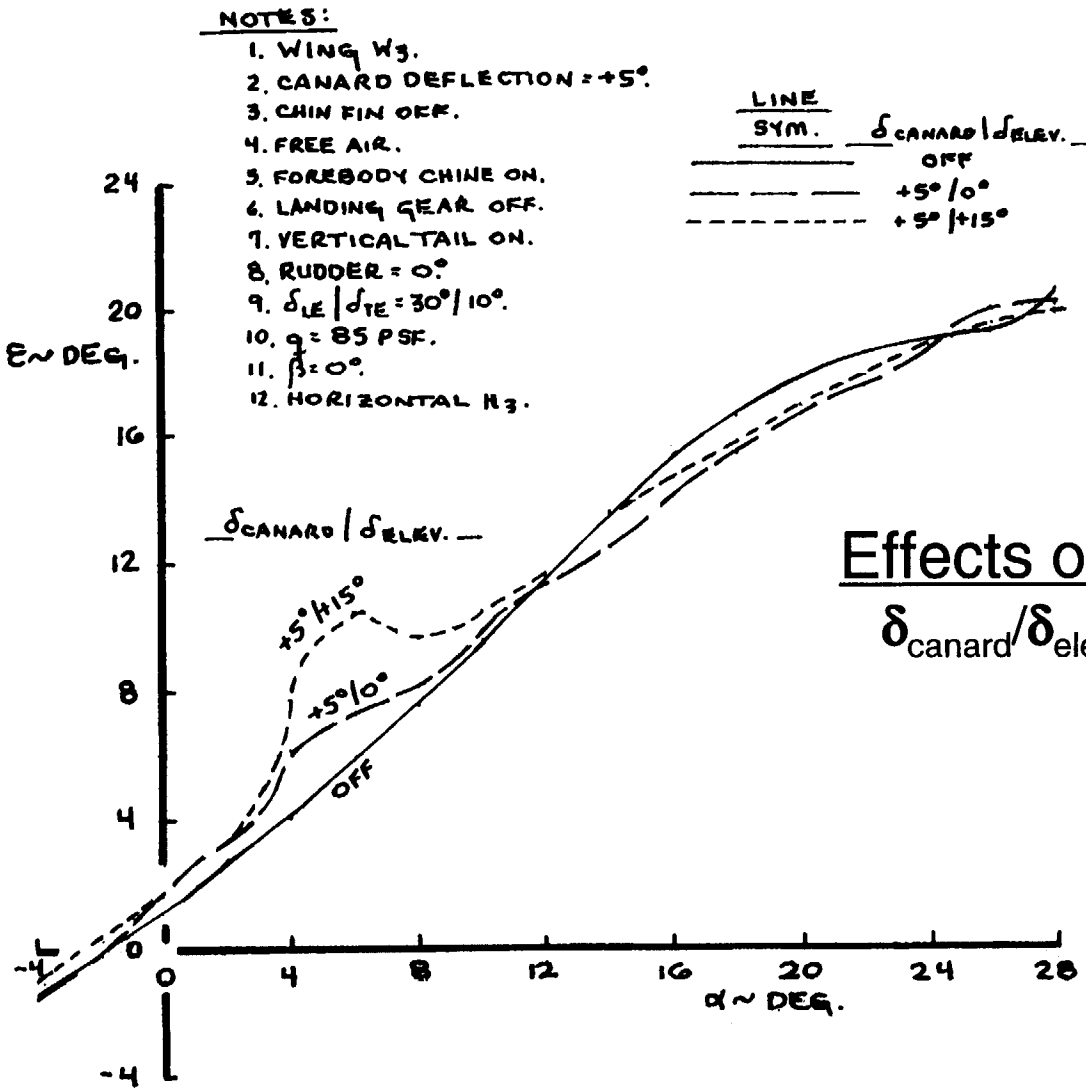

Effects of Canard on Downwash

$\delta_{canard}/\delta_{elev.}$ = OFF, +5°/0°, +5°/+15°

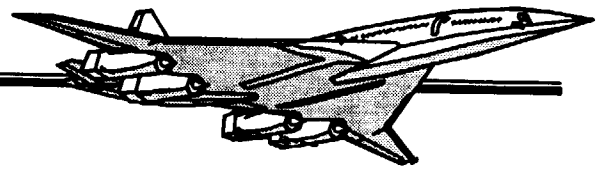

Effects of Canard on Nacelle Inlet Ingestion

Another concern determined during this test entry was found with flow visualization. It would appear that for low angles of attack and any loading on the canard, the shed tip vortices trail aft right into the inboard nacelle inlets. This problem is significant enough to cause a canard with 30° of dihedral to be built for testing in the next high-lift entry at the Ames 12 Ft. Wind Tunnel. While this change might solve the nacelle ingestion problem, a serious concern exists over the effect of raising the canard tips on directional stability and control (See Directional Stability & Control sections of this paper).

Longitudinal Control

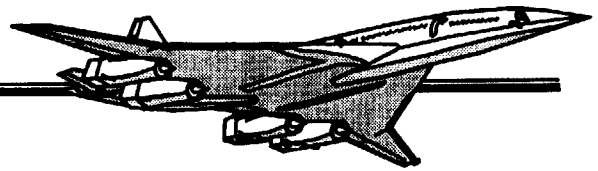

3–View PTC Canard Vortex Traces

HSCT Aerodynamics, Long Beach

M=0.3, AoA=0 deg, Re=8 million, Flap=30/10, Can/Ele=10/15

TCA2.8–28

- Front View
- Bottom View
- Side View

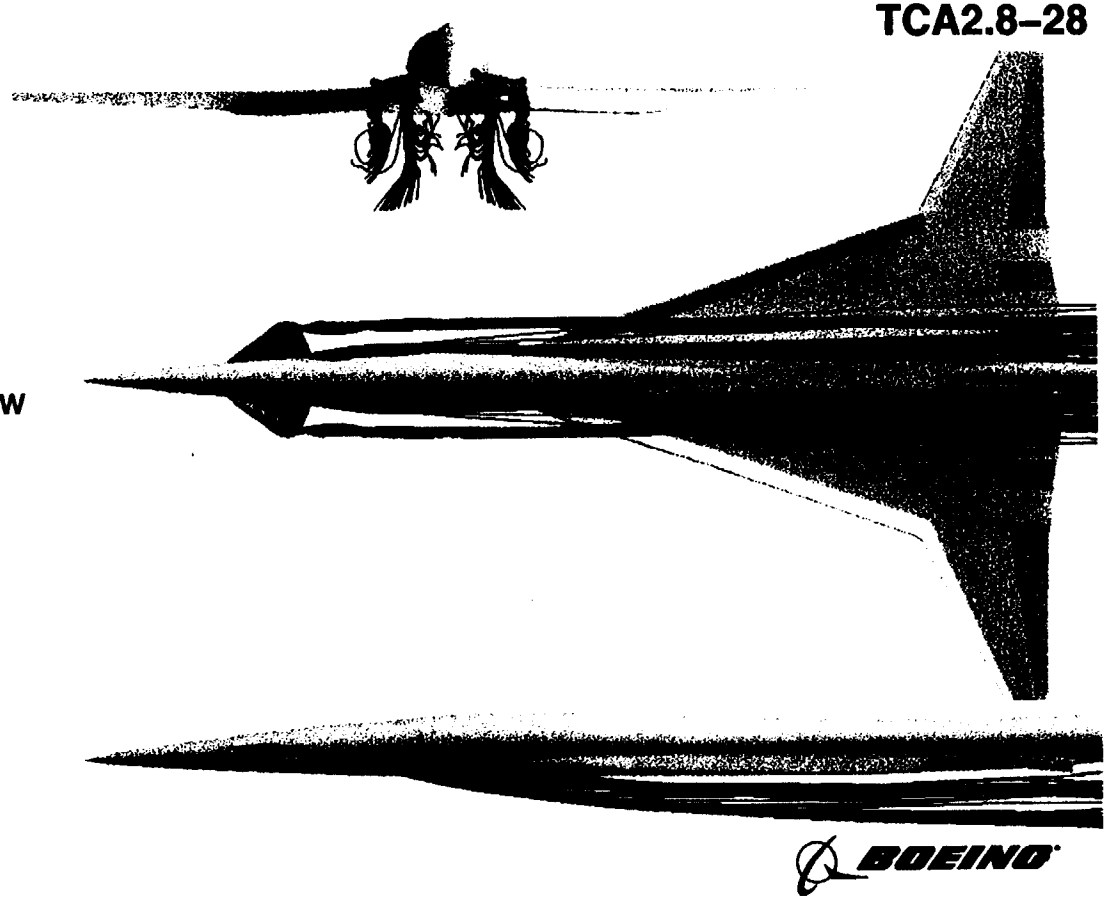

BOEING

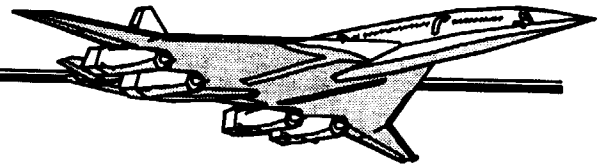

Lateral-Directional Stability

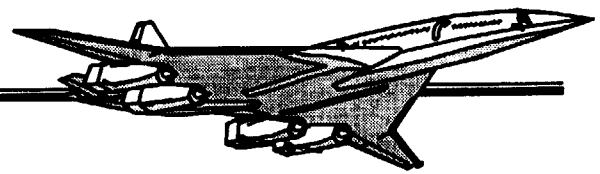

Baseline Directional Stability

Wing W3 ~ Vertical Tail Off and On

The attached shows the yawing moment coefficient versus sideslip data with the vertical tail on and off. Angles of attack of 0°, 10° and 20° are displayed. Note that the vertical tail provides a significant improvement to directional stability. The vertical tail on, $\alpha = 10°$ configuration is the most directionally stable. Also, the vertical tail on, $\alpha = 20°$ condition demonstrates a non-linear, unstable directional state through $\beta = \pm 2°$.

Lateral-Directional Stability

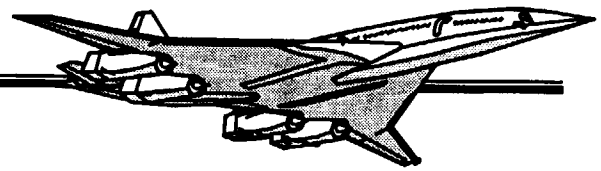

Baseline Directional Stability

Wing W3 ~ Vertical Tail Off and On

Sym.	Line Symbol	Run	Alpha	Vert. Tail
○	———	RUN 319	0	OFF
□	- - - - - - - -	RUN 310	0°	ON
◇	— — —	RUN 320	10°	OFF
○	— · —	RUN 311	10°	ON
△	- · - · - ·	RUN 321	20°	OFF
▽	- · - · - · -	RUN 312	20°	ON

NOTES:
1. HORIZONTAL TAIL ON.
2. STAB./ELEV. = 0°/0°.
3. CANARD OFF.
4. CHINFIN OFF.
5. GEAR OFF.
6. FREE AIR.

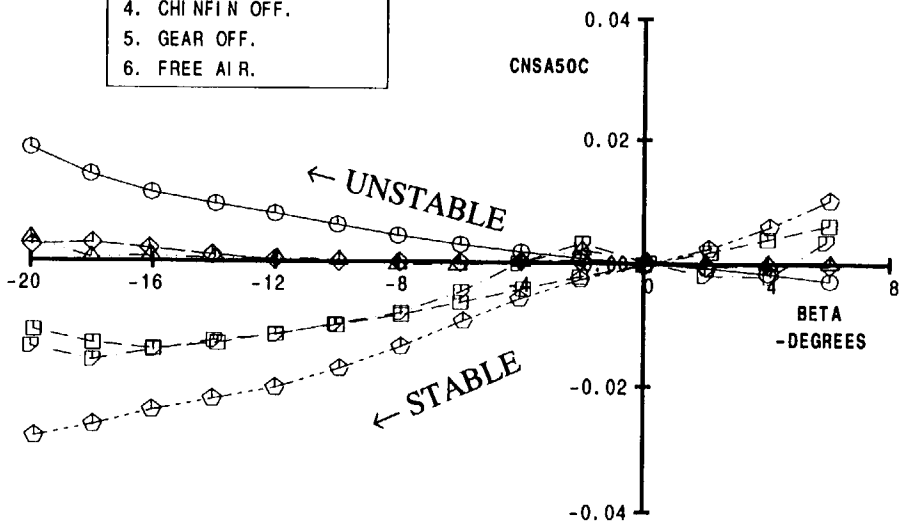

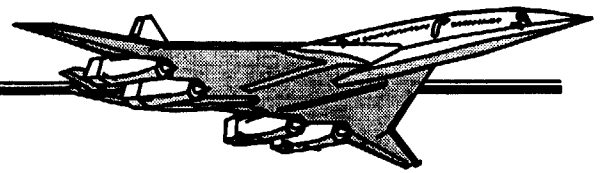

Effects of Canard/Deflection

δ_{CANARD} = OFF, 0°, +15°, -15° ~ α = 0°

The effects of nominal canard deflection on directional stability are shown in the attached chart. The vertical tail is on, the wing W3 leading/trailing edge flaps are at 30°/10° and the model is at an angle of attack of 0°. Note that the δ_C = -15° data provides less directional stability that the other deflections.

Lateral-Directional Stability

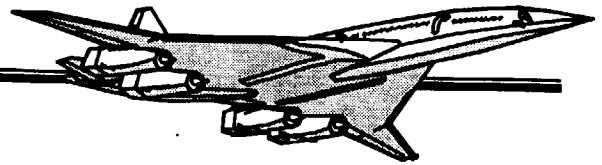

Effects of Canard/Deflection

δ_{CANARD} = OFF, 0°, +15°, -15° ~ α = 0°

Sym.	Line Symbol	Run	Canard
○	———	RUN 310	OFF
□	- - - - - - - -	RUN 478	0°
◇	— — —	RUN 483	15°
⏱	— · · —	RUN 488	-15°

NOTES:
1. HORIZONTAL TAIL ON.
2. STAB./ELEV. = 0°/0°.
3. VERTICAL TAIL ON.
4. CHINFIN OFF.
5. GEAR OFF.
6. FREE AIR.

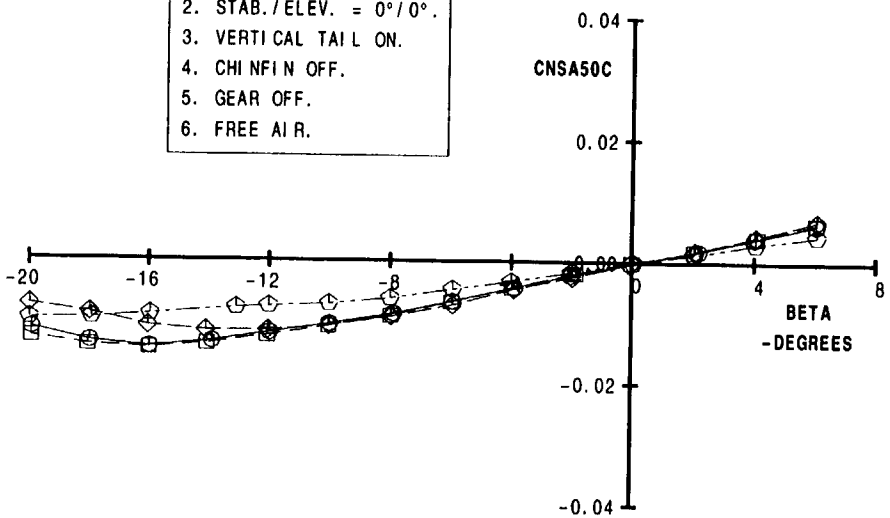

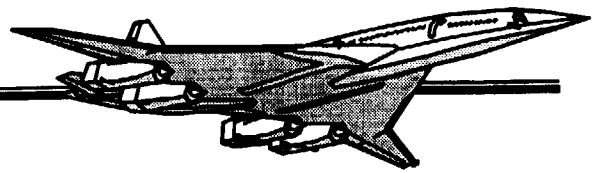

Effects of Canard/Deflection

δ_{CANARD} = OFF, 0°, +25°, -45° ~ α = 0°

The effects of larger positive (+25°) and negative (-45°) canard deflections on directional stability were also examined. Directional testing with the -45° canard deflection resulted in a near neutral stability condition through $\beta = \pm 6°$. Also note that the $\delta_{CANARD} = +25°$ condition becomes unstable beyond $\beta = -14°$. These data are also for an angle of attack of 0°.

Lateral-Directional Stability

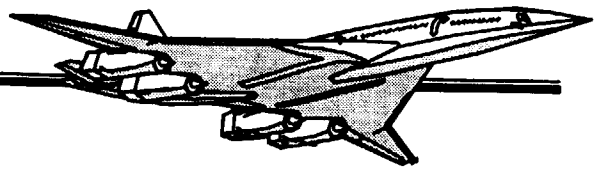

Effects of Canard/Deflection

δ_{CANARD} = OFF, 0°, +25°, -45° ~ α = 0°

Line Sym.	Symbol	Run	Canard
⏀	———	RUN 310	OFF
⏁	--------	RUN 478	0°
◇	— — —	RUN 493	25°
⏀	—·—·—	RUN 409	-45°

NOTES:
1. HORIZONTAL TAIL ON.
2. STAB./ELEV. = 0°/0°.
3. CANARD ELEVATOR = 0°.
4. VERTICAL TAIL ON.
5. CHINFIN OFF.
6. GEAR OFF.
7. FREE AIR.

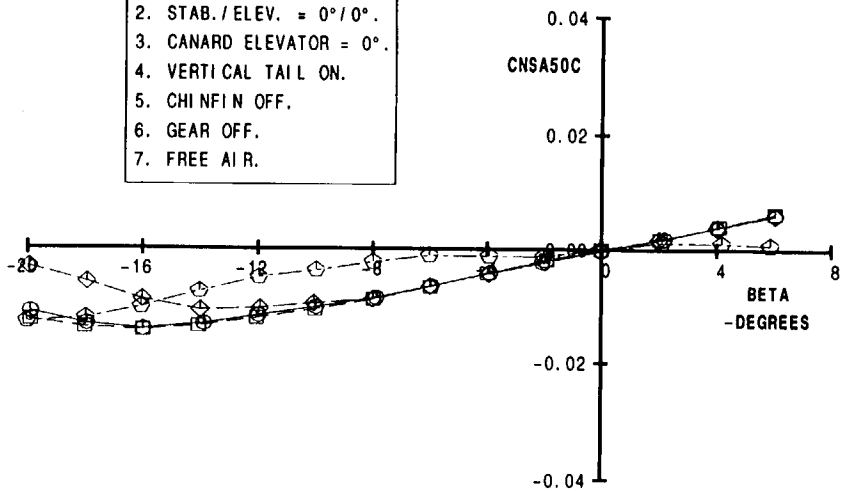

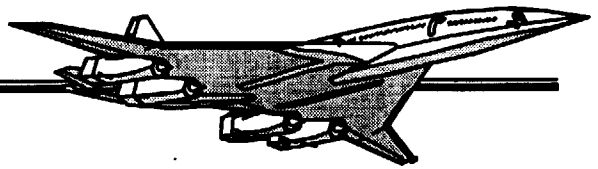

Effects of Canard/Deflection

δ_{CANARD} = OFF, 0°, +15°, -15° ~ α = 10°

For the nominal canard deflections of 0° and ±15°, the effects of angle of attack were also studied. Previously we have observed α = 0° information. Now, the chart below displays directional stability data for 10° angle of attack. The -15° canard data breaks unstable beyond β = -8°. Also observe that the δ_{CANARD} = +15° results are more stable between β = -4° and -12°.

Lateral-Directional Stability

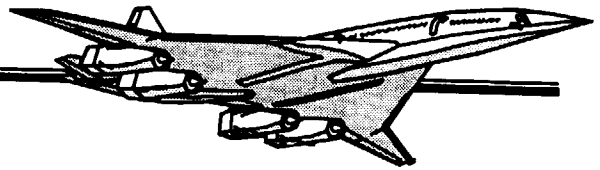

Effects of Canard/Deflection

δ_{CANARD} = OFF, 0°, +15°, -15° ~ α = 10°

Sym.	Line Symbol	Run	Canard
○	———	RUN 311	OFF
□	- - - - - - - -	RUN 479	0°
◇	— — —	RUN 484	15°
○	—·—·—	RUN 489	-15°

NOTES:
1. HORIZONTAL TAIL ON.
2. STAB./ELEV. = 0°/0°.
3. VERTICAL TAIL ON.
4. CHINFIN OFF.
5. GEAR OFF.
6. FREE AIR.

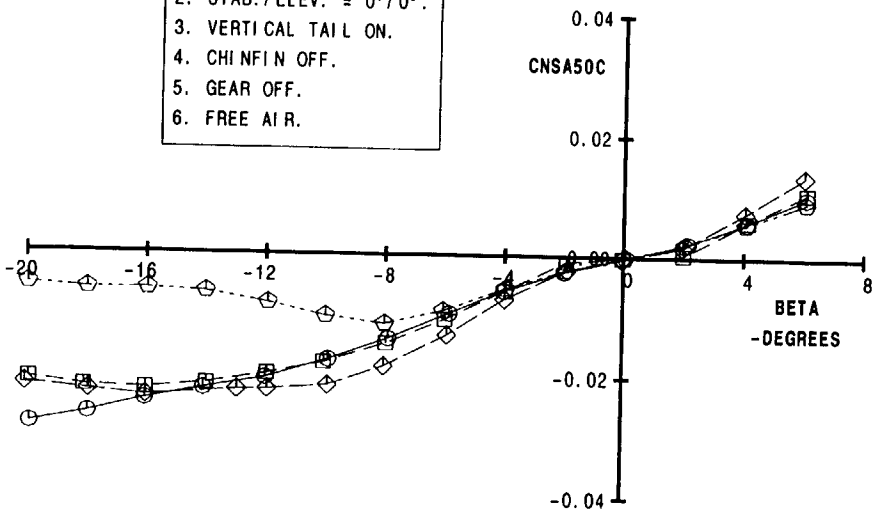

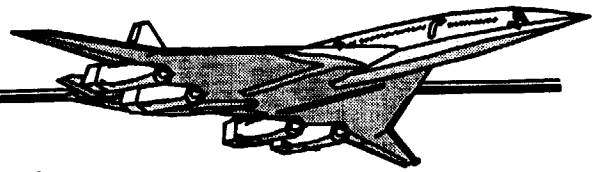

Effects of Canard/Deflection

δ_{CANARD} = OFF, 0°, +15°, -15° ~ α = 20°

The effects of the canard and its deflections were also investigated with the angle of attack at $\alpha = 20°$. Once again, the -15° canard data shows a large reduction in Cn_β, for this condition with sideslip angles more negative than -10°.

This tendency for the directional stability to degrade with negative canard deflection may result from the canard flow going above the wing and interacting with the vertical tail. For more positive canard deflections, the canard wake may be entrained by the wing wake and swept below the vertical tail.

Also note on the data displayed below that having the canard on enhances directional stability through $\beta = \pm 2°$ for this high attitude condition. It is assumed that the canard is reacting like a large forebody chine in this instance.

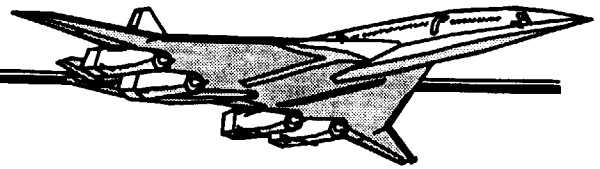

Effects of Canard/Deflection

δ_{CANARD} = OFF, 0°, +15°, -15° ~ α = 20°

Line Sym.	Symbol	Run	Canard
○	———	RUN 312	OFF
□	--------	RUN 480	0°
◇	— — —	RUN 485	15°
○	—·—·—	RUN 490	-15°

NOTES:
1. HORIZONTAL TAIL ON.
2. STAB./ELEV. = 0°/0°.
3. VERTICAL TAIL ON.
4. CHINFIN OFF.
5. GEAR OFF.
6. FREE AIR.

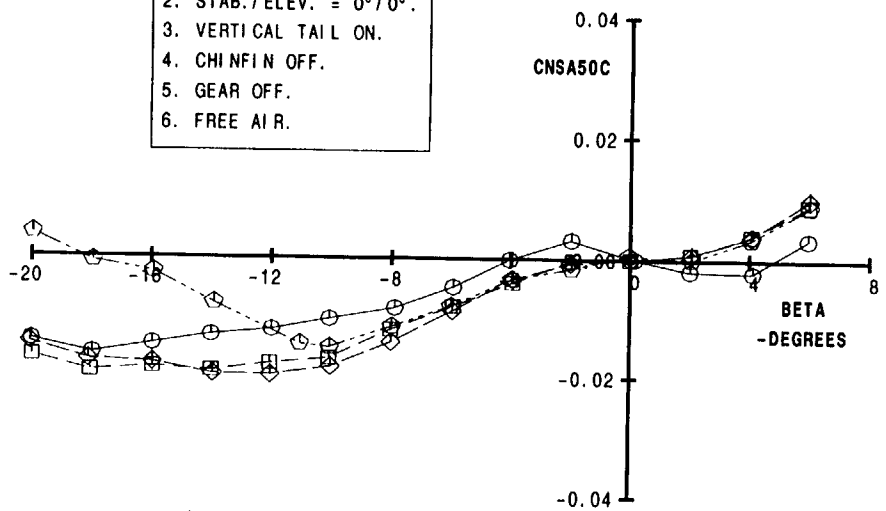

Lateral-Directional Stability

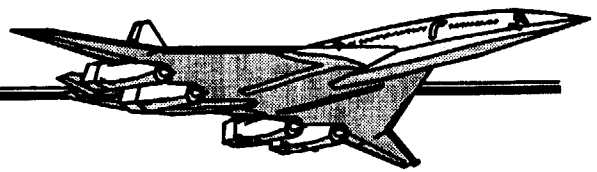

Effects of Canard/Deflection

δ_{CANARD} = OFF, 0°, +15°, -15° ~ $\beta = 0° \rightarrow -4°$ & $\beta = 0° \rightarrow -12°$

Another method of reviewing the directional stability results is presented below. The directional stability derivative Cn_β (dC_{YAW}/d_{BETA}) is plotted against angle of attack for small sideslip angles ($\beta = 0° \rightarrow -4°$) and large sideslip angles ($\beta = 0° \rightarrow -12°$). The same canard deflection angles of OFF, 0°, +15° and -15° are shown. Note that for small sideslip angles, the +15° deflection provides some benefit to directional stability between $\alpha = 0°$ and 20°. However, for the larger sideslip range, the -15° canard degrades Cn_β significantly.

HSR

TCA-4 Stability & Control Test **Lateral-Directional Stability**

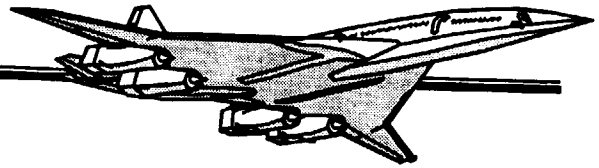

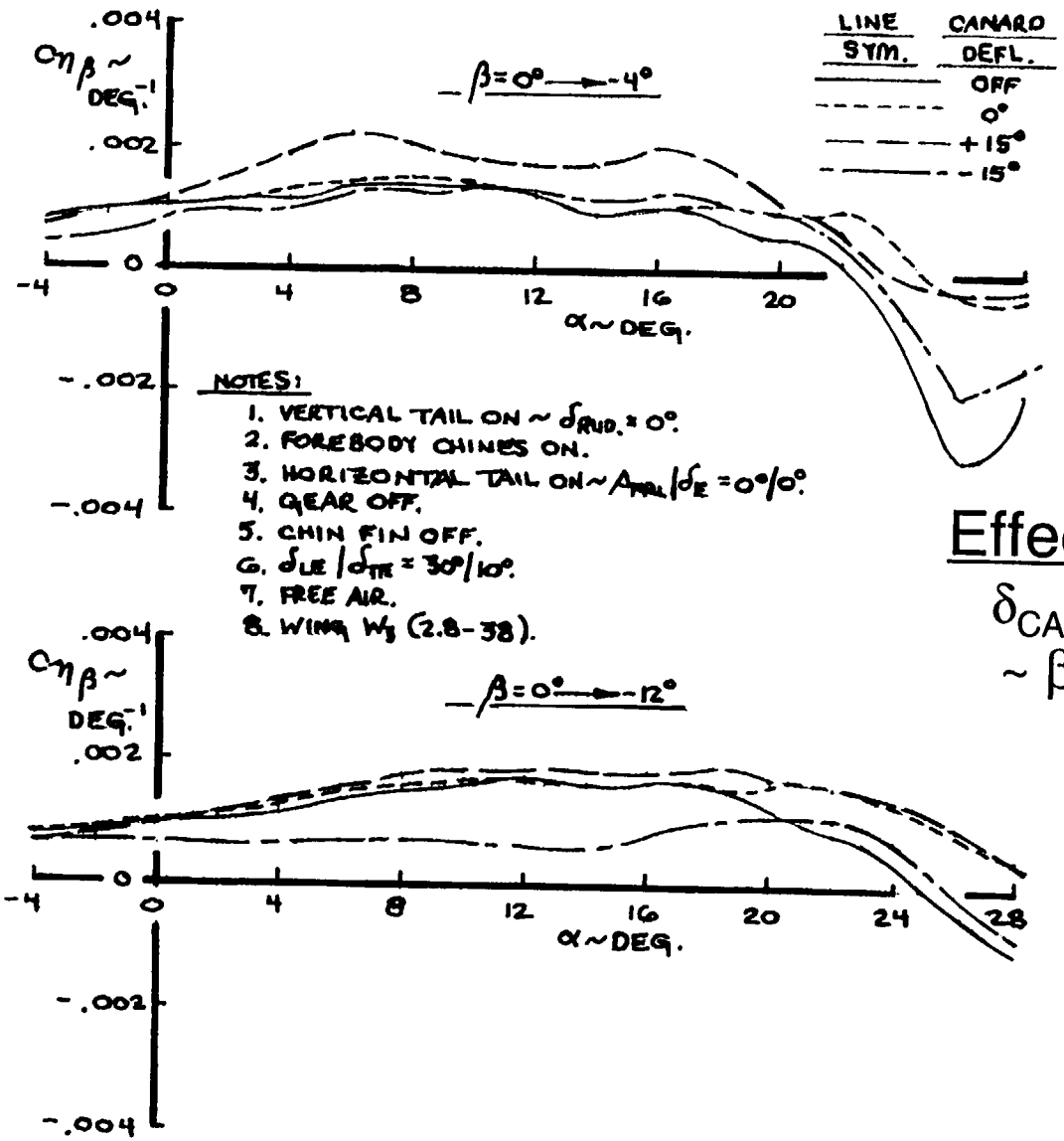

Effects of Canard/Deflection

δ_{CANARD} = OFF, 0°, +15°, -15°

~ $\beta = 0° \rightarrow -4°$ & $\beta = 0° \rightarrow -12°$

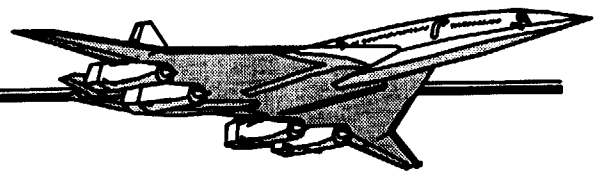

Canard Trailing Vortices

XB-70

The picture on the facing page, of the XB-70 in supersonic flight, provides an excellent visual portrayal of canard tip vortical flow aft in proximity to the vertical tails. When airplane sideslip is encountered, this canard tip vortical flow will decrease directional stability, even to a reversed state.

Test Objectives

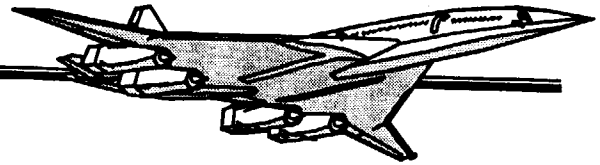

Canard Trailing Vortices

XB-70

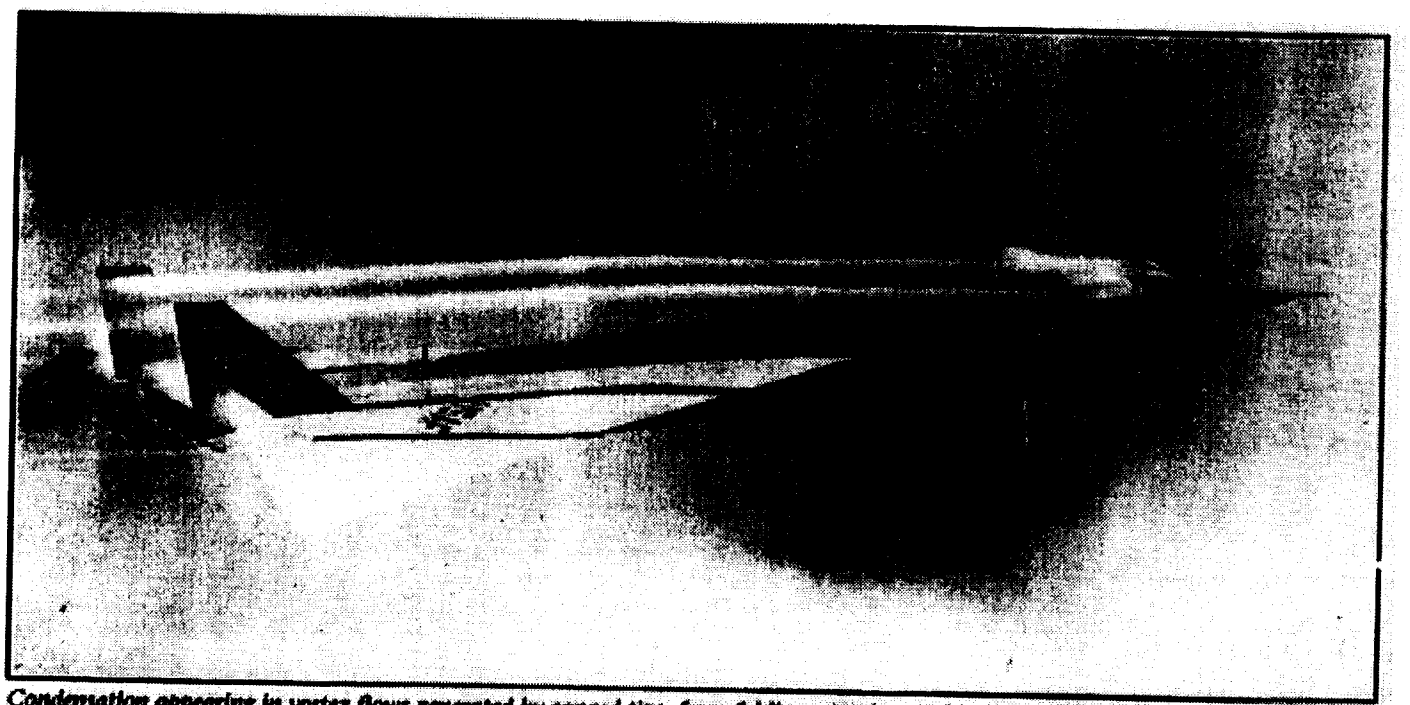

Condensation appearing in vortex flows generated by canard tips, from folding wingtips, and in expansion over the down deflected elevons for XB-70 during cruise at supersonic speeds.

4 • 92

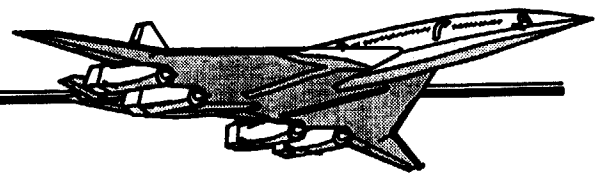

Effects of Wing Planform

Wing W1 vs. W3

Approach Flaps ~ Vertical Tail On ~ Canard Off

The effects of wing planform on directional stability over small and large sideslip ranges are shown. Wing W1 is compared with wing W3. The vertical tail was on, the canard off and the wings were in the approach flaps mode. When the wing W3 data are corrected for span and reference area, the W1 and W3 data compare well out to $\alpha \approx 14° \rightarrow 16°$. The reduced outboard sweep planform (W3) tended to have an increase in directional stability at high angles of attack.

HSR

TCA-4 Stability & Control Test **Lateral-Directional Stability**

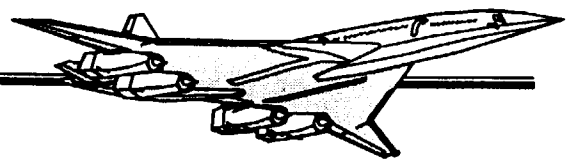

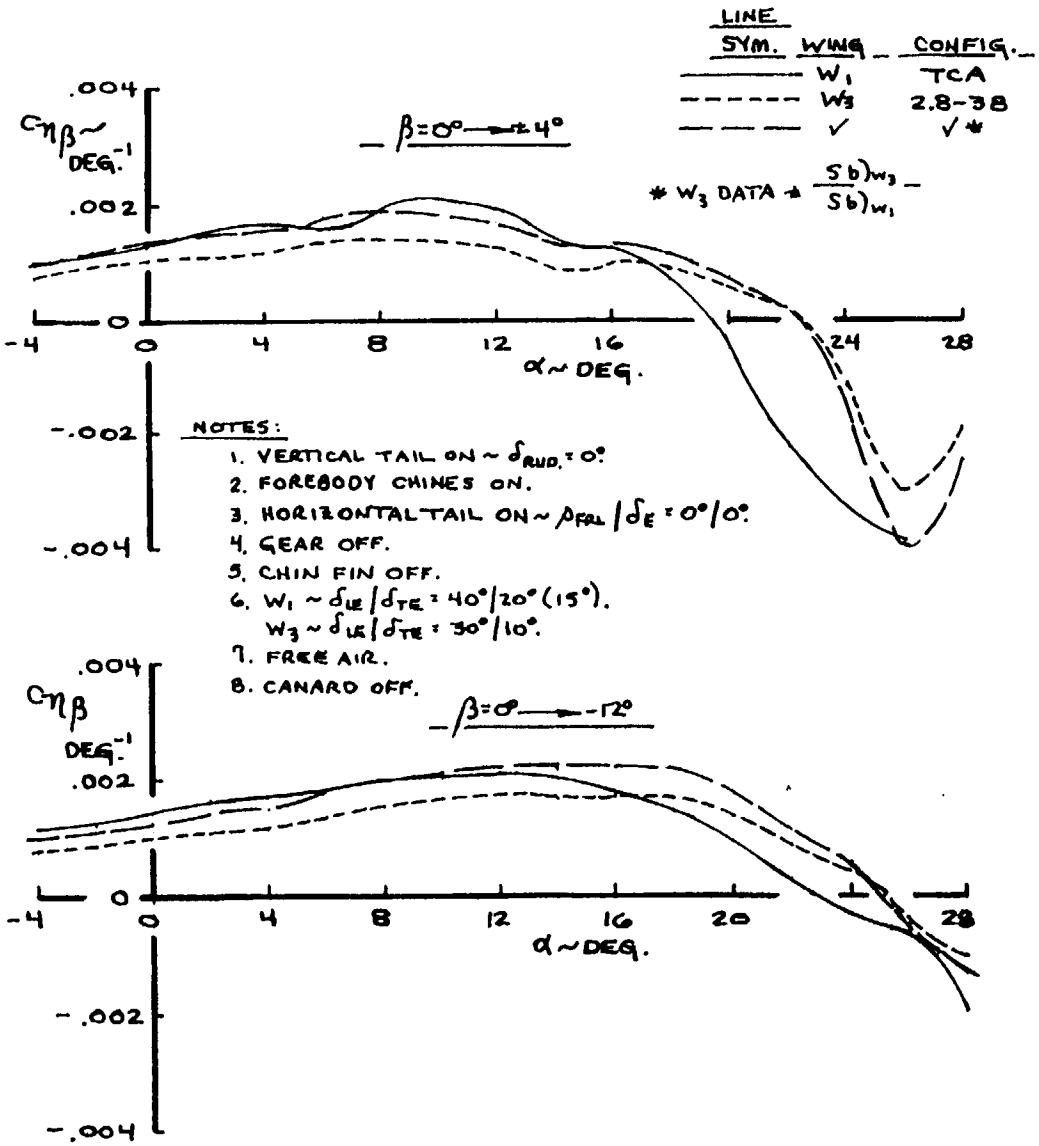

Effects of Wing Planform

Wing W1 vs. W3

Approach Flaps ~ Vertical Tail On

~ Canard Off

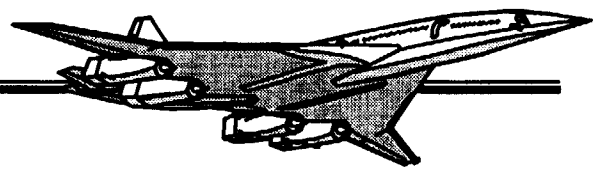

Effects of Wing Planform

Wing W2 vs. W3

Approach Flaps ~ Vertical Tail On ~ Canard On

An additional wing planform comparison was made by relating the wing W2 to wing W3 directional stability levels with the canard and vertical tail on. Here the differences are more subtle.

Lateral-Directional Stability

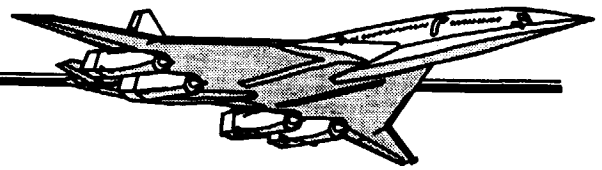

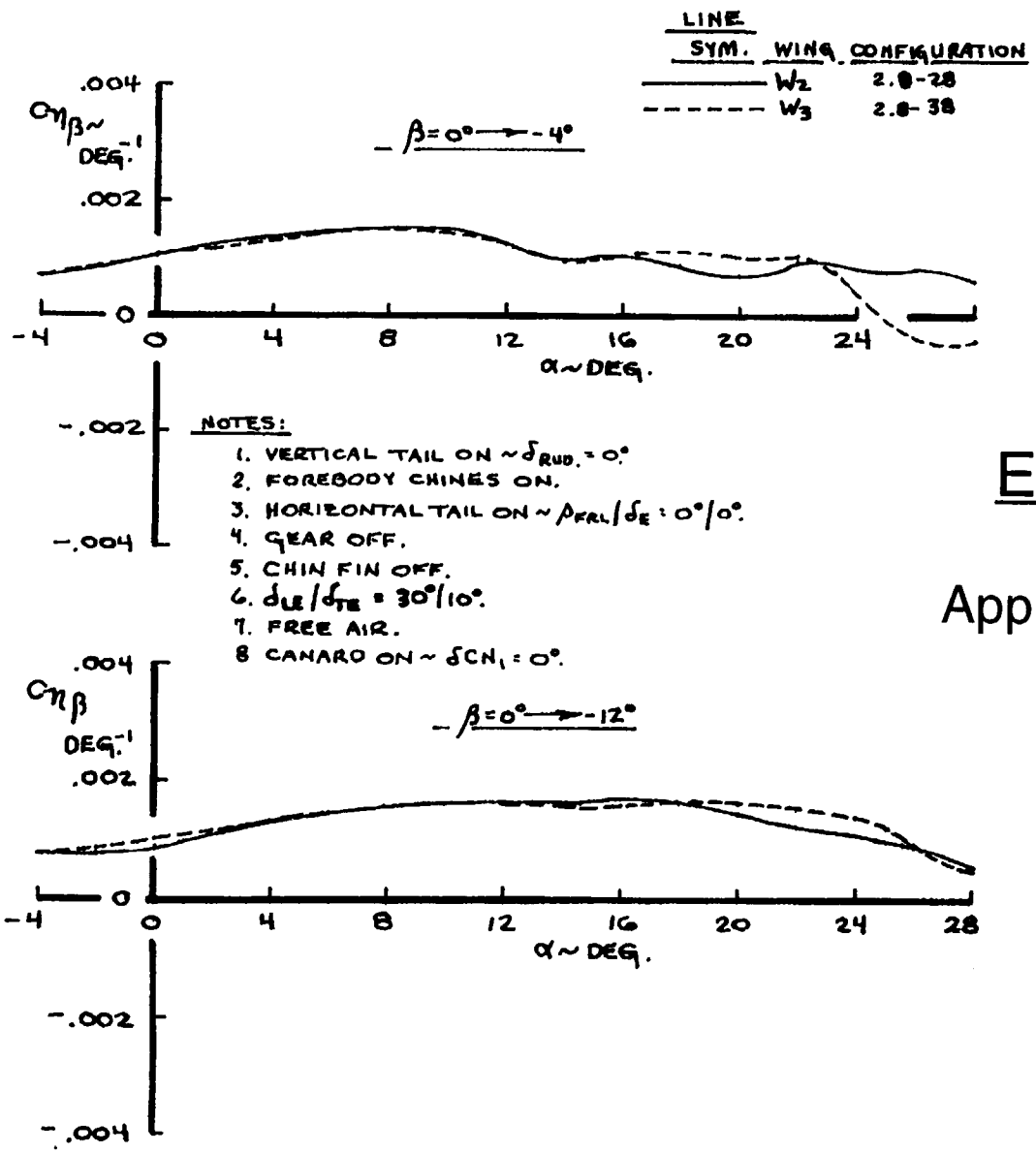

Effects of Wing Planform

Wing W2 vs. W3

Approach Flaps ~ Vertical Tail On

~ Canard On

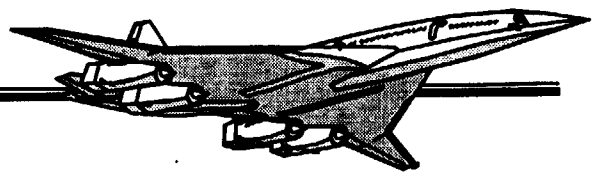

Effects of Wing LE/TE Flap Deflection

Wing W3 ~ Canard On at 0°~ Vertical Tail On

The effects of wing flap deflection on directional stability for wing W3 with the canard and vertical tail on were also analyzed. Once again, the configuration included wing W3 with the vertical tail and canard on at 0°. A clean wing (flaps at 0°/0°) condition was compared to a flaps 30°/10° wing. For the smaller sideslip range, the clean wing condition has better high attitude directional characteristics.

Lateral-Directional Stability

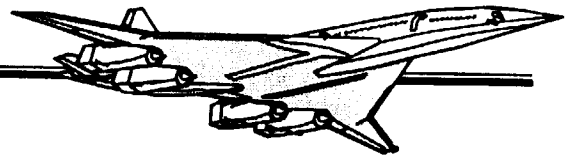

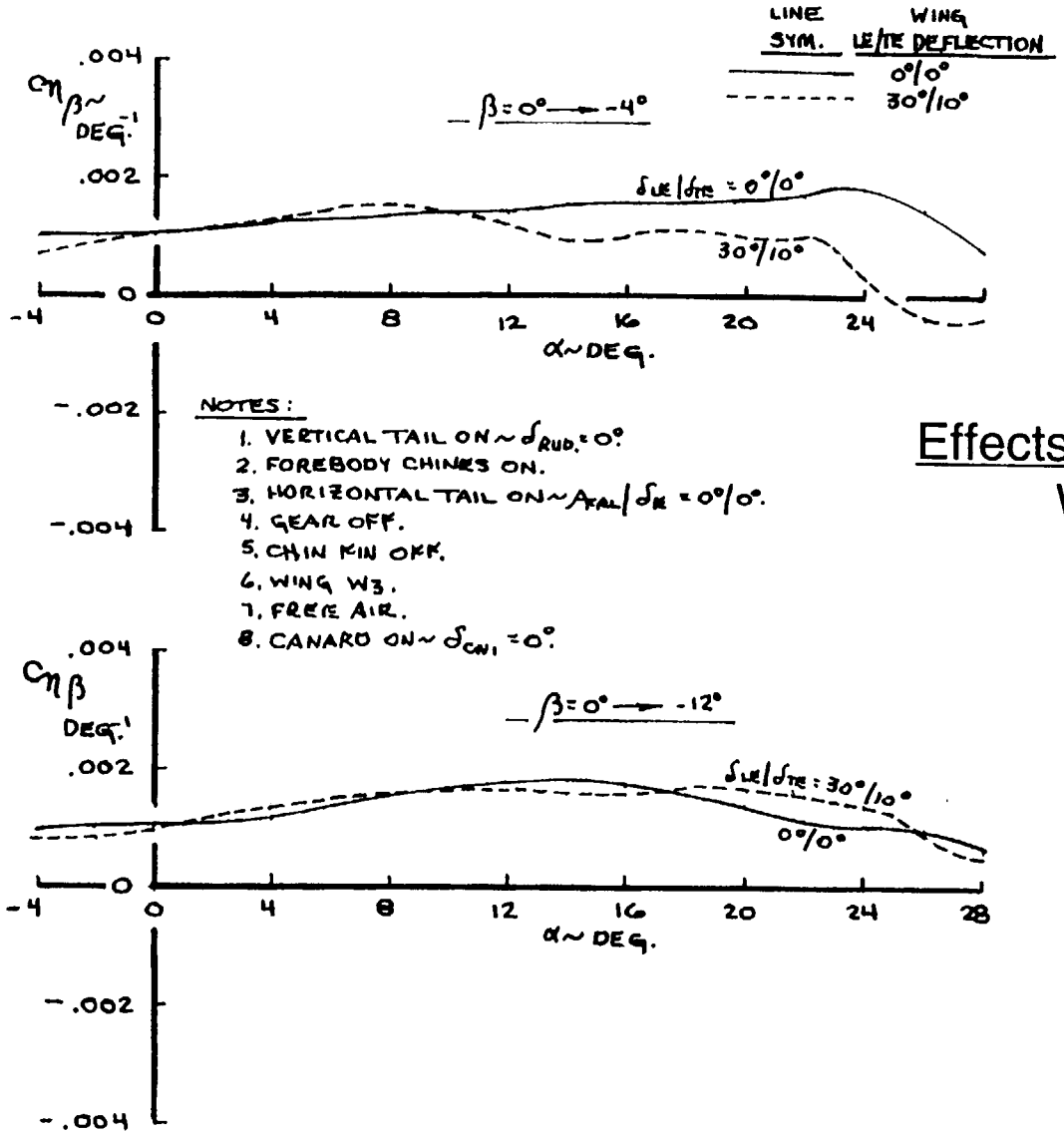

Effects of Wing LE/TE Flap Deflection

Wing W3 ~ Canard On at 0°
~ Vertical Tail On

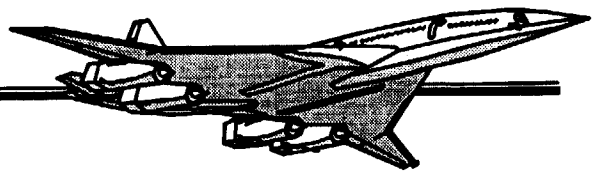

Effects of Chin Fin

Wing W3 ~ Canard On at 0°~ Vertical Tail On

The effects of a forebody chin fin were examined during this test entry. This small (25 ft.^{2}-full scale) surface was added to the configuration to provide side force damping to the airplane lateral bending mode. The +20° deflected chin fin did show a reduction in directional stability from $\alpha = 7°$ to $\alpha = 20°$ for the small sideslip deflection range. The side force control capability will be discussed in the next section.

Lateral-Directional Stability

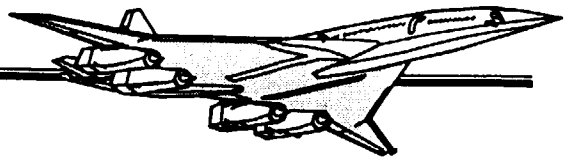

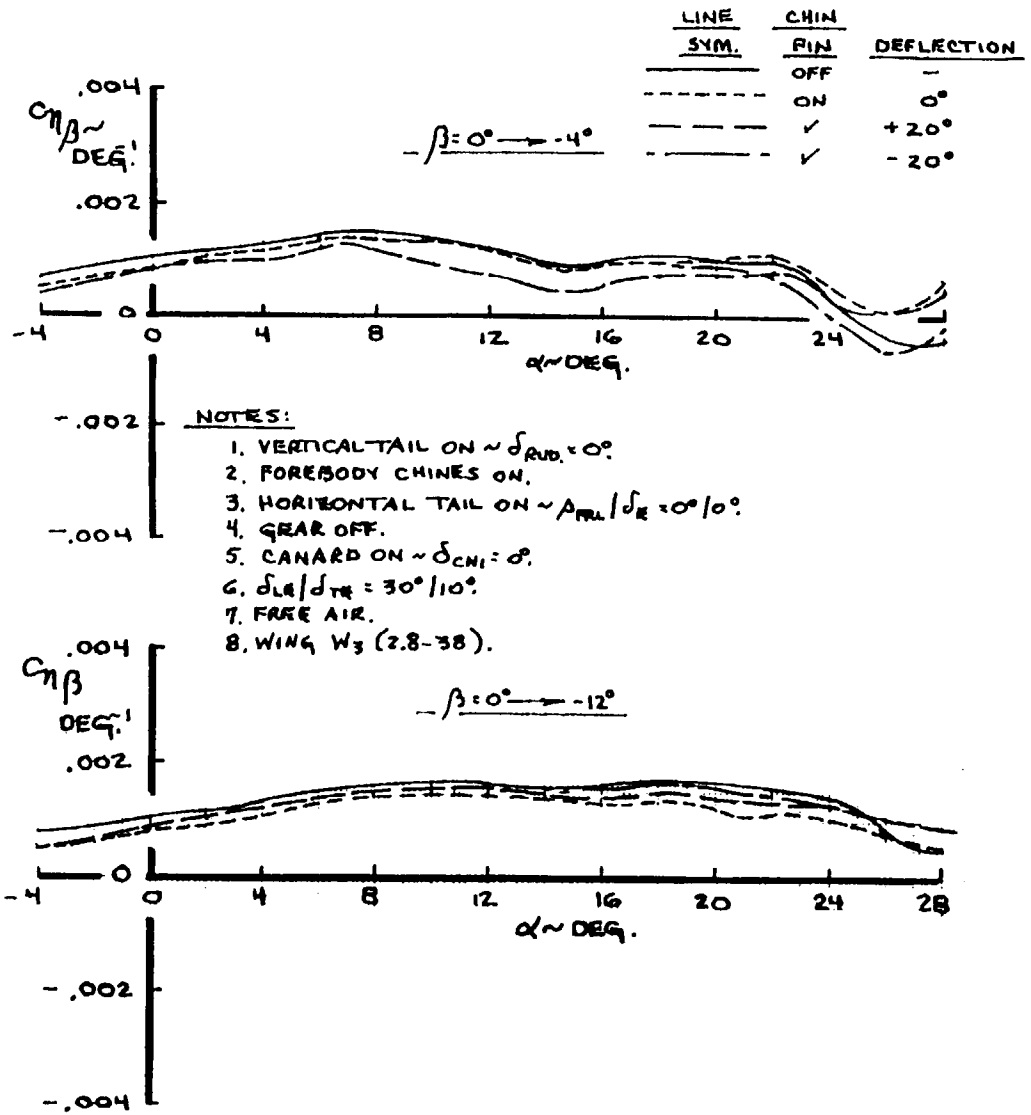

Effects of Chin Fin

Wing W3 ~ Canard On at 0°
~ Vertical Tail On

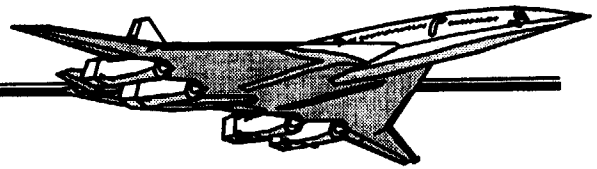

Lateral-Directional Control

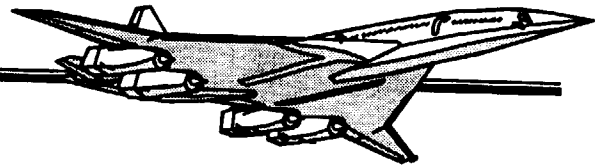

Flaperon Effectiveness

Wing W1 vs. W2 vs. W3

Prior to this test entry, there was concern that the reduced outboard wing sweep of wings W2 and W3 would be more susceptible to separation, reducing flaperon effectiveness at higher angles of attack. The reverse was indeed true, as shown in the attached chart. It is assumed that this enhanced flaperon control results from a higher outboard wing lift.

Lateral-Directional Control

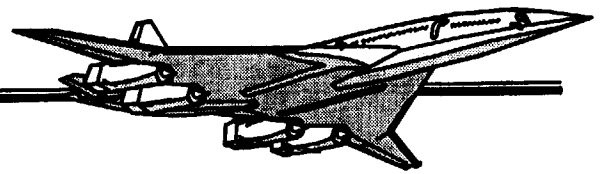

Wing Flaperon Effectiveness

W1 vs. W2 vs. W3

Sym.	Line Symbol	Run	Test	TE (5-8) Deflection	Plnfrm. Config.	Wng	LE
○	———	RUN 579	473	0°/30°/30°/30°	TCA 4	W3	30°
□	- - - - - - -	RUN 581	473	0°/-30°/-30°/-30°	TCA 4	W3	30°
◇	— — —	RUN 906	473	0°/30°/30°/30°	TCA 4	W2	(25°)30°
○	—·—·—	RUN 904	473	0°/-30°/-30°/-30°	TCA 4	W2	(25°)30°
△	·····	292	449	0°/30°/30°/30°	TCA 1	W1	30°
▽	·-·-·-	304	449	0°/-30°/-30°/-30°	TCA 1	W1	30°

TCA 4: BASE RUN (TE=0°/0°/0°/0°), LE = 30°) = RUN 577
TCA 4: BASE RUN (TE=0°/0°/0°/0°), LE=(25°)30°) = RUN 908
TCA 1: BASE RUN (TE=0°/0°/0°/0°), LE = 30°) = RUN 293

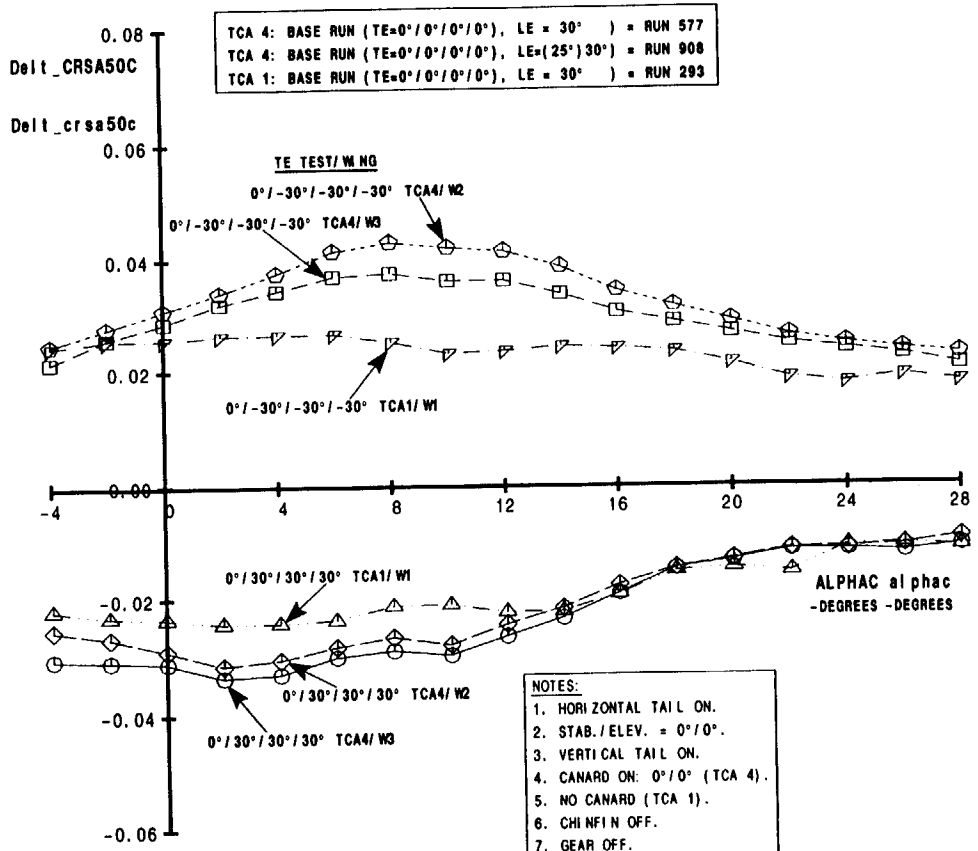

NOTES:
1. HORIZONTAL TAIL ON.
2. STAB./ELEV. = 0°/0°.
3. VERTICAL TAIL ON.
4. CANARD ON: 0°/0° (TCA 4).
5. NO CANARD (TCA 1).
6. CHINFIN OFF.
7. GEAR OFF.
8. FREE AIR.

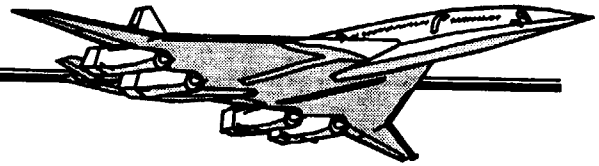

Rudder Effectiveness

Wing W1 vs. W3

Three panel rudder effectiveness was checked on this test entry. After correcting for geometry, the rudder control from TCA-4 was found to agree very well with similar data from TCA-1.

HSR

TCA-4 Stability & Control Test ***Lateral-Directional Control***

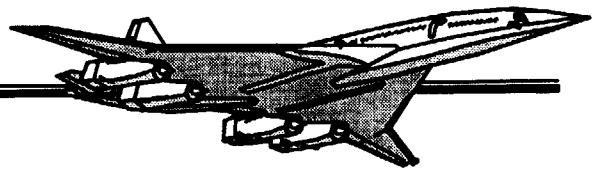

Rudder Effectiveness

Wing W1 vs. W3

Sym.	Line Symbol	Run	Test	Rudder	LE/TE	Plnfrm. Config.	Wing
○	———	RUN 454	473	25°	30°/10°	TCA 4	W3
□	--------	278	449	25°	40°/20°(15°)	TCA 1	W1

TCA 4: BASE RUN (RUD=0°, LE/TE=30°/10°) = RUN 304
TCA 1: BASE RUN (RUD=0°, LE/TE=40°/20°(15°)) = RUN 254

NOTES:
1. HORIZONTAL TAIL ON.
2. VERTICAL TAIL ON.
4. CANARD ON: 0°/0° (TCA 4).
5. NO CANARD (TCA 1).
6. CHINFIN OFF.
7. GEAR OFF.
8. FREE AIR.

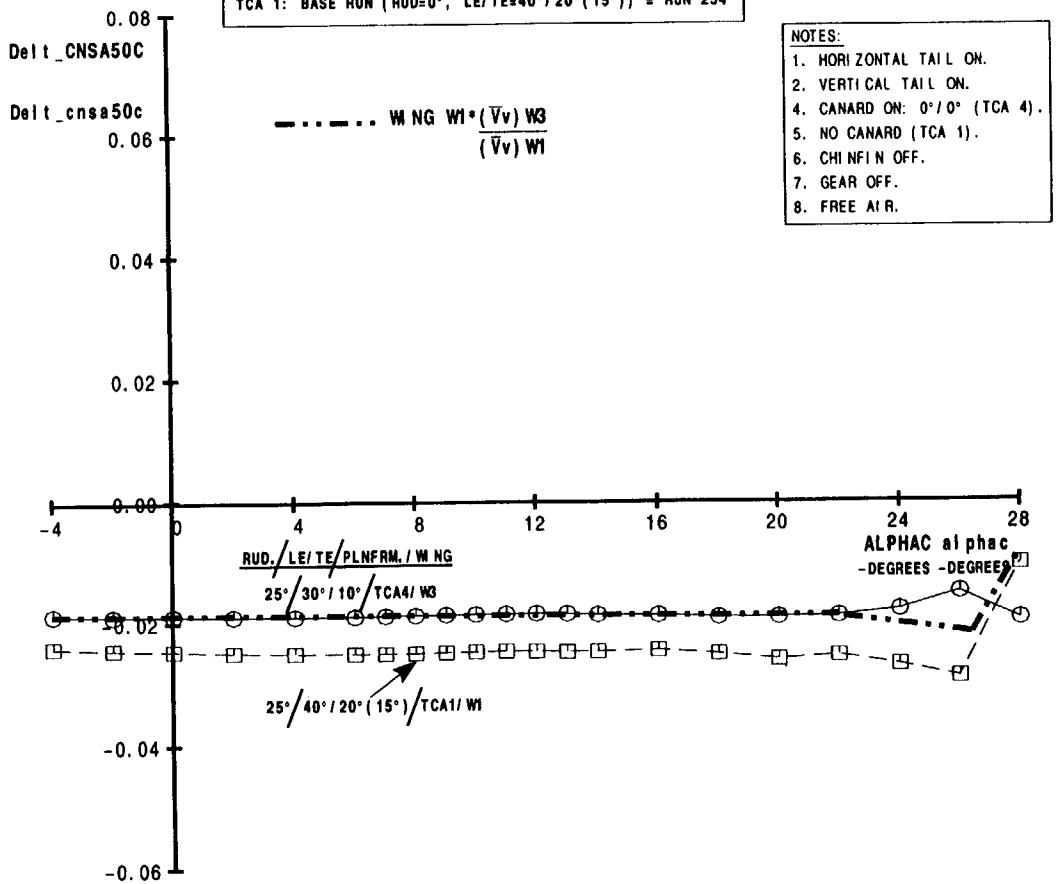

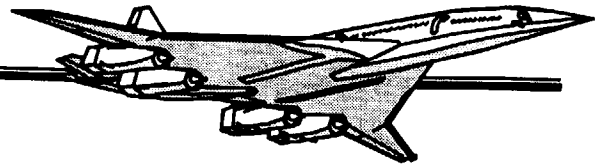

Rudder Effectiveness
Effect of Canard

The effect of the canard on rudder control was briefly investigated. Canard off and canard on at $\delta_c/\delta_e = +15°/0°$ were tested with the vertical tail off, rudder = 0° and +25°. Note that rudder effectiveness deteriorates with increasing angle of attack with the canard on configuration. Since the directional stability was eroded with negative canard deflection angles, this condition will receive special attention during the next test entry, TCA-5.

HSR

TCA-4 Stability & Control Test **Lateral-Directional Control**

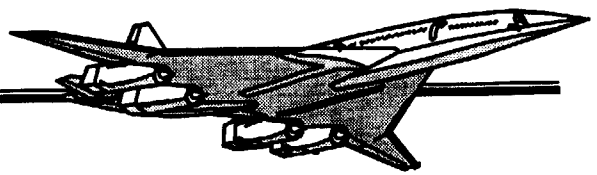

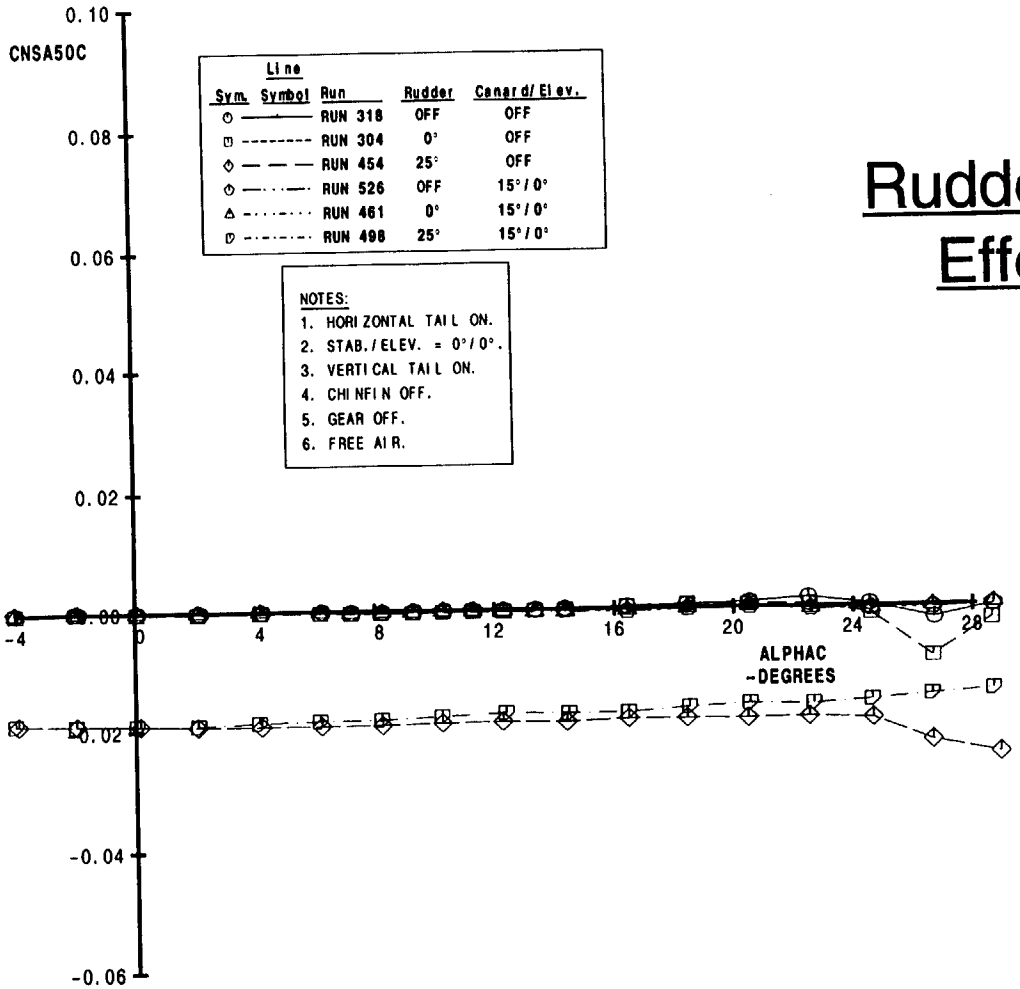

Rudder Effectiveness
Effect of Canard

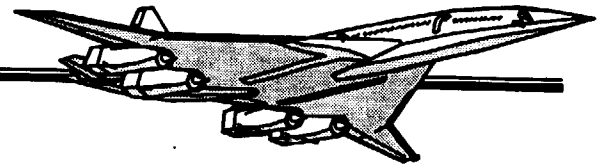

Chin Fin Effectiveness

$\beta = 0°, -4°, -12°$ ~ Canard On

The $25ft^2$ (full scale) chin fin was on the configuration to alleviate the lateral bending mode dynamics thought to be likely with this airplane configuration. The chin fin was found to lose effectiveness with even a moderate angle of attack increase. At high angles of attack, the chin fin demonstrates reversal characteristics. Because of these concerns, the forebody chin fin concept has been eliminated as a lateral control bending mode control surface. A canard with differential elevator dihedral will be evaluated during the next test.

Lateral-Directional Control

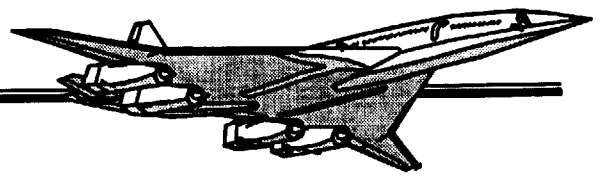

Chin Fin Effectiveness

$\beta = 0°, -4°, -12°$ ~ Canard On

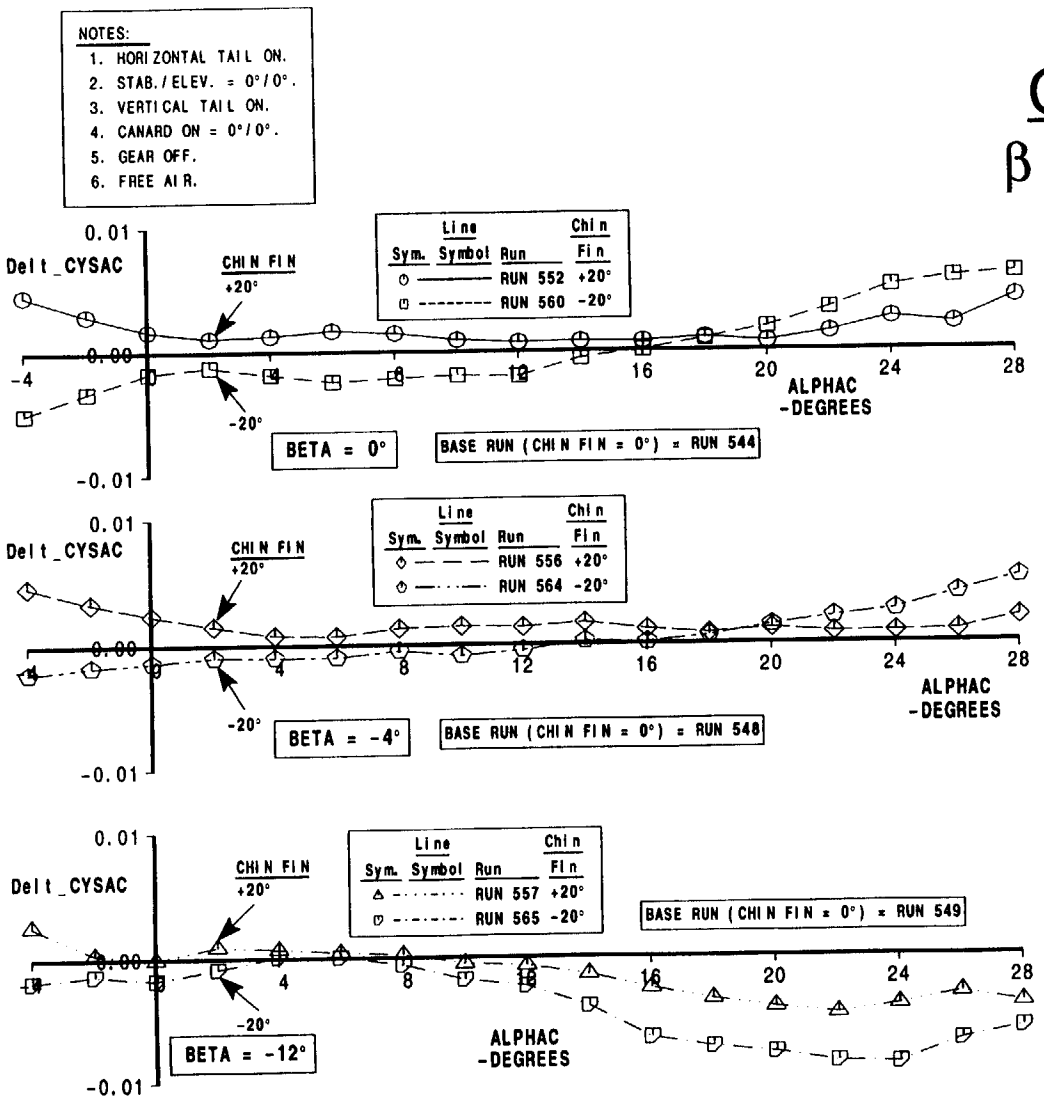

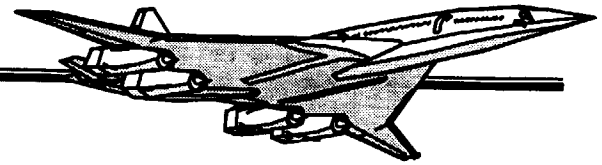

Chin Fin Effectiveness

Forebody Flow Characteristics

David Yeh of Boeing-Long Beach used a CFD generated flowfield to determine model forebody characteristics with a deflected chin fin in place at $\alpha = 0°$ and 10°. It will be seen that at $\alpha = 10°$, a vortex suction force counteracting the deflected chin fin force is produced. This is an excellent example of the usefulness of CFD in assisting stability and control.

Lateral-Directional Control

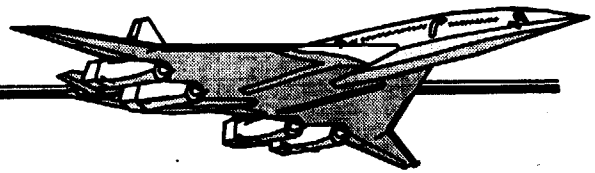

Forebody Chin Fin Flow Characteristics

M=0.3, δ=20°, α=0°

Front View

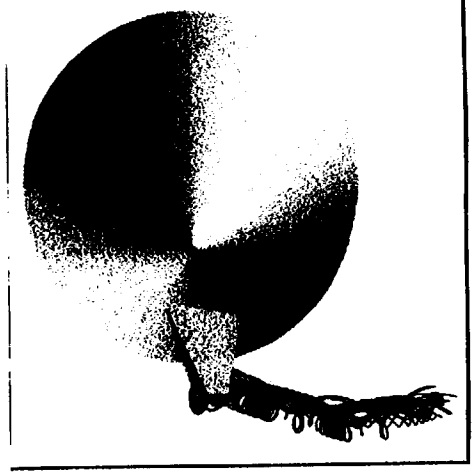

Side View

Bottom View

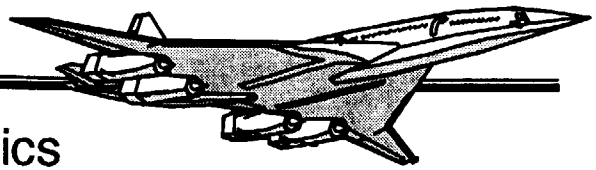

Forebody Chin Fin Flow Characteristics

M=0.3, δ=20°, α=10°

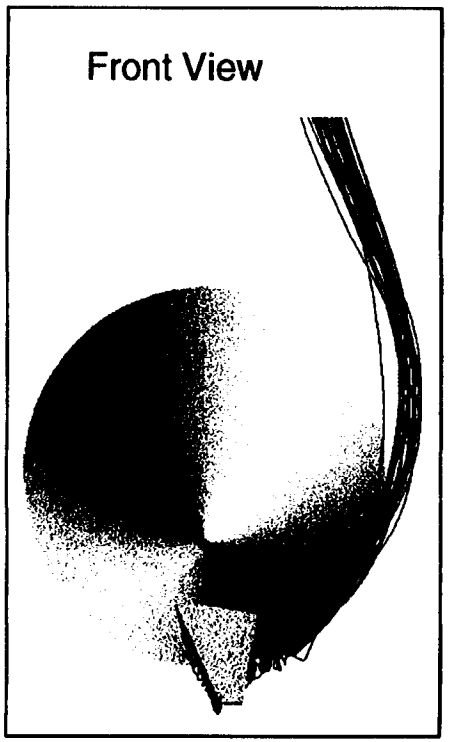

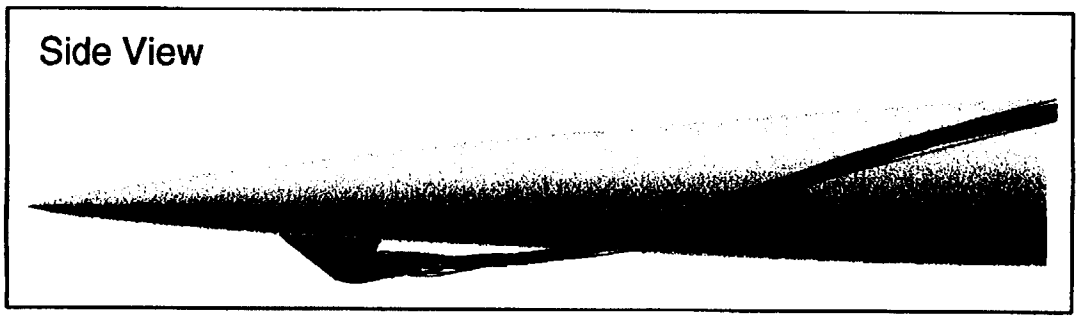

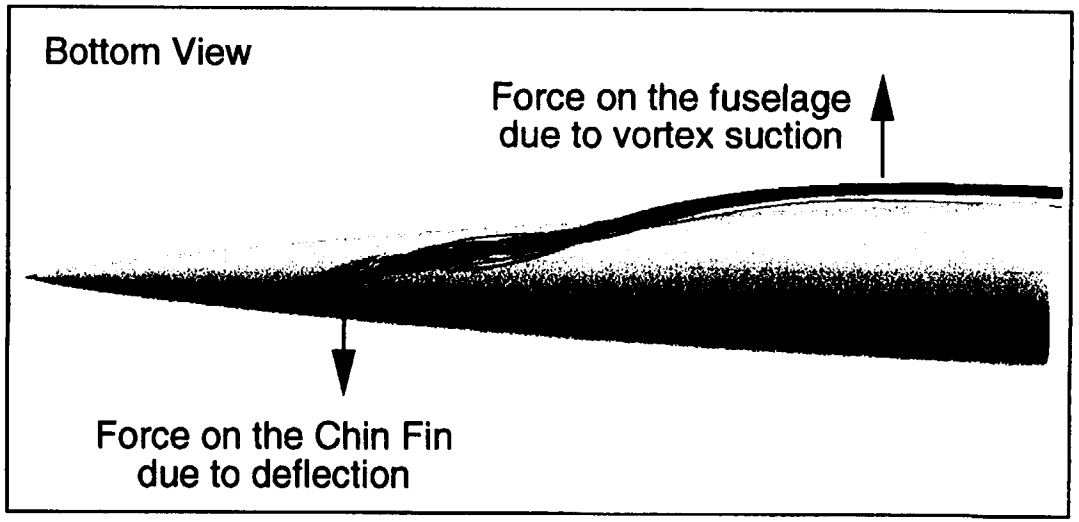

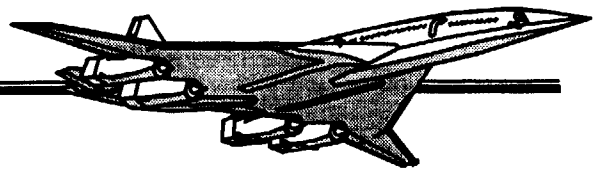

Repeatability

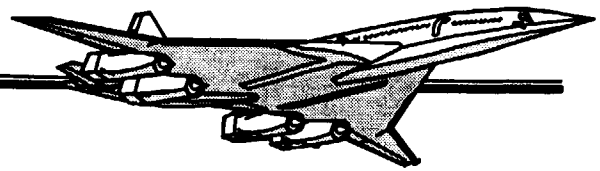

Longitudinal Stability ~ Short Term

Horizontal Tail On ~ Canard Off

Repeatability during TCA-4 was explored in several ways. Three runs were done back-to-back to provide "short-term" repeatability. The data from one such set are shown in the attached plot. Pitching moment repeatability is seen to be very good.

Repeatability

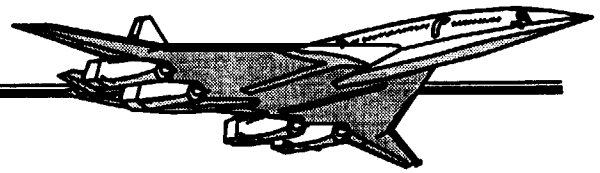

Longitudinal Stability ~ Short Term

Horizontal Tail On ~ Canard Off

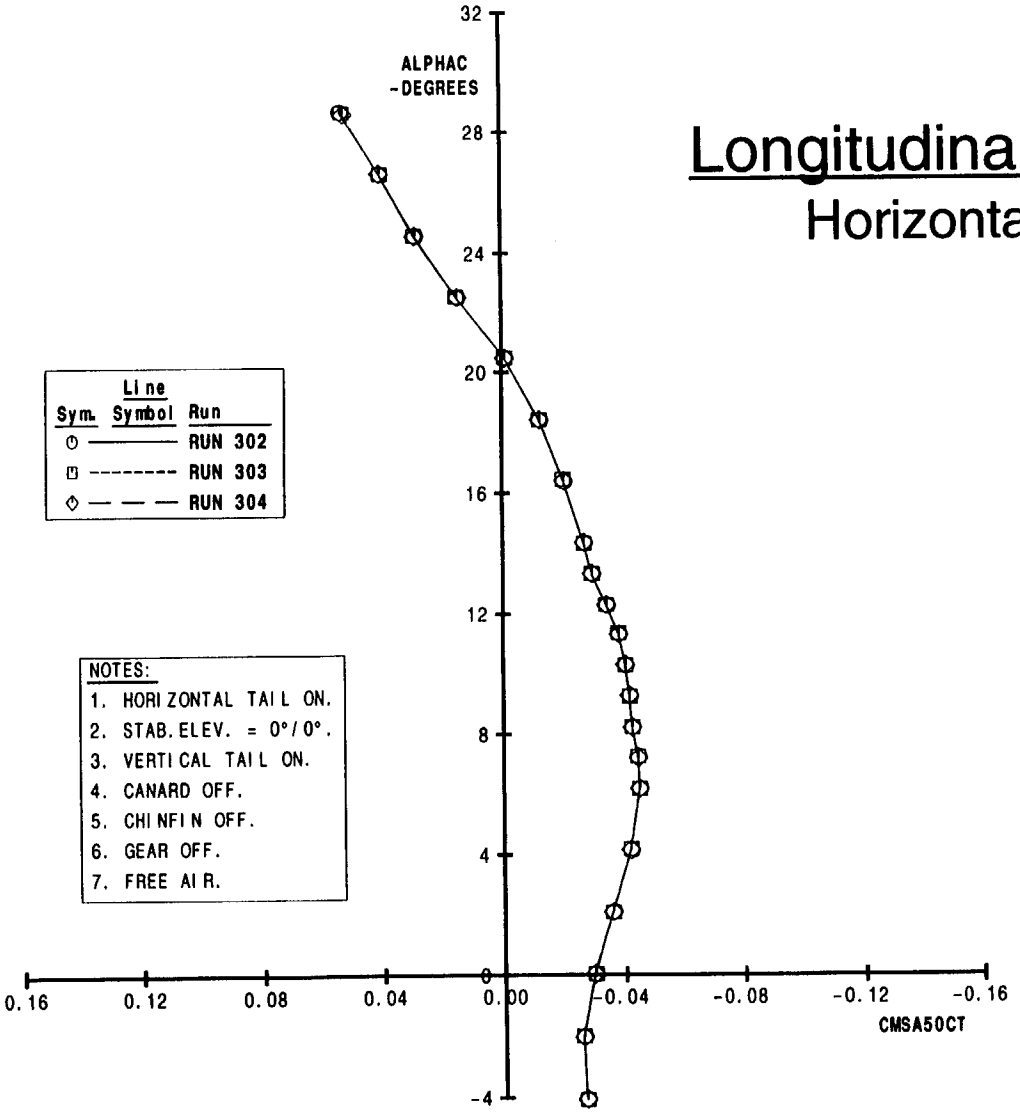

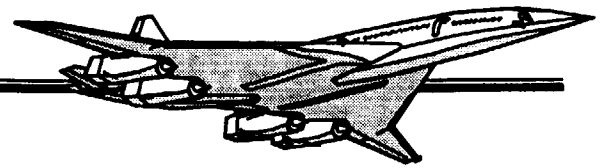

Longitudinal Stability ~ Long Term

Horizontal Tail On ~ Canard On

Another scheme for determining repeatability during this test was to run the same configuration over the course of time, with many different configurations tested in between. This was known as "long-term" repeatability.

HSR

TCA-4 Stability & Control Test

Repeatability

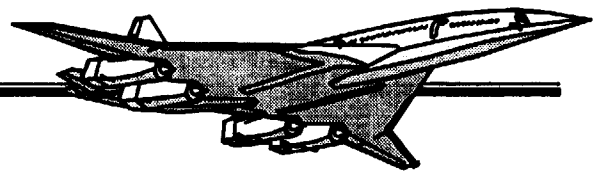

Longitudinal Stability ~ Long Term

Horizontal Tail On ~ Canard On

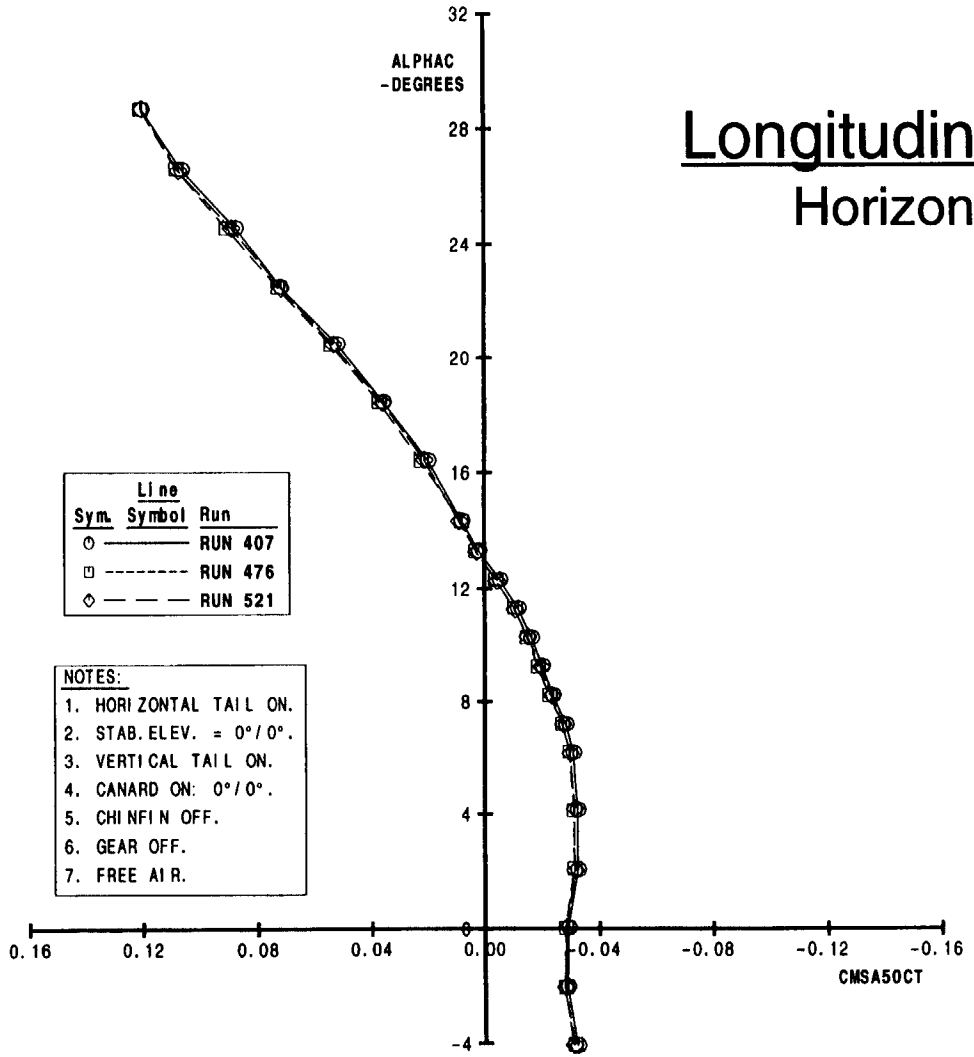

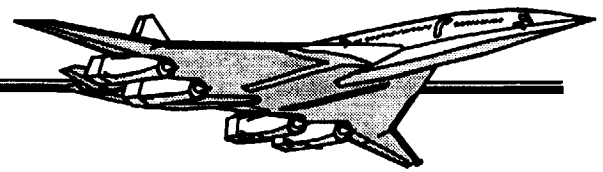

Longitudinal Stability and Control ~ Test-to-Test

Wing W1 ~ Canard Off

Initially, wing W1 was installed. The TCA-4 data were compared to TCA-1 data taken with the same configuration. While the Cm_o levels did not exactly match, the pitching moment curve shapes were very comparable.

HSR

TCA-4 Stability & Control Test

Repeatability

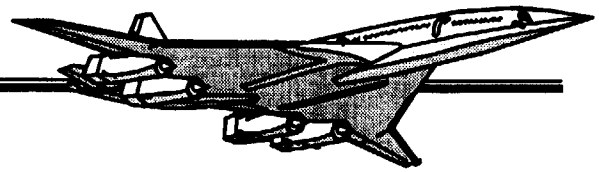

Longitudinal Stability and Control ~ Test-to-Test

Wing W1 ~ Canard Off

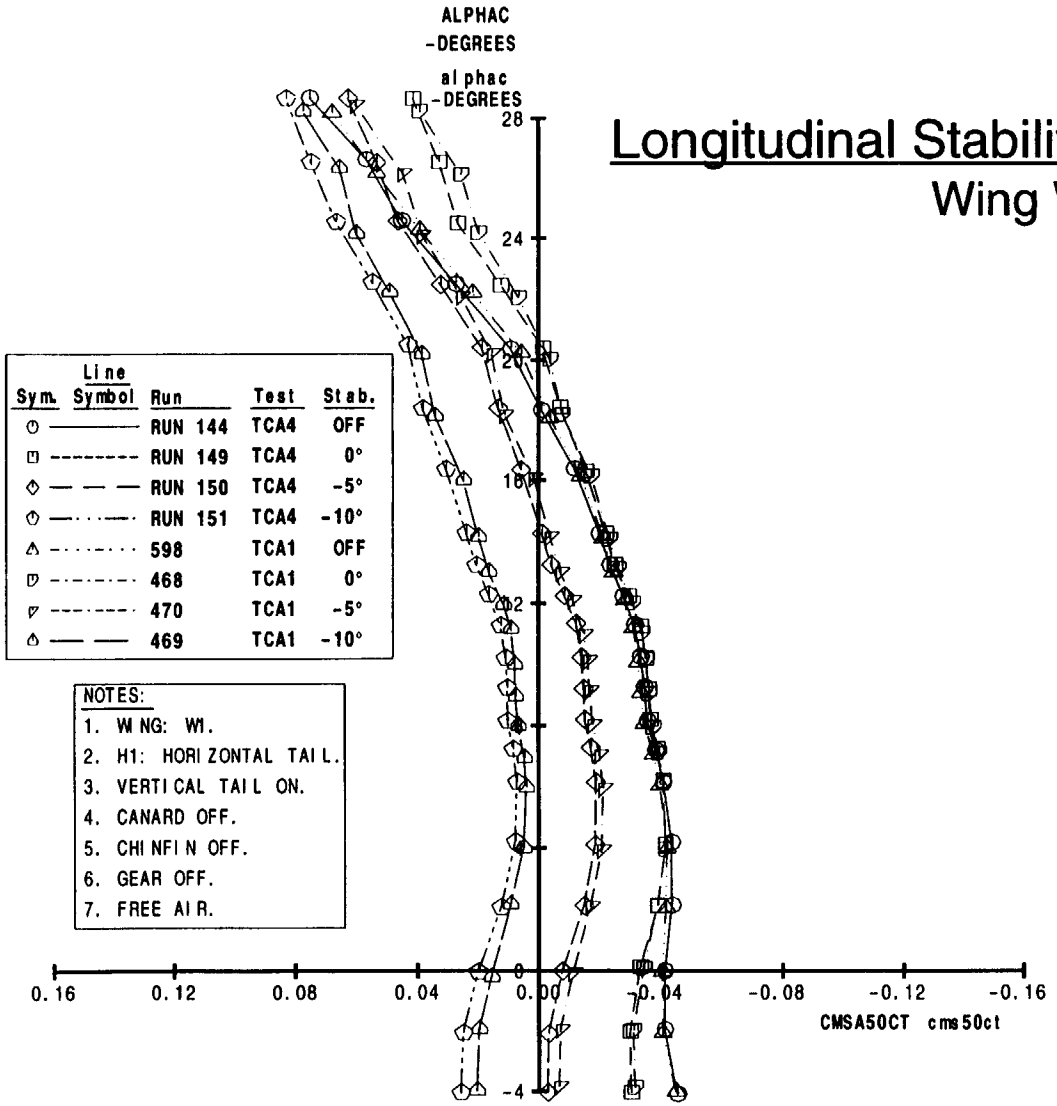

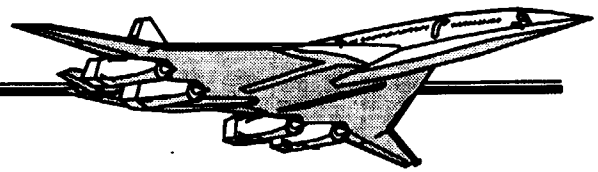

Conclusions

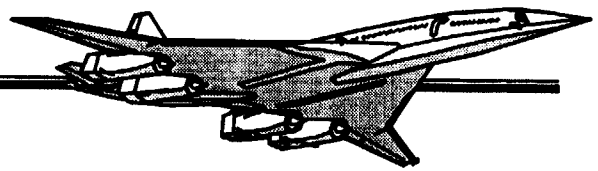

Conclusions--Stability and Control

The TCA-4 test entry answered a number of stability and control questions. Among them were:

1. There were no "showstoppers" associated with the new wing planforms.

2. Ground effects on longitudinal stability were large with the horizontal tail on, but small with the tail off.

3. The addition of the canard decreased pitch stability (as expected).

4. Longitudinal stability/downwash data were altered locally by positive canard/elevator deflections.

5. Negative canard/elevator deflections produced a reduction in directional stability.

(continued on next page)

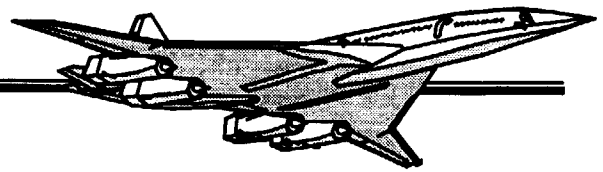

Conclusions--Stability and Control

(continued from previous page)

6. The reduced outboard wing sweep configuration provided increased flaperon effectiveness.

7. Chin fin-induced side force was lower than expected at operating angles of attack. CFD was very useful understanding the associated flow characteristics.

8. With-in test repeatability was good.

   As is the usual situation, additional concerns arose which will need to be answered during the next test entry.

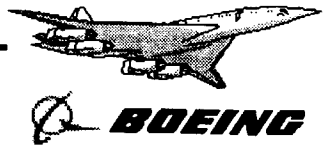

TCA Final Assessment and Test/Theory Comparisons for Sealed Slats

Allen W. Chen

HSR Annual Airframe Technical Review
February 9, 1999

Outline

- The first five items are for the TCA final assessment. The sealed slats are for CFD/test comparisons.

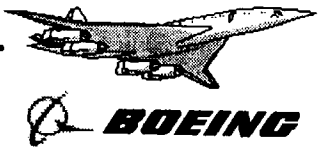

Outline

- Review of exit criteria for TCA final assessment
- Summary of TCA assessment
- Process for assessment
- Review of wind tunnel data
- Assessment
- Seal slats
- Conclusions and recommendations

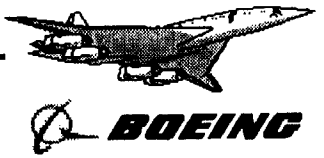

Review of Exit Criteria for TCA Final Assessment

- These are the criteria specified by PCD 2.

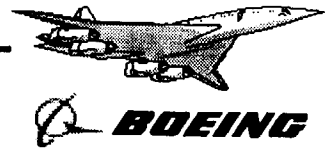

Review of Exit Criteria for TCA Final Assessment

- L/D characteristics
- S & C characteristics
- Assessment of L/D and S & C relative to high-lift technology metrics
- Reynolds number effect on L/D and S & C
- Conclusions and recommendations

Summary of TCA Final Assessment
- High Lift -

- The data from 14x22 has more drag. The reason is not understood. Possible explanation includes differences in upflow and model support interference between 14x22 and the Ames 12-ft.
- 8 M < Re < 37 M in TCA-3 but the Re effect is smaller than what was observed at NTF for the same Reynolds number range.

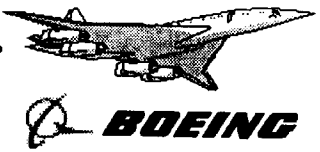

Summary of TCA Final Assessment - High Lift -

- 8.15 (based on 14x22 data) < L/D < 8.89 (based on NTF and 12-ft data)
- Re effect is small for TCA-3
- High Re data from NTF is very valuable
- More complex leading edge devices than the plain flaps are needed to achieve the technology projection

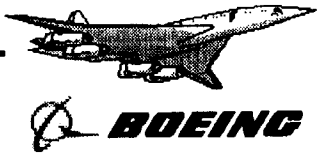

Summary of TCA Final Assessment - Stability and Control -

- The TCA configuration shows a degradation in high attitude longitudinal stability when compared to the Ref. H.
- Stall recovery was enhanced on the TCA model by extending the part-span leading edge flaps inboard to the side to the body.
- Ground effect trends are in good agreement between the TCA and Ref. H.
- A dramatic increase in directional stability is seen with the TCA configuration at high angles of attack for the flaps up condition. For the higher LE and TE flap deflections, the two airplane models have much more similar directional stability characteristics.
- The TCA has less maximum lateral control capability than the Ref. H.

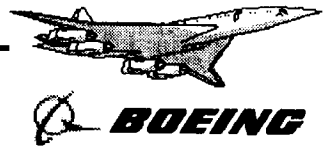

Summary of TCA Final Assessment - Stability and Control -

- dC_L/dC_M at high α worse than Ref. H
- Full-span LE flaps enhance the stall recovery
- Ground effect trend similar to Ref. H
- $dC_n/d\beta$ similar to Ref. H for flaps down
- Less maximum lateral control than Ref. H
- Re effect is small

Process for Assessment

- The tail-off wind tunnel data is corrected for wall effects, model support effects, nacelle internal drag, nacelle base drag, etc.
- The Reynolds number correction depends on the wind tunnel database.

-17.4 8 M to 90 M NTF data with truncated fuselage	-3.7 8 M to 90 M Aft body and tails A389	-7.7 90 M to 206 M full airplane A389	= 28.8 counts 8 M to 206 M
-3.9 37 M to 90 M NTF data with truncated fuselage	-3.7 8 M to 90 M Aft body and tails A389	-7.7 90 M to 206 M full airplane A389	= 15.3 counts 37 M to 206 M

- The geometry increment by AERO3S was applied only when the Ref. H wind tunnel data was used to predict the TCA performance.
- The programmed flap drag polar is the envelope of 169 cases where 13 LE flap deflections are permuted with 13 TE flap deflections.

BOEING

Process for Assessment

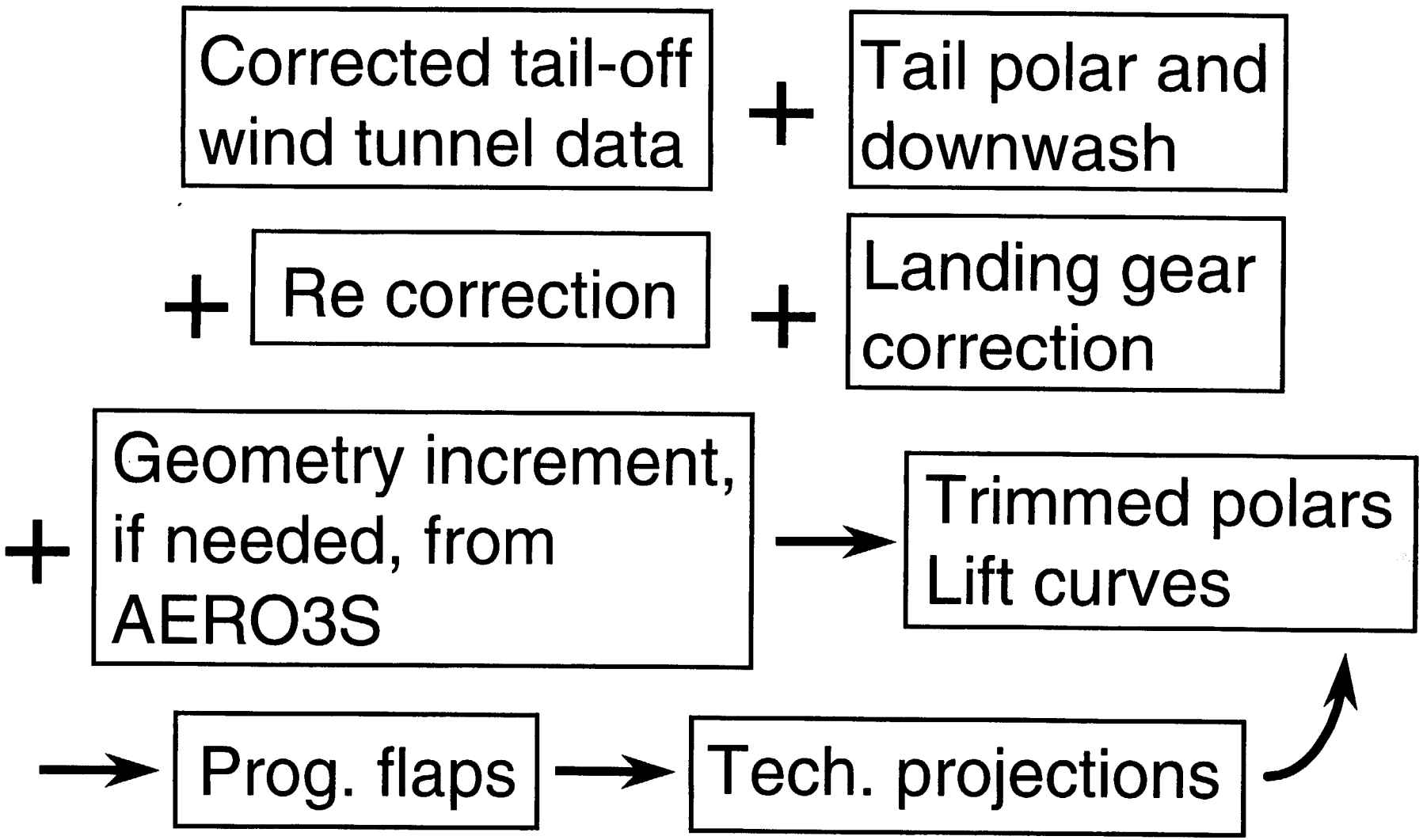

Review of Wind Tunnel Data

- NTF089 was the first test for the TCA planform but the wing sections are not true TCA. It covered 8 M < Re < 90 M.
- TCA-2 was a powered test and the main objective was the effect of power on tail effectiveness.
- TCA-3 had 8 M < Re < 37 M.
- TCA-4 was mainly for planform effect but it also repeated the TCA-3 configuration because TCA-3 showed different L/D than TCA-1.

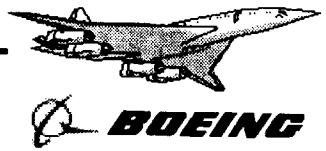

Review of Wind Tunnel Data

- Modified Ref. H (NTF Test 089),
  M ~ 0.3, Re ~ 90 M
- TCA-1 (Langley 14x22 Test 449),
  M ~ 0.24, Re ~ 8 M
- TCA-3 (Ames 12-ft Test 037),
  M ~ 0.24, Re ~ 8 M and 37 M
- TCA-4 (Langley 14x22 Test 473),
  M ~ 0.24, Re ~ 8 M

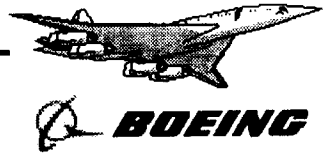

Lift Curves for Various TCA Wind Tunnel Databases

- The modified Ref. H data are for full-span LE 30 and full-span TE 10. TCA data are for full-span LE30 and TE 15/15/15/10 from outboard to inboard. This difference in geometry is the main cause for the difference in C_L.
- All necessary corrections have been applied to these data to make them fully corrected. This includes aft body adjustments (for the modified Ref. H NTF model), tare and interference corrections, wall corrections, nacelle base drag, etc.
- The tare and interference corrections were based on Ref. H corrections. Also, the same corrections were applied to TCA-1, TCA-3, and TCA-4 data although these data were taken in different facilities using different model supports.

BOEING

Lift Curves for Various TCA Wind Tunnel Databases

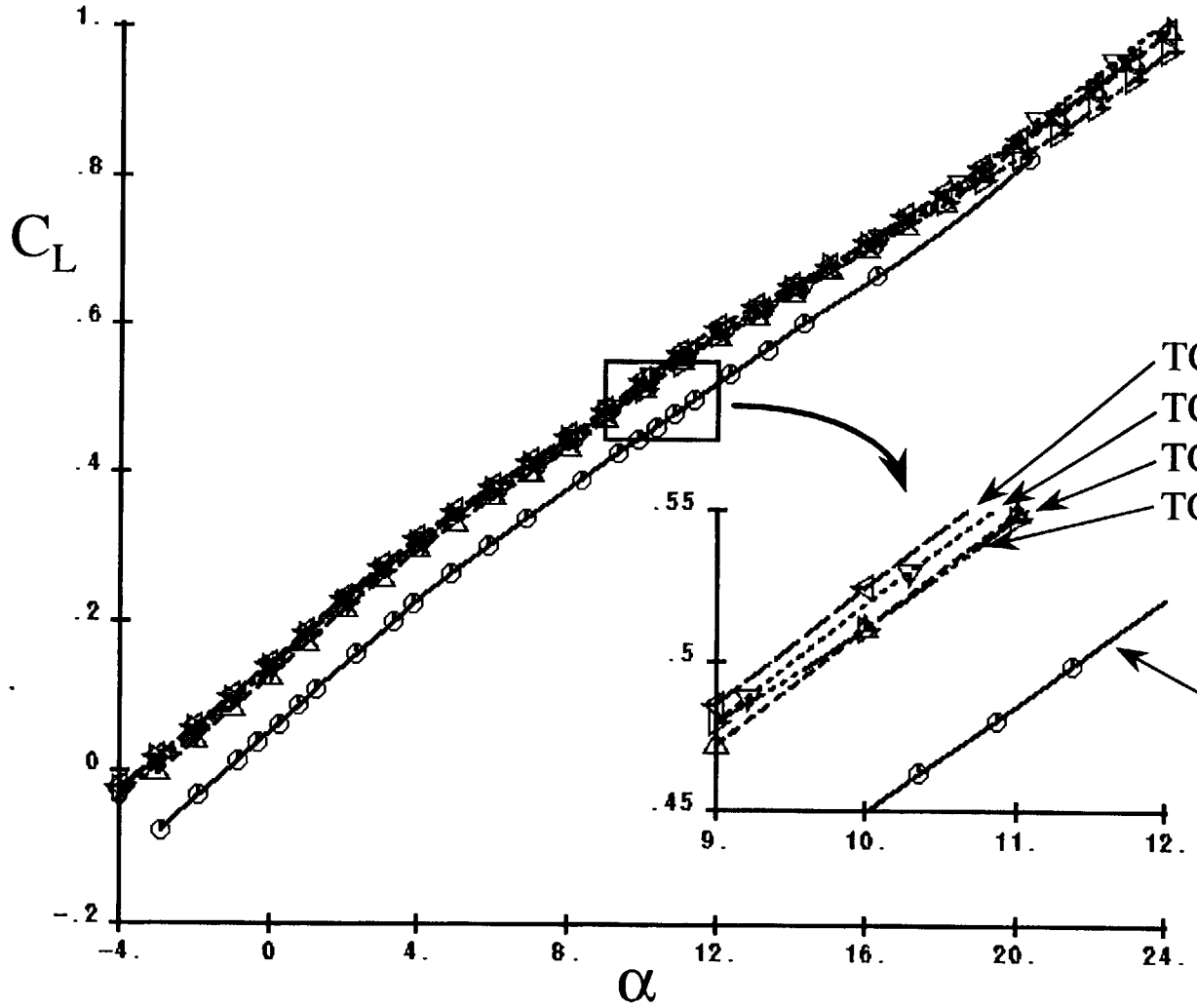

- Sref = 8,500 ft²
- Fully corrected
- Horizontal tail off
- Mod Ref-H data are flaps 30/10. All others are 30/15(10)

TCA-3 (8 M Re)
TCA-4 (8 M Re)
TCA-1 (8 M Re)
TCA-3 (37 M Re)
Flaps LE 30, TE 15/15/15/10

Modified Ref. H (90 M Re)
Flaps LE 30, TE 10

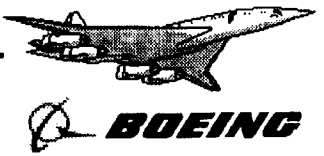

Drag Polars for Various TCA Wind Tunnel Databases

- The modified Ref. H data are for full-span LE 30 and full-span TE 10. TCA data are for full-span LE30 and TE 15/15/15/10 from outboard to inboard.
- All necessary corrections have been applied to these data to make them fully corrected. This includes aft body adjustments (for the modified Ref. H NTF model), tare and interference corrections, wall corrections, nacelle base drag, etc.
- TCA-1 and TCA-4 results show higher drag than TCA-3 at a given C_L. Differences in upflow and model support in different facilities are among the possible causes for this.

BOEING

Drag Polars for Various TCA Wind Tunnel Databases

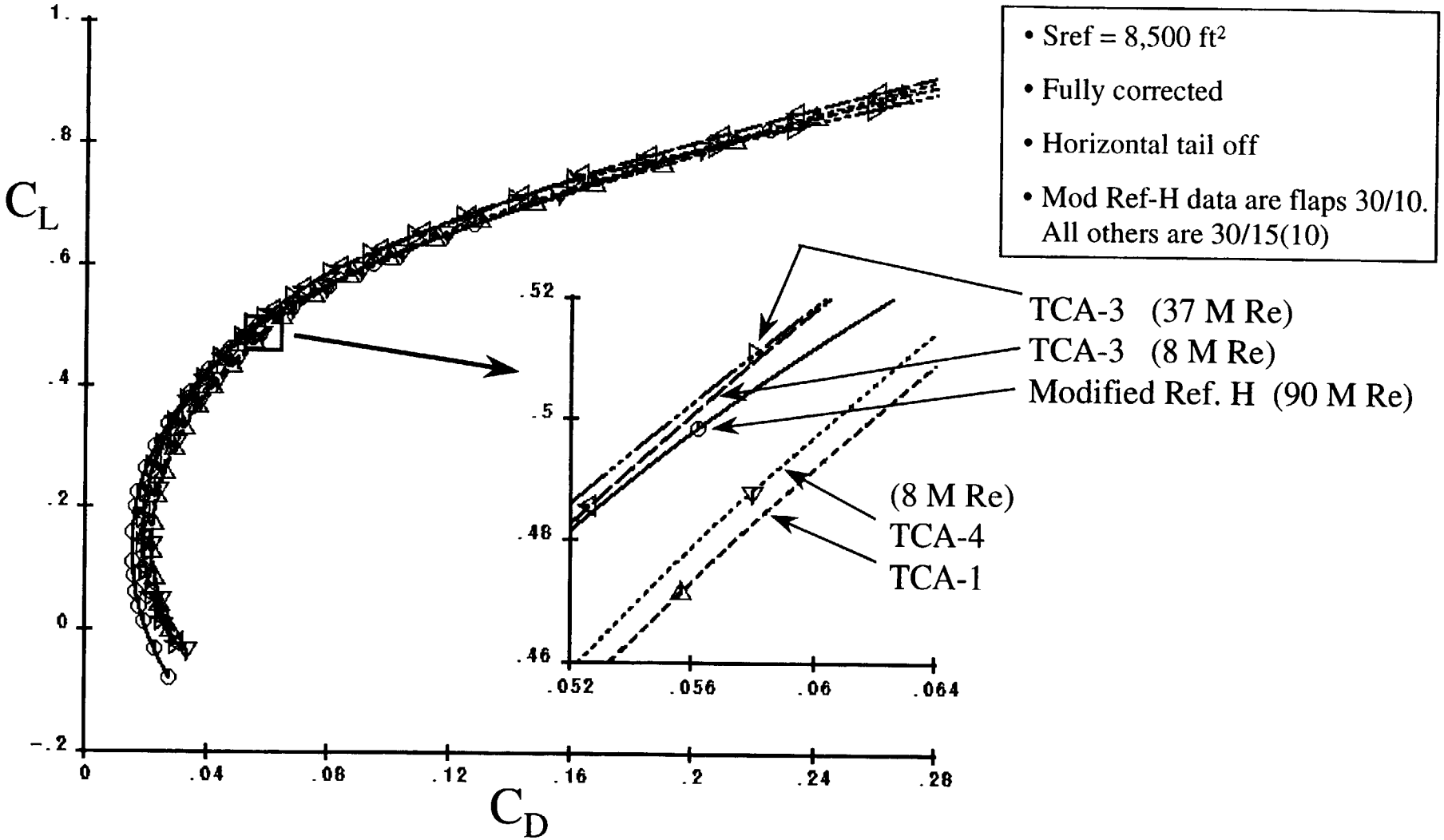

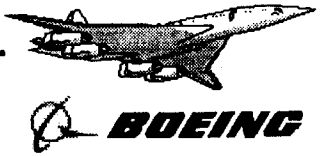

Pitching Moment Curves for Various TCA Wind Tunnel Databases

- The modified Ref. H data are for full-span LE 30 and full-span TE 10. TCA data are for full-span LE30 and TE 15/15/15/10 from outboard to inboard. This explains the more nose down pitching moment of the TCA data.
- All necessary corrections have been applied to these data to make them fully corrected. This includes aft body adjustments (for the modified Ref. H NTF model), tare and interference corrections, wall corrections, nacelle base drag, etc.
- TCA-1 and TCA-4 results tend to be together. TCA-3 results are more nose down than TCA-1 and TCA-4 results for $C_L < 0.7$. For $C_L > 0.7$, the TCA-3 high Re data tend to move toward the 90 M Re modified Ref. H data.

BOEING

Pitching Moment Curves for Various TCA Wind Tunnel Databases

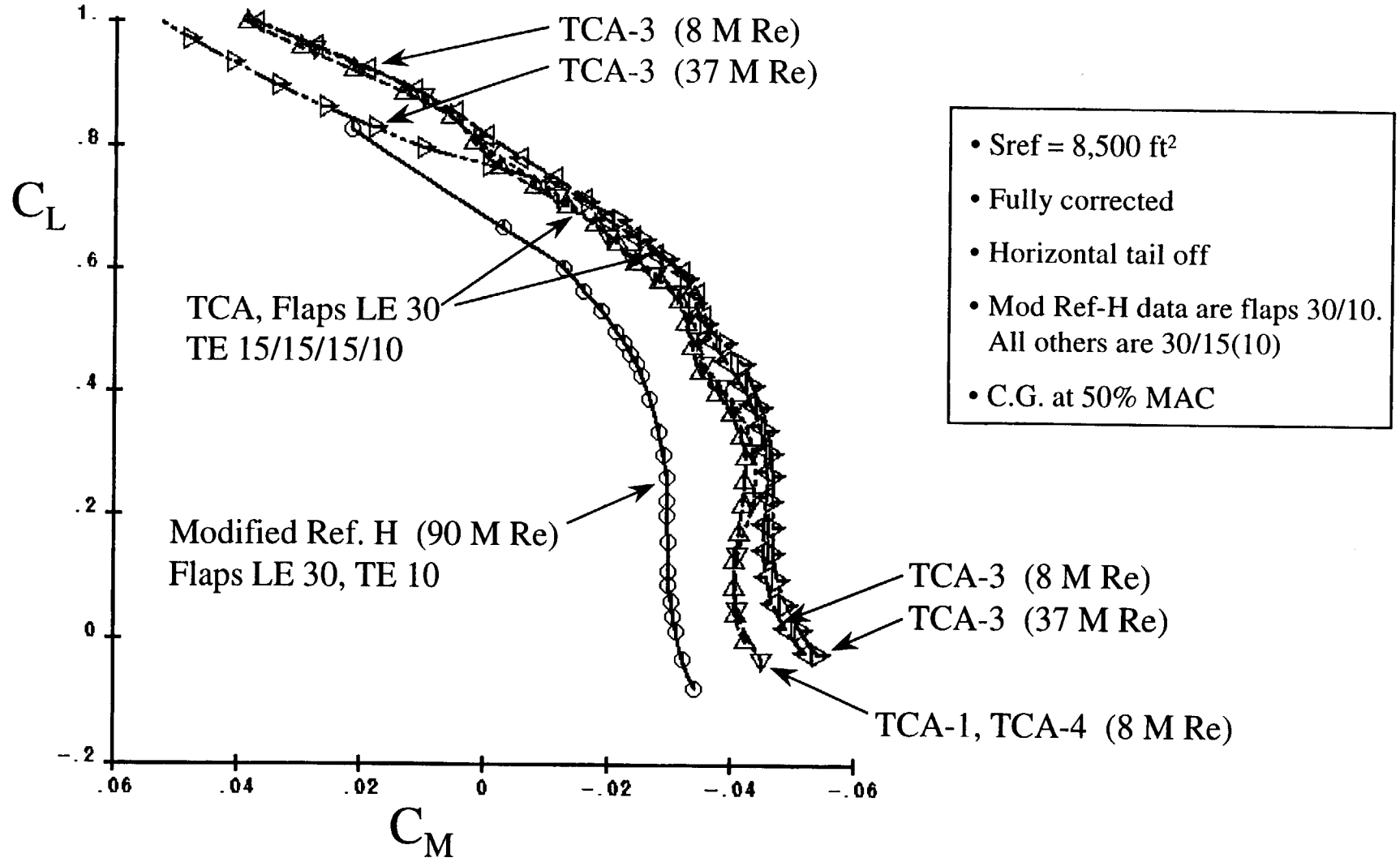

- Sref = 8,500 ft²
- Fully corrected
- Horizontal tail off
- Mod Ref-H data are flaps 30/10. All others are 30/15(10)
- C.G. at 50% MAC

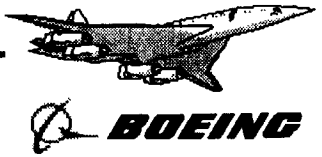

L/D Curves for Various TCA Wind Tunnel Databases

- The modified Ref. H data are for full-span LE 30 and full-span TE 10. TCA data are for full-span LE30 and TE 15/15/15/10 from outboard to inboard.
- All necessary corrections have been applied to these data to make them fully corrected. This includes aft body adjustments (for the modified Ref. H NTF model), tare and interference corrections, wall corrections, nacelle base drag, etc.
- The L/D from TCA-1 and TCA-4 are lower than TCA-3 results throughout the entire C_L range.
- The 90 M Re results for the modified Ref. H has higher L/D than TCA-3, TCA-4, and TCA-1 for $C_L < 0.45$.
- The 90 M Re results for the modified Ref. H has higher L/D than TCA-4, TCA-1, but lower L/D than TCA-3 for $0.45 < C_L < 0.57$.
- The 90 M Re results for the modified Ref. H are almost identical to TCA-4 and TCA-1 results for $C_L > 0.57$.

BOEING

L/D Curves for Various TCA Wind Tunnel Databases

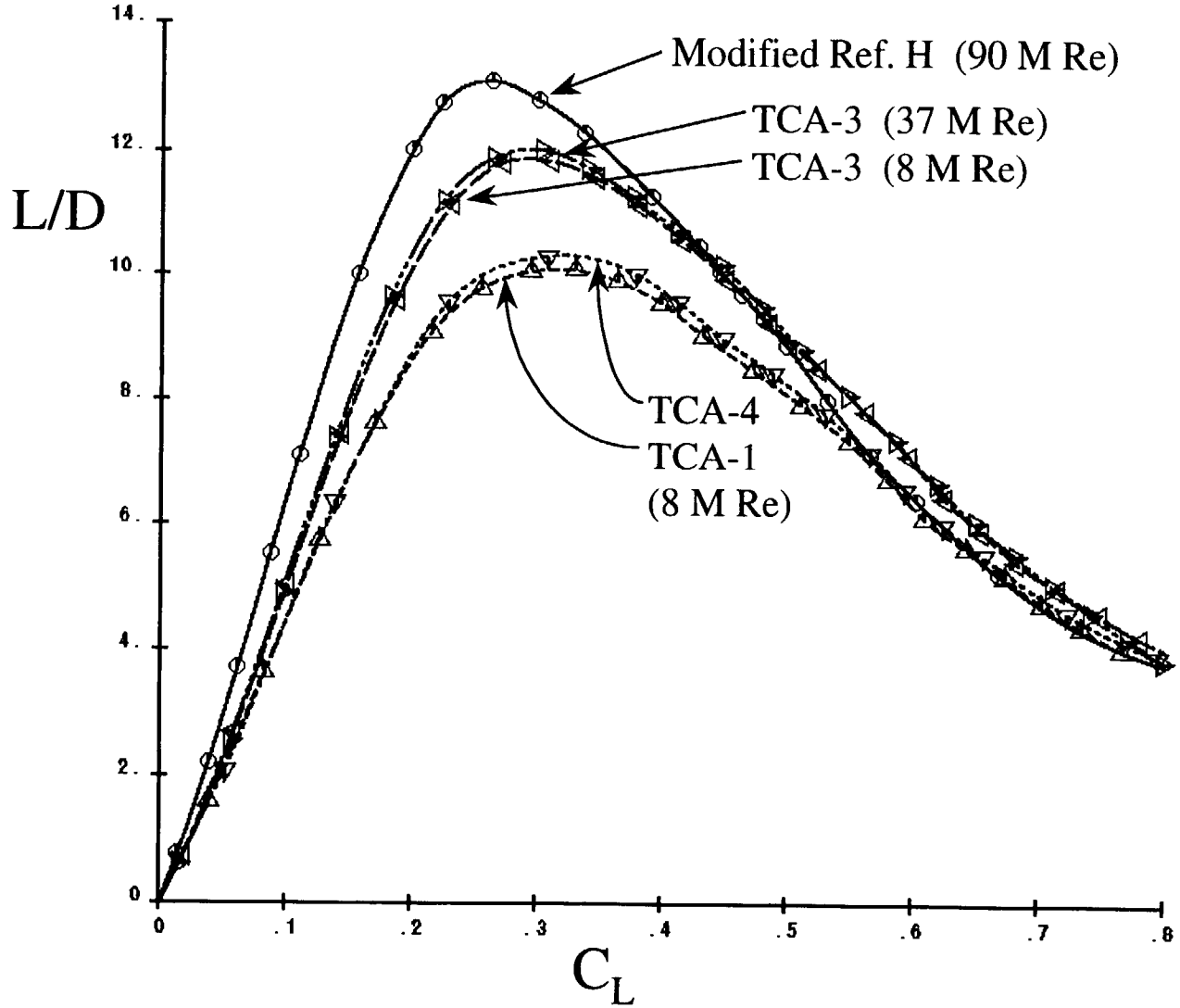

- Sref = 8,500 ft²
- Fully corrected
- Horizontal tail off
- Mod Ref-H data are flaps 30/10. All others are 30/15(10)

Full-Scale Lift Curves in Free Air Climbout Flaps 30/15(10)

- This chart shows the full scale lift curves in free air based on four sets of TCA wind tunnel data. All necessary increments have been applied to the fully corrected wind tunnel data to predict flight levels. This includes Reynolds number scaling and excrescence drag. Additionally, each set of data was trimmed using tail polars and downwash extracted from their respective test.
- All data are based on flaps LE 30 (full span), TE 15/15/15/10 (outboard to inboard). Since wind tunnel data exist for this particular configuration in each test, *AERO3S* was not needed for any of these buildups.
- The results are very close to each other except for $\alpha > 18°$.

BOEING

Full-Scale Lift Curves in Free Air
Climbout Flaps 30/15(10)

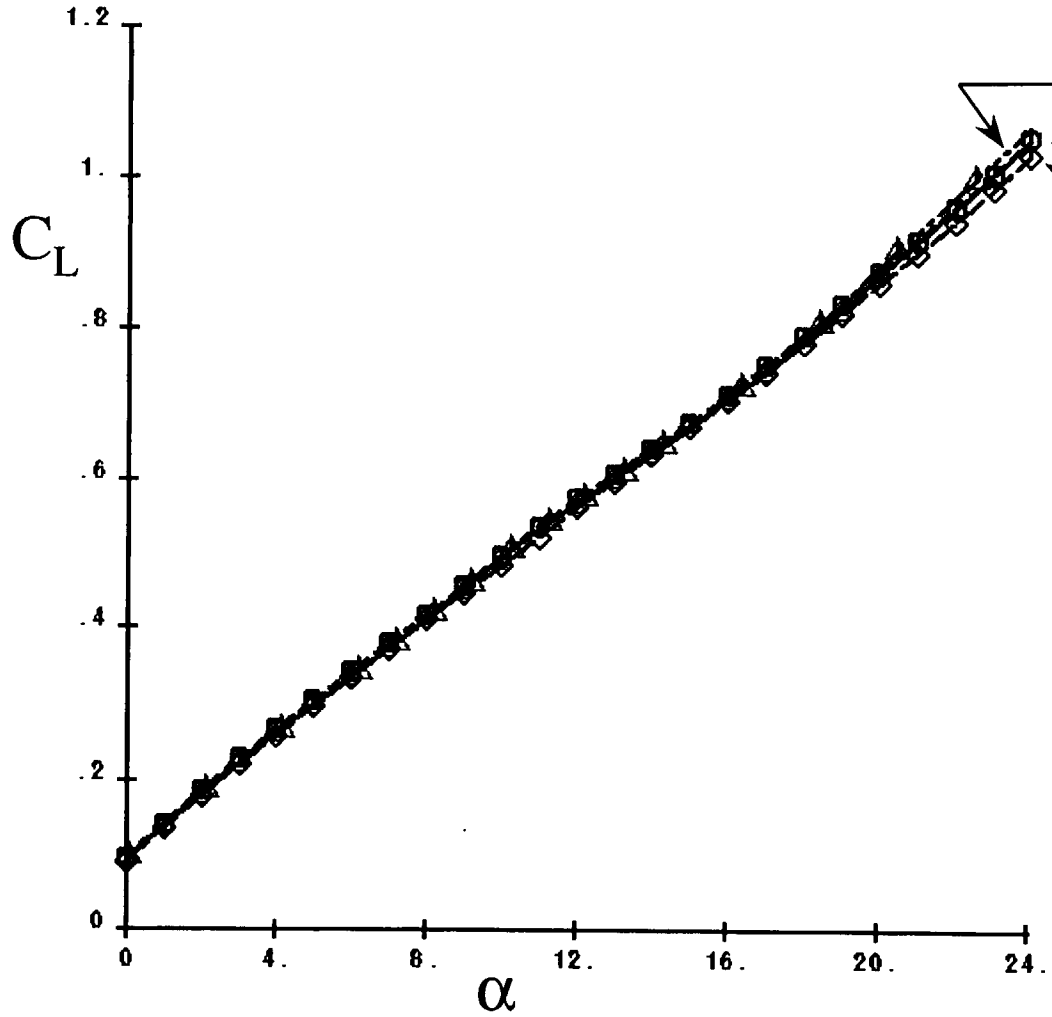

Wind Tunnel Database

- TCA-4 (8 M Re)
- TCA-1 (8 M Re)
- TCA-3 (8 M Re)
- TCA-3 (37 M Re)

- Sref = 8,500 ft²
- No thrust, trimmed data
- Flaps: LE 30, TE 15/15/15/10
- C.G. = 51.5% MAC

Full-Scale Lift Curves in Ground Effect Climbout Flaps 30/15(10)

- This chart shows the full scale lift curves in ground effect based on four sets of TCA wind tunnel data. All necessary increments have been applied to the fully corrected wind tunnel data to predict flight levels. This includes Reynolds number scaling and excrescence drag. Ground effect increments are based on old Ref. H wind tunnel data and cause no change to drag at a constant angle of attack, only lift. Additionally, each set of data was trimmed using tail polars and downwash extracted from their respective test.
- All data are based on flaps LE 30 (full span), TE 15/15/15/10 (outboard to inboard). Since wind tunnel data exist for this particular configuration in each test, *AERO3S* was not needed for any of these buildups.
- Gear is on for these data.
- The results are very close to each other except for $\alpha > 18°$.

BOEING

Full-Scale Lift Curves in Ground Effect
Climbout Flaps 30/15(10)

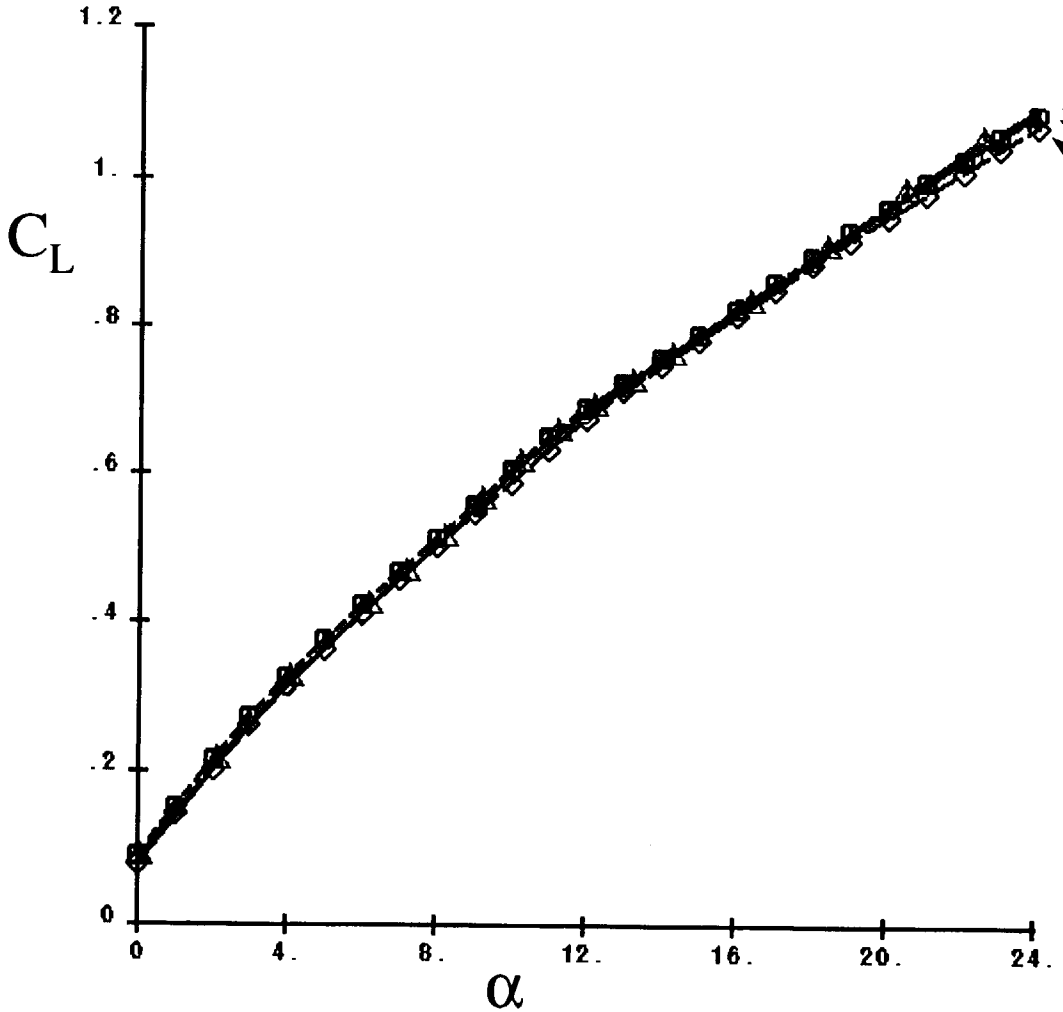

Wind Tunnel Database

TCA-4 (8 M Re)
TCA-1 (8 M Re)
TCA-3 (8 M Re)
TCA-3 (37 M Re)

Ground effect increment from Ref. H data

- Sref = 8,500 ft²
- No thrust, trimmed data
- Flaps: LE 30, TE 15/15/15/10
- C.G. = 51.5% MAC
- Gear ON

Full-Scale Lift Curves in Free Air Landing Flaps 0/30

- This chart shows the full scale lift curves in free air based on three different sets of TCA wind tunnel data that had flap 0/30 data. All necessary increments have been applied to the fully corrected wind tunnel data to predict flight levels. This includes Reynolds number scaling and excrescence drag. Additionally, each set of data were trimmed using tail polars and downwash extracted from their respective test.
- Since wind tunnel data exist for this particular configuration in each test, *AERO3S* was not needed for any of these buildups.
- Gear is on for these data.
- The full scale lift curves based on TCA-3 data have higher C_L, at a given angle of attack, than the one based on TCA-1 data for $\alpha > 2°$.

BOEING

Full-Scale Lift Curves in Free Air
Landing Flaps 0/30

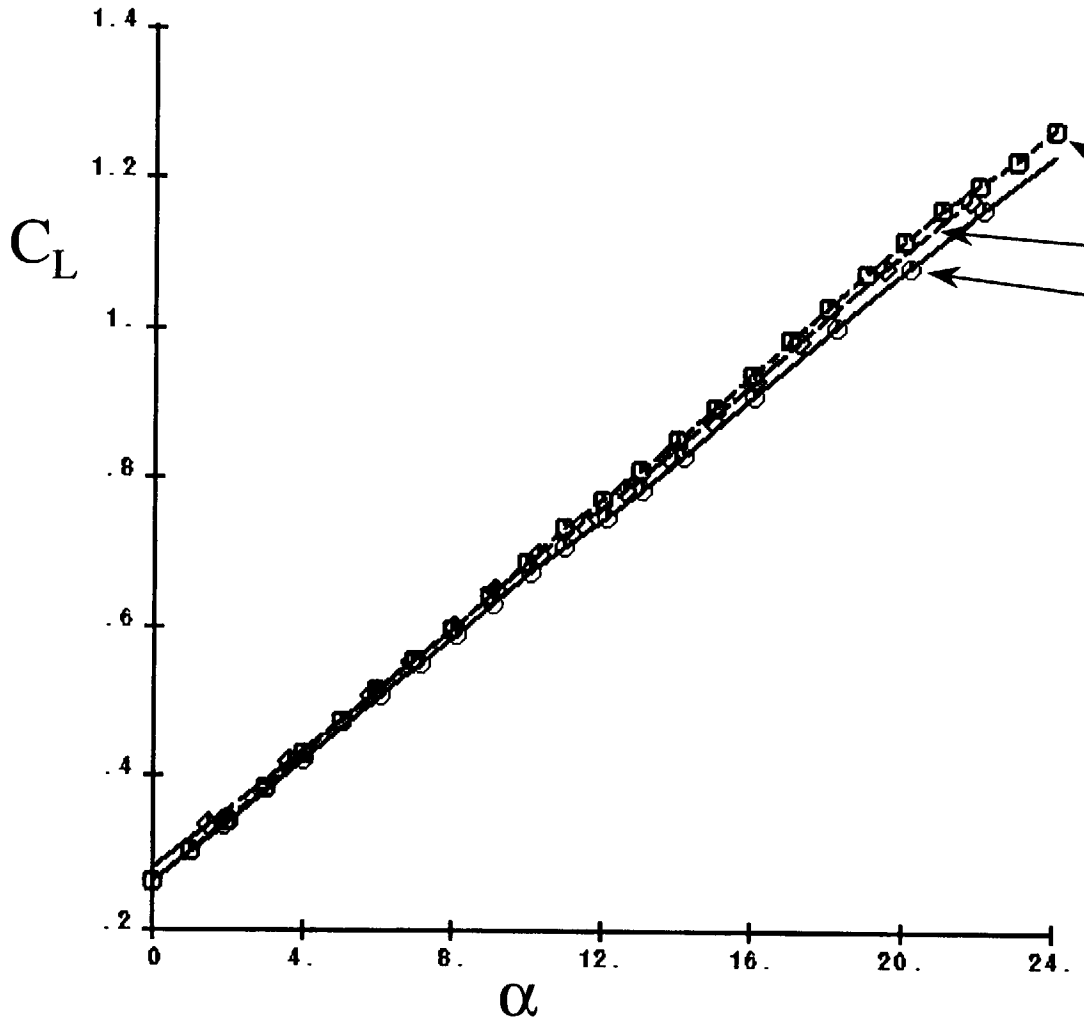

Wind Tunnel Database
TCA-3 (8 M Re)
TCA-3 (37 M Re)
TCA-1 (8 M Re)

- Sref = 8,500 ft^2
- No thrust, trimmed data
- Flaps: LE 0, TE 30
- C.G. = 51.5% MAC
- Gear ON

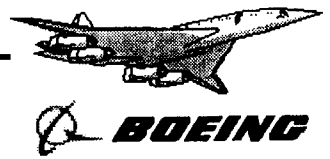

Full-Scale Lift Curves in Ground Effect Landing Flaps 0/30

- This chart shows the full scale lift curves in ground effect based on three different sets of TCA wind tunnel data that had flap 0/30 data. All necessary increments have been applied to the fully corrected wind tunnel data to predict flight levels. This includes Reynolds number scaling and excrescence drag. Ground effect increments are based on old Ref. H wind tunnel data and cause no change to drag at a constant angle of attack, only lift. Additionally, each set of data was trimmed using tail polars and downwash extracted from their respective test.
- Since wind tunnel data exist for this particular configuration in each test, *AERO3S* was not needed for any of these buildups.
- Gear is on for these data.
- The full scale lift curves based on TCA-3 data have higher C_L, at a given angle of attack, than the one based on TCA-1 data for $\alpha > 2°$.

BOEING

Full-Scale Lift Curves in Ground Effect
Landing Flaps 0/30

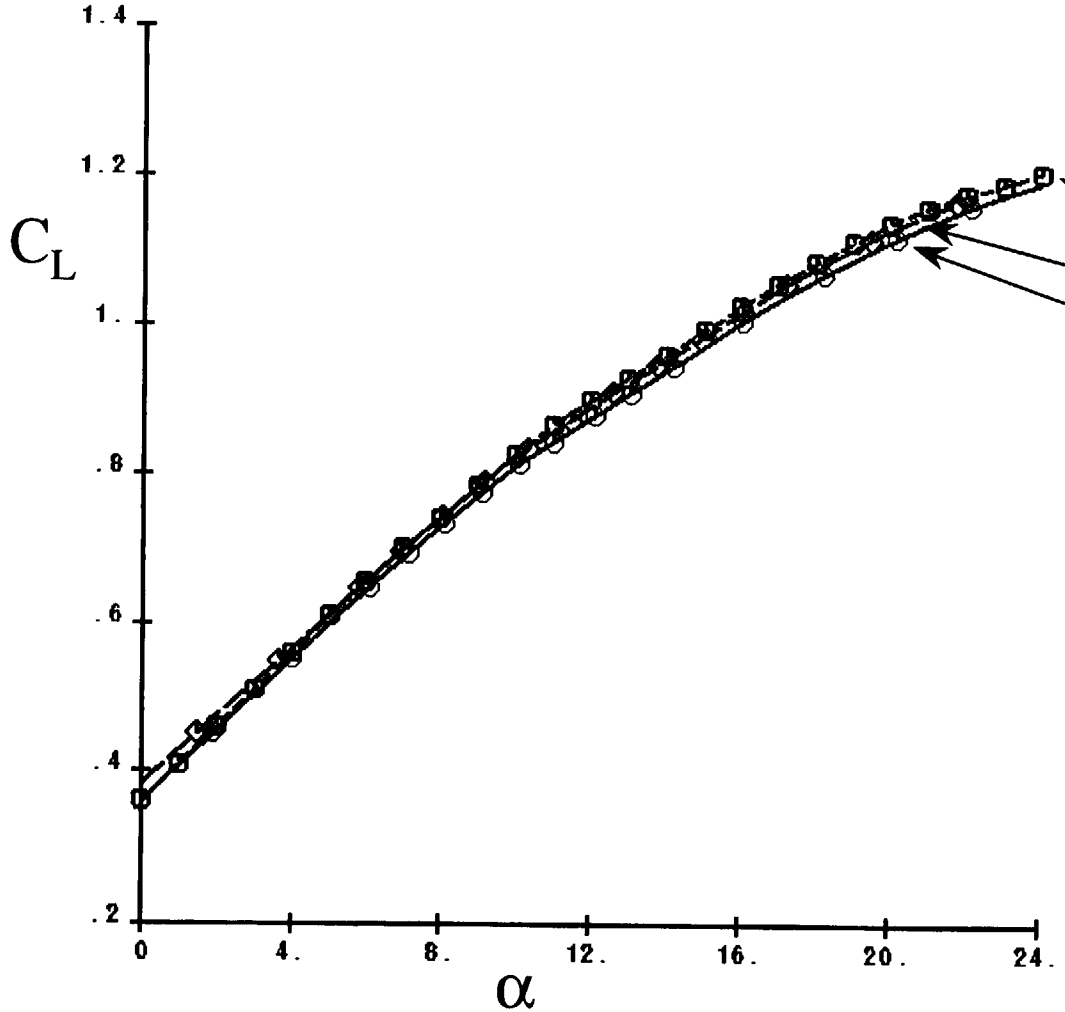

Wind Tunnel Database
TCA-3 (8 M Re)
TCA-3 (37 M Re)
TCA-1 (8 M Re)

Ground effect increment from Ref. H data

- Sref = 8,500 ft²
- No thrust, trimmed data
- Flaps: LE 0, TE 30
- C.G. = 51.5% MAC
- Gear ON

Status L/D Curves for Various TCA Buildups Fixed Flap for Climbout

- This chart shows the full scale status L/D curves in free air based on five different sets of TCA wind tunnel data and the Ref. H wind tunnel data currently used in the Common Process. With the exception of the Ref. H and Mod Ref. H data which are flaps 30/10, all other data are flaps 30/15(10). Ref. H and Mod. Ref. H untrimmed data are trimmed using tail polars and downwash extracted from TCA-1. All other data use tail polars and downwash extracted from their respective tests.
- Geometry increment from *AERO3S* was applied only when the Ref. H wind tunnel data was used. Although the modified Ref. H does not have the same wing sections as the TCA, geometry increments are small.
- None of the predictions reached the technology projection.
- TCA-1 and TCA-4 data resulted in substantially lower L/D levels than the other databases. The differences between these L/D levels shown here are still not fully understood. Differences in upflow and model support in different facilities could be major contributors. Full scale buildups show a spread of about one unit in L/D between these databases at a climbout lift coefficient of $C_L = 0.5$.

BOEING

Status L/D Curves for Various TCA Buildups, Fixed Flap for Climbout

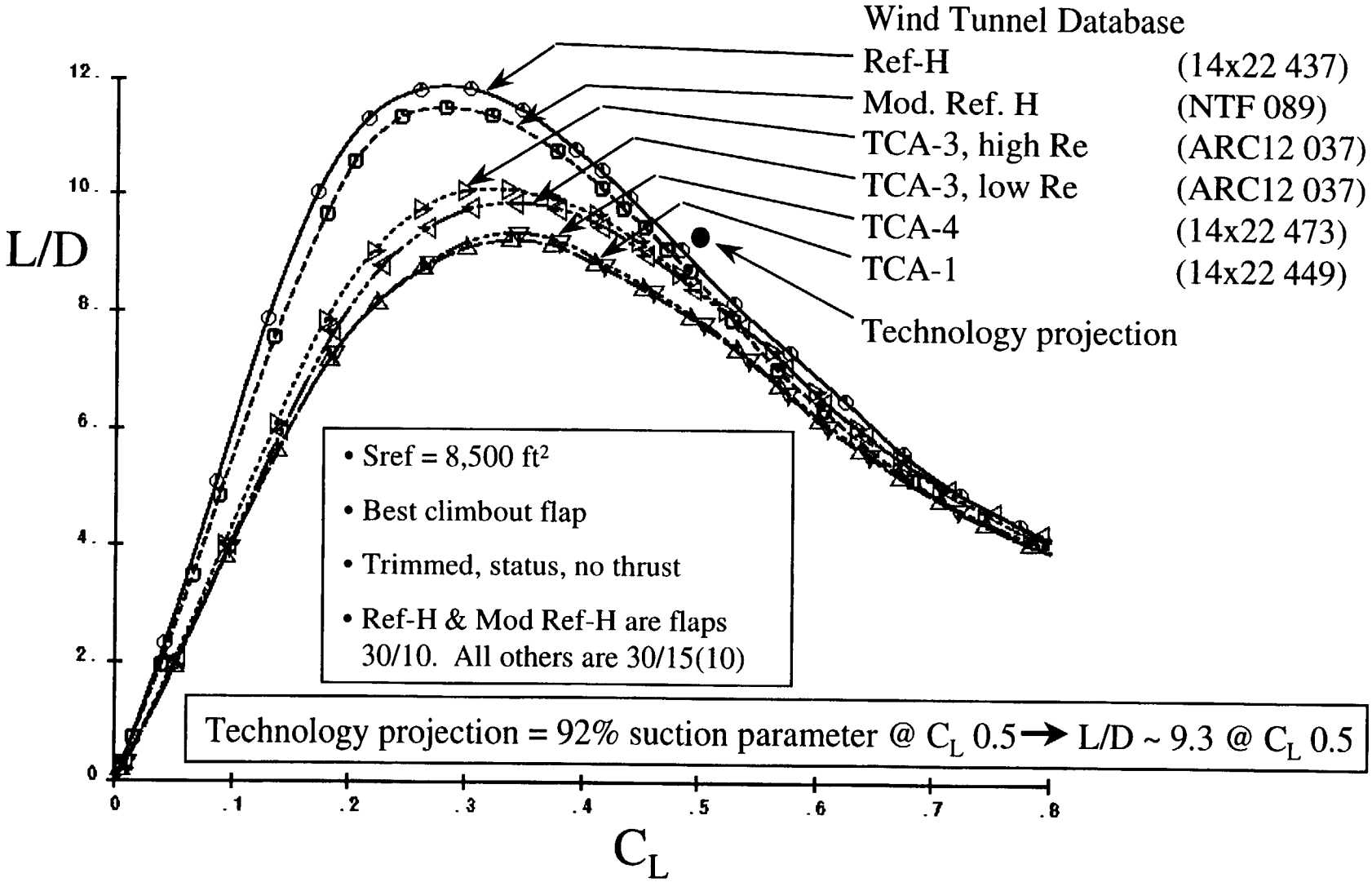

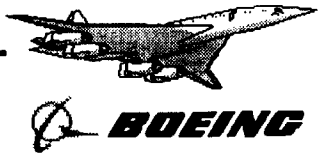

Status L/D Curves for Various TCA Buildups Programmed Flap for Climbout

- This chart shows the full scale status L/D curves in free air based on five different sets of TCA wind tunnel data and the Ref. H wind tunnel data currently used in the Common Process. The data shown are for the programmed flap, or the optimum combination of leading and trailing edge flaps that provides the highest L/D for each C_L. Ref. H and modified Ref. H untrimmed data are trimmed using tail polars and downwash extracted from TCA-1. All other data use tail polars and downwash extracted from their respective tests. Because so many different flap combinations, 169 of them, are necessary for the programmed flap matrix, *AERO3S* was used to predict the lift, drag, and pitching moment for the different configurations. Additionally, *AERO3S* is needed to provide differences between the Ref. H and TCA geometry when using the Ref. H wind tunnel database.
- Again, none of the predictions reached the technology projection.
- Results based on TCA-1 and TCA-4 wind tunnel data show lower L/D's for $C_L < 0.8$.

BOEING

Status L/D Curves for Various TCA Buildups, Programmed Flap for Climbout

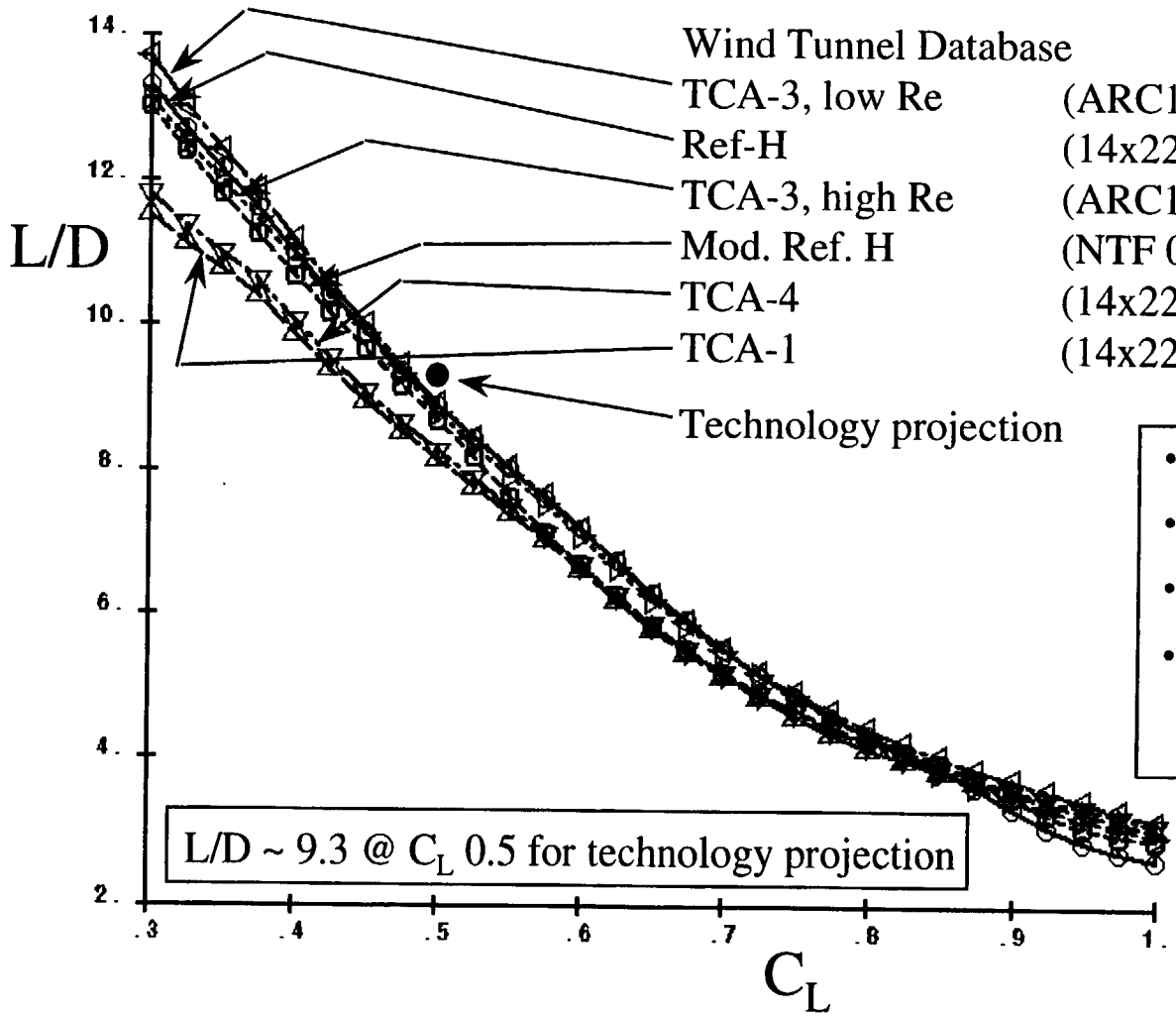

- Sref = 8,500 ft²
- Programmed Flap
- Trimmed, status, no thrust
- Ref-H & Mod Ref-H are based on 30/10 wind tunnel data. All others are based on 30/15(10)

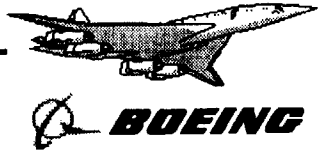

Projected L/D Curves for Various TCA Buildups Programmed Flap for Climbout

- This chart shows the full scale projected L/D curves in free air based on five different sets of TCA wind tunnel data and the Ref. H wind tunnel data currently used in the Common Process. The data shown are for the programmed flap, or the optimum combination of leading and trailing edge flaps that provides the highest L/D for each C_L. Ref. H and modified Ref. H untrimmed data are trimmed using tail polars and downwash extracted from TCA-1. All other data use tail polars and downwash extracted from their respective tests. Because so many different flap combinations, 169 of them, are necessary for the programmed flap matrix, *AERO3S* was used to predict the lift, drag, and pitching moment for the different configurations. Additionally, *AERO3S* is needed to provide differences between the Ref. H and TCA geometry when using the Ref. H wind tunnel database.
- The previous chart illustrates status level L/D curves. From those curves, an increment is applied to the drag levels representing a technology projected that forces the L/D to be a desired value at a $C_L = 0.5$. For the TCA, this desired drag level corresponds to a suction level of 92%, which equates to a projected L/D ~ 9.3.

BOEING

Projected L/D Curves for Various TCA Buildups, Programmed Flap for Climbout

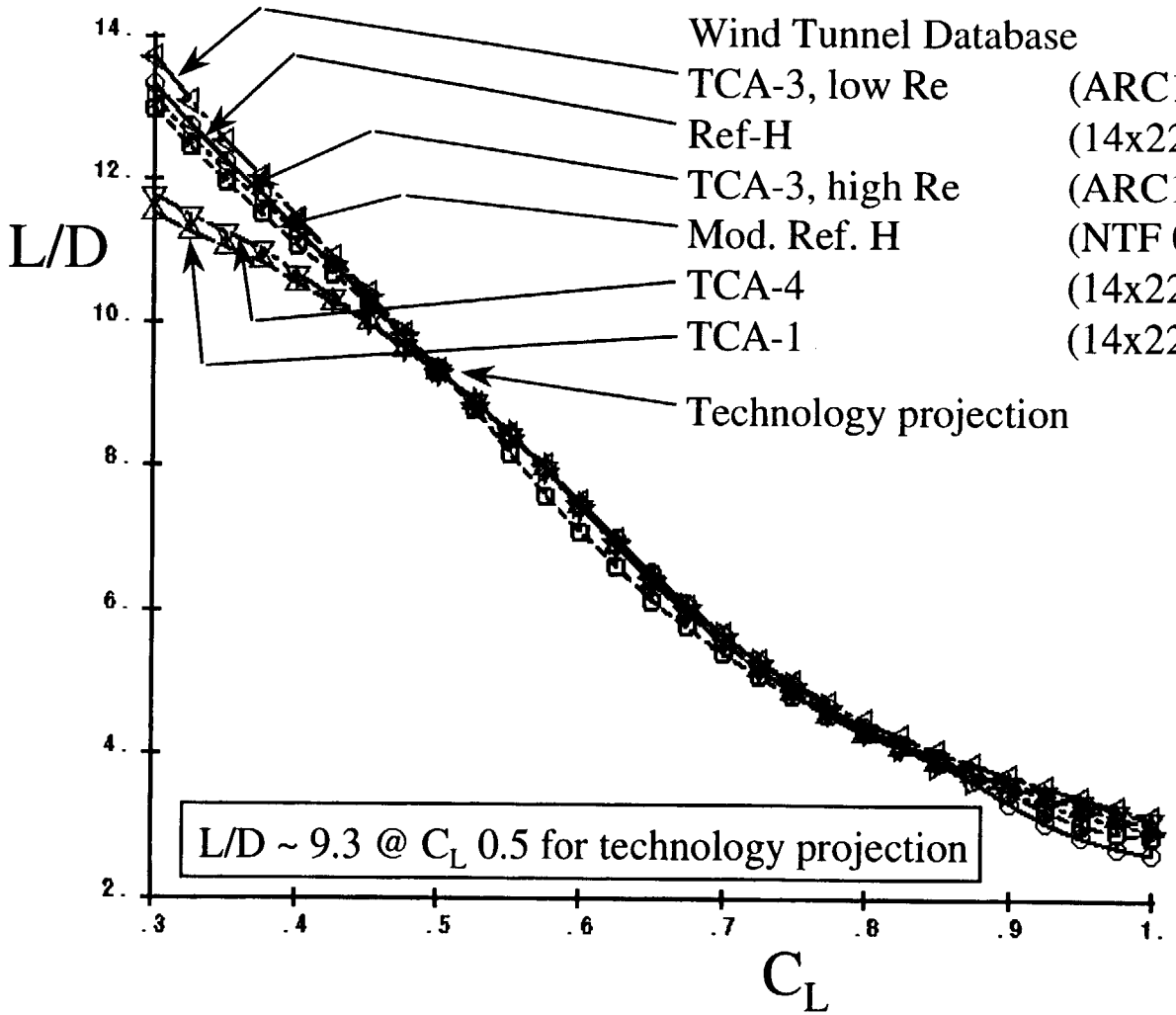

- Sref = 8,500 ft²
- Programmed Flap
- Trimmed, projected, no thrust
- Ref-H & Mod Ref-H are based on 30/10 wind tunnel data. All others are based on 30/15(10)
- Suction parameter = 0.92 @ 0.5 C_L for technology projection

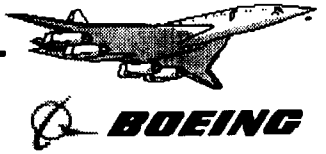

Status Suction Parameter for Various TCA Buildups Programmed Flap for Climbout

- This chart shows the status suction parameter based on five different sets of TCA wind tunnel data and the Ref. H wind tunnel data currently used in the Common Process. The data shown are based on the status programmed flap, or the optimum combination of leading and trailing edge flaps that provides the highest L/D for each C_L.
- The suction parameter is essentially a non-dimensional way of comparing drag levels between configurations of different aspect ratio. For a 2-surface configuration, such as the TCA, the goal is to attain a suction parameter of 92% at a lift coefficient of $C_L = 0.5$.

BOEING

Status Suction Parameter for Various TCA Buildups, Programmed Flap for Climbout

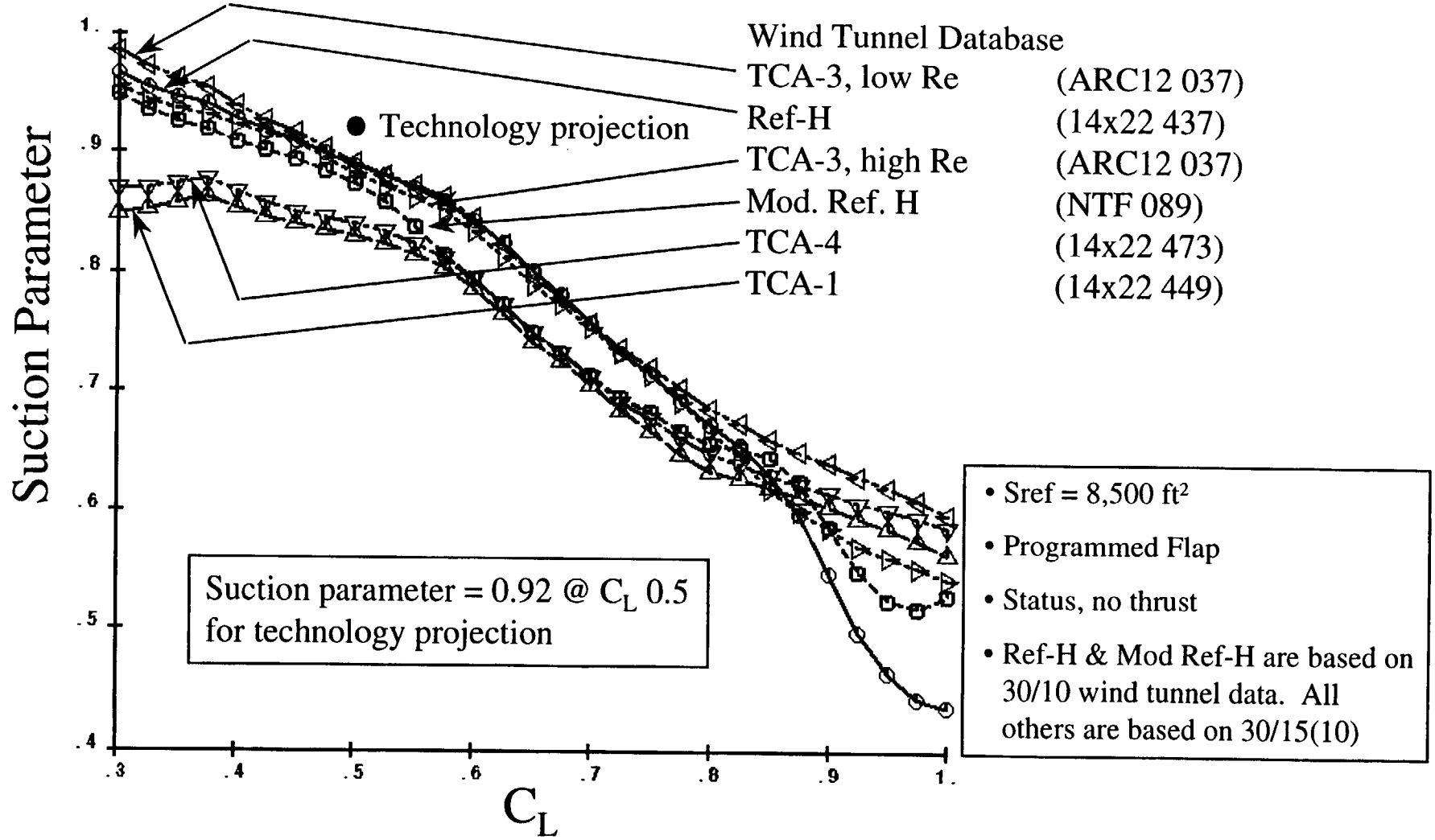

Projected Suction Parameter for Various TCA Buildups Programmed Flap for Climbout

- This chart shows the projected suction parameter based on five different sets of TCA wind tunnel data and the Ref. H wind tunnel data currently used in the Common Process. The data shown are based on the projected programmed flap, or the optimum combination of leading and trailing edge flaps that provides the highest L/D for each C_L.
- The goal is to attain a suction parameter of 92%, or 0.92 at C_L 0.5. The technology projection is applied to the status buildup to force the suction parameter to this level.

BOEING

Projected Suction Parameter for Various TCA Buildups, Programmed Flap for Climbout

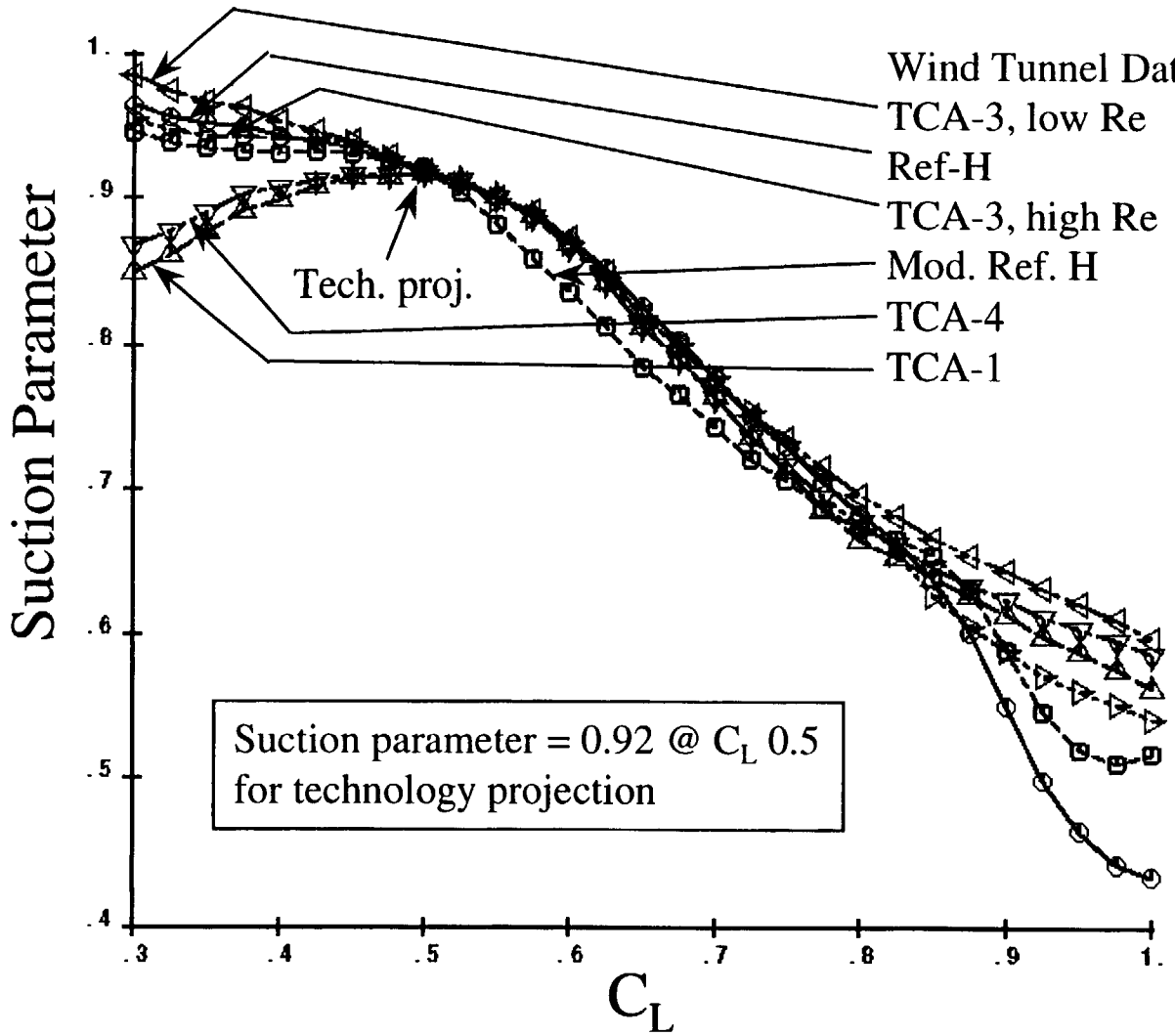

- Sref = 8,500 ft²
- Programmed Flap
- Projected, no thrust
- Ref-H & Mod Ref-H are based on 30/10 wind tunnel data. All others are based on 30/15(10)

Effect of Sealed Slats
TCA-3, Re ~ 8 M and 37 M

- This chart shows the effect of sealed slats on the high-lift performance of the climbout configuration for two Reynolds numbers with nacelles on. The inboard sealed slats did not affect the performance for $0.4 < C_L < 0.9$ at the low Reynolds number, 8 million. The inboard sealed slats did affect the performance for the entire C_L range at the higher Reynolds number, 37 million.

BOEING

Effect of Sealed Slats, TCA-3

Re ~ 8 M

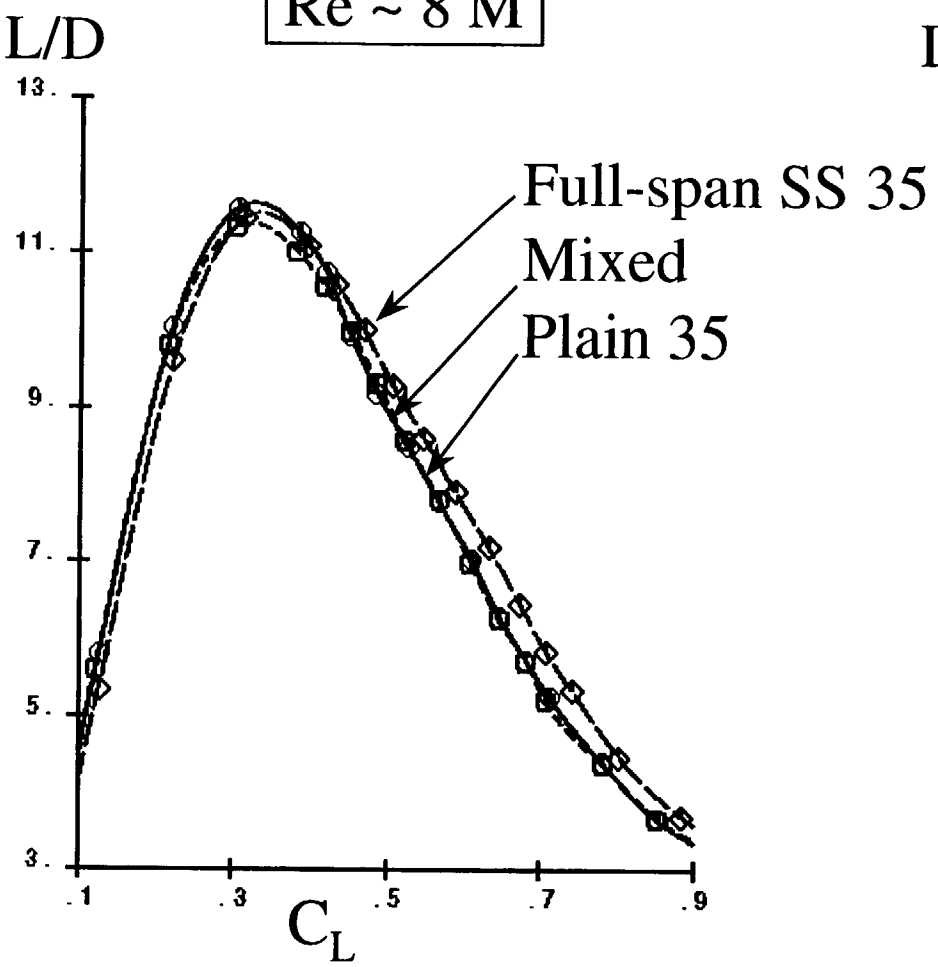

Re ~ 37 M

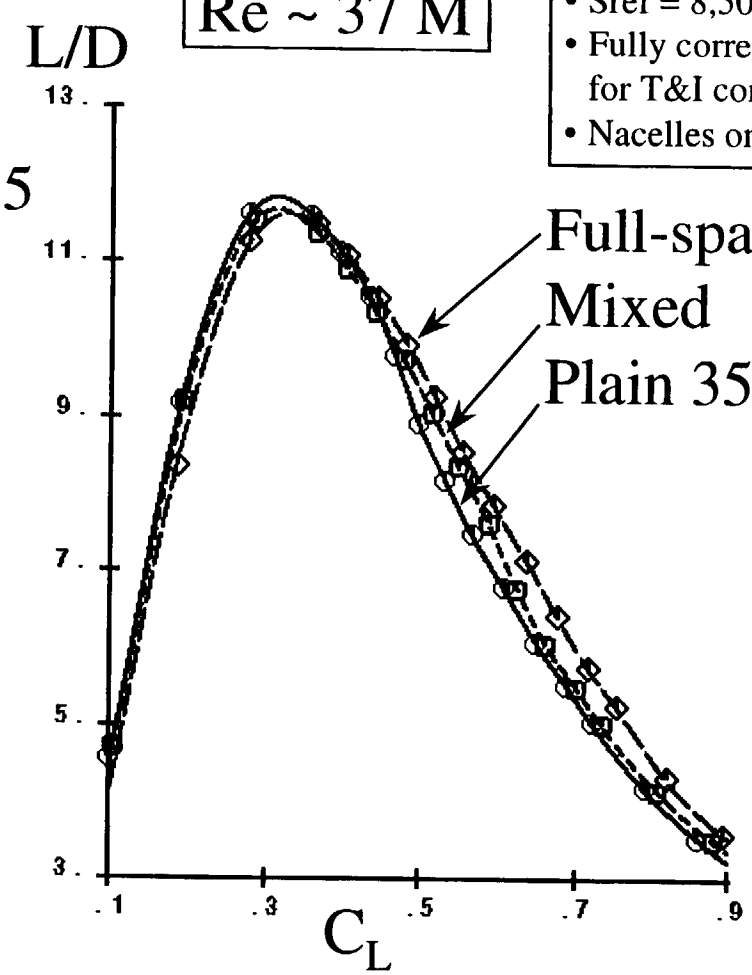

- Sref = 8,500 ft²
- Fully corrected, except for T&I corrections
- Nacelles on

Mixed: inboard SS 35, outboard plain 35

Drag Increment Due to Sealed Slats

- The drag increments due to the sealed slats are shown. Observations made for the previous charts apply here too.

BOEING

Drag Increment Due to Sealed Slats

Base: Full-span plain flaps 35
TCA-3 Data, Nacelles On

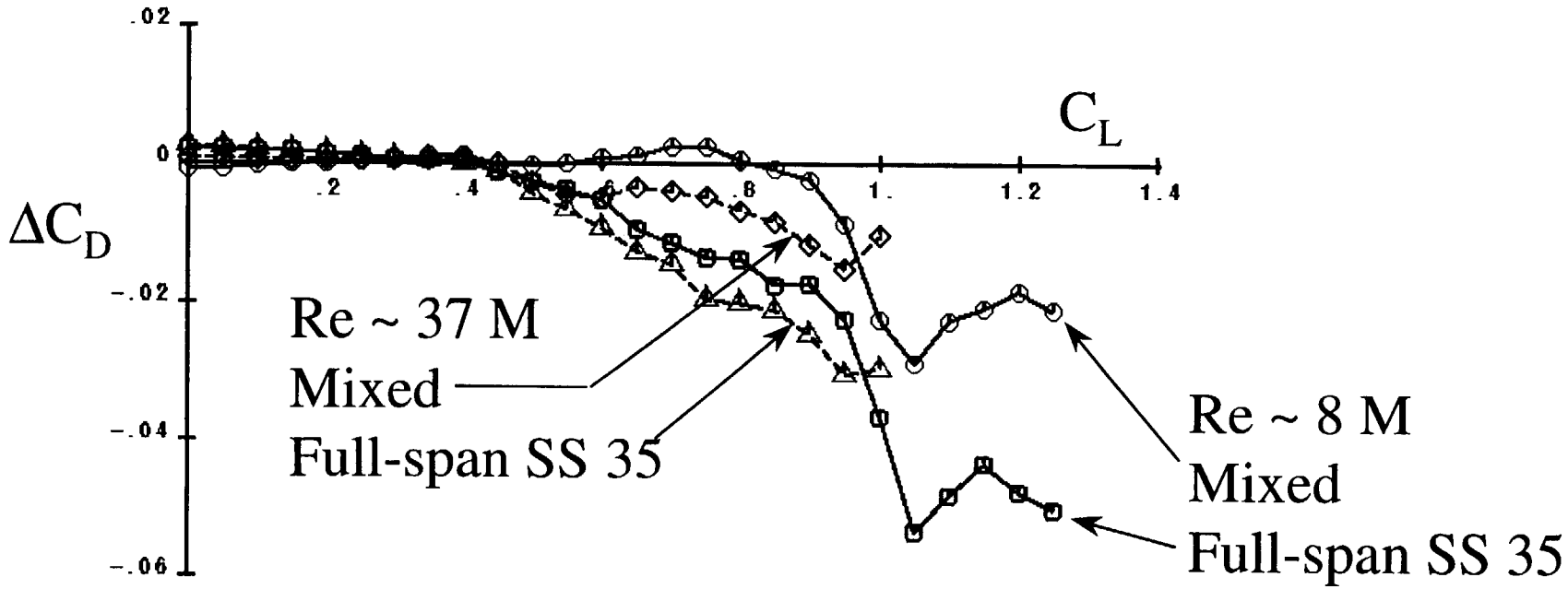

Mixed: inboard SS 35, outboard plain 35

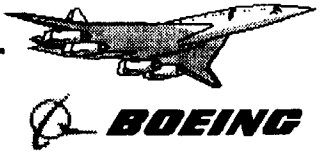

Effect of Sealed Slats
TCA-3, Re ~ 8 M

- The curves on the right are the same ones shown on page 41.
- The effect of the sealed slats, for this Reynolds number, depends on whether the nacelles are on.
- The effect of the PSP (pressure sensitive paint) is insignificant.

BOEING

Effect of Sealed Slats, TCA-3, Re ~ 8 M

W/B, PSP

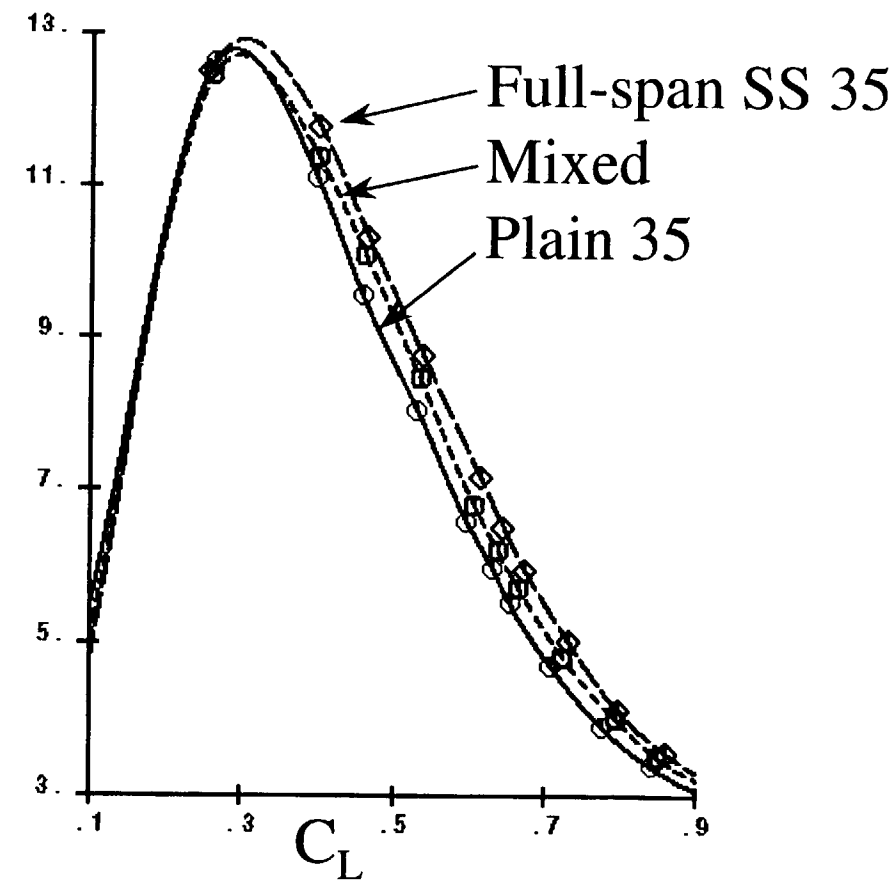

W/B/N/V

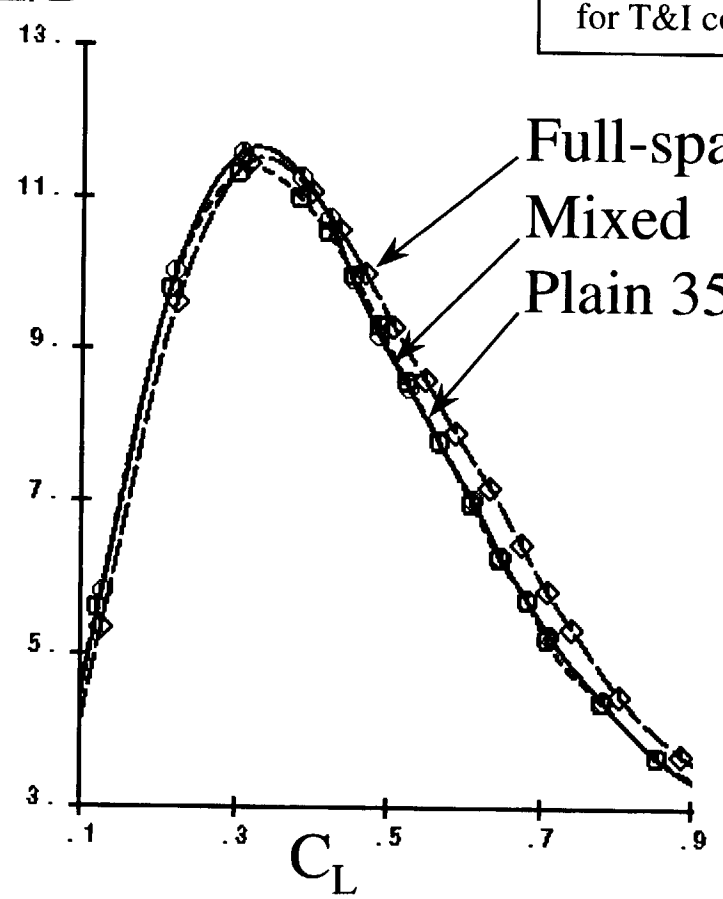

- Sref = 8,500 ft²
- Fully corrected, except for T&I corrections

Mixed: inboard SS 35, outboard plain 35

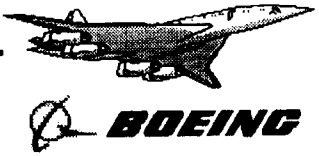

Effect of Sealed Slats on 5% TCA Mach ~ 0.24, Re ~ 8 M

- The effect of the sealed slats was predicted correctly by TNS3DMB, a 3-D multi-block thin layer Navier-Stokes code, in terms of ranking the configuration by their performance.
- The L/D from TNS3DMB is low due to high C_D, a phenomenon observed since 1995.

BOEING

Effect of Sealed Slats on 5% TCA
Mach ~ 0.24, Re ~ 8 M

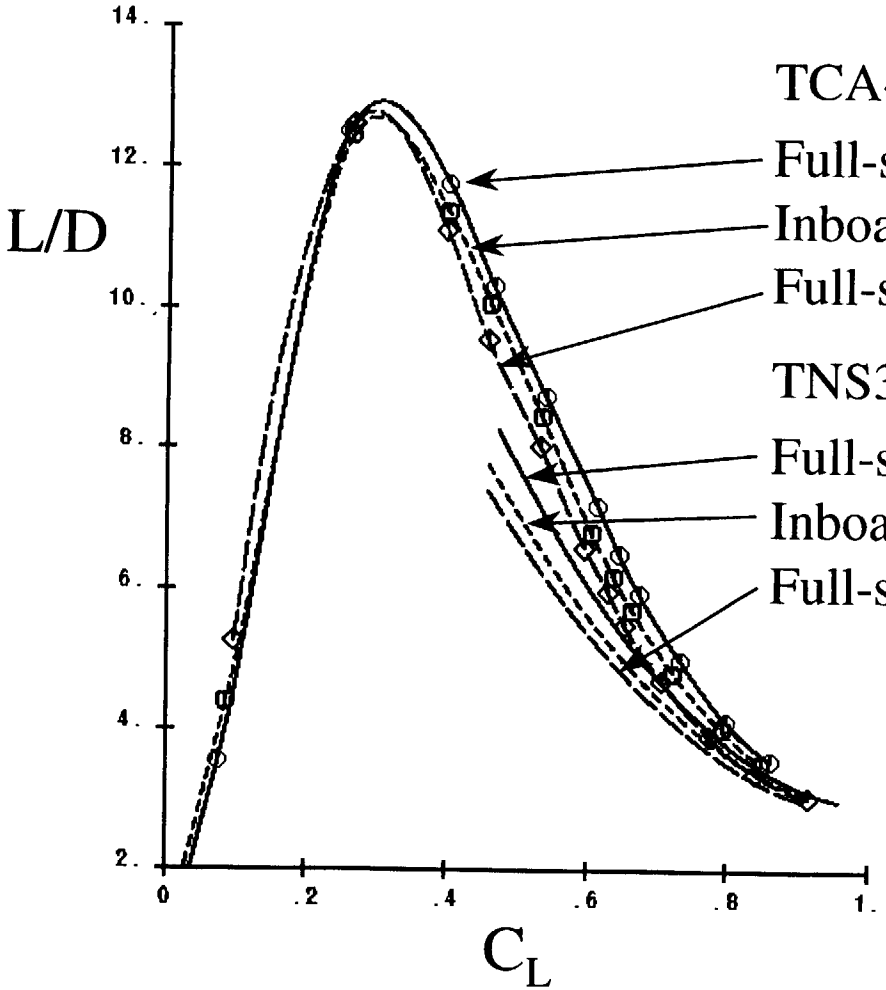

TCA-3 (with PSP)

Full-span sealed slat 35

Inboard SS 35, outboard plain 35

Full-span plain 35

TNS3DMB

Full-span sealed slat 35

Inboard SS 35, outboard plain 35

Full-span plain 35

- Sref = 8,500 ft²
- TCA-3 data fully corrected, except for T&I corrections
- Nacelles off

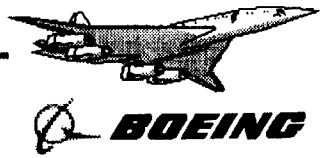

Drag Increment Due to Sealed Slats

- TNS3DMB was able to rank the configurations in terms of the performance. Quantitative difference between the configurations was not captured as well.
- The are three points on each TNS3DMB curves.

BOEING

Drag Increment Due to Sealed Slats

Base: Full-span plain flaps 35
Wing/Body

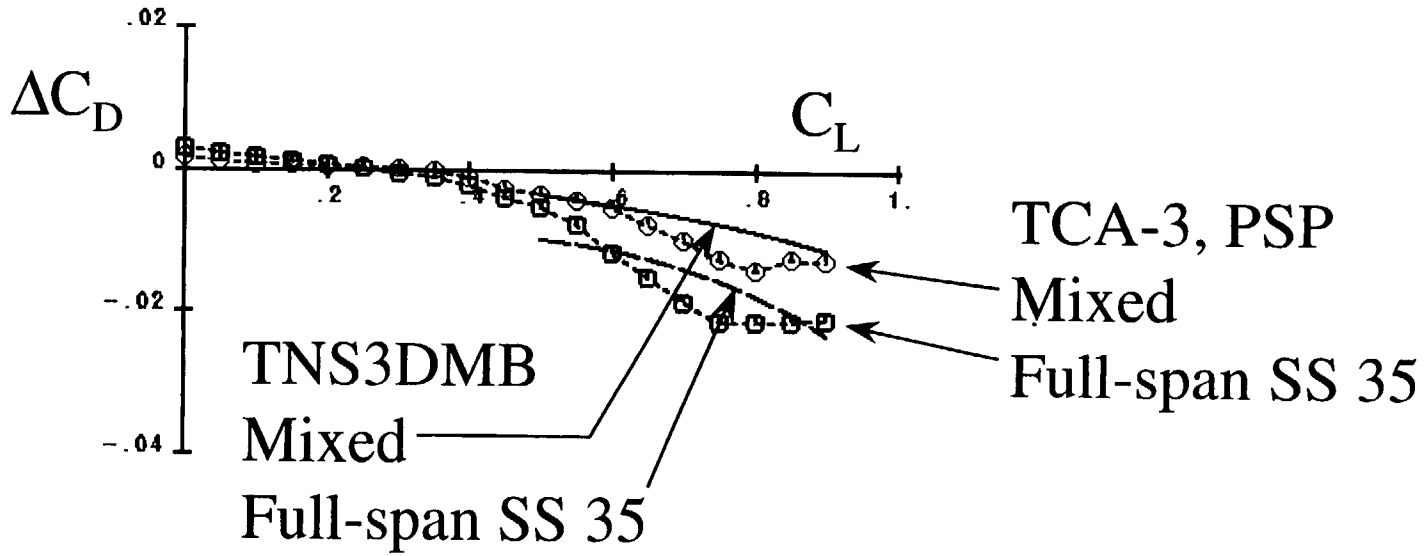

Mixed: inboard SS 35, outboard plain 35

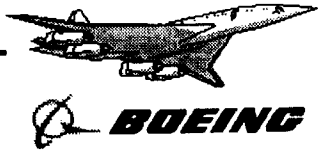

5% TCA W/B Surface Pressures
Mach ~ 0.24, α ~ 10 Degrees, Re ~ 8 M

- PSP data is noisy.
- Forward 30% of the wing has too positive Cp's.
- Areas such as the outboard LE, the outboard LE hinge, the edge between the two outboard TE flaps, all show unreasonable signals.
- Bolt holes such as the ones for mounting the nacelles are also visible on PSP.

BOEING

5% TCA W/B Surface Pressures
Mach ~ 0.24, α ~ 10 Degrees, Re ~ 8 M

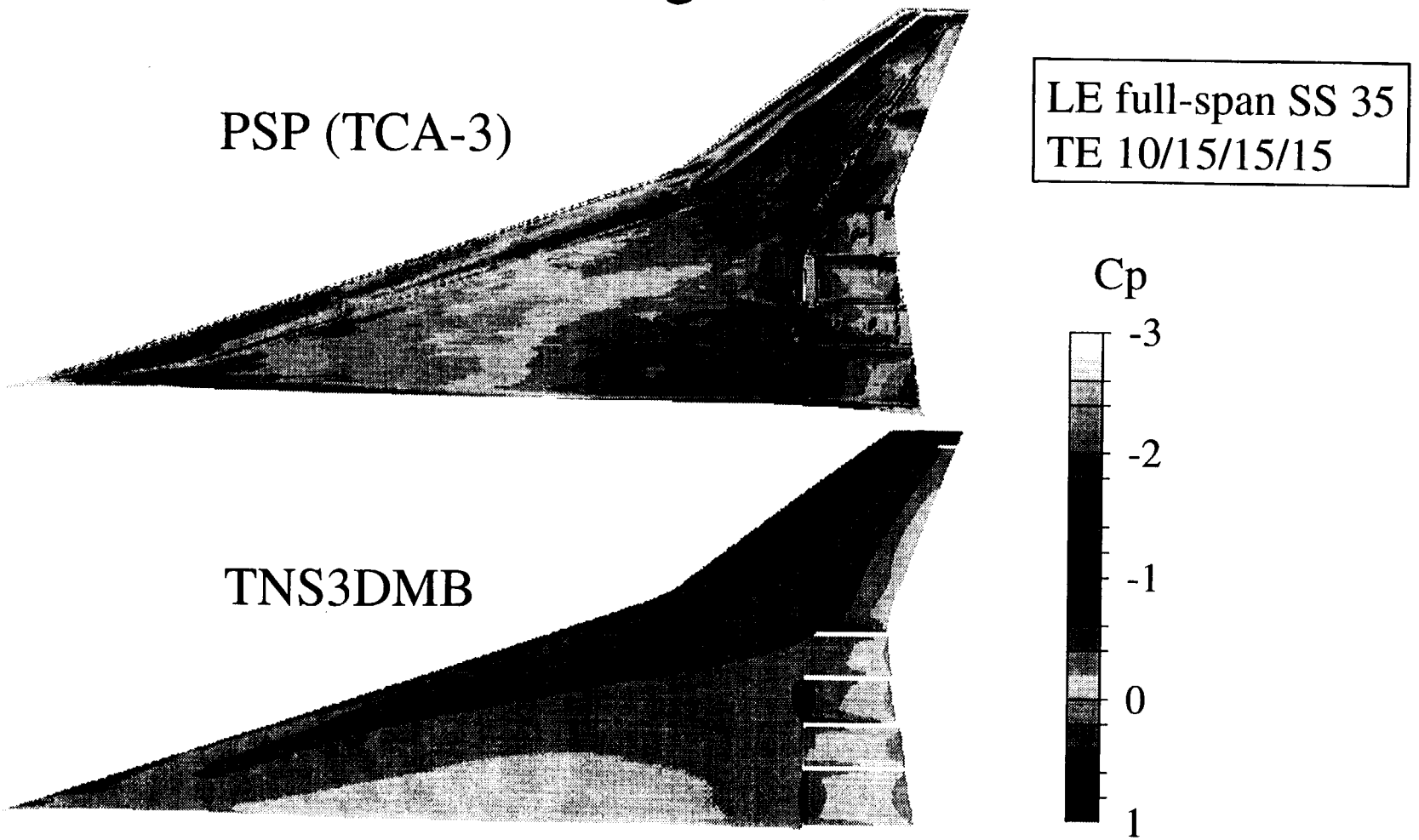

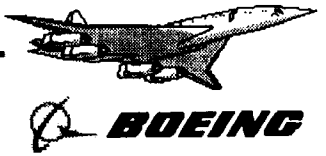

5% TCA W/B Surface Pressures
Mach ~ 0.24, α ~ 10 Degrees, Re ~ 8 M

- PSP data is noisy.
- ESP data is not much better. Leaks are visible.

BOEING

5% TCA W/B Surface Pressures
Mach ~ 0.24, α ~ 10 Degrees, Re ~ 8 M

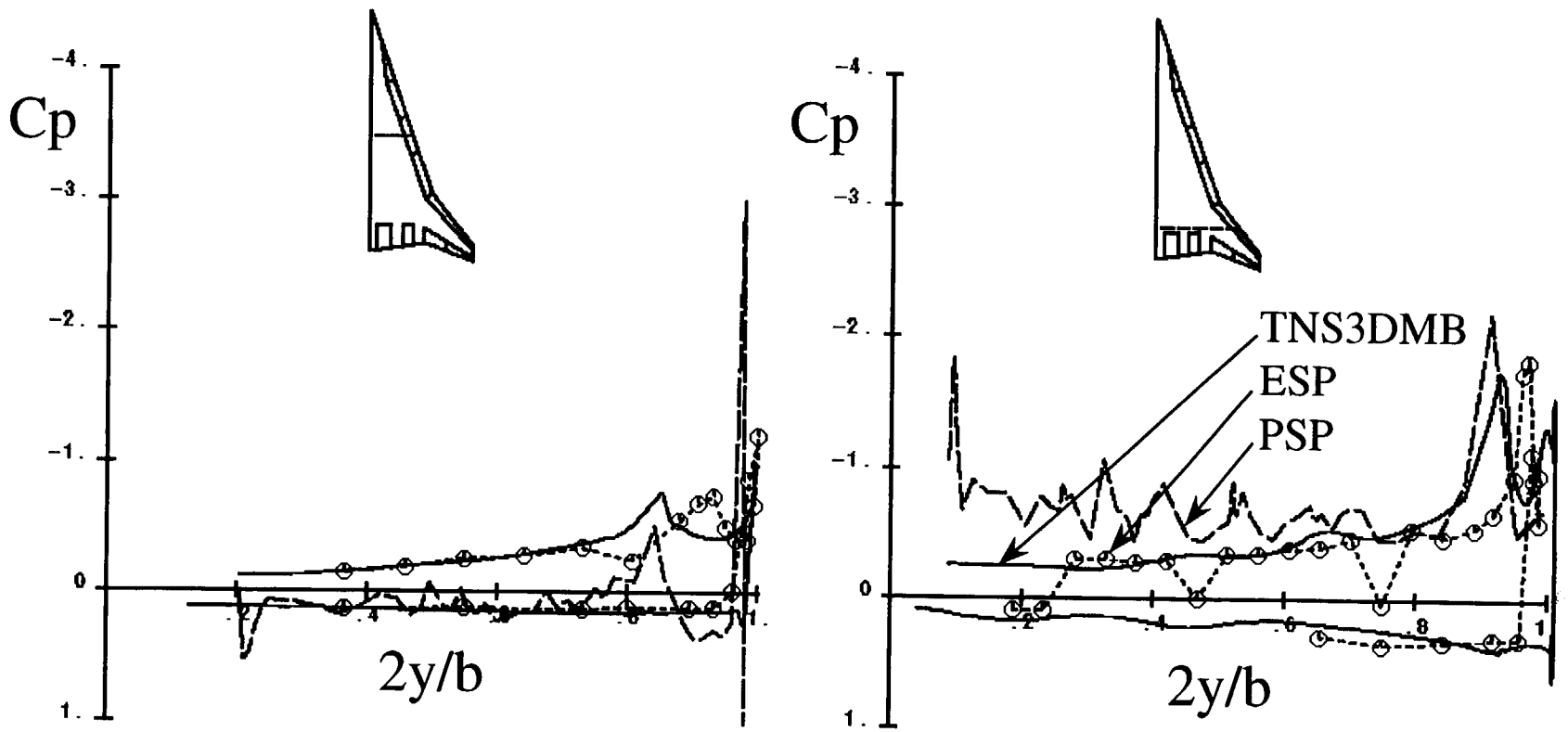

LE full-span SS 35
TE 10/15/15/15

5% TCA W/B Surface Pressures
Mach ~ 0.24, α ~ 10 Degrees, Re ~ 8 M

- PSP data is noisy.
- ESP data is not much better. Leaks are visible.
- PSP Cp at hinge lines on the upper surface are too low.
- Flap Cp's do not make sense.

BOEING

5% TCA W/B Surface Pressures
Mach ~ 0.24, α ~ 10 Degrees, Re ~ 8 M

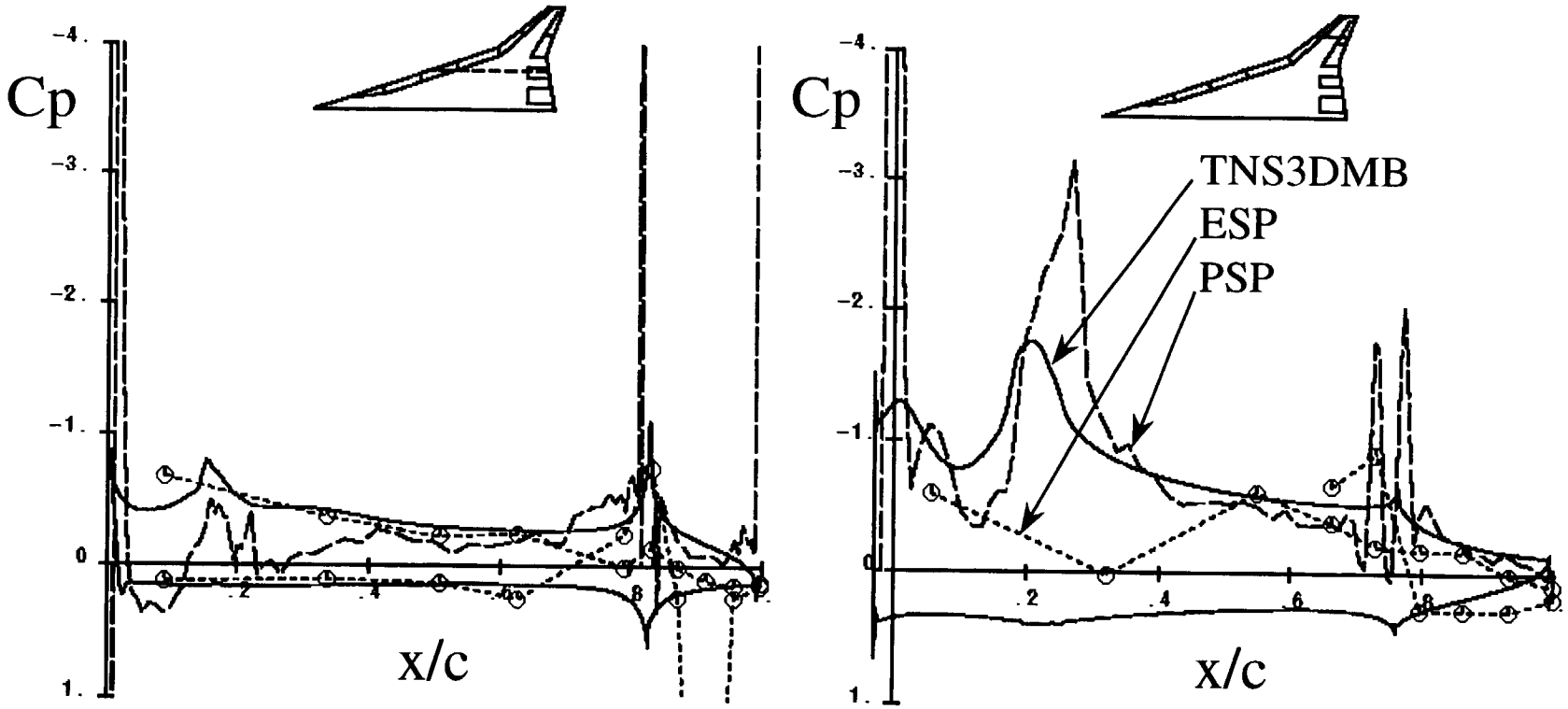

LE full-span SS 35
TE 10/15/15/15

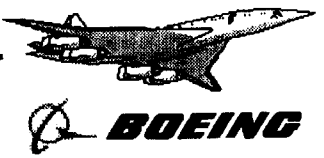

Conclusions

- 14x22 data have higher drag than 12-ft data. The reason is not understood. Differences in upflow and model support between the two facilities could be major contributors.
- Plain flaps, even optimized in the wind tunnel, could not render the technology projection. Sealed slats could.
- The PD process relies heavily on AERO3S for flap optimization. AERO3S is a linear code and therefore does not capture the viscous effect which is significant.
- TNS3DMB captured the effect of the sealed slats at 8 M Reynolds number in terms of ranking various configurations. The L/D level from TNS3DMB is lower than test data, an observation made since 1995.

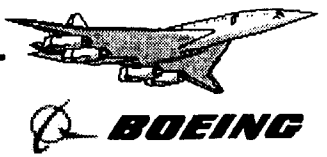

Conclusions

- 8.15 (based on 14x22 data) < TCA L/D < 8.89 (based on NTF and 12-ft data)
- More complex LE devices than the plain flap are needed.
- Flap deflection optimization in the PD process is inadequate.
- TNS3DMB captured the effect of the sealed slats.

Off-Body Upwash Induced by Posts Panel Code A502, Mach 0.3

- Taper generates upflows.
- The 14x22 post seems to generate larger upflows.
- The 12-ft post generates upflows that are more localized.
- Differences in the upflow on the order of 0.6° could cause differences in C_D on the order of 0.005 at $C_L \sim 0.5$.

BOEING

Off-Body Upwash Induced by Posts
Panel Code A502, Mach 0.3

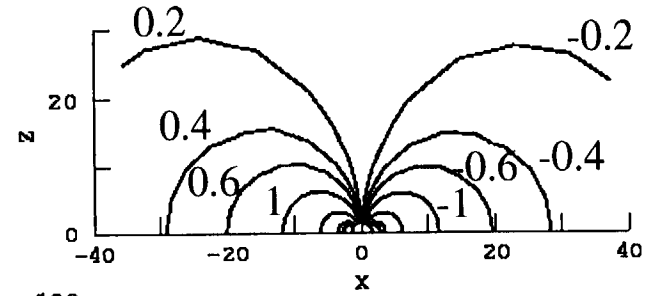

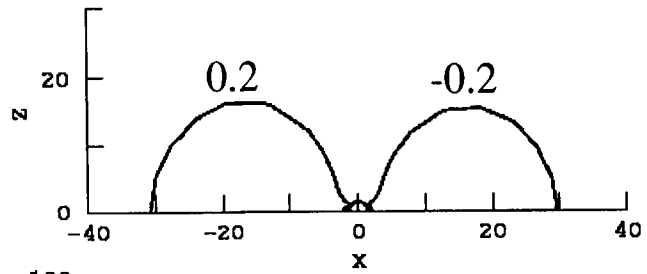

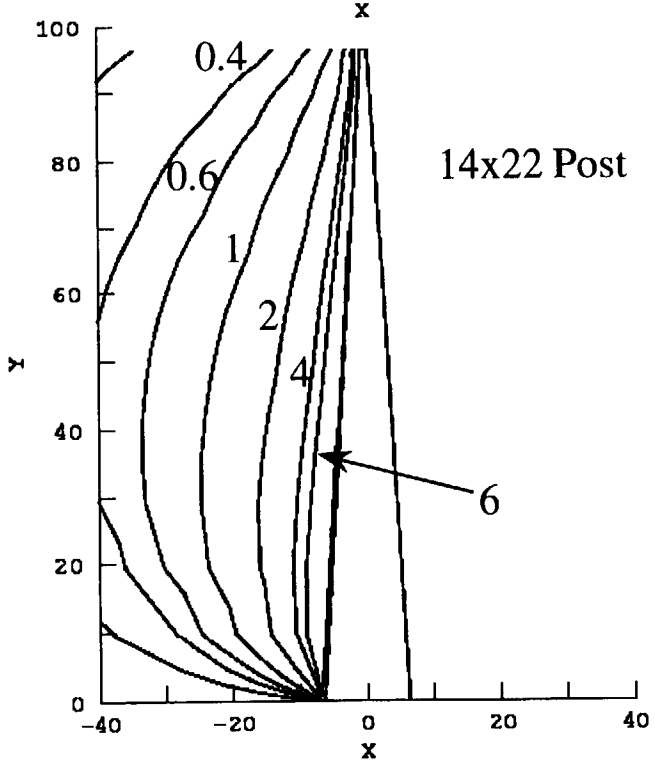

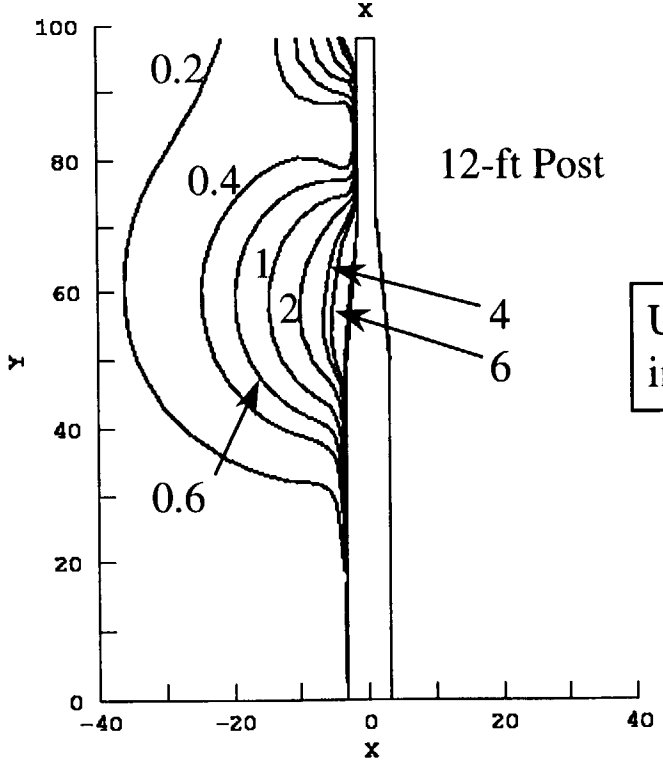

Upwash angles are in degrees

Recommendations (1 of 2)

- Results of the upflow and interference test at 14x22 (Test 442) are inconclusive due to balance problems.

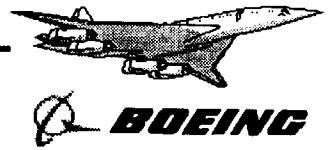

Recommendations (1 of 2)

- Upflow and support interference tests must be conducted in the LaRC 14x22 and ARC 12-ft tunnels if absolute drag levels for post-mounted models are required.
- The preliminary design estimation process should be calibrated/updated with the available wind tunnel data for various wing planforms and flap deflections.

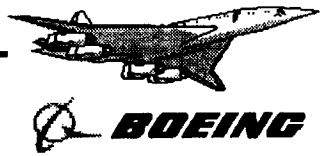

Recommendations - (2 of 2)

- PSP is a technology that needs to be further researched and developed. The outboard wing of HSCT is so thin that there is simply not enough room to place sufficient instrumentation for measuring surface pressures.
- Data needed for test/CFD correlation have not been given sufficiently high priority in almost all the wind tunnel tests. More attention should be given to data such as surface pressure, surface flow patterns, surface skin friction, state of the boundary layer, etc.

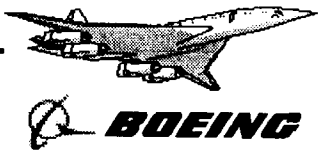

Recommendations (2 of 2)

- The technology projection (suction parameter) should be made a function of the wing planform.
- Continue research on PSP
- Continue test/CFD correlation

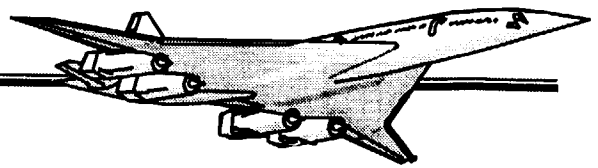

HSR Leading Edge Trade Study

Boeing Commercial Airplane Group
High Lift Aerodynamics
Warren Burggraf

Airframe Annual Review
February 9, 1999

Purpose

- The motivation of this study was to improve the Lift to Drag ratio of the configuration at the critical climb-out condition and thereby reduce the climb-out noise. Lift by itself is not the issue on this airplane but instead drag at the climb-out lift condition.

- This study concentrated on sealed leading edge devices with reductions in wing upper surface curvature when deflected. The reason for this was that recent wind tunnel tests and prior art have shown that these kinds of devices show superior lift to drag characteristics.

- The purpose of the study was to evaluate the impact/advantages relative to the plain flap leading edge of using a sealed slat or a variable camber leading edge on the PTC 1080-1494 wing. The study was an extension of a 1993 study in that new information and methods are now available which impacts the conclusions drawn, in particular new wind tunnel data and new analytical tools (NSU2D).

- Aerodynamics, Structures, Mech/Elec Systems, Weights, and Aero Performance participated in the study.
  - Aerodynamics performed CFD analysis of the devices, assessed the performance, and acted as lead on the study.
  - Structures in conjunction with Aerodynamics prepared drawings of the plain flap, slat and variable camber leading edges concepts and determined the viability of the these concepts.
  - Weights re-evaluated the concepts and determined the weight increments in relation to the plain flap leading edge.
  - Aero Performance prepared sizing charts for performance comparison between the concepts.

Team Members

Aerodynamics	Warren Burggraf (High Lift)
	Servando Flores (High Speed)
Structural Design	Al Falco
Mech/Elec Systems	Ray St. Cyr
Weights	Bill Barclift
Aero Performance	Paul Carpenter

High Lift Wind Tunnel Results

- Because other commercial transports have shown that improved L/D's are achieved when the configurations include a sealed leading edge device with a large wing upper surface radius for the takeoff and climb-out, the design and analysis of these devices have been pursued. Recent wind tunnel tests have supported this position, showing a significantly improved L/D at the important climb-out flight condition, i.e., C_L=0.5.

- The aerodynamic explanation for the drag reduction is the improvement in wing upper surface flow to higher angles of attack by a reduction of the hinge line curvature induced pressure peak.

- The following figure shows the ARC 12ft wind tunnel results of the effect on L/D of the use of sealed slats in place of the plain flap of the current TCA configuration. The three cases shown are an all plain flap configuration , a plain flap inboard and a sealed slat outboard a configuration , and an all-sealed slat configuration.

High Lift Wind Tunnel Results

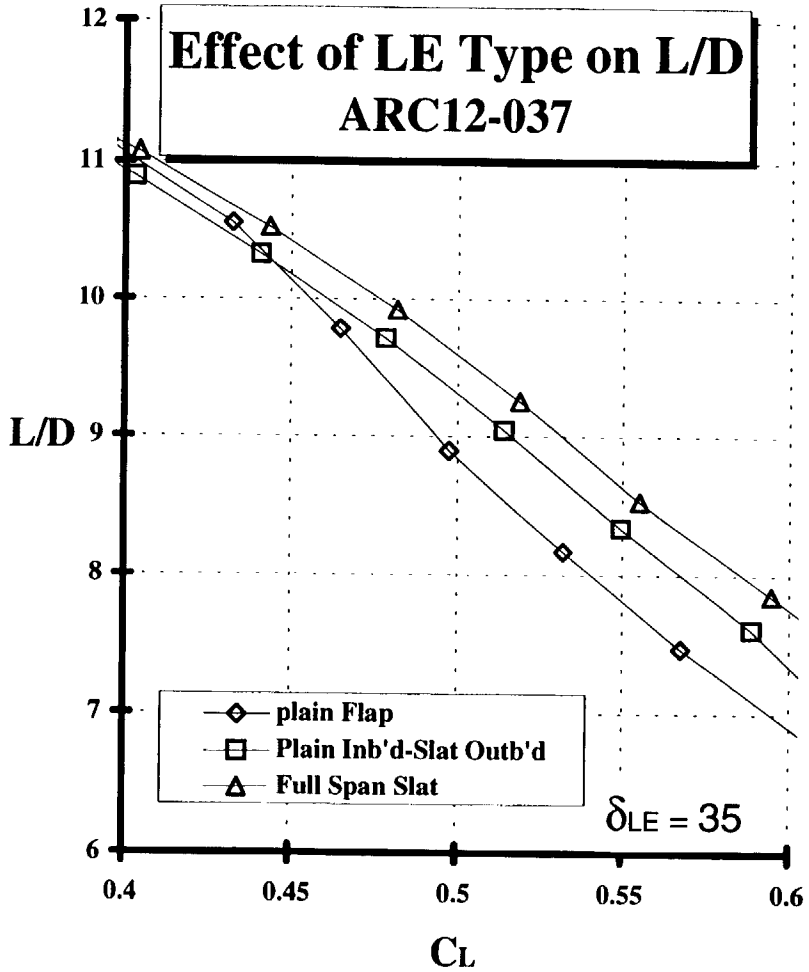

Leading Edge Concepts

Three leading edge device types were studied.

- Baseline plain flap is the simplest of the devices: This concept is a simple rotation around an actuator set as low as possible within the wing so that the upper surface curvature is as low as possible.

- Sealed slat: The leading edge is deflected by a rotating/translating track and the flap trailing edge is sealed against a wiping surface designed for that purpose. Sealing is important to produce a very low drag level at the climb-out flight condition. The motion is such that the wing upper surface curvature is very low compared to the plain flap.

- Variable camber leading edge (VCLE): This device as envisioned during this study is similar to a VCLE device developed by Jim Cole of the Boeing company during the 7-7 program. It is a rotating track driven by a rotary actuator (all within the wing) which bends the leading edge down, providing a very low wing upper surface curvature compared to the plain flap.

Leading Edge Concepts

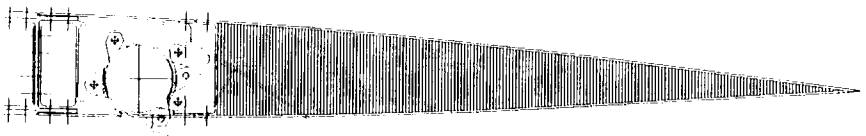

Plain Flap

30 degree deflection
in all cases

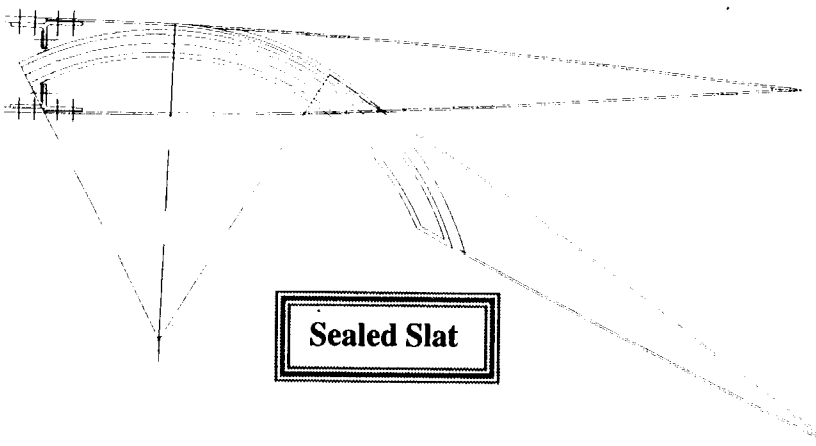

Sealed Slat

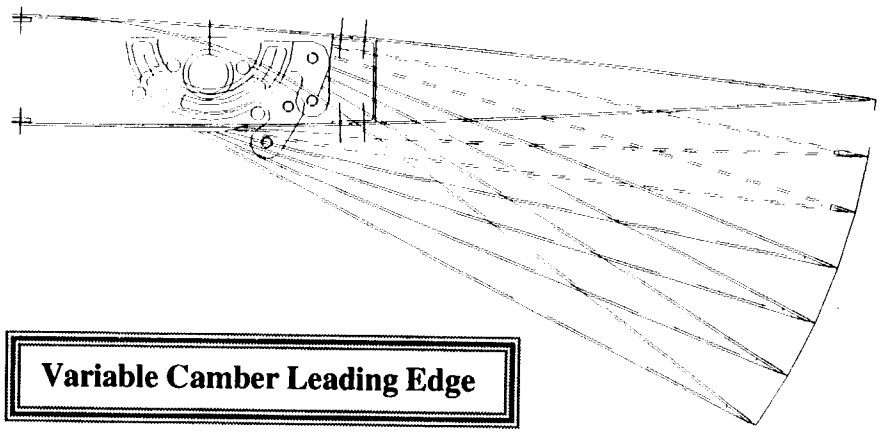

Variable Camber Leading Edge

Ground Rules

The ground rules for this study are in the following chart.

Ground Rules

- Uncycled designs, no optimizations.
- No protrusions when retracted, some allowed when deflected.
- PTC configuration.
- Part span designs allowed if necessary.
- The device is to be operated both transonic and low speed.
- Panel to panel intersections are assumed to be workable.
- The airplane is assumed to be jam tolerant (this is an unfinished task).

High Lift CFD Analysis

- Analytically the method was to use the 2-D CFD program NSU2D to analyze a broad range of leading edge angles to acquire a good understanding of the aerodynamic performance of various leading edge types.
- One variation in leading edge device chord of the slat was analyzed to get the chord effect.
- One representative sectional cut from the wing outboard of the leading edge planform break was analyzed. The section chosen was 1/3 of the distance from the wing planform break to the wing tip, i.e., a wing buttock line 627.3 cut.
- A range of angles of attack were analyzed to get a drag polar for each leading edge deflection angle.
- The trailing edge angle in all cases was 8 degrees since this value was the AERO3S derived optimum for the PTC at the climb-out flight condition.
- Each case required approximately 3/4 hour run time on a SGI Octane work station.
- The following chart shows the cases run.

High Lift CFD Analysis

NSU2D Cases				
δ_{LE}	Plain Flap	Slat	Variable Camber	Half Slat
10	α = -1°,0°,1°,2°	-1°,0°,1°,2°	-1°,0°,1°,2°,3°	-1°,0°,1°,2°
15	1°,2°,3°,4°			
20	1°,2°,3°,4°	2°,3°,4°,5°,6°	1°,2°,3°,4°	1°,2°,3°,4°
24	0°,1°,2°,3°,4°,5°,6°			
30	4°,5°,6°,7°	5°,6°,7°,8°	3°,4°,5°,6°,7°	3°,4°,5°
35	6°,7°,8°	6°,7°,8°,9°,10°	4°,5°,6°,7°	4°,5°,6°,7°
40			5°,6°,7°,8°	5°,6°,7°,8°

High Lift CFD Analysis

- Leading edge surfaces were created at all deflection angles of all leading edge concepts in the PTC wing in the area of interest. The size of the devices were as drawn in the PTC definition with the exception of the half slat which was half the chord of the as drawn leading edge. Device hinge lines were defined by structures, again with the exception of the half slat which used a wing surface radius of curvature scaled to the wing thickness at the device trailing edge.

- The surfaces were then cut at WBL627.3 and the thickness was adjusted for the sweep angle of the wing to get an equivalent non-dimensional 2D section for the analysis.

- The sweep angle used was the 1/4 chord sweep angle of the outboard panel, i.e., 25 degrees.

- The resulting leading edge geometries are shown in the following slide.

High Lift CFD Analysis

PTC Configuration
Equivalent 2-D Leading Edge Sections

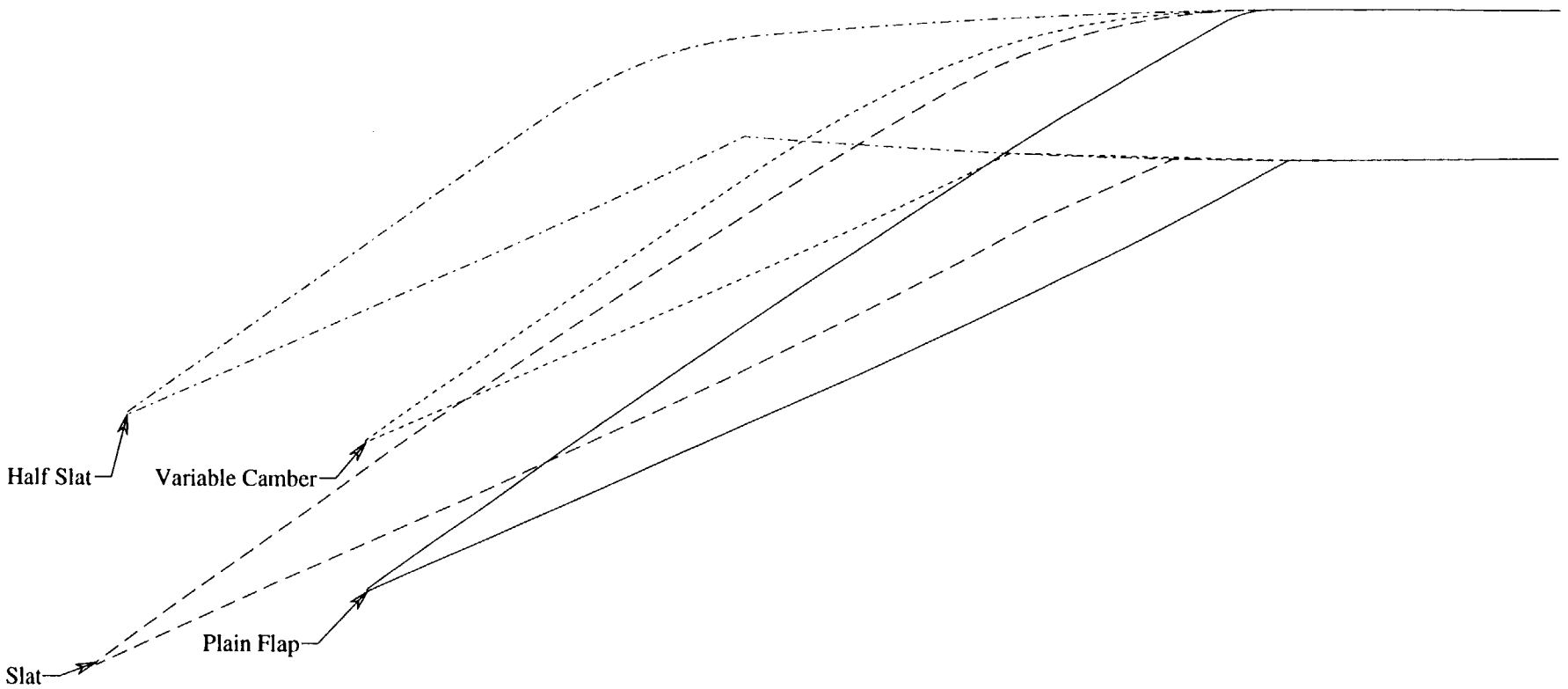

High Lift CFD Analysis

- Drag polars for various leading edge geometries and deflection angles were derived using NSU2D (V.5.0.a), an unstructured grid two dimensional compressible Navier-Stokes code. With these polars the lowest drag leading edge angle for a configuration for any operational lift level can be inferred.

- Examples of the drag polars for the three leading edge types are shown in the following figure.

High Lift CFD Analysis

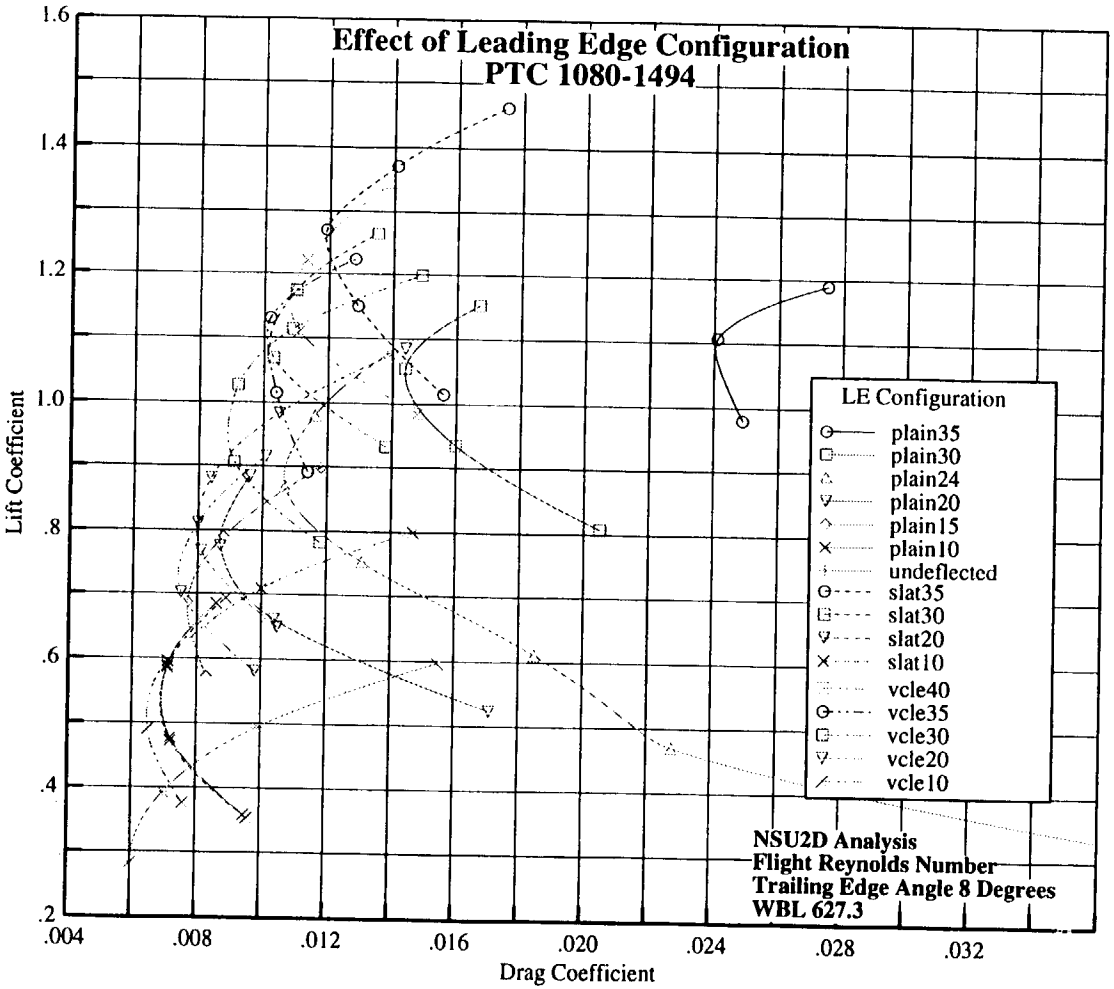

High Lift CFD Analysis

- Minimum drag performance levels of the various leading edge devices as a function of leading edge deflection are shown in the following figure. On the PTC configuration at the climb-out $C_L = 0.5$ the spanload distribution and simple sweep theory gives a 2-D sectional C_l=1.19 at WBL=627.3. Using these charts we find that the optimum slat deflection at this C_l is 33 degrees, whereas for both the VCLE and the half slat the optimum deflection angle is approximately 38.5 degrees. Looking at the drag chart at these angles show that the drag levels of all three types of devices is approximately the same at their optimum deflection angle or C_d=0.0106. The plain flap on the other hand doesn't get to these levels of C_l two dimensionally. To get to these levels on the airplane a leading edge vortex forms and a high drag penalty is imposed.

High Lift CFD Analysis

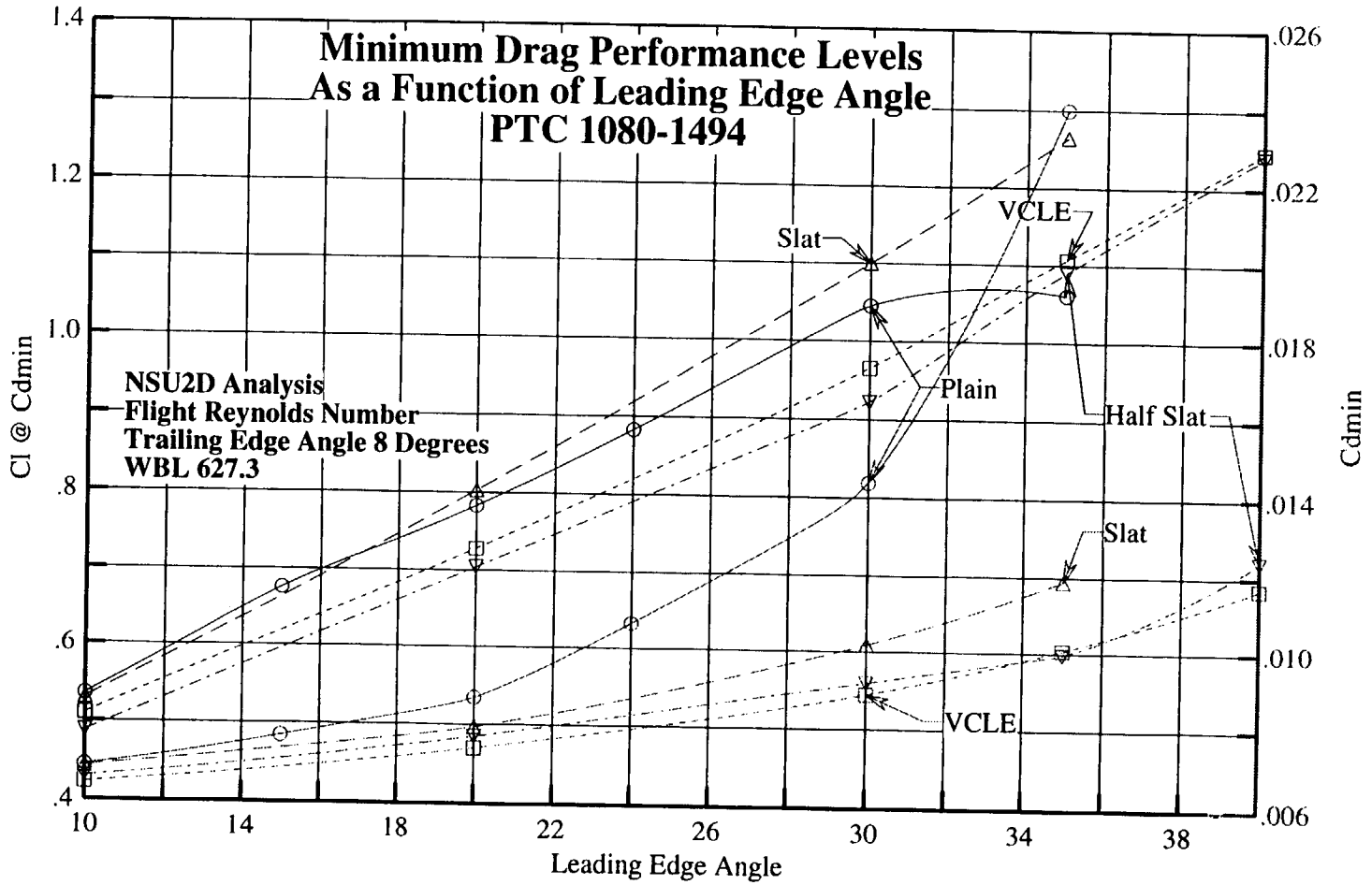

High Lift CFD Analysis

- Since the hinge line radius has a very large effect on drag the question is: "How much radius is necessary to achieve most of the drag improvement from this source?" A series of radius values between the baseline plain flap radius and the slat radius were run to answer this question.
- The leading edge hinge line was moved normal the wing upper surface to the various analyzed values.
- One value of leading edge deflection was analyzed, i.e., 30 degrees, as this is near the climb-out operational value.
- The results show that most of the drag benefit is derived when the radius is on the order of 4.4% of the 2-D chord or greater. This is the 13.14 inch case.
- The following chart illustrates the hinge line radius effect.

High Lift CFD Analysis

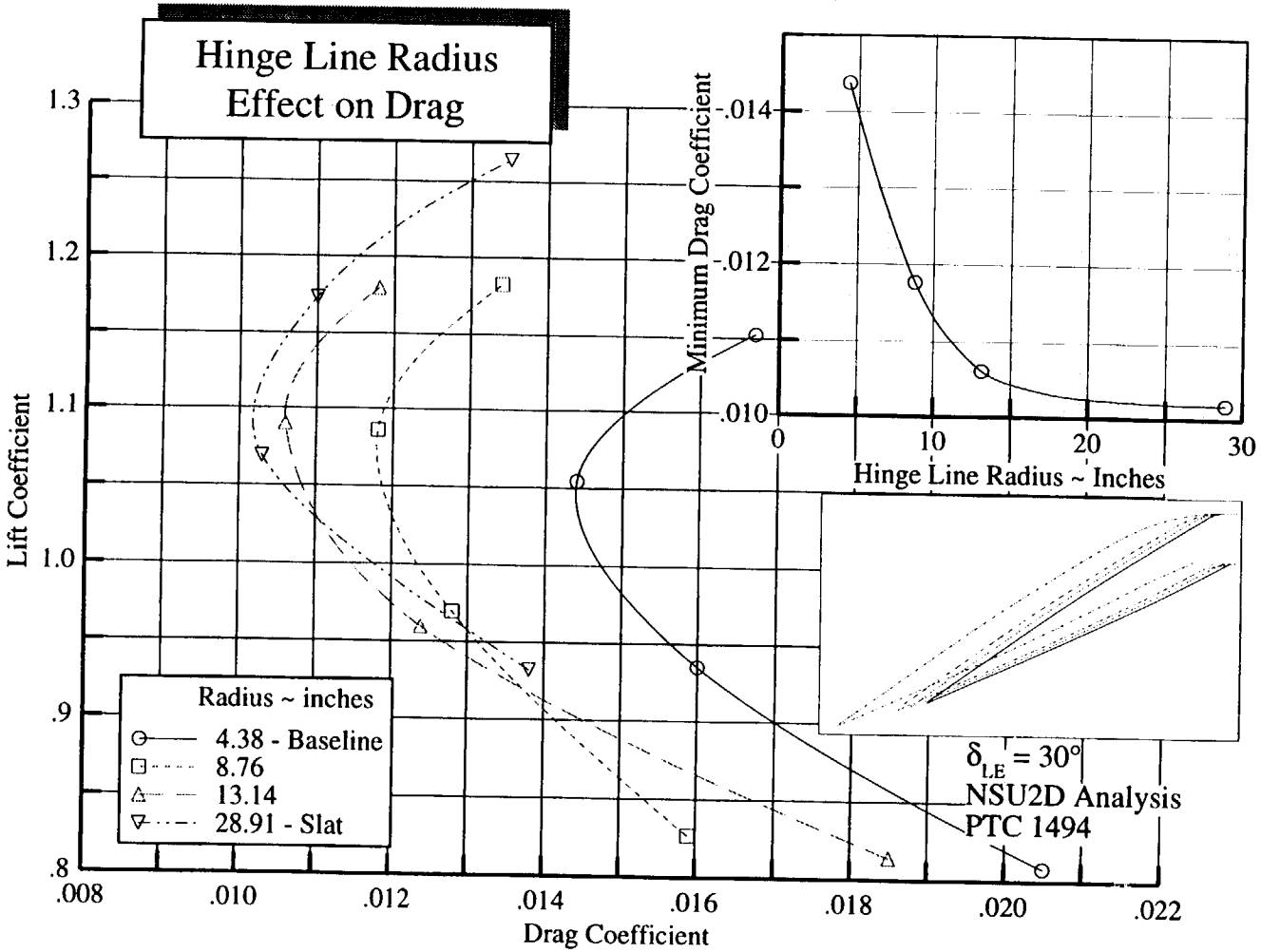

High Speed Aerodynamics

- Linear Potential Analysis
  - AERO3S (Plain and Variable Camber Flaps)
  - A389 (Plain and Variable Camber Flaps)

- Excrescence Analysis
  - ESDU (Plain Flap, Sealed Slat, And Variable Camber Flap)

- High speed, M=0.9 - 2.4, only the the leading edge outboard of the planform break is deflected.

- Sealed Slat had the worst excrescence drag at Mach numbers of 0.9 and 1.2 but shows a benefit at Mach 2.4.

- Variable camber flap showed the best overall performance at all conditions studied.

- The following chart shows the drag results of the high speed analysis.

High Speed Aerodynamics

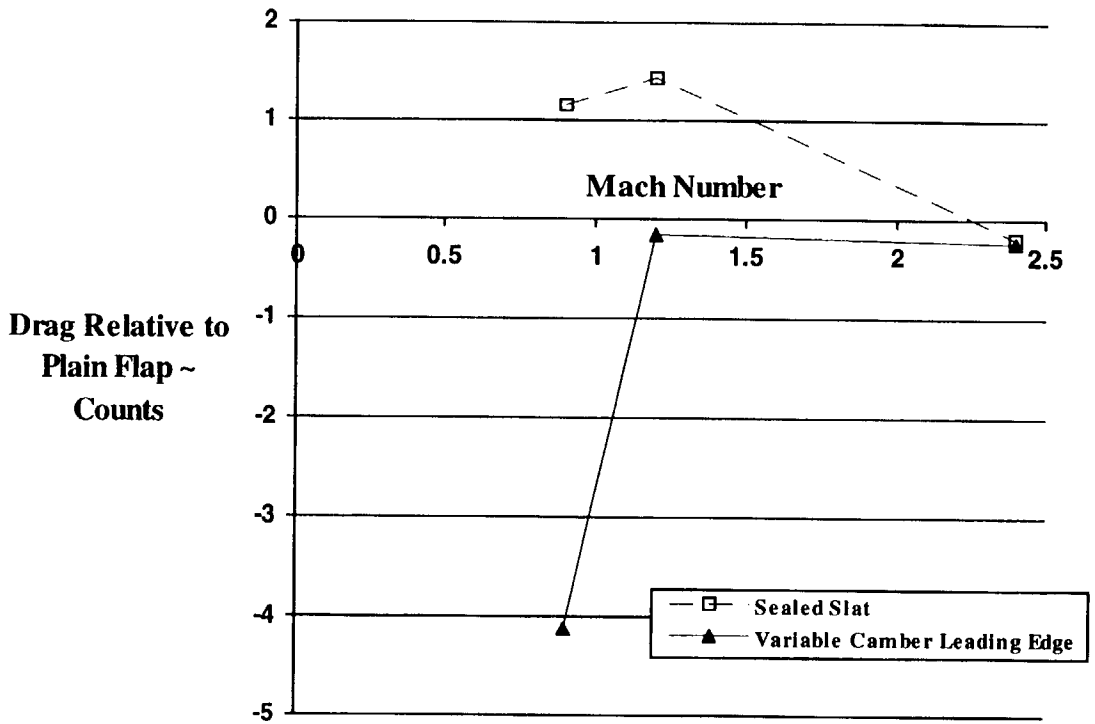

Structural Design

- Only outboard panels #1 and #4 were analyzed.
- 1993 study loads used on all device types.
- The leading edge has 3 inboard panels and to minimize aeroelastic effects 8 outboard panels.
- No design of the corner flap was done but is assumed workable for all device types.
- No flutter analysis was done and this work is left for future study.
- The tapered most inboard panel #11 planform can not be as shown and will depend on device type.
- The following limits apply:

Leading Edge Device Type	Panel #	Structural Deflection Limit	Desired Deflection	Limit Cause
Plain Flap	1	50°	30°	Attachment fittings.
	4	50°	30°	Attachment fittings.
Sealed Slat	1	20°	30°	Track penetrates lower surface at 20° Slat becomes unsealed at 25°.
	4	35°	30°	Track penetrates lower surface, Slat becomes unsealed.
VCLE	1	35°	35°	Track penetrates upper surface.
	4	35°	35°	Track penetrates upper surface.

Structural Design

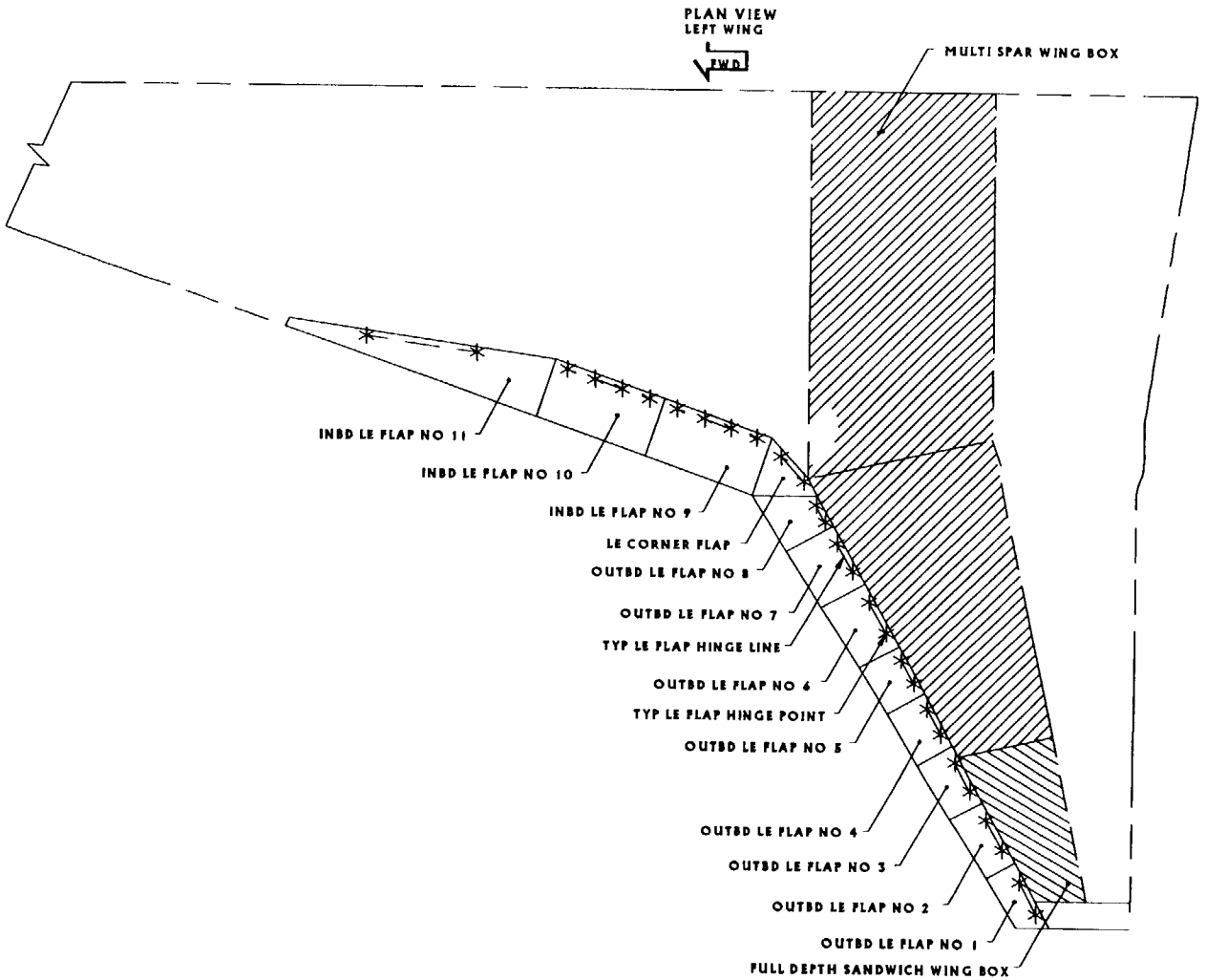

Weights

- The weights of the various devices were assessed using the 1993 analysis. Since this study was a first order detailed structural analysis it was felt that no significant improvement in the weight assessment would be realized over what had been done in the previous study.

- The 1993 study did not explore the use of a sealed slat in the mid-span area of the wing. For this region the current study simply took the ratio of mid-span to outboard ratio of the 1993 study plain flap and applied it to the sealed slat outboard weight to get a weight for the mid-span area.

- The following chart shows the resulting weights of the three device types for the PTC 1080-1494 configuration.

Weights

PTC 1080-1494 Leading Edge Weight

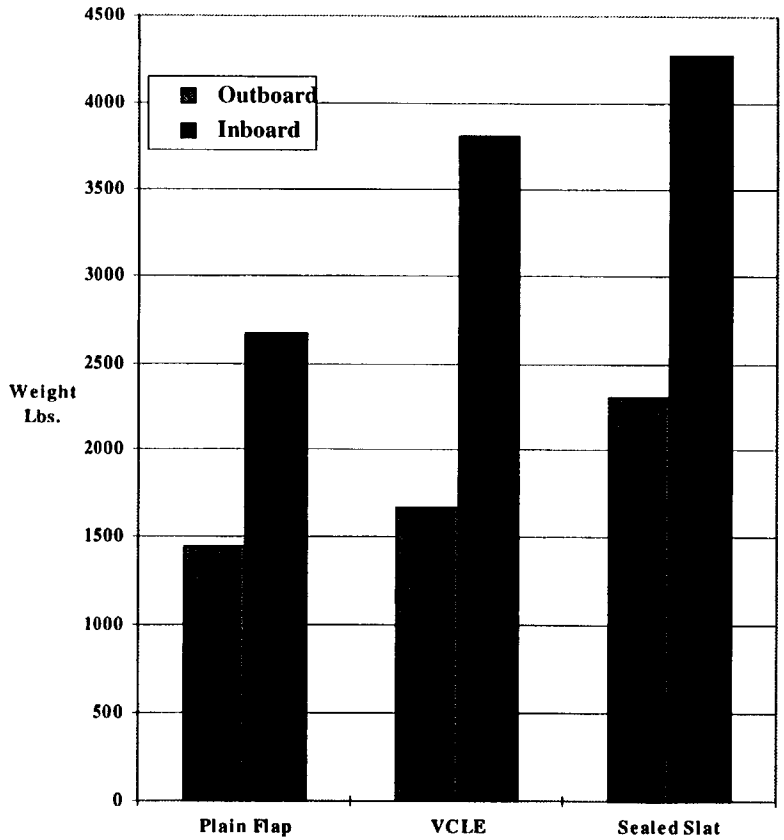

Aerodynamic Performance

- Aerodynamic performance was evaluated relative to the baseline PTC 1080-1504 configuration with both the sealed slat and the variable camber leading edge (VCLE). The configurations included:
  - Plain flap inboard and outboard
  - Plain flap inboard, sealed slat outboard
  - Plain flap inboard, VCLE outboard
  - Sealed slat inboard and outboard
  - VCLE inboard and outboard

- The high lift inputs were status level polar estimates with the wind tunnel increments shown previously. Both the sealed slat and the VCLE were assumed to be aerodynamically equivalent since this was the result of the NSU2D analysis and there was no other data available for the VCLE.
- The high speed inputs were projected level polars with the estimated increments shown previously for each configuration applied.
- The following chart summarizes the performance effects in two ways. One method sizes the wing, engine, and MTOW to the constraints, 5000 mile range and -5 epndb noise; the other fixes the wing, engine, and MTOW, and allows the performance to fall out.

Aerodynamic Performance

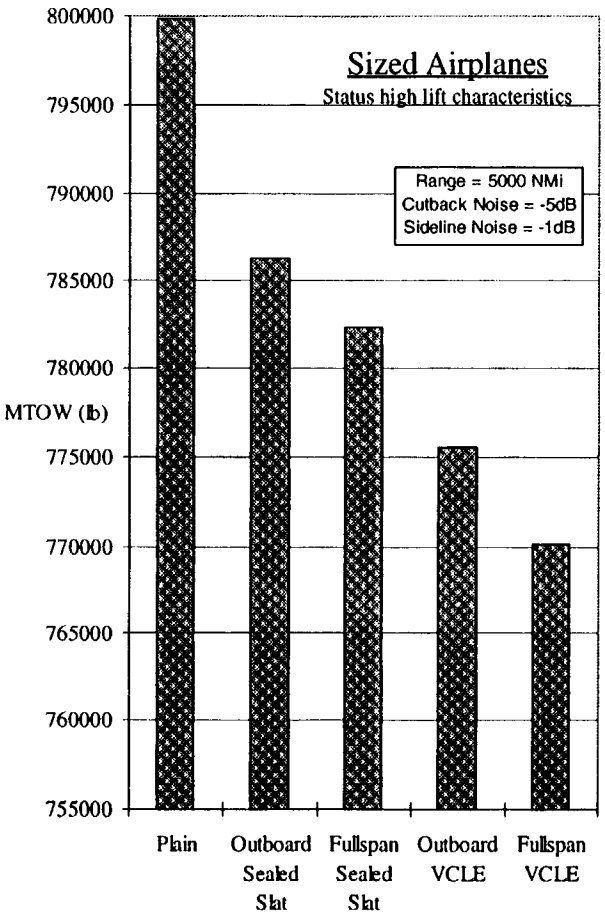

Fixed Sized Airplanes
WA = 764
S_W = 8908 Ft^2
MTOW = 799869 lbs.

	Cutback Noise ΔEPNdb	Sideline Noise ΔEPNdb	Takeoff Field Length ΔFeet	Range ΔN.Mi.
Baseline Plain	0	0	0	0
Outboard Sealed Slats	-1.29	0	-169	-21.3
Fullspan Sealed Slats	-1.93	0	-214	-55
Outboard VCLE	-1.29	0	-169	25.5
Fullspan VCLE	-1.93	0	-214	1.3

Conclusions/Recommendations

- 2-D CFD indicates sealed slat and VCLE are aerodynamically equivalent.
- The VCLE reduces drag at the noise critical climb out lift and at the high speed operating conditions.
- The sealed slat reduces drag at the noise critical climb out lift but high speed shows an increase in drag below M = 2.
- The MTOW of a VCLE equipped PTC configuration with a -5 EPNdb climbout noise level would be 30,000 lbs. lighter than one with a plain flap.
- Wind tunnel testing of the device types is needed to confidently establish the performance levels.
- Further study is needed to establish thermal and flutter limits.

Conclusions/Recommendations

Leading Edge Type	Comments	Advantages	Disadvantages
Plain Flap 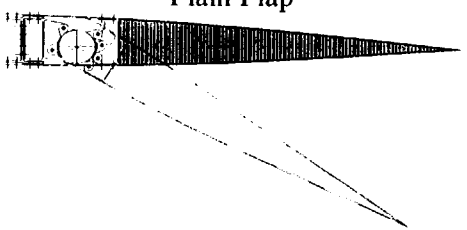	Current baseline. Needs better definition of - panels near wing tip - corner flap - most inboard panel #11	• Simplest design. • Lightest of the devices studied. • Structurally the stiffest. • No front spar penetration. • Clean when deployed Lower high speed drag. • Best deflection capabilities.	• Small hinge line radius, Higher climb-out & high speed drag Difficult high speed integration • Sliding seal at panel trailing edge. • Small step at flap trailing edge (high speed drag). • Complex corner panel design.
Sealed Slat 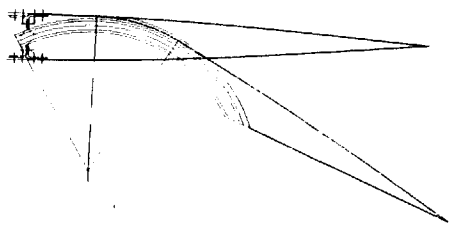	Needs better definition of - panels near wing tip - corner flap - most inboard panel #11	• Larger hinge line radius, Low climb-out drag • Similar to other Boeing products.	• Heaviest of the devices. • Track penetrates front spar. • Structurally softest because of Fowler. (Dynamics problem?) • Sliding seal at panel trailing edge. • More complex design than plain flap (higher cost & maintenance). • Small step at flap trailing edge (high speed drag). • Cluttered under surface when deployed. • Most restricted deflection capabilities. • Complex corner & #11 panel design.
Variable Camber 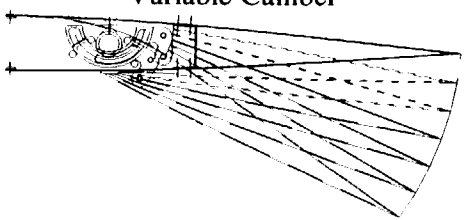	Wing spar top must be piece wise straight. Needs better definition of - panels near wing tip - corner flap - most inboard panel #11	• Larger hinge line radius, Lower climb-out drag. • No sliding seal at panel trailing edge. • No front spar penetration. • No step at panel edge. • Clean when stowed and deployed. Lowest high speed drag. • Carries side load efficiently through skin. • Simplest corner & #11 panel design.	• Heavier than Plain Flap. • Higher stresses in flex panel. • More complex design than plain flap. (higher cost & maintenance) • Unproven design. • Most adversely effected by aeroelastic bending. • Structurally softer than plain flap (stiffer in sideload). • More restricted deflection capabilities.

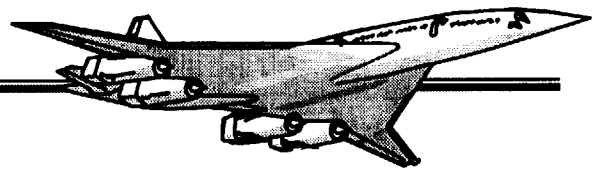

3D CFD Analysis

TNS3DMB L/D Comparisons
TCA 2.8-38
M = 0.247, α = 10, R_{α} = 8X10^6

- TNS3dMB analysis was done on the 2.8-38 configuration in support of the upcoming TCA-5 LaRC 14X22 test.
- The 2.8-38 configuration has higher outboard leading edge sweep than the PTC configuration on which the NSU2d analysis was done. PTC sweep = 32.5 and the 2.8-38 sweep = 38.
- The L/D comparisons of the plain flap and the VCLE shown in the following chart show the VCLE to have higher L/D's at the noise critical C_L = 0.5 condition when the deflection angle is 35 or 40 degrees.
- The situation reverses at the C_L = 0.7 level and then returns at C_L = 1.0.
- The NSU2D analysis predicts the VCLE would perform as well as a sealed slat, at a different deflection angle. These TNS3DMB results show an improvement in ΔL/D of 0.33 @ C_L = 0.5 for the VCLE compared to the plain flap. The TCA-3 test results show a ΔL/D = 0.7 for the sealed slat compared to the plain flap.

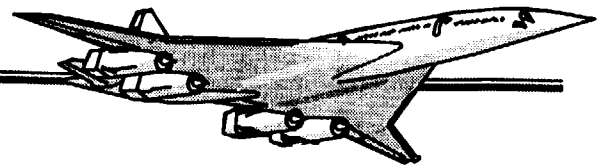

3D CFD Analysis

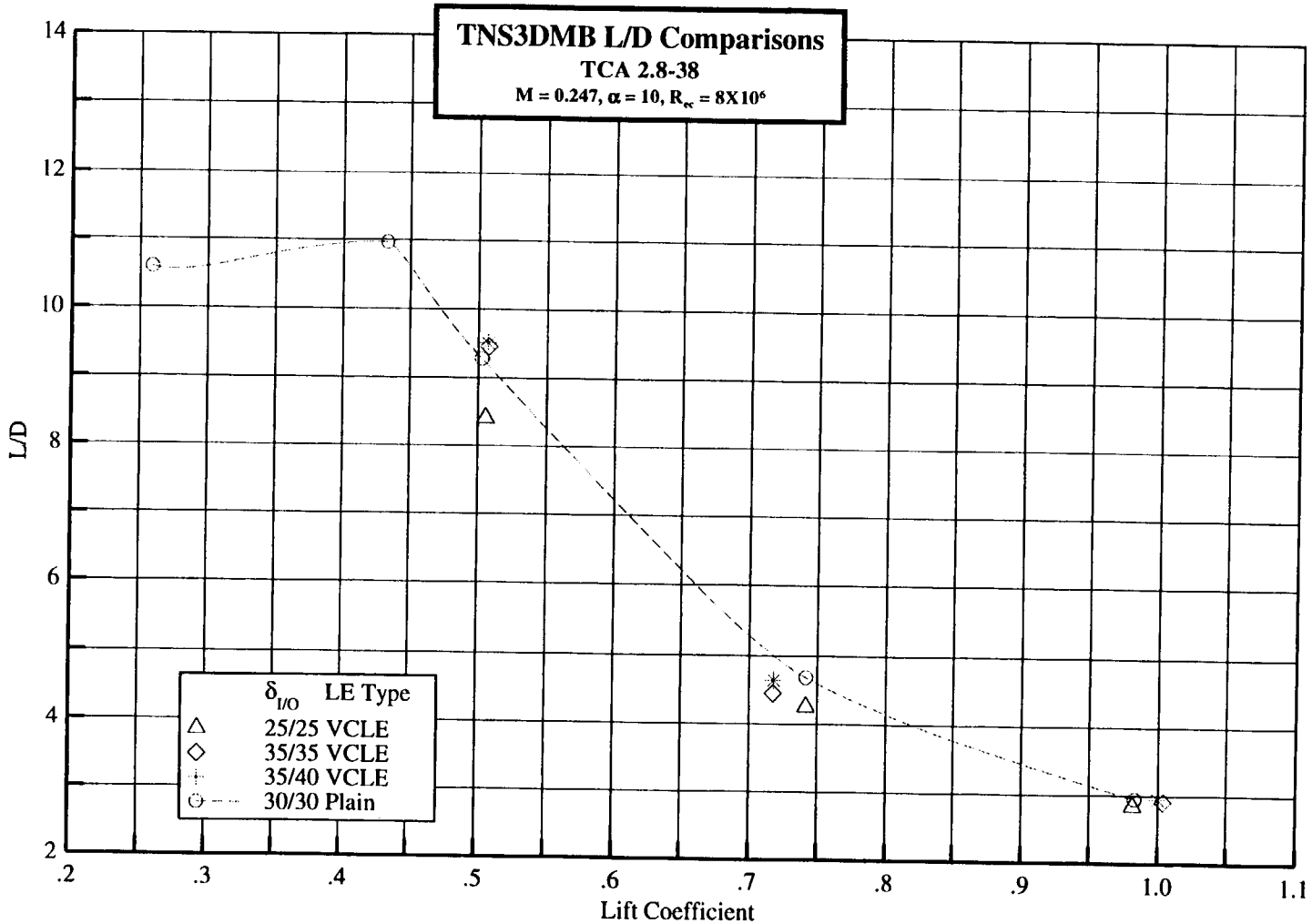

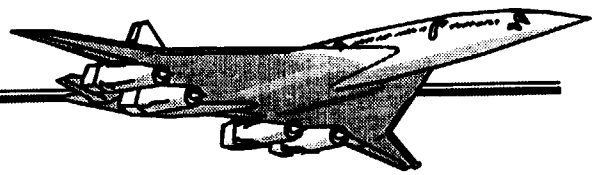

3D CFD Analysis

TNS3DMB Sectional Forces
TCA 2.8-38
M = 0.247, α = 10, R_{cc} = 8X10^6

- Comparisons of the sealed slat and the VCLE TNS3DMB spanloads of lift and drag show the outboard wing lift and drag is improved when the leading edge type is a VCLE. This improvement is due to the elimination of separation at the hinge line and leading edge.

- On the other hand the inboard wing sectional drag is worse with the VCLE. This is not understood at this time. In neither case is there reversed flow on the inboard wing.

The following chart shows these comparisons.

Leading Edge Trade Study

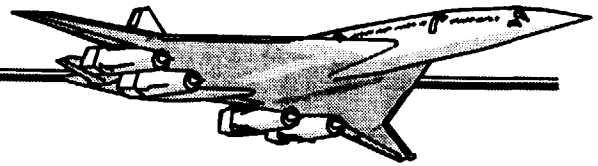

3D CFD Analysis

Effect of Leading Edge Type/Angle, TNS3D Spanloads

TCA 2.8-38, Wing/Body, TE 10 Degrees
Mach = 0.247, Alpha = 10 Degrees, Chord Reynolds Number = 8 Million

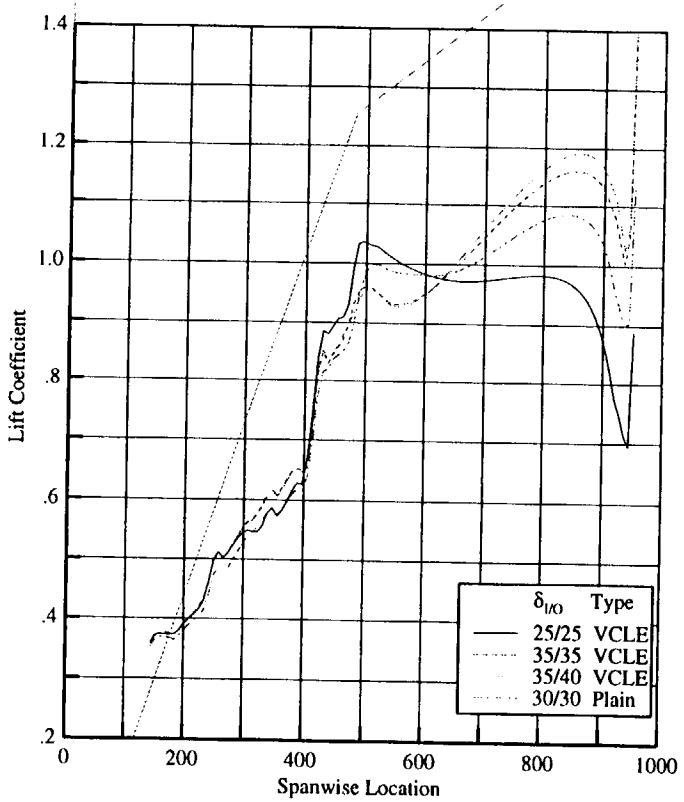

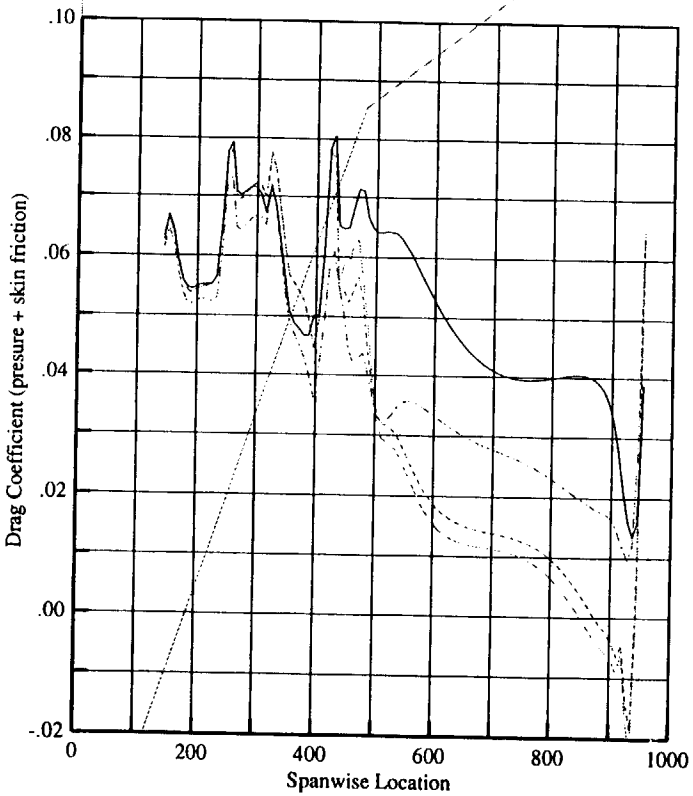

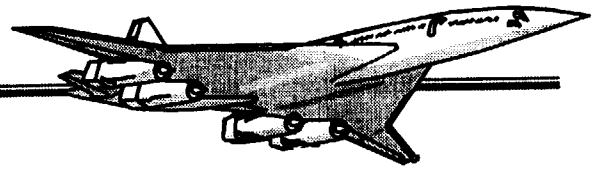

3D CFD Analysis

TNS3DMB Streamwise Skin Friction
TCA 2.8-38 Outboard Wing Panel Upper Surface
M = 0.247, α = 10, R_{∞} = 8X10^6

The inboard wing upper surface of the TCA 2.8-38 configuration show no areas of reversed flow for any of the configurations analyzed.

The facing page shows the areas of negative streamwise skin friction (reversed flow) on upper surface of the outboard panel for both the plain flap and the VCLE.

The following comments apply.

30 Degree Plain Flap

- Flow separated at the hinge line over most of the outboard wing panel upper surface.
- Flow separated on the leading edge over outboard half of the outboard panel upper surface.
- Small separation at the outboard end of the outboard trailing edge flap.
- Changing slat angle positively or negatively would trade leading edge and hingeline separation.

40 Degree VCLE

- Flow attached over most of the wing upper surface except for a small area at the wing tip.
- Trailing Edge separation evident for the plain flap case is nearly eliminated.

Leading Edge Trade Study

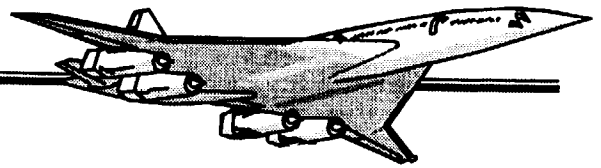

3D CFD Analysis

TNS3DMB Streamwise Skin Friction
TCA 2.8-38 Outboard Wing Panel Upper Surface
M = 0.247, α = 10, R_{cc} = 8X10^6

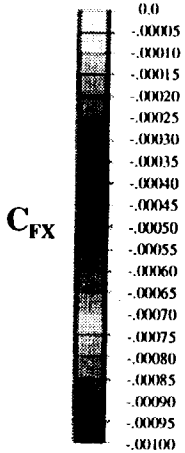

40 Degree VCLE

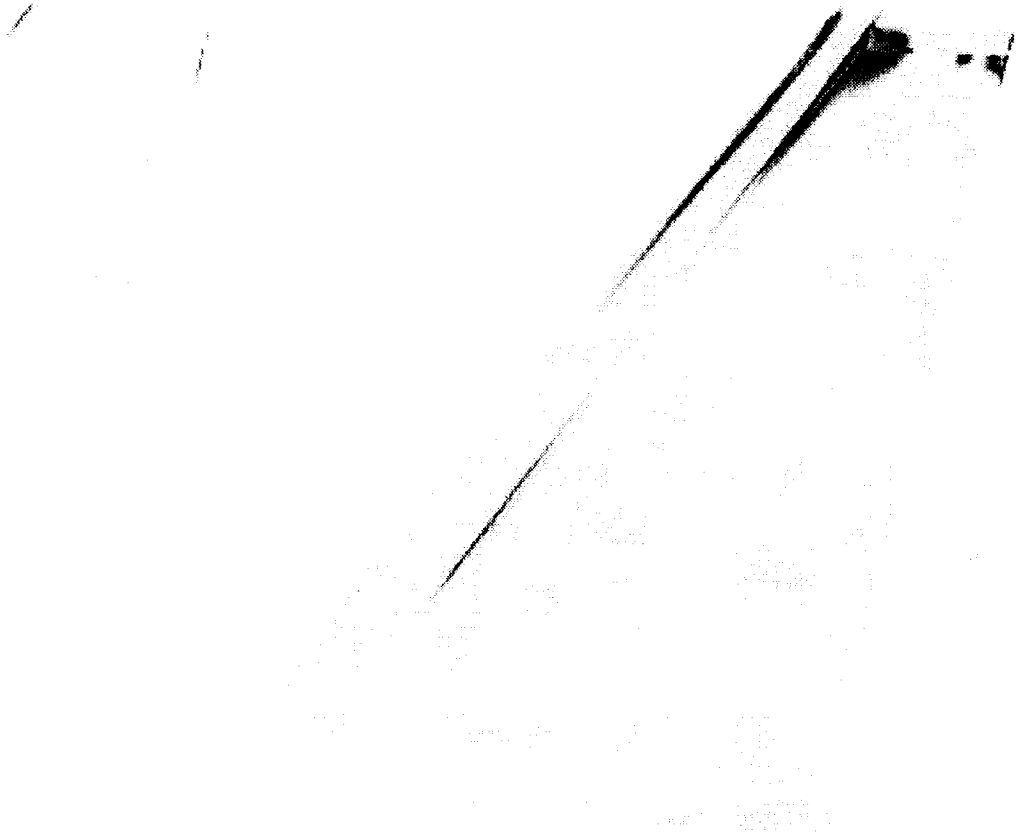

30 Degree Plain Flap

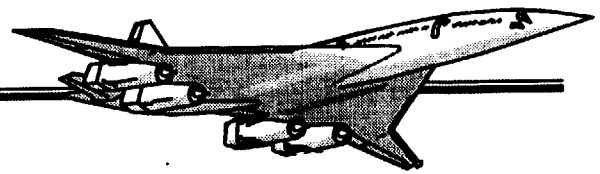

Conclusions

- The TNS3DMB analysis of the variable camber leading edge show improvement in the drag at the noise critical lift level, $C_L = 0.5$, when compared to the plain flap. The improvement is not as great as was seen in the TCA-3 wind tunnel test of the sealed slat.

- Spanwise loading suggests that we need a better understanding of the inboard wing flow as this area is where the drag increases with the VCLE. These analyses would suggest a configuration with a plain flap inboard and a VCLE outboard might be best.

- The 3D analysis agrees with the optimum VCLE outboard deflection angle derived from the 2D analysis, i.e., between 35 and 40 degrees.

- TNS3DMB analysis show a VCLE configuration with no reversed flow as indicated by streamwise skin friction is viable because of low wing upper surface curvature.

- Wind tunnel test data is needed to better understand and support these analyses.

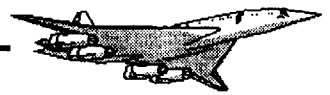

TCA 2.8-38 Outboard LE Flap Chord Study
(and Sliding Hingeline Fairings)

Art Powell
HSCT High Lift
Boeing Phantom Works

HSR Annual Airframe Technical Review
February 9, 1999
Anaheim, CA

This slide shows an outline of the High-Lift Technology program.

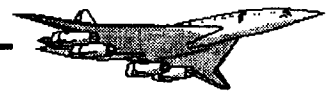

High Lift Technology Development (Task 33)

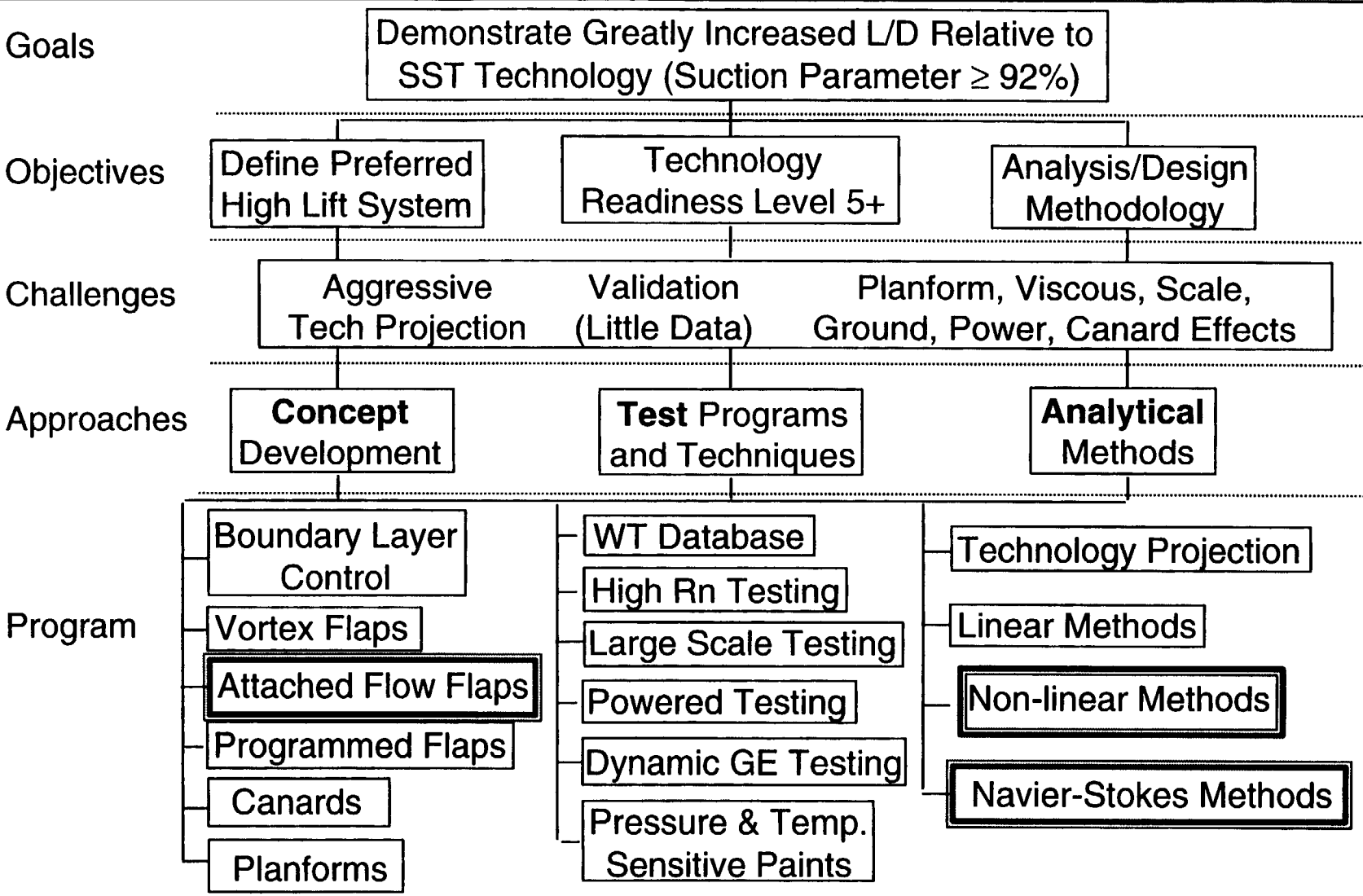

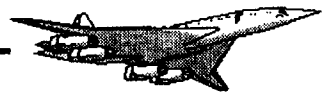

This paper is a brief discussion of some work that was undertaken by the author in support of HSCT high lift technology development. The configuration studied is basically the PTC, but with the 2.8-38 wing.

The 2.8-38 wing features a high-aspect-ratio low-sweep outer panel, occupying the outermost 50% semi-span. This panel is of necessity quite thin, and therefore heavy, so reducing leading-edge flap chord there has the potential for reducing wing weight by enlarging the wing structural box.

TCA-4 experimental oil-flow surface streamline pictures show attached or nearly attached flow over the outer panel at the nearly-optimal 30 degree leading-edge flap deflection and 10 degrees angle-of-attack. Whether or not the leading-edge flap chord could be reduced further depends on whether hingeline separation can be prevented by some means.

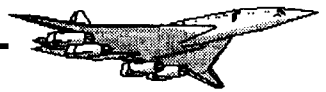

Motivations For Reducing OB LE Flap Chord

Larger, stiffer wing box
Smaller, Lighter actuators
Encouraging results from TCA-4 test
Possibly enabled by Sliding Hingeline Fairing or VCLE concept

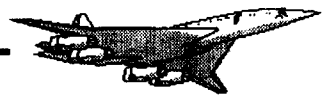

This oil flow picture, taken during the TCA-4 test in the NASA LaRC 14X22-foot wind tunnel shows the three-dimensional character of the flow inboard of the leading-edge sweep break, and what appears to be attached flow over the leading-edge flap hingeline outboard. Upon close inspection it is not clear whether the flow is completely attached; there may be a very short separated region behind the outboard hingeline. This lends encouragement to the prospect of shortening the outboard leading-edge flap chord without adverse effect.

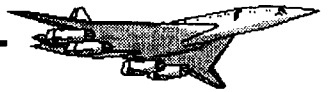

Encouraging Oil Flow Picture from TCA-4

Run 298, Flaps 30/10, α=10 deg.

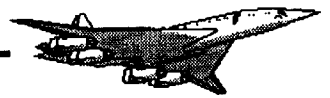

The outer panel from the previous picture has been rotated and contrast increased to facilitate a comparison of surface streamlines with those from a CFL3D solution for the same conditions. It is readily seen that the CFD predicts more spanwise flow than is seen in the wind tunnel. Despite this qualitative difference, close inspection of the two flowfields shows remarkable similarity. Readily visible is the attachment line following the leading-edge separation, the acceleration into the hingeline suction peak, and the largely attached flow over the outer panel. Visible in the CFD streamline trace is a short separated region downstream of the leading-edge flap hingeline, followed by a reattachment line. Upon close inspection these flow features are also visible in the wind-tunnel picture.

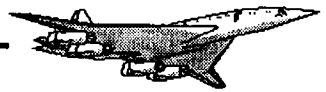

Outer Panel Flowfield Comparison with CFL3D N-S

Flaps 30/10, α=10 deg, R=8m

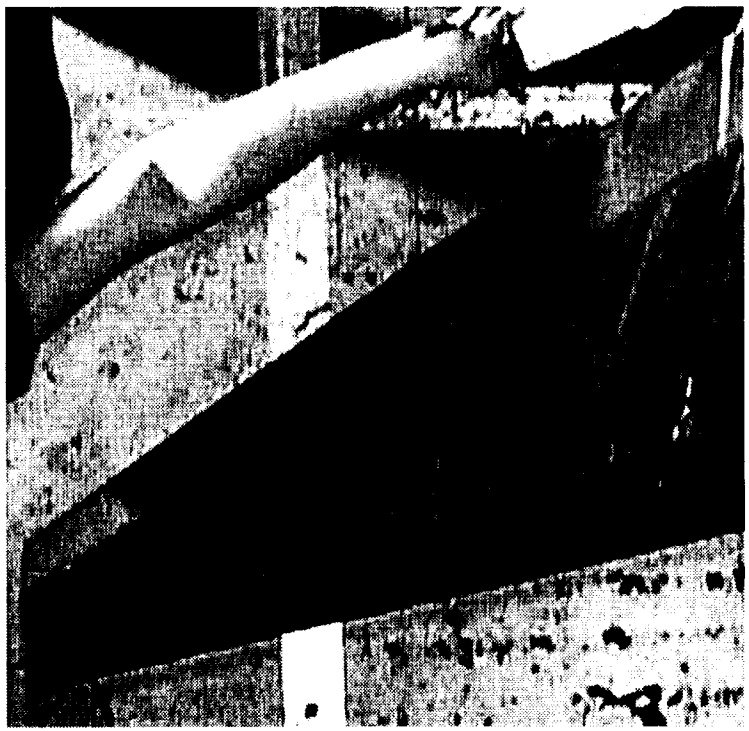

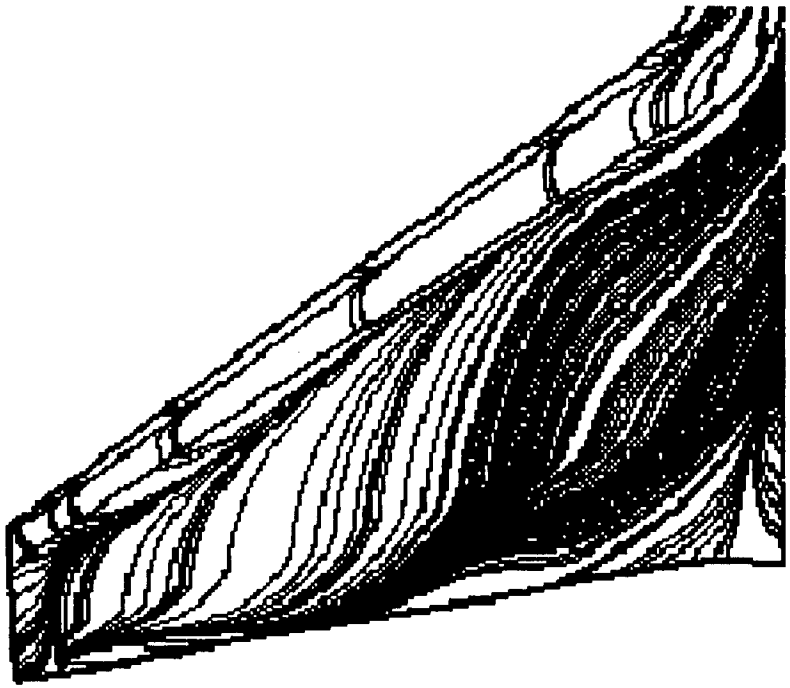

Reducing leading-edge flap chord produces higher leading-edge suction peaks and lower suction peaks at hingeline. The Cp distributions shown here are from CFL3D. Looking at the 70% and 90% span stations as well (not shown) gives convincing evidence that the nominal leading-edge chord distribution is correct for this configuration.

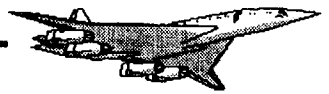

Effect of LE Flap Chord on Cp Distributions

TCA 2.8-38, Flaps 30/10 deg
α=10 deg, R=8m
CFL3D

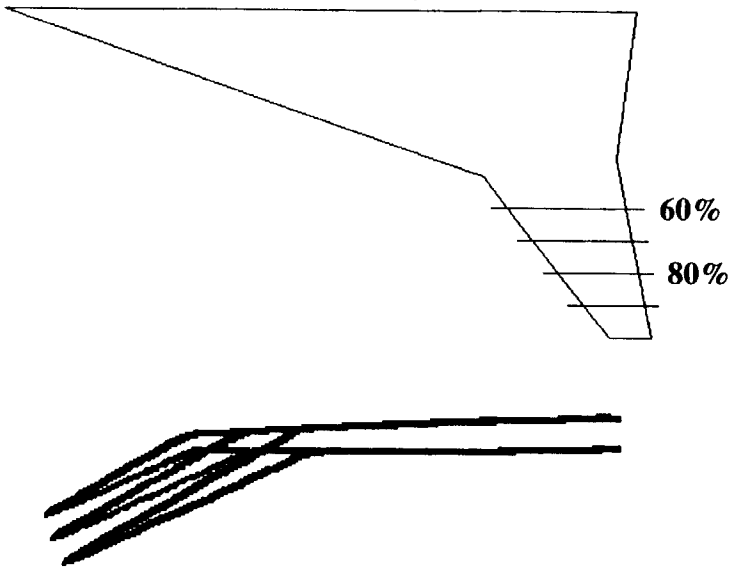

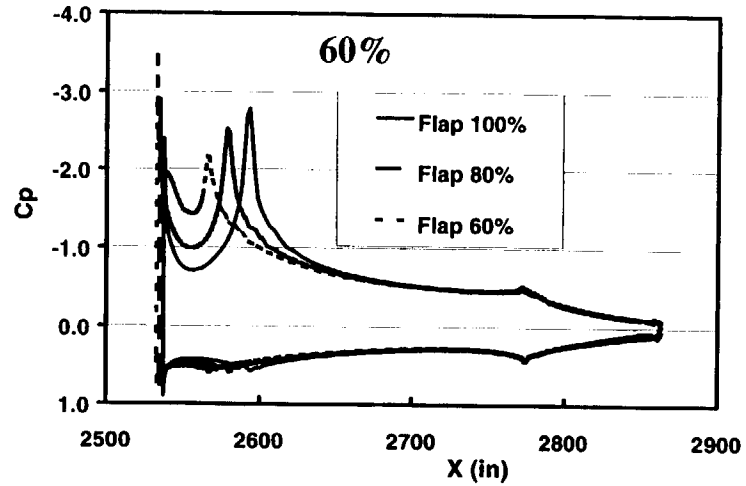

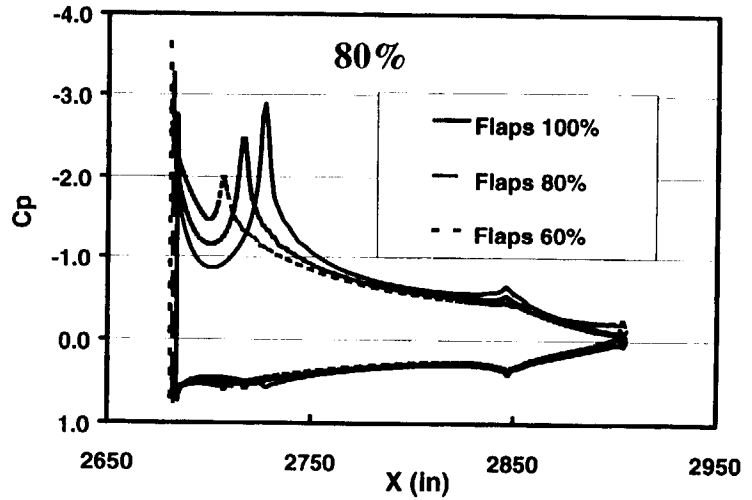

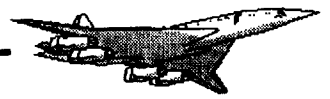

CFL3D Navier-Stokes cases were run for flap chords that were 80% and 60% of the nominal chord as well as the nominal chord baseline. Looking at the surface Cp distributions and in particular the surface streamline patterns for the nominal, 80% and 60% (of nominal) flap cases shows that reducing flap chord increases hingeline separation, despite reduced Cp peak levels. Presumably, the leading-edge suction peak is responsible for progressively weakening the boundary layer as flap chord is reduced. The 60% flap chord case shows reattachment much further aft than the other two cases. The 80% flap chord case shows a small region of hingeline separation which appears to be only slightly worse than that of the nominal-flap-chord case.

A decision was therefore made to concentrate on the 80% nominal flap chord case.

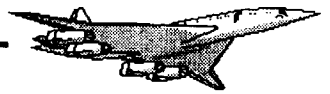

Effect of LE Flap Chord Reduction

CFL3D, M=.3, α=10 deg R=8m, Defl 30/10 deg

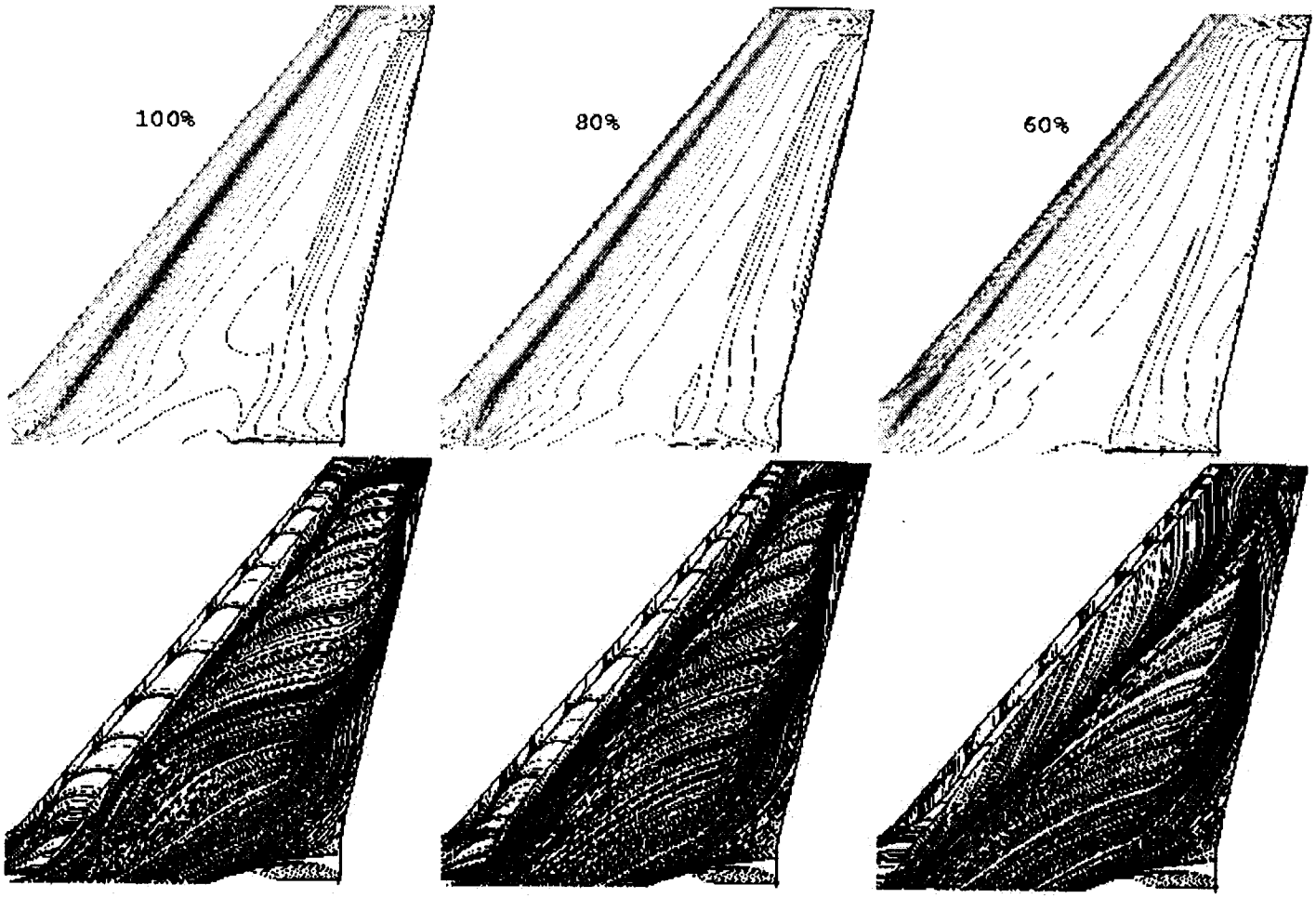

The sliding hingeline fairing idea was originated as a relatively inexpensive way to lower curvatures in the hingeline region, reducing both Cp suction peak and pressure gradients there. The idea is to fix the metal skin to the moving flap piece while allowing sliding motion at the aft end, where a condition of tangency is imposed by some kind of mechanical arrangement. For the purposes of this study the shape of the fairing was assumed to be a cubic passed between two points at which the elevation and slope are specified.

In the plot, the curvatures are compared for a typical outboard station, viewed normal to the hingeline. The curvatures were computed using a simple 3-point algorithm. The region of negative (concave) curvature for the fairing is necessary in order to meet the tangency condition at the aft end of the fairing.

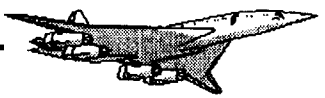

Sliding Hingeline Fairing Idea

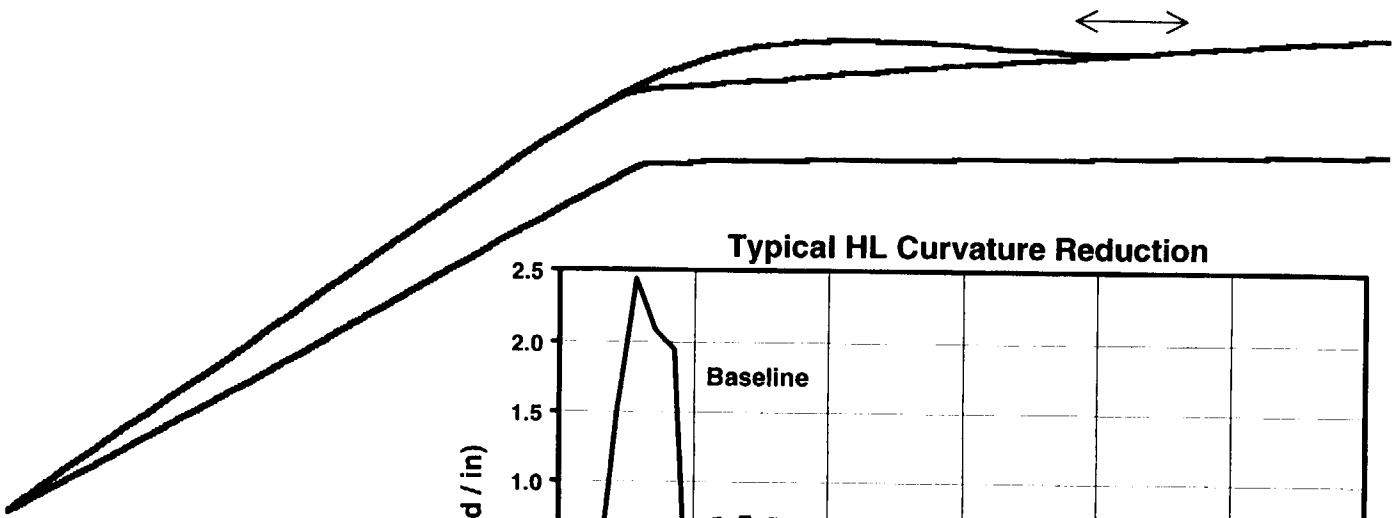

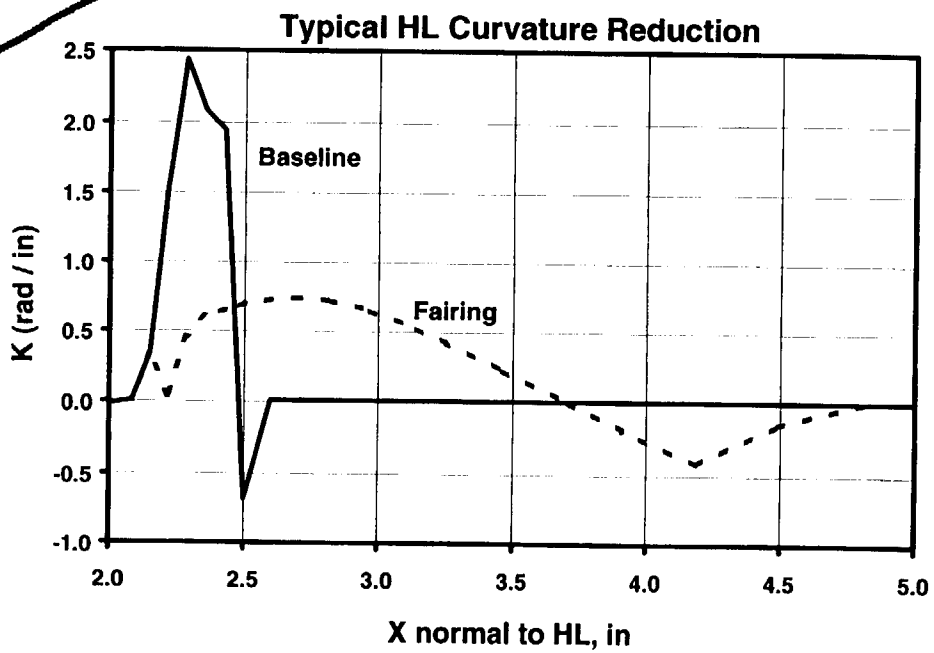

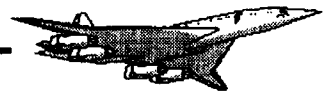

The idea of placing the fairing on the flap ahead of the hingeline was considered, but was ultimately rejected. Enforcing the tangency condition on the front end of the fairing would force the highest curvatures to its aft end, so the fairing is likely to have provided less mitigation of adverse pressure gradients. A simple 2-d panel method calculation confirmed this assertion.

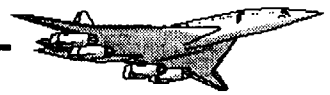

Forward vs. Aft of Hingeline? (2-D)

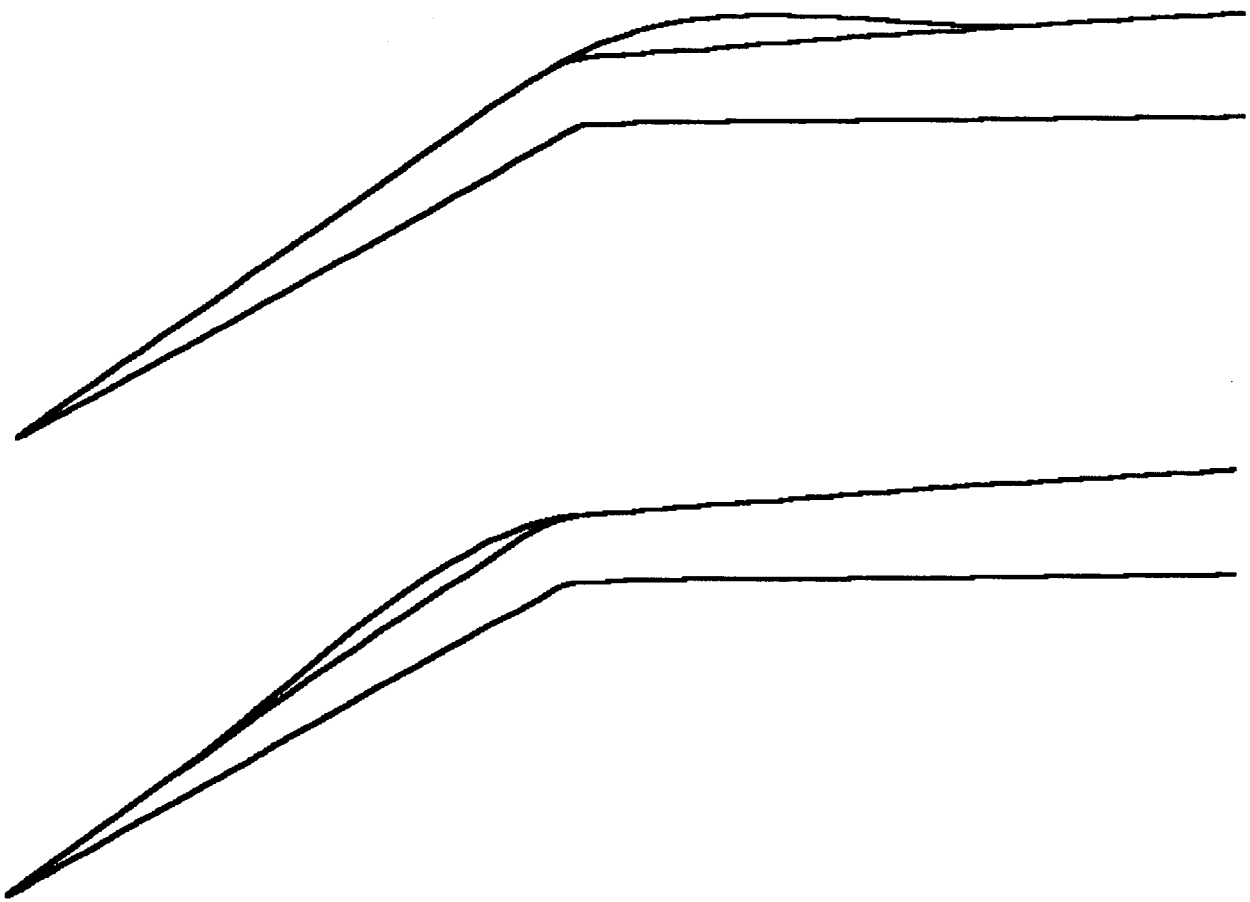

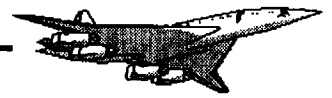

This figure shows the results of a 2-d panel method calculation for the two approaches to fairing the hingeline. As previously noted, placing the fairing on the flap upstream of the hingeline does result in little mitigation of pressure gradients, although the Cp peak is reduced. The aft fairing does a better job of reducing adverse pressure gradients and was chosen for further development in this study.

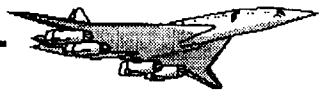

2-D Panel Results

AoA=10 deg

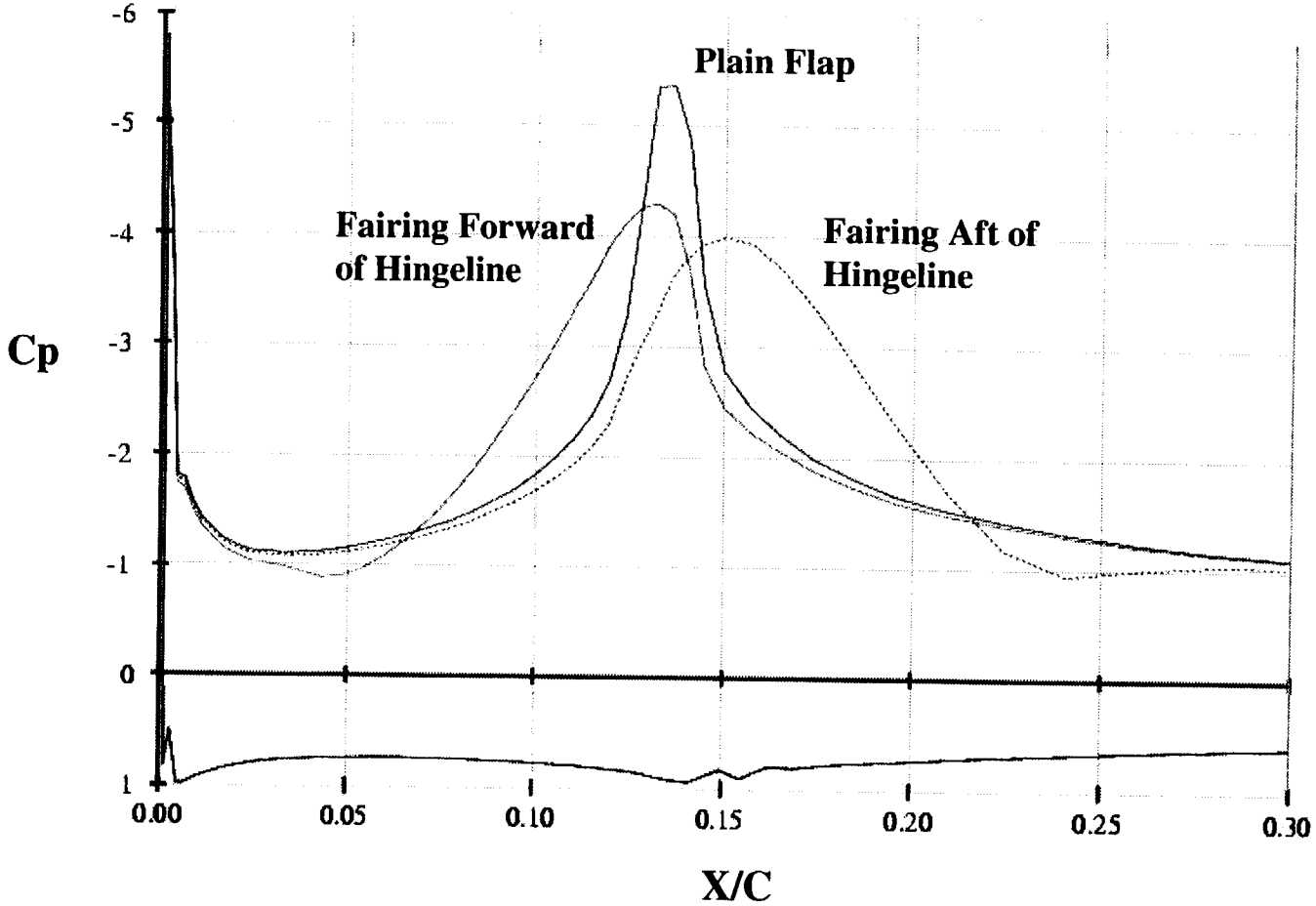

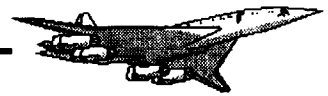

The computed effect of two aft hingeline fairings of different size on chordwise Cp distributions is compared here with the plain flap solution at the 60% semi-span station. The fairing lengths are 67% and 150% of the (80% nominal) leading-edge flap chord. The computation was made using CFL3D in the Navier-Stokes mode. David Yeh's gridding procedures were used, and the turbulence model is Baldwin-Lomax with David's version of the Degani-Schiff modification. The amelioration of the Cp peak and gradient is evident and is greater for the larger fairing.

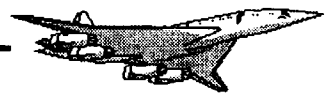

Effect on Streamwise Cp (3-D)

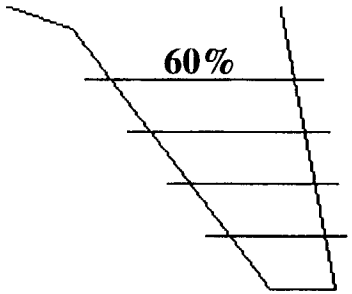

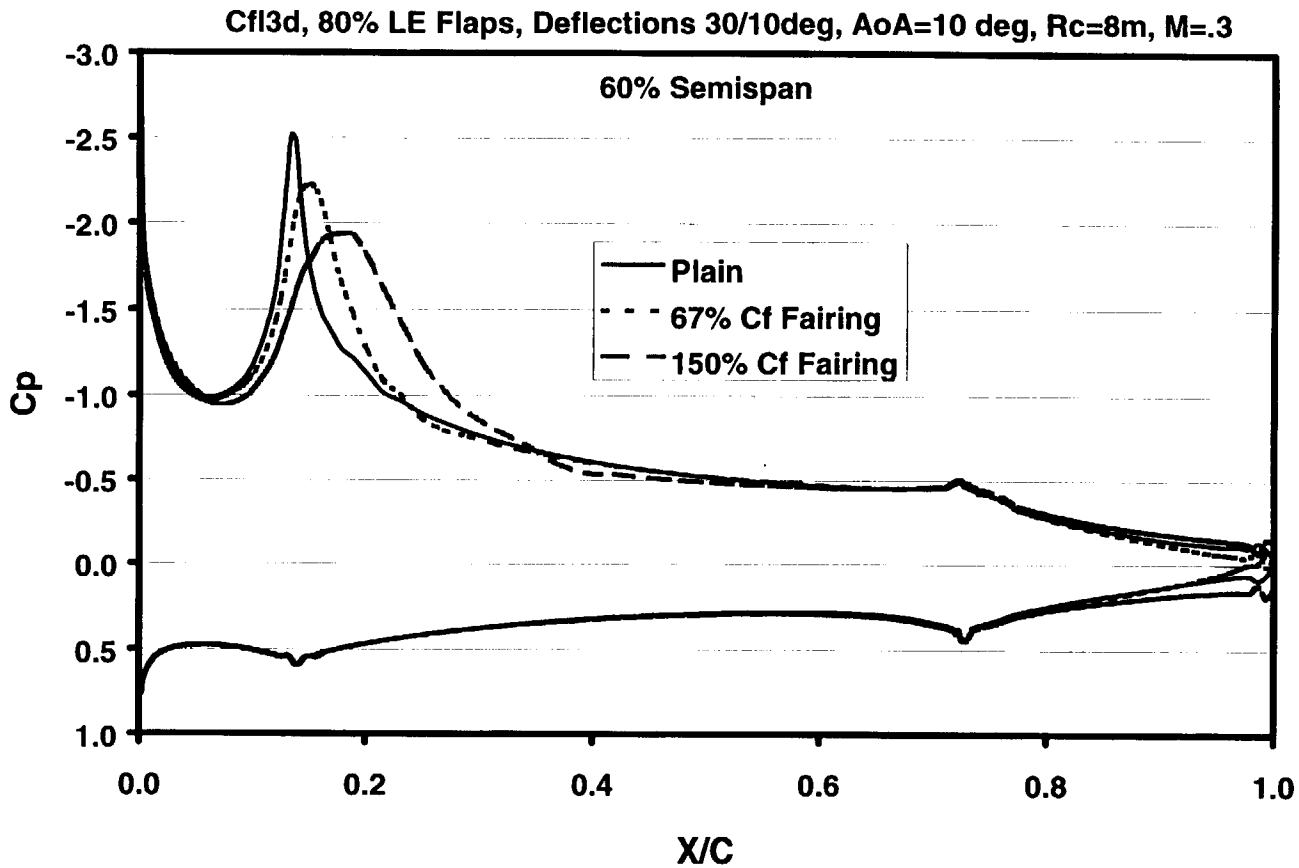

This figure shows the same information and trends at the 80% semi-span station. No particular attempt was made to capture the leading-edge Cp peak.

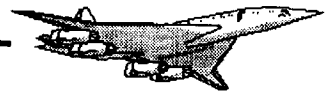

Effect on Streamwise Cp (3-D)

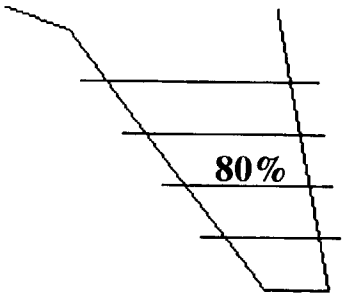

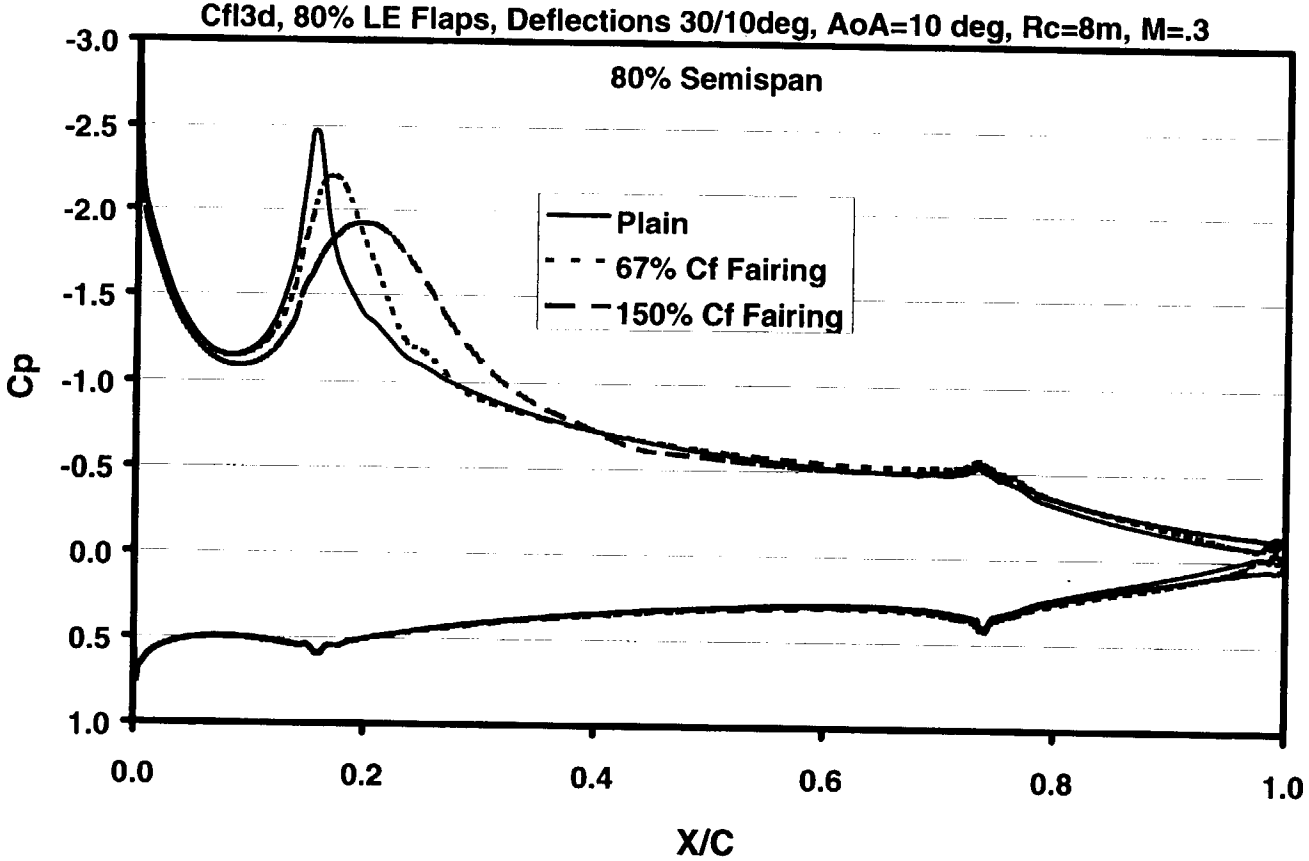

The surface Cp distributions are shown here for the 80% of-nominal-chord plain flap, the 67% fairing, and the 150% fairing. The larger fairing is at the outer limit of practicality; if it were larger it would interfere with the trailing-edge flaps in the vicinity of the wingtip. Apart from confirming that the region of the Cp peak is wider, the pressure plots give little information regarding whether or not the flow is separated.

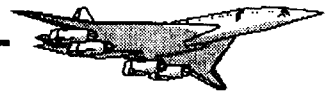

Effect on 3-D Cp Distributions

(80% Nominal LE Flap Chord)

Cfl3d, Flaps 30/10, AoA=10 deg, R=8m

Plain Flap

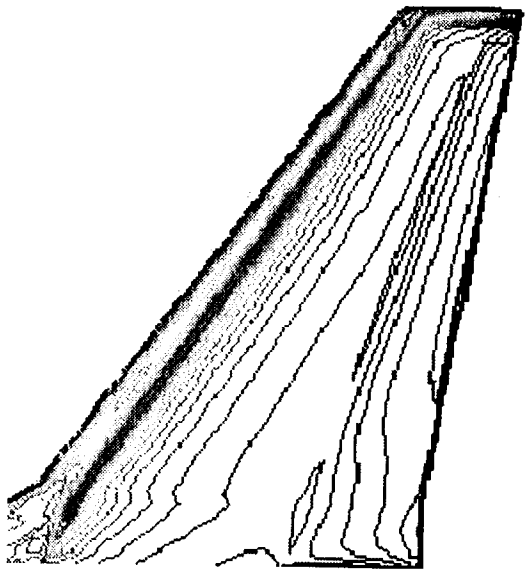

67% Cf Fairing

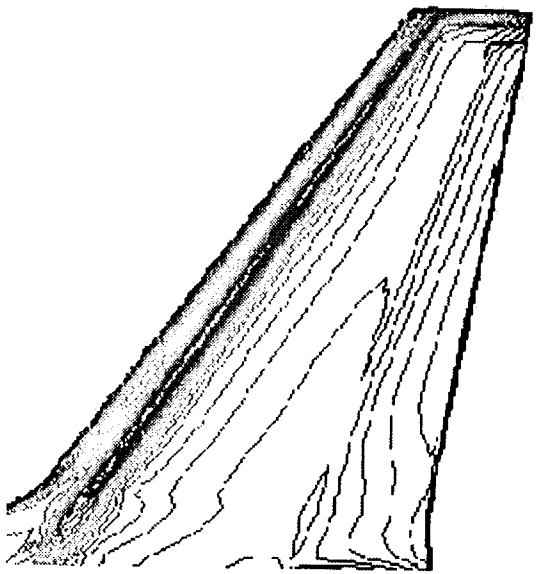

150% Cf Fairing

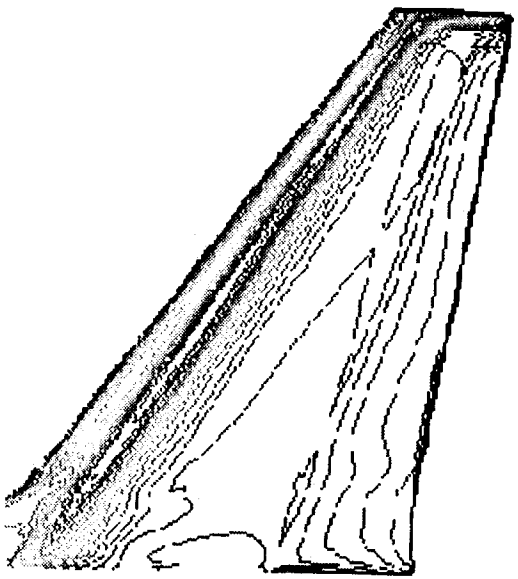

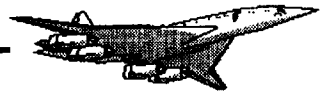

This figure shows CFL3D-computed surface (j=2) streamlines for the same three cases. For purposes of interpretation, note that going outboard, a line upon which others converge signals a separation, whereas one from which others diverge signals a reattachment. For the 67% (local) flap-chord fairing, hinge-line separation clearly is not prevented. The separation point is moved aft to behind the hingeline, but the reattachment line is moved aft as well. It was this result that prompted the formulation of the 150% flap-chord fairing case. Even with the larger fairing, separation is evident, and is only moved aft further into the decelerated region over the fairing bump. This is shown by the surface streamlines curving outboard before separation occurs. The reattachment location is moved aft a similar amount.

Despite the reduction of the hingeline Cp peak and downstream gradient, the use of sliding fairings aft of the hingeline apparently does not permit a 20% reduction in the leading-edge flap chord. It is interesting to note that the effect of the fairings is to increase the extent of separation, in direct opposition to an intuition guided by two-dimensional flow physics!

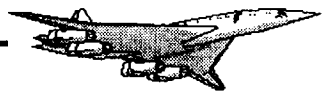

Effect on Surface Streamlines

(80% Nominal LE Flap Chord)

Cfl3d, Flaps 30/10, AoA=10 deg, R=8m

Plain Flap

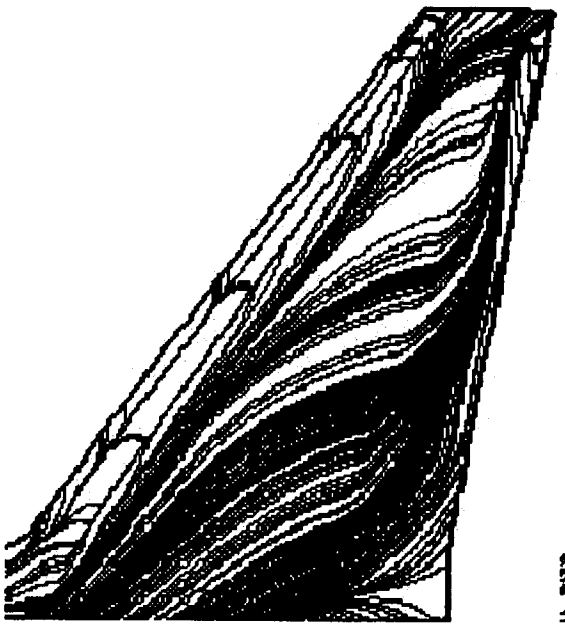

67% Cf Fairing

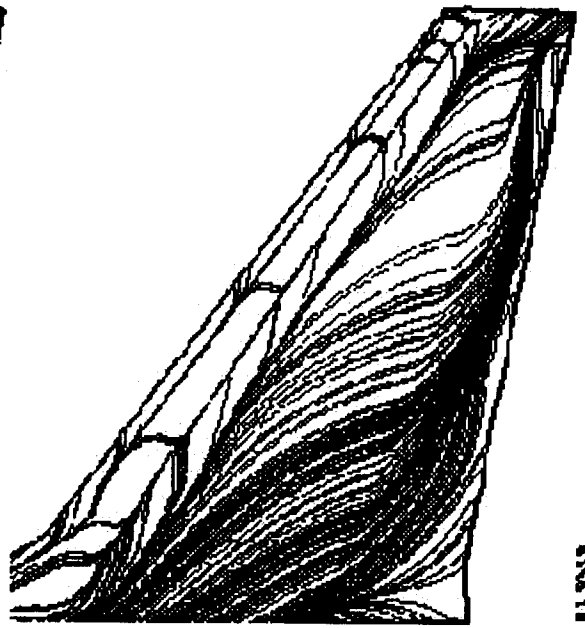

150% Cf Fairing

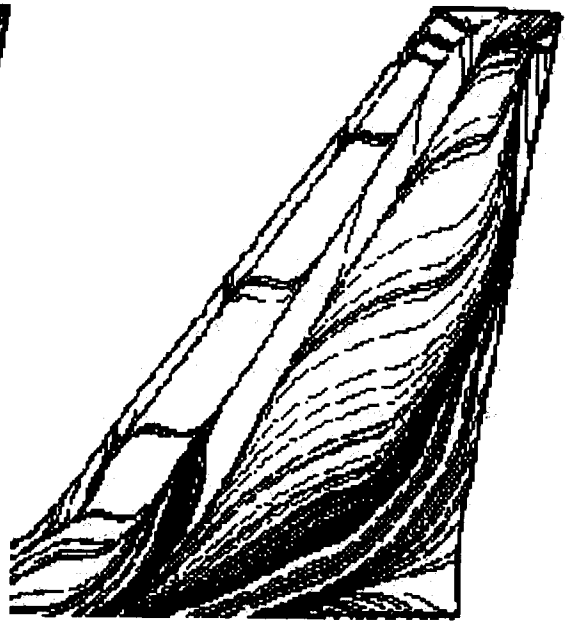

The use of hingeline fairings does not permit a 20% flap chord reduction. Hopefully they can still be useful for nominal-chord flaps in allowing higher flap deflections without hingeline separation. This figure shows chordwise Cp distributions at 60% semispan for 3 cases: plain flaps deflected 30 degrees, plain flaps deflected 35 degrees, and 67%flap-chord faired flaps deflected 35 degrees. The peak for the 35 degree deflection is rather high, but is ameliorated significantly with the addition of the fairing. The 30 degree plain flap underlies the other two curves, and may be hard to see.

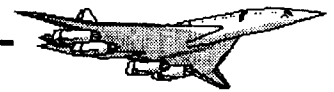

Can Hingeline Fairings Permit Higher L.E. Deflections For Nominal Flap Chords?

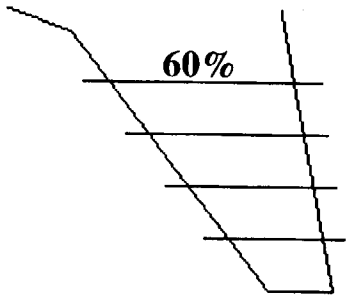

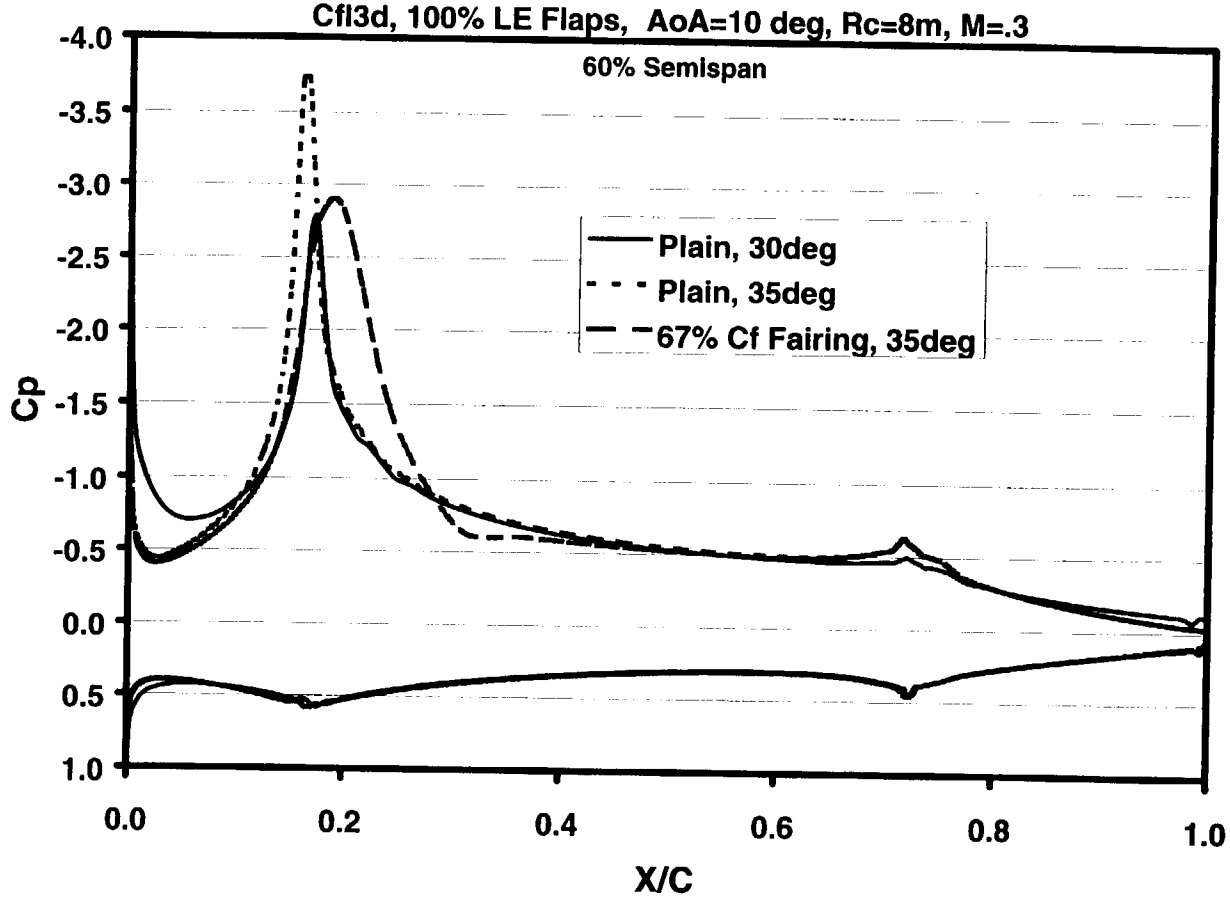

This figure shows the surface Cp distributions for the three cases: Plain flaps deflected 30 degrees, Plain flaps deflected 35 degrees, and flaps deflected 35 degrees with 67% flap-chord hingeline fairings. Again, the Cp peak is spread out by the fairing.

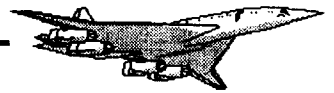

Chordwise Cp Distributions

(Nominal LE Flap Chord)

Cfl3d, Flaps 30/10, AoA=10 deg, R=8m

Plain Flap, 30 deg

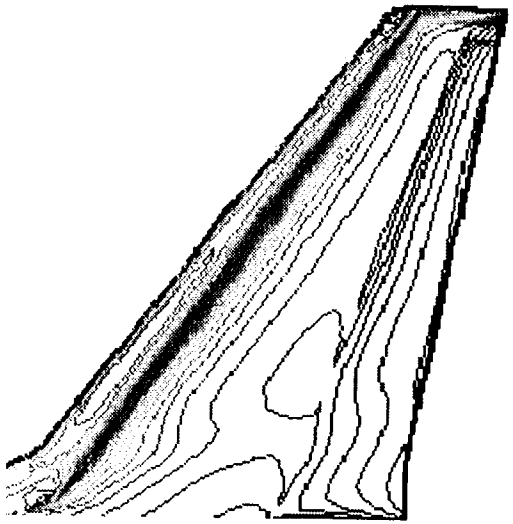

Plain Flap, 35 deg

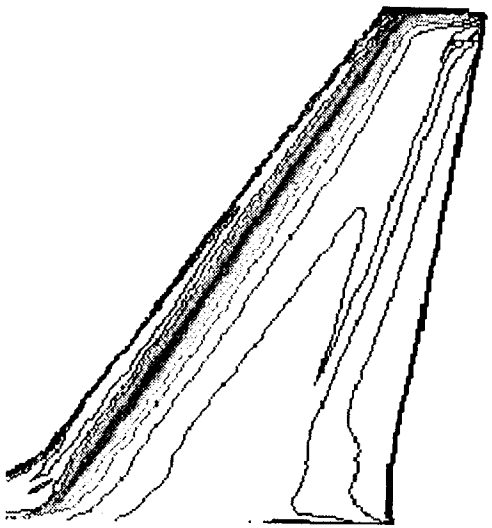

67% Cf Fairing, 35 deg

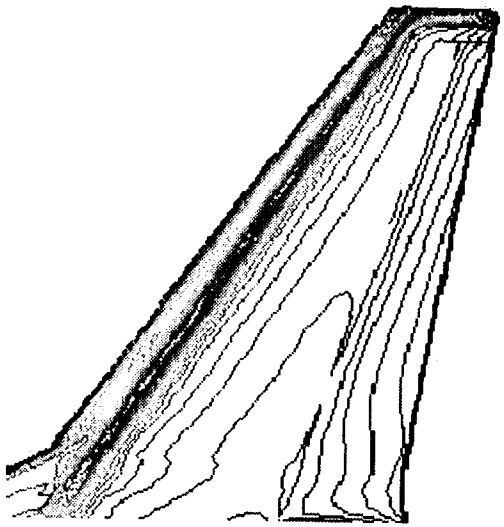

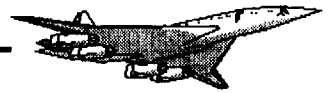

Of perhaps more interest are the surface streamlines. Surprisingly, the separated region on the 35 degree-deflected plain flap hingeline is of about the same width as that for the 30 degree deflection. The effect of the fairing is to move the reattachment line aft, creating a longer separated region. The predicted effect on drag is insignificant, so the fairing again did no good.

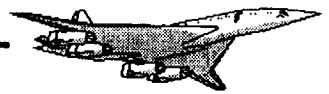

Surface Streamlines
(Nominal LE Flap Chord)

Cfl3d, TE Flaps 10 deg, AoA=10 deg, R=8m

Plain Flap, 30 deg

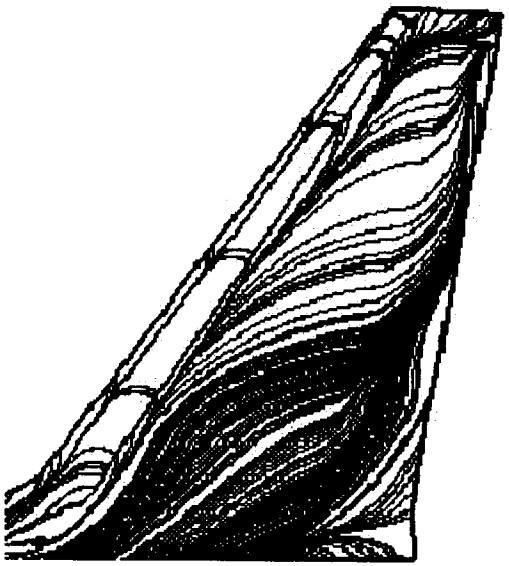

Plain Flap, 35 deg

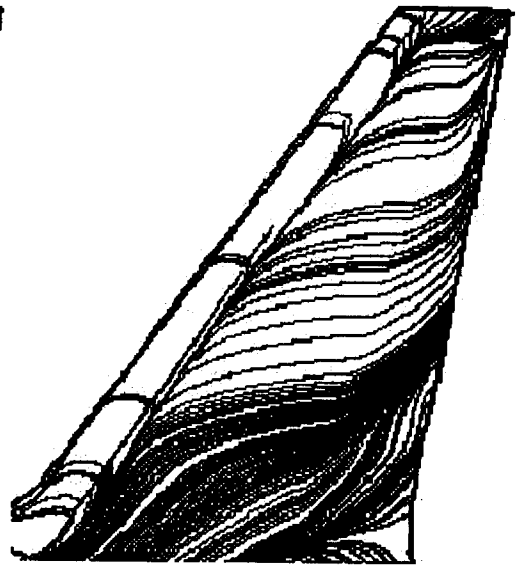

67% Cf Fairing, 35 deg

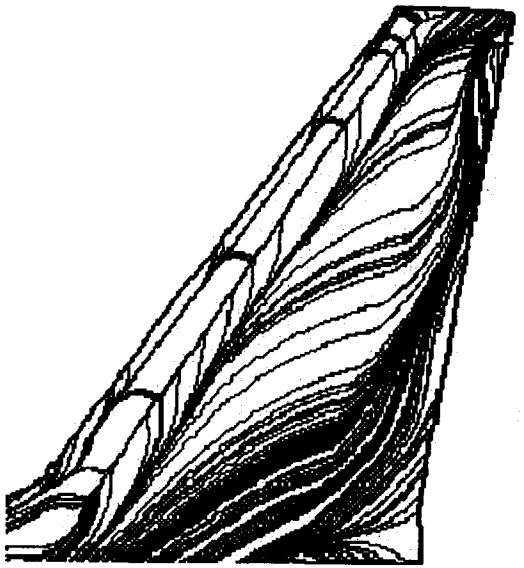

Near-Body Streamlines

In the facing figure, near-body streamlines computed with CFL3D are compared. The purpose was to determine in a relative sense the normal extent of the separated regions for the 35 degree plain flap with and without the hingeline fairing. This gives an indication of whether hingeline separation is really worsened by the presence of the bump. The index J is the c-mesh normal grid level, where J=1 is the surface. Because of the no-slip condition at the wall, the J=2 level was used in the previous surface streamline plots. This is well within the viscous sub-layer.

The CFD solutions for the plain flap and flap with fairing were interrogated at different values of the normal grid index J. As shown in the plots, it is necessary to go to a higher J before evidence of separation is no longer seen when the fairing is used.

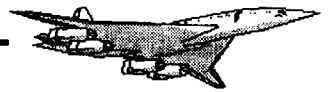

Near-Body Streamlines

Cfl3d, Nominal Chord LE Flaps 35 deg, TE Flaps 10 deg, AoA=10 deg, R=8m

Plain Flap
J=4

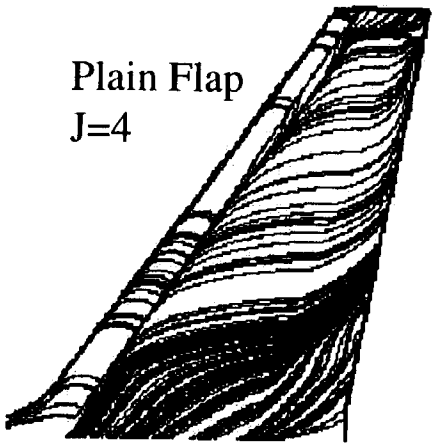

Flow separated at this J-level

With Fairing
J=7

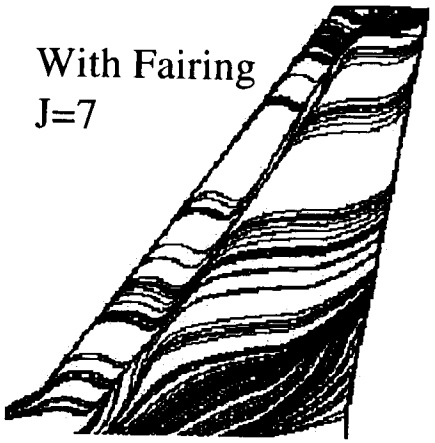

Plain Flap
J=5

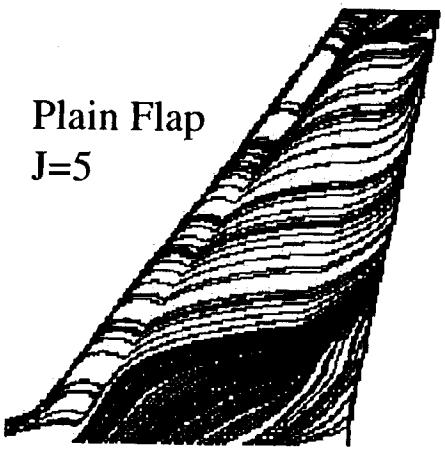

First J-level for attached flow:

With Fairing
J=8

The results of this study are counterintuitive. One would expect smoothing or blending the hingeline to reduce flow separation, yet the reverse was observed computationally. If the flow was computed to be on the verge of separation at 30 degrees deflection for the plain flap, one would expect to see more separation with the flaps deflected 35 degrees. This was not observed computationally. One explanation is that simple 2-D approaches to what constitutes goodness is not applicable at higher sweeps due to 3-D effects. A second explanation is that the fairings extend the adverse gradient region aft making reattachment more difficult. I t would be interesting to see if fairings ahead of the hingeline would have any favorable effect. The conclusions reached here are based on CFD calculations; it remains to be seen whether similar effects will be observed experimentally. This may make a good test case for CFD validation/calibration.

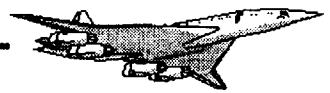

Conclusions and Recommendations

- **CFL3D predicts more spanwise flow than is observed experimentally.**
- **Both 2-D and 3-D methods predict lower suction peaks and weaker gradients for sliding fairings aft of the hingeline.**
- **Notwithstanding the above, CFL3D predicts worse-than-baseline separation where sliding fairings are used aft of the hingeline.**
- **No drag benefits have been identified with hingeline fairings.**
- **A different approach will be necessary if outboard LE flap chord is to be reduced on the 2.8-38 wing.**
- **Sliding hingeline fairings may make a good CFD calibration case. Recommend oil flow visualization testing with wing/body configuration.**

HSR
High Speed Research

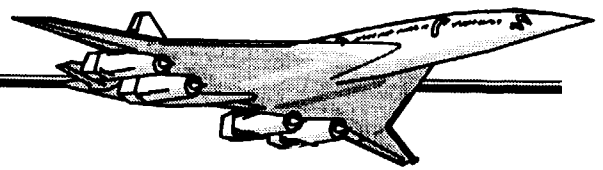

Impact of Wing Planform, Canard, and Leading Edge Flap Type on High Lift Performance and Technology Projection

Boeing Commercial Airplane Group
High Lift Aerodynamics
Paul Meredith

Airframe Annual Review
February 9, 1999

Introduction

L/D Summary

Full Scale Drag Build-ups

- Effects of Wing Planform, Canards, and Sealed Slats

Technology Projection

- Components of Drag
- Limits on Suction Parameter

High Lift Metrics AP-3 and AP-4

Conclusions and Recommendations

L/D Summary

Large variations between status and projected L/D

This slide shows predicted flight status L/D at CL of 0.50 for a variety of configurations and WT data bases. The TCA build-ups show a lot of variation depending on which WT data base is used. The TCA built up from NTF (modified Ref. H) data is felt to be the best estimate of flight since tunnel upflow is measured and there are minimal support interference effects with the straight sting. There is a skin friction correction for the missing aft body and vertical tail.

Referring to the TCA L/Ds, it is seen that a sealed slat is required to meet the technology projection.

Also of interest, the common PD process prediction (based on Ref. H WT data) of the PTC status L/D is very close to the projection while the WT based 2.8-38 L/D status is not so close to the projection. This is further evidence that the PD process is not reliable depending on wing planform and the reference WT data base used.

L/D Summary

Large variations between status and projected L/D

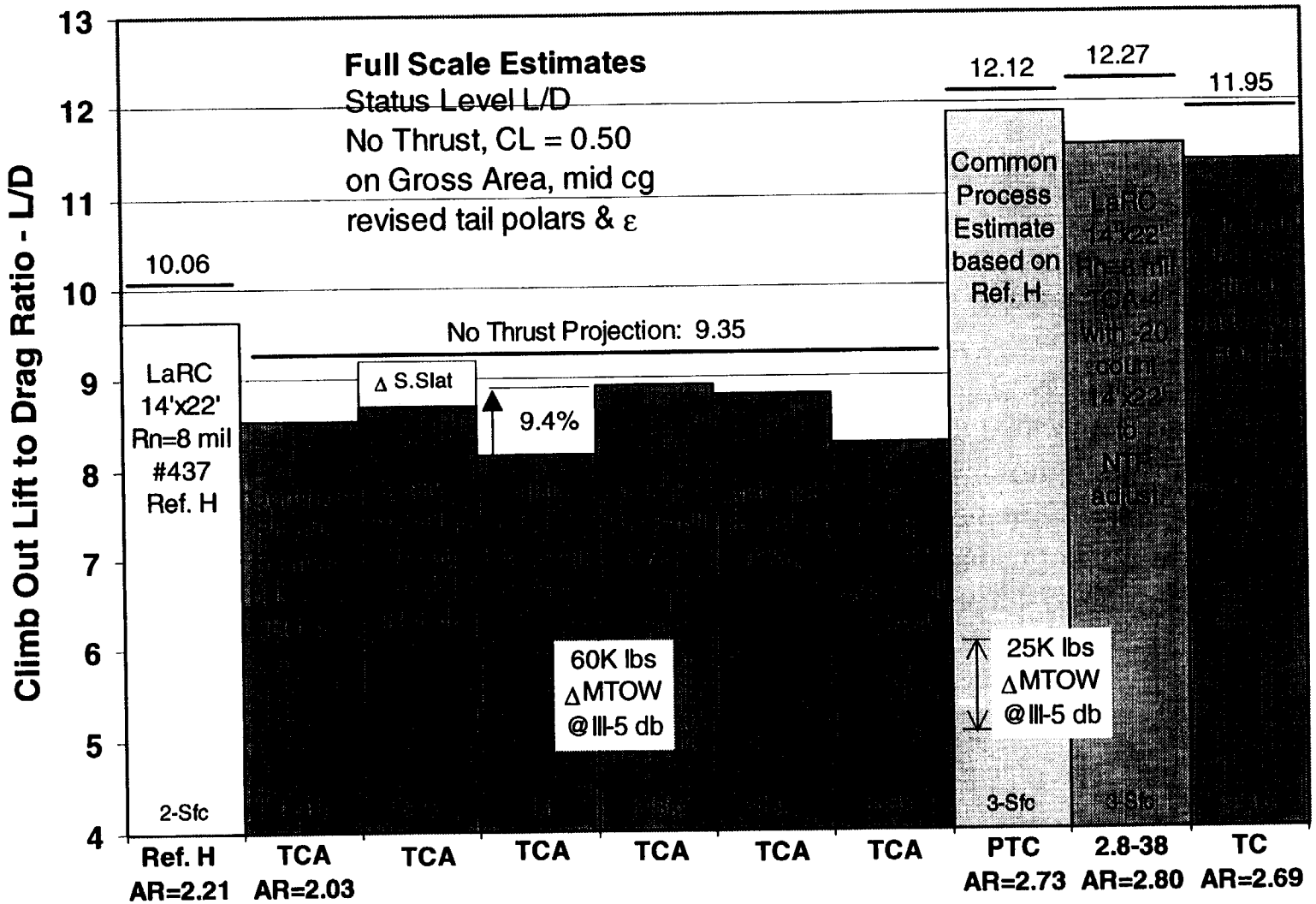

Wing Planforms

Wing 3 has higher AR and lower outboard sweep than Wing 1

This slide shows wing 3 (2.8-38) overlayed on wing 1 (TCA, 2.0-52). The inboard wings are identical. The additional span and reduced outboard sweep of wing 3 are obtained by modifying the outboard wing.

Wing Planforms

Wing 3 has higher AR and lower outboard sweep than Wing 1

Wing 1 (2.0-52, TCA)
Sref = 8500 sqft
AR = 2.027
Outboard Λ_{LE} = 52°

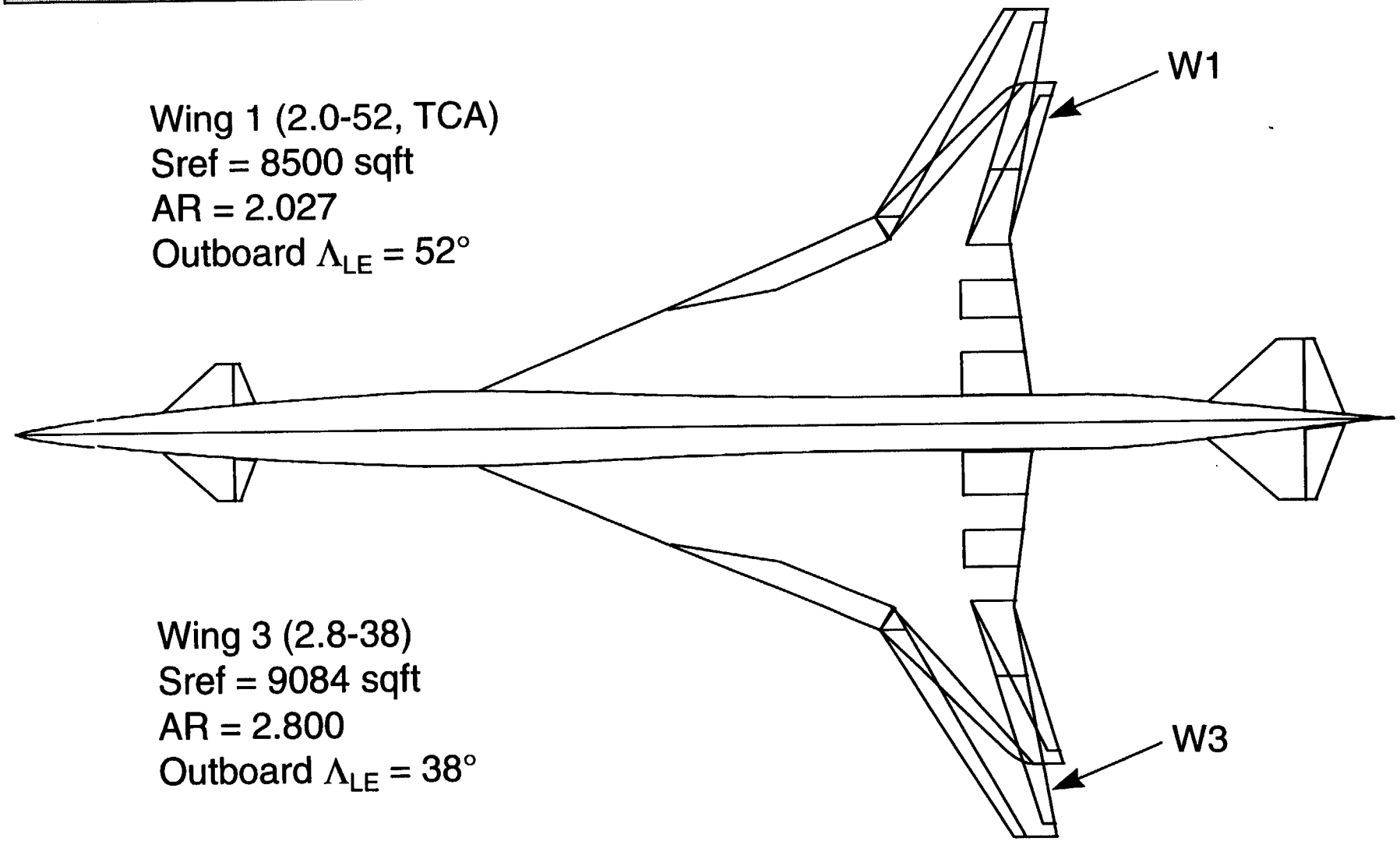

Wing 3 (2.8-38)
Sref = 9084 sqft
AR = 2.800
Outboard Λ_{LE} = 38°

TCA Buildup from NTF Modified Ref.-H

This chart illustrates the drag buildup for the TCA from final, corrected NTF wind tunnel data at a climbout lift coefficient of 0.5 and Reynolds number of 90 million. The data are for flaps 30/10 and come from test NTF089, using the modified Ref-H model which has essentially the same planform as the TCA. An additional 7.1 counts of drag are added to the base wind tunnel data to account for the aft body and vertical tail that did not exist for this sting mounted model.

Skin friction drag is analytically adjusted to account for the expected drag difference between Reynolds numbers of 90 million (NTF) and 200 million (flight).

No configuration differences were applied since the buildup configuration has the same planform as the wind tunnel model. Tail polars and downwash extracted from TCA-1 data are used to trim the tail-off configuration.

14'x22' data indicate that 30/15/10 is a better flap deflection than 30/10 but the NTF model does not have parts for that deflection. Still, the programmed flap increment, which is determined by AERO3S relative to flaps 30/10, is not overly large.

A technology projection of 39.9 counts drag reduction is applied to reach the target suction level of 92% (no thrust).

TCA Buildup from NTF Modified Ref.-H

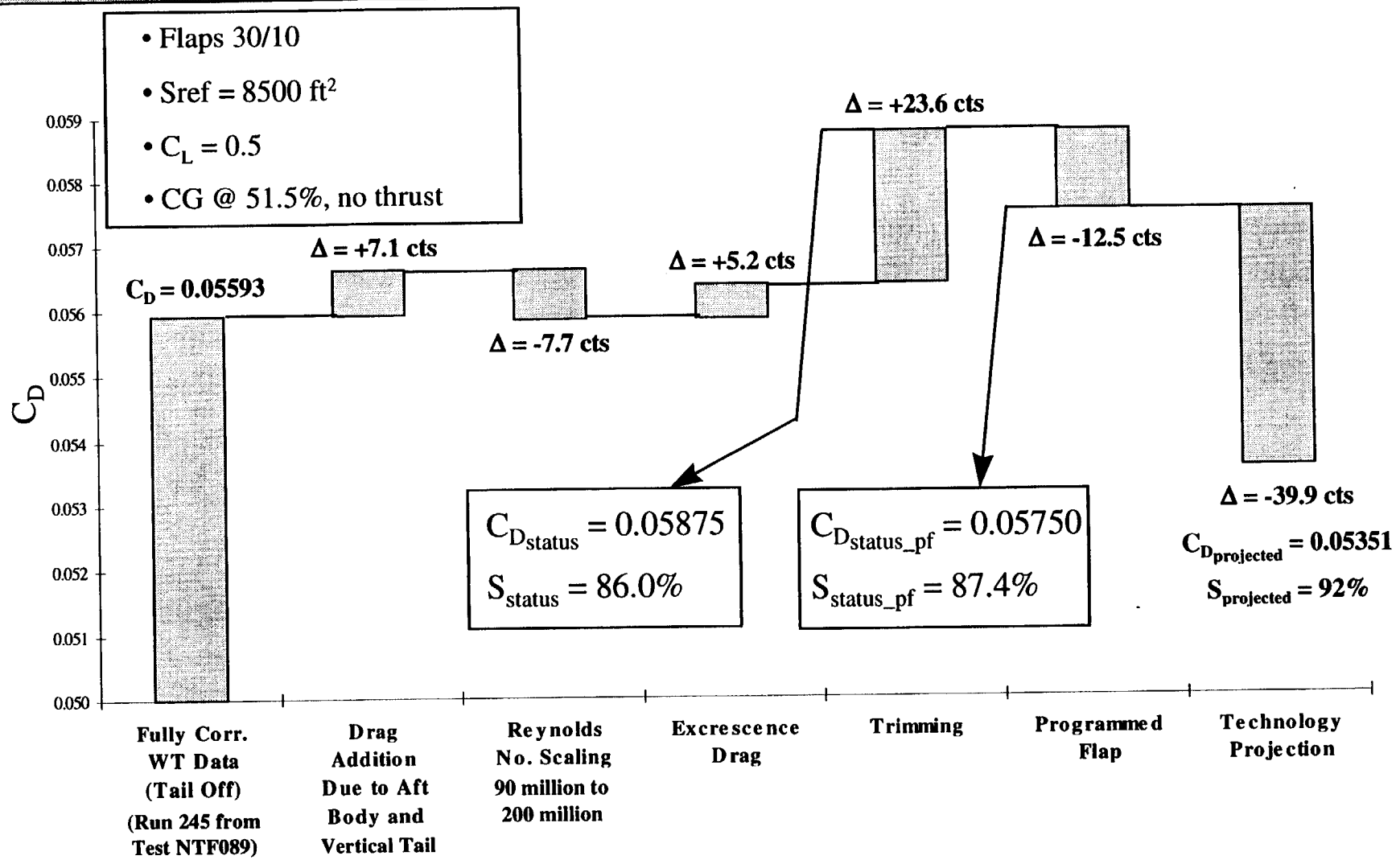

Planform Effect

W3 is more efficient than W1

This slide shows profile drag (CDp = CD - CL^2/πAR) polars for W1 and W3 for flaps up and climbout flaps.

Flaps up, the CDp polars collapse indicating that the wings are perform equally after accounting for induced drag changes due to aspect ratio differences.

With climbout flaps, the CDp polars do not collapse; W3 is more efficient than W1 at a CL of 0.50 having 27 counts less profile drag. This is due to the reduced outboard sweep of W3 and the reduced angle of attack of W3 (due to it's increased lift curve slope). W3 has a more open polar shape which equates to greater leading edge suction or, equivalently, less separated flow.

Planform Effect

W3 is more efficient than W1

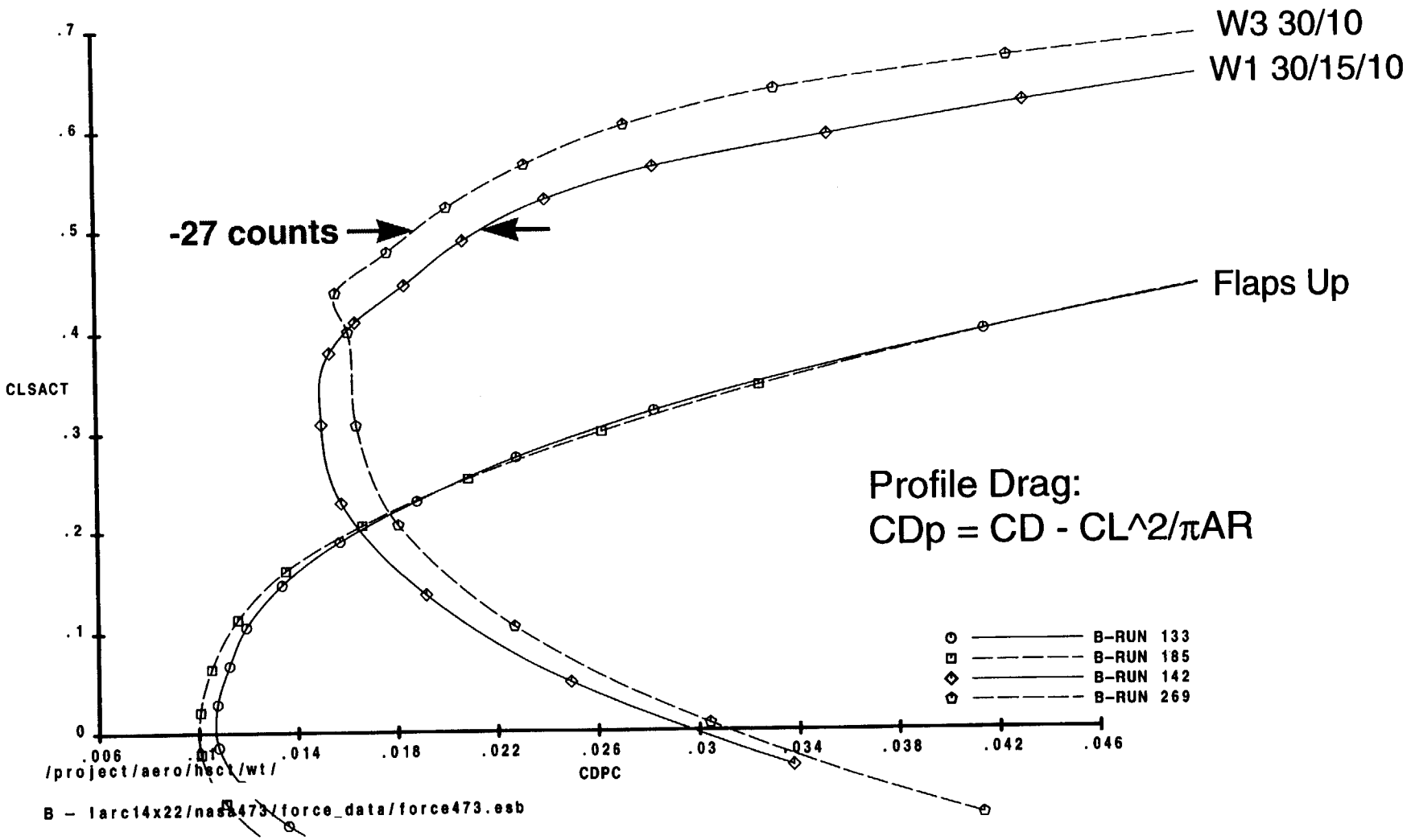

2.8-38 Buildup from adjusted TCA-4 (no canard)

This chart illustrates the drag buildup for the 2-surface (H1 tail only) 2.8-38 from final, corrected 14'x22' wind tunnel data at a climbout lift coefficient of 0.5 and Reynolds number of 8 million. The data are for flaps 30/10 and come from test NASA473, using the modified TCA model.

Ref. H NTF data is used to adjust the drag from 8 million to 90 million Reynolds number. Skin friction drag is analytically adjusted to account for the expected drag difference between Reynolds numbers of 90 million (NTF) and 200 million (flight). A 20 count drag reduction is applied based on drag differences observed for the TCA between the 14'x22' and NTF tunnels. This adjustment makes the 14'x22' based 2.8-38 buildup consistent with the NTF based TCA buildup.

TCA H1 tail polars and downwash (adjusted for wing aspect ratio) extracted from TCA-1 data are used to trim the tail-off configuration. A better approach, not taken because of time limitations, would be to extract the downwash from NASA473. H1 was not tested in NASA473. The resultant trim drag is much larger than for the TCA because of a more negative tail-off pitching moment and reduced wing downwash.

A rather large programmed flap increment is predicted by AERO3S.

A technology projection of 40.1 counts drag reduction is applied to reach the target suction level of 92% (no thrust). This is nearly the same as that applied in the TCA buildup. The improved tail-off performance of wing 3 (2.8-38) relative to wing 1 (TCA) is lost due to increased trim drag.

2.8-38 Buildup from adjusted TCA-4 (no canard)

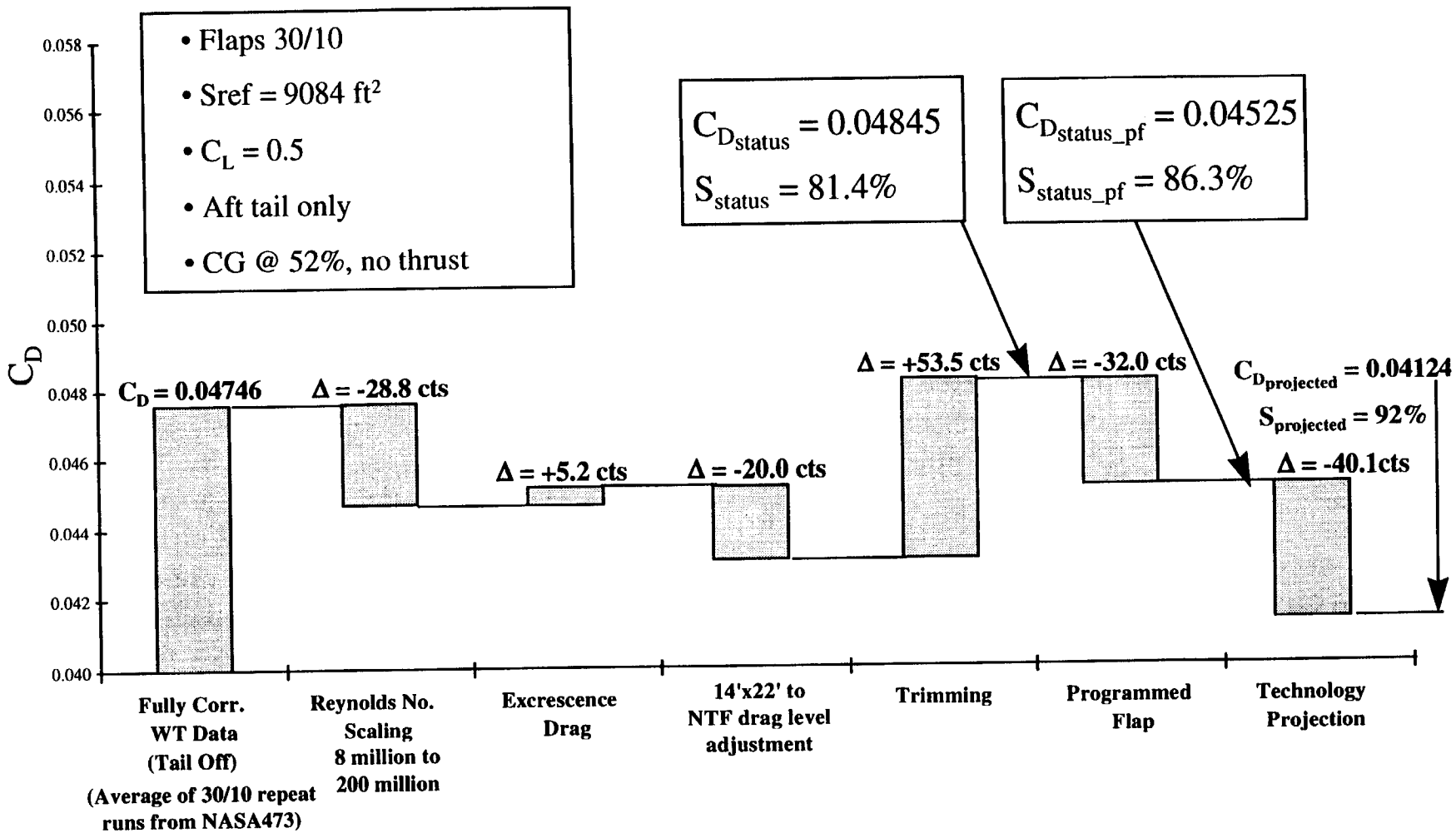

Effect of Canard on Trim Drag

The chart shows tail + trim drag (includes CDo of the trimming surfaces) as a function of the wing/body pitching moment to be trimmed. Curves are shown for the H1 tail only, the H3 tail only (H3 is 2/3 the size of H1), and the CN1 canard with the H3 tail 3-surface configuration.

The data are based on the method adopted for the Common PD Process which is used to predict full scale characteristics for arbitrary HSCT configurations. For 3-surface configurations, trimming becomes a problem as there are an infinite number of canard and tail loading combinations available to trim a given pitching moment. A simple theoretical approach is used to determine the optimum canard load. Any remaining pitching moment is trimmed by the tail. For the 3-surface configuration, most of the trimming is done with the canard.

The addition of a canard gives a large reduction in trim drag relative to trimming with only a tail, about 20 counts less at a pitching moment of -0.03.

The red asterisks are optimum trimming data from the TCA-4 wind tunnel test and are in good agreement with the optimal trimming method employed by the Common PD Process.

Effect of Canard on Trim Drag

Even a small canard provides a large trim drag reduction

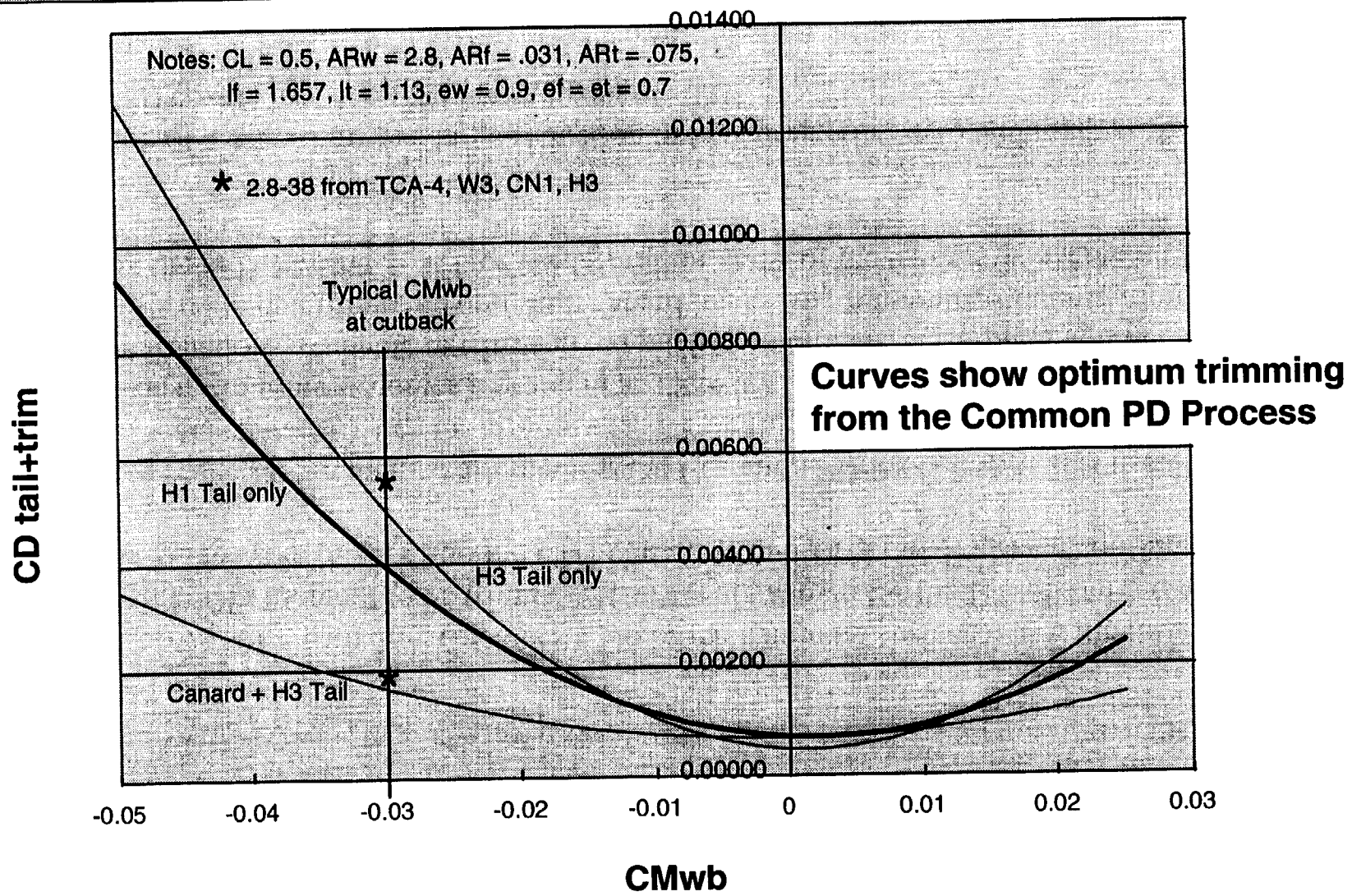

2.8-38 Buildup from adjusted TCA-4 (3-Surface)

This chart illustrates the drag buildup for the 3-surface (CN1 canard with H3 tail) 2.8-38 from final, corrected 14'x22' wind tunnel data at a climbout lift coefficient of 0.5 and Reynolds number of 8 million. The buildup is the same as before with the exception of trimming.

The canard is used to trim the wing/body pitching moment up to its optimal lift or a preset limit. Any remaining pitching moment is trimmed with the tail. Trim drag is only 9.3 counts compared to 53.5 counts with the H1 tail only.

The programmed flap increment is also much smaller than before (-6.8 counts versus -32.0 counts) indicating that the baseline 30/10 flap deflections are nearly optimum for the 3-surface configuration (30/10 was picked as the baseline climb-out flap during the TCA-4 WT test for this reason).

A technology projection of 26.1 counts drag reduction is applied to reach the target suction level of 93% (no thrust). Note that the target suction parameter is increased from 92% to 93% for the addition of a forward trimming surface.

2.8-38 Buildup from adjusted TCA-4 (3-Surface)

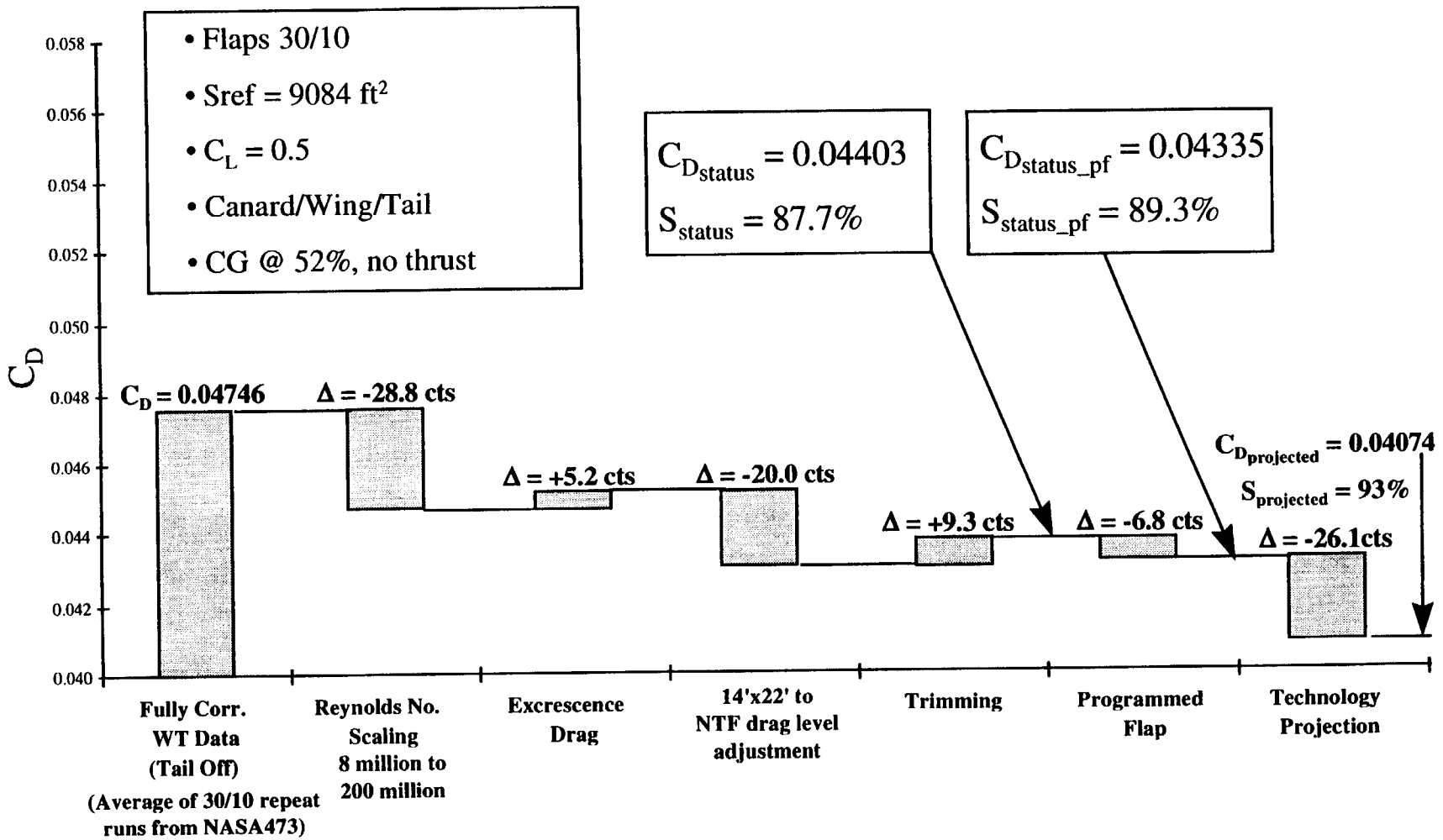

Effect of Sealed Slats

Reduces Viscous Drag Increase with CL

The chart shows TCA drag polars for a configuration having full span plain leading edge flaps and for another having full span sealed slats. The data are from the TCA-3 test in the Ames 12' pressure tunnel. The trailing edge flaps are deflected 15°/10°, the plain LE flaps 30°, and the sealed slats 35° . These are approximately optimum settings for each configuration.

The sealed slat significantly reduces the viscous (as opposed to induced) drag of the wing. At a CL of 0.50, the sealed slats provide a 37 count drag reduction. The reduced upper surface curvature afforded by the sealed slat allows the flap leading edge to be better aligned with the onset flow without causing upper surface flow separation at the hingeline.

Effect of Sealed Slats

Reduces Viscous Drag Increase with CL

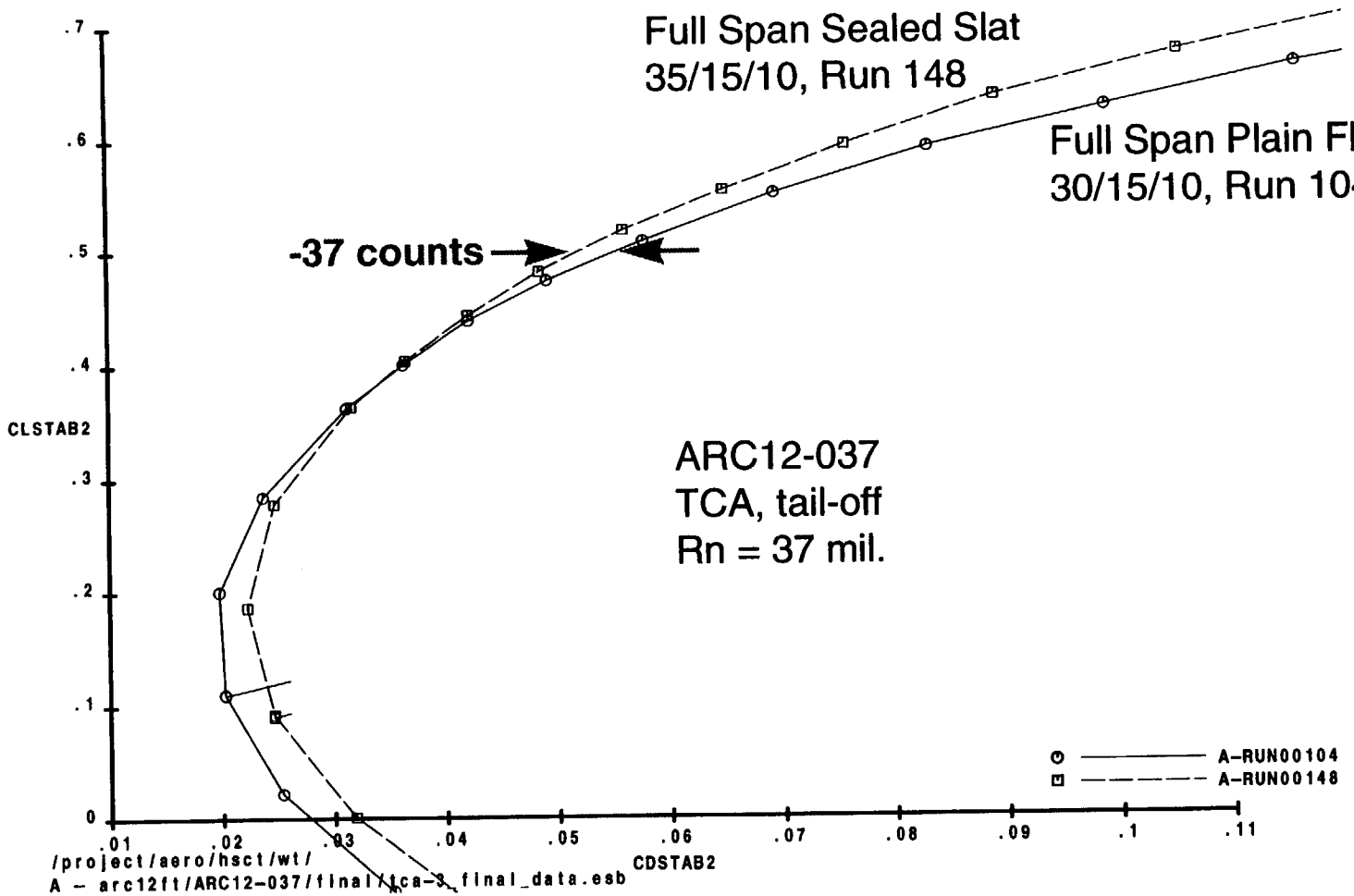

TCA Buildup from Mod Ref H + Sealed Slats

This chart illustrates the drag buildup for the TCA with full span sealed slats. An increment for 35° full span sealed slats relative to 30° full span plain leading edge flaps was obtained from the TCA-3 test in the Ames 12' tunnel. This increment was applied directly to the NTF based TCA buildup shown previously. It is assumed that the -12.5 count programmed flap increment still applies but this is debatable.

The status level suction parameter that results is 91.7%, very near the 92% (no thrust) target; a technology projection of only 2.9 counts drag reduction is needed to reach 92%.

TCA Buildup from Mod Ref H + Sealed Slats

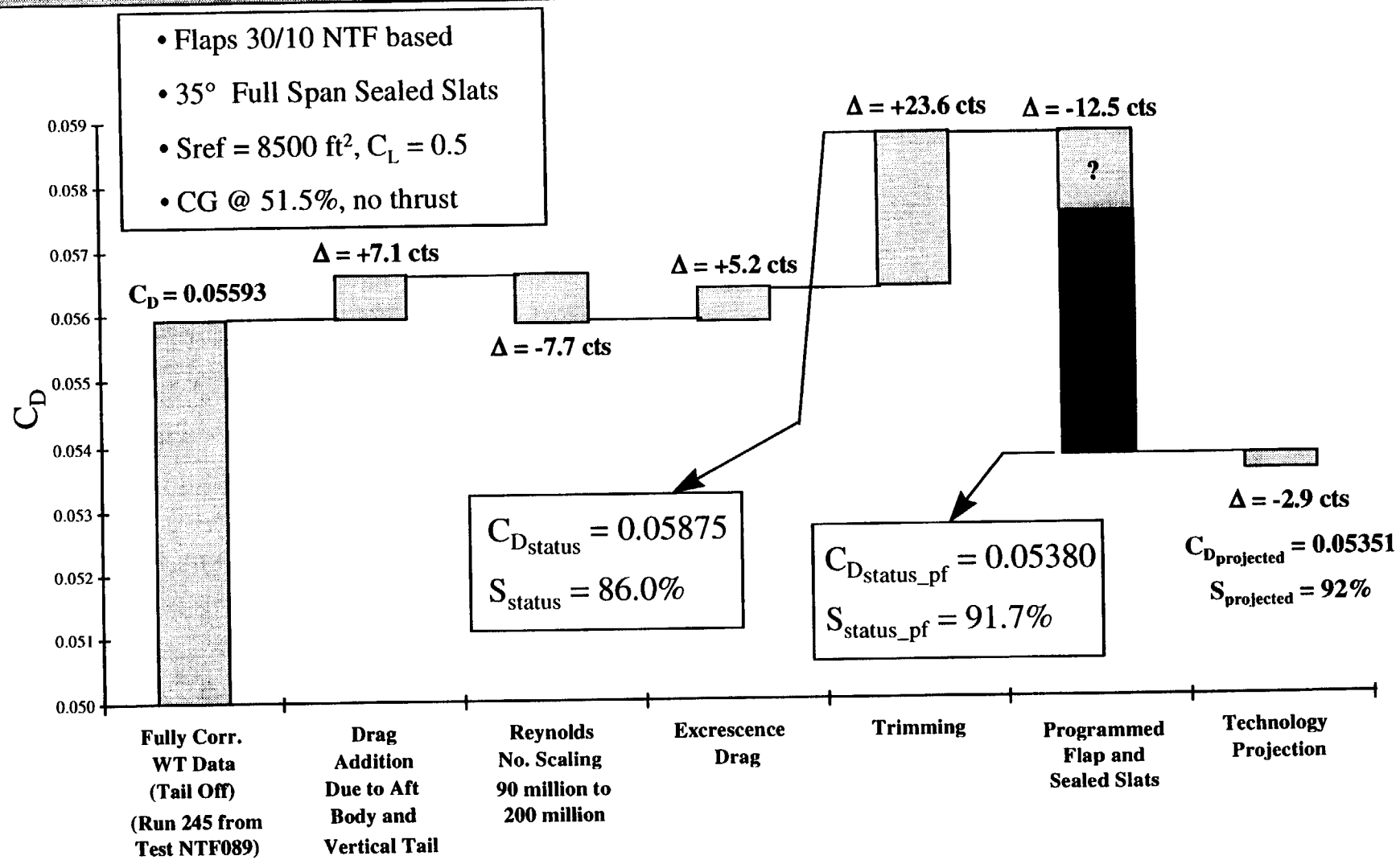

Sealed Slats - Planform Effect

Will W3 get the same benefit as W1?

As before, this slide shows profile drag (CDp = CD - CL^2/πAR) polars for W1 and W3 for flaps up and climbout flaps.

The green star shows W1 CDp at a CL of 0.50 with full span sealed slats, which provide a drag reduction of 37 counts. Note that the resulting drag level is still some 20 counts greater than CDpmin for W1 and that CL at CDpmin (CLp) is about 0.30.

If the same 37 count drag reduction is assumed to apply to W3, the resulting CDp (yellow star) is slightly less than CDpmin (at CLp of 0.40 to 0.43) for W3. This is very unlikely since, as will be shown later, there is always an increase in CDpmin as the CL @ CDpmin is increased. That is, moving the drag bucket to a CL of 0.50 should result in a larger CDpmin than if CLp is at 0.43.

The true effect of sealed slats and variable camber leading edge flaps on higher aspect ratio wings such as W3 will be determined during the TCA-5 WT test at the Ames 12' pressure tunnel.

Sealed Slats - Planform Effect

Will W3 get the same benefit as W1?

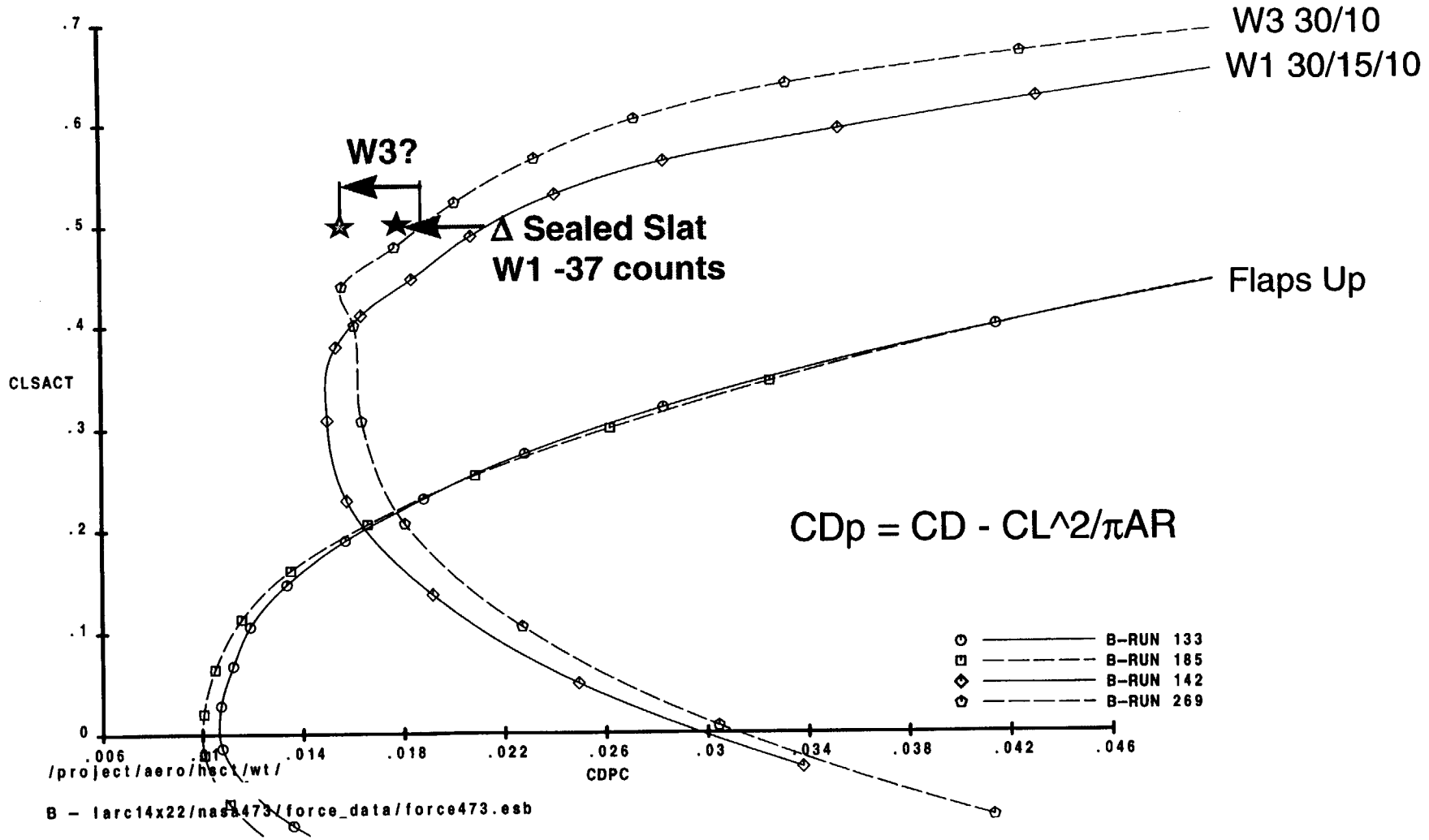

Components of Drag

This slide shows components of drag. The magnitude of the drag increments is representative of a typical HSCT configuration. Starting at CDo,

1) There is drag due to the body being at non-zero angle of attack ($\Delta CD\alpha body$).
2) Viscous drag on the wing increases with CL (ΔCDp).
3) The wing/body combination, flaps up, generates more than the ideal induced drag (ΔCDi).
4) Deflecting the trailing edge flaps further perturbs the span loading away from the ideal due to the cut-outs for the engine nozzles($\Delta CDi\delta f$).
5) Trimming the wing/body pitching moment creates trim drag at typical operating cg's. The increment shown is for trimming with a tail alone; the trim drag is greatly reduced when trimming with a canard ($\Delta CDtrim$).
6) For typical HSCT planforms, at a CL of 0.50, the bulk of the drag is ideal induced drag equal to $CL^2/\pi AR$ (ideal CDi).

Of the above drag components, we can significantly affect only items 2 (ΔCDp) and 5 ($\Delta CDtrim$), the former by the selection of the planform and the LE and TE flap configuration and the later by the selection of the longitudinal trimming configuration (tail only or with a canard). Even so, ΔCDp cannot be reduced to zero nor can $\Delta CDtrim$ for typical operating cg's.

Components of Drag

1 ΔCDαbody

2 ΔCDp (viscous drag)

3 ΔCDi (flaps up)

4 ΔCDi (due to flaps)

5 ΔCDtrim (tail only)

6 CL^2/πAR (ideal CDi)

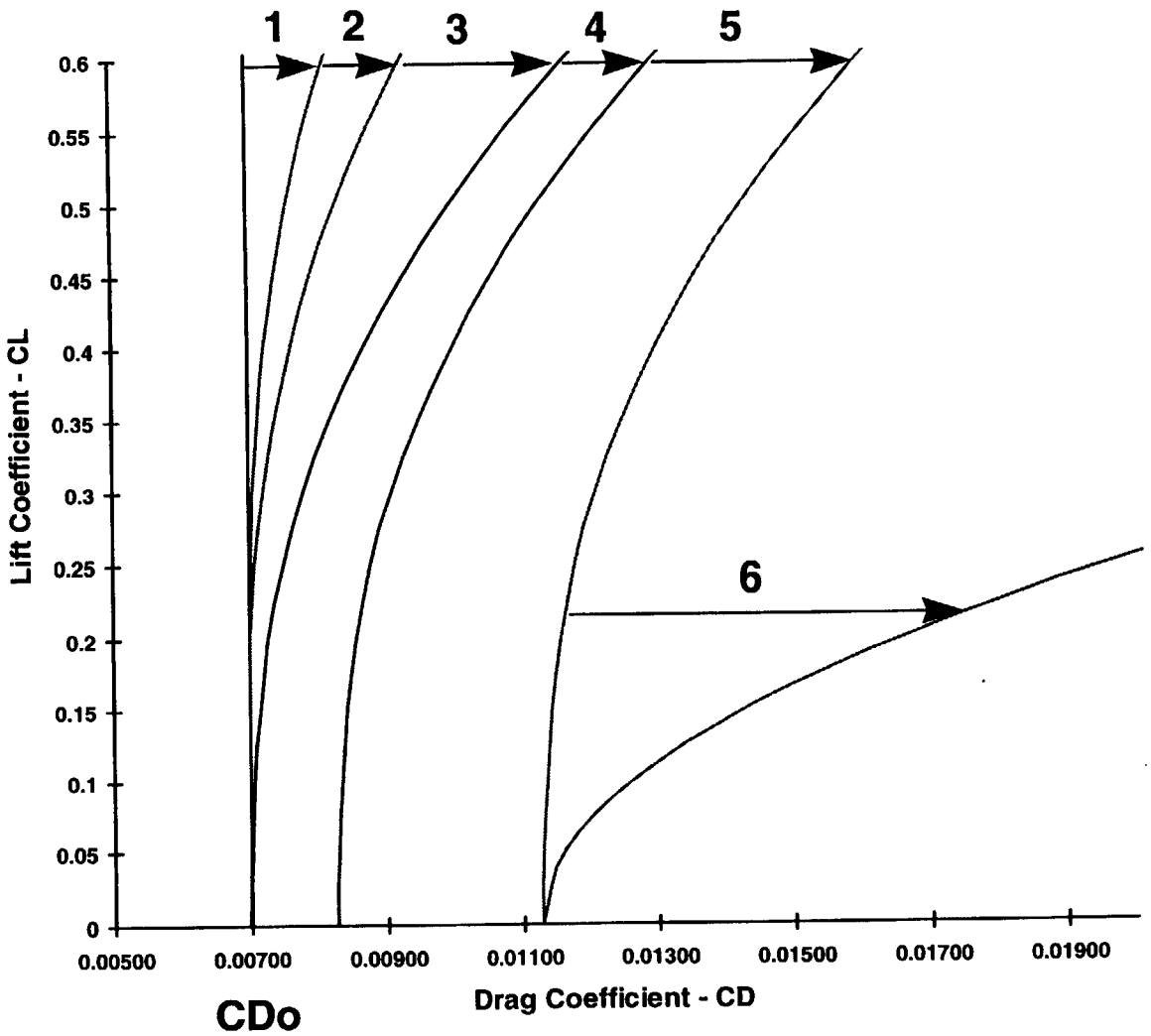

Sectional Profile Drag

Lift is not free, even in 2D

This slide shows two dimensional drag polars for a wing section with a variety of LE flap types and angles. The polars can be used to construct an envelope polar from the locus of Cdpmin's.

To the left, in red, is an idealized polar derived from Helmbold theory. This polar is basically Cdo plus the viscous drag due to generating lift for a fully attached, turbulent flow. Lift is made by accelerating flow over the upper surface which imposes velocity gradients on the boundary layer and increases the drag over that of a flat plate at zero incidence.

Because the idealized polar has fully attached flow, it might be considered as the best possible 2D polar. The 3D equivalent of this idealized viscous polar was used to determine the ΔCDp used in the previous discussion of components of drag.

Sectional Profile Drag

Lift is not free, even in 2D

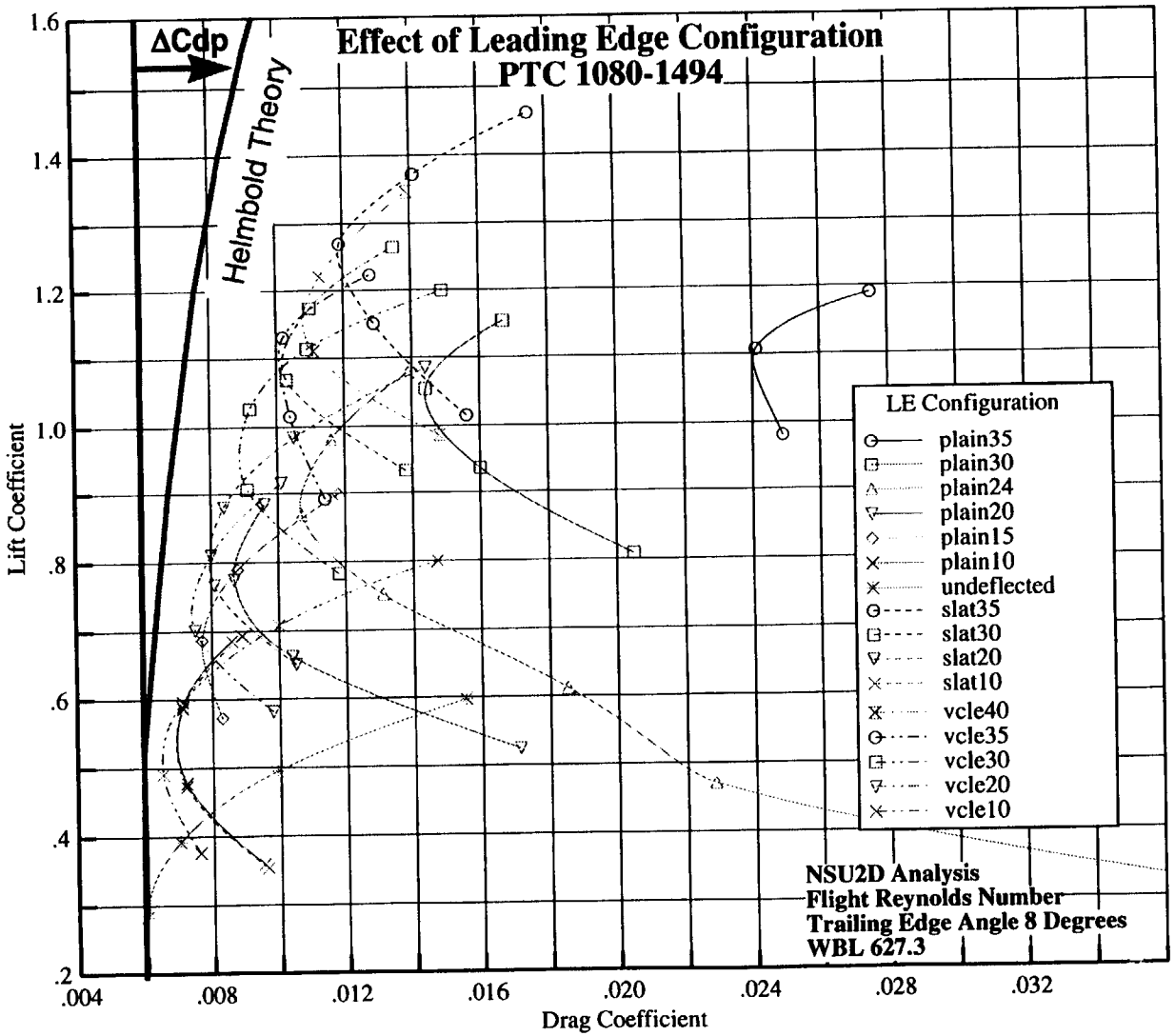

Leading Edge Suction Parameter - S

S is a Measure of Aerodynamic Efficiency

The leading edge suction parameter, S, is the ratio of the difference between the actual drag due to lift and the worst possible drag due to lift (CLtan[CL/CLα]) and the difference between the best possible drag due to lift (CL^2/πAR) and the worst possible drag due to lift.

S = 1 corresponds to full leading edge suction (fully attached flow) while S = 0 corresponds to no leading edge suction (fully separated flow).

The suction parameter is a very useful mesure of aerodynamic efficiency for delta wings that operate with substantial amounts of leading edge separation. It is less useful, or at least overly complicated, for current HSCT configurations which are designed to avoid formation of leading edge vortices.

Leading Edge Suction Parameter - S

S is a Measure of Aerodynamic Efficiency

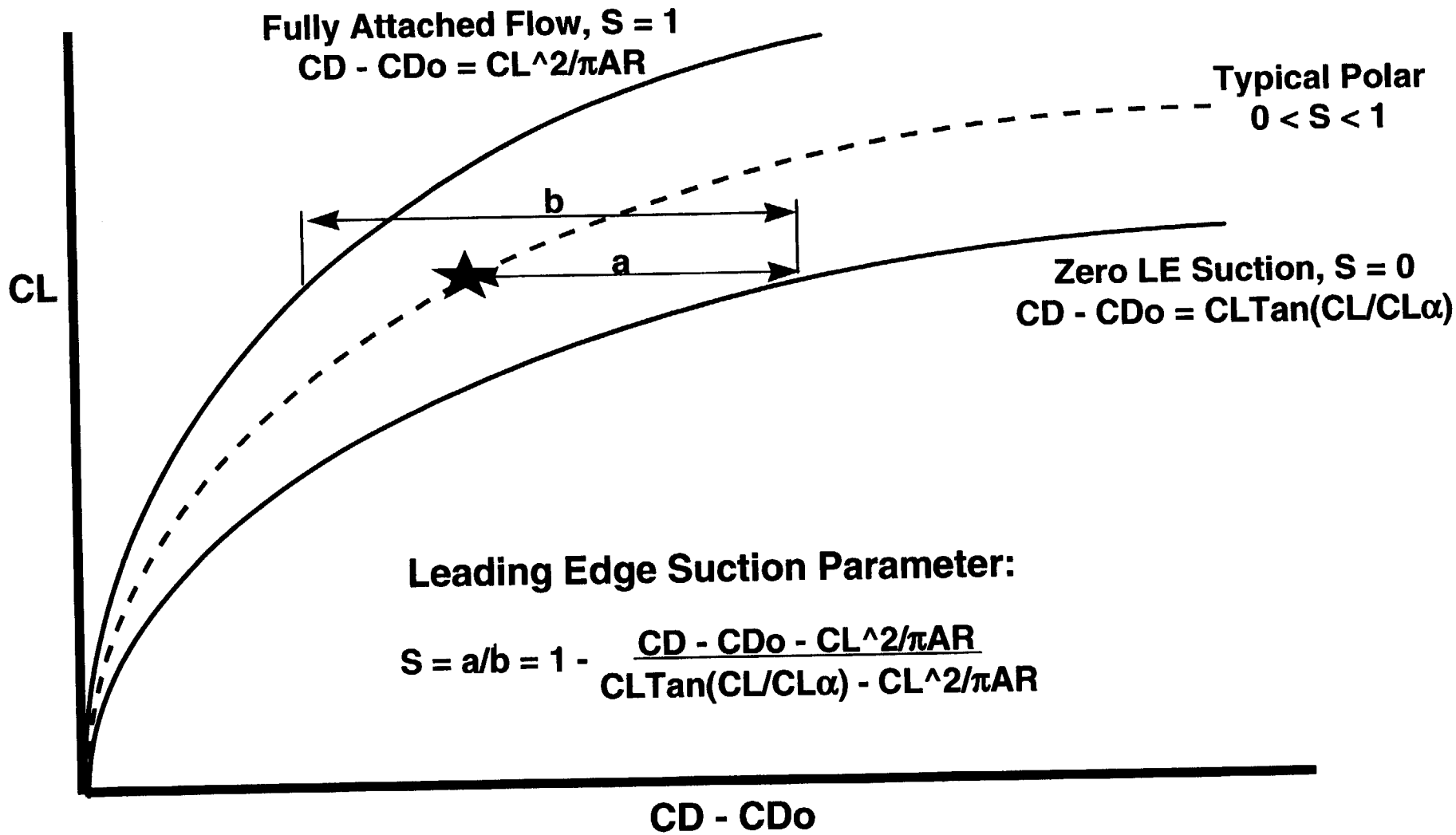

Suction Parameter Limits

Practical Limit is $S \leq 0.95$

This slide shows how the various components of drag limit the achievable suction parameter (S) at the operating CL of 0.50, no thrust. The drag increases shown are roughly the minimum achievable for a practical configuration and thus help to bound the technology projection. A configuration with no trim drag and a complex boundary layer control system could be expected to have a suction parameter of 95% at most.

The slide shows why the high lift technology projections of S = 92% (CL = 0.50, no thrust, no canard) and S = 93% (CL = 0.50, no thrust, with canard) are reasonable limits.

Suction Parameter Limits

Practical Limit is S ≤ 0.95

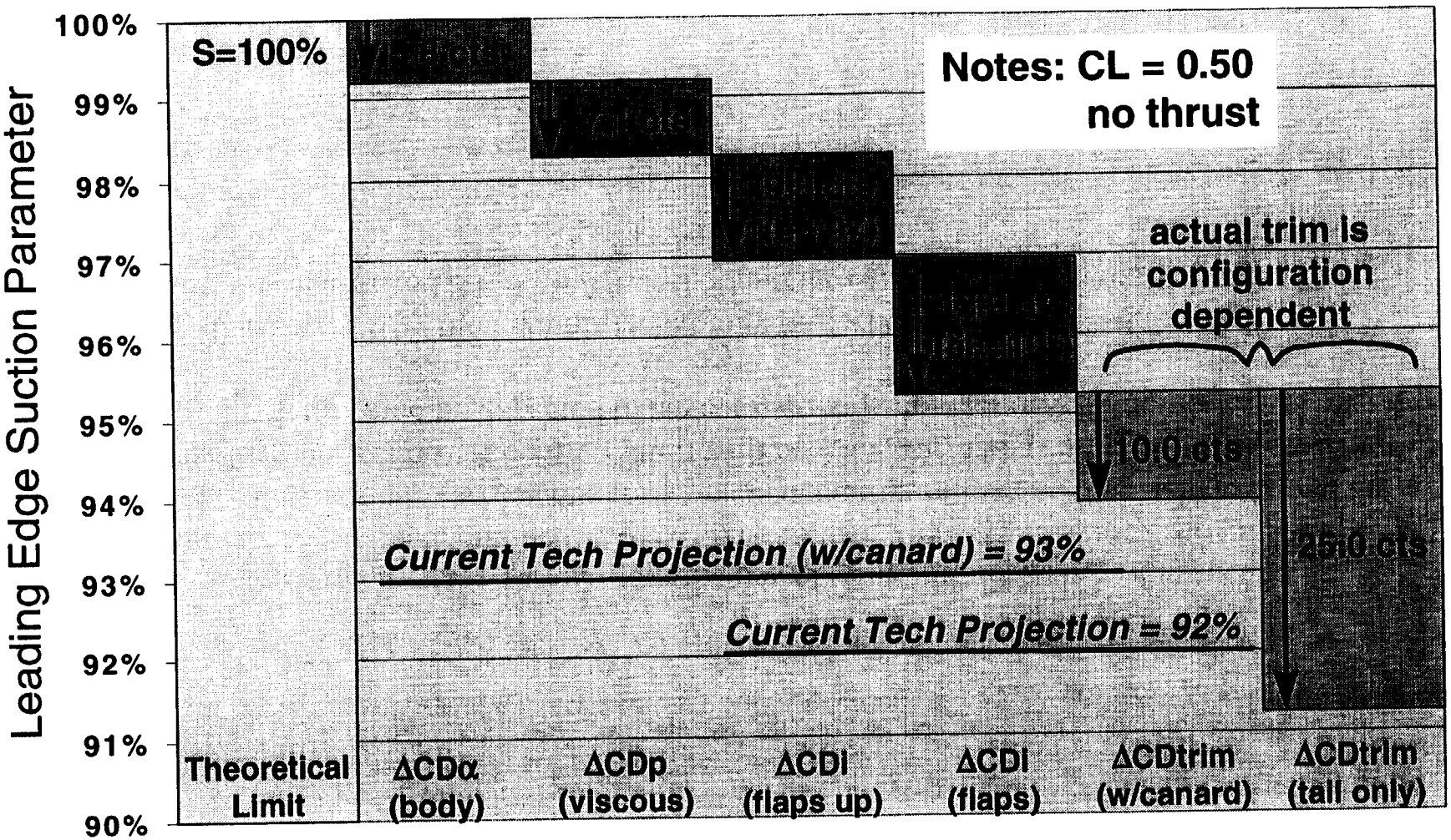

Metric AP-3 - Leading Edge Suction Parameter

Technology Projection is Aggressive

This slide shows the leading edge suction parameter (S) for a variety of configurations. The bars represent the degree of uncertainty in the full scale prediction and the stars within the bars how the actual status level. The horizontal bold lines show the projected suction parameters, 94% without canards and 95% with canards, at a CL of 0.50. Note that for purposes of doing the metrics roll-up, the data on this chart include the thrust vector effect as part of CL and CD, and hence S - these are "with thrust" numbers and are therefore higher than the "no thrust" suction parameters previously discussed.

Much progress was made using the TCA model; with full span sealed slats the TCA exhibits S = 93.7% versus a projection of 94%. The other configurations will also require sealed slats or variable camber leading edge flaps to meet their technology projections.

The difficulty of achieving the projected suction parameters is a measure of the aggressiveness of the technology projection. The previous discussion on suction parameter limits explains this in more detail.

Metric AP-3 - Leading Edge Suction Parameter

Technology Projection is Aggressive

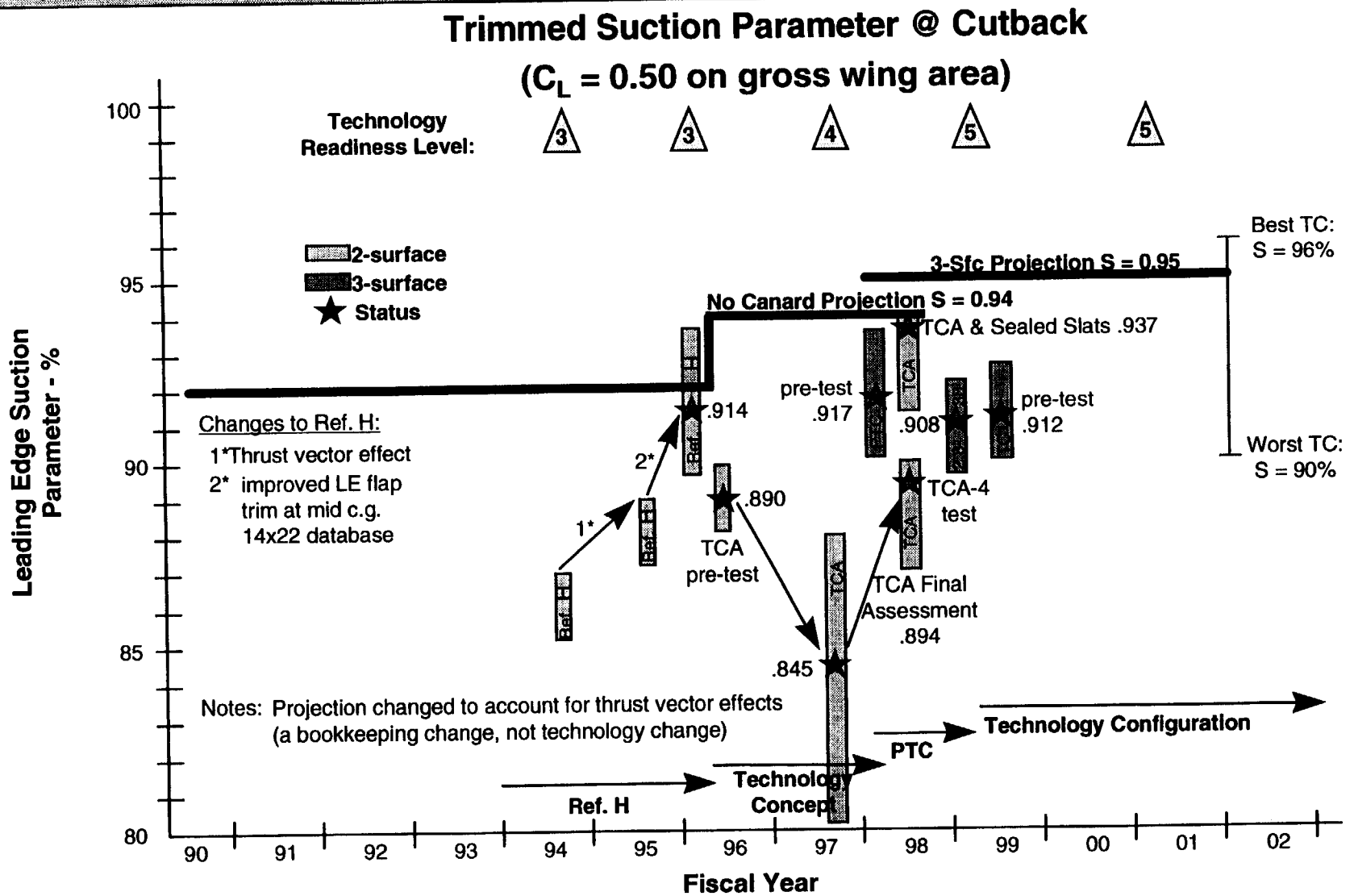

Metric AP-4 - Climb Out Lift/Drag Ratio

Span is our Friend!

This slide shows climb out L/D for a variety of configurations. The bars represent the degree of uncertainty in the full scale prediction and the stars within the bars how the actual status level. The horizontal bold lines show the projected L/Ds which vary widely because of the differences in aspect ratio between the configurations. Note that for purposes of doing the metrics roll-up, the data on this chart include the thrust vector effect as part of CL and CD, and hence L/D - these are "with thrust" numbers and are therefore higher than the "no thrust" L/Ds previously discussed.

The comments regarding AP-3, the suction parameter, pertain here as well.

Finally, while L/D is the parameter which impacts configuration sizing, it is a very poor measure of efficiency since it is largely planform (aspect ratio) dependent. Suction parameter is much more meaningful for comparing the efficiencies of various configurations.

Metric AP-4 - Climb Out Lift/Drag Ratio

Span is our Friend!

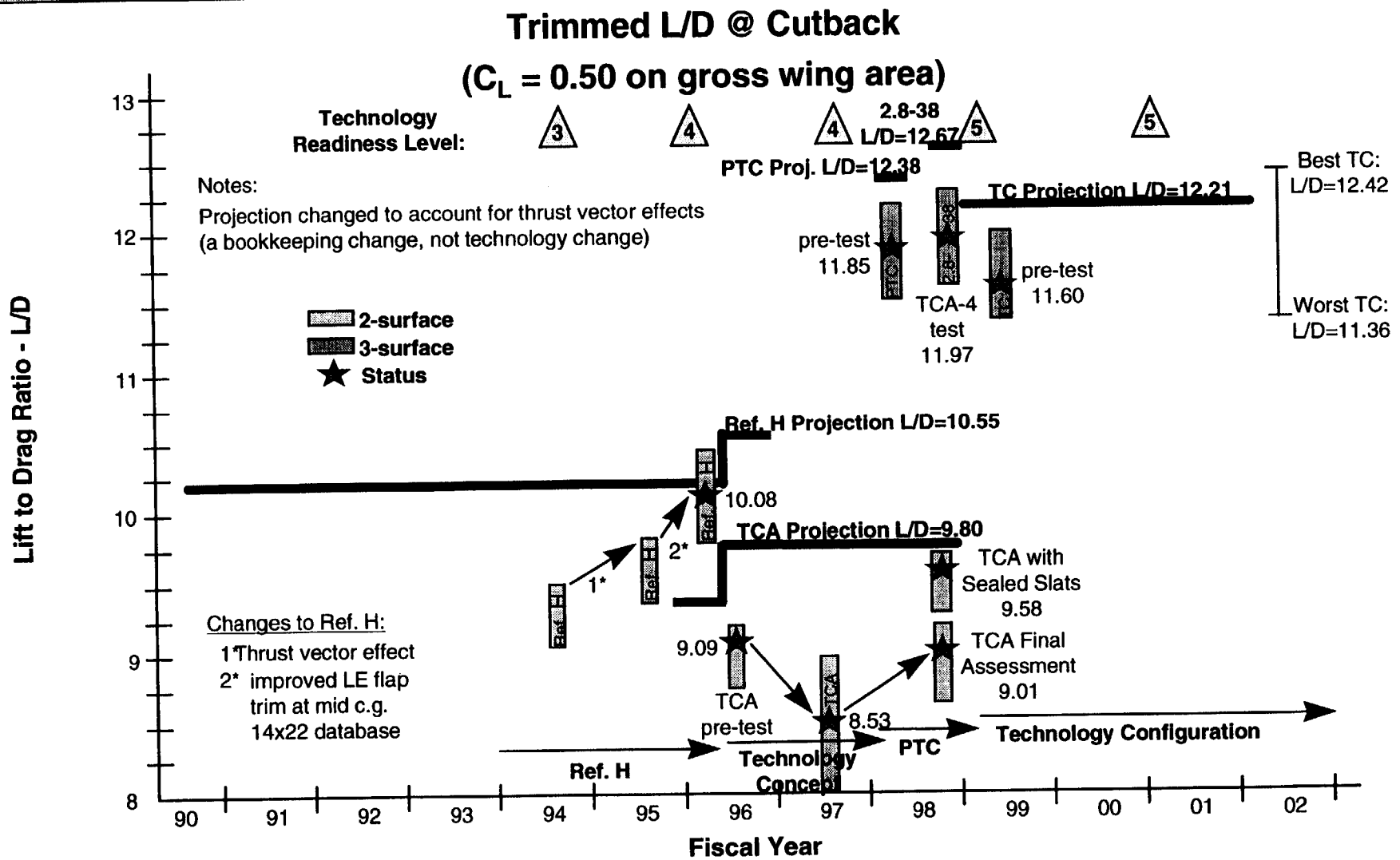

Conclusions

(1) Large variations between status & projected L/D
Variation between wind tunel data bases
Variation caused by PD process (heavy reliance on AERO3S)

(2) W3 (2.8-38) is more efficient than W1 (2.0-52, TCA)
At CL = 0.50, drag is 27 counts less than expected from AR increase
Canard required to exploit wing benefit (reduces trim losses)

(3) Small Canard greatly reduces trim drag
For the 2.8-38 @ CL = 0.50, trim drag is reduced by 44 counts

(4) Sealed Slat or VCLE Flap required to meet Technology Projection
TCA achieves S = 91.7% versus target of 92% (no thrust)
Benefit may be less for wings of higher AR

(6) Current Technology Projection is Aggressive but Reasonable
Difficult to achieve but apparently within reach
Increased projection with canard (93% versus 92%) verified

Recommendations

(1) Reduce variation between WT data bases
For absolute drag levels, need to know upflow, tunnel bouyancy, and support system tare and interference corrections

(2) Improve PD prediction process
Asking too much of AERO3S
Next step is Navier-Stokes but its too slow & costly

(3) Double Technology Projection increase due to canard
Increase ΔSproj from +0.01 to +0.02 (93% to 94%, no thrust)

(4) Update Technology Projection
Should be a function of planform, flap type, and type of trimming

(5) Update Metrics to use no thrust S and L/D

REPORT DOCUMENTATION PAGE

Form Approved
OMB No. 07704-0188

1. AGENCY USE ONLY *(Leave blank)*	2. REPORT DATE	3. REPORT TYPE AND DATES COVERED
	December 1999	Conference Publication

4. TITLE AND SUBTITLE
1999 NASA High-Speed Research Program Aerodynamic Performance Workshop
Volume II—High Lift

5. FUNDING NUMBERS
537-07-51-10

6. AUTHOR(S)
Edited by David E. Hahne

7. PERFORMING ORGANIZATION NAME(S) AND ADDRESS(ES)
NASA Langley Research Center
Hampton, VA 23681-2199

8. PERFORMING ORGANIZATION REPORT NUMBER
L-17911C

9. SPONSORING/MONITORING AGENCY NAME(S) AND ADDRESS(ES)
National Aeronautics and Space Administration
Washington, DC 20546-0001

10. SPONSORING/MONITORING AGENCY REPORT NUMBER
NASA/CP-1999-209704/
VOL2/PT1

11. SUPPLEMENTARY NOTES

12a. DISTRIBUTION/AVAILABILITY STATEMENT
Unclassified–Unlimited
Subject Category 02 Distribution: Nonstandard
Availability: NASA CASI (301) 621-0390

12b. DISTRIBUTION CODE

13. ABSTRACT ***(Maximum 200 words)***

NASA's High-Speed Research Program sponsored the 1999 Aerodynamic Performance Technical Review on February 8-12, 1999 in Anaheim, California. The review was designed to bring together NASA and industry High-Speed Civil Transport (HSCT) Aerodynamic Performance technology development participants in the areas of Configuration Aerodynamics (transonic and supersonic cruise drag prediction and minimization), High Lift, and Flight Controls. The review objectives were to (1) report the progress and status of HSCT aerodynamic performance technology development; (2) disseminate this technology within the appropriate technical communities; and (3) promote synergy among the scientists and engineers working on HSCT aerodynamics. In particular, single and midpoint optimized HSCT configurations, HSCT high-lift system performance predictions, and HSCT simulation results were presented, along with executive summaries for all the Aerodynamic Performance technology areas. The HSR Aerodynamic Performance Technical Review was held simultaneously with the annual review of the following airframe technology areas: Materials and Structures, Environmental Impact, Flight Deck, and Technology Integration. Thus, a fourth objective of the Review was to promote synergy between the Aerodynamic Performance technology area and the other technology areas of the HSR Program.

14. SUBJECT TERMS
High-speed research; High-Speed Civil Transport

15. NUMBER OF PAGES
556

16. PRICE CODE
A24

17. SECURITY CLASSIFICATION OF REPORT	18. SECURITY CLASSIFICATION OF THIS PAGE	19. SECURITY CLASSIFICATION OF ABSTRACT	20. LIMITATION OF ABSTRACT
Unclassified	Unclassified	Unclassified	UL